

**Beyond single biomarker-isotope
studies in paleoclimatology – potential
and limitations of a coupled
 $\delta^2\text{H}_{n\text{-alkane}}-\delta^{18}\text{O}_{\text{sugar}}$ paleohygrometer
approach**

DISSERTATION

zur Erlangung des akademischen Grades eines
Doktors der Naturwissenschaften (Dr. rer. nat.)
an der Fakultät für Biologie, Chemie und Geowissenschaften
der Universität Bayreuth

vorgelegt von

Johannes Hepp

geboren am 26. Oktober 1988 in Ravensburg
Bayreuth, Oktober 2018

Die vorliegende Arbeit wurde in der Zeit von September 2014 bis Oktober 2018 in Bayreuth am Lehrstuhl Geomorphologie und in Halle-Wittenberg an der Professur für Bodenbiogeochemie unter Betreuung von Herrn PD Dr. Michael Zech angefertigt.

Vollständiger Abdruck der von der Fakultät für Biologie, Chemie und Geowissenschaften der Universität Bayreuth genehmigten Dissertation zur Erlangung des akademischen Grades eines Doktors der Naturwissenschaften (Dr. rer. nat.).

Dissertation eingereicht am: 31.10.2018

Zulassung durch die Promotionskommission: 07.11.2018

Wissenschaftliches Kolloquium: 15.02.2019

Amtierender Dekan: Prof. Dr. Stefan Peiffer

Prüfungsausschuss:

PD. Dr. Michael Zech (Gutachter)

Prof. Dr. Eva Lehndorff (Gutachterin)

Prof. Dr. Gerhard Gebauer (Vorsitz)

Prof. Dr. Ludwig Zöllner

Table of Contents

Summary	iii
Zusammenfassung	v
Acknowledgements	vii
Extended Summary	1
1 Introduction	1
2 Compound-specific isotope analyses of biomarkers	3
2.1 Lipid biomarker and compound-specific $\delta^2\text{H}_{n\text{-alkane}}$ analyses	3
2.2 Sugar biomarker and compound-specific $\delta^{18}\text{O}_{\text{sugar}}$ analyses	4
3 Principle of the coupled $\delta^2\text{H}_{n\text{-alkane}}\text{-}\delta^{18}\text{O}_{\text{sugar}}$ paleohygro- meter approach	4
3.1 Biomarker-based leaf water reconstructions	4
3.1.1 Excursus: Uncertainties of the $\delta^2\text{H}_{n\text{-alkane}}$ to $\delta^2\text{H}_{\text{leaf-water}}$ relationship	5
3.1.2 Excursus: Uncertainties of the $\delta^{18}\text{O}_{\text{sugar}}$ to $\delta^{18}\text{O}_{\text{leaf-water}}$ relationship	7
3.2 Leaf water enrichment theory	8
3.3 Reconstruction of plant source water $\delta^2\text{H}$, $\delta^{18}\text{O}$ and RH_{air}	9
4 Results & Discussion	10
4.1 Climate chamber validation study 1 (manuscript 1)	10
4.2 European climate transect validation study 2 (manuscript 2)	12
4.3 Application of the coupled $\delta^2\text{H}_{n\text{-alkane}}\text{-}\delta^{18}\text{O}_{\text{sugar}}$ approach to the terrestrial sedimentary archive of Maundi (manuscript 3)	14
4.4 Source identification of terrestrial versus aquatic sugars in lacustrine systems (manuscript 4)	17
4.5 Application of the coupled $\delta^2\text{H}_{n\text{-alkane}}\text{-}\delta^{18}\text{O}_{\text{sugar}}$ paleohygro- meter approach to the Gemündener Maar sedimentary record (manuscript 5)	18
4.6 Application of the coupled $\delta^2\text{H}_{n\text{-alkane}}\text{-}\delta^{18}\text{O}_{\text{sugar}}$ approach to the Lake Bergsee sedimentary record (manuscript 6)	19
5 Conclusions	21
References	36
Contributions to the included manuscripts	37
Included manuscripts	43
A. Manuscript 1: Hepp et al. (2019c)	45
B. Manuscript 2: Hepp et al. (2019b)	77
C. Manuscript 3: Hepp et al. (2017)	117
D. Manuscript 4: Hepp et al. (2016)	135
E. Manuscript 5: Hepp et al. (2019a)	145
F. Manuscript 6: Hepp et al.	171
Additional publications	203
Versicherungen und Erklärungen	205

Summary

Stable water isotopes have significantly contributed to the reconstruction of climate history qualitatively and quantitatively during the last decades. The hydrogen isotopic composition ($\delta^2\text{H}$) of terrestrial leaf wax-derived n -alkanes is used as source water $\delta^2\text{H}$ recorder, and is often interpreted as $\delta^2\text{H}_{\text{precipitation}}$. However, $\delta^2\text{H}_{n\text{-alkane}}$ is not only influenced by $\delta^2\text{H}_{\text{precipitation}}$ changes, but also by the incorporation of the leaf water enrichment signal caused by evapotranspiration. Therefore, single n -alkane $\delta^2\text{H}$ -based climate proxies are often interpreted only quantitatively. Oxygen isotopic composition ($\delta^{18}\text{O}$) of hemicellulose-derived sugars can be interpreted comparable to the $\delta^2\text{H}$ of n -alkanes. By combining $\delta^2\text{H}_{n\text{-alkane}}$ with $\delta^{18}\text{O}_{\text{sugar}}$ results, potentially a powerful tool is available for disentangling between source water and evapotranspirative enrichment changes. Such a coupled $\delta^2\text{H}_{n\text{-alkane}}-\delta^{18}\text{O}_{\text{sugar}}$ approach was shown to derive quantitative hydroclimate records, i.e. past $\delta^2\text{H}_{\text{source-water}}$, $\delta^{18}\text{O}_{\text{source-water}}$ and relative air humidity (RH_{air}) values, respectively. In previous studies, this coupling was therefore introduced as paleohygrometer approach in analogy to the often used paleothermometer approaches in Quaternary research. Within this PhD thesis I aim at contributing to the validation and the broader application of the coupled $\delta^2\text{H}_{n\text{-alkane}}-\delta^{18}\text{O}_{\text{sugar}}$ paleohygrometer approach, because a detailed validation and particularly the application to lake sediments is still missing.

The first two studies are therefore addressing the validation of the coupled $\delta^2\text{H}_{n\text{-alkane}}-\delta^{18}\text{O}_{\text{sugar}}$ (paleohygrometer) approach. Firstly, leaf sample material from a climate chamber experiment conducted with three different plant species was analyzed. The climate chamber experiment showed that leaf $\delta^2\text{H}_{n\text{-alkane}}$ and $\delta^{18}\text{O}_{\text{sugar}}$ are well correlated with $\delta^2\text{H}_{\text{leaf-water}}$, $\delta^{18}\text{O}_{\text{leaf-water}}$ ($r^2 = 0.45$ and 0.85 , respectively, $p < 0.001$, $n = 24$). RH_{air} was robustly reconstructed based on a simplified Craig-Gordon model. The second validation approach is a European topsoil transect study. It revealed that the coupled $\delta^2\text{H}_{n\text{-alkane}}-\delta^{18}\text{O}_{\text{sugar}}$ approach allows the reconstruction of $\delta^2\text{H}_{\text{source-water}}$, $\delta^{18}\text{O}_{\text{source-water}}$ and mean RH during day-time and vegetation period (RH_{MDV}). However, systematic offsets between biomarker-based (reconstructed) $\delta^2\text{H}_{\text{source-water}}$, $\delta^{18}\text{O}_{\text{source-water}}$ and RH_{MDV} values and a clear larger range compared to $\delta^2\text{H}_{\text{precipitation}}$, $\delta^{18}\text{O}_{\text{precipitation}}$ and climate station RH_{MDV} , respectively, were observed.

The application of the coupled $\delta^2\text{H}_{n\text{-alkane}}-\delta^{18}\text{O}_{\text{sugar}}$ approach to the terrestrial climate archive Maundi (Mt. Kilimanjaro, Tanzania) was successful, allowing the reconstruction of $\delta^2\text{H}_{\text{source-water}}$, $\delta^{18}\text{O}_{\text{source-water}}$ and day-time RH (RH_{D}) throughout the last ~ 100 ka for East African region. The observed strong positive relationship between the biomarker-based $\delta^2\text{H}_{\text{source-water}}$, $\delta^{18}\text{O}_{\text{source-water}}$ and deuterium-excess of leaf water values indicates that an amount effect in precipitation isotope composition seems not to be present on long time scales.

In order to provide the backbone for applying the coupled $\delta^2\text{H}_{n\text{-alkane}}-\delta^{18}\text{O}_{\text{sugar}}$ approach, a source identification study of terrestrial versus aquatic sugar biomarkers in lake sediments was conducted. For Late Glacial-Early Holocene sediments of Lake Gemündener Maar (Western Eifel region, Germany), the results show that arabinose is primarily of terrestrial origin while fucose and xylose stem predominantly from aquatic sources. This allows for using $\delta^{18}\text{O}_{\text{arabinose}}$ and terrestrial $\delta^2\text{H}_{n\text{-alkane}}$ results from Lake Gemündener Maar sediments in a coupled $\delta^2\text{H}_{n\text{-alkane}}-\delta^{18}\text{O}_{\text{sugar}}$ paleohygrometer approach in order to derive a day-time vegetation period RH (RH_{dv}) record. The results challenge the paradigmatic view

that the Younger Dryas is characterized by dry climatic conditions. They rather suggest that a relatively wet phase at the beginning of the Younger Dryas prevailed, which is followed by a more drier ending of the Younger Dryas. Also, large RH_{dv} changes during the Early Holocene were obvious which are more pronounced than the variations during the Allerød-Younger Dryas transition phase.

Finally, I aimed to apply the coupled $\delta^2H_{n\text{-alkane}}-\delta^{18}O_{\text{sugar}}$ approach also to the Late Glacial-Early Holocene sediments of Lake Bergsee (Southern Black Forest, Germany) in order to validate or falsify the findings from Lake Gemündener Maar. However, the source identification strongly suggest that the sugar biomarkers in that lake are primarily of aquatic origin. Hence, a coupling of terrestrial $\delta^2H_{n\text{-alkane}}$ with $\delta^{18}O_{\text{sugar}}$ records was not feasible. At the same time, the coupling of aquatic $\delta^2H_{n\text{-alkane}}$ with $\delta^{18}O_{\text{sugar}}$ records was not possible either, because $n\text{-C}_{23}$ could not be considered as robust aquatic biomarker.

Overall, the findings of the studies I conducted for this thesis highlight the large potential to derive quantitative hydroclimate information from the coupled $\delta^2H_{n\text{-alkane}}-\delta^{18}O_{\text{sugar}}$ (paleohygrometer) approach. At the same time, the reconstruction of $\delta^2H_{\text{leaf-water}}$ from $\delta^2H_{n\text{-alkane}}$ turned out to be a major uncertainty, representing the limitation regarding the reconstruction of rather small variability of $\delta^2H_{\text{source-water}}$, $\delta^{18}O_{\text{source-water}}$ and RH . Furthermore, a clear differentiation between terrestrial or aquatic origins of the $n\text{-alkane}$ and sugar biomarkers seems to be of fundamental importance for a successful application of the coupled $\delta^2H_{n\text{-alkane}}-\delta^{18}O_{\text{sugar}}$ approach to lacustrine archives.

Zusammenfassung

Die Analyse der stabilen Wasserisotope hat in den letzten Dekaden maßgeblich dazu beigetragen die Klimageschichte qualitativ wie auch quantitativ zu erfassen. Zur Rekonstruktion der Isotopenzusammensetzung des Wasserstoffs ($\delta^2\text{H}$) des Wassers, welches Pflanzen aufnehmen, wird oftmals die $\delta^2\text{H}$ von n -Alkan Biomarkern aus Blattwachsen herangezogen. Diese wird wiederum als $\delta^2\text{H}$ des Niederschlags interpretiert. Allerdings werden die $\delta^2\text{H}_{n\text{-Alkan}}$ Werte nicht nur durch Veränderungen in den $\delta^2\text{H}_{\text{Niederschlag}}$ Werten beeinflusst, sondern beinhalten auch ein Anreicherungssignal, welches bei der Evapotranspiration von Blattwasser auftritt. Daher können Klimaproxies, die allein auf $\delta^2\text{H}_{n\text{-Alkan}}$ Ergebnissen basieren, oft nur qualitativ interpretiert werden. Die Interpretation der Isotopenzusammensetzung des Sauerstoffs ($\delta^{18}\text{O}$) von Hemizellulose-bürtigen Zuckern ist vergleichbar mit der Interpretation der $\delta^2\text{H}$ von n -Alkanen. Die Kopplung von Beiden erweist sich als sehr hilfreich um zwischen den Veränderungen im Wasser, welches die Pflanzen aufnehmen und Änderungen in der Evapotranspiration von Blattwasser zu unterscheiden. Solch ein gekoppelter Ansatz kann daher dazu beitragen die hydroklimatischen Bedingungen in der Vergangenheit auch quantitativ zu erfassen. Dazu werden $\delta^2\text{H}_{\text{Wasser}}$ und $\delta^{18}\text{O}_{\text{Wasser}}$ Werte und relative Luftfeuchtigkeiten (RH) rekonstruiert. In vorangegangenen Arbeiten wurde diese Kopplung als Paleohygrometer Ansatz eingeführt, in Analogie zu den in der Quartärforschung oft verwendeten Paleothermometer Ansätzen. In dieser Arbeit will Ich einen Beitrag zur Validierung und der breiteren Anwendung des gekoppelten $\delta^2\text{H}_{n\text{-Alkan}}-\delta^{18}\text{O}_{\text{Zucker}}$ Ansatzes leisten, da eine detaillierte Validierung und insbesondere eine Anwendung auf Seesedimente bislang nicht erfolgt sind.

Die ersten beiden Studien befassen sich mit der Validierung des Ansatzes. Hierfür konnte zum einen auf Blattmaterial eines Klimakammerexperimentes mit drei verschiedenen Pflanzenarten zurückgegriffen werden. Das Klimakammerexperiment zeigt, dass die $\delta^2\text{H}_{n\text{-Alkan}}$ und $\delta^{18}\text{O}_{\text{Zucker}}$ Werte gut mit den $\delta^2\text{H}_{\text{Blattwasser}}$ bzw. $\delta^{18}\text{O}_{\text{Blattwasser}}$ Werten korreliert sind ($r^2 = 0.45$ und 0.85 , $p < 0.001$, $n = 24$). Zudem konnten die RH Bedingungen der Klimakammern mit Hilfe eines simplen Craig-Gordon Modell robust rekonstruiert werden. Als zweiter Validierungsansatz wurden $\delta^2\text{H}_{n\text{-Alkan}}$ und $\delta^{18}\text{O}_{\text{Zucker}}$ in Oberbodenproben eines europäischen Transektes analysiert. $\delta^2\text{H}_{\text{Wasser}}$ und $\delta^{18}\text{O}_{\text{Wasser}}$ sowie RH Werte konnten hiermit rekonstruiert werden. Die RH Werte sind hierbei repräsentativ für die gemittelten Bedingungen während des Tages und der Vegetationsperiode (RH_{MDV}). Jedoch gibt es eine systematische Abweichung zwischen den rekonstruierten $\delta^2\text{H}_{\text{Wasser}}$, $\delta^{18}\text{O}_{\text{Wasser}}$ und RH_{MDV} Werten sowie eine größere Streuung im Vergleich zu $\delta^2\text{H}_{\text{Niederschlag}}$, $\delta^{18}\text{O}_{\text{Niederschlag}}$ und RH_{MDV} Werten der Klimastationen.

Die Anwendung des gekoppelten $\delta^2\text{H}_{n\text{-Alkan}}-\delta^{18}\text{O}_{\text{Zucker}}$ Ansatzes auf das terrestrisches Klimaarchiv Maundi (Mt. Kilimanjaro, Tansania) erlaubte die Rekonstruktion von $\delta^2\text{H}_{\text{Wasser}}$ und $\delta^{18}\text{O}_{\text{Wasser}}$ und Tageszeit RH (RH_{D}) während der letzten ~ 100 ka für die Region Ostafrikas. Es besteht ein starker positiver Zusammenhang zwischen den Biomarkerbasierten $\delta^2\text{H}_{\text{Wasser}}$, $\delta^{18}\text{O}_{\text{Wasser}}$ Werten und dem Deuterium-Exzess des Blattwassers. Dies deutet darauf hin, dass der Niederschlagsmengen-Effekt auf die Niederschlagsisotopie für längere Zeitskalen keinen Einfluss hat.

Um eine solide Basis für die Anwendung des gekoppelten $\delta^2\text{H}_{n\text{-Alkan}}-\delta^{18}\text{O}_{\text{Zucker}}$ Ansatzes auf Seesedimente zu schaffen, wurde zunächst untersucht, wie zwischen dem terrestrischen und aquatischen Beitrag von sedimentären Zuckerbiomarkern unterschieden werden

kann. Für die Spätglazialen-Frühholozänen Sedimente des Gemündener Maars (West-eifel, Deutschland) konnte gezeigt werden, dass Arabinose hauptsächlich terrestrischen Ursprungs ist, während Fucose und Xylose maßgeblich auf aquatischen Eintrag zurückzuführen sind. Basierend auf terrestrischen $\delta^2\text{H}_{n\text{-Alkan}}$ und $\delta^{18}\text{O}_{\text{Arabinose}}$ Ergebnissen, kann damit der gekoppelte $\delta^2\text{H}_{n\text{-Alkan}}\text{-}\delta^{18}\text{O}_{\text{Zucker}}$ paleohygrometer Ansatzes etabliert werden. Die hiermit rekonstruierten RH Werte, welche die RH Bedingungen während der Vegetations- und Tageszeit widerspiegeln (RH_{dv}), stellen die paradigmatische Vorstellung einer trockenen Jüngerer Dryas in Frage. Die Ergebnisse deuten eher darauf hin, dass die Jüngere Dryas relativ feucht begonnen hat und sich erst zum Ende dieser Periode ein trockeneres Klima einstellt hat. Zudem wird offensichtlich, dass die Schwankungen in RH_{dv} im Frühholozän im Vergleich zur Übergangsphase zwischen Allerød und Jüngerer Dryas deutlich höher sind.

Zuletzt sollte der gekoppelte $\delta^2\text{H}_{n\text{-Alkan}}\text{-}\delta^{18}\text{O}_{\text{Zucker}}$ Ansatz auf die Sedimente des Bergsees (Südschwarzwald, Deutschland) übertragen werden. Jedoch zeigte sich, dass die Zuckerbiomarker im Bergsee maßgeblich aquatischen Ursprungs sind, was eine Kopplung von terrestrischen $\delta^2\text{H}_{n\text{-Alkan}}$ mit $\delta^{18}\text{O}_{\text{Zucker}}$ Ergebnissen verhindert. Zudem war auch keine Kopplung von aquatischen $\delta^2\text{H}_{n\text{-Alkan}}$ mit $\delta^{18}\text{O}_{\text{Zucker}}$ Ergebnissen möglich, da $n\text{-C}_{23}$ nicht als robuster aquatischer Biomarker herangezogen werden kann.

Die Ergebnisse der einzelnen Studien dieser Arbeit zeigen das große Potential des gekoppelten $\delta^2\text{H}_{n\text{-Alkan}}$ mit $\delta^{18}\text{O}_{\text{Zucker}}$ Ansatzes zur Ableitung von quantitativen hydroklimatischen Informationen. Es wird jedoch auch offensichtlich, dass insbesondere die Rekonstruktion von $\delta^2\text{H}_{\text{Blattwasser}}$ basierend auf $\delta^2\text{H}_{n\text{-Alkan}}$ Werten fehlerbehaftet sein kann, was die Rekonstruktion von kleinen Schwankungen in $\delta^2\text{H}_{\text{Wasser}}$, $\delta^{18}\text{O}_{\text{Wasser}}$ und RH limitiert. Zudem ist eine deutliche Unterscheidung zwischen terrestrischen und aquatischen Ursprungs der $n\text{-Alkan}$ - und Zuckerbiomarker eine Grundbedingung für die erfolgreiche Anwendung des gekoppelten $\delta^2\text{H}_{n\text{-Alkan}}\text{-}\delta^{18}\text{O}_{\text{Zucker}}$ Ansatzes auf Seesedimentarchive.

Acknowledgements

First of all, I want to thank my first supervisor PD Dr. Michael Zech for convincing me to begin with a PhD research and also to persevere. He came up with the first ideas about the content of this thesis, inspired me to develop new projects and supported me greatly throughout the whole period. I learned a lot from you, thank you very much! Secondly, I am very grateful to Prof. Dr. Bruno Glaser (Group of Soil Biogeochemistry, Martin-Luther-University Halle-Wittenberg). He always stood behind me throughout my PhD time, welcomed me to his working group and provided the laboratory infrastructure of the Soil Biogeochemistry group, which was crucial for this work. Many thanks for your great support during the last years!

I furthermore want to express my deep gratefulness to all the staff of the Soil Biogeochemistry group at the Martin-Luther-University Halle-Wittenberg, namely Marianne Benesch, Steven Polifka, Lucas Bittner, Tobias Bromm, Heike Maennicke, Andrea Lange and Dr. Katja Wiedner. Thank you very much for integrating me into the working group, critical discussion of the results, supporting me with all I needed and also for the hours of relaxing. In particular I want to thank Marianne Benesch for her great logistical support, especially during the first part of my PhD;), for standing hours in front of the measurement device, for the solution of many small problems, in short, for the great collaboration.

My great thanks go furthermore to Prof. Dr. Ludwig Zöller for mentoring me throughout my PhD time and for providing me the infrastructure at the University of Bayreuth. Furthermore, I would like to express my deep gratitude to Prof. em. Dr. Wolfgang Zech. Especially during the first difficult financial phase of my PhD, he was constantly behind me and he was a great mentor to me all the time. I also want to thank the German Environmental Foundation (DBU) for the great support during my PhD via a fellowship. Namely I am very grateful to Dr. Hedda Schlegel-Starmann for mentoring me throughout my not always easy times of funding.

I also want to thank Prof. Dr. Roland Zech and all his staff from his former group of Biogeochemistry and Paleoclimatology at the University of Bern, namely Dr. Lorenz Wüthrich, Dr. Imke Kathrin Schäfer, Marcel Bliedtner and Dr. Jana Zech. Thank you very much for deep discussion of the results, the exchange of measurement difficulties, the great support for solving them and for all the great collaboration. Without you, many manuscripts would not have been possible.

I'm very grateful to Dr. Rolf Siegwolf, Dr. Marco Lehmann and Dr. Matthias Saurer from the former Ecosystem Fluxes Group of the Paul Scherrer Institute, Villigen, Switzerland, for giving me the possibility to use your laboratory devices for ^{18}O measurements. Many thanks for your support, especially when my plans were not successful due to not robust results. It was a great pleasure to work with you together in the laboratory.

Thanks go also to Prof. Dr. Dr. Ingrid Kögel-Knabner from the Chair of Soil Science at the Technical University of Munich for the possibility to use the office infrastructure throughout the last period of my PhD time. I want to express my deep gratitude to Prof. Dr. Kazimierz Rozanski from the Faculty of Physics and Applied Computer Science, AGH University of Science and Technology in Kraków. He taught me not only a lot about leaf or lake water isotope modelling, but I also profited greatly from the constructive and fruitful discussions in which he often pointed to the real origin of the problems and he contributed greatly to

many manuscripts with his broad scientific insight. I learned a lot from him! Furthermore, I want to say many thanks to Dr. Mario Tuthorn. He was supporting me throughout my whole PhD time by discussing results, reviewing and proofreading manuscripts, and for valuable comments.

Finally, I'm very grateful to Dr. Anna-Saskia Kühnel for discussions and valuable comments in any time of the day and in all circumstances. She helped me furthermore a lot concerning questions in R, statistics and \LaTeX . Many thanks for your great support and your deep understanding, especially during the last phase of my PhD. Without you, finishing this thesis would not have been much fun. Many thanks for your great support!

Extended Summary

1 Introduction

The history of human evolution, and especially its cultural history, has always been strongly linked to climate variability (e.g. Behrensmeyer, 2006; Trauth et al., 2007; Sirocko, 2012). This explains why much scientific effort is spent for a better understanding of modern climate systems and climate changes of the past. Stable isotopes have contributed significantly during the last decades to reconstructing qualitatively and quantitatively climate history. For example, the stable oxygen isotopic composition ($\delta^{18}\text{O}$) of deep-sea records serves as proxy for global ice volume and $\delta^{18}\text{O}$, as well as the hydrogen isotope composition ($\delta^2\text{H}$), of ice cores from Antarctica and Greenland are used as proxy for global temperature history (Shackleton, 1987; Petit et al., 1999; Johnsen et al., 2001). With regard to terrestrial climate archives, deriving quantitative paleoclimate information, like relative humidity (RH) and isotope composition of precipitation ($\delta^2\text{H}_{\text{precipitation}}$, $\delta^{18}\text{O}_{\text{precipitation}}$), from biomarker-isotope proxy data could overcome typical limitations of so far applied qualitative interpretation approaches (Feng et al., 2007). Eley and Hren (2018) presented leaf wax-derived *n*-alkane chain-length pattern to derive past vapor pressure deficit changes. Furthermore, Gázquez et al. (2018) showed that triplicate oxygen stable isotope measurements of gypsum can be used for RH_{air} reconstructions. Triplicate oxygen isotope composition was also measured in phytoliths in order to derive RH information for a climate chamber and a topsoil transect study (Alexandre et al., 2018). Rach et al. (2017) used the differences in the hydrogen isotope composition of terrestrial and aquatic *n*-alkanes to calculate a RH_{air} record from the Allerød-Younger Dryas-Early Holocene transition, which were so far only qualitatively interpreted (Rach et al., 2014).

Limitations of single isotope approaches

The hydrogen isotopic composition of terrestrial leaf wax-derived lipid biomarkers (such as long-chain *n*-alkanes and *n*-alkanoic acids) are used as source water hydrogen isotope composition recorders, and are therefore often interpreted as $\delta^2\text{H}_{\text{precipitation}}$ records (e.g. Jacob et al., 2007; Seki et al., 2011; Rach et al., 2014; Muschitiello et al., 2015). Leaf wax $\delta^2\text{H}$ extracted from lacustrine surface sediments (Sauer et al., 2001; Huang et al., 2004; Sachse et al., 2004; Mügler et al., 2008; Rao et al., 2014) and from surface soils (Hou et al., 2008; Rao et al., 2009), also display high correlation with $\delta^2\text{H}_{\text{precipitation}}$. As lipid biomarkers are biosynthesized in the leaves of the plants, this correlation is based on a strong leaf water to precipitation (~plant source water) relationship which occurs when leaf water enrichment is of minor relevance (Sachse et al., 2012). Long-term $\delta^2\text{H}_{\text{precipitation}}$, $\delta^{18}\text{O}_{\text{precipitation}}$ variations show distinct correlation to local air temperature changes in temperate regions (e.g. Stumpp et al., 2014). In tropical regions the precipitation amount seems to play an important role (Dansgaard, 1964; Rozanski et al., 1993), at least on a seasonal time-scale (Rozanski et al., 1996). Araguás-Araguás et al. (2000) point out that effects associated with the moisture source (e.g. the transport history of the moisture or the temperature at the moisture source area) have to be taken into account when $\delta^2\text{H}_{\text{precipitation}}$, $\delta^{18}\text{O}_{\text{precipitation}}$ variations are interpreted. Thus, leaf wax $\delta^2\text{H}$ records in high latitudes were interpreted in terms of a temperature and moisture source proxy (Rach et al., 2014), while in low latitudes

(e.g. in South-East Africa) the interpretation follows the notion of the precipitation amount versus $\delta^2\text{H}_{\text{precipitation}}$, $\delta^{18}\text{O}_{\text{precipitation}}$ (Schefuß et al., 2011). However, when leaf water enrichment caused by evapotranspiration occurs, it is reflected in the leaf wax $\delta^2\text{H}$ signatures (e.g. Kahmen et al., 2013a) which is the reason single leaf wax $\delta^2\text{H}$ -based climate proxies are often interpreted only quantitatively. For a decade, also compound-specific $\delta^{18}\text{O}$ analysis of neutral sugar biomarkers are used in climate studies (Zech and Glaser, 2009; Zech et al., 2013; Zech et al., 2014a). Accordingly $\delta^{18}\text{O}_{\text{sugar}}$ can be interpreted comparable to the leaf wax $\delta^2\text{H}$. If the sugars can be associated with hemicellulose structures of higher vascular plants, they likely reflect the source water signal (i.e. precipitation) modified by evapotranspirative enrichment of leaf water (Tuthorn et al., 2014; Zech et al., 2014b).

Potential of the coupled $\delta^2\text{H}_{n\text{-alkane}}\text{-}\delta^{18}\text{O}_{\text{sugar}}$ approach

Leaf water enrichment is strongly driven by the RH_{air} in the surrounding of the leaves (as reviewed e.g. by Cernusak et al., 2016), which provides large potential to derive quantitative RH values from biomarker-isotopes such as leaf waxes and sugars. Indeed, a coupled approach using cellulose $\delta^2\text{H}$ and $\delta^{18}\text{O}$ values was developed to derive RH values (Voelker et al., 2014). This concept was also applied to sub-fossil wood samples to derive RH changes throughout the Last Glacial Maximum-Early Holocene transition. A conceptual approach of coupling $\delta^2\text{H}_{n\text{-alkane}}$ with $\delta^{18}\text{O}_{\text{sugar}}$ results in order to reconstruct $\delta^2\text{H}_{\text{precipitation}}$, $\delta^{18}\text{O}_{\text{precipitation}}$, as well as the RH_{air} , was recently validated via an Argentinian topsoil climate transect study (Tuthorn et al., 2015). This so-called paleohygrometer approach has the potential to disentangle the source water signal from the modifications caused by leaf water enrichment, overcoming the limitations of single biomarker-isotope approaches (for further details see section 3 and Figure 1). Zech et al. (2013) for the first time introduced this concept to derive RH_{air} and $\delta^2\text{H}_{\text{precipitation}}$, $\delta^{18}\text{O}_{\text{precipitation}}$ records for the last 220 ka from a permafrost paleosol sequence in North-East Siberia. Using n -alkane and sugar biomarkers to gain respective $\delta^2\text{H}$ and $\delta^{18}\text{O}$ results has advantages compared to using cellulose for compound specific $\delta^2\text{H}$ and $\delta^{18}\text{O}$ measurements (e.g. Mayr, 2002). Namely, the new approach overcomes challenges associated with (i) the interpretation of cellulose $\delta^2\text{H}$ results as derived from measurable nitro cellulose derivatives (e.g. Sternberg, 1988) and (ii) the complexity of the extraction, purification and $\delta^{18}\text{O}$ measurements (Mayr, 2002; Saurer and Siegwolf, 2004; Wissel et al., 2008). One essential requirement for a successful application of the coupled $\delta^2\text{H}_{n\text{-alkane}}\text{-}\delta^{18}\text{O}_{\text{sugar}}$ paleohygrometer approach is the biomarker source determination. When n -alkane and sugar biomarkers extracted from lake sediments originate mainly from aquatic sources no quantitative RH reconstructions can be derived (Hepp et al., 2015). Still, disentangling between the lake source water isotope signal ($\delta^2\text{H}_{\text{precipitation}}$, $\delta^{18}\text{O}_{\text{precipitation}}$) and alternations caused by lake water enrichment, both incorporated into the biomarkers, was possible. Overall, the lake water enrichment has to be interpreted in terms of evaporation versus precipitation amount changes (Hepp et al., 2015).

Given the above outlined limitations of single isotope approaches and the potential of the coupled $\delta^2\text{H}_{n\text{-alkane}}\text{-}\delta^{18}\text{O}_{\text{sugar}}$ approach, the following research objectives were addressed within this PhD thesis:

- Validating the coupled $\delta^2\text{H}_{n\text{-alkane}}\text{-}\delta^{18}\text{O}_{\text{sugar}}$ paleohygrometer approach using i) leaf sample material from a climate chamber experiment conducted with three different plant species (Mayr, 2002) and ii) topsoil samples along an European climate transect from Southern Sweden to Southern Germany (Schäfer et al., 2016).

- Application of the coupled $\delta^2\text{H}_{n\text{-alkane}}-\delta^{18}\text{O}_{\text{sugar}}$ approach to a terrestrial climate archive, namely the loess-like paleosol sequence Maundi from the Southern slopes of Mt. Kilimanjaro. This archive offered the potential to establish a first ~ 100 ka RH record for East Africa.
- Source identification of terrestrial versus aquatic sugar biomarkers in a lacustrine study. This forms the basis for the interpretation of $\delta^{18}\text{O}_{\text{sugar}}$ records established from lake sediments.
- Application of the coupled $\delta^2\text{H}_{n\text{-alkane}}-\delta^{18}\text{O}_{\text{sugar}}$ approach to two lake sedimentary archives from the West Eifel maar lake region (Lake Gemündener Maar) and the Southern Black Forest region (Lake Bergsee) in order to derive quantitative hydroclimate information from the Late Glacial-Early Holocene transition.

2 Compound-specific isotope analyses of biomarkers

The 'online' coupling of gas chromatographs via combustion or pyrolysis reactors to isotope ratio mass spectrometers (GC-C,Py-IRMS) developed around 30 years ago (Glaser, 2005; Amelung et al., 2009) augmented compound-specific isotope analyses of biomarkers. While $\delta^{13}\text{C}_{\text{sugar}}$ (e.g. Gross and Glaser, 2004) or $\delta^{13}\text{C}_{n\text{-alkane}}$ and $\delta^2\text{H}_{n\text{-alkane}}$ (e.g. Sessions et al., 1999; Zech and Glaser, 2008) biomarker analyses are nowadays well established in numerous scientific communities ranging from soil and plant science over climate research to forensics (Sachse et al., 2012; Diefendorf and Freimuth, 2016; Tipple et al., 2016; Jansen and Wiesenberg, 2017; Pedentchouk and Zhou, 2018), compound-specific $\delta^{18}\text{O}$ analyses of biomarkers have been realized and published by only three scientific working groups worldwide, hitherto.

2.1 Lipid biomarker and compound-specific $\delta^2\text{H}_{n\text{-alkane}}$ analyses

In order to obtain total lipid extracts from the leaf (manuscript 1), soil (manuscript 2), loess-like paleosol (manuscript 3) and lake sediment samples (manuscripts 5 and 6) three different extraction procedures were performed, i.e. accelerated solvent extraction (manuscript 3; e.g. Zech and Glaser, 2008), microwave extraction (manuscripts 1, 2 and 5; e.g. Veggi et al., 2013) and soxhlet extraction (manuscript 6; e.g. Bourbonniere et al., 1997). Solid phase chromatography via silica gel columns (aminopropyl-silica-gel (Supelco, 45 μm) filled pipettes) are used to separate the total lipid extract into a nonpolar fraction (incl. n -alkanes), a more polar fraction (incl. alcohols) and an acid fraction (incl. n -alkanoic acids). Therefore, the columns were flushed with organic solvents of increasing polarity, i.e. n -hexane, dichloromethane:methanol in a ratio of 1:1 and acetic acid:diethyl ether in a ratio of 1:19 (Hou et al., 2008; Schäfer et al., 2016) to extract the trapped fractions. If necessary (manuscripts 1, 2 and 5), the nonpolar fraction was cleaned over silver-nitrate coated silica gel columns and zeolith columns (Geokleen) in order to obtain a clean n -alkane fraction. Quantification of the n -alkanes was performed on GC to mass spectrometer couplings (manuscripts 1 and 5) and GCs equipped with a flame ionization detector (manuscripts 2, 3 and 6). Compound-specific n -alkane $\delta^2\text{H}$ analyses were performed using

a gas chromatography-isotope ratio mass spectrometry technique consisting of GC online connected via ^2H -pyrolysis reactor to an IRMS. The reactor temperature is thereby set to 1000 °C (GC5 pyrolysis, combustion interface equipped with a CR (ChromeHD) reactor; manuscripts 1 and 5), 1420 °C (in a GC-IRMS coupling of a TRACE GC Ultra and a Delta V Plus IRMS (Thermo Fisher Scientific, Bremen, Germany); manuscript 2), 1445 °C (in a GC-IRMS system equipped with a HP 6890 GC and a DeltaPLUSXL IRMS; manuscript 3) and 1425 °C (for an empty ceramic tube 2H-pyrolysis reactor in the GC IsoLink interface (Thermo Fisher Scientific, Bremen, Germany); manuscript 6). Co-analysing *n*-alkane standard mixtures with known isotope composition (supplied by A. Schimmelmann, University of Indiana) was used for calibration of the lipid $\delta^2\text{H}$ results and checking the precision of the GC-IRMS system. Latter was also ensured by measuring the H_3^+ factor routinely, which stayed constant during the measurement periods.

2.2 Sugar biomarker and compound-specific $\delta^{18}\text{O}_{\text{sugar}}$ analyses

Monosaccharide sugar biomarkers were extracted hydrolytically using 4M trifluoric acid for 4 h at 105 °C from all samples, according to standard procedures (Guggenberger et al., 1994; Amelung et al., 1996). Afterwards, the extracts were cleaned and purified over glass fibre filters followed by XAD-7 (removal of humic-like compounds) and DOWEX 50WX8 (removal of cations) columns. After freezing and freeze-drying the samples, methylboronic acid derivatization was conducted (Knapp, 1979) in order to make the monosaccharides arabinose, fucose, xylose and rhamnose GC-amenable (Gross and Glaser, 2004), allowing for the compound-specific $\delta^{18}\text{O}$ analyses (Zech and Glaser, 2009). Compound-specific $\delta^{18}\text{O}_{\text{sugar}}$ analyses were performed on a GC-IRMS system that was coupled online via an ^{18}O -pyrolysis reactor, which was set to 1280 °C (Zech and Glaser, 2009). The co-analysis of external sugar standards containing arabinose, fucose, xylose and rhamnose in different concentrations and of known isotope compositions ensured the 'Principle of Identical Treatment' standard for stable isotope analysis (according to Werner and Brand, 2001), and allowed furthermore the correction for possibly occurring amount effects (according to Zech and Glaser, 2009).

The compound-specific isotope results are expressed in the common delta notation ($\delta = (R_{\text{sample}} - R_{\text{standard}}) / R_{\text{standard}}$, where $R = ^{18}\text{O}/^{16}\text{O}$ or $^2\text{H}/^1\text{H}$), relative to the Vienna Standard Mean Ocean Water standard (VSMOW; Coplen, 2011).

3 Principle of the coupled $\delta^2\text{H}_{n\text{-alkane}}\text{-}\delta^{18}\text{O}_{\text{sugar}}$ paleohygro-meter approach

3.1 Biomarker-based leaf water reconstructions

The fundamental assumption of the coupled $\delta^2\text{H}_{n\text{-alkane}}\text{-}\delta^{18}\text{O}_{\text{sugar}}$ paleohygro-meter approach is that biomarker isotope signatures reflect primarily the leaf water isotope composition (Figure 1). Hence, when applying biosynthetic fractionation factors leaf water can be reconstructed. Fractionation factors can be derived from the literature. Most likely, appropriate factors are -160‰ for ^2H of *n*-alkanes (ϵ_{bio}^2 ; Sessions et al., 1999; Sachse et al.,

2012) and +27‰ for ^{18}O in sugars ($\epsilon_{\text{bio}}^{18}$ Sternberg et al., 1986; Yakir and DeNiro, 1990; Schmidt et al., 2001; Cernusak et al., 2003):

$$\delta\text{H}_{\text{leaf-water}}^2 = (\delta^2\text{H}_{n\text{-alkane}} - \epsilon_{\text{bio}}^2)/(1 + \epsilon_{\text{bio}}^2/1000) \quad (1)$$

$$\delta^{18}\text{O}_{\text{leaf-water}} = (\delta^{18}\text{O}_{\text{sugar}} - \epsilon_{\text{bio}}^{18})/(1 + \epsilon_{\text{bio}}^{18}/1000) \quad (2)$$

The n -alkane and sugar biomarkers can be related to the epicuticular leaf wax layers (Eglinton and Hamilton, 1967) and to the (leaf) hemicellulose structures of higher vascular plants (e.g. Jia et al., 2008; Zech et al., 2012; Hepp et al., 2016, and references therein), respectively. A large overview of plant cell wall structure and chemical composition is e.g. given in Caffall and Mohnen (2009). The biomarkers thus incorporate the isotope signal of the (leaf) water in which they are biosynthesized. Accordingly the leaf wax n -alkanes and leaf (hemi-)celluloses primarily reflect bulk leaf water during the photosynthetic active period (e.g. Barbour and Farquhar, 2000; Roden et al., 2000; Schmidt et al., 2003; Cernusak et al., 2005; Sachse et al., 2012; Kahmen et al., 2013a).

3.1.1 Excursus: Uncertainties of the $\delta^2\text{H}_{n\text{-alkane}}$ to $\delta^2\text{H}_{\text{leaf-water}}$ relationship

The main uncertainty for n -alkane-based leaf water reconstructions is most likely associated with the rather variable $\delta^2\text{H}_{n\text{-alkane}}$ to $\delta^2\text{H}_{\text{leaf-water}}$ relationship, which results in a large range of ϵ_{bio}^2 (also called $\epsilon_{n\text{-alkane/leaf-water}}$), as presented in the literature (e.g. Feakins and Sessions, 2010; Tipple et al., 2015; Feakins et al., 2016; Freimuth et al., 2017). Based on the therein published $\epsilon_{n\text{-alkane/leaf-water}}$ data of the n -alkanes C_{29} and C_{31} , a large variation of approximately 174‰ (ranging from -66 to -240‰) with a median close to -155‰ can be derived. Furthermore, the timing of leaf wax synthesis could contribute to the wide range of observed $\epsilon_{n\text{-alkane/leaf-water}}$ values. If leaf wax synthesis occurs mainly during leaf flush (Tipple et al., 2013; Gamarra and Kahmen, 2017), the n -alkanes incorporate the source (leaf) water signal during that period (Sachse et al., 2010) and can therefore not be well correlated to the leaf water signals during the whole growing season. For long-chain leaf lipids (from C_{27} to C_{31}), a complete recycling could occur after 71 to 128 days as derived from a labeling experiment of the grass species *Phleum pratense* conducted by Gao et al. (2012). In addition, the influence of storage carbohydrates on the isotope signature of the n -alkanes biosynthesized during leaf flush might be increased (Newberry et al., 2015). However, there is also evidence that n -alkanes reflect more or less continuously the climate conditions during the whole vegetation period (e.g. Newberry et al., 2015; Pedentchouk and Zhou, 2018, and references therein). The n -alkanes of grass species tend to reflect only partially the leaf water signal (Kahmen et al., 2013a; Gamarra et al., 2016). They are considered to be mainly influenced by the source water of the plants (McInerney et al., 2011) due to their leaf growth at the intercalary meristem located at the base of the leaves. Finally, species-specific differences in ϵ_{bio}^2 have to be taken into account (see reviews from Schmidt et al. (2003), Sachse et al. (2012), and Pedentchouk and Zhou (2018), and reference therein), exemplary highlighted by stomatal density effects (Lee et al., 2016) and the carbon as well as the energy metabolism of plants (Cormier et al., 2018; Tipple and Ehleringer, 2018) on ϵ_{bio}^2 .

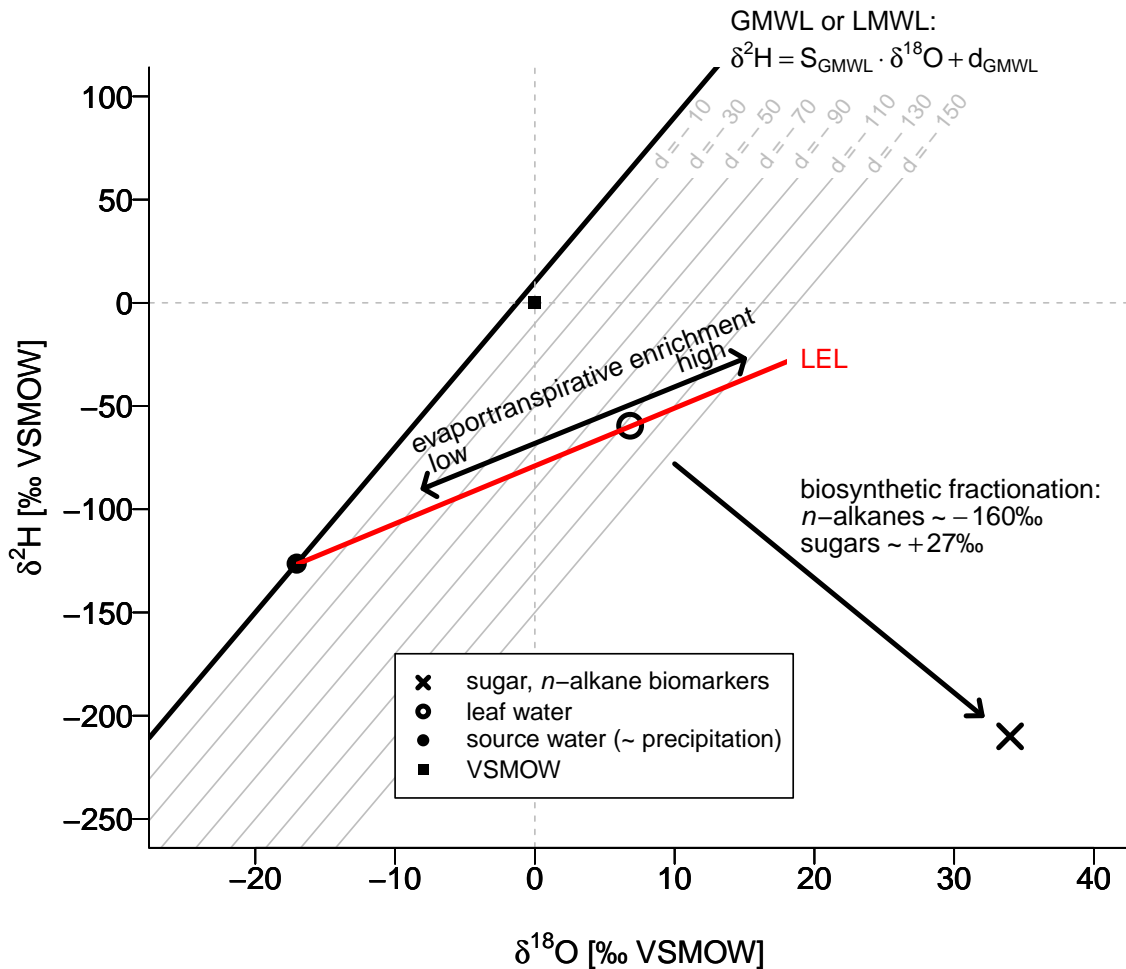


Figure 1: $\delta^2\text{H}$ versus $\delta^{18}\text{O}$ diagram illustrating (i) $\delta^2\text{H}_{n\text{-alkane}}$ versus $\delta^{18}\text{O}_{\text{sugar}}$ (marked with a cross), (ii) the reconstructed leaf water isotope composition by applying biosynthetic fractionation factors (Sessions et al., 1999; Sachse et al., 2012; Schmidt et al., 2001; Cernusak et al., 2003); marked with an open circle), (iii) the possibility to reconstruct source water isotope composition, which could serve as a proxy for precipitation isotope composition, using the intersect between the local evaporation line (LEL) and the global or local meteoric water line (GMWL or LMWL; marked with a filled circle), and finally (iv) the effect of low and high leaf water evapotranspirative enrichment along the LEL on the deuterium-excess (d) of leaf water (which is the parallel distance to the GMWL or LMWL, marked with d letters), possibly serving as quantitative RH proxy (Zech et al., 2013; Tuthorn et al., 2015).

3.1.2 Excursus: Uncertainties of the $\delta^{18}\text{O}_{\text{sugar}}$ to $\delta^{18}\text{O}_{\text{leaf-water}}$ relationship

Uncertainties for reconstructing $\delta^{18}\text{O}_{\text{leaf-water}}$ based on (leaf) hemicellulose sugar $\delta^{18}\text{O}$ are mostly based on cellulose studies. Overall, the influence of (unenriched) source water, which is commonly less enriched than the leaf water, cannot be ruled out. This holds true for dicotyledon plants (e.g. reviews from Barbour, 2007; Sternberg et al., 2006), monocotyledon (grass) species (Helliker and Ehleringer, 2002; Liu et al., 2016; Liu et al., 2017; Lehmann et al., 2017), and surely for stem cellulose (e.g. Roden et al., 2000), but also for leaf cellulose (Wang et al., 1998; Barbour and Farquhar, 2000; Cernusak et al., 2005; Song et al., 2014; Cheesman and Cernusak, 2017; Munksgaard et al., 2017). However, large ranges of the so called damping factor are reported for empirical data (Wang et al., 1998) but also with regard to the theory (Song et al., 2014). The theoretical approach for $\delta^{18}\text{O}$ in (hemi-)cellulose is based on the premise that sucrose exported from photosynthesizing leaves is +27‰ more positive compared to leaf water (Cernusak et al., 2003), which is interpreted as sucrose being in full isotopic equilibrium with the synthesis water. Latter is drawn from the comparison to the equilibrium fractionation effect of the reversible hydration reaction of acetone, which contains only one exchangeable oxygen, with water, resulting in an enrichment of +28, +28 and +26‰ at 15, 25 and 35°C, respectively (Sternberg and DeNiro, 1983).

Also the cellulose biosynthesis is associated with an enrichment of around +27‰ compared to the synthesis water as shown in growth experiments (Sternberg et al., 1986; Yakir and DeNiro, 1990), which is again generally explained via the isotope exchange between the carbonyl oxygen and water (Schmidt et al., 2001). This means that the isotope signal of the leaf water incorporated by the transport sugar sucrose can potentially be dampened by oxygen exchange with local synthesis water during autotrophic, in terms of synthesized from photosynthesis products (sensu Terwilliger et al., 2002), (hemi-)cellulose biosynthesis in any sink tissue. This can be described by the equation of Barbour and Farquhar (2000): $\delta^{18}\text{O}_{(\text{hemi-})\text{cellulose}} = \delta^{18}\text{O}_{\text{source-water}} + (\delta^{18}\text{O}_{\text{leaf-water}} - \delta^{18}\text{O}_{\text{source-water}}) \cdot (1 - p_{\text{ex}} \cdot p_x) + \epsilon_{\text{bio}}^{18}$. Herein, p_x is the proportion of unenriched source water contribution to the local synthesis water and p_{ex} is the proportion of exchangeable oxygen during cellulose synthesis, in multiplication called damping factor.

The exchange is caused by hydration reactions that affect one oxygen when sucrose is cleaved into glucose phosphate, via the reversible conversion to fructose 6-phosphate and fructose 1,6-biphosphate (Waterhouse et al., 2013). A portion of fructose 1,6-biphosphate undergoes a futile cycling through triose phosphates, which allows further three oxygen positions to exchange (Barbour and Farquhar, 2000; Barbour, 2007; Sternberg, 2009; Waterhouse et al., 2013). However the transfer of the cellulose directly to hemicellulose $\delta^{18}\text{O}$ has to be questioned. Pentoses, like the hemicellulose-derived arabinose and xylose, are biosynthesized via decarboxylation of the carbon at position six (C6) from glucose (Altermatt and Neish, 1956; Harper and Bar-Peled, 2002; Burget et al., 2003). Waterhouse et al. (2013) suggested that the oxygens at this glucose C6 position are most strongly affected by the exchange with local water medium (as indicated by 80% exchange during heterotrophic cellulose synthesis).

Thus, most likely at least $\delta^{18}\text{O}$ of hemicellulose-derived pentoses are less effected by potential unenriched source water exchange processes. Still, for stem hemicelluloses from dicotyledonous plants, which grew under controlled climate conditions, a damping factor of

50 to 81% was observed (as highlighted by Sternberg, 2014, based on the data published by Zech et al., 2014b). From the presented theory it is also evident, that biosynthetic fractionation ($\epsilon_{\text{bio}}^{18}$, and also called $\epsilon_{\text{sugar/leaf-water}}$) effects the $\delta^{18}\text{O}_{\text{sugar}}$ signature. Indeed, the temperature dependency of $\epsilon_{\text{bio}}^{18}$ is still under debate (Sternberg and Ellsworth, 2011; Sternberg, 2014 versus Zech et al., 2014c). So far there is evidence that the $\delta^{18}\text{O}$ signature of storage substances like starch, which indeed contribute to leaf cellulose synthesis (e.g. Terwilliger et al., 2001, sensu Terwilliger et al., 2002), can also be described via an +27‰ enriched compared to the synthesis water (as e.g. summarized and suggest by Sternberg (2009). However, the question how strong the $\delta^{18}\text{O}$ imprint of such storage substances is related to $\delta^{18}\text{O}_{\text{leaf-water}}$ is even more important, which cannot be answered here (see e.g. Sternberg et al., 2006; Lehmann et al., 2017, for more details). Sucrose synthesis gradients within a leaf, as well as leaf water inhomogeneity, could lead to weakening the $\delta^{18}\text{O}_{\text{leaf-water}}$ to $\delta^{18}\text{O}_{\text{sugar}}$ relationship, highlighted by a recent study by Lehmann et al. (2017) showing that the bulk leaf water is not always a good substitute of cellulose synthesis water in leaves. Finally, such leaf water inhomogeneities tend to increase under decreasing RH conditions, and vice versa (Santrucek et al., 2007), affecting not only the $\delta^{18}\text{O}_{\text{leaf-water}}$ to $\delta^{18}\text{O}_{\text{sugar}}$ correlation but also the $\delta^2\text{H}_{\text{leaf-water}}$ to $\delta^2\text{H}_{n\text{-alkane}}$ relation.

3.2 Leaf water enrichment theory

The second basic assumption of the paleohygrometer approach concerns leaf water enrichment. Leaf water is commonly enriched compared to the source water utilized by the plants during day time (e.g. the review of Cernusak et al., 2016). This is caused by the evaporation process while the plants transpire water through the stomata (Figure 1). As the leaf water reservoir close to the stomata (at the site where the evaporation takes place) is rather small, it can be assumed that the steady-state conditions occur rather rapidly (Allison et al., 1985; Walker and Brunel, 1990; Bariac et al., 1994; Gat et al., 2007). With the isotope composition of the transpired water being equal to the source water of the plants, the leaf water enrichment can be described via a Craig-Gordon model, given here in δ terms (Equation 3; Flanagan et al., 1991; Roden and Ehleringer, 1999; Barbour et al., 2004):

$$\delta_e \approx \delta_s + \epsilon^* + \epsilon_k + (\delta_a - \delta_s - \epsilon_k) \cdot e_a/e_i. \quad (3)$$

Here, δ_e , δ_s and δ_a are the isotope compositions of evaporative site leaf water, source water and atmospheric water vapor, respectively. The equilibrium enrichment (expressed as $(1-1/\alpha_{L/V}) \cdot 10^{-3}$, where $\alpha_{L/V}$ is the equilibrium fractionation factor between liquid water and water vapour) is included as ϵ^* in ‰. The kinetic fractionation parameters, describing the water vapor diffusion through the stomata and the boundary air layer is expressed as ϵ_k in ‰. Finally, e_a/e_i is the ratio of atmospheric vapor pressure to intracellular vapor pressure, hence a leaf RH realisation. As the ϵ_k values are unknown for paleo applications, due to their dependency on stomatal and boundary layer resistances to the water (vapor) flux (Farquhar et al., 1989), it seems to be appropriate to use more general defined kinetic enrichment parameters (C_k) instead (Craig and Gordon, 1965; Gat and Bowser, 1991). Assuming that leaf temperature is equal to air temperature, the e_a/e_i ratio can be replaced by the air RH. If finally an isotope equilibrium between the source water of the plants and the local atmospheric water vapour is hypothesised, then the term $\delta_a - \delta_s$ can be approximated with $-\epsilon^*$, thus Equation 3 will be simplified to:

$$\delta_e \approx \delta_s + (\epsilon^* + C_k) \cdot (1 - \text{RH}) \quad (4)$$

3.3 Reconstruction of plant source water $\delta^2\text{H}$, $\delta^{18}\text{O}$ and RH_{air}

With the above-presented leaf water enrichment model at hand, both the isotopic composition of plant source water and RH can be reconstructed. Plant source water can be directly linked to soil water and shallow groundwater, which in turn reflect mean annual precipitation (e.g. Herrmann et al., 1987). The isotope composition of global precipitation plots typically along the global meteoric water line (GMWL, with the equation $\delta^2\text{H}_{\text{precipitation}} = 8 \cdot \delta^{18}\text{O}_{\text{precipitation}} + 10$; Dansgaard, 1964) and the isotope composition of local precipitation plots along a local meteoric water line (LMWL, with various equations depending on the locality). These observations can be used for inferring information about the source water of the plants (Figure 1). Plant source water isotope composition can thereby be calculated as the intersect between the local evaporation line, on which the leaf water plots, and the GMWL (Zech et al., 2013) or LMWL. With regard to Equation 4, the slope of the LEL (S_{LEL}) can be derived from Equation 5

$$S_{\text{LEL}} = (\delta_e^2 - \delta_s^2) / (\delta_e^{18} - \delta_s^{18}) \approx (\epsilon_2^* + C_k^2) / (\epsilon_{18}^* + C_k^{18}). \quad (5)$$

The equilibrium fractionation parameters (ϵ_2^* and ϵ_{18}^*) can be calculated according to temperature dependent empirical equations from Horita and Wesolowski (1994). The kinetic fractionation factors (C_k^2 and C_k^{18}) can be derived from Merlivat (1978), who reported maximum values of the molecular water diffusion through a stagnant boundary layer, which seems to be appropriate for leaves. It should be noted that ϵ_k values for broad-leaf trees and shrubs are well in range with the used C_k values (as derived from the supplementary data of Cernusak et al. (2016)). Calculated LEL slopes (Equation 5), only depending on the temperature via the equilibrium fractionation parameters, are well in range with slopes observed in the field and in the laboratory experiments (Zech et al., 2013; Tuthorn et al., 2015 versus Allison et al., 1985; Walker and Brunel, 1990; Bariac et al., 1994; Gat et al., 2007; Tipple et al., 2013). Using the deuterium-excess (d) definition of either the GMWL ($d = \delta^2\text{H} - 8 \cdot \delta^{18}\text{O}$; Dansgaard, 1964) or the LMWL ($d = \delta^2\text{H} - \text{slope of LMWL} \cdot \delta^{18}\text{O}$), the leaf water enrichment model can be described for hydrogen as well as oxygen in a single equation, which can be rearranged in order to calculate RH values (Zech et al., 2013):

$$\text{RH} \approx 1 - (d_e - d_s) / (\epsilon_2^* - S_{\text{GMWL,LMWL}} \cdot \epsilon_{18}^* + C_k^2 - S_{\text{GMWL,LMWL}} \cdot C_k^{18}). \quad (6)$$

Here, d_e and d_s are the deuterium-excess of evaporative site leaf water and source water, respectively, and slopes of the GMWL or LMWL are given as $S_{\text{GMWL,LMWL}}$. When d_s values are achievable from the GMWL or LMWL, then a powerful tool is given for deriving past RH changes via d_e (Zech et al., 2013; Tuthorn et al., 2015), under the assumption that d_e can be derived from the biomarker-based $\delta^2\text{H}_{\text{leaf-water}}$, $\delta^{18}\text{O}_{\text{leaf-water}}$ reconstructions (Equation 1 and Equation 2). Equation 6 requires strictly seen d_e values as input, while the biomarker-based leaf water results rather in a deuterium-excess of (bulk) leaf water (d_l). The d_l values are most likely less enriched than the deuterium-excess at the evaporative site (d_e). It should be noted that differences between d_e and d_l are far below typical analytic errors associated with compound-specific $\delta^2\text{H}_{n\text{-alkane}}$ and $\delta^{18}\text{O}_{\text{sugar}}$ analysis, as derived from d_e and d_l assessment using the complete data sets from Australia (Kahmen et al., 2013b) and Hawaii (Kahmen et al., 2011a), as presented in the supplementary data of Cernusak et al. (2016). The d values were here calculated via a local deuterium-excess formulation using the presented $\delta^2\text{H}$ and $\delta^{18}\text{O}$ of xylem water. Thus a correction

of biomarker-derived d_l values in order to achieve d_e as input for Equation 6 seems to be unnecessary. The here presented approach allows reconstructing RH (particularly of day-time and vegetation time, see Tuthorn et al. (2015) and $\delta^2\text{H}_{\text{precipitation}}$, $\delta^{18}\text{O}_{\text{precipitation}}$ (particularly of weighted mean annual precipitation).

4 Results & Discussion

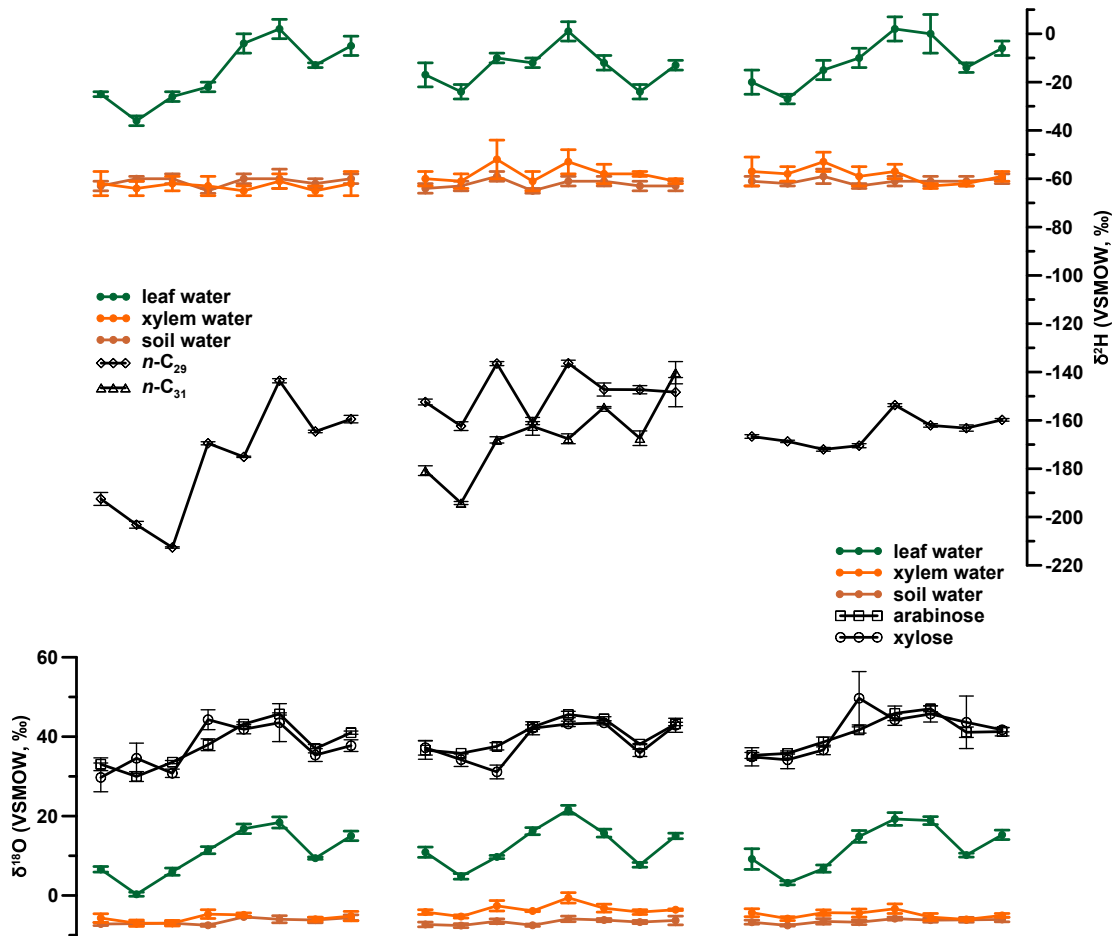
4.1 Climate chamber validation study 1 (manuscript 1)

The overall aim of this study was to validate the coupled $\delta^2\text{H}_{n\text{-alkane}}-\delta^{18}\text{O}_{\text{sugar}}$ paleohygrometer approach by using leaf material from plants grown under controlled climate conditions. A climate chamber experiment, conducted by co-author Christoph Mayr at the Helmholtz Zentrum München during winter 2000/2001 (Mayr, 2002), was used to investigate leaf samples for their $\delta^2\text{H}_{n\text{-alkane}}$ and $\delta^{18}\text{O}_{\text{sugar}}$ values. The three different plant species used in the experiment (*Eucalyptus globulus*, *Vicia faba var. minor* and *Brassica oleracea var. medullosa*) were grown under seven air temperature (T_{air}) and RH_{air} conditions (14, 18, 24 and 30 °C; 21, 24, 32, 48, 49, 50 and 68%) for 56 days. After this period, the plants were harvested and analyzed for $\delta^2\text{H}_{\text{leaf-water}}$, $\delta^{18}\text{O}_{\text{leaf-water}}$. For more details about the experimental set-up and plant related results see Mayr (2002). The analyzed alkanes $n\text{-C}_{29}$ and $n\text{-C}_{31}$ can be associated with the epicuticular leaf wax layers of the plants (Eglinton and Hamilton, 1967), while the extracted monosaccharides arabinose and xylose originate from the hemicellulose structure of the plant leaf cells (Caffall and Mohnen, 2009). The $n\text{-C}_{29}$ and $n\text{-C}_{31}$ $\delta^2\text{H}$ results were combined as weighted mean to $\delta^2\text{H}_{n\text{-alkane}}$ values and the arabinose and xylose $\delta^{18}\text{O}$ values were used to calculate weighted mean $\delta^{18}\text{O}_{\text{sugar}}$ results (Figure 2).

Both biomarker isotope values are highly significantly correlated with the respective leaf water isotope values ($\delta^2\text{H}_{n\text{-alkane}}$ versus $\delta^2\text{H}_{\text{leaf-water}}$ and $\delta^{18}\text{O}_{\text{sugar}}$ versus $\delta^{18}\text{O}_{\text{leaf-water}}$: $r^2 = 0.45$ and 0.85 , $p < 0.001$, $n = 24$). The mean fractionation factors derived from the difference between the biomarkers and the leaf water were -156‰ (within a range from -192 to -133‰) for $\epsilon_{n\text{-alkane}/\text{leaf-water}}$ and $+27.3\text{‰}$ for $\epsilon_{\text{sugar}/\text{leaf-water}}$ (within a range from 23.0 to 32.3‰), which are well in agreement with the literature (Sessions et al., 1999; Kahmen et al., 2011b; Sachse et al., 2012; Sternberg et al., 1986; Yakir and DeNiro, 1990; Schmidt et al., 2001; Cernusak et al., 2003).

In order to evaluate if the principle assumption of the coupled $\delta^2\text{H}_{n\text{-alkane}}-\delta^{18}\text{O}_{\text{sugar}}$ paleohygrometer approach is valid (as outlined in detail in section 3), the measured $\delta^2\text{H}_{\text{leaf-water}}$ and $\delta^{18}\text{O}_{\text{leaf-water}}$ results were used as input variables for calculating RH_{air} via Equation 6 (Figure 3A). The d_e values were derived from the equation $d_e = \delta\text{H}_{\text{leaf-water}}^2 - 8 \cdot \delta^{18}\text{O}_{\text{leaf-water}}$ (according to the equation of Dansgaard (1964) and the GMWL was used as baseline, revealing a d of 10 (used for d_s) and a slope of 8 (Craig, 1961). Modeled RH_{air} values fit very well with the measured RH_{air} values along the 1:1 line (Figure 3A; $R^2 = 0.84$, $\text{RSME} = 6.04\%$). When biomarker-based $\delta^2\text{H}_{\text{leaf-water}}$, $\delta^{18}\text{O}_{\text{leaf-water}}$ values are used (calculated via Equation 1 and Equation 2) for RH_{air} modeling, the RH_{air} predictions are getting worse, but are still significant (Figure 3B, modified from Hepp et al., 2019c). The weaker R^2 when biomarker-based $\delta^2\text{H}_{\text{leaf-water}}$, $\delta^{18}\text{O}_{\text{leaf-water}}$ values are used in comparison to measured values points to one main uncertainty of the coupled $\delta^2\text{H}_{n\text{-alkane}}-\delta^{18}\text{O}_{\text{sugar}}$ paleohygrometer

A) water and biomarker $\delta^2\text{H}$ and $\delta^{18}\text{O}$ values



B) climate chamber conditions

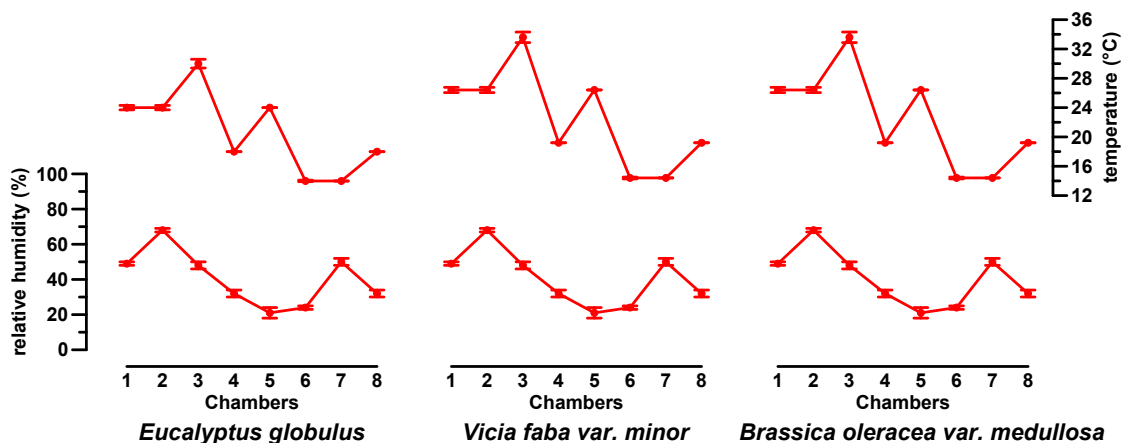


Figure 2: Plant water and climate chamber conditions of the controlled experiment (modified from Hepp et al., 2019c). A) Leaf, xylem and soil water isotope composition (all from Mayr, 2002), along with respective $\delta^2\text{H}_{n\text{-alkane}}$ ($n\text{-C}_{29}$ and $n\text{-C}_{31}$) and $\delta^{18}\text{O}_{\text{sugar}}$ (arabinose and xylose) values. B) Air temperature and relative humidity conditions of the climate chambers (Mayr, 2002).

approach, which is related to the limitations associated with the biomarker-based leaf water reconstruction (see paragraph above). This is understandable when considering the large ranges of the observed $\varepsilon_{n\text{-alkane/leaf-water}}$ and $\varepsilon_{\text{sugar/leaf-water}}$ values as well as the fairly well $\delta^2\text{H}_{n\text{-alkane}}$ to $\delta^2\text{H}_{\text{leaf-water}}$ relationship. Still, the high potential of the coupled $\delta^2\text{H}_{n\text{-alkane}}-\delta^{18}\text{O}_{\text{sugar}}$ paleohygrometer approach is highlighted by robust RH reconstructions, considering an R^2 of 0.54 for the biomarker-based versus measured RH_{air} relationship and an RSME of 10.14% (Figure 3B).

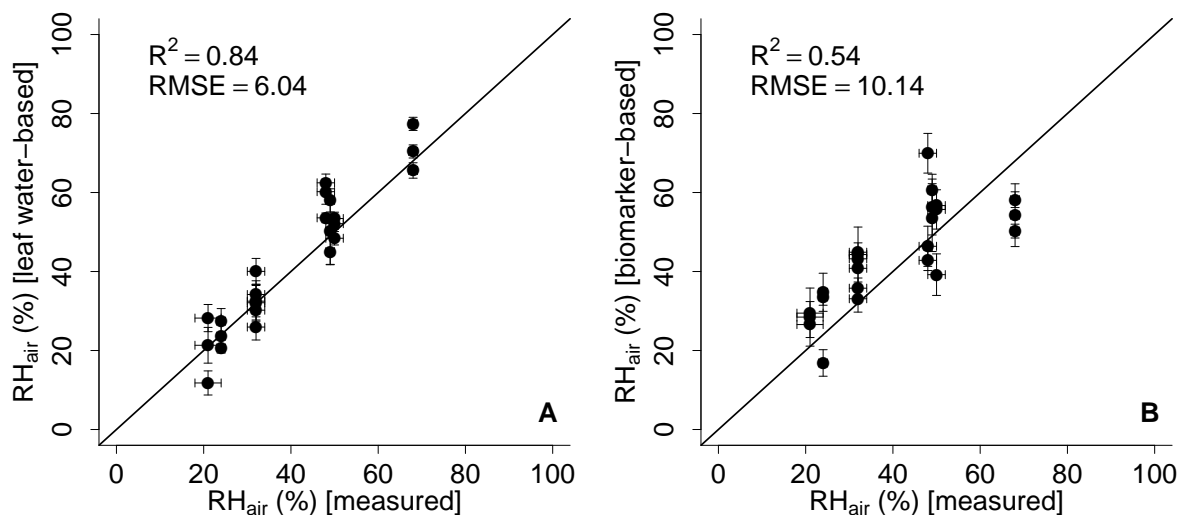


Figure 3: Scatterplots of leaf water- (A) and biomarker-based (B) relative air humidity values (RH_{air}) versus measured RH_{air} values (modified from Hepp et al., 2019c). Black line = 1:1 line; R^2 = coefficient of correlation along the 1:1 line; RMSE = root mean square error in % RH_{air} .

4.2 European climate transect validation study 2 (manuscript 2)

The European topsoil climate transect, established by Imke Kathrin Schäfer and co-authors, allows evaluating the coupled $\delta^2\text{H}_{n\text{-alkane}}-\delta^{18}\text{O}_{\text{sugar}}$ approach under field conditions. For establishing the transect reaching from Southern Sweden to South Germany, topsoil samples (0-5 cm of the Ah horizons) at 16 locations were taken in November 2012. Furthermore, three different vegetation types, i.e. coniferous forest, deciduous forest and grassland were differentiated, which leads in summary to 29 sampling points. Climate variables were derived from the close-by climate station data (climate data were retrieved from the respective German, Danish and Swedish weather observation institutions (DWD, DMI and SMHI); Frich et al., 1997; Laursen et al., 1999; Cappelen, 2002; DWD Climate Data Center, 2018b; DWD Climate Data Center, 2018a; Swedish Meteorological and Hydrological Institute, 2018). From this database, climate variability along the transect regarding long-term mean annual temperatures (T_{MA}) and RH (RH_{MA}), long-term means for the vegetation period (April to October; T_{MV} , RH_{MV}) and finally long-term mean for the day-time (from 7 a.m. to 7 p.m.) and vegetation period (T_{MDV} , RH_{MDV}), were obtained. In addition, long-term mean annual precipitation amount (P_{MA}) was calculated. For two Danish sites long-term means of T_{MDV} were not available (the T_{MV} were used instead). Along the transect, T_{MA} range from 5.3 to 10.6°C and mean annual precipitation (P_{MA}) ranges from 554 to

1769 mm, which is quite comparable to a published Argentinian transect which was used for validating the coupled $\delta^2\text{H}_{n\text{-alkane}}\text{-}\delta^{18}\text{O}_{\text{sugar}}$ paleohygrometer approach (Tuthorn et al., 2015). However, the (weighted) mean annual isotopic composition of precipitation shows smaller variations along the European transect compared to the Argentinian transect. For the Swedish and Danish sites of the European transect, $\delta^2\text{H}_{\text{precipitation}}$ data was gathered from the The Online Isotopes in Precipitation Calculator (called $\delta^2\text{H}_{\text{OIPC}}$, $\delta^{18}\text{O}_{\text{OIPC}}$; Bowen and Revenaugh, 2003; IAEA/WMO, 2015; Bowen, 2018). For the German sites, a regional precipitation $\delta^2\text{H}$ and $\delta^{18}\text{O}$ regionalisation was realized by using long-term data available from 34 German GNIP stations, 4 Austrian ANIP stations (Reutte, Scharnitz, Salzburg, Kufstein) and from Groningen GNIP station, (Stumpp et al., 2014; Geldern et al., 2014; IAEA/WMO, 2018; Umweltbundesamt GmbH, 2018), referred to as $\delta^2\text{H}_{\text{GIPR}}$, $\delta^{18}\text{O}_{\text{GIPR}}$, for more details see manuscript 2. $\delta^2\text{H}_{\text{GIPR,OIPC}}$ and $\delta^{18}\text{O}_{\text{GIPR,OIPC}}$ varies between -52 and -79‰ (= 27‰ range) and between -7.4 and -10.9‰ (= 3.5‰ range), respectively. Along the Argentinian transect, the $\delta^2\text{H}_{\text{OIPC}}$ and $\delta^{18}\text{O}_{\text{OIPC}}$ ranges from -29 to -87‰ (= 58‰ range) and from -5.0 to -11.7‰ (= 6.7‰ range), which is approximately double as large (Tuthorn et al., 2014; Tuthorn et al., 2015). Similar findings are reported for the mean annual RH gradient, which is 25% regarding RH_{MA} along the Argentinian sites (Tuthorn et al., 2015), whereas along the European transect study only a 12% variation can be observed. Therefore, the European topsoil transect can also be seen as a sensitivity test for the coupled $\delta^2\text{H}_{n\text{-alkane}}\text{-}\delta^{18}\text{O}_{\text{sugar}}$ paleohygrometer approach. In summary, 25 samples could be used for coupling of $\delta^2\text{H}_{n\text{-alkane}}$ with $\delta^{18}\text{O}_{\text{sugar}}$ results, which yielded in biomarker-based $\delta^2\text{H}_{\text{source-water}}$, $\delta^{18}\text{O}_{\text{source-water}}$ (~precipitation) and RH_{MDV} values. For $\delta^2\text{H}_{n\text{-alkane}}$ the mean of $\delta^2\text{H}$ of $n\text{-C}_{27}$, $n\text{-C}_{29}$ and $n\text{-C}_{31}$ was used, while for $\delta^{18}\text{O}_{\text{sugar}}$, arabinose and xylose $\delta^{18}\text{O}$ results were combined as weighted means.

The apparent isotope fractionation, calculated as $\epsilon_{n\text{-alkane/precipitation}} = (\delta^2\text{H}_{n\text{-alkane}} - \delta^2\text{H}_{\text{GIPR,OIPC}})/(1 + \delta^2\text{H}_{\text{GIPR,OIPC}}/1000)$ and $\epsilon_{\text{sugar/precipitation}} = (\delta^{18}\text{O}_{\text{sugar}} - \delta^{18}\text{O}_{\text{GIPR,OIPC}})/(1 + \delta^{18}\text{O}_{\text{GIPR,OIPC}}/1000)$, is lower for sugars and more negative for $n\text{-alkanes}$ from grassland compared to the forest sites. This means that $\epsilon_{n\text{-alkane/precipitation}}$ and $\epsilon_{\text{sugar/precipitation}}$ from the grassland sites is closer to the expected ϵ_{bio}^2 and $\epsilon_{\text{bio}}^{18}$ values of -160‰ (Sessions et al., 1999; Sachse et al., 2012) and +27‰ (Sternberg et al., 1986; Yakir and DeNiro, 1990; Schmidt et al., 2001; Cernusak et al., 2003). This finding is well in agreement with recent studies showing that $n\text{-alkanes}$ and cellulose extracted from grass leaves are less sensitive leaf water recorders (McInerney et al., 2011; Kahmen et al., 2013a; Gamarra et al., 2016; Helliker and Ehleringer, 2002). Hence, grass biomarkers reflect the more negative source water signal (~precipitation) rather than the leaf water, which is influenced by evapotranspirative enrichment. Most likely the basal growth form of grass species via an intercalary meristem can explain this effect. Indeed, water sampled from the leaf growth and differentiation zone is close to the source water of grasses (Liu et al., 2017).

The biomarker-based $\delta^2\text{H}_{\text{source-water}}$, $\delta^{18}\text{O}_{\text{source-water}}$ values plot reasonable well close to the 1:1 lines with $\delta^2\text{H}_{\text{GIPR,OIPC}}$ and $\delta^{18}\text{O}_{\text{GIPR,OIPC}}$ but show a much larger range (93 and 12‰ for $\delta^2\text{H}_{\text{source-water}}$ and $\delta^{18}\text{O}_{\text{source-water}}$, respectively; Figure 4A and B). The same holds true for the comparison of biomarker-based with climate station RH_{MVD} . While RH_{MVD} derived from the climate stations show a variation of 17%, the biomarker-based RH_{MVD} show a total range of 40% (Figure 4C). The larger range in the reconstructions could be caused by uncertainties associated with the $\delta^2\text{H}_{\text{leaf-water}}$ reconstruction based on $n\text{-alkane}$ $\delta^2\text{H}$ and a constant ϵ_{bio}^2 factor (see also section 3.1.1). Also the usage of the same LEL slope for the coniferous sites as for deciduous tree and grass sites could lead to the observed large

ranges in the reconstructions. Moreover, systematic offsets between the reconstructed $\delta^2\text{H}_{\text{source-water}}$, $\delta^{18}\text{O}_{\text{source-water}}$ and RH_{MDV} values compared to the GIPR, OIPC precipitation values and the climate station-derived RH_{MDV} are obvious (median $\Delta \delta^2\text{H} \approx -21\text{‰}$, $\Delta \delta^{18}\text{O} \approx -2.9\text{‰}$ and $\Delta \text{RH}_{\text{MDV}} \approx -17.1\%$). With regard to reconstructed $\delta^2\text{H}_{\text{source-water}}$, $\delta^{18}\text{O}_{\text{source-water}}$ this could be caused by the usage of a too steep LEL slope for the coniferous sites. Furthermore, the consideration of the loss of evaporative leaf water enrichment would diminish the negative offset of the grass sites. The study shows therefore the limitations of reconstructing medium variations in precipitation $\delta^2\text{H}$, $\delta^{18}\text{O}$ and RH_{MDV} by using the coupled $\delta^2\text{H}_{n\text{-alkane}}-\delta^{18}\text{O}_{\text{sugar}}$ approach.

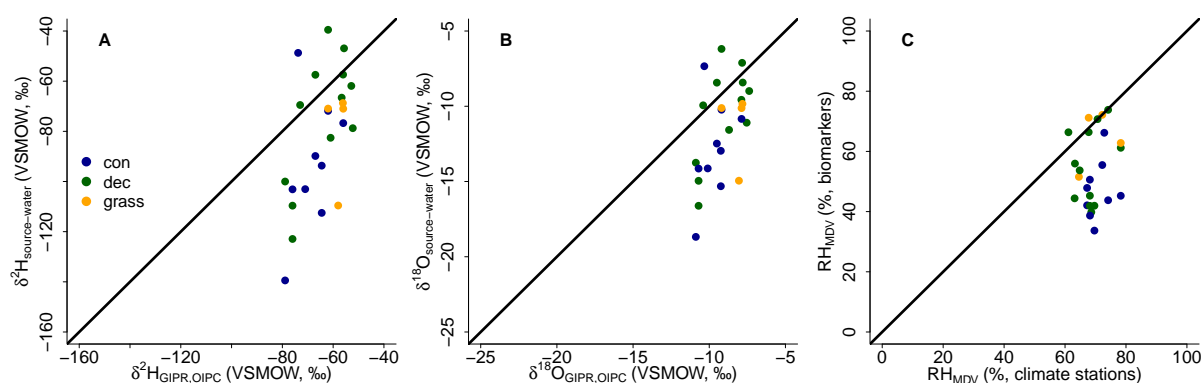


Figure 4: Scatterplots comprising reconstructed source water $\delta^2\text{H}$ versus $\delta^2\text{H}_{\text{GIPR,OIPC}}$ (A), reconstructed source water $\delta^{18}\text{O}$ versus $\delta^{18}\text{O}_{\text{GIPR,OIPC}}$ (B) and reconstructed RH_{MDV} based on the coupled $\delta^2\text{H}_{n\text{-alkane}}-\delta^{18}\text{O}_{\text{sugar}}$ approach versus climate station RH_{MDV} values (C). Abbreviations: con = coniferous forest sites; dec = deciduous forest sites; grass = grassland sites, modified from Hepp et al. (2019b).

4.3 Application of the coupled $\delta^2\text{H}_{n\text{-alkane}}-\delta^{18}\text{O}_{\text{sugar}}$ approach to the terrestrial sedimentary archive of Maundi (manuscript 3)

A first application of the coupled $\delta^2\text{H}_{n\text{-alkane}}-\delta^{18}\text{O}_{\text{sugar}}$ approach within this PhD project was realized on a loess-like paleosol sequence from the Southern slopes of Mt. Kilimanjaro called Maundi (2780 m a.s.l.; $3^{\circ}10'27.5''\text{S}$, $37^{\circ}31'05.8''\text{E}$). The age-depth model suggests that the Maundi record covers approximately the last 100 ka. The sequence was analyzed for $\delta^{18}\text{H}_{\text{sugars}}$ and $\delta^2\text{H}_{\text{methoxyl}}$, $\delta^2\text{H}_{\text{fatty-acids}}$ (n -alkanoic acids) and $\delta^2\text{H}_{n\text{-alkanes}}$ in order to establish a multi-proxy stable isotope record for the Late Quaternary in equatorial East Africa (Figure 5). Pollen results for the same sequence were previously presented by Schüler et al. (2012). The coupled $\delta^2\text{H}_{n\text{-alkanes}}-\delta^{18}\text{O}_{\text{sugars}}$ paleohygrometer approach was used to reconstruct mean RH values during day-time (RH_{HD}) and source water isotope composition ($\delta^2\text{H}_{\text{source-water}}$, $\delta^{18}\text{O}_{\text{source-water}}$). The $\delta^2\text{H}_{\text{fatty-acids}}$ and $\delta^2\text{H}_{n\text{-alkanes}}$ records of Maundi were compared to the $\delta^2\text{H}_{\text{leaf-wax}}$ records of Lake Challa, Lake Tanganyika and Lake Malawi (Tierney et al., 2008; Tierney et al., 2011; Konecky et al., 2011). They all reveal the same trends, i.e. more negative values during the African Humid Period. At the same time, differences regarding the distinct patterns, amplitude and timing of events are also observed (Figure 5).

concerns the intensification of the trade wind inversion, which affects the diurnal atmospheric circulation on the Southern slopes of Mt. Kilimanjaro (Pepin et al., 2010). This can help to explain why the Maundi RH_D record does not show noticeably humid conditions during the Early Holocene, while high lake levels during the Early Holocene document the African Humid Period until ~5 ka as a period with moisture availability in East African region after the interruption caused by the Younger Dryas (Junginger et al., 2014).

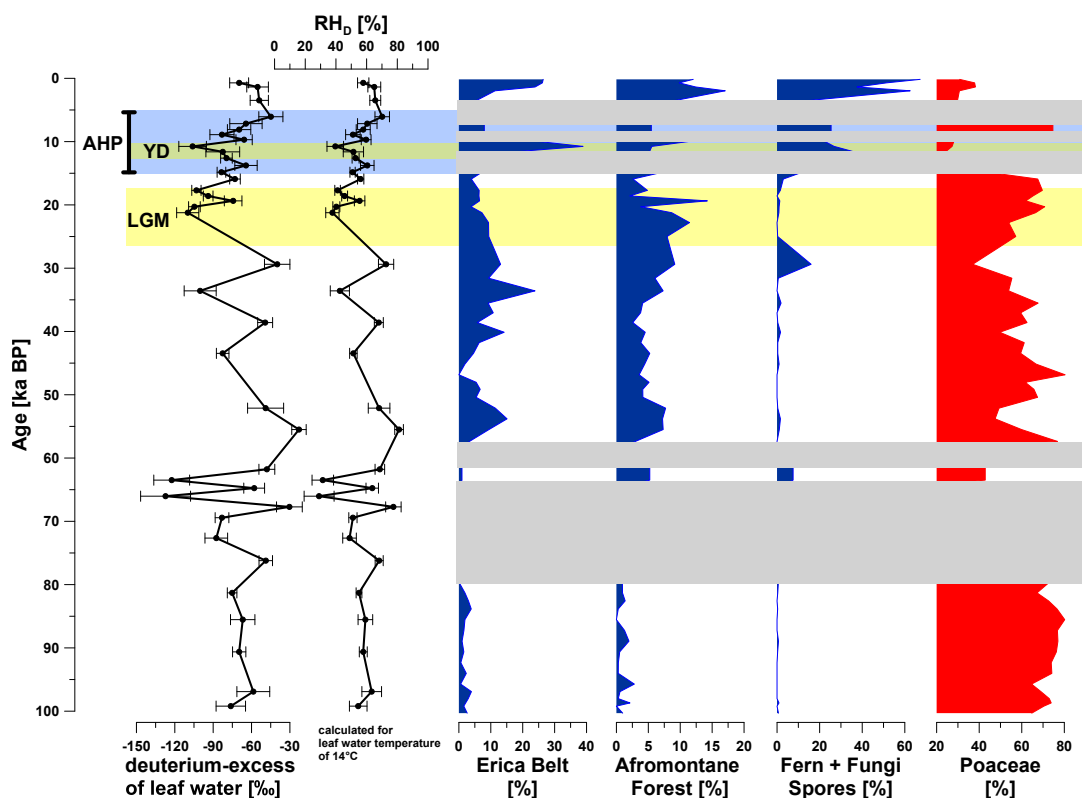


Figure 6: Maundi deuterium-excess of leaf water and reconstructed RH during day-time (RH_D) records, along with selected pollen results from the Maundi loess-like paleosol sequence (Schüler et al., 2012), as modified from Hepp et al. (2017). LGM = Last Glacial Maximum, YD = Younger Dryas, AHP = African Humid Period.

Finally, the highly significant correlation between reconstructed deuterium-excess of leaf water and $\delta^2\text{H}_{\text{source-water}}$, $\delta^{18}\text{O}_{\text{source-water}}$ (Figure 7) reveals that a long-term amount effect cannot explain the pattern of the Maundi $\delta^2\text{H}_{\text{source-water}}$, $\delta^{18}\text{O}_{\text{source-water}}$ records. In modern precipitation, $\delta^2\text{H}$ and $\delta^{18}\text{O}$ for East African regions on a seasonal timescale can be described (Rozanski et al., 1996). However, no clear relationship between $\delta^2\text{H}_{\text{precipitation}}$, $\delta^{18}\text{O}_{\text{precipitation}}$ and precipitation amount is observed on longer (at least inter-annual) time scales (Rozanski et al., 1996; Sundqvist et al., 2013). Most likely effects on local and regional moisture recycling, and therefore the expansion, shrinking (or complete collapse) of montane rainforest on the Southeastern slopes of Mt. Kilimanjaro and changes in regional vegetation cover have to be taken into account for understanding Maundi $\delta^2\text{H}_{\text{source-water}}$, $\delta^{18}\text{O}_{\text{source-water}}$ variations.

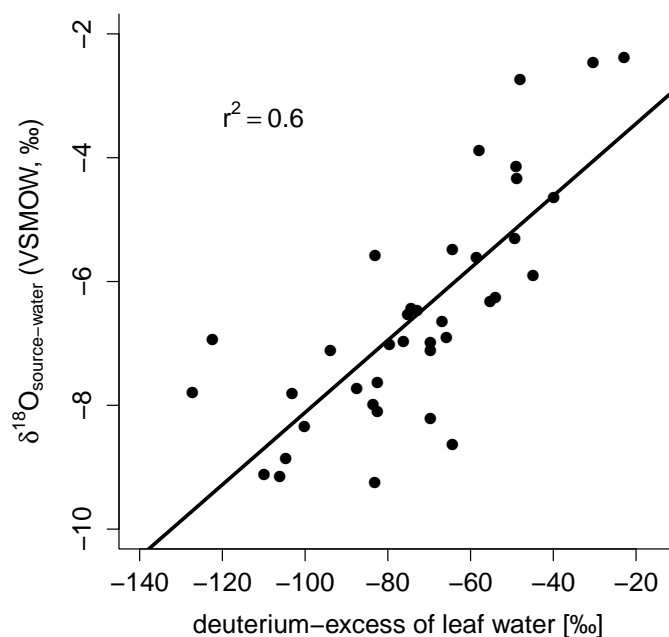


Figure 7: Scatterplot of reconstructed Maundi $\delta^{18}\text{O}_{\text{source-water}}$ versus deuterium-excess of leaf water, revealing a positive correlation with an r^2 of 0.6 (using the data as presented in Tab. 1 of Hepp et al., 2017).

4.4 Source identification of terrestrial versus aquatic sugars in lacustrine systems (manuscript 4)

For a successful application of the coupled $\delta^2\text{H}_{n\text{-alkane}}-\delta^{18}\text{O}_{\text{sugar}}$ paleohygrometer approach to lacustrine archives, the identification of the sedimentary organic matter source, and more specifically the identification of the source of specific biomarkers is essential. With regard to *n*-alkane biomarkers, source identification is mainly based on chain-lengths. Long-chain lipids (*n*-alkanes, *n*-alkanols and *n*-alkanoic acids) are usually interpreted as derived from terrestrial plants because they occur abundantly in epicuticular leaf waxes of higher vascular plants (Eglinton and Hamilton, 1967). By contrast, mid- and short chain lipids are usually associated with submerged aquatic macrophytes (Ficken et al., 2000) or algae. Yet, this source assignment is increasingly challenged (e.g. Hepp et al., 2015; Aichner et al., 2018) and needs careful consideration in every case study. For the sugar biomarkers arabinose, fucose and xylose, a lacustrine sedimentary source identification is presented in this manuscript for the first time.

Sugar biomarkers were extracted from different terrestrial and aquatic plants as well as from various algae species. While vascular plants are characterized by high amounts of arabinose and xylose, algae yielded higher concentrations of fucose (both based on relative sugar biomarker abundances; Figure 8A). In combination with data compiled from the literature this suggests that the ratio of fuc/(ara + xyl) can serve as an additional proxy for differentiating between aquatic versus terrestrial lacustrine sedimentary organic matter input. When additionally taking into account relative sugar biomarker abundances from

soils and sediments (Figure 8B), the ratio of (fuc + xyl)/ara seems to be a helpful proxy for distinguishing aquatic versus terrestrial input in lacustrine archives, too.

Overall, this compilation suggests that sugar biomarkers can serve as valuable complementary proxy for sedimentary source identification and that fucose and xylose can often be related to aquatic sources, whereas arabinose can often be attributed to terrestrial origin. The latter likely holds true for the Lake Gemündener Maar sediments (Figure 8B).

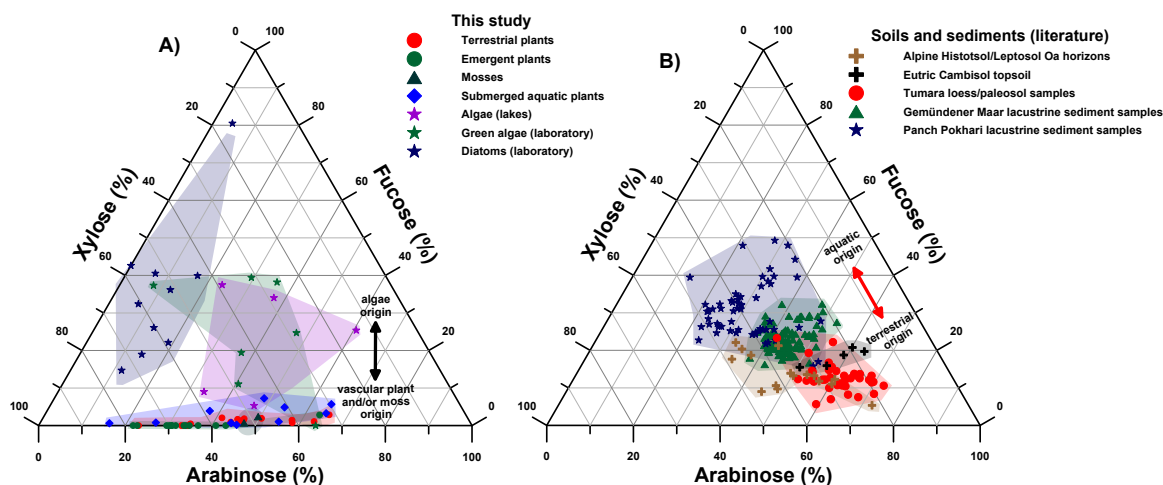


Figure 8: Ternary diagrams illustrating the relative abundances of arabinose, fucose and xylose for the analyzed samples presented in manuscript 4 (Hepp et al., 2016) (A), as well as for soil and sediment data compiled from the literature, i.e. alpine soils (Prietz et al., 2013), topsoil samples (Bock et al., 2007), loess/paleosol samples (Zech et al., 2013) and lacustrine sediments (Zech et al., 2014a) (B). Figure modified from Hepp et al. (2016).

4.5 Application of the coupled $\delta^2\text{H}_{n\text{-alkane}}\text{-}\delta^{18}\text{O}_{\text{sugar}}$ paleohygrometer approach to the Gemündener Maar sedimentary record (manuscript 5)

The above-presented source identification study of terrestrial versus aquatic sugars in lacustrine systems (manuscript 4) provides the basis for applying the coupled $\delta^2\text{H}_{n\text{-alkane}}\text{-}\delta^{18}\text{O}_{\text{sugar}}$ paleohygrometer approach to the Late Glacial-Early Holocene Lake Gemündener Maar sediment archive. The Lake is located in the Western Eifel region (50°10'39.853"N, 6°50'12.912"E; 407 m a.s.l.), Germany, within the ancient volcanic field (Sirocko et al., 2013). The weighted mean $\delta^2\text{H}$ of the alkanes $n\text{-C}_{27}$ and $n\text{-C}_{29}$ as well as $\delta^{18}\text{O}_{\text{arabinose}}$ are used to derive RH day-time and vegetation period (RH_{dv}), because they are considered to record the past $\delta^2\text{H}_{\text{leaf-water}}$ and $\delta^{18}\text{O}_{\text{leaf-water}}$.

Interestingly, the results suggest that the Younger Dryas was not uniformly dry but two-phased with regard to RH. The first phase is characterised by RH_{dv} values similar to the Allerød level; only the end of the Younger Dryas is characterised by drier climatic conditions (Figure 9). This contradicts earlier results suggesting (i) continuously dry conditions throughout the Younger Dryas (Rach et al., 2014) and (ii) a two-phasing with a dry and

cold first period that is followed by increasing wetness and higher temperatures during the second Younger Dryas phase (Brauer et al., 1999). Moreover, the Lake Gemündener Maar RH record reveals quite high variability during the Early Holocene, compared to the Younger Dryas and the Allerød sections. So far, it is uncertain how strong the solar activity influenced this unexpected finding in Late Glacial-Early Holocene RH history over Central Europe.

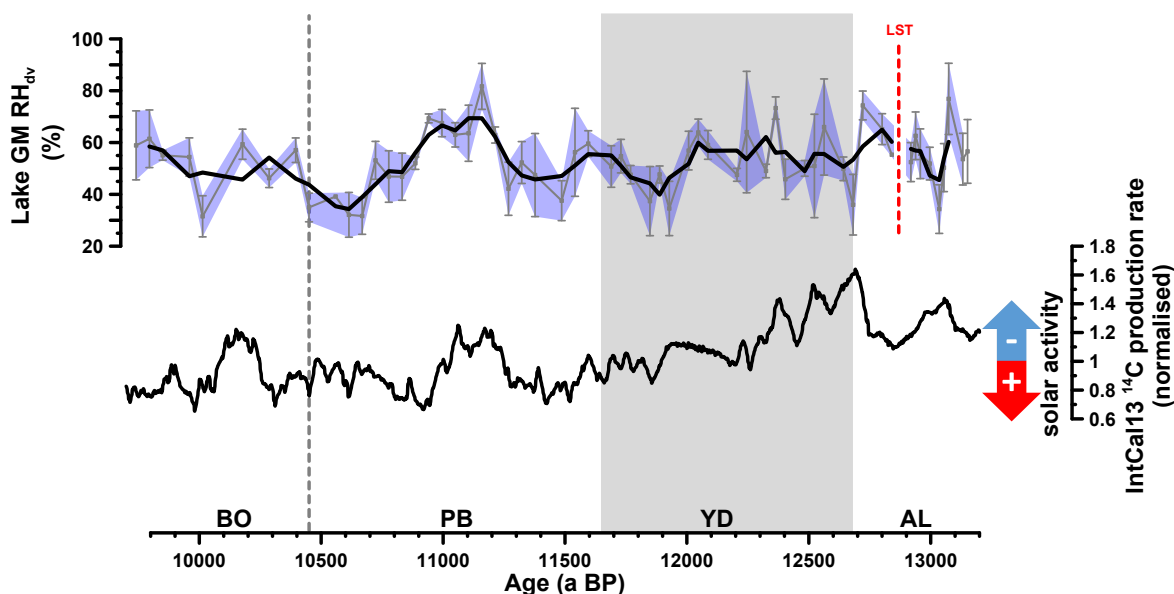


Figure 9: A) Lake Gemündener Maar relative humidity record during day-time and vegetation period (RH_{dv}) along with B) the IntCal 13 ^{14}C production rate (Muscheler et al., 2014), which can be interpreted as solar activity proxy (Stuiver and Braziunas, 1988). Bold line in RH_{dv} plot = 3 point running mean; Error bars and shaded area represents uncertainties associated with $\delta^2H_{n-alkane}$ and $\delta^{18}O_{sugar}$ measurements. AL = Allerød, LST = Laacher See Tephra, YD = Younger Dryas, PB = Preboreal, BO = Boreal. Figure modified from Hepp et al. (2019a).

4.6 Application of the coupled $\delta^2H_{n-alkane}-\delta^{18}O_{sugar}$ approach to the Lake Bergsee sedimentary record (manuscript 6)

The second application of the coupled $\delta^2H_{n-alkane}-\delta^{18}O_{sugar}$ approach to a lake sedimentary archive was conducted on samples from Lake Bergsee, Southern Black Forest, Germany (7°56'11"E, 47°34'20"N; 382 m a.s.l.; Becker et al., 2006). The investigated core section covers, like the Lake Gemündener Maar study, the Late Glacial to Early Holocene transition, i.e. a time span between 16,000 to 10,750 a cal BP. As highlighted by Hepp et al. (2015) (section 4.4 and manuscript 4) and Hepp et al. (2019a) (section 4.5 and manuscript 5), the biomarker source identification is essential for interpreting the compound-specific isotope results. For the biomarker source identification, n -alkane and sugar biomarker pattern were analyzed in detail and, for potentially coupling $\delta^2H_{n-alkane}$ with $\delta^{18}O_{sugar}$ results, alkanes with the chain length $n-C_{23}$, $n-C_{25}$, $n-C_{27}$, $n-C_{29}$ and $n-C_{31}$ as well as the sugars arabinose, fucose and xylose were analyzed for their δ^2H and $\delta^{18}O$ isotope signatures, respectively.

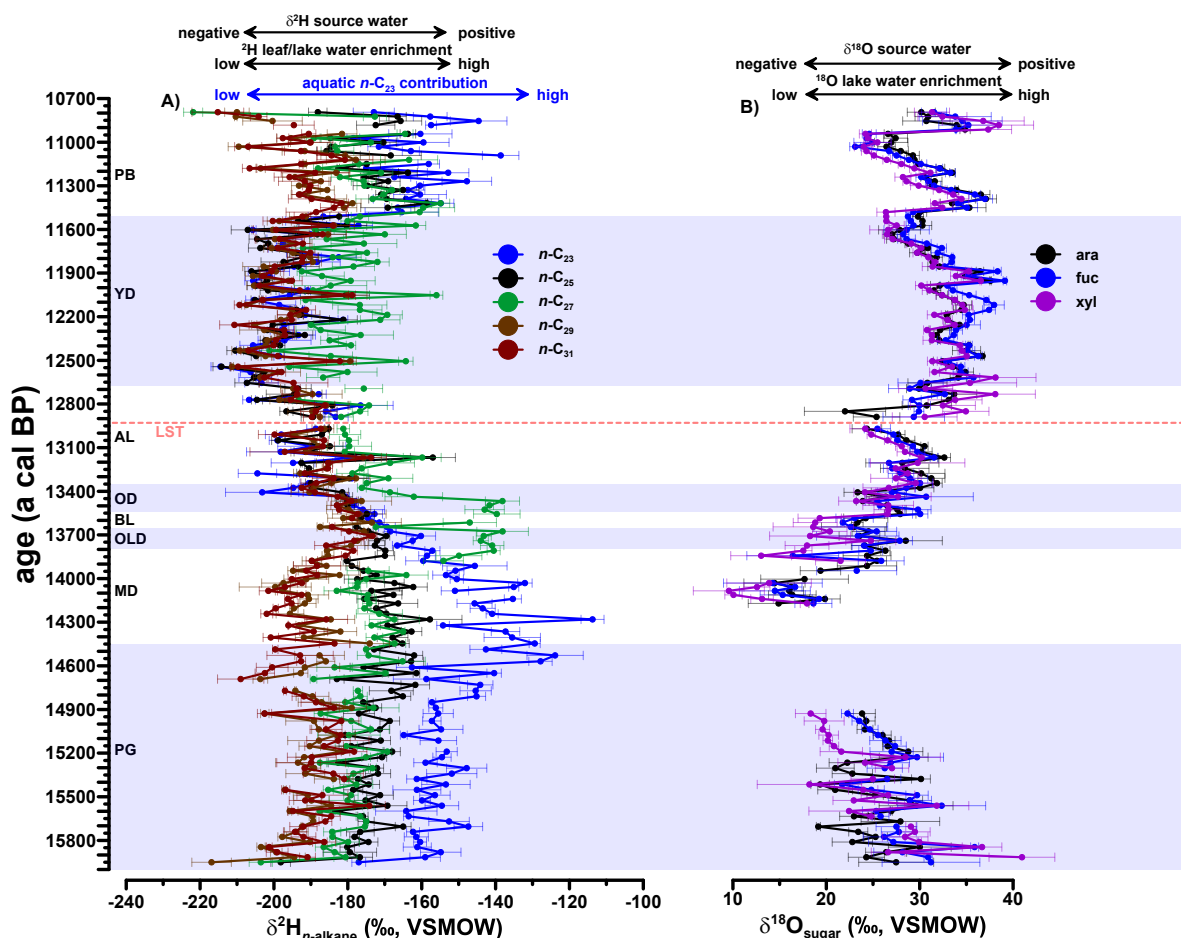


Figure 10: A) $\delta^2\text{H}_{n\text{-alkane}}$ records ($n\text{-C}_{23}$, $n\text{-C}_{25}$, $n\text{-C}_{27}$, $n\text{-C}_{29}$ and $n\text{-C}_{31}$) and B) $\delta^{18}\text{O}_{\text{sugar}}$ records (arabinose, fucose, xylose) of Lake Bergsee. Background colors show time periods (according to Litt et al., 2001): PB = Preboreal, YD = Younger Dryas, AL = Allerød, OD = Older Dryas, BL = Bølling, OLD = Oldest Dryas, MD = Meiendorf, PG = Pleniglacial. LST = Laacher See Tephra.

An unambiguous bulk source determination turned out to be not possible for Lake Bergsee based on the bulk results. Regarding the n -alkane biomarkers, however, it can be assumed that the long-chain homologues ($n\text{-C}_{27}$, $n\text{-C}_{29}$ and $n\text{-C}_{31}$) originate from terrestrial sources (Eglinton and Hamilton, 1967), i.e. from leaf waxes of higher terrestrial plants grown in the Lake Bergsee catchment. The short-chain compound ($n\text{-C}_{23}$) reflect most likely a mixture between the input from submerged aquatic organisms (e.g. Ficken et al., 2000) and from terrestrial plants, as shown also by Aichner et al. (2018) for a lacustrine record from Poland. Sedimentary sugars are interpreted to be primarily aquatic-derived, based on the sugar ratios developed from manuscript 4 (Figure 8). Accordingly, $\delta^{18}\text{O}_{\text{sugar}}$ (arabinose, xylose and fucose) are presumably good $\delta^{18}\text{O}_{\text{lake-water}}$ recorders, while $\delta^2\text{H}_{n\text{-alkane}}$ values from long-chain n -alkane ($n\text{-C}_{27}$, $n\text{-C}_{29}$ and $n\text{-C}_{31}$) should reflect paleo $\delta^2\text{H}_{\text{leaf-water}}$.

The origin of the n -alkane and sugar biomarkers becomes also obvious when describing the biomarker-based isotope records (Figure 10). When the $n\text{-C}_{29}$ and $n\text{-C}_{31}$ alkanes originate from grasses (e.g. *Poaceae*) and $n\text{-C}_{27}$ from trees (e.g. *Betula*), in average +17‰ more positive $n\text{-C}_{27}$ $\delta^2\text{H}$ values can be explained with the fact that n -alkanes from grasses are typically less sensitive leaf water enrichment recorders (McInerney et al., 2011; Kahmen et al., 2013a). The $n\text{-C}_{25}$ $\delta^2\text{H}$ record seems to be a mixture between tree (*Betula*)

and grass (*Poaceae*) input, because the values are close to $n\text{-C}_{27}$ during the Pleniglacial, Meindorf and the Preboreal, while during Oldest Dryas, Bølling, Older Dryas, Allerød and Younger Dryas the $n\text{-C}_{25}$ $\delta^2\text{H}$ record resemble the $n\text{-C}_{29}$, $n\text{-C}_{31}$ ones. For long-chain n -alkanes, often an $\varepsilon_{\text{bio}}^2$ factor of -160‰ is assumed, based on findings from Sachse et al. (2006) and Sessions et al. (1999). For $n\text{-C}_{23}$ $\delta^2\text{H}$ data from *Potamogeton* and surface sediments, however, a smaller fractionation factor during biosynthesis of -82 to -88‰ is suggested (Aichner et al., 2010). Offsets between Lake Bergsee $n\text{-C}_{23}$ $\delta^2\text{H}$ and $n\text{-C}_{27}$, $n\text{-C}_{29}$, $n\text{-C}_{31}$ $\delta^2\text{H}$ records could therefore result from variable aquatic contribution of $n\text{-C}_{23}$. The main influencing factors on n -alkane $\delta^2\text{H}$ are highlighted in Figure 10A.

The Lake Bergsee $\delta^{18}\text{O}_{\text{sugar}}$ records can be interpreted in terms of reflecting changes in (i) $\delta^{18}\text{O}$ of source water (\sim local precipitation) and (ii) ^{18}O lake water enrichment (as illustrated in Figure 10B). This can explain why the $\delta^{18}\text{O}_{\text{sugar}}$ record of Lake Bergsee reveals opposite trends and a much higher amplitude compared to precipitation records based on carbonate $\delta^{18}\text{O}$ (Mayer and Schwark, 1999; Wurth et al., 2004). Focusing on the Younger Dryas-Preboreal transition, a shift of $\sim 5\text{‰}$ is obvious in $\delta^{18}\text{O}_{\text{sugar}}$ record, based on average values for both periods. This is well in agreement with a reconstructed $\delta^{18}\text{O}_{\text{lake-water}}$ shift of around 6‰ from Lake Gosciadz (Rozanski et al., 2010).

Due to the mixed origin of $n\text{-C}_{23}$ in Lake Bergsee sediments (= mixture between aquatic and terrestrial sources) a coupling between $\delta^2\text{H}_{n\text{-alkane}}$ ($n\text{-C}_{23}$) and $\delta^{18}\text{O}_{\text{sugar}}$ according to Hepp et al. (2015) was not possible. The large potential of the coupled $\delta^2\text{H}_{n\text{-alkane}}\text{-}\delta^{18}\text{O}_{\text{sugar}}$ approach for disentangling lake or leaf water enrichments from source water changes could therefore not be utilized in this study. Moreover, our results are in line with other publications emphasising that caution has to be taken when applying the classical n -alkane chain-length interpretation to lacustrine archives (Hepp et al., 2015; Duan et al., 2016; Liu and Liu, 2016; Rao et al., 2016).

5 Conclusions

The following conclusions can be drawn from the results and discussions presented in this thesis dealing with the coupled $\delta^2\text{H}_{n\text{-alkane}}\text{-}\delta^{18}\text{O}_{\text{sugar}}$ approach:

- The analysis of the leaf material from the climate chamber experiment shows that $\delta^2\text{H}_{n\text{-alkane}}\text{-}\delta^{18}\text{O}_{\text{sugar}}$ are well correlated with $\delta^2\text{H}_{\text{leaf-water}}$, $\delta^{18}\text{O}_{\text{leaf-water}}$ ($r^2 = 0.45$ and 0.85 , respectively, $p < 0.001$, $n = 24$). Moreover, RH_{air} can be robustly reconstructed based on measured $\delta^2\text{H}_{\text{leaf-water}}$, $\delta^{18}\text{O}_{\text{leaf-water}}$ values as well as on $\delta^2\text{H}_{n\text{-alkane}}$, $\delta^{18}\text{O}_{\text{sugar}}$ -derived leaf water isotope composition by using a simplified Craig-Gordon model. This highlights the large potential of the coupled $\delta^2\text{H}_{n\text{-alkane}}\text{-}\delta^{18}\text{O}_{\text{sugar}}$ paleohygrometer approach. From the topsoil transect study, it can be concluded that such an $\delta^2\text{H}_{n\text{-alkane}}\text{-}\delta^{18}\text{O}_{\text{sugar}}$ approach allows the reconstruction of $\delta^2\text{H}_{\text{source-water}}$, $\delta^{18}\text{O}_{\text{source-water}}$ and RH_{MDV} values. However, also systematical offsets between biomarker-based (reconstructed) $\delta^2\text{H}_{\text{source-water}}$, $\delta^{18}\text{O}_{\text{source-water}}$ and RH_{MDV} values compared to precipitation $\delta^2\text{H}_{\text{GIPR,OIPC}}$, $\delta^{18}\text{O}_{\text{GIPR,OIPC}}$ and climate station RH_{MDV} values, respectively, are observed. Thus, both studies imply that the uncertainty of reconstructing $\delta^2\text{H}_{\text{leaf-water}}$ based on $\delta^2\text{H}_{n\text{-alkane}}$ values (which is also present in data compiled from literature, see section 3.1.1) represents one clear limitation of the coupled $\delta^2\text{H}_{n\text{-alkane}}\text{-}\delta^{18}\text{O}_{\text{sugar}}$ approach regarding the reconstruction of rather small variability in $\delta^2\text{H}_{\text{source-water}}$, $\delta^{18}\text{O}_{\text{source-water}}$ and RH records.

- The application of the coupled $\delta^2\text{H}_{n\text{-alkane}}\text{-}\delta^{18}\text{O}_{\text{sugar}}$ approach to the terrestrial climate archive Maundi was still successful in terms of establishing $\delta^2\text{H}_{\text{source-water}}$, $\delta^{18}\text{O}_{\text{source-water}}$ and RH_D records for the last ~ 100 ka for the East African region. The results indicate that leaf water enrichment can mask changes in precipitation isotope composition, both incorporated in $\delta^2\text{H}_{n\text{-alkane}}$ and $\delta^{18}\text{O}_{\text{sugar}}$. The coupled $\delta^2\text{H}_{n\text{-alkane}}\text{-}\delta^{18}\text{O}_{\text{sugar}}$ approach is shown to have the potential to disentangle between those signals. A strong relationship between biomarker-based $\delta^2\text{H}_{\text{source-water}}$, $\delta^{18}\text{O}_{\text{source-water}}$ and RH_D furthermore points against the presence of an amount effect on $\delta^2\text{H}_{\text{precipitation}}$ and $\delta^{18}\text{O}_{\text{precipitation}}$ isotope composition on long-time scales.
- The source identification study of terrestrial versus aquatic sugar biomarkers in lake sediments shows in general that the relative abundances of arabinose, fucose and xylose can be used to distinguish between algae and terrestrial plant sources. Arabinose from Late Glacial-Early Holocene Lake Gemündener Maar sediments is primarily of terrestrial origin, whereas fucose and xylose stem predominately from aquatic sources.
- The $\delta^{18}\text{O}_{\text{arabinose}}$ and terrestrial $\delta^2\text{H}_{n\text{-alkane}}$ ($n\text{-C}_{27}$, $n\text{-C}_{29}$) results derived from Lake Gemündener Maar sediments were used in a coupled $\delta^2\text{H}_{n\text{-alkane}}\text{-}\delta^{18}\text{O}_{\text{sugar}}$ paleohygrometer approach. The established RH_{dv} record challenges that the Younger Dryas was characterized by overall dry climatic conditions. There was rather a relatively wet phase at the beginning of the Younger Dryas, which is followed by a drier late Younger Dryas. Furthermore, large RH_{dv} changes during the Early Holocene are observed, which are even more pronounced than the variations during the Allerød-Younger Dryas transition. Unlike the Lake Gemündener Maar study, the coupled $\delta^2\text{H}_{n\text{-alkane}}\text{-}\delta^{18}\text{O}_{\text{sugar}}$ approach could not be applied to Lake Bergsee Late Glacial-Early Holocene sediments. While the long-chain n -alkanes can be attributed to terrestrial sources and the sugars to primarily aquatic sources, $n\text{-C}_{23}$ is most likely a mixture of both origins. A clear differentiation between terrestrial or aquatic origins of the n -alkane and sugar biomarkers seems to be fundamental for a successful application of the coupled $\delta^2\text{H}_{n\text{-alkane}}\text{-}\delta^{18}\text{O}_{\text{sugar}}$ approach to lacustrine archives.

References

- Aichner, B., U. Herzs Schuh, H. Wilkes, A. Vieth, and J. Böhner (2010). “ δD values of *n*-alkanes in Tibetan lake sediments and aquatic macrophytes - A surface sediment study and application to a 16 ka record from Lake Koucha”. *Organic Geochemistry* 41.8, pp. 779–790. DOI: <http://dx.doi.org/10.1016/j.orggeochem.2010.05.010>.
- Aichner, B., F. Ott, M. Słowiński, A. M. Noryśkiewicz, A. Brauer, and D. Sachse (2018). “Leaf wax *n*-alkane distributions record ecological changes during the Younger Dryas at Trzechowskie paleolake (Northern Poland) without temporal delay”. *Climate of the Past Discussions* March, pp. 1–29. DOI: 10.5194/cp-2018-6.
- Alexandre, A., A. Landais, C. Vallet-Coulomb, C. Piel, S. Devidal, S. Pauchet, C. Sonzogni, M. Couapel, M. Pasturel, P. Cornuault, J. Xin, J. C. Mazur, F. Prié, I. Bentaleb, E. Webb, F. Chalié, and J. Roy (2018). “The triple oxygen isotope composition of phytoliths as a proxy of continental atmospheric humidity: Insights from climate chamber and climate transect calibrations”. *Biogeosciences* 15.10, pp. 3223–3241. DOI: 10.5194/bg-15-3223-2018.
- Allison, G., J. R. Gat, and F. W. J. Leaney (1985). “The relationship between deuterium and oxygen-18 delta values in leaf water”. *Chemical Geology* 58, pp. 145–156.
- Altermatt, H. and A. Neish (1956). “The biosynthesis of cell wall carbohydrates: III. Further studies on formation of cellulose and xylan from labeled monosaccharides in wheat plants”. *Canadian Journal of Biochemistry and Physiology* 34.3, pp. 405–413. DOI: 10.1139/o56-042.
- Amelung, W., S. Brodowski, A. Sandhage-Hofmann, and R. Bol (2009). “Chapter 6 Combining Biomarker with Stable Isotope Analyses for Assessing the Transformation and Turnover of Soil Organic Matter”. *Advances in Agronomy*. Vol. 100. C. Academic Press, pp. 155–250. DOI: 10.1016/S0065-2113(08)00606-8.
- Amelung, W., M. Cheshire, and G. Guggenberger (1996). “Determination of neutral and acidic sugars in soil by capillary gas-liquid chromatography after trifluoroacetic acid hydrolysis”. *Soil Biology and Biochemistry* 28.12, pp. 1631–1639.
- Araguás-Araguás, L, K Froehlich, and K Rozanski (2000). “Deuterium and oxygen-18 isotope composition of precipitation and atmospheric moisture”. *Hydrological Processes* 14.8, pp. 1341–1355. DOI: 10.1002/1099-1085(20000615)14:8<1341::AID-HYP983>3.0.CO;2-Z.
- Barbour, M. M. and G. D. Farquhar (2000). “Relative humidity-and ABA-induced variation in carbon and oxygen isotope ratios of cotton leaves”. *Plant, Cell & Environment* 23.5, pp. 473–485.
- Barbour, M. M. (2007). “Stable oxygen isotope composition of plant tissue: a review”. *Functional Plant Biology* 34, pp. 83–94. DOI: <http://dx.doi.org/10.1071/FP06228>.
- Barbour, M. M., J. S. Roden, G. D. Farquhar, and J. R. Ehleringer (2004). “Expressing leaf water and cellulose oxygen isotope ratios as enrichment above source water reveals evidence of a Pécelet effect”. *Oecologia* 138.3, pp. 426–435. DOI: 10.1007/s00442-003-1449-3.
- Bariac, T, J Gonzalez-Dunia, N Katerji, O Béthenod, J. M. Bertolini, and A Mariotti (1994). “Spatial variation of the isotopic composition of water (^{18}O , 2H) in the soil-plant-atmo-

- sphere system, 2. Assessment under field conditions". *Chemical Geology* 115, pp. 317–333.
- Becker, A., B. Ammann, F. S. Anselmetti, A. M. Hirt, M. Magny, L. Millet, A.-M. Rachoud, G. Sampietro, and C. Wüthrich (2006). "Paleoenvironmental studies on Lake Bergsee, Black Forest, Germany". *Neues Jahrbuch für Geologie und Paläontologie - Abhandlungen* 240.3, pp. 405–445.
- Behrensmeyer, A. K. (2006). "Climate Change and Human Evolution". *Science* 311. January, pp. 476–478.
- Bock, M., B. Glaser, and N. Millar (2007). "Sequestration and turnover of plant- and microbially derived sugars in a temperate grassland soil during 7 years exposed to elevated atmospheric pCO₂". *Global Change Biology* 13.2, pp. 478–490. DOI: 10.1111/j.1365-2486.2006.01303.x.
- Bourbonniere, R. A., S. L. Telford, L. A. Ziolkowski, J. Lee, M. S. Evans, and P. A. Meyers (1997). "Biogeochemical marker profiles in cores of dated sediments from large North American lakes". *Molecular Markers in Environmental Geochemistry*. Ed. by R. P. Eganhouse. Washington, DC: American Chemical Society, pp. 133–150.
- Bowen, G. J. (2018). *The Online Isotopes in Precipitation Calculator, version 3.1*. Tech. rep.
- Bowen, G. J. and J. Revenaugh (2003). "Interpolating the isotopic composition of modern meteoric precipitation". *Water Resources Research* 39.10, pp. 1–13. DOI: 10.1029/2003WR002086.
- Brauer, A., C. Endres, C. Günter, T. Litt, M. Stebich, and J. F. W. Negendank (1999). "High resolution sediment and vegetation responses to Younger Dryas climate change in varved lake sediments from Meerfelder Maar, Germany". *Quaternary Science Reviews* 18.3, pp. 321–329. DOI: 10.1016/S0277-3791(98)00084-5.
- Burget, E. G., R. Verma, M. Mølhøj, and W.-D. Reiter (2003). "The Biosynthesis of L-Arabinose in Plants: Molecular Cloning and Characterization of a Golgi-Localized UDP-D-Xylose 4-Epimerase Encoded by the MUR4 Gene of Arabidopsis". *Plant Cell* 15. February, pp. 523–531. DOI: 10.1105/tpc.008425.response.
- Caffall, K. H. and D. Mohnen (2009). "The structure, function, and biosynthesis of plant cell wall pectic polysaccharides". *Carbohydrate Research* 344.14, pp. 1879–1900. DOI: 10.1016/j.carres.2009.05.021.
- Cappelen, J. (2002). *Danish Climatological Normals 1971-2000 - for selected stations*. Tech. rep. Technical Report 02-12: Danish Meteorological Institute, p. 40.
- Cernusak, L. A., G. D. Farquhar, and J. S. Pate (2005). "Environmental and physiological controls over oxygen and carbon isotope composition of Tasmanian blue gum, *Eucalyptus globulus*". *Tree Physiology* 25.2, pp. 129–146. DOI: 10.1093/treephys/25.2.129.
- Cernusak, L. A., S. C. Wong, and G. Farquhar (2003). "Oxygen isotope composition of phloem sap in relation to leaf water in *Ricinus communis*". *Functional Plant Biology* 30.10, pp. 1059–1070.
- Cernusak, L. A., M. M. Barbour, S. K. Arndt, A. W. Cheesman, N. B. English, T. S. Feild, B. R. Helliker, M. M. Holloway-Phillips, J. A. Holtum, A. Kahmen, F. A. Mcinerney, N. C. Munksgaard, K. A. Simonin, X. Song, H. Stuart-Williams, J. B. West, and G. D. Farquhar (2016). "Stable isotopes in leaf water of terrestrial plants". *Plant Cell and Environment* 39.5, pp. 1087–1102. DOI: 10.1111/pce.12703.

- Cheesman, A. W. and L. A. Cernusak (2017). "Infidelity in the outback: Climate signal recorded in $\Delta^{18}\text{O}$ of leaf but not branch cellulose of eucalypts across an Australian aridity gradient". *Tree Physiology* 37.5, pp. 554–564. DOI: 10.1093/treephys/tpw121.
- Coplen, T. B. (2011). "Guidelines and recommended terms for expression of stable-isotope-ratio and gas-ratio measurement results". *Rapid Communications in Mass Spectrometry* 25.17, pp. 2538–2560. DOI: 10.1002/rcm.5129.
- Cormier, M.-A., R. Werner, P. Sauer, D. Gröcke, L. M.C., T. Wieloch, J. Schleucher, and A. Kahmen (2018). " ^2H fractionations during the biosynthesis of carbohydrates and lipids imprint a metabolic signal on the $\delta^2\text{H}$ values of plant organic compounds". *New Phytologist* February. DOI: 10.1111/nph.15016.
- Craig, H (1961). "Isotopic Variations in Meteoric Waters". *Science* 133, pp. 1702–1703.
- Craig, H and L. I. Gordon (1965). *Deuterium and oxygen-18 variations in the ocean and the marine atmosphere*. Ed. by E Tongiorgi. Pisa: Lischi and Figli, pp. 9–130.
- Dansgaard, W (1964). "Stable isotopes in precipitation". *Tellus* 16.4, pp. 436–468. DOI: 10.1111/j.2153-3490.1964.tb00181.x.
- Diefendorf, A. F. and E. J. Freimuth (2016). "Extracting the most from terrestrial plant-derived *n*-alkyl lipids and their carbon isotopes from the sedimentary record: A review". *Organic Geochemistry* 103.January, pp. 1–21. DOI: 10.1016/j.orggeochem.2016.10.016.
- Duan, Y., Y. Zhao, Y. Wu, J. He, L. Xu, X. Zhang, L. Ma, and R. Qian (2016). " δD values of *n*-alkanes in sediments from Gahai Lake, Gannan, China: implications for sources of organic matter". *Journal of Paleolimnology* 56.2-3, pp. 95–107. DOI: 10.1007/s10933-016-9895-1.
- DWD Climate Data Center (2018a). *Historical annual precipitation observations for Germany*. Tech. rep.
- DWD Climate Data Center (2018b). *Historical hourly station observations of 2m air temperature and humidity for Germany*. Tech. rep.
- Eglinton, G. and R. J. Hamilton (1967). "Leaf Epicuticular Waxes". *Science* 156.3780, pp. 1322–1335. DOI: 10.1126/science.156.3780.1322.
- Eley, Y. L. and M. T. Hren (2018). "Reconstructing vapor pressure deficit from leaf wax lipid molecular distributions". *Scientific Reports* 8.1, pp. 1–8. DOI: 10.1038/s41598-018-21959-w.
- Farquhar, G. D., K. T. Hubick, A. G. Condon, and R. A. Richards (1989). "Carbon Isotope Fractionation and Plant Water-Use Efficiency". *Stable Isotopes in Ecological Research. Ecological Studies (Analysis and Synthesis)*. Ed. by P. W. Rundel, J. R. Ehleringer, and K. A. Nagy. Vol. 68. New York: Springer-Verlag. Chap. 2, pp. 21–40. DOI: 10.1007/978-1-4612-3498-2_2.
- Feakins, S. J. and A. L. Sessions (2010). "Controls on the D/H ratios of plant leaf waxes in an arid ecosystem". *Geochimica et Cosmochimica Acta* 74.7, pp. 2128–2141. DOI: <http://dx.doi.org/10.1016/j.gca.2010.01.016>.
- Feakins, S. J., L. P. Bentley, N. Salinas, A. Shenkin, B. Blonder, G. R. Goldsmith, C. Ponton, L. J. Arvin, M. S. Wu, T. Peters, A. J. West, R. E. Martin, B. J. Enquist, G. P. Asner, and Y. Malhi (2016). "Plant leaf wax biomarkers capture gradients in hydrogen isotopes of precipitation from the Andes and Amazon". *Geochimica et Cosmochimica Acta* 182, pp. 155–172. DOI: 10.1016/j.gca.2016.03.018.

- Feng, X., A. L. Reddington, A. M. Faiia, E. S. Posmentier, Y. Shu, and X. Xu (2007). "The changes in North American atmospheric circulation patterns indicated by wood cellulose". *Geology* 35.2, pp. 163–166. DOI: 10.1130/G22884A.1.
- Ficken, K., B. Li, D. Swain, and G. Eglinton (2000). "An *n*-alkane proxy for the sedimentary input of submerged/floating freshwater aquatic macrophytes". *Organic Geochemistry* 31.78, pp. 745–749. DOI: [http://dx.doi.org/10.1016/S0146-6380\(00\)00081-4](http://dx.doi.org/10.1016/S0146-6380(00)00081-4).
- Flanagan, L. B., J. P. Comstock, and J. R. Ehleringer (1991). "Comparison of Modeled and Observed Environmental Influences on the Stable Oxygen and Hydrogen Isotope Composition of Leaf Water in *Phaseolus vulgaris* L." *Plant Physiology* 96, pp. 588–596.
- Freimuth, E. J., A. F. Diefendorf, and T. V. Lowell (2017). "Hydrogen isotopes of *n*-alkanes and *n*-alkanoic acids as tracers of precipitation in a temperate forest and implications for paleorecords". *Geochimica et Cosmochimica Acta* 206, pp. 166–183. DOI: 10.1016/j.gca.2017.02.027.
- Frich, P., S. Rosenørn, H. Madsen, and J. J. Jensen (1997). *Observed Precipitation in Denmark, 1961-90*. Tech. rep. Technical Report 97-8: Danish Meteorological Institute, p. 40.
- Gamarra, B., D. Sachse, and A. Kahmen (2016). "Effects of leaf water evaporative ^2H -enrichment and biosynthetic fractionation on leaf wax *n*-alkane $\delta^2\text{H}$ values in C3 and C4 grasses". *Plant, Cell and Environment* 39, pp. 2390–2403. DOI: 10.1111/pce.12789.
- Gamarra, B. and A. Kahmen (2017). "Low secondary leaf wax *n*-alkane synthesis on fully mature leaves of C3 grasses grown at controlled environmental conditions and variable humidity". *Rapid Communications in Mass Spectrometry* 31, pp. 218–226. DOI: 10.1002/rcm.7770.
- Gao, L., A. Burnier, and Y. Huang (2012). "Quantifying instantaneous regeneration rates of plant leaf waxes using stable hydrogen isotope labeling". *Rapid Communications in Mass Spectrometry* 26.2, pp. 115–122. DOI: 10.1002/rcm.5313.
- Gasse, F. (2000). "Hydrological changes in the African tropics since the Last Glacial Maximum". *Quaternary Science Reviews* 19, pp. 189–211.
- Gasse, F., V. Lédée, M. Massault, and J.-C. Fontes (1989). "Water-level fluctuations of Lake Tanganyika in phase with oceanic changes during the last glaciation and deglaciation". *Nature* 342.6245, pp. 57–59.
- Gat, J. R. and C. J. Bowser (1991). "The heavy isotope enrichment of water in coupled evaporative systems". *Stable Isotope Geochemistry: A Tribute to Samuel Epstein*. Ed. by H. P. Taylor, J. R. O'Neil, and I. R. Kaplan. Vol. 3. Lancaster: The Geochemical Society, pp. 159–168.
- Gat, J. R., D. Yakir, G. Goodfriend, P. Fritz, P. Trumborn, J. Lipp, I. Gev, E. Adar, and Y. Waisel (2007). "Stable isotope composition of water in desert plants". *Plant and Soil* 298.1–2, pp. 31–45. DOI: 10.1007/s11104-007-9321-6.
- Gázquez, F., M. Morellón, T. Bauska, D. Herwartz, J. Surma, A. Moreno, M. Staubwasser, B. Valero-Garcés, A. Delgado-Huertas, and D. A. Hodell (2018). "Triple oxygen and hydrogen isotopes of gypsum hydration water for quantitative paleo-humidity reconstruction". *Earth and Planetary Science Letters* 481, pp. 177–188. DOI: 10.1016/j.epsl.2017.10.020.
- Geldern, R. van, A. Baier, H. L. Subert, S. Kowol, L. Balk, and J. A. C. Barth (2014). "(Table S1) Stable isotope composition of precipitation sampled at Erlangen, Germany between

- 2010 and 2013 for station GeoZentrum located at Erlangen city center". *In supplement to: van Geldern, R et al. (2014): Pleistocene paleo-groundwater as a pristine fresh water resource in southern Germany – evidence from stable and radiogenic isotopes. Science of the Total Environment, 496, 107-115, <https://doi.org/10.1016/j.panga.2014.08.012>. PANGAEA. DOI: 10.1594/PANGAEA.833837.*
- Glaser, B. (2005). "Compound-specific stable-isotope ($\delta^{13}\text{C}$) analysis in soil science". *Journal of Plant Nutrition and Soil Science* 168.5, pp. 633–648. DOI: 10.1002/jpln.200521794.
- Gross, S. and B. Glaser (2004). "Minimization of carbon addition during derivatization of monosaccharides for compound-specific $\delta^{13}\text{C}$ analysis in environmental research". *Rapid Communications in Mass Spectrometry* 18, pp. 2753–2764. DOI: 10.1002/rcm.1684.
- Guggenberger, G., B. T. Christensen, and W. Zech (1994). "Land-use effects on the composition of organic matter in particle-size separates of soil: I. Lignin and carbohydrate signature". *European Journal of Soil Science* 45. December, pp. 449–458.
- Harper, A. D. and M. Bar-Peled (2002). "Biosynthesis of UDP-Xylose. Cloning and Characterization of a Novel Arabidopsis Gene Family, UXS, Encoding Soluble and Putative Membrane-Bound UDP-Glucuronic Acid Decarboxylase Isoforms". *Gene* 130. December, pp. 2188–2198. DOI: 10.1104/pp.009654.2188.
- Helliker, B. R. and J. R. Ehleringer (2002). "Grass blades as tree rings: environmentally induced changes in the oxygen isotope ratio of cellulose along the length of grass blades". *New Phytologist* 155, pp. 417–424.
- Hepp, J., M. Tuthorn, R. Zech, I. Mügler, F. Schlütz, W. Zech, and M. Zech (2015). "Reconstructing lake evaporation history and the isotopic composition of precipitation by a coupled $\delta^{18}\text{O}$ – $\delta^2\text{H}$ biomarker approach". *Journal of Hydrology* 529, pp. 622–631.
- Hepp, J., M. Rabus, T. Anhäuser, T. Bromm, C. Laforsch, F. Sirocko, B. Glaser, and M. Zech (2016). "A sugar biomarker proxy for assessing terrestrial versus aquatic sedimentary input". *Organic Geochemistry* 98, pp. 98–104. DOI: 10.1016/j.orggeochem.2016.05.012.
- Hepp, J., R. Zech, K. Rozanski, M. Tuthorn, B. Glaser, M. Greule, F. Keppler, Y. Huang, W. Zech, and M. Zech (2017). "Late Quaternary relative humidity changes from Mt. Kilimanjaro, based on a coupled ^2H – ^{18}O biomarker paleohygrometer approach". *Quaternary International* 438, pp. 116–130. DOI: 10.1016/j.quaint.2017.03.059.
- Hepp, J., L. Wüthrich, T. Bromm, M. Bliedtner, I. K. Schäfer, B. Glaser, K. Rozanski, F. Sirocko, R. Zech, and M. Zech (2019a). "How dry was the Younger Dryas? Evidence from a coupled $\delta^2\text{H}$ – $\delta^{18}\text{O}$ biomarker paleohygrometer, applied to the Lake Gemündener Maar sediments, Western Eifel, Germany". *Climate of the Past* 15, 713–733. DOI: 10.5194/cp-15-713-2019.
- Hepp, J., I. K. Schäfer, V. Lanny, J. Franke, M. Bliedtner, K. Rozanski, B. Glaser, M. Zech, T. I. Eglinton, and R. Zech (2019b). "Evaluation of bacterial glycerol dialkyl glycerol tetraether and ^2H – ^{18}O biomarker proxies along a Central European topsoil transect". *Biogeosciences Discussions* under review, pp. 1–27. DOI: 10.5194/bg-2019-197.
- Hepp, J., B. Glaser, D. Juchelka, C. Mayr, K. Rozanski, I. K. Schäfer, W. Stichler, M. Tuthorn, R. Zech, and M. Zech (2019c). "Validation of a coupled $\delta^2\text{H}_{n\text{-alkane}}$ – $\delta^{18}\text{O}_{\text{sugar}}$ paleohygrometer approach based on a climate chamber experiment". *Biogeosciences Discussions* under review, pp. 1–30. DOI: 10.5194/bg-2019-427.

- Herrmann, A., P. Maloszewski, and W. Stichler (1987). "Changes of ^{18}O contents of precipitation water during seepage in the unsaturated zone". *Proceedings of International Symposium on Groundwater Monitoring and Management, 23 - 28 March*. Dresden: Institut of Water Management Berlin (GDR) with support of UNESCO, p. 22.
- Horita, J. and D. J. Wesolowski (1994). "Liquid-vapor fractionation of oxygen and hydrogen isotopes of water from the freezing to the critical temperature". *Geochimica et Cosmochimica Acta* 58.16, pp. 3425–3437. DOI: [http://dx.doi.org/10.1016/0016-7037\(94\)90096-5](http://dx.doi.org/10.1016/0016-7037(94)90096-5).
- Hou, J., W. J. D'Andrea, and Y. Huang (2008). "Can sedimentary leaf waxes record D/H ratios of continental precipitation? Field, model, and experimental assessments". *Geochimica et Cosmochimica Acta* 72, pp. 3503–3517. DOI: [10.1016/j.gca.2008.04.030](https://doi.org/10.1016/j.gca.2008.04.030).
- Huang, Y., B. Shuman, Y. Wang, and T. W. Iii (2004). "Hydrogen isotope ratios of individual lipids in lake sediments as novel tracers of climatic and environmental change: a surface sediment test". *Journal of Paleolimnology* 31, pp. 363–375.
- IAEA/WMO (2015). *Global Network of Isotopes in Precipitation. The GNIP Database*. Tech. rep.
- IAEA/WMO (2018). *Global Network of Isotopes in Precipitation. The GNIP Database*. Tech. rep.
- Jacob, J., Y. Huang, J. R. Disnar, A. Sifeddine, M. Boussafir, A. L. Spadano Albuquerque, and B. Turcq (2007). "Paleohydrological changes during the last deglaciation in Northern Brazil". *Quaternary Science Reviews* 26.7-8, pp. 1004–1015. DOI: [10.1016/j.quascirev.2006.12.004](https://doi.org/10.1016/j.quascirev.2006.12.004).
- Jansen, B. and G. L. Wiesenberg (2017). "Opportunities and limitations related to the application of plant-derived lipid molecular proxies in soil science". *Soil* 3.4, pp. 211–234. DOI: [10.5194/soil-3-211-2017](https://doi.org/10.5194/soil-3-211-2017).
- Jia, G., J. Dungait, E. Bingham, M. Valiranta, A. Korhola, and R. Evershed (2008). "Neutral monosaccharides as biomarker proxies for bog-forming plants for application to palaeovegetation reconstruction in ombrotrophic peat deposits". *Organic Geochemistry* 39.12, pp. 1790–1799. DOI: [10.1016/j.orggeochem.2008.07.002](https://doi.org/10.1016/j.orggeochem.2008.07.002).
- Johnsen, S. J., D. Dahl-Jensen, N. Gundestrup, J. P. Steffensen, H. B. Clausen, H. Miller, V. Masson-Delmotte, A. E. Sveinbjörnsdottir, and J. White (2001). "Oxygen isotope and palaeotemperature records from six Greenland ice-core stations: Camp Century, Dye-3, GRIP, GISP2, Renland and NorthGRIP". *Journal of Quaternary Science* 16.4, pp. 299–307. DOI: [10.1002/jqs.622](https://doi.org/10.1002/jqs.622).
- Junginger, A., S. Roller, L. A. Olaka, and M. H. Trauth (2014). "The effects of solar irradiation changes on the migration of the Congo Air Boundary and water levels of paleo-Lake Suguta, Northern Kenya Rift, during the African Humid Period (15 – 5 ka BP)". *Palaeogeography, Palaeoclimatology, Palaeoecology* 396, pp. 1–16. DOI: [10.1016/j.palaeo.2013.12.007](https://doi.org/10.1016/j.palaeo.2013.12.007).
- Kahmen, A., T. E. Dawson, A. Vieth, and D. Sachse (2011b). "Leaf wax *n*-alkane δD values are determined early in the ontogeny of *Populus trichocarpa* leaves when grown under controlled environmental conditions". *Plant, Cell and Environment* 34.10, pp. 1639–1651. DOI: [10.1111/j.1365-3040.2011.02360.x](https://doi.org/10.1111/j.1365-3040.2011.02360.x).
- Kahmen, A., D. Sachse, S. K. Arndt, K. P. Tu, H. Farrington, P. M. Vitousek, and T. E. Dawson (2011a). "Cellulose $\delta^{18}\text{O}$ is an index of leaf-to-air vapor pressure difference

- (VPD) in tropical plants". *Proceedings of the National Academy of Sciences of the United States of America* 108.5, pp. 1981–1986. DOI: 10.1073/pnas.1018906108.
- Kahmen, A., E. Schefuß, and D. Sachse (2013a). "Leaf water deuterium enrichment shapes leaf wax *n*-alkane δ D values of angiosperm plants I: Experimental evidence and mechanistic insights". *Geochimica et Cosmochimica Acta* 111, pp. 39–49.
- Kahmen, A., B. Hoffmann, E. Schefuß, S. K. Arndt, L. A. Cernusak, J. B. West, and D. Sachse (2013b). "Leaf water deuterium enrichment shapes leaf wax *n*-alkane δ D values of angiosperm plants II: Observational evidence and global implications". *Geochimica et Cosmochimica Acta* 111, pp. 50–63. DOI: 10.1016/j.gca.2012.09.004.
- Konecky, B. L., J. M. Russell, T. C. Johnson, E. T. Brown, M. A. Berke, J. P. Werne, and Y. Huang (2011). "Atmospheric circulation patterns during late Pleistocene climate changes at Lake Malawi, Africa". *Earth and Planetary Science Letters* 312.3-4, pp. 318–326. DOI: 10.1016/j.epsl.2011.10.020.
- Laursen, E. V., R. S. Thomsen, and J. Cappelen (1999). *Observed Air Temperature, Humidity, Pressure, Cloud Cover and Weather in Denmark - with Climatological Standard Normals, 1961-90*. Tech. rep. Technical Report 99-5: Danish Meteorological Institute, p. 142.
- Lee, H., S. J. Feakins, and L. d.S. L. Sternberg (2016). "Carbon and hydrogen isotopic effects of stomatal density in *Arabidopsis thaliana*". *Geochimica et Cosmochimica Acta* 179, pp. 275–286. DOI: 10.1016/j.gca.2016.01.029.
- Lehmann, M. M., B. Gamarra, A. Kahmen, R. T. Siegwolf, and M. Saurer (2017). "Oxygen isotope fractionations across individual leaf carbohydrates in grass and tree species". *Plant Cell and Environment* 40.8, pp. 1658–1670. DOI: 10.1111/pce.12974.
- Litt, T., A. Brauer, T. Goslar, J. Merkt, K. Balaga, H. Müller, M. Ralska-Jasiewiczowa, M. Stebich, and J. F. W. Negendank (2001). "Correlation and synchronisation of Lateglacial continental sequences in northern central Europe based on annually laminated lacustrine sediments". *Quaternary Science Reviews* 20, pp. 1233,1249.
- Liu, H. T., X. Y. Gong, R. Schäufele, F. Yang, R. T. Hirl, A. Schmidt, and H. Schnyder (2016). "Nitrogen fertilization and $\delta^{18}\text{O}$ of CO_2 have no effect on ^{18}O -enrichment of leaf water and cellulose in *Cleistogenes squarrosa* (C_4) – is VPD the sole control?" *Plant Cell and Environment* 39.12, pp. 2701–2712. DOI: 10.1111/pce.12824.
- Liu, H. T., R. Schäufele, X. Y. Gong, and H. Schnyder (2017). "The $\delta^{18}\text{O}$ and $\delta^2\text{H}$ of water in the leaf growth-and-differentiation zone of grasses is close to source water in both humid and dry atmospheres". *New Phytologist* 214.4, pp. 1423–1431. DOI: 10.1111/nph.14549.
- Liu, H. and W. Liu (2016). "*n*-Alkane distributions and concentrations in algae, submerged plants and terrestrial plants from the Qinghai-Tibetan Plateau". *Organic Geochemistry* 99, pp. 10–22. DOI: 10.1016/j.orggeochem.2016.06.003.
- Mayer, B. and L. Schwark (1999). "A 15,000-year stable isotope record from sediments of Lake Steisslingen, Southwest Germany". *Chemical Geology* 161.1, pp. 315–337. DOI: 10.1016/S0009-2541(99)00093-5.
- Mayr, C. (2002). "Möglichkeiten der Klimarekonstruktion im Holozän mit $\delta^{13}\text{C}$ - und $\delta^2\text{H}$ -Werten von Baum-Jahrringen auf der Basis von Klimakammerversuchen und Rezentstudien". PhD thesis. PhD thesis, Ludwig-Maximilians-Universität München. GSF-Bericht 14/02, 152 pp, p. 152.
- McGlue, M. M., K. E. Lezzar, A. S. Cohen, J. M. Russell, J.-J. Tierceline, A. A. Felton, E. Mbede, and H. H. Nkotalu (2007). "Seismic records of late Pleistocene aridity in Lake

- Tanganyika, tropical East Africa”. *Journal of Paleolimnology* 40.2, pp. 635–653. DOI: 10.1007/s10933-007-9187-x.
- McInerney, F. A., B. R. Helliker, and K. H. Freeman (2011). “Hydrogen isotope ratios of leaf wax *n*-alkanes in grasses are insensitive to transpiration”. *Geochimica et Cosmochimica Acta* 75.2, pp. 541–554. DOI: 10.1016/j.gca.2010.10.022.
- Merlivat, L. (1978). “Molecular diffusivities of H₂¹⁶O, HD¹⁶O, and H₂¹⁸O in gases”. *The Journal of Chemical Physics* 69.6, pp. 2864–2871. DOI: <http://dx.doi.org/10.1063/1.436884>.
- Moernaut, J, D Verschuren, F Charlet, I Kristen, M Fagot, and M. D. Batist (2010). “The seismic-stratigraphic record of lake-level fluctuations in Lake Challa: Hydrological stability and change in equatorial East Africa over the last 140 kyr”. *Earth and Planetary Science Letters* 290.1-2, pp. 214–223. DOI: 10.1016/j.epsl.2009.12.023.
- Mügler, I., D. Sachse, M. Werner, B. Xu, G. Wu, T. Yao, and G. Gleixner (2008). “Effect of lake evaporation on δD values of lacustrine *n*-alkanes: A comparison of Nam Co (Tibetan Plateau) and Holzmaar (Germany)”. *Organic Geochemistry* 39.6, pp. 711–729.
- Munksgaard, N. C., A. W. Cheesman, N. B. English, C. Zwart, A. Kahmen, and L. A. Cernusak (2017). “Identifying drivers of leaf water and cellulose stable isotope enrichment in Eucalyptus in northern Australia”. *Oecologia* 183.1, pp. 31–43. DOI: 10.1007/s00442-016-3761-8.
- Muscheler, R., F. Adolphi, and M. F. Knudsen (2014). “Assessing the differences between the IntCal and Greenland ice-core time scales for the last 14,000 years via the common cosmogenic radionuclide variations”. *Quaternary Science Reviews* 106, pp. 81–87. DOI: 10.1016/j.quascirev.2014.08.017.
- Muschitiello, F., F. S. R. Pausata, J. E. Watson, R. H. Smittenberg, A. A. M. Salih, S. J. Brooks, N. J. Whitehouse, A. Karlatou-Charalampopoulou, and B. Wohlfarth (2015). “Fennoscandian freshwater control on Greenland hydroclimate shifts at the onset of the Younger Dryas”. *Nature Communications* 6, p. 8939. DOI: 10.1038/ncomms9939. arXiv: 9809069v1 [arXiv:gr-qc].
- Newberry, S. L., A. Kahmen, P. Dennis, and A. Grant (2015). “*n*-Alkane biosynthetic hydrogen isotope fractionation is not constant throughout the growing season in the riparian tree *Salix viminalis*”. *Geochimica et Cosmochimica Acta* 165, pp. 75–85. DOI: 10.1016/j.gca.2015.05.001.
- Otto-Bliesner, B. L., J. M. Russell, P. U. Clark, Z. Liu, J. T. Overpeck, B. Konecky, P. DeMenocal, S. E. Nicholson, F. He, and Z. Lu (2014). “Coherent changes of southeastern equatorial and northern African rainfall during the last deglaciation”. *Science* 346.6214, pp. 1223–1227.
- Pedentchouk, N. and Y. Zhou (2018). “Factors Controlling Carbon and Hydrogen Isotope Fractionation During Biosynthesis of Lipids by Phototrophic Organisms”. *Hydrocarbons, Oils and Lipids: Diversity, Origin, Chemistry and Fate. Handbook of Hydrocarbon and Lipid Microbiology*. Ed. by H. Wilkes. Cham: Springer, pp. 1–24.
- Pepin, N. C., W. J. Duane, and D. R. Hardy (2010). “The montane circulation on Kilimanjaro, Tanzania and its relevance for the summit ice fields: Comparison of surface mountain climate with equivalent reanalysis parameters”. *Global and Planetary Change* 74.2, pp. 61–75. DOI: 10.1016/j.gloplacha.2010.08.001.
- Petit, J. R., J Jouzel, D Raynaud, N. I. Barkov, J.-M. Barnola, I Basile, M Bender, J Chappellaz, M Davis, G Delaygue, M Delmotte, V. M. Kotlyakov, M Legrand, V. Y. Lipenkov, C Lorius, L Pépin, C Ritz, E Saltzman, and M Stievenard (1999). “Climate and atmo-

- spheric history of the past 420,000 years from the Vostok ice core, Antarctica". *Nature* 399, pp. 429–436.
- Prietzl, J., N. Dechamps, and S. Spielvogel (2013). "Analysis of non-cellulosic polysaccharides helps to reveal the history of thick organic surface layers on calcareous Alpine soils". *Plant and Soil* 365.1-2, pp. 93–114. DOI: 10.1007/s11104-012-1340-2.
- Rach, O., A. Brauer, H. Wilkes, and D. Sachse (2014). "Delayed hydrological response to Greenland cooling at the onset of the Younger Dryas in western Europe". *Nature Geoscience* 7.2, pp. 109–112.
- Rach, O., A. Kahmen, A. Brauer, and D. Sachse (2017). "A dual-biomarker approach for quantification of changes in relative humidity from sedimentary lipid D/H ratios". *Climate of the Past* 13, pp. 741–757. DOI: 10.5194/cp-2017-7.
- Rao, Z., Z. Zhu, G. Jia, A. C. G. Henderson, Q. Xue, and S. Wang (2009). "Compound specific δD values of long chain *n*-alkanes derived from terrestrial higher plants are indicative of the δD of meteoric waters: Evidence from surface soils in eastern China". *Organic Geochemistry* 40.8, pp. 922–930. DOI: <http://dx.doi.org/10.1016/j.orggeochem.2009.04.011>.
- Rao, Z., G. Jia, M. Qiang, and Y. Zhao (2014). "Assessment of the difference between mid- and long chain compound specific $\delta D_{n-alkanes}$ values in lacustrine sediments as a paleoclimatic indicator". *Organic Geochemistry* 76, pp. 104–117. DOI: 10.1016/j.orggeochem.2014.07.015.
- Rao, Z., M. Qiang, G. Jia, Y. Li, D. Dan, and F. Chen (2016). "A 15 ka lake water δD record from Genggahai Lake, northeastern Tibetan Plateau, and its paleoclimatic significance". *Organic Geochemistry* 97, pp. 5–16. DOI: 10.1016/j.orggeochem.2016.03.007.
- Roden, J. S. and J. R. Ehleringer (1999). "Observations of Hydrogen and Oxygen Isotopes in Leaf Water Confirm the Craig-Gordon Model under Wide-Ranging Environmental Conditions". *Plant Physiology* 120.August, pp. 1165–1173.
- Roden, J. S., G. Lin, and J. R. Ehleringer (2000). "A mechanistic model for interpretation of hydrogen and oxygen isotope ratios in tree-ring cellulose". *Geochimica et Cosmochimica Acta* 64.1, pp. 21–35.
- Rozanski, K., L. Araguás-Araguás, and R. Gonfiantini (1993). "Isotopic patterns in modern global precipitation". *Climate change in continental isotopic records*, pp. 1–36.
- Rozanski, K., L. Araguás-Araguás, and R. Gonfiantini (1996). "Isotope patterns of precipitation in the East African region". *The Limnology, climatology and paleoclimatology of the East African Lakes*, pp. 79–94.
- Rozanski, K., M. A. Klisch, P. Wachniew, Z. Gorczyca, T. Goslar, T. W. Edwards, and A. Shemesh (2010). "Oxygen-isotope geothermometers in lacustrine sediments: New insights through combined $\delta^{18}O$ analyses of aquatic cellulose, authigenic calcite and biogenic silica in Lake Gościąg, central Poland". *Geochimica et Cosmochimica Acta* 74.10, pp. 2957–2969. DOI: 10.1016/j.gca.2010.02.026.
- Sachse, D., J. Radke, and G. Gleixner (2004). "Hydrogen isotope ratios of recent lacustrine sedimentary *n*-alkanes record modern climate variability". *Geochimica et Cosmochimica Acta* 68.23, pp. 4877–4889. DOI: <http://dx.doi.org/10.1016/j.gca.2004.06.004>.
- Sachse, D., J. Radke, and G. Gleixner (2006). " δD values of individual *n*-alkanes from terrestrial plants along a climatic gradient - Implications for the sedimentary biomarker record". *Organic Geochemistry* 37.4, pp. 469–483.

- Sachse, D., G. Gleixner, H. Wilkes, and A. Kahmen (2010). "Leaf wax *n*-alkane δD values of field-grown barley reflect leaf water δD values at the time of leaf formation". *Geochimica et Cosmochimica Acta* 74.23, pp. 6741–6750. DOI: 10.1016/j.gca.2010.08.033.
- Sachse, D., I. Billault, G. Bowen, Y. Chikaraishi, T. Dawson, S. Feakins, K. Freeman, C. Magill, F. McInerney, M. van der Meer, P. Polissar, R. Robins, J. Sachs, H.-L. Schmidt, A. Sessions, J. White, and J. West (2012). "Molecular Paleohydrology: Interpreting the Hydrogen-Isotopic Composition of Lipid Biomarkers from Photosynthesizing Organisms". *Annual Reviews* 40, pp. 221–249. DOI: 10.1146/annurev-earth-042711-105535.
- Santrucek, J., J. Kveton, J. Setlik, and L. Bulickova (2007). "Spatial Variation of Deuterium Enrichment in Bulk Water of Snowgum Leaves". *Plant Physiology* 143.1, pp. 88–97. DOI: 10.1104/pp.106.089284.
- Sauer, P. E., T. I. Eglinton, J. M. Hayes, A. Schimmelmann, and A. L. Sessions (2001). "Compound-specific D/H ratios of lipid biomarkers from sediments as a proxy for environmental and climatic conditions". *Geochimica et Cosmochimica Acta* 65.2, pp. 213–222. DOI: [http://dx.doi.org/10.1016/S0016-7037\(00\)00520-2](http://dx.doi.org/10.1016/S0016-7037(00)00520-2).
- Saurer, M. and R. Siegwolf (2004). "Pyrolysis Techniques for Oxygen Isotope Analysis of Cellulose". *Handbook of Stable Isotope Analytical Techniques*. Ed. by P. de Groot. Volume-I. April. Elsevier B.V., pp. 497–506. DOI: 10.1016/B978-044451114-0/50025-9.
- Schäfer, I. K., V. Lanny, J. Franke, T. I. Eglinton, M. Zech, B. Vysloužilová, and R. Zech (2016). "Leaf waxes in litter and topsoils along a European transect". *SOIL* 2, pp. 551–564. DOI: 10.5194/soil-2-551-2016.
- Schefuß, E., H. Kuhlmann, G. Mollenhauer, M. Prange, and J. Pätzold (2011). "Forcing of wet phases in southeast Africa over the past 17,000 years". *Nature* 480, pp. 509–512. DOI: 10.1038/nature10685.
- Schmidt, H.-L., R. A. Werner, and A. Roßmann (2001). " ^{18}O Pattern and biosynthesis of natural plant products". *Phytochemistry* 58.1, pp. 9–32. DOI: [http://dx.doi.org/10.1016/S0031-9422\(01\)00017-6](http://dx.doi.org/10.1016/S0031-9422(01)00017-6).
- Schmidt, H.-L., R. A. Werner, and W. Eisenreich (2003). "Systematics of 2H patterns in natural compounds and its importance for the elucidation of biosynthetic pathways". *Phytochemistry Reviews* 2.1-2, pp. 61–85. DOI: 10.1023/B:PHYT.00000004185.92648.ae.
- Scholz, C. A., T. C. Johnson, A. S. Cohen, J. W. King, J. A. Peck, J. T. Overpeck, M. R. Talbot, E. T. Brown, L. Kalindekaffe, P. Y. O. Amoako, R. P. Lyons, T. M. Shanahan, I. S. Castañeda, C. W. Heil, S. L. Forman, L. R. McHargue, K. R. Beuning, J. Gomez, and J. Pierson (2007). "East African megadroughts between 135 and 75 thousand years ago and bearing on early-modern human origins". *PNAS* 104.42, pp. 16416–16421.
- Schüler, L., A. Hemp, W. Zech, and H. Behling (2012). "Vegetation, climate and fire-dynamics in East Africa inferred from the Maundi crater pollen record from Mt Kilimanjaro during the last glacial-interglacial cycle". *Quaternary Science Reviews* 39, pp. 1–13. DOI: 10.1016/j.quascirev.2012.02.003.
- Seki, O., P. A. Meyers, S. Yamamoto, K. Kawamura, T. Nakatsuka, W. Zhou, and Y. Zheng (2011). "Plant-wax hydrogen isotopic evidence for postglacial variations in delivery of precipitation in the monsoon domain of China". *Geology* 39.9, pp. 875–878. DOI: 10.1130/G32117.1.

- Sessions, A. L., T. W. Burgoyne, A. Schimmelmann, and J. M. Hayes (1999). "Fractionation of hydrogen isotopes in lipid biosynthesis". *Organic Geochemistry* 30, pp. 1193–1200.
- Shackleton, N. J. (1987). "Oxygen Isotopes, Ice Volume and Sea Level". *Quaternary Science Reviews* 6, pp. 183–190.
- Sirocko, F (2012). *Wetter, Klima, Menschheitsentwicklung: Von der Eiszeit bis ins 21. Jahrhundert*. Wiss. Buchges., p. 208.
- Sirocko, F., S. Dietrich, D. Veres, P. Grootes, K. Schaber-Mohr, K. Seelos, M.-J. Nadeau, B. Kromer, L. Rothacker, M. Röhner, M. Krbetschek, P. Appleby, U. Hambach, C. Rolf, M. Sudo, and S. Grim (2013). "Multi-proxy dating of Holocene maar lakes and Pleistocene dry maar sediments in the Eifel, Germany". *Quaternary Science Reviews* 62, pp. 56–76.
- Song, X., G. D. Farquhar, A. Gessler, and M. M. Barbour (2014). "Turnover time of the non-structural carbohydrate pool influences $\delta^{18}\text{O}$ of leaf cellulose". *Plant Cell and Environment* 37.11, pp. 2500–2507. DOI: 10.1111/pce.12309.
- Sternberg, L, M. C. Pinzon, W. T. Anderson, and A. H. Jahren (2006). "Variation in oxygen isotope fractionation during cellulose synthesis: intramolecular and biosynthetic effects". *Plant, Cell & Environment* 29.10, pp. 1881–1889. DOI: 10.1111/j.1365-3040.2006.01564.x.
- Sternberg, L. and P. F. V. Ellsworth (2011). "Divergent Biochemical Fractionation, Not Convergent Temperature, Explains Cellulose Oxygen Isotope Enrichment across Latitudes". *PLoS ONE* 6.11, e28040. DOI: 10.1371/journal.pone.0028040.
- Sternberg, L. D.S.L. O. (2009). "Oxygen stable isotope ratios of tree-ring cellulose: The next phase of understanding". *New Phytologist* 181.3, pp. 553–562. DOI: 10.1111/j.1469-8137.2008.02661.x.
- Sternberg, L. d.S.L. O. and M. J. D. DeNiro (1983). "Biogeochemical implications of the isotopic equilibrium fractionation factor between the oxygen atoms of acetone and water". *Geochimica et Cosmochimica Acta* 47.12, pp. 2271–2274. DOI: 10.1016/0016-7037(83)90049-2.
- Sternberg, L. S. L., M. J. DeNiro, and R. A. Savidge (1986). "Oxygen Isotope Exchange between Metabolites and Water during Biochemical Reactions Leading to Cellulose Synthesis". *Plant Physiology* 82, pp. 423–427.
- Sternberg, L. S. L. (1988). "D/H ratios of environmental water recored by D/H ratios of plants lipids". *Nature* 336, pp. 403–405. DOI: 10.1038/332141a0.
- Sternberg, L. (2014). "Comment on "Oxygen isotope ratios ($^{18}\text{O}/^{16}\text{O}$) of hemicellulose-derived sugar biomarkers in plants, soils and sediments as paleoclimate proxy I: Insight from a climate chamber experiment" by Zech et al. (2014)". *Geochimica et Cosmochimica Acta* 141, pp. 677–679. DOI: 10.1016/j.gca.2014.04.051.
- Stuiver, M. and T. F. Braziunas (1988). "The Solar Component of the Atmospheric ^{14}C Record". *Secular Solar and Geomagnetic Variations in the Last 10,000 Years*. Ed. by F. Stephenson and A. Wolfendale. 236th ed. Dordrecht: Springer, pp. 245–266.
- Stumpp, C., J. Klaus, and W. Stichler (2014). "Analysis of long-term stable isotopic composition in German precipitation". *Journal of Hydrology* 517, pp. 351–361. DOI: 10.1016/j.jhydrol.2014.05.034.
- Sundqvist, H. S., K Holmgren, J Fohlmeister, Q Zhang, M Bar Matthews, C Spötl, and H Körnich (2013). "Evidence of a large cooling between 1690 and 1740 AD in southern Africa". *Scientific Reports* 3.1767, pp. 1–6. DOI: 10.1038/srep01767.
- Swedish Meteorological and Hydrological Institute (2018). *SMHI Open Data Meteorological Observations*. Tech. rep.

- Talbot, M. R. and D. A. Livingstone (1989). "Hydrogen index and carbon isotopes of lacustrine organic matter as lake level indicators". *Palaeogeography, Palaeoclimatology, Palaeoecology* 70.1–3, pp. 121–137. DOI: [http://dx.doi.org/10.1016/0031-0182\(89\)90084-9](http://dx.doi.org/10.1016/0031-0182(89)90084-9).
- Terwilliger, V. J., K. Kitajima, D. J. Le Roux-Swarthout, S. Mulkey, and S. J. Wright (2001). "Intrinsic water-use efficiency and heterotrophic investment in tropical leaf growth of two Neotropical pioneer tree species as estimated from $\delta^{13}\text{C}$ values". *New Phytologist* 152.2, pp. 267–281. DOI: [10.1046/j.0028-646X.2001.00252.x](https://doi.org/10.1046/j.0028-646X.2001.00252.x).
- Terwilliger, V. J., J. L. Betancourt, S. W. Leavitt, and P. K. Van De water (2002). "Leaf cellulose δD and $\delta^{18}\text{O}$ trends with elevation differ in direction among co-occurring, semi-arid plant species". *Geochimica et Cosmochimica Acta* 66.22, pp. 3887–3900. DOI: [10.1016/S0016-7037\(02\)00964-X](https://doi.org/10.1016/S0016-7037(02)00964-X).
- Tierney, J. E., J. M. Russell, Y. Huang, J. S. Sinninghe Damsté, E. C. Hopmans, and A. S. Cohen (2008). "Northern Hemisphere Controls on Tropical Southeast African Climate During the Past 60,000 Years". *Science* 322, pp. 252–255. DOI: [10.1126/science.1160485](https://doi.org/10.1126/science.1160485).
- Tierney, J. E., J. M. Russell, J. S. Sinninghe Damsté, Y. Huang, and D. Verschuren (2011). "Late Quaternary behavior of the East African monsoon and the importance of the Congo Air Boundary". *Quaternary Science Reviews* 30.7-8, pp. 798–807. DOI: [10.1016/j.quascirev.2011.01.017](https://doi.org/10.1016/j.quascirev.2011.01.017).
- Tipple, B. J. and J. R. Ehleringer (2018). "Distinctions in heterotrophic and autotrophic-based metabolism as recorded in the hydrogen and carbon isotope ratios of normal alkanes". *Oecologia* 187.4, pp. 1053–1075. DOI: [10.1007/s00442-018-4189-0](https://doi.org/10.1007/s00442-018-4189-0).
- Tipple, B. J., M. A. Berke, C. E. Doman, S. Khachatryan, and J. R. Ehleringer (2013). "Leaf-wax *n*-alkanes record the plant-water environment at leaf flush". *Proceedings of the National Academy of Sciences* 110.7, pp. 2659–2664. DOI: [10.1073/pnas.1213875110](https://doi.org/10.1073/pnas.1213875110).
- Tipple, B. J., M. A. Berke, B. Hambach, J. S. Roden, and J. R. Ehleringer (2015). "Predicting leaf wax *n*-alkane $^2\text{H}/^1\text{H}$ ratios: Controlled water source and humidity experiments with hydroponically grown trees confirm predictions of Craig-Gordon model". *Plant, Cell and Environment* 38.6, pp. 1035–1047. DOI: [10.1111/pce.12457](https://doi.org/10.1111/pce.12457).
- Tipple, B. J., B. Hambach, J. E. Barnette, L. A. Chesson, and J. R. Ehleringer (2016). "The influences of cultivation setting on inflorescence lipid distributions, concentrations, and carbon isotope ratios of *Cannabis sp.*" *Forensic Science International* 262.March, pp. 233–241. DOI: [10.1016/j.forsciint.2016.03.029](https://doi.org/10.1016/j.forsciint.2016.03.029).
- Trauth, M. H., M. A. Maslin, A. L. Deino, M. R. Strecker, A. G. N. Bergner, and M. Dühnforth (2007). "High- and Low- latitude forcing of Plio-Pleistocene East African climate and human evolution". *Journal of Human Evolution* 53, pp. 475–486. DOI: [10.1016/j.jhevol.2006.12.009](https://doi.org/10.1016/j.jhevol.2006.12.009).
- Tuthorn, M., M. Zech, M. Ruppenthal, Y. Oelmann, A. Kahmen, H. F. del Valle, W. Wilcke, and B. Glaser (2014). "Oxygen isotope ratios ($^{18}\text{O}/^{16}\text{O}$) of hemicellulose-derived sugar biomarkers in plants, soils and sediments as paleoclimate proxy II: Insight from a climate transect study". *Geochimica et Cosmochimica Acta* 126.0, pp. 624–634. DOI: <http://dx.doi.org/10.1016/j.gca.2013.11.002>.
- Tuthorn, M., R. Zech, M. Ruppenthal, Y. Oelmann, A. Kahmen, H. del Valle, T. Eglinton, K. Rozanski, and M. Zech (2015). "Coupling $\delta^2\text{H}$ and $\delta^{18}\text{O}$ biomarker results yields information on relative humidity and isotopic composition of precipitation - a climate transect

- validation study". *Biogeosciences* 12, pp. 3913–3924. DOI: 10.5194/bg-12-3913-2015.
- Umweltbundesamt GmbH (2018). *Erhebung der Wassergüte in Österreich gemäß Hydrographiegesetz i.d.F. des BGBl. Nr. 252/90 (gültig bis Dezember 2006) bzw. Gewässerzustandsüberwachung in Österreich gemäß Wasserrechtsgesetz, BGBl. I Nr. 123/06, i.d.g.F.; BMLFUW, Sektion IV / Abteilung 3 N*. Tech. rep.
- Veggi, P. C., J. Martinez, and M. A. A. Meireles (2013). "Fundamentals of Microwave Extraction". *Microwave-assisted Extraction for Bioactive Compounds: Theory and Practice*. Ed. by F. Chemat and G. Cravotto. Boston, MA: Springer US, pp. 15–52. DOI: 10.1007/978-1-4614-4830-3_2.
- Verschuren, D., J. S. S. Damsté, J. Moernaut, I. Kristen, M. Blaauw, M. Fagot, G. H. Haug, and C. project members (2009). "Half-precessional dynamics of monsoon rainfall near the East African Equator". *Nature* 462.7273, pp. 637–641. DOI: 10.1038/nature08520.
- Voelker, S. L., J. R. Brooks, F. C. Meinzer, J. Roden, A. Pazdur, S. Pawelczyk, P. Hartsough, K. Snyder, L. Plavcova, and J. Santrucek (2014). "Reconstructing relative humidity from plant $\delta^{18}\text{O}$ and δD as deuterium deviations from the global meteoric water line". *Ecological Applications* 24.5, pp. 960–975. DOI: 10.1890/13-0988.1.
- Walker, C. D. and J.-P. Brunel (1990). "Examining Evapotranspiration in a Semi-Arid Region using Stable Isotopes of Hydrogen and Oxygen". *Journal of Hydrology* 118, pp. 55–75.
- Wang, X.-F., D. Yakir, and M. Avisha (1998). "Non-climatic variations in the oxygen isotopic composition of plants". *Global Change Biology* 4, pp. 835–849.
- Waterhouse, J. S., S. Cheng, D. Juchelka, N. J. Loader, D. McCarroll, V. R. Switsur, and L. Gautam (2013). "Position-specific measurement of oxygen isotope ratios in cellulose: Isotopic exchange during heterotrophic cellulose synthesis". *Geochimica et Cosmochimica Acta* 112.0, pp. 178–191. DOI: <http://dx.doi.org/10.1016/j.gca.2013.02.021>.
- Werner, R. A. and W. A. Brand (2001). "Referencing strategies and techniques in stable isotope ratio analysis". *Rapid Communications in Mass Spectrometry* 15.7, pp. 501–519. DOI: 10.1002/rcm.258.
- Wissel, H., C. Mayr, and A. Lücke (2008). "A new approach for the isolation of cellulose from aquatic plant tissue and freshwater sediments for stable isotope analysis". *Organic Geochemistry* 39.11, pp. 1545–1561. DOI: <http://dx.doi.org/10.1016/j.orggeochem.2008.07.014>.
- Wurth, G., S. Niggemann, D. K. Richter, and A. Mangini (2004). "The Younger Dryas and Holocene climate record of a stalagmite from Hölloch Cave (Bavarian Alps, Germany)". *Journal of Quaternary Science* 19.3, pp. 291–298. DOI: 10.1002/jqs.837.
- Yakir, D. and M. J. DeNiro (1990). "Oxygen and Hydrogen Isotope Fractionation during Cellulose Metabolism in *Lemna gibba* L." *Plant Ecology* 93, pp. 325–332.
- Zech, M. and B. Glaser (2008). "Improved compound-specific $\delta^{13}\text{C}$ analysis of *n*-alkanes for application in palaeoenvironmental studies". *Rapid Communications in Mass Spectrometry* 22, pp. 135–142. DOI: 10.1002/rcm.
- Zech, M. and B. Glaser (2009). "Compound-specific $\delta^{18}\text{O}$ analyses of neutral sugars in soils using gas chromatography-pyrolysis-isotope ratio mass spectrometry: problems, possible solutions and a first application". *Rapid Communications in Mass Spectrometry* 23, pp. 3522–3532. DOI: 10.1002/rcm.

- Zech, M., R. A. Werner, D. Juchelka, K. Kalbitz, B. Buggle, and B. Glaser (2012). "Absence of oxygen isotope fractionation/exchange of (hemi-) cellulose derived sugars during litter decomposition". *Organic Geochemistry* 42.12, pp. 1470–1475. DOI: <http://dx.doi.org/10.1016/j.orggeochem.2011.06.006>.
- Zech, M., M. Tuthorn, F. Detsch, K. Rozanski, R. Zech, L. Zöller, W. Zech, and B. Glaser (2013). "A 220 ka terrestrial $\delta^{18}\text{O}$ and deuterium excess biomarker record from an eolian permafrost paleosol sequence, NE-Siberia". *Chemical Geology* 360-361, pp. 220–230. DOI: <http://dx.doi.org/10.1016/j.chemgeo.2013.10.023>.
- Zech, M., M. Tuthorn, F. Schlütz, W. Zech, and B. Glaser (2014a). "A 16-ka $\delta^{18}\text{O}$ record of lacustrine sugar biomarkers from the High Himalaya reflects Indian Summer Monsoon variability". *Journal of Paleolimnology* 51, pp. 241–251. DOI: [10.1007/s10933-013-9744-4](https://doi.org/10.1007/s10933-013-9744-4).
- Zech, M., C. Mayr, M. Tuthorn, K. Leiber-Sauheidl, and B. Glaser (2014b). "Oxygen isotope ratios ($^{18}\text{O}/^{16}\text{O}$) of hemicellulose-derived sugar biomarkers in plants, soils and sediments as paleoclimate proxy I: Insight from a climate chamber experiment". *Geochimica et Cosmochimica Acta* 126.0, pp. 614–623. DOI: <http://dx.doi.org/10.1016/j.gca.2013.10.048>.
- Zech, M., C. Mayr, M. Tuthorn, K. Leiber-Sauheidl, and B. Glaser (2014c). "Reply to the comment of Sternberg on "Zech et al. (2014) Oxygen isotope ratios ($^{18}\text{O}/^{16}\text{O}$) of hemicellulose-derived sugar biomarkers in plants, soils and sediments as paleoclimate proxy I: Insight from a climate chamber experiment. GCA". *Geochimica et Cosmochimica Acta* 141.0, pp. 680–682. DOI: [10.1016/j.gca.2014.04.051](https://doi.org/10.1016/j.gca.2014.04.051).

Contributions to the included manuscripts

The presented cumulative thesis is comprised of 6 manuscripts prepared with the contributions from all co-authors. A record of the specific author contribution is given below:

Manuscript 1: Validation of a coupled $\delta^2\text{H}_{n\text{-alkane}}\text{-}\delta^{18}\text{O}_{\text{sugar}}$ paleohygrometer approach based on a climate chamber experiment

Johannes Hepp:	laboratory work ($\delta^{18}\text{O}$ of sugars), modeling, discussion of results, manuscript preparation, publication handling (60%)
Bruno Glaser:	discussion of results, comments on the manuscript (3%)
Dieter Juchelka:	comments on the manuscript (2%)
Christoph Mayr:	climate chamber experiment, discussion of results, comments on the manuscript (7%)
Kazimierz Rozanski:	discussion of results, comments on the manuscript (5%)
Imke Kathrin Schäfer:	laboratory work ($\delta^2\text{H}$ of n -alkanes), data preparation and evaluation, comments on the manuscript (5%)
Willibald Stichler:	climate chamber experiment, comments on the manuscript (2%)
Mario Tuthorn:	laboratory work ($\delta^{18}\text{O}$ of sugars), data preparation and evaluation, discussion of results, comments on the manuscript (7%)
Roland Zech:	laboratory work ($\delta^2\text{H}$ of n -alkanes), discussion of results, comments on the manuscript (2%)
Michael Zech:	discussion of results, comments on the manuscript (7%)

Manuscript 2: Evaluation of bacterial glycerol dialkyl glycerol tetraether and ^2H - ^{18}O biomarker proxies along a Central European topsoil transect

Johannes Hepp:	laboratory work ($\delta^{18}\text{O}$ of sugars and pH), data evaluation and preparation, performed coupled ^2H - ^{18}O biomarker approach modelling, discussion of results, manuscript preparation, publication handling (40%)
Imke Kathrin Schäfer:	data evaluation and preparation ($\delta^2\text{H}$ of <i>n</i> -alkanes and GDGT's), discussion of results, manuscript preparation (30%)
Verena Lanny:	field work, laboratory work ($\delta^2\text{H}$ of <i>n</i> -alkanes and GDGT's), discussion of results, comments on the manuscript (6%)
Jörg Franke:	statistical analysis, discussion of results, comments on the manuscript (2%)
Marcel Bliedtner:	assistance with laboratory work ($\delta^2\text{H}$ of <i>n</i> -alkanes and GDGT's), discussion of results, comments on the manuscript (2%)
Kazimierz Rozanski:	assistance with coupled ^2H - ^{18}O biomarker approach modelling, discussion of the $\delta^2\text{H}$ and $\delta^{18}\text{O}$ results, comments on the manuscript (5%)
Bruno Glaser:	discussion of the $\delta^2\text{H}$ and $\delta^{18}\text{O}$ results, comments on the manuscript (2%)
Michael Zech:	discussion of the $\delta^2\text{H}$ and $\delta^{18}\text{O}$ results, comments on the manuscript (3%)
Timothy Eglinton:	discussion of the GDGT results, comments on the manuscript (2%)
Roland Zech:	study design, discussion of results, comments on the manuscript (8%)

Manuscript 3: Late Quaternary relative humidity changes from Mt. Kilimanjaro, based on a coupled ^2H - ^{18}O biomarker paleohygrometer approach

Johannes Hepp:	data evaluation and compilation, discussion of results, manuscript preparation, publication handling (51%)
Roland Zech:	laboratory work ($\delta^2\text{H}$ of <i>n</i> -alkanes and fatty acids), data preparation, discussion of the results, comments on the manuscript (10%)
Kazimierz Rozanski:	assistance with modelling, comments on the manuscript (7%)
Mario Tuthorn:	laboratory work ($\delta^{18}\text{O}$ of sugars), discussion of the results, comments on the manuscript (7%)
Bruno Glaser:	discussion of results, comments on the manuscript (3%)
Markus Greule:	laboratory work ($\delta^2\text{H}$ of methoxyl groups), data preparation, discussion of results, comments on the manuscript (3%)
Frank Keppler:	laboratory work ($\delta^2\text{H}$ of methoxyl groups), discussion of results, comments on the manuscript (3%)
Yongsong Huang:	laboratory work ($\delta^2\text{H}$ of <i>n</i> -alkanes and fatty acids), comments on the manuscript (3%)
Wolfgang Zech:	field work, comments on the manuscript (3%)
Michael Zech:	laboratory work ($\delta^{18}\text{O}$ of sugars), data preparation, discussion of the results, comments on the manuscript (10%)

Manuscript 4: A sugar biomarker proxy for assessing terrestrial versus aquatic sedimentary input

Johannes Hepp:	field work (recent plant samples), laboratory work (sugar measurements of recent plant, sediment and algae samples), data preparation and evaluation of recent plant, sediment and algae samples, discussion of results, manuscript preparation, publication handling (65%)
Max Rabus:	laboratory work (algae cultures), discussion of results, comments on the manuscript (5%)
Tobias Anhäuser:	field work (recent plant and sediment), comments on the manuscript (3%)
Tobias Bromm:	Lake Gemündener Maar (GM) sediment samples, laboratory work (sugar measurements of lake GM sediment samples), data preparation and evaluation of lake GM sediment samples, comments on the manuscript (4%)
Christian Laforsch:	laboratory work (algae cultures), discussion of results, comments on the manuscript (5%)
Frank Sirocko:	Lake GM sediment samples, comments on the manuscript (3%)
Bruno Glaser:	discussion of results, comments on the manuscript (3%)
Michael Zech:	field work (recent plant and sediment sample samples), Lake GM sediment samples, assistance with data preparation and evaluation, discussion of results, comments on the manuscript (12%)

Manuscript 5: How dry was the Younger Dryas? Evidence from a coupled $\delta^2\text{H}$ - $\delta^{18}\text{O}$ biomarker paleohygrometer, applied to the Lake Gemündener Maar sediments, Western Eifel, Germany

Johannes Hepp:	data evaluation and compilation, modelling, discussion of results, co-writing an earlier version of the manuscript, manuscript preparation of the actual version, publication handling (52%)
Lorenz Wüthrich:	laboratory work ($\delta^2\text{H}$ of <i>n</i> -alkanes), data preparation and evaluation, discussion of results, manuscript preparation of an earlier version of the manuscript, comments on the actual version of the manuscript (15%)
Tobias Bromm:	laboratory work ($\delta^{18}\text{O}$ of sugars), data preparation and evaluation, discussion of results, comments on the manuscript (3%)
Marcel Bliedtner:	laboratory work ($\delta^2\text{H}$ of <i>n</i> -alkanes), data preparation and evaluation, discussion of results, comments on the manuscript (3%)
Imke Kathrin Schäfer:	laboratory work ($\delta^2\text{H}$ of <i>n</i> -alkanes), data preparation and evaluation, discussion of results, comments on the manuscript (3%)
Bruno Glaser:	discussion of results, comments on the manuscript (2%)
Kazimierz Rozanski:	assistance with modelling, discussion of results, comments on the manuscript (6%)
Frank Sirocko:	lake coring, chronology, discussion of results, comments on the manuscript (3%)
Roland Zech:	discussion of results, co-writing an earlier version of the manuscript (6%)
Michael Zech:	core sampling, assistance with laboratory work, discussion of results, co-writing an earlier version of the manuscript, comments on the actual version of the manuscript (7%)

Manuscript 6: Late Glacial to Early Holocene $\delta^2\text{H}_{n\text{-alkane}}$ and $\delta^{18}\text{O}$ records from Lake Bergsee, Black Forest, Germany – potential and limitations

Johannes Hepp:	core sampling, laboratory work (bulk measurements, sugar and $\delta^{18}\text{O}$ of sugars, n -alkanes and $\delta^2\text{H}$ of n -alkanes), data preparation, evaluation and compilation, discussion of results, manuscript preparation (60%)
Lucas Kämpf:	core sampling, laboratory work (sugars and $\delta^{18}\text{O}$ of sugars), discussion of results, comments on the manuscript (5%)
Damien Rius:	lake coring, chronology, pollen results, discussion of the results, comments on the manuscript (5%)
Mario Tuthorn:	laboratory work (bulk measurements, sugar and $\delta^{18}\text{O}$ of sugars), discussion of results, comments on the manuscript (5%)
Lucas Bittner:	laboratory work ($\delta^{18}\text{O}$ of sugar), data evaluation, discussion of results, comments on the manuscript (3%)
Laurent Millet:	lake coring, chronology, pollen results, discussion of the results, comments on the manuscript (3%)
Fanny Dupart-Oualid:	pollen analysis, discussion of results, comments on the manuscript (2%)
Bruno Glaser:	discussion of the results, comments of the manuscript (2%)
Michael Zech:	core sampling, assistance with laboratory work ($\delta^{18}\text{O}$ of sugars and $\delta^2\text{H}$ of n -alkanes), discussion of results, comments on the manuscript (15%)

Included manuscripts

A. Manuscript 1: Hepp et al. (2019c)

submitted to *Biogeosciences*, published in *Biogeosciences Discussion*

<https://doi.org/10.5194/bg-2019-427>

<https://doi.org/10.5194/bg-2019-427>

Preprint. Discussion started: 4 November 2019

© Author(s) 2019. CC BY 4.0 License.



1 **Validation of a coupled $\delta^2\text{H}_{n\text{-alkane}}\text{-}\delta^{18}\text{O}_{\text{sugar}}$ paleohygrometer**
2 **approach based on a climate chamber experiment**

3
4 Johannes Hepp^{a,b,1,*,#}, Bruno Glaser^b, Dieter Juchelka^c, Christoph Mayr^{d,e,2}, Kazimierz Rozanski^f, Imke
5 Kathrin Schäfer^g, Willibald Stichler^h, Mario Tuthorn^{c,3}, Roland Zech^{g,i,4}, Michael Zech^{b,j,5,#}

6
7 ^aChair of Geomorphology and BayCEER, University of Bayreuth, Universitätsstrasse 30, D-95440
8 Bayreuth, Germany

9 ^bInstitute of Agronomy and Nutritional Sciences, Soil Biogeochemistry, Martin-Luther-University Halle-
10 Wittenberg, Von-Seckendorff-Platz 3, D-06120 Halle (Saale), Germany

11 ^cThermo Fisher Scientific, Hanna-Kunath-Str. 11, D-28199 Bremen, Germany

12 ^dInstitute of Geography, Friedrich-Alexander-University Erlangen-Nürnberg, Wetterkreuz 15, D-91058
13 Erlangen, Germany

14 ^eGeoBio-Center & Earth and Environmental Sciences, Ludwig-Maximilian University Munich, Richard-
15 Wagner-Str. 10, D-80333 München, Germany

16 ^fFaculty of Physics and Applied Computer Science, AGH University of Science and Technology, Al.
17 Mickiewicza 30, PL-30-059 Kraków, Poland

18 ^gInstitute of Geography and Oeschger Centre for Climate Research, University of Bern, Hallerstrasse
19 12, CH-3012 Bern, Switzerland

20 ^hHelmholtz Zentrum München, German Research Center for Environmental Health, Ingolstädter
21 Landstrasse 1, D-85764 Neuherberg, Germany

22 ⁱInstitute of Geography, Chair of Physical Geography, Friedrich-Schiller University of Jena,
23 Löbdergraben 32, D-07743 Jena, Germany

24 ^jInstitute of Geography, Heisenberg Chair of Physical Geography with focus on paleoenvironmental
25 research, Technical University of Dresden, Helmholtzstrasse 10, D-01062 Dresden, Germany

26
27 *corresponding author: johannes-hepp@gmx.de

28 #all other co-authors are listed alphabetically

¹Present address: Chair of Geomorphology and BayCEER, University of Bayreuth, Universitätsstrasse 30, D-95440 Bayreuth, Germany

²Present address: Institute of Geography, Friedrich-Alexander-University Erlangen-Nürnberg, Wetterkreuz 15, D-91058 Erlangen, Germany

³Present address: Thermo Fisher Scientific, Hanna-Kunath-Str. 11, D-28199 Bremen, Germany

⁴Present address: Institute of Geography, Chair of Physical Geography, Friedrich-Schiller University of Jena, Löbdergraben 32, D-07743 Jena, Germany

⁵Present address: Institute of Geography, Heisenberg Chair of Physical Geography with focus on paleoenvironmental research, Technical University of Dresden, Helmholtzstrasse 10, D-01062 Dresden, Germany

<https://doi.org/10.5194/bg-2019-427>

Preprint. Discussion started: 4 November 2019

© Author(s) 2019. CC BY 4.0 License.



29 Keywords

30 hydrogen stable isotopes, oxygen stable isotopes, hemicellulose sugars, leaf waxes, leaf water
31 enrichment, deuterium-excess, relative humidity

32 Abstract

33 The hydrogen isotopic composition of leaf wax-derived biomarkers, e.g. long chain n -alkanes ($\delta^2\text{H}_n$ -
34 alkane), is widely applied in paleoclimatology research. However, a direct reconstruction of the isotopic
35 composition of paleoprecipitation based on $\delta^2\text{H}_{n\text{-alkane}}$ alone can be challenging due to the overprint of
36 the source water isotopic signal by leaf-water enrichment. The coupling of $\delta^2\text{H}_{n\text{-alkane}}$ with $\delta^{18}\text{O}$ of
37 hemicellulose-derived sugars ($\delta^{18}\text{O}_{\text{sugar}}$) has the potential to disentangle this effect and additionally
38 allow relative humidity reconstructions. Here, we present $\delta^2\text{H}_{n\text{-alkane}}$ as well as $\delta^{18}\text{O}_{\text{sugar}}$ results obtained
39 from leaves of the plant species *Eucalyptus globulus*, *Vicia faba* var. *minor* and *Brassica oleracea* var.
40 *medullosa*, which were grown under controlled conditions. We addressed the questions (i) do $\delta^2\text{H}_n$ -
41 alkane and $\delta^{18}\text{O}_{\text{sugar}}$ values allow precise reconstructions of leaf water isotope composition, (ii) how
42 accurately does the reconstructed leaf-water-isotope composition enables relative humidity (RH)
43 reconstruction in which the plants grew, and (iii) does the coupling of $\delta^2\text{H}_{n\text{-alkane}}$ and $\delta^{18}\text{O}_{\text{sugar}}$ enable a
44 robust source water calculation?

45 For all investigated species, the alkane $n\text{-C}_{29}$ was most abundant and therefore used for compound-
46 specific $\delta^2\text{H}$ measurements. For *Vicia faba*, additionally the $\delta^2\text{H}$ values of $n\text{-C}_{31}$ could be evaluated
47 robustly. With regard to hemicellulose-derived monosaccharides, arabinose and xylose were most
48 abundant and their $\delta^{18}\text{O}$ values were therefore used to calculate weighted mean leaf $\delta^{18}\text{O}_{\text{sugar}}$ values.
49 Both $\delta^2\text{H}_{n\text{-alkane}}$ and $\delta^{18}\text{O}_{\text{sugar}}$ yielded significant correlations with $\delta^2\text{H}_{\text{leaf-water}}$ and $\delta^{18}\text{O}_{\text{leaf-water}}$,
50 respectively ($r^2 = 0.45$ and 0.85 , respectively; $p < 0.001$, $n = 24$). Mean fractionation factors between
51 biomarkers and leaf water were found to be -156‰ (ranging from -133 to -192‰) for $\epsilon_{n\text{-alkane/leaf-water}}$
52 and $+27.3\text{‰}$ (ranging from $+23.0$ to 32.3‰) for $\epsilon_{\text{sugar/leaf-water}}$, respectively. Using rearranged Craig-
53 Gordon equations with either T_{air} or T_{leaf} and measured $\delta^2\text{H}_{\text{leaf-water}}$ or $\delta^{18}\text{O}_{\text{leaf-water}}$ as input variables, we
54 furthermore modeled climate chamber RH_{air} and RH_{leaf} values. Modelled RH_{air} values, from the more
55 simplified Craig-Gordon model, turned out to be most accurate and correlate highly significantly with
56 measured RH_{air} values ($R^2 = 0.84$, $p < 0.001$; $\text{RMSE} = 6\%$). When combining $\delta^2\text{H}_{\text{leaf-water}}$ and $\delta^{18}\text{O}_{\text{leaf-water}}$
57 values that are calculated from the alkane and sugar biomarkers instead of actually measured $\delta^2\text{H}_{\text{leaf-}}$
58 water and $\delta^{18}\text{O}_{\text{leaf-water}}$ as input variables, the correlation of modelled RH_{air} values with measured RH_{air}
59 values is getting worse, but is still highly significant with $R^2 = 0.54$, $p < 0.001$; $\text{RMSE} = 10\%$. This
60 highlights the potential of the coupled $\delta^2\text{H}_{n\text{-alkane}}\text{-}\delta^{18}\text{O}_{\text{sugar}}$ paleohygrometer approach for suitable
61 relative humidity reconstructions. Finally, the reconstructed source water isotope composition ($\delta^2\text{H}_s$
62 and $\delta^{18}\text{O}_s$) as calculated from the coupled approach matches the source water in the climate chamber
63 experiment ($\delta^2\text{H}_{\text{tank-water}}$ and $\delta^{18}\text{O}_{\text{tank-water}}$).
64

<https://doi.org/10.5194/bg-2019-427>

Preprint. Discussion started: 4 November 2019

© Author(s) 2019. CC BY 4.0 License.



65 1 Introduction

66 Leaf-wax-derived biomarkers, such as long chain n -alkanes, and their stable hydrogen isotopic
67 composition ($\delta^2\text{H}_{n\text{-alkane}}$) are widely applied in paleoclimatology research. Sedimentary $\delta^2\text{H}_{n\text{-alkane}}$ values
68 correlate with $\delta^2\text{H}$ of precipitation (Huang et al., 2004; Mügler et al., 2008; Sachse et al., 2004; Sauer
69 et al., 2001), confirming the high potential of $\delta^2\text{H}_{n\text{-alkane}}$ to establish $\delta^2\text{H}$ records of past precipitation
70 (Hou et al., 2008; Rao et al., 2009; Sachse et al., 2012). However, the alteration of the isotopic signal
71 as a result of the often unknown amount of leaf water enrichment caused by evapotranspiration can
72 be several tens of per mil. This poses a challenge for accurate data interpretation (e.g. Zech et al.,
73 2015), especially in respect of single proxy ($\delta^2\text{H}_{n\text{-alkane}}$)-based climate records. Apart from studies of
74 sedimentary cellulose (Heyng et al., 2014; Wissel et al., 2008), the oxygen stable isotope composition
75 of sugar biomarkers ($\delta^{18}\text{O}_{\text{sugar}}$) emerged as complementary paleoclimate proxy during the last decade
76 (Hepp et al., 2015, 2017, Zech et al., 2013a, 2014a). The interpretation of the $\delta^{18}\text{O}_{\text{sugar}}$ values is
77 comparable to those of $\delta^2\text{H}_{n\text{-alkane}}$. When sugars originate primarily from leaf biomass of higher
78 terrestrial plants, they reflect the plant source water (which is often directly linked to the local
79 precipitation) modified by evapotranspirative enrichment of the leaf water (Tuthorn et al., 2014; Zech
80 et al., 2014a). The coupling of $\delta^2\text{H}_{n\text{-alkane}}$ with $\delta^{18}\text{O}_{\text{sugar}}$ values allows quantification of leaf-water isotopic
81 enrichment and relative air humidity (Zech et al., 2013a). This approach was validated by Tuthorn et
82 al. (2015) by applying it to topsoil samples along a climate transect in Argentina. Accordingly, the
83 biomarker-derived relative air humidity values correlate significantly with actual air relative humidity
84 from the respective study sites, highlighting the potential of the $\delta^2\text{H}_{n\text{-alkane}}\text{-}\delta^{18}\text{O}_{\text{sugar}}$ paleohygrometer
85 approach.

86 The coupled approach is based on the observation that the isotope signature of precipitation
87 ($\delta^2\text{H}_{\text{precipitation}}$ and $\delta^{18}\text{O}_{\text{precipitation}}$) typically plots on or adjacent to the global meteoric water line (GMWL),
88 in a $\delta^2\text{H}\text{-}\delta^{18}\text{O}$ diagram. The GMWL is characterized by the equation $\delta^2\text{H}_{\text{precipitation}} = 8 \cdot \delta^{18}\text{O}_{\text{precipitation}} + 10$
89 (Dansgaard, 1964). In most cases, the local precipitation can be directly linked to the source water of
90 plants, which is indeed soil water and eventually shallow groundwater. The isotopic composition of
91 xylem water of plants readily reflects these sources (e.g. Dawson, 1993). However, leaf-derived
92 biomarkers reflect the leaf water isotope composition, which is, unlike xylem water, prone to
93 evapotranspiration (e.g. Barbour and Farquhar, 2000; Helliker and Ehleringer, 2002; Cernusak et al.,
94 2003; Barbour et al., 2004; Cernusak et al., 2005; Feakins and Sessions, 2010; Kahmen et al., 2011;
95 Sachse et al., 2012; Kahmen, Schefuß, et al., 2013; Tipple et al., 2013; Lehmann et al., 2017; Liu et al.,
96 2017). During daytime, the leaf water is typically enriched in the heavy isotope compared to the source
97 water because of the evapotranspirative enrichment through the stomata. Thereby, lighter water
98 isotopes evaporate preferentially, which results in a deuterium-excess in the remaining water
99 compared to the precipitation water ($d = \delta^2\text{H} - 8 \cdot \delta^{18}\text{O}$; according to Dansgaard, 1964). The degree of
100 evapotranspirative enrichment is mainly controlled by the relative air humidity in the direct
101 surrounding of the plant leaves (e.g. Cernusak et al., 2016). Although the biomarkers reflect the
102 isotopic composition of leaf water, there is still a modification by the so-called biosynthetic
103 fractionation during the biosynthesis, leading to an offset between leaf water and biomarker isotope
104 composition. In case the biosynthetic fractionation is known and constant, there is a great potential
105 that relative humidity can be derived from coupling $\delta^2\text{H}_{n\text{-alkane}}$ and $\delta^{18}\text{O}_{\text{sugar}}$ values.

106 The overall aim of this study is to evaluate the $\delta^2\text{H}_{n\text{-alkane}}\text{-}\delta^{18}\text{O}_{\text{sugar}}$ paleohygrometer approach by
107 applying it to plant leaf material from three different plants grown in a climate chamber experiment
108 under well controlled conditions. More specifically, we address the following questions:

- 109 (i) which homologue and specific monosaccharide can be used to gain $\delta^2\text{H}_{n\text{-alkane}}$ and $\delta^{18}\text{O}_{\text{sugar}}$
110 results for the climate chamber plants leaf material, respectively,

<https://doi.org/10.5194/bg-2019-427>

Preprint. Discussion started: 4 November 2019

© Author(s) 2019. CC BY 4.0 License.



- 111 (ii) how precisely do $\delta^2\text{H}_{n\text{-alkane}}$ and $\delta^{18}\text{O}_{\text{sugar}}$ values allow reconstructing $\delta^2\text{H}$ and $\delta^{18}\text{O}$ of leaf
112 water, respectively,
113 (iii) how accurately does the leaf-water-isotope composition reflect the relative humidity
114 conditions,
115 (iv) and does the coupling of $\delta^2\text{H}_{n\text{-alkane}}$ and $\delta^{18}\text{O}_{\text{sugar}}$ enable a robust source water calculation
116 and how reliable are relative humidity reconstructions?
117

118 2 Material and Methods

119 2.1 Climate chamber experiment

120 A phytotron experiment was conducted at the Helmholtz Zentrum München in Neuherberg during
121 winter 2000/2001 (Mayr, 2002). Three different dicotyledon plant species (*Eucalyptus globulus*, *Vicia*
122 *faba* var. *minor* and *Brassica oleracea* var. *medullosa*) were grown in eight chambers for 56 days under
123 seven distinct climatic conditions (same conditions in chambers 4 and 8). Air temperature (T_{air}) were
124 set to 14, 18, 24 and 30°C and relative humidity (RH_{air}) to around 20, 30, 50, and 70% between 11
125 a.m. and 4 p.m. (Fig. 1B). During the rest of the day typical natural diurnal variations were aimed for
126 (details in Mayr, 2002). Furthermore, uniform irrigation conditions were guaranteed via an automatic
127 irrigation system, which was controlled by tensiometers installed in 9 cm substrate depth. The tank
128 water used for irrigation was sampled periodically (intervals of one to three days) over the whole
129 experiment and revealed only minor variability in its isotope composition ($\delta^{18}\text{O}_{\text{tank-water}} = -10.7 \pm 0.3\%$
130 standard deviation (σ); $\delta^2\text{H}_{\text{tank-water}} = -7 \pm 1\%$ σ). Once a week, soil water (via ceramic cups in 13 cm soil
131 depth) and atmospheric water vapor (via dry ice condensation traps) was sampled ($\delta^2\text{H}_{\text{soil-water}}$, $\delta^{18}\text{O}_{\text{soil-}}$
132 water and $\delta^2\text{H}_{\text{atmospheric-water-vapor}}$, $\delta^{18}\text{O}_{\text{atmospheric-water-vapor}}$). Additionally, leaf temperatures (T_{leaf}) were
133 derived from gas exchange measurements, at least once a week (Mayr, 2002).

134 In order to analyze stable hydrogen and oxygen isotopic composition of leaf ($\delta^2\text{H}_{\text{leaf-water}}$, $\delta^{18}\text{O}_{\text{leaf-water}}$)
135 and stem water, the plants were harvested at the end of the experiment. The vacuum distillation
136 method was used for the extraction of the plant water. It should be noted that stem water is a mixture
137 between phloem and xylem water, while the latter should reflect the isotopic composition of the soil
138 water. For simplification, stem water is referred to as xylem water in the following ($\delta^2\text{H}_{\text{xylem-water}}$,
139 $\delta^{18}\text{O}_{\text{xylem-water}}$).

140 For more details about the experiment, the reader is referred to the original publication (Mayr, 2002).
141

142 2.2 Leaf biomarker extraction and compound-specific stable isotope analysis

143 A total of 24 leaf samples were prepared according to Schäfer et al. (2016) for compound specific $\delta^2\text{H}$
144 measurements of *n*-alkanes, at the Institute of Geography, Group of Biogeochemistry and
145 Paleoclimate, University of Bern. Microwave extraction with 15 ml dichloromethane (DCM)/methanol
146 (MeOH) 9:1 (v:v) at 100°C for 1 h was conducted. The resulting total lipid extract was purified and
147 separated using aminopropyl-silica-gel (Supelco, 45 μm) pipette columns. The hydrocarbon fraction
148 (containing *n*-alkanes) was eluted with *n*-hexane and cleaned via silver nitrate-coated silica gel pipettes
149 (Supelco, 60-200 mesh) and zeolite (Geokleen Ltd.) columns. The $\delta^2\text{H}$ measurements of the highest
150 concentrated *n*-alkanes (*n*-C₂₉ and *n*-C₃₁) were performed on a GC-²H-pyrolysis-IRMS system, equipped
151 with an Agilent 7890A gas chromatograph (GC) and IsoPrime 100 isotope-ratio-mass spectrometer
152 (IRMS) coupled with a GC5 pyrolysis/combustion interface operating in pyrolysis modus with a Cr
153 (ChromeHD) reactor at 1000°C. The compound-specific $\delta^2\text{H}$ values were calibrated against a standard
154 alkane mix (*n*-C₂₇, *n*-C₂₉, *n*-C₃₃) with known isotope composition (A. Schimmelmann, University of
155 Indiana), measured twice every six sample injections. Standard deviation of the triplicate

<https://doi.org/10.5194/bg-2019-427>

Preprint. Discussion started: 4 November 2019

© Author(s) 2019. CC BY 4.0 License.



156 measurements were typically $\leq 5\%$. The H^{3+} factor stayed constant during the course of the
157 measurements.

158

159 Additionally, the leaf samples were dried and finely ground in preparation for $\delta^{18}O$ analysis of
160 hemicellulose-derived sugars (modified from Zech and Glaser, 2009) at the Institute of Agronomy and
161 Nutritional Sciences, Soil Biogeochemistry, Martin-Luther-University Halle-Wittenberg. The
162 hemicellulose sugars were hydrolytically extracted for 4 h at 105°C using 4M trifluoroacetic acid
163 (Amelung et al., 1996) and purified via XAD-7 and Dowex 50WX8 columns. Prior to the methylboronic-
164 acid (MBA) derivatization (4 mg of MBA in 400 μ l dry pyridine for 1 h at 60°C), the cleaned sugars were
165 frozen and freeze-dried overnight (Knapp, 1979). Compound-specific $\delta^{18}O$ measurements were
166 performed on a Trace GC 2000 coupled to a Delta V Advantage IRMS via an ^{18}O -pyrolysis reactor (GC
167 IsoLink) and a ConFlo IV interface (all devices from Thermo Fisher Scientific, Bremen, Germany). The
168 sample batches were measured along with embedded co-derivatized standard batches, which
169 contained arabinose, fucose, xylose, and rhamnose in different concentrations of known $\delta^{18}O$ value.
170 The $\delta^{18}O$ values of the standard sugars were determined via temperature conversion/elemental
171 analysis-IRMS coupling at the Institute of Plant Sciences, ETH Zurich, Switzerland (Zech and Glaser,
172 2009). This procedure allows corrections for possible amount dependencies (Zech and Glaser, 2009)
173 and ensures the “Principle of Identical Treatment” (Werner and Brand, 2001). Standard deviations for
174 the triplicate measurements were 0.9‰ and 2.2‰ (average over all investigated samples) for
175 arabinose and xylose, respectively. We focus on arabinose and xylose in this study because they were
176 (i) the dominant peaks in all chromatograms, and (ii) previously found to strongly predominate over
177 fucose (and rhamnose) in terrestrial plants, soils (Hepp et al., 2016).

178

179 All δ values are expressed in per mil as isotope ratios ($R = ^{18}O/^{16}O$ or $^2H/^1H$) relative to the Vienna
180 Standard Mean Ocean Water (VSMOW) standard in the common delta notation
181 ($\delta = R_{\text{sample}} - R_{\text{standard}}/R_{\text{standard}}$; e.g. Coplen, 2011).

182

183 2.3 Framework for coupling $\delta^2H_{n\text{-alkane}}$ with $\delta^{18}O_{\text{sugar}}$ results

184 2.3.1 Deuterium-excess of leaf water and relative humidity

185 The coupled approach is based on the observation that isotope composition of global precipitation
186 plots typically close to the GMWL ($\delta^2H_{\text{precipitation}} = 8 \cdot \delta^{18}O_{\text{precipitation}} + 10$; Dansgaard, 1964; Fig. 2). The
187 soil water and shallow groundwater, which acts as source water for plants, can often directly be related
188 to the local precipitation. However, especially during daytime leaf water is typically enriched compared
189 to the precipitation due to evapotranspiration through the stomata, therefore plotting right of the
190 GMWL (Fig. 2; e.g. Allison et al., 1985; Bariac et al., 1994; Walker and Brunel, 1990). The leaf water
191 reservoir at the evaporative sites is frequently assumed to be in isotope steady-state (Allison et al.,
192 1985; Bariac et al., 1994; Gat et al., 2007; Walker and Brunel, 1990), meaning that the isotope
193 composition of the transpired water vapor is in isotopic equilibrium with the source water utilized by
194 the plants during the transpiration process. The Craig-Gordon model (e.g. Flanagan et al., 1991; Roden
195 and Ehleringer, 1999) approximates the isotope processes in leaf water in δ terms (e.g. Barbour et al.,
196 2004):

$$\delta_e \approx \delta_s + \epsilon^* + \epsilon_k + (\delta_a - \delta_s - \epsilon_k) \frac{e_a}{e_i}, \quad (\text{Equation 1})$$

197 where δ_e , δ_s and δ_a are the hydrogen and oxygen isotopic compositions of leaf water at the evaporative
198 sites, source water and atmospheric water vapor, respectively. The equilibrium enrichment (ϵ^*) is
199 expressed as $(1-1/\alpha_{LV}) \cdot 10^3$, where α_{LV} is the equilibrium fractionation between liquid and vapor in

<https://doi.org/10.5194/bg-2019-427>

Preprint. Discussion started: 4 November 2019

© Author(s) 2019. CC BY 4.0 License.



200 per mil. The kinetic fractionation parameter (ϵ_k) describes the water vapor diffusion from intracellular
201 air space through the stomata and the boundary layer into to the atmosphere, and e_a/e_i is the ratio of
202 the atmospheric to intracellular vapor pressure.

203

204 In a $\delta^2\text{H}-\delta^{18}\text{O}$ diagram, the isotope composition of the leaf water as well as the source water can be
205 described as deuterium-excess (d) values by using the equation of Dansgaard (1964), with $d = \delta^2\text{H} - 8 \cdot$
206 $\delta^{18}\text{O}$. This allows rewriting the Eq. 1, in which hydrogen and oxygen isotopes have to be handled in
207 separate equations, in one equation:

$$d_e \approx d_s + (\epsilon_2^* - 8 \cdot \epsilon_{18}^*) + (C_k^2 - 8 \cdot C_k^{18}) + [d_a - d_s - (C_k^2 - 8 \cdot C_k^{18})] \cdot \frac{e_a}{e_i}, \quad (\text{Equation 2})$$

208 where d_e , d_s and d_a are the deuterium excess values of leaf water at the evaporative sites, source water
209 and atmospheric water vapor, respectively. The kinetic fractionation parameter (ϵ_k) is typically related
210 to stomatal and boundary layer resistances to water flux (Farquhar et al., 1989). We used the kinetic
211 enrichment factor (C_k) instead of ϵ_k to be close to paleo studies where direct measurements of such a
212 plant physiological parameter are not available. The kinetic enrichment factor is derived from a more
213 generalized form of the Craig-Gordon model for describing the kinetic isotope enrichment for ^2H and
214 ^{18}O (C_k^2 and C_k^{18} , respectively) (Craig and Gordon, 1965; Gat and Bowser, 1991). If the plant source
215 water and the local atmospheric water vapor are in isotope equilibrium, the term $\delta_a - \delta_s$ in Eq. 1 can
216 be approximated by $-\epsilon^*$. Thus, Eq. 2 can be reduced to:

$$d_e \approx d_s + (\epsilon_2^* - 8 \cdot \epsilon_{18}^* + C_k^2 - 8 \cdot C_k^{18}) \cdot \left(1 - \frac{e_a}{e_i}\right). \quad (\text{Equation 3})$$

217 The actual atmospheric vapor pressure (e_a) and the leaf vapor pressure (e_i) in kPa can be derived from
218 Eqs. 4 and 5 by using T_{air} and T_{leaf} , respectively:

$$e_a = 0.61365 \cdot e^{[17.502 \cdot T_{\text{air}} / (T_{\text{air}} + 240.97)]} \cdot \text{RH}_{\text{air}} \quad (\text{Equation 4})$$

$$e_i = 0.61365 \cdot e^{[17.502 \cdot T_{\text{leaf}} / (T_{\text{leaf}} + 240.97)]}, \quad (\text{Equation 5})$$

219 where e_a/e_i is the relative humidity calculated with the saturation vapor pressure when the leaf
220 temperature is used in the denominator rather than the air temperature (Eq. 5), ranging between 0
221 and 1. In order to increase the comparability to RH_{air} , the e_a/e_i ratio calculated with T_{leaf} in Eq. 5 can be
222 converted into RH_{leaf} by multiplication with 100. When T_{air} is used in Eq. 5, e_a/e_i represents RH_{air} (also
223 ranging between 0 and 1, representing 0 to 100% relative humidity when multiplying with 100). It
224 should be noted that the differences between measured RH_{leaf} and T_{leaf} with the respective air
225 parameters (RH , T_{air}) are not very pronounced in most cases (Mayr, 2002; Kahmen et al., 2011b),
226 revealing rather the same trends and magnitude (Fig. 1B).

227 With Eqs. 2 and 3, two equations are given to derive relative humidity values by rearranging them,
228 resulting in RH_{air} and RH_{leaf} , respectively, by using either T_{air} or T_{leaf} for ϵ^* (Eqs. 6 and 7):

$$\text{RH}_{\text{leaf/air}} \approx \frac{d_e - d_s - (\epsilon_2^* - 8 \cdot \epsilon_{18}^*) - (C_k^2 - 8 \cdot C_k^{18})}{d_a - d_s - (C_k^2 - 8 \cdot C_k^{18})}, \quad (\text{Equation 6})$$

$$\text{RH}_{\text{leaf/air}} \approx 1 - \frac{d_e - d_s}{(\epsilon_2^* - 8 \cdot \epsilon_{18}^* + C_k^2 - 8 \cdot C_k^{18})}. \quad (\text{Equation 7})$$

229 Equilibrium fractionation parameters (ϵ_2^* and ϵ_{18}^*) are derived from empirical equations of Horita and
230 Wesolowski (1994) by using either the climate chamber T_{air} or T_{leaf} values. The kinetic fractionation
231 parameters (C_k^2 and C_k^{18}) for ^2H and ^{18}O , respectively, are set to 25.1 and 28.5‰ according to Merlivat
232 (1978), who reported maximum values during the molecular diffusion process of water through a
233 stagnant boundary layer. It should be noted that ϵ_k values of broadleaf trees and shrubs over broad

<https://doi.org/10.5194/bg-2019-427>

Preprint. Discussion started: 4 November 2019

© Author(s) 2019. CC BY 4.0 License.



234 climatic conditions are well in the range with used C_k^2 and C_k^{18} values, revealing 23.9 ± 0.9 and 26.7%
235 ± 1.0 for ϵ_k^2 and ϵ_k^{18} , respectively (derived from supplementary data of Cernusak et al., 2016).
236 If $\delta^2\text{H}_{\text{leaf-water}}$ and $\delta^{18}\text{O}_{\text{leaf-water}}$ can be reconstructed from the measured δ values of n -alkanes and sugars
237 biomarkers, this framework provides a powerful tool to establish relative humidity records from
238 sedimentary archives (Hepp et al., 2017; Zech et al., 2013a). To reconstruct the isotope composition of
239 leaf water it is assumed that fractionation factors of -160% for ^2H of alkanes $n\text{-C}_{29}$ and $n\text{-C}_{31}$ (ϵ_{bio}^2 ;
240 Sachse et al., 2012; Sessions et al., 1999), and $+27\%$ for ^{18}O of the hemicellulose-derived sugars
241 arabinose and xylose ($\epsilon_{\text{bio}}^{18}$; Cernusak et al., 2003; Schmidt et al., 2001; Sternberg et al., 1986; Yakir
242 and DeNiro, 1990) can be applied:

$$\text{alkane-based } \delta^2\text{H}_{\text{leaf-water}} = (\delta^2\text{H}_{n\text{-alkane}} - \epsilon_{\text{bio}}^2)/(1 + \epsilon_{\text{bio}}^2/1000) \quad (\text{Equation 8})$$

$$\text{sugar-based } \delta^{18}\text{O}_{\text{leaf-water}} = (\delta^{18}\text{O}_{\text{sugar}} - \epsilon_{\text{bio}}^{18})/(1 + \epsilon_{\text{bio}}^{18}/1000). \quad (\text{Equation 9})$$

243

244 2.3.2 Isotope composition of plant source water

245 In a $\delta^2\text{H}$ - $\delta^{18}\text{O}$ diagram, the hydrogen and oxygen isotope composition of the plant source water ($\delta^2\text{H}_s$
246 and $\delta^{18}\text{O}_s$, respectively) can be assessed via the slope of the individual leaf water evapotranspiration
247 lines (LEL's; Craig and Gordon, 1965; Gat and Bowser, 1991). Depending on the degree of
248 simplification, the LEL slope (S_{LEL}) can be derived from Eq. 10 (consistent to Eq. 2) and Eq. 11 (consistent
249 to Eq. 3):

$$S_{\text{LEL}} \approx \frac{\epsilon_2^* + C_k^2 + (\delta_a^2 - \delta_s^2 - C_k^2) \cdot \frac{e_a}{e_i}}{\epsilon_{18}^* + C_k^{18} + (\delta_a^{18} - \delta_s^{18} - C_k^{18}) \cdot \frac{e_a}{e_i}}, \quad (\text{Equation 10})$$

$$S_{\text{LEL}} \approx \frac{\epsilon_2^* + C_k^2 \cdot \left(1 - \frac{e_a}{e_i}\right)}{\epsilon_{18}^* + C_k^{18} \cdot \left(1 - \frac{e_a}{e_i}\right)} \approx \frac{\epsilon_2^* + C_k^2}{\epsilon_{18}^* + C_k^{18}}, \quad (\text{Equation 11})$$

250 where all parameters are defined as in section 2.3.1. The $\delta^2\text{H}_s$ and $\delta^{18}\text{O}_s$ values can then be calculated
251 for each leaf water data point via the intersect between the individual LEL's with the GMWL. The model
252 results (from Eqs. 10 and 11) can be furthermore compared to the slope calculated by Eq. 12, using the
253 measured $\delta^2\text{H}_{\text{leaf-water}}$, $\delta^{18}\text{O}_{\text{leaf-water}}$ and $\delta^2\text{H}_{\text{tank-water}}$, $\delta^{18}\text{O}_{\text{tank-water}}$ values (Craig and Gordon, 1965; Gat and
254 Bowser, 1991).

$$S_{\text{LEL}} = \frac{\delta^2\text{H}_{\text{leaf-water}} - \delta^2\text{H}_{\text{tank-water}}}{\delta^{18}\text{O}_{\text{leaf-water}} - \delta^{18}\text{O}_{\text{tank-water}}} \quad (\text{Equation 12})$$

255

256 2.4 Modeling and isotope fractionation calculations

257 Relative humidity (Eq. 6), deuterium-excess values of leaf water (d_e , Eq. 2) and S_{LEL} values (Eq. 10) were
258 modeled leading to less simplified results, because the measured δ_a values are used explicitly.
259 Equations 7, 3 and 11 were therefore used to obtain RH, d_e and S_{LEL} results, representing a more
260 simplified model approach because $\delta_a - \delta_s$ are approximated by $-\epsilon^*$. This model procedure allows
261 furthermore the comparison of scenarios based on air or leaf temperature (T_{air} or T_{leaf}). In Eqs. 6 and
262 7, the reconstructed (biomarker-based) deuterium-excess $S_{\text{leaf-water}}$ was used as additional input, as
263 gained from Eqs. 8 and 9. The modeled LEL slopes (Eqs. 10 and 11) were used to derive source water
264 isotope composition ($\delta^2\text{H}_s$, $\delta^{18}\text{O}_s$). In all equations presented in section 2.3 to gain the model results
265 (Eqs. 2 to 8), $\delta^2\text{H}_{\text{atmospheric-water-voupor}}$, $\delta^{18}\text{O}_{\text{atmospheric-water-voupor}}$ and $\delta^2\text{H}_{\text{tank-water}}$, $\delta^{18}\text{O}_{\text{tank-water}}$ were used for δ_a
266 and δ_s (therefore also for d_a and d_s). All other input parameters were set as described in section 2.3. In
267 order to provide an 1σ range bracketing the modeled results (d_e , RH_{air} , RH_{leaf} , S_{LEL} , $\delta^2\text{H}_s$, $\delta^{18}\text{O}_s$), the

https://doi.org/10.5194/bg-2019-427

Preprint. Discussion started: 4 November 2019

© Author(s) 2019. CC BY 4.0 License.



268 calculations were also run with values generated by subtracting/adding the individual σ to the average.
269 This procedure was also used to derive measured deuterium-excess_{leaf-water} and S_{LEL} uncertainties.
270 Model quality was overall assessed by calculating the coefficient of determination [$R^2 = 1 -$
271 $\frac{\sum(\text{modeled} - \text{measured})^2}{\sum(\text{measured} - \text{measured mean})^2}$] and the root mean square error
272 $\left[\text{RMSE} = \sqrt{\left(\frac{1}{n} \cdot \sum(\text{modeled} - \text{measured})^2 \right)} \right]$. The R^2 is not equal to the r^2 , which provides here the
273 fraction of variance explained by a linear regression between a dependent (y) and an explanatory
274 variable [$r^2 = 1 - \frac{\sum(y - \text{fitted } y)^2}{\sum(y - \text{mean } y)^2}$] (R Core Team, 2015).

275
276 The fractionation between the measured leaf biomarkers and leaf water can be described by the
277 following equations (Eq. 10 and 11; e.g. Coplen, 2011):

$$\epsilon_{n\text{-alkane}/\text{leaf-water}} = (\delta^2\text{H}_{n\text{-alkane}} - \delta^2\text{H}_{\text{leaf-water}}) / (1 + \delta^2\text{H}_{\text{leaf-water}}/1000) \quad (\text{Equation 13})$$

$$\epsilon_{\text{sugar}/\text{leaf-water}} = (\delta^{18}\text{O}_{\text{sugar}} + \delta^{18}\text{O}_{\text{leaf-water}}) / (1 + \delta^{18}\text{O}_{\text{leaf-water}}/1000). \quad (\text{Equation 14})$$

278 For Eqs. 8 and 9 (biomarker-based leaf water reconstruction) as well as for Eqs. 13 and 14, the 1σ
279 range were calculated by subtracting/adding the individual σ , analogous to the modeling results.

280
281 All calculations and statistical analysis were realized in R (version 3.2.2; R Core Team, 2015).

282

283 3 Results and Discussion

284 3.1 Compound-specific isotope results of leaf wax-derived *n*-alkanes and hemicellulose- 285 derived sugars

286 All investigated leaf material showed a dominance of C_{29} *n*-alkanes. The dominance of *n*- C_{29} in *Brassica*
287 *oleracea* and *Eucalyptus globulus* was also reported by Ali et al. (2005) and Herbin and Robins (1968).
288 *Vicia faba* leaf samples additionally revealed a high abundance of C_{31} *n*-alkanes. This agrees with results
289 from Maffei (1996) and enables a robust determination of compound-specific $\delta^2\text{H}$ values for C_{29} and
290 C_{31} . The $\delta^2\text{H}_{n\text{-alkane}}$ values of *Vicia faba* are therefore calculated as weighted mean.

291 The top of Fig. 1A illustrates the $\delta^2\text{H}_{n\text{-alkane}}$ results along with isotopic data for leaf, xylem and soil water
292 (the latter were originally published in Mayr 2002). In addition the climate chamber conditions (RH_{air} ,
293 RH_{leaf} , T_{air} and T_{leaf}) are displayed (all from Mayr, 2002; Fig. 1B). For more details about the (plant) water
294 isotope results, climate chamber conditions as well as not shown plant physiological properties the
295 reader is referred to Mayr (2002). The $\delta^2\text{H}_{n\text{-alkane}}$ values range from -213 to -144‰ over all plant species.
296 As revealed by overlapping notches in the respective boxplots, no statistically significant differences in
297 the median values between the three plant species can be described (Fig. S1A; McGill et al., 1978). Fig.
298 1A moreover shows that $\delta^2\text{H}_{n\text{-alkane}}$ values range largest for *Eucalyptus globulus* compared to the other
299 two plants. However, the low number of samples per plant species prohibits a robust interpretation.

300

301

(Fig. 1)

302

303 The investigated leaf samples yielded substantially higher amounts of arabinose and xylose compared
304 to fucose and rhamnose. This is in agreement with sugar patterns reported for higher plants (D'Souza
305 et al., 2005; Hepp et al., 2016; Jia et al., 2008; Prietzel et al., 2013; Zech et al., 2012, 2014a) and
306 hampers a robust data evaluation of fucose and rhamnose. The $\delta^{18}\text{O}$ values of the investigated
307 pentoses arabinose and xylose range from 30 to 47‰ and 30 to 50‰, respectively, and are shown

<https://doi.org/10.5194/bg-2019-427>

Preprint. Discussion started: 4 November 2019

© Author(s) 2019. CC BY 4.0 License.



308 along with isotopic data for leaf, xylem and soil water (Mayr 2002) in the bottom of Fig. 1A. No
309 considerable difference in the $\delta^{18}\text{O}$ values of arabinose and xylose can be seen in the $\delta^{18}\text{O}$ pentose
310 data. This is in line with findings from Zech and Glaser (2009), Zech et al. (2012), Zech et al. (2013b)
311 and Zech et al. (2014b) but contradicting with slightly more positive $\delta^{18}\text{O}_{\text{arabinose}}$ values compared to
312 $\delta^{18}\text{O}_{\text{xylose}}$ values reported by Zech et al. (2013a) and Tuthorn et al. (2014). Overall, the two sugars
313 display very similar results (Fig. 1; $r^2 = 0.7$, $p < 0.001$, $n = 24$). The $\delta^{18}\text{O}$ values of arabinose and xylose
314 can therefore be combined as a weighted mean (as $\delta^{18}\text{O}_{\text{sugar}}$ values) for further data interpretation.
315 The $\delta^{18}\text{O}_{\text{sugar}}$ values are not significantly different between the three investigated plant species.

316

317 The compound-specific isotope results of leaf hemicellulose-derived sugars and leaf wax-derived *n*-
318 alkanes can be compared with leaf, xylem, soil and tank water (compare Fig. 1A and Fig. 2). This
319 comparison reveals that soil and xylem water plot close to the tank water, whereas leaf water shows
320 a clear evapotranspirative enrichment. This enrichment strongly differs between the climate
321 chambers, depending mainly on T and RH conditions. The biomarker results furthermore follow the
322 leaf water with a certain offset (ϵ_{bio}).

323

(Fig. 2)

324

325 3.2 Do *n*-alkane and sugar biomarkers reflect the isotope composition of leaf water?

326 The $\delta^2\text{H}_{n\text{-alkane}}$ dataset reveals a significant correlation with $\delta^2\text{H}_{\text{leaf-water}}$ of 0.45 (r^2) using all plant species
327 with $p < 0.001$ (Fig. 3A). A slope of 1.1 and an intercept of -152‰ furthermore characterize the
328 relationship. It seems that each plant type shows a different $\delta^2\text{H}_{n\text{-alkane}}$ to $\delta^2\text{H}_{\text{leaf-water}}$ relation, with the
329 highest slope for *Vicia faba* and the lowest for *Brassica oleracea*. However, we argue that the number
330 of replicates for each plant species is simply too low to interpret this finding robustly. A highly
331 significant correlation is also observed for the correlation between $\delta^{18}\text{O}_{\text{sugar}}$ and $\delta^{18}\text{O}_{\text{leaf-water}}$ ($r^2 = 0.84$,
332 $p < 0.001$; Fig. 3B). The regression reveals a slope of 0.74 and an intercept of 30.7‰.

333

(Fig. 3)

334

335

336 Since it is well known that measured leaf water is not always equal to the specific water pool in which
337 the *n*-alkanes are biosynthesized (e.g. Tipple et al., 2015), the correlation reveals a rather low r^2 (Fig.
338 3A). Furthermore, NADPH is acting also as hydrogen source during *n*-alkane biosynthesis, which is
339 clearly more negative than the biosynthetic water pool (Schmidt et al., 2003), further contributing to
340 a weakening of the $\delta^2\text{H}_{n\text{-alkane}}$ to $\delta^2\text{H}_{\text{leaf-water}}$ relationship. The correlation between the deuterium
341 contents of leaf wax *n*-alkanes and leaf water presented here is still well in range with the literature.
342 Feakins and Sessions (2010) presented *n*-alkane (C_{29} and C_{31}) and leaf water $\delta^2\text{H}$ data from typical plant
343 species (excluding grasses) along a southern California aridity gradient, revealing that only $\delta^2\text{H}$ of *n*- C_{29}
344 is significantly correlated with leaf water ($r^2 = 0.24$, $p < 0.1$, $n = 16$; based on the associated
345 supplementary data). Another field dataset from the temperate forest at Brown's Lake Bog, Ohio, USA
346 revealed significant correlations between $\delta^2\text{H}$ of *n*- C_{29} and *n*- C_{31} with leaf water of the species *Prunus*
347 *serotina*, *Acer saccharinum*, *Quercus rubra*, *Quercus alba*, and *Ulmus americana* ($r^2 = 0.49$, $p < 0.001$,
348 $n = 38$; $r^2 = 0.59$, $p < 0.001$, $n = 29$; as derived from the supplement material of Freimuth et al., 2017).
349 Data from a controlled climate chamber experiment using two tree species show a highly significant
350 relationship between leaf wax *n*-alkanes $\delta^2\text{H}$ and leaf water (with C_{31} of *Betula occidentalis* and C_{29} of
351 *Populus fremontii*; $r^2 = 0.96$, $p < 0.001$, $n = 24$; derived from supplementary data of Tipple et al., 2015).
352 It is conformed that leaf wax *n*-alkanes of dicotyledonous plants largely incorporate the leaf water

<https://doi.org/10.5194/bg-2019-427>

Preprint. Discussion started: 4 November 2019

© Author(s) 2019. CC BY 4.0 License.



353 isotope signal, while in monocotyledonous plants (e.g. grasses) the *n*-alkanes are more strongly
 354 affected by the source water due to the leaf growth at the intercalary meristem (Kahmen et al., 2013).
 355 The observed slope of the $\delta^{18}\text{O}_{\text{sugar}}$ to $\delta^{18}\text{O}_{\text{leaf-water}}$ relationship (Fig. 3B) could serve as indicator for a
 356 leaf water (enrichment) signal transfer damping of approximately 26%. The theory behind the signal
 357 damping is adopted from the cellulose research (e.g. Barbour and Farquhar, 2000). Barbour and
 358 Farquhar (2000) related the extent of the signal damping to the proportion of unenriched source
 359 water, which contribute to the local synthesis water pool and to the proportion of exchangeable
 360 oxygen during cellulose synthesis. Here calculated damping factor would be well in the range of values
 361 reported for cellulose synthesis in *Gossypium hirsutum* leaves (between 35 and 38%; Barbour and
 362 Farquhar, 2000), for *Eucalyptus globulus* leaf samples (38%; Cernusak et al., 2005) and for five C_3 and
 363 C_4 grasses (25%; Helliker and Ehleringer, 2002). Recently Cheesman and Cernusak (2017) provided
 364 damping factors for leaf cellulose synthesis based on plant data grown under same conditions at
 365 Jerusalem Botanical Gardens published by Wang et al. (1998), ranging between 4 and 100% with a
 366 mean of 49%, revealing large variations among and between ecological groups (namely conifers,
 367 deciduous, evergreen and shrubs). A large range of damping factors associated with leaf cellulose was
 368 also reported by Song et al. (2014) for *Ricinus communis* grown under controlled conditions. A common
 369 disadvantage of the above-mentioned studies is the absence of direct measurements of the proportion
 370 of depleted source water contribution to the local synthesis water (as noticed by Liu et al., 2017), which
 371 largely contribute to the extent of the damping factor (Barbour and Farquhar, 2000). However, when
 372 transferring cellulose results to pentoses, such as hemicellulose-derived arabinose and xylose, it should
 373 be noted that they are biosynthesized via decarboxylation of the carbon at position six (C6) from
 374 glucose (Altermatt and Neish, 1956; Burget et al., 2003; Harper and Bar-Peled, 2002). Waterhouse et
 375 al. (2013) showed that the oxygen atoms at C6 position in glucose moieties, used for heterotrophic
 376 cellulose synthesis, are strongly affected by the exchange with local water (up to 80%). Based on these
 377 findings, it can be suggested that the influence of the non-enriched source water during the synthesis
 378 of leaf hemicelluloses is rather small.

3.3 Fractionation factors between biomarkers and leaf water

380 In order to explore possible species-specific effects on the fractionation between the biomarkers and
 381 the leaf water, boxplots of the individual plant species of $\epsilon_{n\text{-alkane/leaf-water}}$ and $\epsilon_{\text{sugar/leaf-water}}$ values are
 382 shown in Fig. 4. Median $\epsilon_{n\text{-alkane/leaf-water}}$ values are -155‰ for *Brassica oleracea*, -164‰ for *Eucalyptus*
 383 *globulus* and -149‰ for *Vicia faba* (Fig. 4A), with an overall mean value of -156‰ (ranging from -133
 384 to -192‰). Median $\epsilon_{\text{sugar/leaf-water}}$ values of +27.0‰ for *Brassica oleracea*, +26.6‰ for *Eucalyptus*
 385 *globulus*, +26.8‰ for *Vicia faba* are shown in Fig. 4B. The overall $\epsilon_{\text{sugar/leaf-water}}$ average value of the
 386 three investigated species is +27.3‰ (ranging from +23.0 to +32.3‰). In both plots, no difference
 387 between the individual species seems to be observable.

388

389

390

(Fig. 4)

391

392

393

394

395

396

397

398

The boxplots of $\epsilon_{n\text{-alkane/leaf-water}}$ reveal that the median of the three investigated plant species can be
 statistically not distinguished, due to overlapping notches (Fig. 4A). It should be noted that due to the
 low sample number from each species, the 95% confidence interval is larger than the interquartile
 range in some cases. However, it seems that at least small species-specific differences cannot be ruled
 out. Our $\epsilon_{n\text{-alkane/leaf-water}}$ values resemble well the data from a laboratory study (Kahmen et al., 2011),
 reporting a median value of -162‰ for *n*- C_{25} , *n*- C_{27} and *n*- C_{29} of *Populus trichocarpa*. Furthermore, they
 are well comparable to climate chamber data of *Betula occidentalis* (*n*- C_{31}) and *Populus fremontii* (*n*-

<https://doi.org/10.5194/bg-2019-427>

Preprint. Discussion started: 4 November 2019

© Author(s) 2019. CC BY 4.0 License.



399 C₂₉) from Tipple et al. (2015), reporting a median $\epsilon_{n\text{-alkane/leaf-water}}$ value of -155‰. In addition, field
 400 experiments reveal similar median values of -151‰ (for *n*-C₂₉) and -142‰ (for *n*-C₃₁) from typical plant
 401 species (excluding grasses) from southern California (Feakins and Sessions, 2010) and -144‰ (for *n*-
 402 C₂₉, of the species *Prunus serotina*, *Acer saccharinum*, *Quercus rubra*, *Quercus alba* and *Ulmus*
 403 *americana*) from the temperate forest at Brown's Lake Bog, Ohio, USA. The large range in $\epsilon_{\text{xylem-water/leaf-}}$
 404 water values from our study (-192 to -133‰) is also obvious in the respective laboratory and field studies
 405 (-198 to -115‰, derived from *n*-C₂₉ and *n*-C₃₁ data from Feakins and Sessions, 2010; Kahmen et al.,
 406 2011a; Tipple et al., 2015; Freimuth et al., 2017). This could point to a specific water pool being used
 407 rather than bulk leaf water during biosynthesis (Sachse et al., 2012; Schmidt et al., 2003). In more
 408 detail, alkane synthesis takes place by modifying/expanding fatty acids in the cytosol, while fatty acids
 409 are synthesized in the chloroplasts (Schmidt et al., 2003). Thus, the cytosol as well as chloroplast water
 410 is one hydrogen source. However hydrogen can additionally be added to the alkanes and fatty acids
 411 by NADPH which originates from different sources (photosynthesis and pentose phosphate cycle,
 412 Schmidt et al., 2003). It is therefore challenging to measure directly the water pool in which the alkanes
 413 are biosynthesized (Tipple et al., 2015). Moreover, biosynthetic and metabolic pathways in general
 414 (Kahmen et al., 2013; Sessions et al., 1999; Zhang et al., 2009), the carbon and energy metabolism of
 415 plants more specifically (Cormier et al., 2018) and the number of carbon atoms of the *n*-alkane chains
 416 (Zhou et al., 2010) may have an influence on the fractionation. Our $\epsilon_{n\text{-alkane/leaf-water}}$ values correlate with
 417 T_{air} (Fig. S2A), whereas the correlation with RH_{air} (Fig. S2B) is not significant. This could point to a
 418 relationship between $\epsilon_{\text{xylem-water/leaf-water}}$ and plant physiological processes (affecting various plants
 419 differently).

420 The $\epsilon_{\text{sugar/leaf-water}}$ values (Fig. 4B) do not correlate significantly with T_{air} , but significantly with RH_{air} (Fig.
 421 S2C and D). A temperature dependence of the $\epsilon_{\text{sugar/leaf-water}}$ is not supported by this experiment, in
 422 contrast to results from Sternberg and Ellsworth (2011), where a temperature effect on oxygen
 423 fractionation during heterotrophic cellulose biosynthesis is observed. The here observed fractionation
 424 between hemicellulose-derived sugars and leaf water, with regard to $\epsilon_{\text{sugar/leaf-water}}$ values, is well in
 425 range with values reported for sucrose (exported from photosynthesizing leaves) and leaf water, which
 426 was shown to be +27‰ (Cernusak et al., 2003). Also the cellulose biosynthesis is associated with an
 427 enrichment of around +27‰ compared to the synthesis water as shown in growth experiments
 428 (Sternberg et al., 1986; Yakir and DeNiro, 1990). The relatively uniform fractionation is explained via
 429 the isotope exchange between the carbonyl oxygens of the organic molecules and the surrounding
 430 water (cf. Schmidt et al., 2001). This equilibrium fractionation effect was indeed described earlier by
 431 the reversible hydration reaction of acetone in water by Sternberg and DeNiro (1983) to be +28, +28
 432 and +26‰ at 15, 25 and 35°C, respectively. However, the observed range of approximately 9‰ (Fig.
 433 4B) could indicate that partially more than the oxygen equilibrium fractionation between organic
 434 molecules and medium water have to be considered. Presumably, isotopic as well as sucrose synthesis
 435 gradients within the leaf have to be taken into account when interpreting leaf sugar oxygen isotopic
 436 compositions and their correlation to leaf water (Lehmann et al., 2017). Lehmann et al. (2017) reported
 437 on a fractionation between sucrose and leaf water of +33.1‰. Based on this they proposed a
 438 conceptual scheme how such gradients can lead to discrepancies between the isotopic composition of
 439 the bulk leaf water and the synthesis water, while the latter is incorporated into the carbohydrates,
 440 and thus fractionation determination based on bulk leaf water can exceed the common average of
 441 +27‰. Also Mayr et al. (2015) found a fractionation between aquatic cellulose $\delta^{18}\text{O}$ and lake water
 442 larger than this value of around +29‰.

443 3.4 Strong control of relative humidity over deuterium-excess of leaf water

<https://doi.org/10.5194/bg-2019-427>

Preprint. Discussion started: 4 November 2019

© Author(s) 2019. CC BY 4.0 License.



445 The correlations between leaf water-based and measured RH_{air} or RH_{leaf} as well as modeled d_e and
 446 measured deuterium-excess_{leaf-water} are illustrated in Fig. 5A, B, D and E. Furthermore, modeled LEL
 447 slopes are compared to measured LEL slopes in Fig. 5C and F. In red, the results of the less simplified
 448 models are displayed (Eqs. 6, 2 and 10), in black the results of the more simplified models are shown
 449 (Eqs. 7, 3 and 11).

450

451

(Fig. 5)

452

453 Evidence for the strong control of relative humidity on deuterium-excess of leaf water comes from
 454 multivariate regression analysis between the measured deuterium-excess_{leaf-water} values versus RH_{air} ,
 455 RH_{leaf} and T_{air} , T_{leaf} . The results reveal that the deuterium-excess_{leaf-water} significantly correlates with RH_{air}
 456 of the climate chambers ($p < 0.001$), with an r^2 of 0.92. When RH_{leaf} and T_{leaf} values are used, the r^2 is
 457 0.84 and deuterium-excess_{leaf-water} correlates significantly with RH_{leaf} ($p < 0.001$). The strong control of
 458 relative humidity on deuterium-excess of leaf water is furthermore supported by the significant
 459 correlations between calculated versus measured RH_{air} values (Fig. 5A), regardless of whether the Eq.
 460 6 or 7 were used (representing a lower and higher degree of simplification). This is in line with the
 461 strong correlation between modeled d_e based on T_{air} and measured deuterium-excess_{leaf-water} values
 462 (Fig. 5B). When modeled RH_{leaf} values are compared to the measured ones, the correlation is less
 463 strong compared to RH_{air} (Fig. 5D vs. 5A), represented by lower R^2 and higher RMSE values. Clearly
 464 more data points are lying above the 1:1 line with regard to RH_{leaf} , compared to RH_{air} . On the same
 465 basis, the T_{leaf} -based d_e shows a weaker correlation to the measured values than the T_{air} -based d_e (Fig.
 466 5E vs. 5B). The generally better model performance when T_{air} is used (in contrast to T_{leaf}) could point
 467 to the fact that T_{leaf} does not well represent the actual conditions in the leaves. For the correlation
 468 between modeled and measured RH_{leaf} this means that the measured RH_{leaf} values do not reflect the
 469 real conditions because measured RH_{leaf} is calculated via $e_l/e_a * 100$ with T_{leaf} as input for the e_a equation
 470 (see section 2.3). In fact, the RH model results do not differ from each other and can be well compared
 471 to the measured RH_{air} , while the measured RH_{leaf} values reveal an average offset of approximately 9%
 472 with regard to the median values (Figure S3A). This can be explained by the small difference in ϵ^*
 473 calculated either with T_{leaf} or T_{air} . Moreover, when T_{leaf} values are used to model d_e , the match to T_{air} -
 474 based d_e and measured deuterium-excess_{leaf-water} values is weaker (Fig. 5B vs. E; Fig. S3B). This offset is
 475 caused by higher T_{leaf} values (compared to T_{air} ; Fig. 1), which are leading to more negative modeled d_e
 476 values.

477 Overall, the modeled d_e values show a high agreement with measured deuterium-excess of leaf water
 478 despite without being too positive, which can be expected from the literature. This is because bulk leaf
 479 is less enriched than the leaf water at the evaporative sites, which is however, the output of the Craig-
 480 Gordon-based leaf water enrichment model (e.g. Allison et al., 1985; Barbour et al., 2004; Cernusak et
 481 al., 2016; section 2.3). Especially under low relative humidity conditions, the discrepancy between
 482 Craig-Gordon model results and the measured values is shown to be more pronounced, associated
 483 with higher transpiration fluxes and higher isotope heterogeneity within the leaf water due to a non-
 484 uniform closure of the stomata (Flanagan et al., 1991; Santrucek et al., 2007). An overestimation of the
 485 Craig-Gordon models can hardly be observed here (Fig. 5B and 5E). However, based on the accepted
 486 leaf water enrichment theory (e.g. Cernusak et al., 2016), higher transpiration rates (e.g. under low
 487 humidity conditions) should still lead to a larger discrepancy between Craig-Gordon modelled and
 488 measured leaf water, because the back diffusion of enriched leaf water from the evaporative sites
 489 should get lower the higher the transpiration flux is. Why there is no difference between modeled and

<https://doi.org/10.5194/bg-2019-427>

Preprint. Discussion started: 4 November 2019

© Author(s) 2019. CC BY 4.0 License.



490 measured deuterium-excess of leaf water in here presented climate chamber experiment is not
491 comprehensible.

492 The simplified model variants show generally a better correspondence between calculated and
493 measured deuterium-excess of leaf water, based on R^2 and RMSE, than the less simplified models. This
494 does not seem to be related to the slope of the LEL because it can only be linked to the measured
495 values based on the less simplified models (Fig. 5C and 5F). The simplified air and leaf temperature
496 based slopes average at 2.7 and 2.6, respectively, with a common range between 2.5 and 2.8. The
497 average is well in agreement with the mean measured S_{LEL} of 2.9. In addition, a regression through the
498 tank water and all leaf water points reveals a slope of 2.7 (± 0.02 , based on subtracting/adding the
499 individual σ ; $r^2 = 0.98$, $n = 48$, $p < 0.001$). This could be the reason why the more simplified models are
500 still more accurate, despite the less simplified models do not reflect well the range of the measured
501 S_{LEL} , which vary between 2.4 and 3.8. Much better matches are found for the less simplified LEL slopes
502 (T_{air} based: 2.6 and 3.8, T_{leaf} based: 2.5 and 3.5; Fig. 5C and 5F). Indeed the measured as well as the
503 calculated S_{LEL} depend on the e_a/e_i ratio (hence RH_{leaf} and RH_{air} regarding T_{leaf} or T_{air} is used for
504 calculations, respectively) and on $\delta_a - \delta_s$, in line with the theory and literature (see section 2.3; e.g.
505 Allison et al., 1985). The higher accuracy of the simpler models would therefore imply that the S_{LEL}
506 depend only on equilibrium and kinetic fractionation parameters for both isotopes, which would valid
507 for isotope equilibrium conditions between the tank water (the water source of the plants) and the
508 atmospheric water vapor, allowing the usage of the unambiguous approximation $\delta_a - \delta_s = -\epsilon^*$. Indeed,
509 close-to equilibrium conditions between the tank water and the atmospheric water vapor are observed
510 for the climate chambers 4 to 6 and 8, while the others are characterized by a slight disequilibrium
511 conditions. However, the degree of uncertainty seems to be higher when using d_a values, by the
512 probably inadequate representation of the measured $\delta^2H_{atmospheric-water-vapor}$ and $\delta^{18}O_{atmospheric-water-vapor}$
513 with the actual conditions influencing the plants in the climate chamber, leading to a generally better
514 performance of the more simplified model variants.

515

516 3.5 Coupling $\delta^2H_{n-alkane}$ and $\delta^{18}O_{sugar}$ – Potential and limitations

517 One of the advantages of the proposed coupled $\delta^2H_{n-alkane}$ - $\delta^{18}O_{sugar}$ approach is a more robust
518 reconstruction of the isotope composition of the source water, which can often be directly linked to
519 the local precipitation signal (Hepp et al., 2015, 2017; Tuthorn et al., 2015; Zech et al., 2013a).
520 Therefore, Fig. 6 shows boxplots for measured leaf water, biomarker-based (reconstructed) leaf water,
521 measured source water (tank water; see section 2.1), biomarker-based source water (using
522 reconstructed leaf water as origin for the LEL's) and leaf-water-based source water values (using
523 measured leaf water as origin for the LEL's). Source water isotope compositions were calculated via
524 the slopes of the LEL's and the GMWL. The numbers (1-4) mark the available scenarios for source water
525 reconstruction (see section 2.4): 1) S_{LEL} calculated with the more simplified Eq. 11 with T_{air} , 2) as 1 but
526 with T_{leaf} , 3) S_{LEL} calculated with Eq. 10 with T_{air} , 4) as 3 but with T_{leaf} . Fig. 6 clearly shows that the n -
527 alkane and sugar biomarkers reflect leaf water rather than tank water used for irrigation. For δ^2H ,
528 neither the range nor the median of the $\delta^2H_{leaf-water}$ are well captured by the alkane-based leaf water
529 values. However, the overlapping notches do not support a statistical difference in the median values
530 (Fig. 6A). The medians are still on average 13‰ more positive than the measured $\delta^2H_{tank-water}$. A higher
531 agreement between measured and modeled values is observed from leaf water-based δ^2H_s compared
532 to $\delta^2H_{tank-water}$. The average offset is reduced to 2‰ and the range is reduced by approximately 70‰,
533 compared to the biomarker-based reconstruction. Besides the more simplified leaf water-based δ^2H_s
534 using T_{leaf} for calculating ϵ^* (scenario 2 in Fig. 6A), no statistical significant difference can be seen
535 between the leaf water-based δ^2H_s and the $\delta^2H_{tank-water}$, with regard to the overlapping notches.

<https://doi.org/10.5194/bg-2019-427>

Preprint. Discussion started: 4 November 2019

© Author(s) 2019. CC BY 4.0 License.



536

537

(Fig. 6)

538

539 For $\delta^{18}\text{O}$, the sugar-based leaf water values are in agreement with the measured ones with regard to
 540 the median values, as supported by the largely overlapping notches (Fig. 6B). The range of the
 541 reconstructed leaf water is in the order of 6‰ smaller than for the measured $\delta^{18}\text{O}_{\text{leaf-water}}$ dataset. All
 542 reconstructed $\delta^{18}\text{O}_s$ values, regardless whether they are biomarker- or leaf water-based, are
 543 comparable to the measured $\delta^{18}\text{O}_{\text{tank-water}}$. While the biomarker-based datasets depict an average
 544 offset of 2‰, the leaf water-based values only differ by 0.3‰ from the tank water $\delta^{18}\text{O}$ values,
 545 referring to the medians. As for $\delta^2\text{H}$, the same leaf water-based $\delta^{18}\text{O}_s$ scenario (more simplified leaf
 546 water-based model using T_{leaf} for calculating ϵ^* , scenario 2 in Fig. 6B) do not show overlapping notches
 547 with $\delta^{18}\text{O}_{\text{tank-water}}$, while the other leaf water-based source water reconstructions do. In addition, the
 548 range in the leaf water-based $\delta^{18}\text{O}_{\text{source-water}}$ values is considerable smaller than for the biomarker-based
 549 once (9‰ reduction). The overall larger range in modeled $\delta^2\text{H}_s$ and $\delta^{18}\text{O}_s$ compared to measured
 550 $\delta^2\text{H}_{\text{tank-water}}$ and $\delta^{18}\text{O}_{\text{tank-water}}$ can be related to uncertainties in S_{LEL} modeling (see equations in section
 551 2.3.2). Bariac et al. (1994) mentioned that they found no agreement between the intersect of modeled
 552 LEL's with the GMWL and the plant source water. Allison et al. (1985) explained such results with
 553 changing environmental conditions, leading to various LEL's with a locus line not necessarily passing
 554 the $\delta^2\text{H}_s$ and $\delta^{18}\text{O}_s$ data point, in a system that approaches rapidly new steady-state conditions.

555

556 Finally, the alkane and sugar-based leaf water values were used to reconstruct RH_{air} and RH_{leaf} . While
 557 the measured RH_{air} is well captured by the biomarker-based air relative humidity values ($R^2 = 0.54$ and
 558 0.48 for the more and less simplified models, respectively, Fig. 7A), the correlations are weak between
 559 the reconstructed leaf relative humidity values and the measured RH_{leaf} ($R^2 = 0.09$ and -0.04 for the
 560 more and less simplified models, respectively, Fig. 7B). The measured RH_{air} is reconstructed most
 561 accurate by the biomarker-based air relative humidity values (Fig. 7A). As for leaf water-based RH
 562 reconstructions, a difference between biomarker-based RH_{air} and RH_{leaf} is observed (compare Fig. 7B
 563 with 7A). This can be explained by the small difference between T_{leaf} and T_{air} , used for ϵ^* calculations
 564 in the respective equations. The better performance of the more simplified models compared to the
 565 less simplified ones, in general, and the fact that T_{air} seems to be the better model input compared to
 566 T_{leaf} , more specifically, can be explained as for the leaf water-based application (see section 3.3). The
 567 T_{leaf} as well as the measured $\delta^2\text{H}_{\text{atmospheric-water-vapor}}$ and $\delta^{18}\text{O}_{\text{atmospheric-water-vapor}}$ values seem to be less
 568 representative for the conditions affecting the climate chamber plant leaves.

569

(Fig. 7)

570

571

572 Overall, a lower coefficient of determination of the biomarker-based model results compared to the
 573 leaf water-based reconstructions (compare Fig. 5A and D with Fig. 7A and B) is observed. This can be
 574 attributed to the uncertainties in leaf water reconstructed using $\delta^2\text{H}_{n\text{-alkane}}$ and $\delta^{18}\text{O}_{\text{sugar}}$ datasets as
 575 discussed in section 3.2. The limitations regarding deuterium arose from the rather weak relationship
 576 between the $\delta^2\text{H}$ of the n -alkanes and the leaf water, probably linked with the large range in the
 577 fractionation between n -alkanes and leaf water ($\epsilon^2_{n\text{-alkane/leaf-water}}$). The applied equation to
 578 reconstructed $\delta^2\text{H}_{\text{leaf-water}}$ by using $\delta^2\text{H}_{n\text{-alkane}}$ and a constant biosynthetic fractionation of -160‰ (Eq.
 579 13) was considered to be suitable (Sachse et al., 2012; Sessions et al., 1999), but introduce also some
 580 uncertainty for the final relative humidity reconstruction. With regard to oxygen, the relatively large
 581 variations in $\epsilon_{\text{sugar/leaf-water}}$ of 9‰ have to be considered (Fig. 4B), because in the $\delta^{18}\text{O}_{\text{leaf-water}}$

<https://doi.org/10.5194/bg-2019-427>

Preprint. Discussion started: 4 November 2019

© Author(s) 2019. CC BY 4.0 License.



582 reconstructions a fixed value of +27‰ is used (Eq. 14). Such a uniform biosynthetic fractionation is an
583 approximation which may not always be fulfilled, as shown in the literature (e.g. Sternberg and
584 Ellsworth, 2011; Lehmann et al., 2017). Especially the underestimation of the biomarker-based RH_{air}
585 values under the 68% relative humidity conditions, as well as the large range in reconstructed RH_{air}
586 values for the 48, 49, 50% RH_{air} chambers can be attributed to the leaf water reconstruction
587 uncertainties. It should be mentioned that using Eqs. 8 and 9 to calculate leaf water isotope
588 composition based on the biomarkers via a biosynthetic fractionation values implies that the
589 fractionation process in principle can be treated as single process with a unique source. While this
590 approximation can be questioned (see discussion in section 3.2), the overall approximation between
591 biomarker-based and measured RH_{air} highlights the potential of the approach (Hepp et al., 2017;
592 Tuthorn et al., 2015; Zech et al., 2013a), also for future paleo-applications.

593

594 4 Conclusions

595 The climate chamber results and discussion suggest that leaf wax-derived *n*-alkane and hemicellulose-
596 derived sugar biomarkers are valuable $\delta^2H_{leaf-water}$ and $\delta^{18}O_{leaf-water}$ recorders, respectively. The coupling
597 of $\delta^2H_{n-alkane}$ and $\delta^{18}O_{sugar}$ results allows moreover a robust RH_{air} reconstruction of the chambers in
598 which the plants were grown, by using simplified Craig-Gordon equations. With regard to the research
599 questions, we summarize as follows:

600

- 601 (i) Alkanes with the chain-length *n*-C₂₉ were found to be suitable abundant for compound-
602 specific δ^2H measurements in the leaf samples from all investigated species (*Eucalyptus*
603 *globulus*, *Vicia faba* var. *minor* and *Brassica oleracea* var. *medullosa*). For *Vicia faba*,
604 additionally *n*-C₃₁ could be evaluated robustly. $\delta^{18}O_{sugar}$ values could be obtained for the
605 hemicellulose-derived monosaccharides arabinose and xylose.
- 606 (ii) Both the $\delta^2H_{n-alkane}$ and $\delta^{18}O_{sugar}$ values yielded highly significant correlations with δ^2H_{leaf-}
607 $water$ and $\delta^{18}O_{leaf-water}$ ($r^2 = 0.45$ and 0.85 , respectively; $p < 0.001$, $n = 24$). Mean fractionation
608 factors between biomarkers and leaf water were found to be -156‰ (ranging from -133
609 to -192‰) for $\epsilon_{n-alkane/leaf-water}$ and +27.3‰ (ranging from +23.0 to +32.3‰) for $\epsilon_{sugar/leaf-water}$.
- 610 (iii) Using measured leaf water isotope composition ($\delta^2H_{leaf-water}$ and $\delta^{18}O_{leaf-water}$) in a less (Eq.
611 6) and a more simplified rearranged Craig-Gordon model (Eq. 7), RH_{air} and RH_{leaf} can be
612 derived, by using either T_{air} or T_{leaf} . Most accurately, the RH_{air} values via Eq. 7 can be
613 reconstructed, with a calculated R^2 of 0.84 ($p < 0.001$) between measured and modeled
614 RH_{air} and a RMSE of 6%. RH_{leaf} reconstructions seemed less robust.
- 615 (iv) Reconstructed source water isotope composition (δ^2H_s , $\delta^{18}O_s$) are in range with the
616 measured tank water ($\delta^2H_{tank-water}$, $\delta^{18}O_{tank-water}$). However, modeled δ^2H_s and $\delta^{18}O_s$ show a
617 clear large range compared to $\delta^2H_{tank-water}$ and $\delta^{18}O_{tank-water}$. The uncertainties for source
618 water determination are thus considerably higher compared to the relative humidity
619 reconstructions. Still, the coupled δ^2H - $\delta^{18}O$ approach enables a back calculation of the
620 plant source water. Uncertainties, with regard to relative humidity reconstructions via
621 biomarker-based leaf water isotope composition, arose from leaf water reconstructions
622 and model uncertainties, as shown in conclusions ii) and iii). Overall, the biomarker-based
623 and measured RH_{air} correlation with a R^2 of 0.54 ($p < 0.001$) and a RMSE of 10% highlights
624 the great potential of the coupled $\delta^2H_{n-alkane}$ - $\delta^{18}O_{sugar}$ paleohygrometer approach for
625 reliable relative humidity reconstructions.

626

<https://doi.org/10.5194/bg-2019-427>

Preprint. Discussion started: 4 November 2019

© Author(s) 2019. CC BY 4.0 License.



627 **Acknowledgements**

628 We would like to thank M. Bliedtner and J. Zech (both University of Bern) for help during lipid
629 biomarker and $\delta^2\text{H}_{n\text{-alkane}}$ analysis. We thank M. Benesch (Martin-Luther-University Halle-Wittenberg)
630 and M. Schaarschmidt (University of Bayreuth) for laboratory assistance during sugar biomarker and
631 $\delta^{18}\text{O}_{\text{sugar}}$ analysis. The research was partly funded by the Swiss National Science Foundation (PP00P2
632 150590). We also acknowledge N. Orłowski (University of Freiburg), M. M. Lehmann (Swiss Federal
633 Institute WSL, Birmensdorf) and L. Wüthrich (University of Bern) for helpful discussions. Involvement
634 of K. Rozanski was supported by AGH UST statutory task No. 11.11.220.01/1 within subsidy of the
635 Ministry of Science and Higher Education. J. Hepp greatly acknowledges the support given by the
636 German Federal Environmental Foundation. The experiment carried out by C. Mayr was gratefully
637 supported by the HGF-project “Natural climate variations from 10,000 years to the present” (project
638 no. 01SF9813). The experiments were possible due to the assistance of J.B. Winkler, H. Lowag, D.
639 Strube, A. Kruse, D. Arthofer, H. Seidlitz, D. Schneider, H. D. Payer, and other members of the Helmholtz
640 Zentrum München.

641

642

643 **Author contributions**

644 J. Hepp and M. Zech wrote the paper; C. Mayr was responsible for the climate chamber experiment
645 together with W. Stichler and provided the leaf samples and the data; M. Zech and R. Zech were
646 responsible for compound-specific isotope analysis on the biomarkers; J. Hepp, M. Tuthorn and I. K.
647 Schäfer did laboratory work and data evaluation of the biomarker compound-specific isotope analysis;
648 B. Glaser, D. Juchelka, K. Rozanski and all co-authors contributed to the discussion and commented on
649 the manuscript.

<https://doi.org/10.5194/bg-2019-427>

Preprint. Discussion started: 4 November 2019

© Author(s) 2019. CC BY 4.0 License.



650 References

- 651 Ali, H. a. M., Mayes, R. W., Hector, B. L., Verma, a. K. and Ørskov, E. R.: The possible use of n-alkanes,
652 long-chain fatty alcohols and long-chain fatty acids as markers in studies of the botanical
653 composition of the diet of free-ranging herbivores, *The Journal of Agricultural Science*, 143(1),
654 85–95, doi:10.1017/S0021859605004958, 2005.
- 655 Allison, G. B., Gat, J. R. and Leaney, F. W. J.: The relationship between deuterium and oxygen-18 delta
656 values in leaf water, *Chemical Geology*, 58, 145–156, 1985.
- 657 Altermatt, H. A. and Neish, A. C.: The biosynthesis of cell wall carbohydrates: III. Further studies on
658 formation of cellulose and xylan from labeled monosaccharides in wheat plants, *Canadian
659 Journal of Biochemistry and Physiology*, 34(3), 405–413, doi:10.1139/o56-042, 1956.
- 660 Amelung, W., Cheshire, M. V. and Guggenberger, G.: Determination of neutral and acidic sugars in soil
661 by capillary gas-liquid chromatography after trifluoroacetic acid hydrolysis, *Soil Biology and
662 Biochemistry*, 28(12), 1631–1639, 1996.
- 663 Barbour, M. M. and Farquhar, G. D.: Relative humidity-and ABA-induced variation in carbon and oxygen
664 isotope ratios of cotton leaves, *Plant, Cell & Environment*, 23(5), 473–485, 2000.
- 665 Barbour, M. M., Roden, J. S., Farquhar, G. D. and Ehleringer, J. R.: Expressing leaf water and cellulose
666 oxygen isotope ratios as enrichment above source water reveals evidence of a Péclet effect,
667 *Oecologia*, 138(3), 426–435, doi:10.1007/s00442-003-1449-3, 2004.
- 668 Bariac, T., Gonzalez-Dunia, J., Katerji, N., Béthenod, O., Bertolini, J. M. and Mariotti, A.: Spatial variation
669 of the isotopic composition of water (^{18}O , ^2H) in the soil-plant-atmosphere system, 2.
670 Assessment under field conditions, *Chemical Geology*, 115, 317–333, 1994.
- 671 Burget, E. G., Verma, R., Mølhøj, M. and Reiter, W.-D.: The Biosynthesis of L-Arabinose in Plants:
672 Molecular Cloning and Characterization of a Golgi-Localized UDP-D-Xylose 4-Epimerase Encoded
673 by the MUR4 Gene of Arabidopsis, *Plant Cell*, 15(February), 523–531,
674 doi:10.1105/tpc.008425.response, 2003.
- 675 Cernusak, L. A., Wong, S. C. and Farquhar, G. D.: Oxygen isotope composition of phloem sap in relation
676 to leaf water in *Ricinus communis*, *Functional Plant Biology*, 30(10), 1059–1070, 2003.
- 677 Cernusak, L. A., Farquhar, G. D. and Pate, J. S.: Environmental and physiological controls over oxygen
678 and carbon isotope composition of Tasmanian blue gum, *Eucalyptus globulus*, *Tree Physiology*,
679 25(2), 129–146, doi:10.1093/treephys/25.2.129, 2005.
- 680 Cernusak, L. A., Barbour, M. M., Arndt, S. K., Cheesman, A. W., English, N. B., Feild, T. S., Helliker, B. R.,
681 Holloway-Phillips, M. M., Holtum, J. A. M., Kahmen, A., Mcinerney, F. A., Munksgaard, N. C.,
682 Simonin, K. A., Song, X., Stuart-Williams, H., West, J. B. and Farquhar, G. D.: Stable isotopes in
683 leaf water of terrestrial plants, *Plant Cell and Environment*, 39(5), 1087–1102,
684 doi:10.1111/pce.12703, 2016.
- 685 Cheesman, A. W. and Cernusak, L. A.: Infidelity in the outback: Climate signal recorded in $\Delta^{18}\text{O}$ of leaf
686 but not branch cellulose of eucalypts across an Australian aridity gradient, *Tree Physiology*,
687 37(5), 554–564, doi:10.1093/treephys/tpw121, 2017.
- 688 Coplen, T. B.: Guidelines and recommended terms for expression of stable-isotope-ratio and gas-ratio
689 measurement results, *Rapid Communications in Mass Spectrometry*, 25(17), 2538–2560,
690 doi:10.1002/rcm.5129, 2011.
- 691 Cormier, M.-A., Werner, R. A., Sauer, P. E., Gröcke, D. R., M.C., L., Wieloch, T., Schleucher, J. and
692 Kahmen, A.: ^2H fractionations during the biosynthesis of carbohydrates and lipids imprint a
693 metabolic signal on the $\delta^2\text{H}$ values of plant organic compounds, *New Phytologist*, 218(2), 479–
694 491, doi:10.1111/nph.15016, 2018.
- 695 Craig, H. and Gordon, L. I.: Deuterium and oxygen-18 variations in the ocean and the marine
696 atmosphere, in *Proceedings of a Conference on Stable Isotopes in Oceanographic Studies and
697 Palaeotemperatures*, edited by E. Tongiorgi, pp. 9–130, Lischi and Figli, Pisa., 1965.
- 698 D'Souza, F., Garg, A. and Bhosle, N. B.: Seasonal variation in the chemical composition and
699 carbohydrate signature compounds of biofilm, *Aquatic Microbial Ecology*, 41(2), 199–207,
700 doi:10.3354/ame041199, 2005.
- 701 Dansgaard, W.: Stable isotopes in precipitation, *Tellus*, 16(4), 436–468, doi:10.1111/j.2153-

<https://doi.org/10.5194/bg-2019-427>

Preprint. Discussion started: 4 November 2019

© Author(s) 2019. CC BY 4.0 License.



- 702 3490.1964.tb00181.x, 1964.
- 703 Dawson, T. E.: Hydraulic lift and water use by plants: implications for water balance, performance and
704 plant-plant interactions, *Oecologia*, 95(4), 565–574, 1993.
- 705 Farquhar, G. D., Hubick, K. T., Condon, A. G. and Richards, R. A.: Carbon Isotope Fractionation and Plant
706 Water-Use Efficiency, in *Stable Isotopes in Ecological Research. Ecological Studies (Analysis and
707 Synthesis)*, vol. 68, edited by P. W. Rundel, J. R. Ehleringer, and K. A. Nagy, pp. 21–40, Springer-
708 Verlag, New York., 1989.
- 709 Feakins, S. J. and Sessions, A. L.: Controls on the D/H ratios of plant leaf waxes in an arid ecosystem,
710 *Geochimica et Cosmochimica Acta*, 74(7), 2128–2141,
711 doi:<http://dx.doi.org/10.1016/j.gca.2010.01.016>, 2010.
- 712 Flanagan, L. B., Comstock, J. P. and Ehleringer, J. R.: Comparison of Modeled and Observed
713 Environmental Influences on the Stable Oxygen and Hydrogen Isotope Composition of Leaf
714 Water in *Phaseolus vulgaris* L., *Plant Physiology*, (96), 588–596, 1991.
- 715 Freimuth, E. J., Diefendorf, A. F. and Lowell, T. V.: Hydrogen isotopes of *n*-alkanes and *n*-alkanoic acids
716 as tracers of precipitation in a temperate forest and implications for paleorecords, *Geochimica
717 et Cosmochimica Acta*, 206, 166–183, doi:10.1016/j.gca.2017.02.027, 2017.
- 718 Gat, J. R. and Bowser, C. J.: The heavy isotope enrichment of water in coupled evaporative systems, in
719 *Stable Isotope Geochemistry: A Tribute to Samuel Epstein*, vol. 3, edited by H. P. Taylor, J. R.
720 O’Neil, and I. R. Kaplan, pp. 159–168, The Geochemical Society, Lancaster., 1991.
- 721 Gat, J. R., Yakir, D., Goodfriend, G., Fritz, P., Trumborn, P., Lipp, J., Gev, I., Adar, E. and Waisel, Y.: Stable
722 isotope composition of water in desert plants, *Plant and Soil*, 298(1–2), 31–45,
723 doi:10.1007/s11104-007-9321-6, 2007.
- 724 Harper, A. D. and Bar-Peled, M.: Biosynthesis of UDP-Xylose. Cloning and Characterization of a Novel
725 Arabidopsis Gene Family, UXS, Encoding Soluble and Putative Membrane-Bound UDP-
726 Glucuronic Acid Decarboxylase Isoforms, *Gene*, 130(December), 2188–2198,
727 doi:10.1104/pp.009654.2188, 2002.
- 728 Helliker, B. R. and Ehleringer, J. R.: Differential ¹⁸O enrichment of leaf cellulose in C3 versus C4 grasses,
729 *Functional Plant Biology*, 29, 435–442, 2002.
- 730 Hepp, J., Tuthorn, M., Zech, R., Mügler, I., Schlütz, F., Zech, W. and Zech, M.: Reconstructing lake
731 evaporation history and the isotopic composition of precipitation by a coupled $\delta^{18}\text{O}$ – $\delta^2\text{H}$
732 biomarker approach, *Journal of Hydrology*, 529, 622–631, 2015.
- 733 Hepp, J., Rabus, M., Anhäuser, T., Bromm, T., Laforsch, C., Sirocco, F., Glaser, B. and Zech, M.: A sugar
734 biomarker proxy for assessing terrestrial versus aquatic sedimentary input, *Organic
735 Geochemistry*, 98, 98–104, doi:10.1016/j.orggeochem.2016.05.012, 2016.
- 736 Hepp, J., Zech, R., Rozanski, K., Tuthorn, M., Glaser, B., Greule, M., Keppler, F., Huang, Y., Zech, W. and
737 Zech, M.: Late Quaternary relative humidity changes from Mt. Kilimanjaro, based on a coupled
738 ²H–¹⁸O biomarker paleohygrometer approach, *Quaternary International*, 438, 116–130,
739 doi:10.1016/j.quaint.2017.03.059, 2017.
- 740 Herbin, G. A. and Robins, P. A.: Studies on plant cuticular waxes-II. Alkanes from members of the genus
741 *Agave* (Agavaceae), the genera *Kalanchoe*, *Echeveria*, *Crassula* and *Sedum* (Crassulaceae) and
742 the genus *Eucalyptus* (Myrtaceae) with an examination of Hutchinson, *Phytochemistry*, 7(1951),
743 257–268, 1968.
- 744 Heyng, A., Mayr, C., Lücke, A., Wissel, H. and Striewski, B.: Late Holocene hydrologic changes in
745 northern New Zealand inferred from stable isotope values of aquatic cellulose in sediments from
746 Lake Pupuke, *Journal of Paleolimnology*, 51(4), 485–497, doi:10.1007/s10933-014-9769-3, 2014.
- 747 Horita, J. and Wesolowski, D. J.: Liquid-vapor fractionation of oxygen and hydrogen isotopes of water
748 from the freezing to the critical temperature, *Geochimica et Cosmochimica Acta*, 58(16), 3425–
749 3437, doi:[http://dx.doi.org/10.1016/0016-7037\(94\)90096-5](http://dx.doi.org/10.1016/0016-7037(94)90096-5), 1994.
- 750 Hou, J., D’Andrea, W. J. and Huang, Y.: Can sedimentary leaf waxes record D/H ratios of continental
751 precipitation? Field, model, and experimental assessments, *Geochimica et Cosmochimica Acta*,
752 72, 3503–3517, doi:10.1016/j.gca.2008.04.030, 2008.
- 753 Huang, Y., Shuman, B., Wang, Y. and Iii, T. W.: Hydrogen isotope ratios of individual lipids in lake
754 sediments as novel tracers of climatic and environmental change: a surface sediment test,

<https://doi.org/10.5194/bg-2019-427>

Preprint. Discussion started: 4 November 2019

© Author(s) 2019. CC BY 4.0 License.



- 755 Journal of Paleolimnology, 31, 363–375, 2004.
- 756 Jia, G., Dungait, J. A. J., Bingham, E. M., Valiranta, M., Korhola, A. and Evershed, R. P.: Neutral
757 monosaccharides as biomarker proxies for bog-forming plants for application to
758 palaeovegetation reconstruction in ombrotrophic peat deposits, *Organic Geochemistry*, 39(12),
759 1790–1799, doi:10.1016/j.orggeochem.2008.07.002, 2008.
- 760 Kahmen, A., Sachse, D., Arndt, S. K., Tu, K. P., Farrington, H., Vitousek, P. M. and Dawson, T. E.: Cellulose
761 $\delta^{18}\text{O}$ is an index of leaf-to-air vapor pressure difference (VPD) in tropical plants, *Proceedings of*
762 *the National Academy of Sciences of the United States of America*, 108(5), 1981–1986,
763 doi:10.1073/pnas.1018906108, 2011a.
- 764 Kahmen, A., Dawson, T. E., Vieth, A. and Sachse, D.: Leaf wax *n*-alkane δD values are determined early
765 in the ontogeny of *Populus trichocarpa* leaves when grown under controlled environmental
766 conditions, *Plant, Cell and Environment*, 34(10), 1639–1651, doi:10.1111/j.1365-
767 3040.2011.02360.x, 2011b.
- 768 Kahmen, A., Schefuß, E. and Sachse, D.: Leaf water deuterium enrichment shapes leaf wax *n*-alkane δD
769 values of angiosperm plants I: Experimental evidence and mechanistic insights, *Geochimica et*
770 *Cosmochimica Acta*, 111, 39–49, 2013.
- 771 Knapp, D. R.: *Handbook of Analytical Derivatization Reactions*, John Wiley & Sons, New York,
772 Chichester, Brisbane, Toronto, Singapore., 1979.
- 773 Lehmann, M. M., Gamarra, B., Kahmen, A., Siegwolf, R. T. W. and Saurer, M.: Oxygen isotope
774 fractionations across individual leaf carbohydrates in grass and tree species, *Plant Cell and*
775 *Environment*, 40(8), 1658–1670, doi:10.1111/pce.12974, 2017.
- 776 Liu, H. T., Schäufele, R., Gong, X. Y. and Schnyder, H.: The $\delta^{18}\text{O}$ and $\delta^2\text{H}$ of water in the leaf growth-
777 and-differentiation zone of grasses is close to source water in both humid and dry atmospheres,
778 *New Phytologist*, 214(4), 1423–1431, doi:10.1111/nph.14549, 2017.
- 779 Maffei, M.: Chemotaxonomic significance of leaf wax *n*-alkanes in the umbelliferae, cruciferae and
780 leguminosae (subf. Papilionoideae), *Biochemical Systematics and Ecology*, 24(6), 531–545,
781 doi:10.1016/0305-1978(96)00037-3, 1996.
- 782 Mayr, C.: Möglichkeiten der Klimarekonstruktion im Holozän mit $\delta^{13}\text{C}$ - und $\delta^2\text{H}$ -Werten von Baum-
783 Jahrringen auf der Basis von Klimakammerversuchen und Rezentstudien, PhD thesis, Ludwig-
784 Maximilians-Universität München. GSF-Bericht 14/02, 152 pp., 2002.
- 785 Mayr, C., Laprida, C., Lücke, A., Martín, R. S., Massaferro, J., Ramón-Mercau, J. and Wissel, H.: Oxygen
786 isotope ratios of chironomids, aquatic macrophytes and ostracods for lake-water isotopic
787 reconstructions - Results of a calibration study in Patagonia, *Journal of Hydrology*, 529(P2), 600–
788 607, doi:10.1016/j.jhydrol.2014.11.001, 2015.
- 789 McGill, R., Tukey, J. W. and Larsen, W. A.: Variations of Box Plots, *The American Statistician*, 32(1), 12–
790 16, 1978.
- 791 Merlivat, L.: Molecular diffusivities of H_2^{16}O , HD^{16}O , and H_2^{18}O in gases, *The Journal of Chemical*
792 *Physics*, 69(6), 2864–2871, doi:http://dx.doi.org/10.1063/1.436884, 1978.
- 793 Mügler, I., Sachse, D., Werner, M., Xu, B., Wu, G., Yao, T. and Gleixner, G.: Effect of lake evaporation
794 on δD values of lacustrine *n*-alkanes: A comparison of Nam Co (Tibetan Plateau) and Holzmaar
795 (Germany), *Organic Geochemistry*, 39(6), 711–729, 2008.
- 796 Prietzel, J., Dechamps, N. and Spielvogel, S.: Analysis of non-cellulosic polysaccharides helps to reveal
797 the history of thick organic surface layers on calcareous Alpine soils, *Plant and Soil*, 365(1–2),
798 93–114, doi:10.1007/s11104-012-1340-2, 2013.
- 799 R Core Team: R: A Language and Environment for Statistical Computing, [online] Available from:
800 <https://www.r-project.org/>, 2015.
- 801 Rao, Z., Zhu, Z., Jia, G., Henderson, A. C. G., Xue, Q. and Wang, S.: Compound specific δD values of long
802 chain *n*-alkanes derived from terrestrial higher plants are indicative of the δD of meteoric
803 waters: Evidence from surface soils in eastern China, *Organic Geochemistry*, 40(8), 922–930,
804 doi:http://dx.doi.org/10.1016/j.orggeochem.2009.04.011, 2009.
- 805 Roden, J. S. and Ehleringer, J. R.: Observations of Hydrogen and Oxygen Isotopes in Leaf Water Confirm
806 the Craig-Gordon Model under Wide-Ranging Environmental Conditions, *Plant Physiology*,
807 120(August), 1165–1173, 1999.

<https://doi.org/10.5194/bg-2019-427>

Preprint. Discussion started: 4 November 2019

© Author(s) 2019. CC BY 4.0 License.



- 808 Sachse, D., Radke, J. and Gleixner, G.: Hydrogen isotope ratios of recent lacustrine sedimentary *n*-
809 alkanes record modern climate variability, *Geochimica et Cosmochimica Acta*, 68(23), 4877–
810 4889, doi:<http://dx.doi.org/10.1016/j.gca.2004.06.004>, 2004.
- 811 Sachse, D., Billault, I., Bowen, G. J., Chikaraishi, Y., Dawson, T. E., Feakins, S. J., Freeman, K. H., Magill,
812 C. R., McInerney, F. A., van der Meer, M. T. J., Polissar, P., Robins, R. J., Sachs, J. P., Schmidt, H.-
813 L., Sessions, A. L., White, J. W. C. and West, J. B.: Molecular Paleohydrology: Interpreting the
814 Hydrogen-Isotopic Composition of Lipid Biomarkers from Photosynthesizing Organisms, *Annual*
815 *Reviews*, 40, 221–249, doi:10.1146/annurev-earth-042711-105535, 2012.
- 816 Santrucek, J., Kveton, J., Setlik, J. and Bulickova, L.: Spatial Variation of Deuterium Enrichment in Bulk
817 Water of Snowgum Leaves, *Plant Physiology*, 143(1), 88–97, doi:10.1104/pp.106.089284, 2007.
- 818 Sauer, P. E., Eglinton, T. I., Hayes, J. M., Schimmelmann, A. and Sessions, A. L.: Compound-specific D/H
819 ratios of lipid biomarkers from sediments as a proxy for environmental and climatic conditions,
820 *Geochimica et Cosmochimica Acta*, 65(2), 213–222, doi:[http://dx.doi.org/10.1016/S0016-](http://dx.doi.org/10.1016/S0016-7037(00)00520-2)
821 [7037\(00\)00520-2](http://dx.doi.org/10.1016/S0016-7037(00)00520-2), 2001.
- 822 Schäfer, I. K., Lanny, V., Franke, J., Eglinton, T. I., Zech, M., Vysloužilová, B. and Zech, R.: Leaf waxes in
823 litter and topsoils along a European transect, *SOIL*, 2, 551–564, doi:10.5194/soil-2-551-2016,
824 2016.
- 825 Schmidt, H.-L., Werner, R. A. and Roßmann, A.: ¹⁸O Pattern and biosynthesis of natural plant products,
826 *Phytochemistry*, 58(1), 9–32, doi:[http://dx.doi.org/10.1016/S0031-9422\(01\)00017-6](http://dx.doi.org/10.1016/S0031-9422(01)00017-6), 2001.
- 827 Schmidt, H.-L., Werner, R. A. and Eisenreich, W.: Systematics of ²H patterns in natural compounds and
828 its importance for the elucidation of biosynthetic pathways, *Phytochemistry Reviews*, 2(1–2),
829 61–85, doi:10.1023/B:PHYT.0000004185.92648.ae, 2003.
- 830 Sessions, A. L., Burgoyne, T. W., Schimmelmann, A. and Hayes, J. M.: Fractionation of hydrogen
831 isotopes in lipid biosynthesis, *Organic Geochemistry*, 30, 1193–1200, 1999.
- 832 Song, X., Farquhar, G. D., Gessler, A. and Barbour, M. M.: Turnover time of the non-structural
833 carbohydrate pool influences δ18O of leaf cellulose, *Plant Cell and Environment*, 37(11), 2500–
834 2507, doi:10.1111/pce.12309, 2014.
- 835 Sternberg, L. and Ellsworth, P. F. V.: Divergent Biochemical Fractionation, Not Convergent
836 Temperature, Explains Cellulose Oxygen Isotope Enrichment across Latitudes, *PLoS ONE*, 6(11),
837 e28040, doi:10.1371/journal.pone.0028040, 2011.
- 838 Sternberg, L. da S. L. O. and DeNiro, M. J. D.: Biogeochemical implications of the isotopic equilibrium
839 fractionation factor between the oxygen atoms of acetone and water, *Geochimica et*
840 *Cosmochimica Acta*, 47(12), 2271–2274, doi:10.1016/0016-7037(83)90049-2, 1983.
- 841 Sternberg, L. S. L., DeNiro, M. J. and Savidge, R. A.: Oxygen Isotope Exchange between Metabolites and
842 Water during Biochemical Reactions Leading to Cellulose Synthesis, *Plant Physiology*, 82, 423–
843 427, 1986.
- 844 Tipple, B. J., Berke, M. A., Doman, C. E., Khachatryan, S. and Ehleringer, J. R.: Leaf-wax *n*-alkanes
845 record the plant-water environment at leaf flush, *Proceedings of the National Academy of*
846 *Sciences*, 110(7), 2659–2664, doi:10.1073/pnas.1213875110, 2013.
- 847 Tipple, B. J., Berke, M. A., Hambach, B., Roden, J. S. and Ehleringer, J. R.: Predicting leaf wax *n*-alkane
848 ²H/¹H ratios: Controlled water source and humidity experiments with hydroponically grown
849 trees confirm predictions of Craig-Gordon model, *Plant, Cell and Environment*, 38(6), 1035–
850 1047, doi:10.1111/pce.12457, 2015.
- 851 Tuthorn, M., Zech, M., Ruppenthal, M., Oelmann, Y., Kahmen, A., del Valle, H. F., Wilcke, W. and Glaser,
852 B.: Oxygen isotope ratios (¹⁸O/¹⁶O) of hemicellulose-derived sugar biomarkers in plants, soils and
853 sediments as paleoclimate proxy II: Insight from a climate transect study, *Geochimica et*
854 *Cosmochimica Acta*, 126, 624–634, doi:<http://dx.doi.org/10.1016/j.gca.2013.11.002>, 2014.
- 855 Tuthorn, M., Zech, R., Ruppenthal, M., Oelmann, Y., Kahmen, A., del Valle, H. F., Eglinton, T., Rozanski,
856 K. and Zech, M.: Coupling δ²H and δ¹⁸O biomarker results yields information on relative humidity
857 and isotopic composition of precipitation - a climate transect validation study, *Biogeosciences*,
858 12, 3913–3924, doi:10.5194/bg-12-3913-2015, 2015.
- 859 Walker, C. D. and Brunel, J.-P.: Examining Evapotranspiration in a Semi-Arid Region using Stable
860 Isotopes of Hydrogen and Oxygen, *Journal of Hydrology*, 118, 55–75, 1990.

<https://doi.org/10.5194/bg-2019-427>

Preprint. Discussion started: 4 November 2019

© Author(s) 2019. CC BY 4.0 License.



- 861 Wang, X.-F., Yakir, D. and Avisha, M.: Non-climatic variations in the oxygen isotopic composition of
862 plants, *Global Change Biology*, 4, 835–849, 1998.
- 863 Waterhouse, J. S., Cheng, S., Juchelka, D., Loader, N. J., McCarroll, D., Switsur, V. R. and Gautam, L.:
864 Position-specific measurement of oxygen isotope ratios in cellulose: Isotopic exchange during
865 heterotrophic cellulose synthesis, *Geochimica et Cosmochimica Acta*, 112(0), 178–191,
866 doi:<http://dx.doi.org/10.1016/j.gca.2013.02.021>, 2013.
- 867 Werner, R. A. and Brand, W. A.: Referencing strategies and techniques in stable isotope ratio analysis,
868 *Rapid Communications in Mass Spectrometry*, 15(7), 501–519, doi:10.1002/rcm.258, 2001.
- 869 Wissel, H., Mayr, C. and Lücke, A.: A new approach for the isolation of cellulose from aquatic plant
870 tissue and freshwater sediments for stable isotope analysis, *Organic Geochemistry*, 39(11),
871 1545–1561, doi:<http://dx.doi.org/10.1016/j.orggeochem.2008.07.014>, 2008.
- 872 Yakir, D. and DeNiro, M. J.: Oxygen and Hydrogen Isotope Fractionation during Cellulose Metabolism
873 in *Lemna gibba* L., *Plant Ecology*, 93, 325–332, 1990.
- 874 Zech, M. and Glaser, B.: Compound-specific $\delta^{18}\text{O}$ analyses of neutral sugars in soils using gas
875 chromatography-pyrolysis-isotope ratio mass spectrometry: problems, possible solutions and a
876 first application, *Rapid Communications in Mass Spectrometry*, 23, 3522–3532,
877 doi:10.1002/rcm, 2009.
- 878 Zech, M., Werner, R. A., Juchelka, D., Kalbitz, K., Buggle, B. and Glaser, B.: Absence of oxygen isotope
879 fractionation/exchange of (hemi-) cellulose derived sugars during litter decomposition, *Organic*
880 *Geochemistry*, 42(12), 1470–1475, doi:<http://dx.doi.org/10.1016/j.orggeochem.2011.06.006>,
881 2012.
- 882 Zech, M., Tuthorn, M., Detsch, F., Rozanski, K., Zech, R., Zöller, L., Zech, W. and Glaser, B.: A 220 ka
883 terrestrial $\delta^{18}\text{O}$ and deuterium excess biomarker record from an eolian permafrost paleosol
884 sequence, NE-Siberia, *Chemical Geology*, 360–361, 220–230,
885 doi:<http://dx.doi.org/10.1016/j.chemgeo.2013.10.023>, 2013a.
- 886 Zech, M., Tuthorn, M., Glaser, B., Amelung, W., Huwe, B., Zech, W., Zöller, L. and Löffler, J.: Natural
887 abundance of $\delta^{18}\text{O}$ of sugar biomarkers in topsoils along a climate transect over the Central
888 Scandinavian Mountains, Norway, *Journal of Plant Nutrition and Soil Science*, 176(1), 12–15,
889 doi:10.1002/jpln.201200365, 2013b.
- 890 Zech, M., Mayr, C., Tuthorn, M., Leiber-Sauheitl, K. and Glaser, B.: Oxygen isotope ratios ($^{18}\text{O}/^{16}\text{O}$) of
891 hemicellulose-derived sugar biomarkers in plants, soils and sediments as paleoclimate proxy I:
892 Insight from a climate chamber experiment, *Geochimica et Cosmochimica Acta*, 126(0), 614–
893 623, doi:<http://dx.doi.org/10.1016/j.gca.2013.10.048>, 2014a.
- 894 Zech, M., Mayr, C., Tuthorn, M., Leiber-Sauheitl, K. and Glaser, B.: Reply to the comment of Sternberg
895 on “Zech et al. (2014) Oxygen isotope ratios ($^{18}\text{O}/^{16}\text{O}$) of hemicellulose-derived sugar biomarkers
896 in plants, soils and sediments as paleoclimate proxy I: Insight from a climate chamber
897 experiment. *GCA, Geochimica et Cosmochimica Acta*, 141(0), 680–682,
898 doi:10.1016/j.gca.2014.04.051, 2014b.
- 899 Zech, M., Zech, R., Rozanski, K., Gleixner, G. and Zech, W.: Do *n*-alkane biomarkers in soils/sediments
900 reflect the $\delta^2\text{H}$ isotopic composition of precipitation? A case study from Mt. Kilimanjaro and
901 implications for paleoaltimetry and paleoclimate research, *Isotopes in Environmental and*
902 *Health Studies*, 51(4), 508–524, doi:10.1080/10256016.2015.1058790, 2015.
- 903 Zhang, X., Gillespie, A. L. and Sessions, A. L.: Large D/H variations in bacterial lipids reflect central
904 metabolic pathways, *PNAS*, 106(31), 12580–12586, 2009.
- 905 Zhou, Y., Grice, K., Stuart-Williams, H., Farquhar, G. D., Hocart, C. H., Lu, H. and Liu, W.: Biosynthetic
906 origin of the saw-toothed profile in $\delta^{13}\text{C}$ and $\delta^2\text{H}$ of *n*-alkanes and systematic isotopic differences
907 between *n*-, *iso*- and *anteiso*-alkanes in leaf waxes of land plants, *Phytochemistry*, 71(4), 388–
908 403, doi:10.1016/j.phytochem.2009.11.009, 2010.

<https://doi.org/10.5194/bg-2019-427>

Preprint. Discussion started: 4 November 2019

© Author(s) 2019. CC BY 4.0 License.



909 Figure captions

910 **Fig. 1:** A: Plant water (leaf water, xylem water and soil water) isotope compositions (in green, orange
911 and brown, respectively) and the isotope composition of the investigated leaf biomarkers (leaf wax *n*-
912 alkanes *n*-C₂₉ and *n*-C₃₁ as open diamonds and triangles, respectively; hemicellulose-derived sugars:
913 arabinose and xylose as open squares and circles, respectively) for the three plants *Eucalyptus*
914 *globulus*, *Vicia faba* and *Brassica oleracea* grown in the climate chambers. B: Associated climate
915 chamber conditions (leaf temperature and relative humidity in green and air temperature and relative
916 humidity in red). Error bars represent analytical standard deviation of the respective measurements
917 (see section 2.2 and Mayr, 2002).

918

919 **Fig. 2:** $\delta^2\text{H}$ - $\delta^{18}\text{O}$ diagram illustrating the isotope composition of the biomarkers, comprising $\delta^2\text{H}$ values
920 of the leaf wax *n*-alkanes (C₂₉ for *Eucalyptus globulus* and *Brassica oleracea*; weighted mean of C₂₉ and
921 C₃₁ for *Vicia faba*) and $\delta^{18}\text{O}$ values of the hemicellulose-derived sugars arabinose and xylose (black
922 crosses) and the measured isotope compositions of leaf water (green squares), xylem water (orange
923 squares), soil water (brown squares), atmospheric water vapor (red squares) and the tank water used
924 for irrigation (blue triangle), which plot very close to the global meteoric water line.
925

926 **Fig. 3:** Scatterplots depicting the relationships between the compound-specific biomarker isotope
927 composition and the respective leaf water values (A: $\delta^2\text{H}_{n\text{-alkane}}$ vs. $\delta^2\text{H}_{\text{leaf-water}}$; B: $\delta^{18}\text{O}_{\text{sugar}}$ vs. $\delta^{18}\text{O}_{\text{leaf-}}$
928 *water*). *Brassica oleracea*, *Eucalyptus globulus* and *Vicia faba* samples are shown in purple, orange and
929 black, respectively. Error bars of the δ values represent standard deviation of repeated measurements
930 (see section 2.2 and Mayr, 2002).

931

932 **Fig. 4:** Boxplots comprising the plant-specific fractionation between the biomarkers and the leaf water
933 (A: $\epsilon_{n\text{-alkane}/\text{leaf-water}}$ according Eq. 8; B: $\epsilon_{\text{sugar}/\text{leaf-water}}$ according to Eq. 9). *Brassica oleracea*, *Eucalyptus*
934 *globulus* and *Vicia faba* samples are shown in purple, orange and black, respectively. Boxplots show
935 median (thick black line), interquartile range (IQR) with upper (75%) and lower (25%) quartiles, lower
936 and upper whiskers, which are restricted to $1.5 \cdot \text{IQR}$. Outside the $1.5 \cdot \text{IQR}$ space, the data points are
937 marked with a dot. The notches extend to $\pm 1.58 \cdot \text{IQR} / \sqrt{n}$, by convention and give a 95%
938 confidence interval for the difference of two medians (McGill et al., 1978).
939

940 **Fig. 5:** Scatterplots illustrating the correlation between leaf water-based and measured air/leaf relative
941 humidity [modeled vs. measured RH_{air} (A) and RH_{leaf} (B)], modeled vs. measured leaf water deuterium-
942 excess [T_{air} -based (B) and T_{leaf} -based (E) d_e vs. deuterium-excess_{leaf-water}] and modeled vs. measured LEL
943 slopes [T_{air} -based (C) and T_{leaf} -based (F) vs. measured slopes]. In red, the results of the less simplified
944 models are displayed (Eq. 2 for d_e , Eq. 6 for RH and Eq. 10 for S_{LEL}) and in black the results of the more
945 simplified models are shown (Eq. 3 and d_e , Eq. 7 for RH and Eq. 11 for S_{LEL}). Black lines indicate the 1:1
946 relationship. R^2 and RMSE are calculated as described in section 2.4, while the RMSE values have the
947 dimensions of the respective variables. Error bars for the measured RH values represent analytical
948 standard deviations (see Mayr, 2002). For the uncertainties of the calculated and modeled variables
949 see section 2.4.
950

951 **Fig. 6:** Boxplots showing the measured leaf water in comparison to the biomarker-based leaf water
952 (according Eqs. 8 and 9), tank water, source water calculated with biomarker-based leaf water values
953 and source water based on measured leaf water. Source water isotope compositions were calculated
954 via the slopes of the LEL's (either with biomarker-based or measured leaf water values) and the GMWL.

<https://doi.org/10.5194/bg-2019-427>

Preprint. Discussion started: 4 November 2019

© Author(s) 2019. CC BY 4.0 License.



955 The numbers (1-4) mark the available scenarios for source water reconstruction (see section 2.4): 1 =
956 S_{LEL} calculated according more simplified Eq. 11 with T_{air} , 2 = as 1 but with T_{leaf} , 3 = S_{LEL} calculated
957 according less simplified Eq. 10 with T_{air} , 4 = as 3 but with T_{leaf} . Boxplots show median (thick black line),
958 interquartile range (IQR) with upper (75%) and lower (25%) quartiles, lower and upper whiskers, which
959 are restricted to $1.5 \cdot IQR$. Outside the $1.5 \cdot IQR$ space, the data points are marked with a dot. The
960 notches are extend to $\pm 1.58 \cdot IQR / \sqrt{n}$, by convention and give a 95% confidence interval for the
961 difference of two medians (McGill et al., 1978).

962

963 **Fig. 7:** Scatterplots depicting the relationship between biomarker-based (modeled) and measured
964 air/leaf relative humidity [RH_{air} (A) and RH_{leaf} (B)]. Black lines indicate the 1:1 relationship. R^2 and RMSE
965 was calculated as described in section 2.4, while the RMSE values have the dimensions of the
966 respective variables. Error bars for the measured values represent analytical standard deviations (see
967 Mayr, 2002). For uncertainty calculation of the modeled properties, see section 2.4. In addition, the
968 leaf water-based air/leaf relative humidity results (from Fig. 5A and D) are shown in light colors for
969 comparison.

970

971 **Fig. S1:** Boxplots comprising the plant-specific $\delta^2H_{n-alkane}$ (A) and $\delta^{18}O_{sugar}$ values (B). *Brassica oleracera*,
972 *Eucalyptus globulus* and *Vicia faba* samples are shown in purple, orange and black, respectively.
973 Boxplots show median (thick black line), interquartile range (IQR) with upper (75%) and lower (25%)
974 quartiles, lower and upper whiskers, which are restricted to $1.5 \cdot IQR$. Outside the $1.5 \cdot IQR$ space, the
975 data points are marked with a dot. The notches are extend to $\pm 1.58 \cdot IQR / \sqrt{n}$, by convention and give
976 a 95% confidence interval for the difference of two medians (McGill et al., 1978).

977

978 **Fig. S2:** Scatterplots of the fractionation between the biomarkers and leaf water vs. air temperature,
979 air relative humidity (A and B: $\epsilon_{n-alkane/leaf-water}$ according Eq. 13; C and D $\epsilon_{sugar/leaf-water}$ according Eq. 14).
980 *Brassica oleracera*, *Eucalyptus globulus* and *Vicia faba* samples are shown in purple, orange and black,
981 respectively. Error bars for the measured values represent analytical standard deviations of repeated
982 measurements (see section 2.2 and Mayr, 2002). For uncertainty calculation of the ϵ values, see section
983 2.4.

984

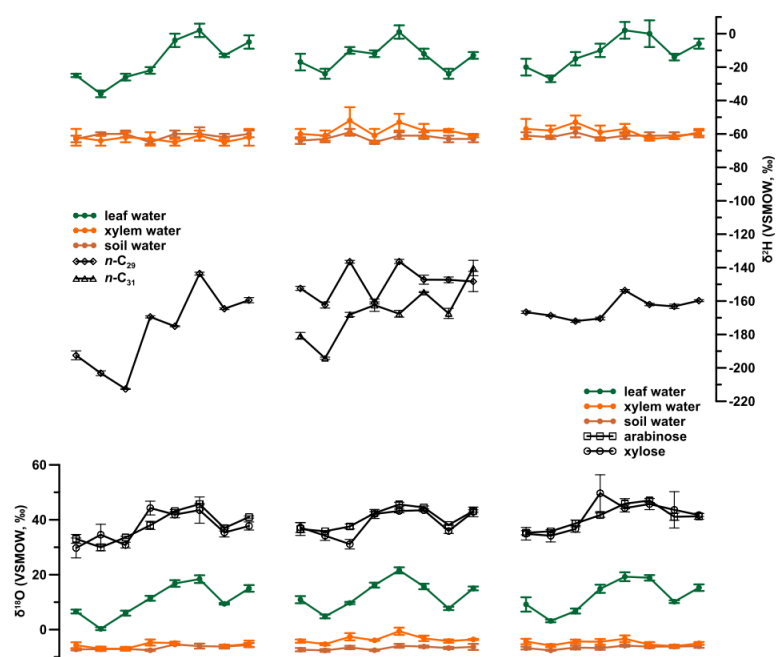
985 **Fig. S3:** Boxplots comprising measured and modeled RH (A) and deuterium-excess values (B). The
986 numbers (1-2) mark the two available models for $RH_{leaf/air}$ and d_e reconstruction (see section 2.4): 1 =
987 more simplified models (Eq. 3 for d_e and Eq. 7 for RH), 2 = less simplified models (Eq. 2 for d_e and Eq. 6
988 for RH). Boxplots show median (thick black line), interquartile range (IQR) with upper (75%) and lower
989 (25%) quartiles, lower and upper whiskers, which are restricted to $1.5 \cdot IQR$. Outside the $1.5 \cdot IQR$ space,
990 the data points are marked with a dot. The notches are extend to $\pm 1.58 \cdot IQR / \sqrt{n}$, by convention and
991 give a 95% confidence interval for the difference of two medians (McGill et al., 1978).

https://doi.org/10.5194/bg-2019-427
 Preprint. Discussion started: 4 November 2019
 © Author(s) 2019. CC BY 4.0 License.

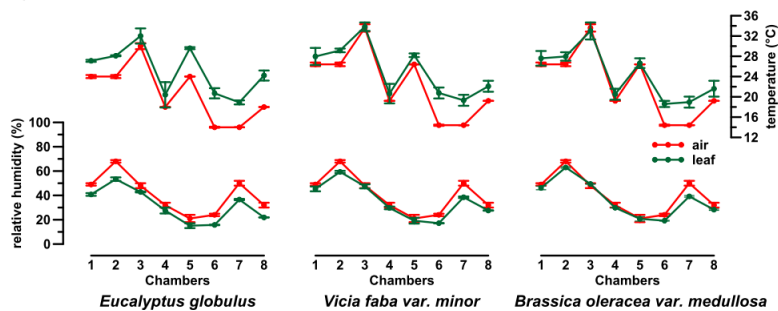


992 Fig. 1

A) water and biomarker $\delta^2\text{H}/\delta^{18}\text{O}$ values



B) climate chamber conditions

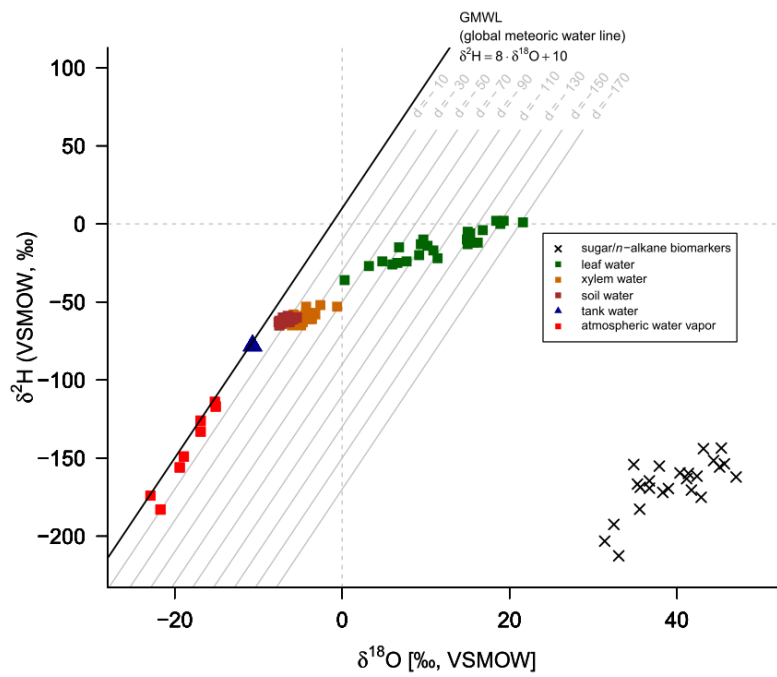


993

<https://doi.org/10.5194/bg-2019-427>
 Preprint. Discussion started: 4 November 2019
 © Author(s) 2019. CC BY 4.0 License.



994 Fig. 2

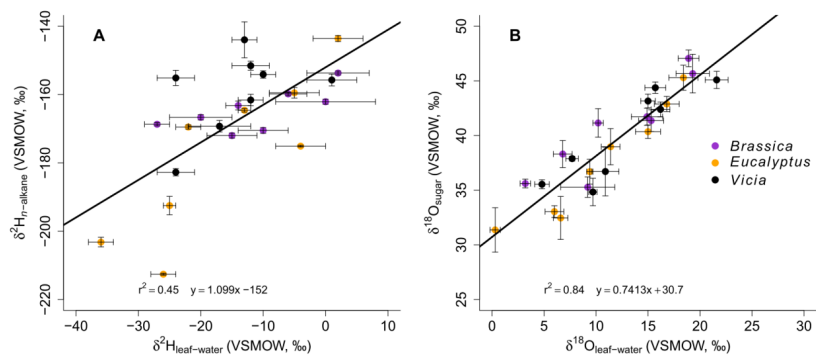


995
 996

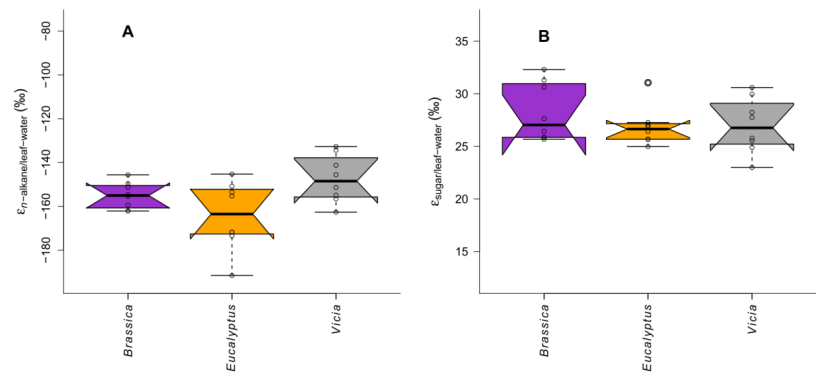
<https://doi.org/10.5194/bg-2019-427>
 Preprint. Discussion started: 4 November 2019
 © Author(s) 2019. CC BY 4.0 License.



997 Fig. 3



998 Fig. 4
 999

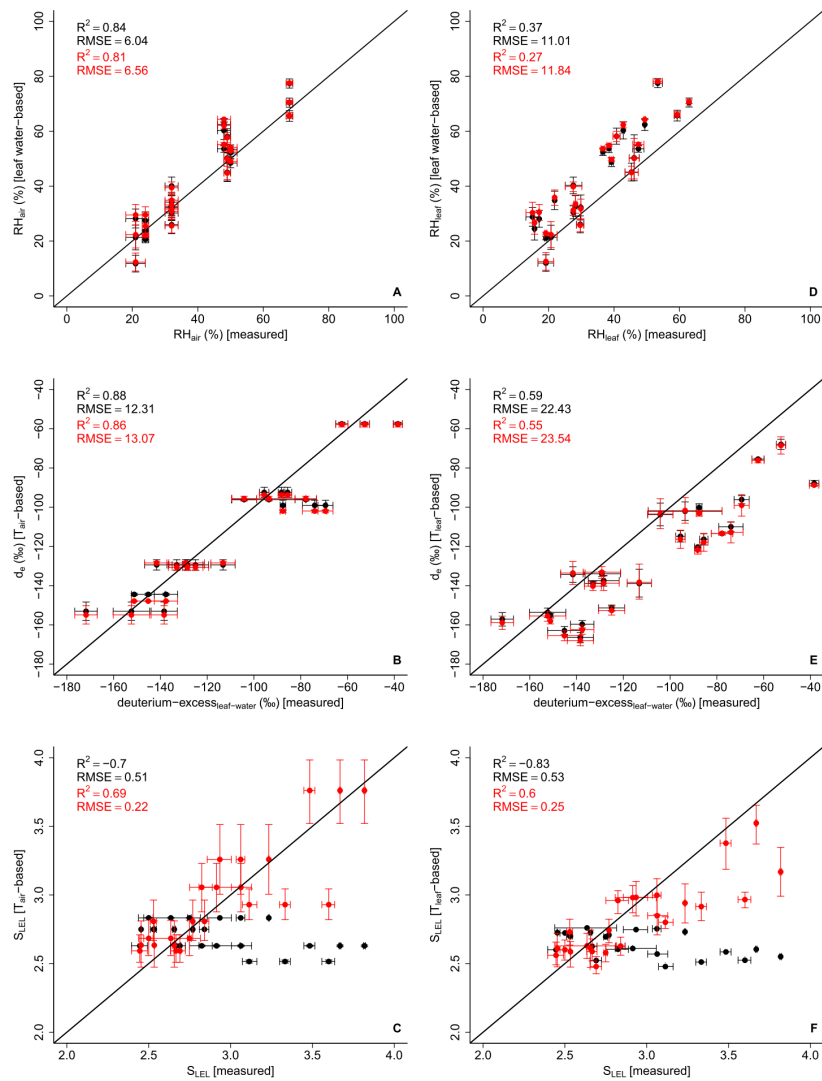


1000
 1001

<https://doi.org/10.5194/bg-2019-427>
 Preprint. Discussion started: 4 November 2019
 © Author(s) 2019. CC BY 4.0 License.



1002 Fig. 5

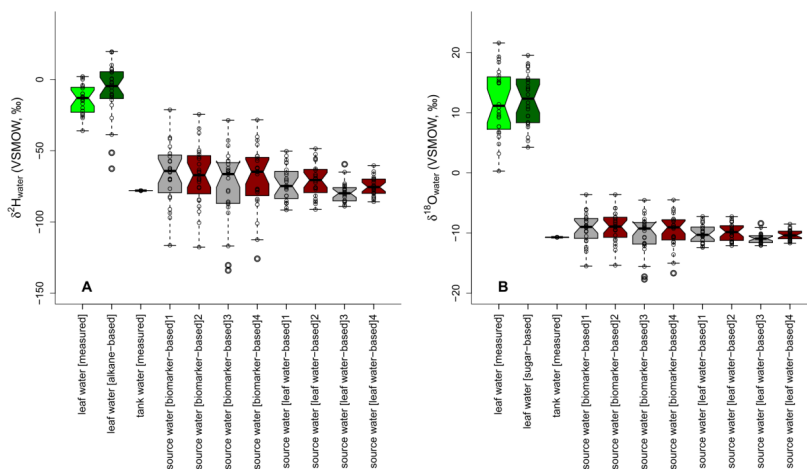


1003
 1004

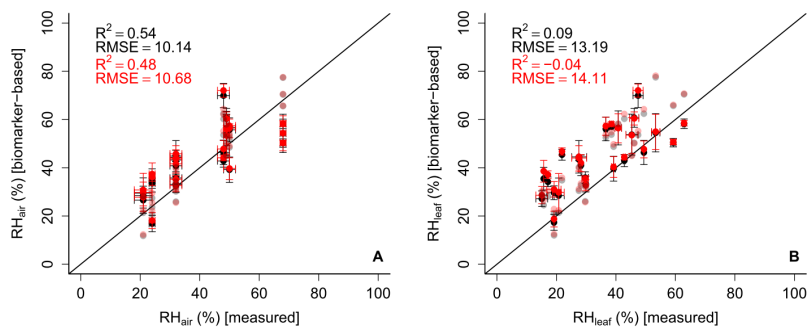
https://doi.org/10.5194/bg-2019-427
 Preprint. Discussion started: 4 November 2019
 © Author(s) 2019. CC BY 4.0 License.



1005 Fig. 6



1006 Fig. 7
 1007

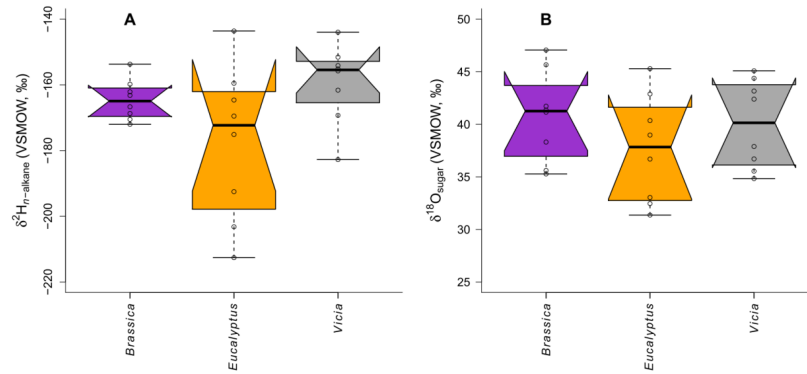


1008
 1009

<https://doi.org/10.5194/bg-2019-427>
 Preprint. Discussion started: 4 November 2019
 © Author(s) 2019. CC BY 4.0 License.



1010 **Fig. S1**

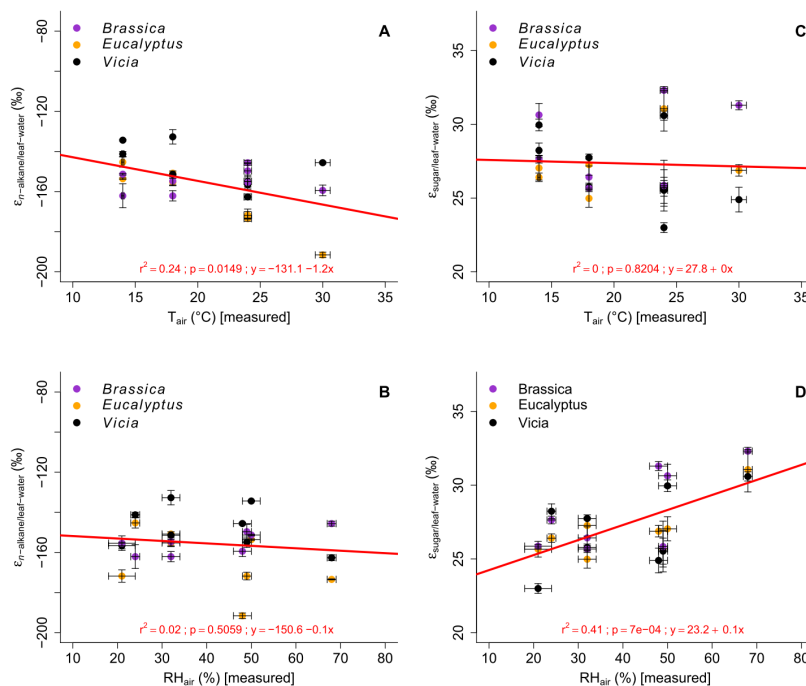


1011
 1012

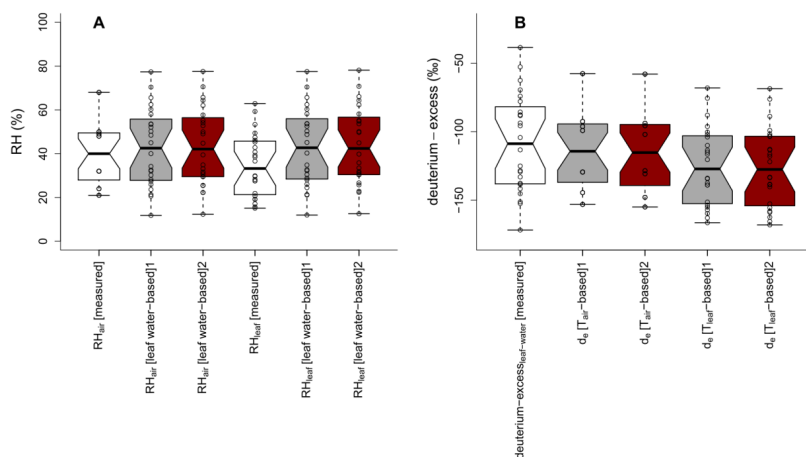
https://doi.org/10.5194/bg-2019-427
 Preprint. Discussion started: 4 November 2019
 © Author(s) 2019. CC BY 4.0 License.



1013 Fig. S2



1014 Fig. S3
 1015



1016

B. Manuscript 2: Hepp et al. (2019b)

submitted to *Biogeosciences*, published in *Biogeosciences Discussion*

<https://doi.org/10.5194/bg-2019-197>

<https://doi.org/10.5194/bg-2019-197>
Preprint. Discussion started: 29 May 2019
© Author(s) 2019. CC BY 4.0 License.



1 **Evaluation of bacterial glycerol dialkyl glycerol tetraether and ²H-**
2 **¹⁸O biomarker proxies along a Central European topsoil transect**

3 Johannes Hepp^{1,2,*}, Imke K. Schäfer³, Verena Lanny⁴, Jörg Franke³, Marcel
4 Bliedtner^{3,a}, Kazimierz Rozanski⁵, Bruno Glaser², Michael Zech^{2,6}, Timothy I.
5 Eglinton⁴, Roland Zech^{3,a}

6 ¹Chair of Geomorphology and BayCEER, University of Bayreuth, 95440 Bayreuth, Germany and

7 ²Institute of Agronomy and Nutritional Sciences, Soil Biogeochemistry, Martin-Luther-University
8 Halle-Wittenberg, 06120 Halle, Germany

9 ³Institute of Geography and Oeschger Centre for Climate Change Research, University of Bern, 3012
10 Bern, Switzerland

11 ⁴Department of Earth Science, ETH Zurich, 8092 Zurich, Switzerland

12 ⁵Faculty of Physics and Applied Computer Science, AGH University of Science and Technology, 30-
13 059 Kraków, Poland

14 ⁶Institute of Geography, Faculty of Environmental Sciences, Technical University of Dresden, 01062
15 Dresden, Germany

16 ^anow at Institute of Geography, Chair of Physical Geography, Friedrich-Schiller University of Jena,
17 07743 Jena, Germany

18

19 *corresponding author (johannes-hepp@gmx.de)

<https://doi.org/10.5194/bg-2019-197>
Preprint. Discussion started: 29 May 2019
© Author(s) 2019. CC BY 4.0 License.



20 **Keywords**

21 Leaf wax *n*-alkanes, hemicellulose sugars, pH, temperature, CBT, MBT^{*}, precipitation
22 $\delta^2\text{H}/\delta^{18}\text{O}$, relative humidity

23 **Abstract**

24 Molecular fossils, like bacterial branched glycerol dialkyl glycerol tetraethers (brGDGTs), and
25 the stable isotopic composition of biomarkers, such as $\delta^2\text{H}$ of leaf wax-derived *n*-alkanes ($\delta^2\text{H}_{n\text{-alkane}}$)
26 or $\delta^{18}\text{O}$ of hemicellulose-derived sugars ($\delta^{18}\text{O}_{\text{sugar}}$) are increasingly used for the
27 reconstruction of past climate and environmental conditions. Plant-derived $\delta^2\text{H}_{n\text{-alkane}}$ and
28 $\delta^{18}\text{O}_{\text{sugar}}$ values record the isotopic composition of plant source water ($\delta^2\text{H}/\delta^{18}\text{O}_{\text{source-water}}$),
29 which usually reflects mean annual precipitation ($\delta^2\text{H}/\delta^{18}\text{O}_{\text{precipitation}}$), modulated by
30 evapotranspirative leaf water enrichment and biosynthetic fractionation. Accuracy and
31 precision of respective proxies should be ideally evaluated at a regional scale. For this study,
32 we analysed topsoils below coniferous and deciduous forests, as well as grassland soils along a
33 Central European transect in order to investigate the variability and robustness of various
34 proxies, and to identify effects related to vegetation. Soil pH-values derived from brGDGTs
35 correlate reasonably well with measured soil pH-values, but systematically overestimate them
36 ($\Delta\text{pH} = 0.6 \pm 0.6$). The branched vs. isoprenoid tetraether index (BIT) can give some indication
37 whether the pH reconstruction is reliable. Temperatures derived from brGDGTs overestimate
38 mean annual air temperatures slightly ($\Delta T_{\text{MA}} = 0.5^\circ\text{C} \pm 2.4$). Apparent isotopic fractionation ($\epsilon_{n\text{-alkane/precipitation}}$
39 and $\epsilon_{\text{sugar/precipitation}}$) is lower for grassland sites than for forest sites due to “signal
40 damping”, i.e. grass biomarkers do not record the full evapotranspirative leaf water enrichment.
41 Coupling $\delta^2\text{H}_{n\text{-alkane}}$ with $\delta^{18}\text{O}_{\text{sugar}}$ allows to reconstruct the stable isotopic composition of the
42 source water more accurately than without the coupled approach ($\Delta\delta^2\text{H} = \sim 21\text{‰} \pm 22$ and
43 $\Delta\delta^{18}\text{O} = \sim 2.9\text{‰} \pm 2.8$). Similarly, relative humidity during daytime and vegetation period
44 (RH_{MDV}) can be reconstructed using the coupled isotope approach ($\Delta\text{RH}_{\text{MDV}} = \sim 17 \pm 12$).
45 Especially for coniferous sites, reconstructed RH_{MDV} values as well as source water isotope
46 composition underestimate the measured values. This can be likely explained by understory
47 grass vegetation at the coniferous sites contributing significantly to the *n*-alkane pool but only
48 marginally to the sugar pool in the topsoil. The large uncertainty likely reflect the fact that
49 biosynthetic fractionation is not constant, as well as microclimate variability. Overall, GDGTs
50 and the coupled $\delta^2\text{H}_{n\text{-alkane}}\text{-}\delta^{18}\text{O}_{\text{sugar}}$ approach have great potential for more quantitative
51 paleoclimate reconstructions.

<https://doi.org/10.5194/bg-2019-197>
 Preprint. Discussion started: 29 May 2019
 © Author(s) 2019. CC BY 4.0 License.



52 **1 Introduction**

53 Information about the variability and consequences of past climate changes is a prerequisite for
 54 precise predictions regarding the present climate change. Molecular fossils, so called
 55 biomarkers, climate proxies have great potential to enhance our understanding about variations
 56 of past climate and environmental changes. Lipid biomarkers in particular, are increasingly
 57 used for paleoclimate and environmental reconstructions (e.g. Brinchat et al., 2000; Eglinton and
 58 Eglinton, 2008; Rach et al., 2014; Romero-Viana et al., 2012; Schreuder et al., 2016). However
 59 strengths and limitations of respective proxies need known (Dang et al., 2016). For this,
 60 calibrations using modern reference samples are essential.

61 Terrestrial branched glycerol dialkyl glycerol tetraethers (brGDGTs) that are synthesized in the
 62 cell membranes of anaerobe heterotrophic soil bacteria (Oppermann et al., 2010; Weijers et al.,
 63 2010) have great potential for the reconstruction of past environmental conditions (e.g. Coffinet
 64 et al., 2017; Schreuder et al., 2016; Zech et al., 2012), although some uncertainties exist.
 65 Calibration studies suggest that the relative abundance of the individual brGDGTs varies with
 66 mean annual air temperature (T_{MA}) and soil pH (Peterse et al., 2012; Weijers et al., 2007), at
 67 least across large, global climate gradients or along pronounced altitudinal gradients (Wang et
 68 al., 2017). However, in arid regions the production of brGDGT is limited, while isoprenoidal
 69 GDGTs (iGDGTs) produced by archaea provide the dominant part of the overall soil GDGT
 70 pool (Anderson et al., 2014; Dang et al., 2016; Dirghangi et al., 2013; Wang et al., 2013; Xie
 71 et al., 2012). The ratio of brGDGTs vs. isoprenoid GDGTs (BIT) can be used as indication
 72 whether a reconstruction of T_{MA} and pH will be reliable. Moreover, Mueller-Niggemann et al.
 73 (2016) revealed an influence of the vegetation cover on the brGDGT producing soil microbes.
 74 From field experiments, it is known, that vegetation type and mulching practice strongly effect
 75 soil temperature and moisture (Awe et al., 2015; Liu et al., 2014). Thus, multiple factors can be
 76 expected to influence soil microbial communities and GDGT production. So far, little is known
 77 about the variability of GDGT proxies on a regional scale, and a calibration study with small
 78 climate gradient but with different vegetation types might be useful.

79 Compound specific stable hydrogen isotopes of leaf wax biomarkers, such as long chain *n*-
 80 alkanes ($\delta^2H_{n-alkanes}$) record the isotopic signal of precipitation and therefore past climate and
 81 environmental conditions (Sachse et al., 2004, 2006). However, various influencing factors are
 82 known all along the way from the moisture source to leaf waxes (Pedentchouk and Zhou, 2018
 83 and Sachse et al., 2012 for review). One is the evapotranspiration of leaf water (Feakins and
 84 Sessions, 2010; Kahmen et al., 2013; Zech et al., 2015), which is strongly driven by relative air
 85 humidity (RH; e.g. Cernusak et al., 2016 for review). In addition, a strong precipitation signal
 86 is known to be incorporated into long chain leaf waxes (Hou et al., 2008; Rao et al., 2009;
 87 Sachse et al., 2004). In paleoclimate studies, it is often not feasible to disentangle between the
 88 evapotranspirative enrichment from the precipitation signal. Zech et al. (2013) proposed to
 89 couple $\delta^2H_{n-alkane}$ results with oxygen stable isotopes of hemicellulose-derived sugars ($\delta^{18}O_{sugar}$).
 90 Assuming constant biosynthetic fractionation factors (ϵ_{bio}) for the different compound classes
 91 (*n*-alkanes and hemicellulose sugars), the coupling enables the reconstruction of the isotopic
 92 composition of leaf water, RH and $\delta^2H/\delta^{18}O$ of plant source water ($\approx \delta^2H/\delta^{18}O$ of precipitation;
 93 Tuthorn et al., 2015). So far, a detailed evaluation of this approach on the European scale, as
 94 well as concerning possible effects related to vegetation changes is missing.

<https://doi.org/10.5194/bg-2019-197>
Preprint. Discussion started: 29 May 2019
© Author(s) 2019. CC BY 4.0 License.



95 We analysed topsoil samples under coniferous, deciduous and grassland vegetation along a
96 Central European transect in order to estimate the variability of the biomarker proxies. More
97 specifically, we aim to test whether:

98 (i) the vegetation type has an influence on the brGDGT proxies, the $\delta^2\text{H}_{n\text{-alkane}}$ and the $\delta^{18}\text{O}_{\text{sugar}}$
99 stable isotopic composition, as well as on reconstructed $\delta^2\text{H}/\delta^{18}\text{O}_{\text{source-water}}$ and RH.

100 (ii) the published brGDGT proxies used for reconstructing mean annual temperature and soil
101 pH are sensitive enough to reflect the medium changes in temperature and soil pH along our
102 transect.

103 (iii) the coupled $\delta^2\text{H}_{n\text{-alkane}}-\delta^{18}\text{O}_{\text{sugar}}$ approach faithfully reflects $\delta^2\text{H}/\delta^{18}\text{O}$ of precipitation and
104 RH along the transect.

105

106 2 Material and methods

107 2.1 Geographical setting and sampling

108 In November 2012, we collected topsoil samples (0-5 cm depth) at 16 locations along a transect
109 from Southern Germany to Southern Sweden (Fig. 1A) and distinguished between sites with
110 coniferous forest (con, $n = 9$), deciduous forest (dec, $n = 14$) and grassland (grass, $n = 6$)
111 vegetation cover (for more details see Schäfer et al. (2016) and Tab. S1).

112

113 2.2 Database of instrumental climate variables and isotope composition of precipitation

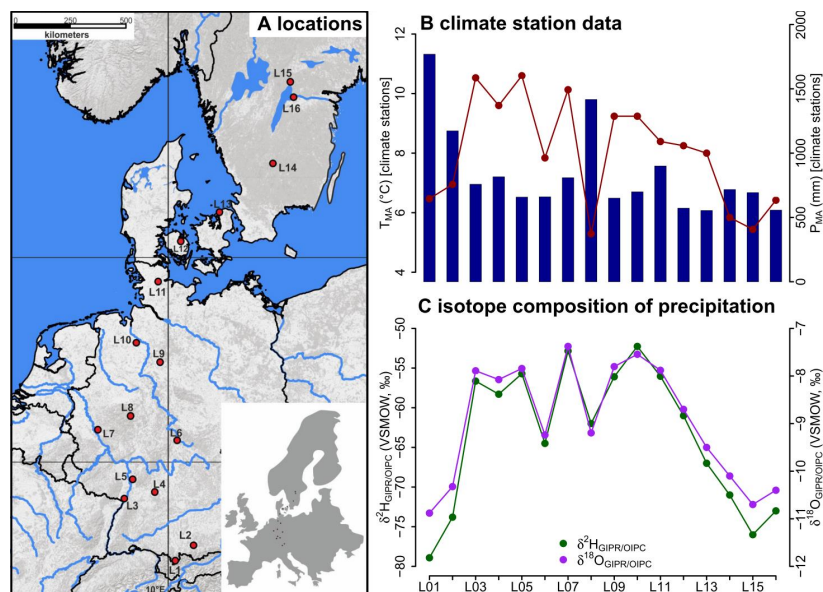
114 Climate data was derived from close-by weather observation stations operating by the regional
115 institutions (Deutscher Wetterdienst (DWD) for Germany, Danmarks Meteorologiske Institut
116 (DMI) for Denmark and the Sveriges Meteorologiska och Hydrologiska Institute (SMHI) for
117 Sweden). The DWD provides hourly data for each station (DWD Climate Data Center, 2018b),
118 enabling not only the calculation of T_{MA} , but also of the mean annual relative air humidity
119 (RH_{MA}), mean temperature and relative air humidity during the vegetation period (T/RH_{MV}),
120 and of daytime temperature and relative humidity averages over the vegetation period
121 (T/RH_{MDV}). In addition, annual precipitation observations were used to derive the mean annual
122 precipitation amount (P_{MA} ; DWD Climate Data Center, 2018b). From the DMI, the respective
123 climate variables were derived from published technical reports (Cappelen, 2002; Frich et al.,
124 1997; Laursen et al., 1999). The SMHI provides open data from which we derived the climate
125 variables for the Swedish sites (Swedish Meteorological and Hydrological Institute, 2018). For
126 more details about the climate database used for calculations and comparisons, the reader is
127 referred to Tab. S2.

128 For comprising German precipitation $\delta^2\text{H}/\delta^{18}\text{O}$ along the transect, we realized a regionalisation
129 (called $\delta^2\text{H}/\delta^{18}\text{O}_{\text{GIPR}}$) using online available data from 34 German GNIP stations, 4 Austrian
130 ANIP stations and the Groningen GNIP station (van Geldern et al., 2014; IAEA/WMO, 2018;
131 Stumpp et al., 2014; Umweltbundesamt GmbH, 2018), following the approach of Schlotter
132 (2007). However, instead of the multivariate regression procedure applied by Schlotter (2007),
133 we used a random forest approach (Hothorn et al., 2006; Strobl et al., 2007, 2008) to describe
134 the relationship of squared latitude, latitude, longitude and altitude vs. long term weighted
135 means of precipitation $\delta^2\text{H}/\delta^{18}\text{O}$, and realized the prediction for the study sites. For the Danish

https://doi.org/10.5194/bg-2019-197
 Preprint. Discussion started: 29 May 2019
 © Author(s) 2019. CC BY 4.0 License.



136 and Swedish sites, such a procedure was not possible. Hence, the annual precipitation $\delta^2\text{H}/\delta^{18}\text{O}$
 137 values were derived from the Online Isotopes in Precipitation Calculator (OIPC, version 3.1),
 138 therefore called $\delta^2\text{H}/\delta^{18}\text{O}_{\text{OIPC}}$ (Bowen, 2018; Bowen and Revenaugh, 2003; IAEA/WMO,
 139 2015). The finally used $\delta^2\text{H}/\delta^{18}\text{O}_{\text{GIPR/OIPC}}$ data are given in Tab. S1.
 140 The T_{MA} along the transect ranges from 5.3 to 10.6°C, and P_{MA} ranges from 554 to 1769 mm
 141 (Fig. 1B). Precipitation $\delta^2\text{H}/\delta^{18}\text{O}$ shows moderate changes along the transect, $\delta^2\text{H}_{\text{GIPR/OIPC}}$
 142 varies between -52 and -79‰, and $\delta^{18}\text{O}_{\text{GIPR/OIPC}}$ ranges from -7.4 to -10.9‰ (Fig. 1C).
 143 Correlations between $\delta^{18}\text{O}_{\text{GIPR/OIPC}}$ and P_{MA} , altitude of the locations, T_{MA} are given in the
 144 supplementary material (Fig. S1 to S3), along with a $\delta^2\text{H}_{\text{GIPR/OIPC}}$ vs. $\delta^{18}\text{O}_{\text{GIPR/OIPC}}$ scatter plot
 145 (Fig. S4).



146 **Fig. 1.** (A) Sample locations (red dots, map source: US National Park Service), (B) variations
 147 of mean annual air temperature (T_{MA}) and mean annual precipitation (P_{MA}) derived from close-
 148 by climate station data, and (C) hydrogen and oxygen stable isotope composition of
 149 precipitation ($\delta^2\text{H}_{\text{GIPR/OIPC}}$ and $\delta^{18}\text{O}_{\text{GIPR/OIPC}}$, respectively) as derived for the sampled transect
 150 locations (see section 2.2 GIPR $\delta^2\text{H}/\delta^{18}\text{O}$ generation procedure). The reader is referred to
 151 section 2.2 (and Tab. S1 and S2) for database and reference information of data plotted in (B)
 152 and (C).
 153

154

155 2.3 Soil extractions and analysis

156 2.3.1 GDGTs and pH

157 A detailed description of sample preparation for lipid analysis can be found in Schäfer et al.
 158 (2016). Briefly, 1–6 g freeze-dried and grounded soil sample was microwave extracted with 15

<https://doi.org/10.5194/bg-2019-197>
Preprint. Discussion started: 29 May 2019
© Author(s) 2019. CC BY 4.0 License.



159 ml dichloromethane (DCM)/methanol (MeOH) 9:1 (*v:v*) at 100°C for 1 h. Extracts were
160 separated over aminopropyl silica gel (Supelco, 45 µm) pipette columns. The nonpolar fraction
161 (including *n*-alkanes) was eluted with hexane and further purified over AgNO₃ coated silica
162 pipette columns (Supelco, 60-200 mesh) and zeolite (Geokleen Ltd.). The GDGT-containing
163 fraction was eluted with DCM:MeOH 1:1 (*v:v*), re-dissolved in hexane/isopropanol (IPA) 99:1
164 (*v:v*) and transferred over 0.45 µm PTFE filters into 300 µl inserts. For quantification, a known
165 amount of a C₄₆ diol standard was added after transfer. The samples were analysed at ETH
166 Zurich using an Agilent 1260 Infinity series HPLC–atmospheric chemical pressure ionization
167 mass spectrometer (HPLC–APCI-MS) equipped with a Grace Prevail Cyano column (150 mm
168 × 2.1 mm; 3 µm). The GDGTs were eluted isocratically with 90% A and 10% B for 5 min and
169 then with a linear gradient to 18% B for 34 min at 0.2 ml min⁻¹, where A=hexane and
170 B=hexane/isopropanol (9:1, *v:v*). Injection volume was 10 µl and single ion monitoring of
171 [M+H]⁺ was used to detect GDGTs.

172 The pH of the samples was measured in the laboratory of the Soil Biogeochemistry group,
173 Institute of Agronomy and Nutritional Sciences, Martin-Luther-University Halle-Wittenberg,
174 in a 1:3 soil:water (*w/v*) mixture.

175

176 2.3.2 δ²H_{*n*-alkane}

177 The hydrogen isotopic composition of the highest concentrated *n*-alkanes (*n*-C₂₅, *n*-C₂₇, *n*-C₂₉,
178 *n*-C₃₁, and *n*-C₃₃) was determined using a TRACE GC Ultra Gas Chromatography connected to
179 a Delta V Plus Isotope Ratio Mass Spectrometer via a ²H pyrolysis reactor (GC-²H-Py-IRMS;
180 Thermo Scientific, Bremen, Germany) at the ETH Zurich. The compound-specific ²H/¹H ratios
181 were calibrated against an external standard with C₁₅ – C₃₅ homologues. External standard
182 mixtures (A4 mix from A. Schimmelmann, University of Indiana) were run between the
183 samples for multipoint linear normalization. The H⁺³ factor was determined on each
184 measurement day and was constant throughout the periods of the sample batches. Samples were
185 analysed in duplicates, and results typically agreed within 4% (average difference = 1.4%). All
186 δ²H values are expressed relative to the Vienna Standard Mean Ocean Water (V-SMOW).

187

188 2.3.3 δ¹⁸O_{sugar}

189 Hemicellulose sugars were extracted and purified using a slightly modified standard procedure
190 (Amelung et al., 1996; Guggenberger et al., 1994; Zech and Glaser, 2009). Briefly, myoinositol
191 was added to the samples prior to extraction as first internal standard. The sugars were released
192 hydrolytically using 4M trifluoroacetic acid for 4 h at 105°C, cleaned over glass fiber filters and
193 further purified using XAD and Dowex columns. Before derivatization with methylboronic acid
194 (Knapp, 1979), the samples were frozen, freeze-dried, and 3-O-methylglucose in dry pyridine
195 was added as second internal standard. Compound-specific hemicellulose sugar ¹⁸O
196 measurements were performed in the laboratory of the Soil Biogeochemistry group, Institute of
197 Agronomy and Nutritional Sciences, Martin-Luther-University Halle-Wittenberg, using GC-
198 ¹⁸O-Py-IRMS (all devices from Thermo Fisher Scientific, Bremen, Germany). Standard
199 deviations of the triplicate measurements were 1.4‰ (over 29 investigated samples) for
200 arabinose and xylose, respectively. We focus on these two hemicellulose-derived neutral sugars

https://doi.org/10.5194/bg-2019-197
 Preprint. Discussion started: 29 May 2019
 © Author(s) 2019. CC BY 4.0 License.



201 arabinose and xylose as they strongly predominate over fucose in terrestrial plants, soils and
 202 sediments (Hepp et al., 2016 and references therein). Rhamnose concentrations were too low to
 203 obtain reliable $\delta^{18}\text{O}$ results. All $\delta^{18}\text{O}$ values are expressed relative to the Vienna Standard Mean
 204 Ocean Water (V-SMOW).

205

206 2.4 Theory and Calculations

207 2.4.1 Calculations used for the GDGT-based reconstructions

208 The branched and isoprenoid tetraether (BIT) index is calculated according to Hopmans et al.
 209 (2004), for structures see Fig. S5:

$$210 \quad \text{BIT} = \frac{\text{Ia} + \text{IIa} + \text{IIIa}}{\text{Ia} + \text{IIa} + \text{IIIa} + \text{crenarchaeol}} \quad (1)$$

211 The cyclopentane moiety number of brGDGTs correlates negatively with soil pH (Weijers et
 212 al., 2007), which led to the development of the cyclization of branched tetraethers (CBT) ratio.
 213 CBT and the CBT based pH (pH_{CBT}) were calculated according to Peterse et al. (2012):

$$214 \quad \text{CBT} = -\log \frac{\text{Ib} + \text{IIb}}{\text{Ia} + \text{IIa}}, \quad (2)$$

$$215 \quad \text{pH}_{\text{CBT}} = 7.9 - 1.97 \times \text{CBT}. \quad (3)$$

216 The number of methyl groups in brGDGTs correlates negatively with T_{MA} and soil pH (Peterse
 217 et al., 2012; Weijers et al., 2007). Thus, the ratio of the methylation of branched tetraethers
 218 (MBT) ratio and the CBT ratio can be used to reconstruct T_{MA} . We use the equation given by
 219 Peterse et al. (2012):

$$220 \quad \text{MBT}' = \frac{\text{Ia} + \text{Ib} + \text{Ic}}{\text{Ia} + \text{Ib} + \text{Ic} + \text{IIa} + \text{IIb} + \text{IIc} + \text{IIIa}}, \quad (4)$$

$$221 \quad T_{\text{MA}} = 0.81 - 5.67 \times \text{CBT} + 31.0 \times \text{MBT}'. \quad (5)$$

222

223 2.4.2 Calculations and concepts used for the coupled $\delta^2\text{H}$ - $\delta^{18}\text{O}$ approach

224 The apparent fractionation is calculated according to Cernusak et al. (2016):

$$225 \quad \varepsilon_{n\text{-alkane/precipitation}} = \left(\frac{\delta^2\text{H}_{n\text{-alkane}} - \delta^2\text{H}_{\text{GIPR/OIPC}}}{1 + \delta^2\text{H}_{\text{GIPR/OIPC}}/1000} \right), \quad (6)$$

$$226 \quad \varepsilon_{\text{sugar/precipitation}} = \left(\frac{\delta^{18}\text{O}_{\text{sugar}} - \delta^{18}\text{O}_{\text{GIPR/OIPC}}}{1 + \delta^{18}\text{O}_{\text{GIPR/OIPC}}/1000} \right). \quad (7)$$

227 The isotopic composition of leaf water ($\delta^2\text{H}/\delta^{18}\text{O}_{\text{leaf water}}$) can be calculated using ε_{bio} for $\delta^2\text{H}_{n\text{-alkane}}$
 228 alkane (-160‰, Sachse et al., 2012; Sessions et al., 1999) and $\delta^{18}\text{O}_{\text{sugar}}$ (+27‰, Cernusak et al.,
 229 2003; Schmidt et al., 2001):

$$230 \quad \delta^2\text{H}_{\text{leaf water}} = \left(\frac{1000 + \delta^2\text{H}_{n\text{-alkane}}}{1000 + \varepsilon_{\text{bio}}(n\text{-alkane})} \right) \times 10^3 - 1000, \quad (8)$$

$$231 \quad \delta^{18}\text{O}_{\text{leaf water}} = \left(\frac{1000 + \delta^{18}\text{O}_{\text{sugar}}}{1000 + \varepsilon_{\text{bio}}(\text{sugar})} \right) \times 10^3 - 1000. \quad (9)$$

232 Zech et al. (2013) introduced the conceptual model for the coupled $\delta^2\text{H}_{n\text{-alkane}}$ - $\delta^{18}\text{O}_{\text{sugar}}$ approach
 233 in detail. Briefly, the coupled approach is based on the following assumptions (illustrated in
 234 Fig. 8): (i) The isotopic composition of precipitation, which is set to be equal to the plant source
 235 water, typically plots along the global meteoric water line (GMWL; $\delta^2\text{H} = 8 \times \delta^{18}\text{O} + 10$) in a

https://doi.org/10.5194/bg-2019-197
 Preprint. Discussion started: 29 May 2019
 © Author(s) 2019. CC BY 4.0 License.



236 $\delta^{18}\text{O}$ vs. $\delta^2\text{H}$ space (Craig, 1961); (ii) Source water uptake by plants does not lead to any
 237 fractionation (e.g. Dawson et al., 2002), and significant evaporation of soil water can be
 238 excluded; (iii) Evapotranspiration leads to enrichment of the remaining leaf water along the
 239 local evaporation line (LEL; Allison et al., 1985; Bariac et al., 1994; Walker and Brunel, 1990),
 240 compared to the source water taken up by the plant; (iv) The biosynthetic fractionation is
 241 assumed to be constant. In addition, isotopic equilibrium between plant source water (~
 242 weighted mean annual precipitation) and the local atmospheric water vapour is assumed.
 243 Further assumption concerns the isotope steady-state in the evaporating leaf water reservoir.
 244 The coupled approach allows for reconstructing the isotopic composition of plant source water
 245 ($\delta^2\text{H}/\delta^{18}\text{O}_{\text{source-water}}$) from the reconstructed leaf water, by calculating the intercepts of the LELs
 246 with the GMWL (Zech et al., 2013). The slope of the LEL (S_{LEL}) can be assessed by the
 247 following equation (Gat, 1971):

$$248 \quad S_{\text{LEL}} = \frac{\varepsilon_2^* + C_k^2}{\varepsilon_{18}^* + C_k^{18}}, \quad (10)$$

249 where ε^* are equilibrium isotope fractionation factors and C_k are kinetic fractionation factors.
 250 The latter equals to 25.1‰ and 28.5‰, for C_k^2 and C_k^{18} , respectively (Merlivat, 1978). The
 251 equilibrium fractionation factors can be derived from empirical equations (Horita and
 252 Wesolowski, 1994) by using T_{MDV} values. For two Danish sites T_{MDV} are not available, instead
 253 T_{MV} is used here (section 2.2 and Tab. S2).

254 In a $\delta^{18}\text{O}$ - $\delta^2\text{H}$ diagram, the distance of the leaf water from the GMWL define the deuterium-
 255 excess of leaf water ($d_{\text{leaf-water}} = \delta^2\text{H}_{\text{leaf-water}} - 8 \times \delta^{18}\text{O}_{\text{leaf-water}}$, according Dansgaard, (1964); Fig.
 256 8). To convert $d_{\text{leaf-water}}$ into mean RH during daytime and vegetation period (RH_{MDV}), a
 257 simplified Craig-Gordon model can be applied (Zech et al., 2013):

$$258 \quad \text{RH} = 1 - \frac{\Delta d}{\varepsilon_2^* - 8 \times \varepsilon_{18}^* + C_k^2 - 8 \times C_k^{18}}, \quad (11)$$

259 where Δd is the difference in $d_{\text{leaf-water}}$ and the deuterium-excess of source water ($d_{\text{source-water}}$).

260

261 2.5 Statistics

262 In the statistical analysis we checked sample distributions for normality (Shapiro and Wilk,
 263 1965) and for equal variance (Levene, 1960). If normality and equal variances are given, we
 264 perform an Analysis of Variance (ANOVA). If that is not the case, we conduct the non-
 265 parametric Kruskal-Wallis Test. ANOVA or Kruskal-Wallis are used to find significant
 266 differences ($\alpha=0.05$) between the vegetation types (deciduous, conifer and grass).

267 In order to describe the relation along a 1:1 line, the coefficient of correlation (R^2) was
 268 calculated as $R^2 = 1 - \frac{\sum(\text{modeled} - \text{measured})^2}{\sum(\text{measured} - \text{measured mean})^2}$. The small
 269 r^2 is taken as coefficient of correlation of a linear regression between a dependent (y) and
 270 explanatory variable(s). The root mean square error (RMSE) of the relationships was calculated

271 as $\text{RMSE} = \sqrt{\left(\frac{1}{n} \cdot \sum(\text{modeled} - \text{measured})^2\right)}$. All data plotting and statistical analysis was
 272 realized in R (version 3.2.2; R Core Team, 2015).

273

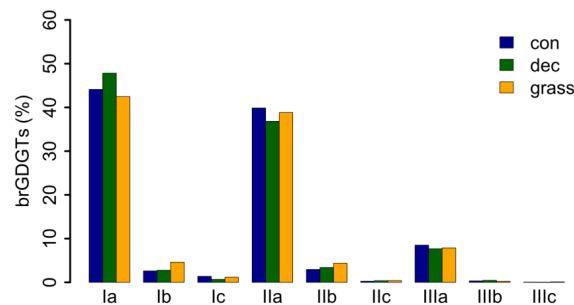
https://doi.org/10.5194/bg-2019-197
 Preprint. Discussion started: 29 May 2019
 © Author(s) 2019. CC BY 4.0 License.



274 3 Results and Discussion

275 3.1 GDGT concentrations

276 GDGT Ia has the highest concentration under all vegetation types, followed by GDGT IIa and
 277 GDGT IIIa (Fig. 2). GDGT Ib, IIb and Ic occur in minor, GDGT IIc and IIIb only in trace
 278 amounts. GDGT IIIc was below the detection limit in most of the samples (Tab. S3). Although
 279 other studies document an influence of the vegetation cover on soil temperature and soil water
 280 content, which control the microbial community composition in soils (Awe et al., 2015; Liu et
 281 al., 2014; Mueller-Niggemann et al., 2016), we find no statistically different pattern of the
 282 individual brGDGTs.



283

284 **Fig. 2.** Mean concentrations of individual brGDGTs as percentage of all brGDGTs for the three
 285 investigated types. Abbreviations: con = coniferous forest sites (n=9); dec = deciduous forest
 286 sites (n=14); grass = grassland sites (n=6).

287 Total concentrations of brGDGTs range from 0.32 to 9.17 $\mu\text{g/g}$ dry weight and tend to be
 288 highest for the coniferous samples and lowest for the grasses (Fig. 3A, Tab. S3). Bulk brGDGT
 289 concentrations lie within ranges of other studies examining soils of mid latitude regions (Huguet
 290 et al., 2010b, 2010a; Weijers et al., 2011). Similar concentrations in coniferous and deciduous
 291 samples imply that brGDGT production does not strongly vary in soils below different forest
 292 types. The grass samples show lower brGDGT concentrations compared to the forest samples,
 293 but this is probably mainly due to ploughing of the grass sites and hence admixing of mineral
 294 subsoil material. Anyhow, the differences in brGDGT concentrations are not significant (p-
 295 value = 0.06).

296

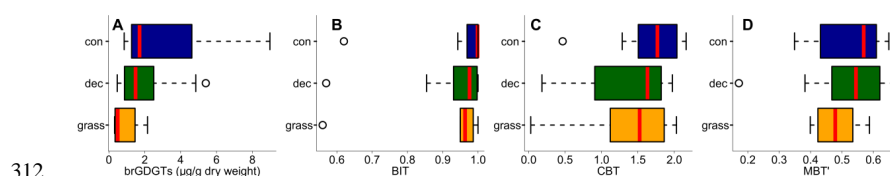
297 3.2 BIT index

298 Most of the samples have a BIT index higher than 0.9 (Fig 3B and Tab. S3). The BIT-values
 299 are typical for soils in humid and temperate climate regions (Weijers et al., 2006). However,
 300 outliers exist. The most likely source of iGDGTs in soils are Thaumarchaeota, i.e. aerobic
 301 ammonia oxidizing archaea producing Crenarchaeol and its regioisomer (Schouten et al., 2013
 302 and references therein), precipitation amounts drop below 700-800 mm (Dang et al., 2016;
 303 Dirghangi et al., 2013). The P_{MA} data of our sampling sites mostly show precipitation > 550
 304 mm (Fig. 1B), but one has to be aware that this data is based on the climate station nearest to
 305 the respective sampling locations and microclimate effects, such as sunlight exposure, canopy

https://doi.org/10.5194/bg-2019-197
 Preprint. Discussion started: 29 May 2019
 © Author(s) 2019. CC BY 4.0 License.



306 cover or exposition might have a pronounced influence on the brGDGT vs. iGDGT distribution.
 307 Mueller-Niggemann et al. (2016) found higher BIT indices in upland soils compared to paddy
 308 soils and stated that the management type also influences BIT values in soils. Along our
 309 transect, grass sites tend to have slightly lower BIT-values than forest sites, probably due to the
 310 absence of a litter layer and hence, no isolation mechanism preventing evaporation of soil water.
 311 Anyhow, differences between vegetation types are not significant (p-value = 0.32).



312
 313 **Fig. 3.** (A) Total concentrations of brGDGTs in $\mu\text{g g}^{-1}$ dry weight, as well as (B) BIT, (C) CBT
 314 and (D) MBT'. Abbreviations: con = coniferous forest sites (n=9); dec = deciduous forest sites
 315 (n=14); grass = grassland sites (n=6). Box plots show median (red line), interquartile range
 316 (IQR) with upper (75%) and lower (25%) quartiles, lowest whisker still within 1.5IQR of lower
 317 quartile, and highest whisker still within 1.5IQR of upper quartile, dots mark outliers.

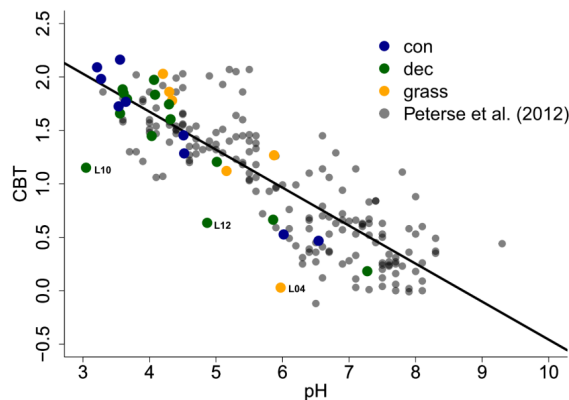
318

319 3.3 CBT-derived pH

320 The CBT ratio shows a pronounced variation independent of vegetation type with values
 321 between 0.03 and 2.16 (Fig 3C). The coniferous samples tend to be highest, but the differences
 322 between vegetation types are not significant (p-value = 0.48). The CBT index can be related to
 323 pH in acidic and/or humid soils (e.g. Dirghangi et al., 2013; Mueller-Niggemann et al., 2016;
 324 Peterse et al., 2012; Weijers et al., 2007) but might be an indicator of soil water content and
 325 hence, precipitation in more arid and alkaline soils (e.g. Dang et al., 2016). There is a
 326 pronounced correlation between CBT and soil pH (Fig. 4), which is in good agreement with
 327 other studies from mid latitude regions where precipitation is relatively high (Anderson et al.,
 328 2014 and references therein). Moreover, the CBT to pH relationship in terms of slope and
 329 intersect in our dataset ($\text{CBT} = -0.47 \times \text{pH} + 3.5$, $r^2 = 0.7$, p-value < 0.0001, n = 29) is well
 330 comparable to the correlation described for the global calibration dataset of Peterse et al. (2012)
 331 ($\text{CBT} = -0.36 \times \text{pH} + 3.1$, $r^2 = 0.7$, p-value < 0.0001, n = 176).

332 However, there are some outliers in the CBT-pH correlation, which need a further examination
 333 (see locations grass L04, dec L10 and dec L12 as marked in Figs. 4 and 5). The outliers show
 334 lower BIT indices (< 0.85, Tab. S3). Even though the data from the nearest climate station
 335 suggest no abnormal P_{MA} . Local effects such as differences in the amount of sunlight exposure,
 336 nutrient availability for brGDGT producing organisms or, most likely soil water content might
 337 influence the brGDGT production at these locations (Anderson et al., 2014; Dang et al., 2016).
 338 A lower BIT index as well as a lower CBT occur when soil water content decreases (Dang et
 339 al., 2016; Sun et al., 2016) or when aeration is high and less anoxic microhabitats for GDGT
 340 producing microbes exist (e.g. Dirghangi et al., 2013).

https://doi.org/10.5194/bg-2019-197
 Preprint. Discussion started: 29 May 2019
 © Author(s) 2019. CC BY 4.0 License.

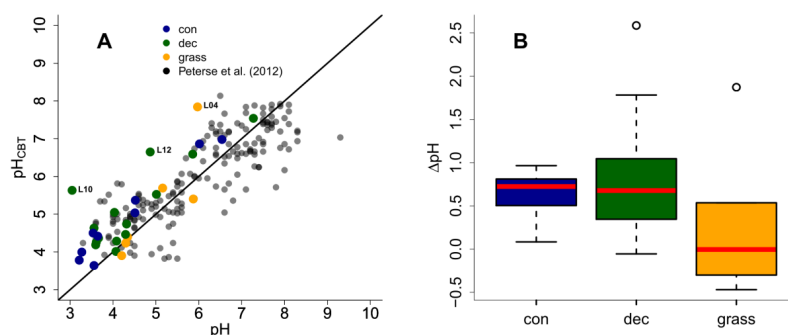


341

342 **Fig. 4.** CBT to pH relationship in our dataset in comparison to the global calibration dataset
 343 from Peterse et al. (2012) ($CBT = -0.36 \times pH + 3.1$, $r^2 = 0.7$, p -value < 0.0001 , $n = 176$, black
 344 line). Abbreviations: con = coniferous forest sites ($n=9$); dec = deciduous forest sites ($n=14$);
 345 grass = grassland sites ($n=6$).

346

347 As the CBT and pH are similarly correlated in our dataset and the global dataset of Peterse et
 348 al. (2012), the CBT-derived pH correlated well with the actual pH (Fig. 5A; $R^2 = 0.3$).
 349 Expressed as ΔpH (CBT-derived pH - measured pH), there is a tendency that the GDGTs result
 350 in an overestimation of the real pH for the forest sites (Fig. B). Yet a Kruskal-Wallis test shows
 351 no statistically significant difference between the vegetation types, with a p -value of 0.13. The
 352 overall ΔpH of 0.6 ± 0.6 shows that the reconstruction of soil pH using brGDGTs works well
 353 along this transect.



354

355 **Fig. 5.** (A) Correlation between measured pH and reconstructed soil pH (pH_{CBT}) from our
 356 transect data in comparison to the global calibration dataset from Peterse et al. (2012) ($R^2 = 0.7$,
 357 $RMSE = 0.75$, $n = 176$). Black line indicates the 1:1 relationship. (B) Boxplots of ΔpH (refers
 358 to $pH_{CBT} - pH$). Box plots show median (red line), interquartile range (IQR) with upper (75%)

https://doi.org/10.5194/bg-2019-197
 Preprint. Discussion started: 29 May 2019
 © Author(s) 2019. CC BY 4.0 License.

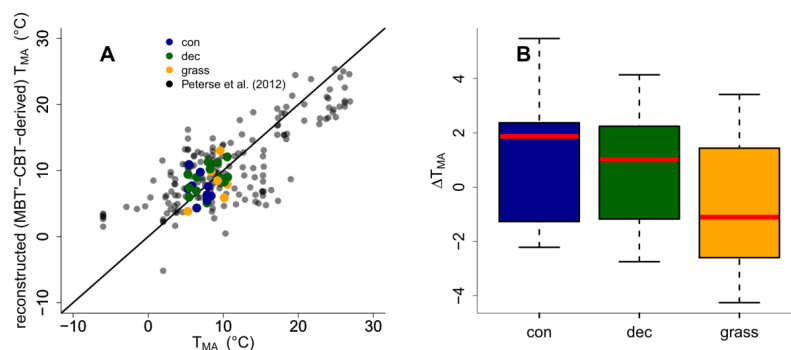


359 and lower (25%) quartiles, lowest whisker still within 1.5IQR of lower quartile, and highest
 360 whisker still within 1.5IQR of upper quartile, dots mark outliers. Abbreviations: con =
 361 coniferous forest sites (n=9); dec = deciduous forest sites (n=14); grass = grassland sites (n=6).

362

363 3.4 MBT^l-CBT-derived T_{MA} reconstructions

364 The MBT^l shows high variability with values ranging from 0.17 to 0.67 no statistical
 365 differences between vegetation types (p-value = 0.54; Fig. 3D, Tab. S3). When comparing
 366 reconstructed (MBT^l-CBT-derived) T_{MA} with climate station T_{MA}, the data plot close to the 1:1
 367 line, and fit well into the global dataset of Peterse et al. (2012) (Fig. 7A). The ΔT_{MA} reveal an
 368 overall offset of $0.5^{\circ}\text{C} \pm 2.4$ and there is no statistically difference between vegetation types
 369 (Fig. 7B). The standard deviation in ΔT_{MA} of ± 2.4 is well in line with the RMSE of 5.0 for the
 370 global calibration dataset (Peterse et al., 2012).



371 **Fig. 6.** (A) Correlation between climate station T_{MA} and reconstructed (MBT^l-CBT-derived)
 372 T_{MA}. For comparison, the global calibration dataset from Peterse et al. (2012) is shown. The
 373 black line indicates the 1:1 relationship. (B) Boxplots of ΔT_{MA} (refers to reconstructed T_{MA}-
 374 T_{MA} from climate stations) in the different vegetation types from our transect study. Box plots
 375 show median (red line), interquartile range (IQR) with upper (75%) and lower (25%) quartiles,
 376 lowest whisker still within 1.5IQR of lower quartile, and highest whisker still within 1.5IQR of
 377 upper quartile, dots mark outliers. Abbreviations: con = coniferous forest sites (n=9); dec =
 378 deciduous forest sites (n=14); grass = grassland sites (n=6).

380

381 3.5 Apparent fractionation of $\delta^2\text{H}$ and $\delta^{18}\text{O}$ in the different vegetation types

382 The $\delta^2\text{H}$ values could be obtained for *n*-alkanes C₂₇, C₂₉ and C₃₁ in all samples and additionally
 383 at two locations for *n*-C₂₅ and *n*-C₃₃ at six other locations. The $\delta^2\text{H}_{n\text{-alkane}}$ values, calculated as
 384 mean of *n*-C₂₅ to *n*-C₃₁ $\delta^2\text{H}$, ranges from -156 to -216‰. Pooled standard deviations show an
 385 overall average of 3.6‰. The $\delta^{18}\text{O}_{\text{sugar}}$ values, calculated as the area weighted means for
 386 arabinose and xylose, ranges from 27.7 to 39.4‰. The average weighted mean standard
 387 deviation is 1.4‰. The compound-specific isotope data is summarized along with the
 388 calculations in Tab. S4.

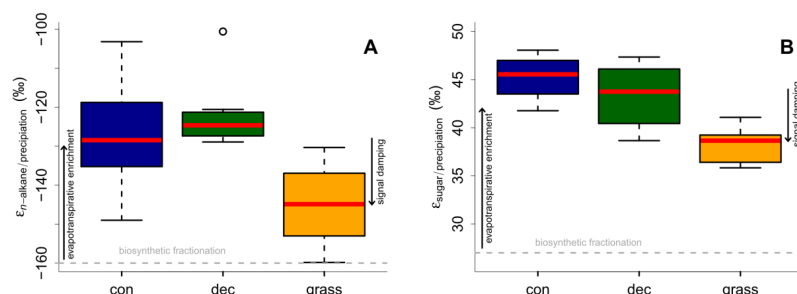
https://doi.org/10.5194/bg-2019-197
 Preprint. Discussion started: 29 May 2019
 © Author(s) 2019. CC BY 4.0 License.



389 Apparent fractionation ($\epsilon_{n\text{-alkane/precipitation}}$) is on the order of -120 to -150‰, i.e. a bit less than
 390 the biosynthetic fraction of -160‰. This implies that evapotranspirative enrichment is ~ 10 to
 391 40‰ (Fig. 7A). $\epsilon_{n\text{-alkane/precipitation}}$ is lower for grass sites compared to the forest sites. Differences
 392 are significant between deciduous and grass sites (p-value = 0.005). This finding supports the
 393 results of other studies (Kahmen et al., 2013; Liu and Yang, 2008; McInerney et al., 2011), and
 394 can be named “signal damping”. Grasses do not only incorporate the evaporatively-enriched
 395 leaf water only but also unenriched leaf water in the growth and differentiation zone of grasses
 396 (Gamarra et al., 2016; Liu et al., 2017).

397 The grass-derived hemicellulose sugar biomarkers do not fully record the evapotranspirative
 398 enrichment of the leaf water, either, as indicated by lower apparent fractionation ($\epsilon_{\text{sugar/precipitation}}$)
 399 in Fig. 7B. The differences are significant between forest and grass sites (p-value < 0.005). This
 400 is in agreement with a study on cellulose extracted from grass blades (Helliker and Ehleringer,
 401 2002), and again, the “signal damping” can be explained with incorporation of enriched leaf
 402 water and non-enriched stem water.

403 Based on the comparison of evapotranspirative enrichment between forest and grass sites, the
 404 “signal damping” can be quantified to be ~ 31% for the hemicellulose sugars, and ~ 49% for
 405 the *n*-alkanes. This is in agreement with other studies that reported a loss of 22% of the leaf
 406 water enrichment for hemicellulose sugars (Helliker and Ehleringer, 2002) and 39 to 62% loss
 407 of the leaf water enrichment for *n*-alkanes (Gamarra et al., 2016).



408

409 **Fig. 7.** Apparent fractionation (A) $\epsilon_{n\text{-alkane/precipitation}}$ and (B) $\epsilon_{\text{sugar/precipitation}}$. Biosynthetic
 410 fractionation factors according to section 2.4.2. Box plots show median (red line), interquartile
 411 range (IQR) with upper (75%) and lower (25%) quartiles, lowest whisker still within 1.5IQR
 412 of lower quartile, and highest whisker still within 1.5IQR of upper quartile, dots mark outliers.
 413 Abbreviations: con = coniferous forest sites (n=9); dec = deciduous forest sites (n=11 and 14
 414 for *n*-alkanes and sugars, respectively); grass = grassland sites (n=4 and 6 for *n*-alkanes and
 415 sugars, respectively). The figure conceptually illustrates the effect of biosynthetic fractionation
 416 and evapotranspirative enrichment as well as “signal damping”.

417

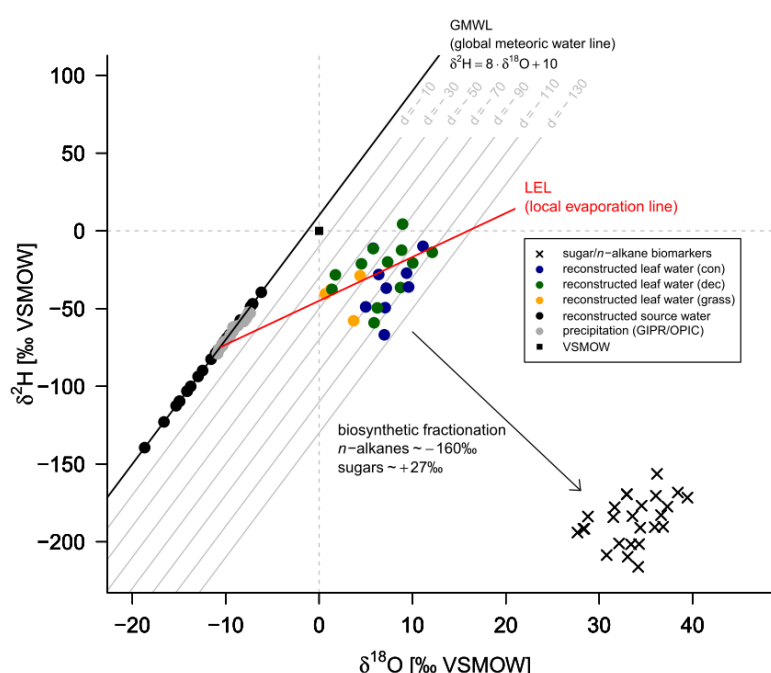
418 3.6 $\delta^2\text{H}/\delta^{18}\text{O}_{\text{source-water}}$ reconstructions

419 The $\delta^2\text{H}$ versus $\delta^{18}\text{O}$ diagram shown in Fig. 8 graphically illustrates the reconstruction of
 420 $\delta^2\text{H}/\delta^{18}\text{O}_{\text{leaf-water}}$ (colored dots) from $\delta^2\text{H}_{n\text{-alkane}}/\delta^{18}\text{O}_{\text{sugar}}$ (crosses), as well as the reconstruction

https://doi.org/10.5194/bg-2019-197
 Preprint. Discussion started: 29 May 2019
 © Author(s) 2019. CC BY 4.0 License.



421 of $\delta^2\text{H}/\delta^{18}\text{O}_{\text{source-water}}$ (black dots). For reconstructing $\delta^2\text{H}/\delta^{18}\text{O}_{\text{source-water}}$, LELs with an average
 422 slope of 2.8 ± 0.1 (Eq. 10) can be generated through every leaf water point and the intercepts of
 423 these LELs with the GMWL.



424
 425 **Fig. 8.** $\delta^2\text{H}$ vs. $\delta^{18}\text{O}$ diagram illustrating $\delta^2\text{H}_{n\text{-alkane}}$ and $\delta^{18}\text{O}_{\text{sugar}}$, reconstructed $\delta^2\text{H}/\delta^{18}\text{O}_{\text{leaf-water}}$
 426 (according Eqs. 8 and 9) and reconstructed $\delta^2\text{H}/\delta^{18}\text{O}_{\text{source-water}}$ in comparison to GIPR/OIPC-
 427 based $\delta^2\text{H}/\delta^{18}\text{O}_{\text{precipitation}}$. Abbreviations: con = coniferous forest sites (n=9); dec = deciduous
 428 forest sites (n=11); grass = grassland sites (n=4).

429

430 The reconstructed $\delta^2\text{H}/\delta^{18}\text{O}_{\text{source-water}}$ results can be compared with the $\delta^2\text{H}/\delta^{18}\text{O}_{\text{GIPR/OIPC}}$ data
 431 (Fig. 9). This comparison reveals that the coupled $\delta^2\text{H}_{n\text{-alkane}}-\delta^{18}\text{O}_{\text{sugar}}$ approach yields more
 432 accurate $\delta^2\text{H}/\delta^{18}\text{O}_{\text{source-water}}$ results than hitherto applied $\delta^2\text{H}_{n\text{-alkane}}$ single isotope approaches.
 433 However, the range of the reconstructed $\delta^2\text{H}/\delta^{18}\text{O}_{\text{source-water}}$ values is clearly larger than in
 434 $\delta^2\text{H}/\delta^{18}\text{O}_{\text{GIPR/OIPC}}$ values. $\delta^2\text{H}$ is systematically underestimated by $\sim 21\text{‰} \pm 22$ (Fig. 9B) and
 435 $\delta^{18}\text{O}$ by $\sim 2.9\text{‰} \pm 2.8$ (Fig. 9D). The type of vegetation seems to be not particularly relevant (p-
 436 value = 0.18 for $\Delta\delta^2\text{H}$ and p-value = 0.34 for $\Delta\delta^{18}\text{O}$). Nevertheless, the systematic offsets tend
 437 to be lowest for the deciduous sites ($\Delta\delta^2\text{H}/\Delta\delta^{18}\text{O}$ is closer to zero with $\sim -5\text{‰} \pm 15$ and $\sim -1.1\text{‰}$
 438 ± 2.1), followed by grass sites ($\sim -14\text{‰} \pm 20$ and $\sim -2.1\text{‰} \pm 2.6$). In comparison, the coniferous
 439 sites show the largest offsets ($\sim -23\text{‰} \pm 26$ for $\Delta\delta^2\text{H}$ $\sim -3.0\text{‰} \pm 3.3$ for $\Delta\delta^{18}\text{O}$). Differences are,
 440 however, not statistically significant. The systematic offset and the large variability might have

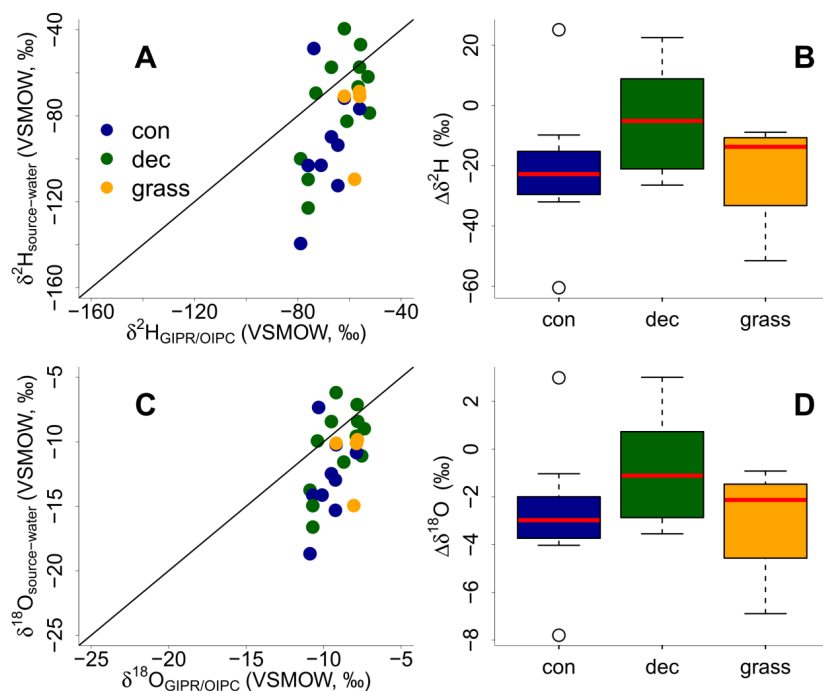
<https://doi.org/10.5194/bg-2019-197>
Preprint. Discussion started: 29 May 2019
© Author(s) 2019. CC BY 4.0 License.



441 more specific reasons, and we suggest that this is related to the type of vegetation. Deciduous
442 trees produce lots of leaf waxes and sugars (e.g. Prietzel et al., 2013; Zech et al., 2012a), and
443 all biomarkers reflect and record the evapotranspirative enrichment of the leaf water (e.g.
444 Cernusak et al., 2016; Tuthorn et al., 2014). The coupled approach and the leaf water
445 reconstruction based on the *n*-alkane and sugar biomarkers thus works well. However,
446 coniferous trees produce quite low amounts of *n*-alkanes (Diefendorf and Freimuth, 2016; Zech
447 et al., 2012a), while sugar concentrations are as high as in other vascular plants (e.g. Hepp et
448 al., 2016; Prietzel et al., 2013). For the coniferous soil samples this means that the *n*-alkanes
449 stem most likely from the understory whereas the sugars originate from grasses and coniferous
450 needles. When the understory is dominated by grass species then the *n*-alkane biomarkers do
451 not record the full leaf water enrichment signal, whereas the sugars from the needles do. The
452 reconstructed leaf water for the coniferous sites is therefore too negative concerning $\delta^2\text{H}$, and
453 reconstructed $\delta^2\text{H}/\delta^{18}\text{O}_{\text{source-water}}$ values thus also become too negative (Fig. 8). Concerning the
454 grass sites the following explanation can be found. Correcting for “signal damping” makes the
455 reconstructed leaf water points more positive and shifts them in Fig. 8 up and right. As the
456 “signal damping” is stronger for $\delta^2\text{H}$ than for $\delta^{18}\text{O}$ the corrected leaf water points are now above
457 the uncorrected ones. The corrected leaf water points leads to more positive reconstructed
458 $\delta^2\text{H}/\delta^{18}\text{O}_{\text{source-water}}$ values for the grass sites.

459 Vegetation type specific rooting depths could partly cause the overall high variability in
460 reconstructed $\delta^2\text{H}/\delta^{18}\text{O}_{\text{source-water}}$. Deep rooting species most likely use the water from deeper
461 soil horizons and/or shallow ground water, which is equal to the (weighted) mean annual
462 precipitation (e.g. Herrmann et al., 1987). Shallow rooting plants take up water from upper soil
463 horizons, which is influenced by seasonal variations in $\delta^2\text{H}/\delta^{18}\text{O}_{\text{precipitation}}$ and by soil water
464 enrichment (Dubbart et al., 2013). Thus, the overall assumption that the source water of the
465 plants reflects the local (weighted) mean precipitation might be not fully valid for all sites.
466 Moreover, a partly contribution of root-derived rather than leaf-derived sugar biomarkers in our
467 topsoil samples is very likely. This does, by contrast, not apply for *n*-alkanes, which are hardly
468 produced in roots (Zech et al., 2012b and the discussion).

https://doi.org/10.5194/bg-2019-197
 Preprint. Discussion started: 29 May 2019
 © Author(s) 2019. CC BY 4.0 License.



469
 470 **Fig. 9.** Correlation of reconstructed $\delta^2\text{H}/\delta^{18}\text{O}_{\text{source-water}}$ vs. precipitation $\delta^2\text{H}/\delta^{18}\text{O}_{\text{GIPR/OIPC}}$ (A and
 471 C). Black lines indicate 1:1 relationship. Differences between reconstructed source water and
 472 precipitation ($\Delta\delta^2\text{H}/\delta^{18}\text{O} = \delta^2\text{H}/\delta^{18}\text{O}_{\text{source-water}} - \delta^2\text{H}/\delta^{18}\text{O}_{\text{GIPR/OIPC}}$) for the three different
 473 vegetation types (B and D). Box plots show median (red line), interquartile range (IQR) with
 474 upper (75%) and lower (25%) quartiles, lowest whisker still within 1.5IQR of lower quartile,
 475 and highest whisker still within 1.5IQR of upper quartile. Abbreviations: con = coniferous
 476 forest sites (n=9); dec = deciduous forest sites (n=11); grass = grassland sites (n=4).

477 Moreover, the high variability within the vegetation types could be caused by variability in ϵ_{bio}
 478 of ^2H in *n*-alkanes, as well as ^{18}O in sugars. There is an ongoing discussion about the correct
 479 ϵ_{bio} for ^{18}O in hemicellulose sugars (Sternberg, 2014 vs. Zech et al., 2014), and ϵ_{bio} is probably
 480 not constant over all vegetation types. This translates into errors concerning leaf water
 481 reconstruction and thus for reconstructing $\delta^2\text{H}/\delta^{18}\text{O}_{\text{source-water}}$ values (Eq. 9 and Fig. 8).
 482 Likewise, the ϵ_{bio} values reported in the literature for ^2H of *n*-alkanes can be off from -160‰
 483 by tens of permille (Feakins and Sessions, 2010; Tipple et al., 2015; Feakins et al., 2016;
 484 Freimuth et al., 2017). The degree to which hydrogen originates from NADPH rather than leaf
 485 water is important, because NADPH is more negative (Schmidt et al., 2003). The wide range
 486 in biosynthetic ^2H fractionation factors is therefore also related to the carbon and energy
 487 metabolism state of plants (Cormier et al., 2018).

https://doi.org/10.5194/bg-2019-197
 Preprint. Discussion started: 29 May 2019
 © Author(s) 2019. CC BY 4.0 License.

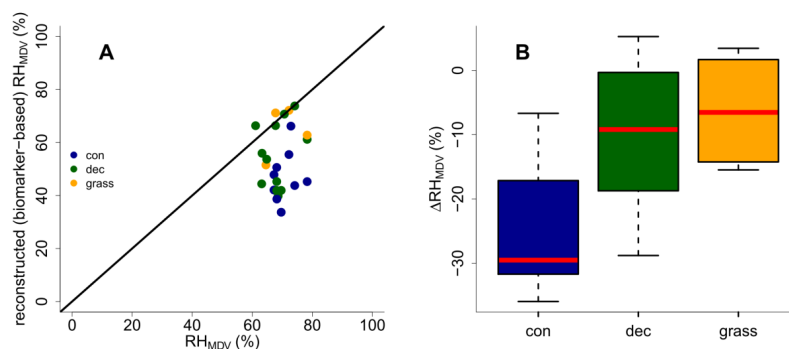


488 3.7 RH reconstruction

489 Reconstructed RH_{MDV} ranges from 34 to 74%, while RH_{MDV} from climate station data range
 490 from 61 to 78% (Fig. 10A). Biomarker-based values thus systematically underestimate the
 491 station data ($\Delta RH_{MDV} = -17\% \pm 12$; Fig. 10B). Yet the offsets are much less for deciduous tree
 492 and grass sites ($\Delta RH_{MDV} = -10\% \pm 12$ and $-7\% \pm 9$, respectively). The offsets for the coniferous
 493 sites are $-30\% \pm 11$, and significantly larger than for the deciduous and grass sites (p -values <
 494 0.05).

495 Too low reconstructed RH_{MDV} values for the coniferous sites make sense in view of the
 496 previously discussed option that soils contain n -alkanes from the understory (which is
 497 dominated by grass species), while sugars stem from needles and grasses. As explained earlier
 498 already, the “signal damping” leads to too negative reconstructed $\delta^2H_{leaf-water}$ (whereas $\delta^{18}O$ is
 499 affected less by the “signal damping”), and too negative $\delta^2H_{leaf-water}$ translates into
 500 overestimated d -excess and underestimated RH values. In Fig. 8, a correction for this require
 501 moving the coniferous leaf water data points upwards towards more positive δ^2H values, thus
 502 the distance between the leaf water and the source water is reduced.

503 The underestimation of RH for the deciduous and grass sites could be partly associated with the
 504 use of the GMWL as baseline for the coupled $\delta^2H_{n-alkane}-\delta^{18}O_{sugar}$ approach. The deuterium-
 505 excess of the LMWLs is generally lower than the +10‰ of the GMWL, while the slopes of the
 506 LMWLs are well comparable to the GMWL (Stumpp et al., 2014). In addition, if soil water
 507 evaporation occurred before water uptake by the plants, this would lead to an underestimation
 508 of biomarker-based RH_{MDV} values. It can be furthermore assumed that plant metabolism is
 509 highest during times with direct sunshine and high irradiation, i.e. during noon at sunny days.
 510 The relevant RH could therefore be lower than the climate station-derived RH_{MDV} . Indeed,
 511 already climate station RH_{MDV} is considerable lower than RH_{MA} and RH_{MV} (Tab. S1).



512

513 **Fig. 10.** (A) Comparison of reconstructed (biomarker-based) RH_{MDV} values and climate station
 514 RH_{MDV} data. The black line indicates the 1:1 relationship. (B) Differences between
 515 reconstructed and climate station RH_{MDV} values ($\Delta RH_{MDV} = \text{reconstructed} - \text{climate station}$
 516 RH_{MDV}) for the three different vegetation types along the transect. Abbreviations: con =
 517 coniferous forest sites ($n=9$); dec = deciduous forest sites ($n=11$); grass = grassland sites ($n=4$).

https://doi.org/10.5194/bg-2019-197
 Preprint. Discussion started: 29 May 2019
 © Author(s) 2019. CC BY 4.0 License.



518 The uncertainty of reconstructed RH_{MDV} values are large for all three investigated vegetation
 519 types, and again these uncertainties are probably also related to ε_{bio} , which is most likely not
 520 constant as assumed for our calculations. Moreover, microclimate variability is underestimated
 521 in our approach. As mentioned in sections 2.4.2 and 3.6, in the coupled approach not only the
 522 source water of the plants is equated with (weighted) mean annual precipitation, but also an
 523 isotopic equilibrium between the source water and the (local) atmospheric water vapour is
 524 assumed. However, in areas with distinct seasonality this might be not fully valid. To account
 525 for this lack of equilibrium between precipitation and local atmospheric water vapour, apparent
 526 ε values can be calculated with data from Jacob and Sonntag, (1991). As shown by Hepp et al.
 527 (2018) those values can be used to achieve alternative RH reconstructions based on the coupled
 528 $\delta^2H_{n\text{-alkane}}\text{-}\delta^{18}O_{\text{sugar}}$ approach. Such calculated RH_{MDV} values are on average 1.5% more
 529 negative than the original values. However, this difference in RH is far below the analytical
 530 uncertainties of the compound-specific biomarker isotope analysis.

531 Finally, the integration time of the investigated topsoils has to be discussed. Unfortunately, no
 532 ^{14}C dates are available for the soil samples. However, most likely the organic matter has been
 533 built up over a longer timescale than the available climate data, which is used for comparison.
 534 In combination with vegetation changes/management changes throughout that period, this
 535 could surely lead to a less tight relationship of the reconstructions compared to the climate
 536 station data. Root input of arabinose and xylose seems to be of minor relevance in our topsoil
 537 samples. Otherwise, the reconstructed $\delta^{18}O_{\text{sugar}}$ values would be too negative resulting in
 538 RH_{MDV} overestimations, which is not observed.

539

540 4 Conclusions

541 We were able to show that

- 542 (i) the vegetation type does not significantly influence the brGDGT concentrations and
 543 proxies, yet the coniferous sites tend to have higher brGDGT concentrations, BIT
 544 indices and CBT/MBT³ ratios, while grass sites tend to be lowest.
- 545 (ii) CBT faithfully records soil pH with a median ΔpH of 0.6 ± 0.6 . The CBT
 546 overestimates the real pH particularly at the forest sites.
- 547 (iii) CBT-MBT³-derived T_{MA} reflect the climate station-derived T_{MA} values with a
 548 median ΔT_{MA} of $0.5^\circ C \pm 2.4$, but again slightly too high reconstruction for the forest
 549 sites were observed.
- 550 (iv) differences in the apparent fractionation between the investigated vegetation types
 551 are caused by “signal damping”, i.e. the grasses do not see and record the full
 552 evaporative enrichment of leaf water.
- 553 (v) the reconstructed $\delta^2H/\delta^{18}O_{\text{source-water}}$ reflects the $\delta^2H/\delta^{18}O_{GIPR/OIPC}$ with a systematic
 554 offset for δ^2H of $\sim -21\% \pm 22$ and for $\delta^{18}O$ of $\sim -2.9\% \pm 2.8$ (based on overall medians
 555 of $\Delta\delta^2H/\delta^{18}O$). This is caused by too negative reconstructions for coniferous and
 556 grass sites. For coniferous sites, this can be explained with *n*-alkanes originating
 557 from understory grasses, and for the grass sites the “signal damping” more effect
 558 δ^2H than $\delta^{18}O$. This leads to too negative reconstructed $\delta^2H_{\text{leaf-water}}$ values and thus
 559 to too negative $\delta^2H/\delta^{18}O_{\text{source-water}}$ reconstruction.

https://doi.org/10.5194/bg-2019-197
 Preprint. Discussion started: 29 May 2019
 © Author(s) 2019. CC BY 4.0 License.



560 (vi) reconstructed (biomarker-based) RH_{MDV} values tend to underestimate climate
 561 station-derived RH_{MDV} values ($\Delta RH_{MDV} = \sim -17\% \pm 12$). For coniferous sites the
 562 underestimations are strongest, which can be explained with understory grasses
 563 being the main source of *n*-alkanes for the investigated soils under coniferous
 564 forests.

565 Overall, our study highlights the great potential of GDGTs and the coupled $\delta^2H_{n\text{-alkane}}\text{-}\delta^{18}O_{\text{sugar}}$
 566 approach for more quantitative paleoclimate reconstructions. Taking into account effects of
 567 different vegetation types improves correlations and reconstructions. This holds particularly
 568 true for the coupled $\delta^2H_{n\text{-alkane}}\text{-}\delta^{18}O_{\text{sugar}}$ approach, which is affected by “signal damping” of the
 569 grass vegetation. Assuming constant biosynthetic fractionation is likely a considerable source
 570 of uncertainty. Climate chamber experiments would be very useful to further evaluate and refine
 571 the coupled $\delta^2H_{n\text{-alkane}}\text{-}\delta^{18}O_{\text{sugar}}$ approach, because uncertainties related to microclimate
 572 variability can be reduced. Field experiments like ours suffer from the fact that biomarker pools
 573 in the sampled topsoils may have been affected by past vegetation and climate changes.

574

575 Acknowledgements

576 We thank L. Wüthrich, H. Veit, T. Sprafke, A. Groos (all University of Bern), A. Kühnel
 577 (Technical University of Munich) for constructive discussions and statistical advices, and M.
 578 Schaarschmidt (University of Bayreuth), C. Heinrich and M. Benesch (Martin-Luther-
 579 University Halle-Wittenberg) for laboratory assistance during $\delta^{18}O_{\text{sugar}}$ analysis and pH
 580 measurements, respectively. The Swiss National Science Foundation (PP00P2 150590) funded
 581 this research. J. Hepp greatly acknowledges the support by the German Federal Environmental
 582 Foundation (DBU) in form of his PhD-fellowship.

583

584 References

- 585 Allison, G. B., Gat, J. R. and Leaney, F. W. J.: The relationship between deuterium and oxygen-
 586 18 delta values in leaf water, *Chemical Geology*, 58, 145–156, 1985.
- 587 Amelung, W., Cheshire, M. V. and Guggenberger, G.: Determination of neutral and acidic
 588 sugars in soil by capillary gas-liquid chromatography after trifluoroacetic acid hydrolysis,
 589 *Soil Biology and Biochemistry*, 28(12), 1631–1639, 1996.
- 590 Anderson, V. J., Shanahan, T. M., Saylor, J. E., Horton, B. K. and Mora, A. R.: Sources of local
 591 and regional variability in the MBT'/CBT paleotemperature proxy: Insights from a
 592 modern elevation transect across the Eastern Cordillera of Colombia, *Organic
 593 Geochemistry*, 69, 42–51, doi:10.1016/j.orggeochem.2014.01.022, 2014.
- 594 Awe, G. O., Reichert, J. M. and Wendroth, O. O.: Temporal variability and covariance
 595 structures of soil temperature in a sugarcane field under different management practices
 596 in southern Brazil, *Soil and Tillage Research*, 150, 93–106,
 597 doi:10.1016/j.still.2015.01.013, 2015.
- 598 Bariat, T., Gonzalez-Dunia, J., Katerji, N., Béthenod, O., Bertolini, J. M. and Mariotti, A.:
 599 Spatial variation of the isotopic composition of water (^{18}O , 2H) in the soil-plant-
 600 atmosphere system, 2. Assessment under field conditions, *Chemical Geology*, 115, 317–

<https://doi.org/10.5194/bg-2019-197>
Preprint. Discussion started: 29 May 2019
© Author(s) 2019. CC BY 4.0 License.



- 601 333, 1994.
- 602 Bowen, G. J.: The Online Isotopes in Precipitation Calculator, version 3.1., 2018.
- 603 Bowen, G. J. and Revenaugh, J.: Interpolating the isotopic composition of modern meteoric
604 precipitation, *Water Resources Research*, 39(10), 1–13, doi:10.1029/2003WR002086,
605 2003.
- 606 Brincat, D., Yamada, K., Ishiwatari, R., Uemura, H. and Naraoka, H.: Molecular-isotopic
607 stratigraphy of long-chain *n*-alkanes in Lake Baikal Holocene and glacial age sediments,
608 *Organic Geochemistry*, 31(4), 287–294, doi:10.1016/S0146-6380(99)00164-3, 2000.
- 609 Cappelen, J.: Danish Climatological Normals 1971–2000 - for selected stations., 2002.
- 610 Cernusak, L. A., Wong, S. C. and Farquhar, G. D.: Oxygen isotope composition of phloem sap
611 in relation to leaf water in *Ricinus communis*, *Functional Plant Biology*, 30(10), 1059–
612 1070, 2003.
- 613 Cernusak, L. A., Barbour, M. M., Arndt, S. K., Cheesman, A. W., English, N. B., Feild, T. S.,
614 Helliker, B. R., Holloway-Phillips, M. M., Holtum, J. A. M., Kahmen, A., McInerney, F.
615 A., Munksgaard, N. C., Simonin, K. A., Song, X., Stuart-Williams, H., West, J. B. and
616 Farquhar, G. D.: Stable isotopes in leaf water of terrestrial plants, *Plant Cell and
617 Environment*, 39(5), 1087–1102, doi:10.1111/pce.12703, 2016.
- 618 Coffinet, S., Hugué, A., Anquetil, C., Derenne, S., Pedentchouk, N., Bergonzini, L.,
619 Omuombo, C., Williamson, D., Jones, M., Majule, A. and Wagner, T.: Evaluation of
620 branched GDGTs and leaf wax *n*-alkane $\delta^2\text{H}$ as (paleo) environmental proxies in East
621 Africa, *Geochimica et Cosmochimica Acta*, 198, 182–193,
622 doi:10.1016/j.gca.2016.11.020, 2017.
- 623 Cormier, M.-A., Werner, R. A., Sauer, P. E., Gröcke, D. R., M.C., L., Wieloch, T., Schleucher,
624 J. and Kahmen, A.: ^2H fractionations during the biosynthesis of carbohydrates and lipids
625 imprint a metabolic signal on the $\delta^2\text{H}$ values of plant organic compounds, *New
626 Phytologist*, 218(2), 479–491, doi:10.1111/nph.15016, 2018.
- 627 Craig, H.: Isotopic Variations in Meteoric Waters, *Science*, 133, 1702–1703, 1961.
- 628 Dang, X., Yang, H., Naafs, B. D. A., Pancost, R. D. and Xie, S.: Evidence of moisture control
629 on the methylation of branched glycerol dialkyl glycerol tetraethers in semi-arid and arid
630 soils, *Geochimica et Cosmochimica Acta*, 189, 24–36, doi:10.1016/j.gca.2016.06.004,
631 2016.
- 632 Dansgaard, W.: Stable isotopes in precipitation, *Tellus*, 16(4), 436–468, doi:10.1111/j.2153-
633 3490.1964.tb00181.x, 1964.
- 634 Dawson, T. E., Mambelli, S., Plamboeck, A. H., Templer, P. H. and Tu, K. P.: Stable Isotopes
635 in Plant Ecology, *Annual Review of Ecology and Systematics*, 33(1), 507–559,
636 doi:10.1146/annurev.ecolsys.33.020602.095451, 2002.
- 637 Diefendorf, A. F. and Freimuth, E. J.: Extracting the most from terrestrial plant-derived *n*-alkyl
638 lipids and their carbon isotopes from the sedimentary record: A review, *Organic
639 Geochemistry*, 103(January), 1–21, doi:10.1016/j.orggeochem.2016.10.016, 2016.
- 640 Dirghangi, S. S., Pagani, M., Hren, M. T. and Tipple, B. J.: Distribution of glycerol dialkyl
641 glycerol tetraethers in soils from two environmental transects in the USA, *Organic
642 Geochemistry*, 59, 49–60, doi:10.1016/j.orggeochem.2013.03.009, 2013.

<https://doi.org/10.5194/bg-2019-197>
 Preprint. Discussion started: 29 May 2019
 © Author(s) 2019. CC BY 4.0 License.



- 643 Dubbert, M., Cuntz, M., Piayda, A., Maguás, C. and Werner, C.: Partitioning evapotranspiration
 644 - Testing the Craig and Gordon model with field measurements of oxygen isotope ratios
 645 of evaporative fluxes, *Journal of Hydrology*, 496, 142–153,
 646 doi:10.1016/j.jhydrol.2013.05.033, 2013.
- 647 DWD Climate Data Center: Historical annual precipitation observations for Germany. [online]
 648 Available from: [ftp://ftp-](ftp://ftp-cdc.dwd.de/pub/CDC/observations_germany/climate/hourly/precipitation/historical/)
 649 [cdc.dwd.de/pub/CDC/observations_germany/climate/hourly/precipitation/historical/](ftp://ftp-cdc.dwd.de/pub/CDC/observations_germany/climate/hourly/precipitation/historical/)
 650 (Accessed 20 September 2018a), 2018.
- 651 DWD Climate Data Center: Historical hourly station observations of 2m air temperature and
 652 humidity for Germany. [online] Available from: [ftp://ftp-](ftp://ftp-cdc.dwd.de/pub/CDC/observations_germany/climate/hourly/air_temperature/historical/)
 653 [cdc.dwd.de/pub/CDC/observations_germany/climate/hourly/air_temperature/historical/](ftp://ftp-cdc.dwd.de/pub/CDC/observations_germany/climate/hourly/air_temperature/historical/)
 654 (Accessed 19 September 2018b), 2018.
- 655 Eglinton, T. I. and Eglinton, G.: Molecular proxies for paleoclimatology, *Earth and Planetary*
 656 *Science Letters*, 275(1), 1–16, 2008.
- 657 Feakins, S. J. and Sessions, A. L.: Controls on the D/H ratios of plant leaf waxes in an arid
 658 ecosystem, *Geochimica et Cosmochimica Acta*, 74(7), 2128–2141,
 659 doi:<http://dx.doi.org/10.1016/j.gca.2010.01.016>, 2010.
- 660 Feakins, S. J., Bentley, L. P., Salinas, N., Shenkin, A., Blonder, B., Goldsmith, G. R., Ponton,
 661 C., Arvin, L. J., Wu, M. S., Peters, T., West, A. J., Martin, R. E., Enquist, B. J., Asner, G.
 662 P. and Malhi, Y.: Plant leaf wax biomarkers capture gradients in hydrogen isotopes of
 663 precipitation from the Andes and Amazon, *Geochimica et Cosmochimica Acta*, 182, 155–
 664 172, doi:10.1016/j.gca.2016.03.018, 2016.
- 665 Freimuth, E. J., Diefendorf, A. F. and Lowell, T. V.: Hydrogen isotopes of *n*-alkanes and *n*-
 666 alkanolic acids as tracers of precipitation in a temperate forest and implications for
 667 paleorecords, *Geochimica et Cosmochimica Acta*, 206, 166–183,
 668 doi:10.1016/j.gca.2017.02.027, 2017.
- 669 Frich, P., Rosenørn, S., Madsen, H. and Jensen, J. J.: Observed Precipitation in Denmark, 1961-
 670 90., 1997.
- 671 Gamarra, B., Sachse, D. and Kahmen, A.: Effects of leaf water evaporative ²H-enrichment and
 672 biosynthetic fractionation on leaf wax *n*-alkane $\delta^2\text{H}$ values in C3 and C4 grasses, *Plant,*
 673 *Cell and Environment Environment*, 39, 2390–2403, doi:10.1111/pce.12789, 2016.
- 674 Gat, J. R.: Comments on the Stable Isotope Method in Regional Groundwater Investigations,
 675 *Water Resources Research*, 7(4), 980–993, doi:10.1029/WR007i004p00980, 1971.
- 676 van Geldern, R., Baier, A., Subert, H. L., Kowol, S., Balk, L. and Barth, J. A. C.: (Table S1)
 677 Stable isotope composition of precipitation sampled at Erlangen, Germany between 2010
 678 and 2013 for station GeoZentrum located at Erlangen city center, in In supplement to: van
 679 Geldern, R et al. (2014): Pleistocene paleo-groundwater as a pristine fresh water resource
 680 in southern Germany – evidence from stable and radiogenic isotopes. *Science of the Total*
 681 *Environment*, 496, 107-115, <https://doi.org/10.1016/j.panga.2014.07.014>, 2014.
- 682 Guggenberger, G., Christensen, B. T. and Zech, W.: Land-use effects on the composition of
 683 organic matter in particle-size separates of soil: I. Lignin and carbohydrate signature,
 684 *European Journal of Soil Science*, 45(December), 449–458, 1994.
- 685 Helliker, B. R. and Ehleringer, J. R.: Grass blades as tree rings: environmentally induced
 686 changes in the oxygen isotope ratio of cellulose along the length of grass blades, *New*

<https://doi.org/10.5194/bg-2019-197>
Preprint. Discussion started: 29 May 2019
© Author(s) 2019. CC BY 4.0 License.



Biogeosciences
Discussions
Open Access
EGU

- 687 Phytologist, 155, 417–424, 2002.
- 688 Hepp, J., Rabus, M., Anhäuser, T., Bromm, T., Laforsch, C., Sirocko, F., Glaser, B. and Zech,
689 M.: A sugar biomarker proxy for assessing terrestrial versus aquatic sedimentary input,
690 Organic Geochemistry, 98, 98–104, doi:10.1016/j.orggeochem.2016.05.012, 2016.
- 691 Hepp, J., Wüthrich, L., Bromm, T., Bliedtner, M., Schäfer, I. K., Glaser, B., Rozanski, K.,
692 Sirocko, F., Zech, R. and Zech, M.: How dry was the Younger Dryas? Evidence from a
693 coupled $\delta^2\text{H}$ - $\delta^{18}\text{O}$ biomarker paleohygrometer, applied to the Lake Gemündener Maar
694 sediments, Western Eifel, Germany, Climate of the Past Discussions, (September), 1–44,
695 doi:10.5194/cp-2018-114, 2018a.
- 696 Hepp, J., Schäfer, I., Tuthorn, M., Glaser, B., Juchelka, D., Rozanski, K., Stichler, W., Zech,
697 R., Mayr, C. and Zech, M.: Validation of acoupled $\delta^2\text{H}_{n\text{-alkane}}$ - $\delta^{18}\text{O}_{\text{sugar}}$ paleohygrometer
698 approach based on a climate chamber experiment, submitted to GCA, 2018b.
- 699 Herrmann, A., Maloszewski, P. and Stichler, W.: Changes of ^{18}O contents of precipitation water
700 during seepage in the unsaturated zone, in Proceedings of International Symposium on
701 Groundwater Monitoring and Management, 23 - 28 March, p. 22, Institut of Water
702 Management Berlin (GDR) with support of UNESCO, Dresden., 1987.
- 703 Hopmans, E. C., Weijers, J. W. H., Schefuß, E., Herfort, L., Sinninghe Damsté, J. S. and
704 Schouten, S.: A novel proxy for terrestrial organic matter in sediments based on branched
705 and isoprenoid tetraether lipids, Earth and Planetary Science Letters, 224(1–2), 107–116,
706 doi:10.1016/j.epsl.2004.05.012, 2004.
- 707 Horita, J. and Wesolowski, D. J.: Liquid-vapor fractionation of oxygen and hydrogen isotopes
708 of water from the freezing to the critical temperature, Geochimica et Cosmochimica Acta,
709 58(16), 3425–3437, doi:http://dx.doi.org/10.1016/0016-7037(94)90096-5, 1994.
- 710 Hothorn, T., Bühlmann, P., Dudoit, S., Molinaro, A. and Van Der Laan, M. J.: Survival
711 ensembles, Biostatistics, 7(3), 355–373, doi:10.1093/biostatistics/kxj011, 2006.
- 712 Hou, J., D’Andrea, W. J. and Huang, Y.: Can sedimentary leaf waxes record D/H ratios of
713 continental precipitation? Field, model, and experimental assessments, Geochimica et
714 Cosmochimica Acta, 72, 3503–3517, doi:10.1016/j.gca.2008.04.030, 2008.
- 715 Hugué, A., Fosse, C., Metzger, P., Fritsch, E. and Derenne, S.: Occurrence and distribution of
716 extractable glycerol dialkyl glycerol tetraethers in podzols, Organic Geochemistry, 41(3),
717 291–301, doi:10.1016/j.orggeochem.2009.10.007, 2010a.
- 718 Hugué, A., Fosse, C., Laggoun-Défarge, F., Toussaint, M. L. and Derenne, S.: Occurrence and
719 distribution of glycerol dialkyl glycerol tetraethers in a French peat bog, Organic
720 Geochemistry, 41(6), 559–572, doi:10.1016/j.orggeochem.2010.02.015, 2010b.
- 721 IAEA/WMO: Global Network of Isotopes in Precipitation. The GNIP Database., 2015.
- 722 IAEA/WMO: Global Network of Isotopes in Precipitation. The GNIP Database., 2018.
- 723 Jacob, H. and Sonntag, C.: An 8-year record of the seasonal- variation of ^2H and ^{18}O in
724 atmospheric water vapor and precipitation at Heidelberg, Tellus, 43B(3), 291–300, 1991.
- 725 Kahmen, A., Schefuß, E. and Sachse, D.: Leaf water deuterium enrichment shapes leaf wax *n*-
726 alkane δD values of angiosperm plants I: Experimental evidence and mechanistic
727 insights, Geochimica et Cosmochimica Acta, 111, 39–49, doi:10.1016/j.gca.2012.09.004,
728 2013.

<https://doi.org/10.5194/bg-2019-197>
 Preprint. Discussion started: 29 May 2019
 © Author(s) 2019. CC BY 4.0 License.



Biogeosciences
 Discussions
 Open Access

- 729 Knapp, D. R.: Handbook of Analytical Derivatization Reactions, John Wiley & Sons, New
 730 York, Chichester, Brisbane, Toronto, Singapore., 1979.
- 731 Laursen, E. V., Thomsen, R. S. and Cappelen, J.: Observed Air Temperature, Humidity,
 732 Pressure, Cloud Cover and Weather in Denmark - with Climatological Standard Normals,
 733 1961-90., 1999.
- 734 Levene, H.: Robust Tests for Equality of Variances, in Contributions to Probability and
 735 Statistics: Essays in Honor of Harold Hotelling, vol. 69, edited by I. Olkin, pp. 78–92,
 736 Stanford University Press, Palo Alto, California., 1960.
- 737 Liu, W. and Yang, H.: Multiple controls for the variability of hydrogen isotopic compositions
 738 in higher plant *n*-alkanes from modern ecosystems, *Global Change Biology*, 14(9), 2166–
 739 2177, doi:10.1111/j.1365-2486.2008.01608.x, 2008.
- 740 Liu, Y., Wang, J., Liu, D., Li, Z., Zhang, G., Tao, Y., Xie, J., Pan, J. and Chen, F.: Straw
 741 mulching reduces the harmful effects of extreme hydrological and temperature conditions
 742 in citrus orchards, *PLoS ONE*, 9(1), 1–9, doi:10.1371/journal.pone.0087094, 2014.
- 743 McNerney, F. A., Helliker, B. R. and Freeman, K. H.: Hydrogen isotope ratios of leaf wax *n*-
 744 alkanes in grasses are insensitive to transpiration, *Geochimica et Cosmochimica Acta*,
 745 75(2), 541–554, doi:10.1016/j.gca.2010.10.022, 2011.
- 746 Merlivat, L.: Molecular diffusivities of H₂¹⁶O, HD¹⁶O, and H₂¹⁸O in gases, *The Journal of*
 747 *Chemical Physics*, 69(6), 2864–2871, doi:http://dx.doi.org/10.1063/1.436884, 1978.
- 748 Mueller-Niggemann, C., Utami, S. R., Marxen, A., Mangelsdorf, K., Bauersachs, T. and
 749 Schwark, L.: Distribution of tetraether lipids in agricultural soils - Differentiation
 750 between paddy and upland management, *Biogeosciences*, 13(5), 1647–1666,
 751 doi:10.5194/bg-13-1647-2016, 2016.
- 752 Oppermann, B. I., Michaelis, W., Blumenberg, M., Frerichs, J., Schulz, H. M., Schippers, A.,
 753 Beaubien, S. E. and Krüger, M.: Soil microbial community changes as a result of long-
 754 term exposure to a natural CO₂vent, *Geochimica et Cosmochimica Acta*, 74(9), 2697–
 755 2716, doi:10.1016/j.gca.2010.02.006, 2010.
- 756 Pedentchouk, N. and Zhou, Y.: Factors Controlling Carbon and Hydrogen Isotope Fractionation
 757 During Biosynthesis of Lipids by Phototrophic Organisms, in *Hydrocarbons, Oils and*
 758 *Lipids: Diversity, Origin, Chemistry and Fate. Handbook of Hydrocarbon and Lipid*
 759 *Microbiology*, edited by H. Wilkes, pp. 1–24, Springer, Cham., 2018.
- 760 Peterse, F., van der Meer, J., Schouten, S., Weijers, J. W. H., Fierer, N., Jackson, R. B., Kim,
 761 J. H. and Sinninghe Damsté, J. S.: Revised calibration of the MBT-CBT paleotemperature
 762 proxy based on branched tetraether membrane lipids in surface soils, *Geochimica et*
 763 *Cosmochimica Acta*, 96, 215–229, doi:10.1016/j.gca.2012.08.011, 2012.
- 764 Prietzel, J., Dechamps, N. and Spielvogel, S.: Analysis of non-cellulosic polysaccharides helps
 765 to reveal the history of thick organic surface layers on calcareous Alpine soils, *Plant and*
 766 *Soil*, 365(1–2), 93–114, doi:10.1007/s11104-012-1340-2, 2013.
- 767 R Core Team: R: A Language and Environment for Statistical Computing, [online] Available
 768 from: <https://www.r-project.org/>, 2015.
- 769 Rach, O., Brauer, A., Wilkes, H. and Sachse, D.: Delayed hydrological response to Greenland
 770 cooling at the onset of the Younger Dryas in western Europe, *Nature Geoscience*, 7(1),
 771 109–112, doi:10.1038/ngeo2053, 2014.

<https://doi.org/10.5194/bg-2019-197>
Preprint. Discussion started: 29 May 2019
© Author(s) 2019. CC BY 4.0 License.



- 772 Rao, Z., Zhu, Z., Jia, G., Henderson, A. C. G., Xue, Q. and Wang, S.: Compound specific δD
773 values of long chain *n*-alkanes derived from terrestrial higher plants are indicative of the
774 δD of meteoric waters: Evidence from surface soils in eastern China, *Organic*
775 *Geochemistry*, 40(8), 922–930, doi:<http://dx.doi.org/10.1016/j.orggeochem.2009.04.011>,
776 2009.
- 777 Romero-Viana, L., Kienel, U. and Sachse, D.: Lipid biomarker signatures in a hypersaline lake
778 on Isabel Island (Eastern Pacific) as a proxy for past rainfall anomaly (1942-2006AD),
779 *Palaeogeography, Palaeoclimatology, Palaeoecology*, 350–352, 49–61,
780 doi:[10.1016/j.palaeo.2012.06.011](http://dx.doi.org/10.1016/j.palaeo.2012.06.011), 2012.
- 781 Sachse, D., Radke, J. and Gleixner, G.: Hydrogen isotope ratios of recent lacustrine sedimentary
782 *n*-alkanes record modern climate variability, *Geochimica et Cosmochimica Acta*, 68(23),
783 4877–4889, doi:<http://dx.doi.org/10.1016/j.gca.2004.06.004>, 2004.
- 784 Sachse, D., Radke, J. and Gleixner, G.: δD values of individual *n*-alkanes from terrestrial plants
785 along a climatic gradient – Implications for the sedimentary biomarker record, *Organic*
786 *Geochemistry*, 37, 469–483, doi:[10.1016/j.orggeochem.2005.12.003](http://dx.doi.org/10.1016/j.orggeochem.2005.12.003), 2006.
- 787 Sachse, D., Billault, I., Bowen, G. J., Chikaraishi, Y., Dawson, T. E., Feakins, S. J., Freeman,
788 K. H., Magill, C. R., McInerney, F. A., van der Meer, M. T. J., Polissar, P., Robins, R. J.,
789 Sachs, J. P., Schmidt, H.-L., Sessions, A. L., White, J. W. C. and West, J. B.: Molecular
790 Paleohydrology: Interpreting the Hydrogen-Isotopic Composition of Lipid Biomarkers
791 from Photosynthesizing Organisms, *Annual Reviews*, 40, 221–249,
792 doi:[10.1146/annurev-earth-042711-105535](http://dx.doi.org/10.1146/annurev-earth-042711-105535), 2012.
- 793 Schäfer, I. K., Lanny, V., Franke, J., Eglinton, T. I., Zech, M., Vysloužilová, B. and Zech, R.:
794 Leaf waxes in litter and topsoils along a European transect, *SOIL*, 2, 551–564,
795 doi:[10.5194/soil-2-551-2016](http://dx.doi.org/10.5194/soil-2-551-2016), 2016.
- 796 Schlotter, D.: The spatio-temporal distribution of $\delta^{18}O$ and δ^2H of precipitation in Germany -
797 an evaluation of regionalization methods, Albert-Ludwigs-Universität Freiburg im
798 Breisgau. [online] Available from: [http://www.hydrology.uni-](http://www.hydrology.uni-freiburg.de/abschluss/Schlotter_D_2007_DA.pdf)
799 [freiburg.de/abschluss/Schlotter_D_2007_DA.pdf](http://www.hydrology.uni-freiburg.de/abschluss/Schlotter_D_2007_DA.pdf), 2007.
- 800 Schmidt, H.-L., Werner, R. A. and Roßmann, A.: ^{18}O Pattern and biosynthesis of natural plant
801 products, *Phytochemistry*, 58(1), 9–32, doi:[http://dx.doi.org/10.1016/S0031-](http://dx.doi.org/10.1016/S0031-9422(01)00017-6)
802 [9422\(01\)00017-6](http://dx.doi.org/10.1016/S0031-9422(01)00017-6), 2001.
- 803 Schmidt, H.-L., Werner, R. A. and Eisenreich, W.: Systematics of 2H patterns in natural
804 compounds and its importance for the elucidation of biosynthetic pathways,
805 *Phytochemistry Reviews*, 2(1–2), 61–85, doi:[10.1023/B:PHYT.0000004185.92648.ae](http://dx.doi.org/10.1023/B:PHYT.0000004185.92648.ae),
806 2003.
- 807 Schouten, S., Hopmans, E. C. and Sinninghe Damsté, J. S.: The organic geochemistry of
808 glycerol dialkyl glycerol tetraether lipids: A review, *Organic Geochemistry*, 54, 19–61,
809 doi:[10.1016/j.orggeochem.2012.09.006](http://dx.doi.org/10.1016/j.orggeochem.2012.09.006), 2013.
- 810 Schreuder, L. T., Beets, C. J., Prins, M. A., Hatté, C. and Peterse, F.: Late Pleistocene climate
811 evolution in Southeastern Europe recorded by soil bacterial membrane lipids in Serbian
812 loess, *Palaeogeography, Palaeoclimatology, Palaeoecology*, 449, 141–148,
813 doi:[10.1016/j.palaeo.2016.02.013](http://dx.doi.org/10.1016/j.palaeo.2016.02.013), 2016.
- 814 Sessions, A. L., Burgoyne, T. W., Schimmelmann, A. and Hayes, J. M.: Fractionation of
815 hydrogen isotopes in lipid biosynthesis, *Organic Geochemistry*, 30, 1193–1200, 1999.

<https://doi.org/10.5194/bg-2019-197>
 Preprint. Discussion started: 29 May 2019
 © Author(s) 2019. CC BY 4.0 License.



Biogeosciences
 Discussions
 Open Access
 EGU

- 816 Shapiro, S. S. and Wilk, M. B.: An Analysis of Variance Test for Normality, *Biometrika*,
 817 52(3/4), 591–611, doi:biomet/52.3-4.591, 1965.
- 818 Sternberg, L. S. L.: Comment on “Oxygen isotope ratios ($^{18}\text{O}/^{16}\text{O}$) of hemicellulose-derived
 819 sugar biomarkers in plants, soils and sediments as paleoclimate proxy I: Insight from a
 820 climate chamber experiment” by Zech et al. (2014), *Geochimica et Cosmochimica Acta*,
 821 141, 677–679, doi:10.1016/j.gca.2014.04.051, 2014.
- 822 Strobl, C., Boulesteix, A. L., Zeileis, A. and Hothorn, T.: Bias in random forest variable
 823 importance measures: Illustrations, sources and a solution, *BMC Bioinformatics*, 8,
 824 doi:10.1186/1471-2105-8-25, 2007.
- 825 Strobl, C., Boulesteix, A. L., Kneib, T., Augustin, T. and Zeileis, A.: Conditional variable
 826 importance for random forests, *BMC Bioinformatics*, 9, 1–11, doi:10.1186/1471-2105-9-
 827 307, 2008.
- 828 Stumpp, C., Klaus, J. and Stichler, W.: Analysis of long-term stable isotopic composition in
 829 German precipitation, *Journal of Hydrology*, 517, 351–361,
 830 doi:10.1016/j.jhydrol.2014.05.034, 2014.
- 831 Sun, C. J., Zhang, C. L., Li, F. Y., Wang, H. Y. and Liu, W. G.: Distribution of branched
 832 glycerol dialkyl glycerol tetraethers in soils on the Northeastern Qinghai-Tibetan Plateau
 833 and possible production by nitrite-reducing bacteria, *Science China Earth Sciences*, 59(9),
 834 1834–1846, doi:10.1007/s11430-015-0230-2, 2016.
- 835 Swedish Meteorological and Hydrological Institute: SMHI Open Data Meteorological
 836 Observations., 2018.
- 837 Tipple, B. J., Berke, M. A., Hambach, B., Roden, J. S. and Ehleringer, J. R.: Predicting leaf
 838 wax *n*-alkane $^2\text{H}/^1\text{H}$ ratios: Controlled water source and humidity experiments with
 839 hydroponically grown trees confirm predictions of Craig-Gordon model, *Plant, Cell and*
 840 *Environment*, 38(6), 1035–1047, doi:10.1111/pce.12457, 2015.
- 841 Tuthorn, M., Zech, M., Ruppenthal, M., Oelmann, Y., Kahmen, A., del Valle, H. F., Wilcke,
 842 W. and Glaser, B.: Oxygen isotope ratios ($^{18}\text{O}/^{16}\text{O}$) of hemicellulose-derived sugar
 843 biomarkers in plants, soils and sediments as paleoclimate proxy II: Insight from a climate
 844 transect study, *Geochimica et Cosmochimica Acta*, 126, 624–634,
 845 doi:http://dx.doi.org/10.1016/j.gca.2013.11.002, 2014.
- 846 Tuthorn, M., Zech, R., Ruppenthal, M., Oelmann, Y., Kahmen, A., del Valle, H. F., Eglington,
 847 T., Rozanski, K. and Zech, M.: Coupling $\delta^2\text{H}$ and $\delta^{18}\text{O}$ biomarker results yields
 848 information on relative humidity and isotopic composition of precipitation - a climate
 849 transect validation study, *Biogeosciences*, 12, 3913–3924, doi:10.5194/bg-12-3913-
 850 2015, 2015.
- 851 Umweltbundesamt GmbH: Erhebung der Wassergüte in Österreich gemäß Hydrographiegesetz
 852 i.d.F. des BGBl. Nr. 252/90 (gültig bis Dezember 2006) bzw.
 853 Gewässerzustandsüberwachung in Österreich gemäß Wasserrechtsgesetz, BGBl. I Nr.
 854 123/06, i.d.g.F.; BMLFUW, Sektion IV / Abteilung 3 N. [online] Available from:
 855 <https://wasser.umweltbundesamt.at/h2odb/fivestep/abfrageQdPublic.xhtml> (Accessed 20
 856 September 2018), 2018.
- 857 Walker, C. D. and Brunel, J.-P.: Examining Evapotranspiration in a Semi-Arid Region using
 858 Stable Isotopes of Hydrogen and Oxygen, *Journal of Hydrology*, 118, 55–75, 1990.
- 859 Wang, C., Hren, M. T., Hoke, G. D., Liu-Zeng, J. and Garziona, C. N.: Soil *n*-alkane δD and

<https://doi.org/10.5194/bg-2019-197>
Preprint. Discussion started: 29 May 2019
© Author(s) 2019. CC BY 4.0 License.



Biogeosciences
Discussions
Open Access
EGU

- 860 glycerol dialkyl glycerol tetraether (GDGT) distributions along an altitudinal transect
861 from southwest China: Evaluating organic molecular proxies for paleoclimate and
862 paleoelevation, *Organic Geochemistry*, 107, 21–32,
863 doi:10.1016/j.orggeochem.2017.01.006, 2017.
- 864 Wang, H., Liu, W., Zhang, C. L., Liu, Z. and He, Y.: Branched and isoprenoid tetraether (BIT)
865 index traces water content along two marsh-soil transects surrounding Lake Qinghai:
866 Implications for paleo-humidity variation, *Organic Geochemistry*, 59, 75–81,
867 doi:10.1016/j.orggeochem.2013.03.011, 2013.
- 868 Weijers, J. W. H., Schouten, S., Spaargaren, O. C. and Sinninghe Damsté, J. S.: Occurrence
869 and distribution of tetraether membrane lipids in soils: Implications for the use of the
870 TEX₈₆ proxy and the BIT index, *Organic Geochemistry*, 37(12), 1680–1693,
871 doi:10.1016/j.orggeochem.2006.07.018, 2006.
- 872 Weijers, J. W. H., Schouten, S., van den Donker, J. C., Hopmans, E. C. and Sinninghe Damsté,
873 J. S.: Environmental controls on bacterial tetraether membrane lipid distribution in soils,
874 *Geochimica et Cosmochimica Acta*, 71(3), 703–713, doi:10.1016/j.gca.2006.10.003,
875 2007.
- 876 Weijers, J. W. H., Wiesenberg, G. L. B., Bol, R., Hopmans, E. C. and Pancost, R. D.: Carbon
877 isotopic composition of branched tetraether membrane lipids in soils suggest a rapid
878 turnover and a heterotrophic life style of their source organism(s), *Biogeosciences*, 7(9),
879 2959–2973, doi:10.5194/bg-7-2959-2010, 2010.
- 880 Weijers, J. W. H., Steinmann, P., Hopmans, E. C., Schouten, S. and Sinninghe Damsté, J. S.:
881 Bacterial tetraether membrane lipids in peat and coal: Testing the MBT-CBT temperature
882 proxy for climate reconstruction, *Organic Geochemistry*, 42(5), 477–486,
883 doi:10.1016/j.orggeochem.2011.03.013, 2011.
- 884 Xie, S., Pancost, R. D., Chen, L., Evershed, R. P., Yang, H., Zhang, K., Huang, J. and Xu, Y.:
885 Microbial lipid records of highly alkaline deposits and enhanced aridity associated with
886 significant uplift of the Tibetan Plateau in the Late Miocene, *Geology*, 40(4), 291–294,
887 doi:10.1130/G32570.1, 2012.
- 888 Zech, M. and Glaser, B.: Compound-specific $\delta^{18}\text{O}$ analyses of neutral sugars in soils using gas
889 chromatography-pyrolysis-isotope ratio mass spectrometry: problems, possible solutions
890 and a first application, *Rapid Communications in Mass Spectrometry*, 23, 3522–3532,
891 doi:10.1002/rcm, 2009.
- 892 Zech, M., Rass, S., Bugge, B., Löscher, M. and Zöller, L.: Reconstruction of the late
893 Quaternary paleoenvironments of the Nussloch loess paleosol sequence, Germany, using
894 *n*-alkane biomarkers, *Quaternary Research*, 78(2), 226–235,
895 doi:10.1016/j.yqres.2012.05.006, 2012a.
- 896 Zech, M., Kreutzer, S., Goslar, T., Meszner, S., Krause, T., Faust, D. and Fuchs, M.: Technical
897 Note: *n*-Alkane lipid biomarkers in loess: post-sedimentary or syn-sedimentary?,
898 *Discussions, Biogeosciences*, 9, 9875–9896, doi:10.5194/bgd-9-9875-2012, 2012b.
- 899 Zech, M., Tuthorn, M., Detsch, F., Rozanski, K., Zech, R., Zöller, L., Zech, W. and Glaser, B.:
900 A 220 ka terrestrial $\delta^{18}\text{O}$ and deuterium excess biomarker record from an eolian
901 permafrost paleosol sequence, NE-Siberia, *Chemical Geology*,
902 doi:10.1016/j.chemgeo.2013.10.023, 2013.
- 903 Zech, M., Mayr, C., Tuthorn, M., Leiber-Sauheitl, K. and Glaser, B.: Reply to the comment of

<https://doi.org/10.5194/bg-2019-197>
Preprint. Discussion started: 29 May 2019
© Author(s) 2019. CC BY 4.0 License.

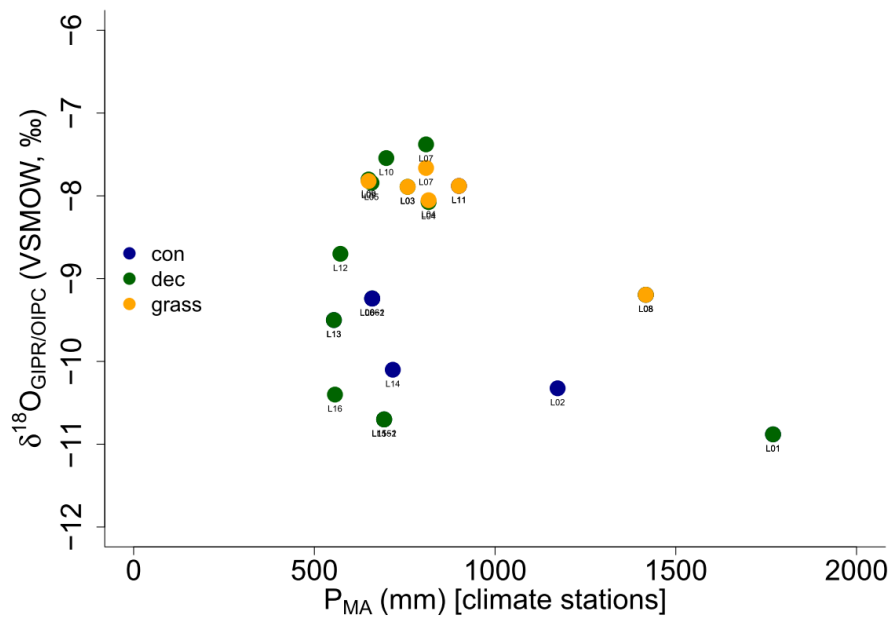


- 904 Sternberg on “Zech et al. (2014) Oxygen isotope ratios ($^{18}\text{O}/^{16}\text{O}$) of hemicellulose-
905 derived sugar biomarkers in plants, soils and sediments as paleoclimate proxy I: Insight
906 from a climate chamber experiment. *GCA, Geochimica et Cosmochimica Acta*, 141(0),
907 680–682, doi:10.1016/j.gca.2014.04.051, 2014.
- 908 Zech, M., Zech, R., Rozanski, K., Gleixner, G. and Zech, W.: Do *n*-alkane biomarkers in
909 soils/sediments reflect the $\delta^2\text{H}$ isotopic composition of precipitation? A case study from
910 Mt. Kilimanjaro and implications for paleoaltimetry and paleoclimate research, *Isotopes*
911 in Environmental and Health Studies, 51(4), 508–524,
912 doi:10.1080/10256016.2015.1058790, 2015.
- 913 Zech, R., Gao, L., Tarozo, R. and Huang, Y.: Branched glycerol dialkyl glycerol tetraethers in
914 Pleistocene loess-paleosol sequences: Three case studies, *Organic Geochemistry*, 53, 38–
915 44, doi:10.1016/j.orggeochem.2012.09.005, 2012c.

1 **Supplementary figures**

2

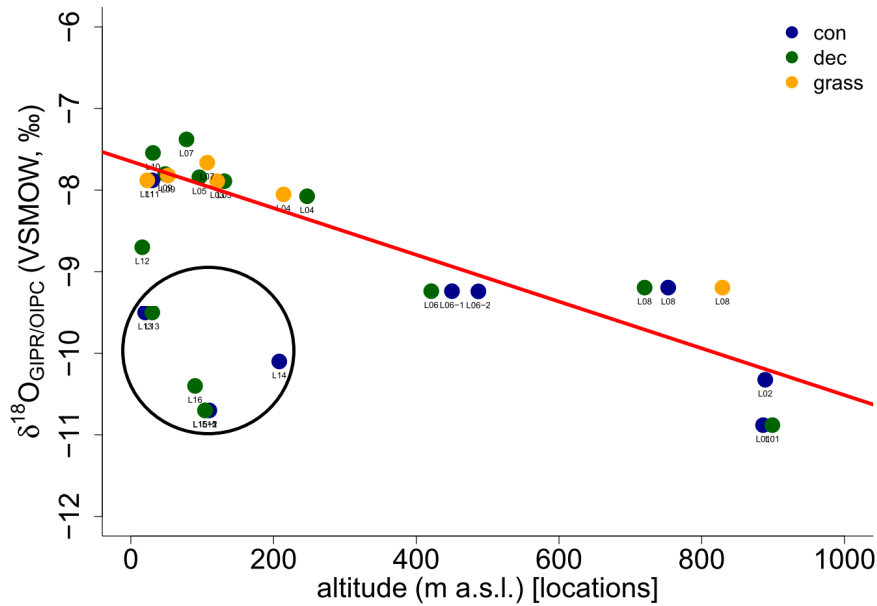
3



4

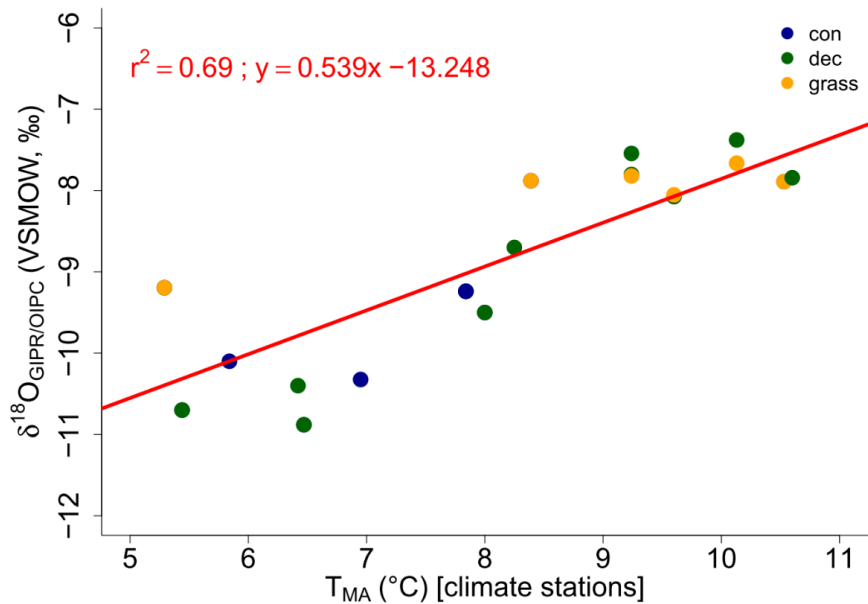
5 **Fig. S1.** Comparison between $\delta^{18}\text{O}_{\text{GIPR/OIPC}}$ values vs. P_{MA} for the three different vegetation
6 types along the transect. All data points are marked with the location names. Abbreviations:
7 con = coniferous forest sites (n=9); dec = deciduous forest sites (n=11); grass = grassland sites
8 (n=4).

9

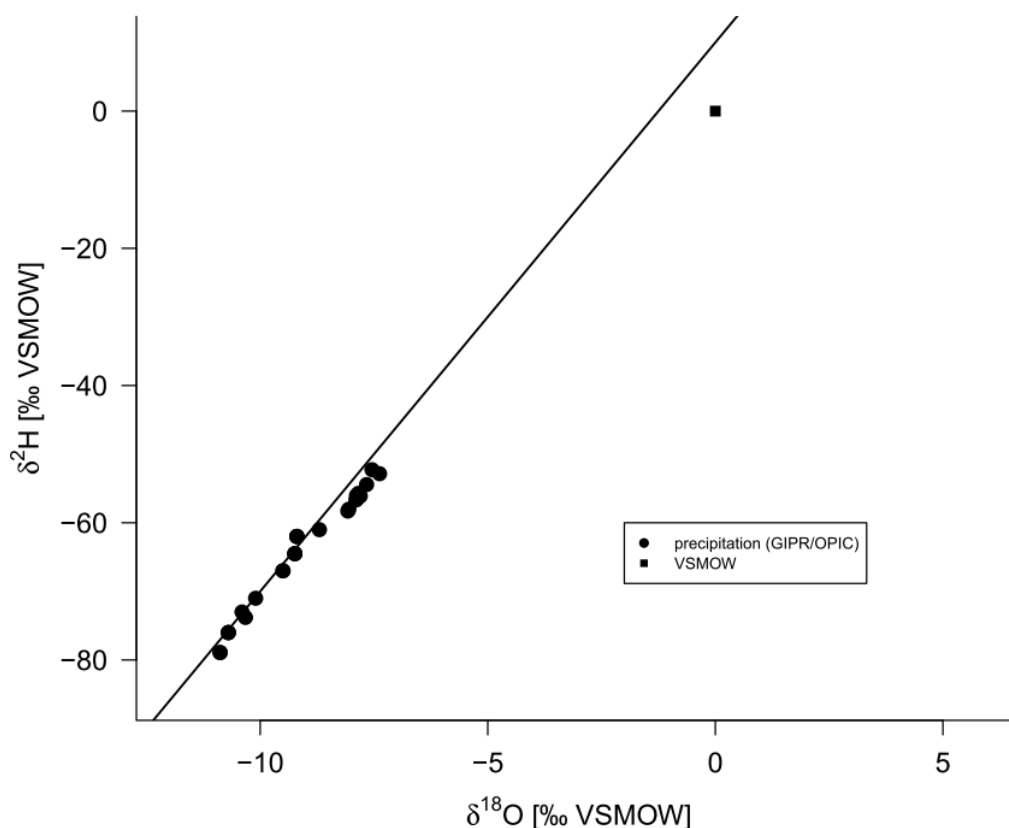


10

11 **Fig. S2.** Comparison between $\delta^{18}\text{O}_{\text{GIPR/OIPC}}$ values vs. location altitudes for the three different
 12 vegetation types along the transect. The red line represents the regression line throughout all
 13 German sites. All data points are marked with the location names. Swedish and Danish sites
 14 are boarded in black. Abbreviations: con = coniferous forest sites (n=9); dec = deciduous forest
 15 sites (n=11); grass = grassland sites (n=4).



16 **Fig. S3.** Comparison between $\delta^{18}\text{O}_{\text{GIPR/OIPC}}$ values vs. T_{MA} for the three different vegetation
 17 types along the transect. The red line represents the regression line throughout all sites.
 18 Abbreviations: con = coniferous forest sites (n=9); dec = deciduous forest sites (n=11); grass =
 19 grassland sites (n=4).



20 **Fig. S4.** $\delta^2\text{H}_{\text{GIPR/OIPC}}$ vs. $\delta^{18}\text{O}_{\text{GIPR/OIPC}}$ diagram along the transect. The black line represents the
 21 global meteoric water line (GMWL; $\delta^2\text{H} = 8 \times \delta^{18}\text{O} + 10$; Dansgaard, 1964).

22

23 Based on the values quoted in the Tabs. S1 and S2, $\delta^{18}\text{O}$ is plotted as functions of the reported
 24 environmental parameters (climate station P_{MA} , location altitude and T_{MA} ; Figs. S1 to S3).

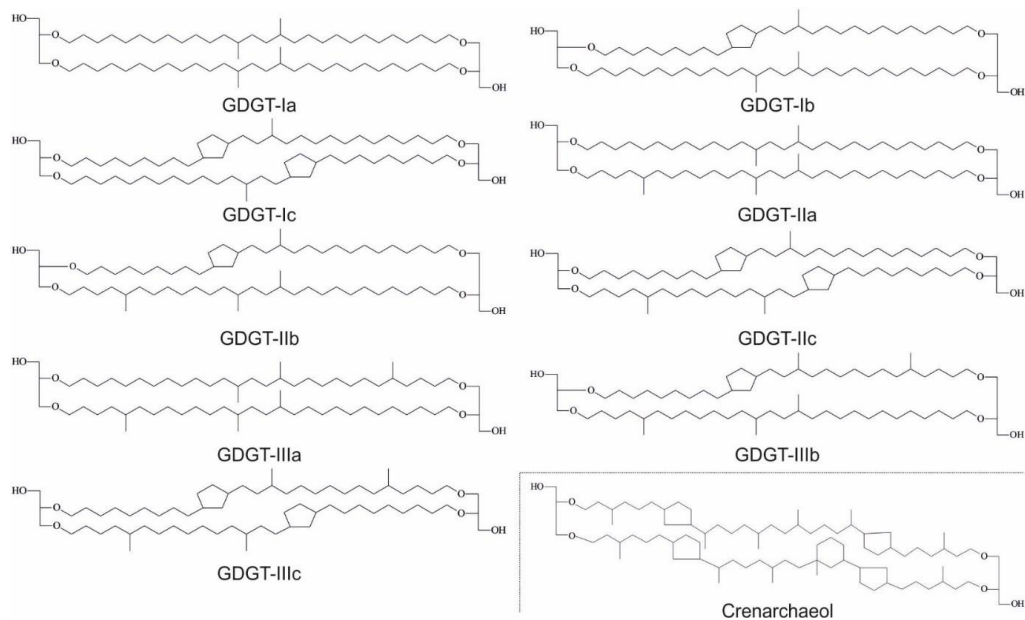
25 It is worth to note that the five points representing Danish and Swedish sites (L12 to L16) form
 26 a separate group in Figs. S2 and S3, with clear more negative $\delta^{18}\text{O}$ values. All other
 27 (continental) sites show a regular altitude effect (decreasing $\delta^{18}\text{O}$ values with increasing
 28 altitude; red trend in Fig. S3). All Danish and Swedish isotope signatures of precipitation are
 29 shifted from the trend line by ca 2 to 2.5‰ towards more negative $\delta^{18}\text{O}$ values. One would
 30 rather expect more enriched values due to relative proximity to the sea. It should be noted that
 31 those values were derived from OIPC, while the $\delta^{18}\text{O}$ data for the German sites is derived from
 32 GNIP/ANIP data (see section 2.2 for more details).

33 The precipitation $\delta^{18}\text{O}$ shows the expected relationship with T_{MA} (Fig. S4). The slope of this
 34 relationship (ca. 0.54‰/°C) is in the range of the slope of δ -T spatial relationship observed at
 35 mid latitudes of the northern hemisphere (e.g. Rozanski et al., 1993).

36 It is apparent from the above Fig. S5 that the data points plot along the GMWL. Only more
 37 positive $\delta^{18}\text{O}$ values cluster below the line, indicating most probably some evaporation

38 enrichment effects (partial evaporation of raindrops and/or evaporation effects in the rain
39 gauges).

40



41 **Fig. S5.** Structures of brGDGTs and Crenarchaeol mentioned.

42

43 Literature

44 Dansgaard, W.: Stable isotopes in precipitation, *Tellus*, 16(4), 436–468, doi:10.1111/j.2153-
45 3490.1964.tb00181.x, 1964.

46 Rozanski, K., Araguás-Araguás, L. and Gonfiantini, R.: Isotopic patterns in modern global
47 precipitation, *Climate change in continental isotopic records*, 1–36, 1993.

48 **Supplementary data**

49 **Tab. S1.** Location characterization, GIPR and OIPC data.

Location	Vegetation	Characterization	Precipitation $\delta^2\text{H}$ (‰)	Precipitation $\delta^{18}\text{O}$ source (‰)
L01	con	spruce forest, steep hillside	-78.9	-10.9
L01	dec	beech forest, close to fir stand	-78.9	GIPR ^{A,B,C,D}
L02	con	fir forest	-73.8	GIPR ^{A,B,C,D}
L03	dec	beeches, oaks, limes, sparse pines	-56.6	-10.3
L03	grass	glade, next to farmland and fruit trees (apple, plum)	-56.6	GIPR ^{A,B,C,D}
L04	dec	beech forest, sparse firs and oaks	-58.3	-7.9
L04	grass	grassland in the valley, next to beech forest	-58.0	GIPR ^{A,B,C,D}
L05	dec	oak forest, sparse beeches, elms and pines	-55.7	-8.1
L06	dec	beech forest, steep hillside	-64.5	GIPR ^{A,B,C,D}
L06-1	con1	sparse pine forest with grass layer	-64.5	-9.2
L06-2	con2	sparse larch forest with grass layer	-64.5	GIPR ^{A,B,C,D}
L07	dec	beeches, acers, elms, oaks	-52.8	-9.2
L07	grass	heath	-54.4	GIPR ^{A,B,C,D}
L08	con	luxuriant spruce forest	-62.0	-7.7
L08	dec	young beech forest at hillside, close to spruce stand	-62.0	GIPR ^{A,B,C,D}
L08	grass	heath, small shrubs, close to spruce stand, initially cleared	-62.0	-9.2
L09	dec	birch forest with small oaks, sparse poplars, surrounded by farmland	-56.1	GIPR ^{A,B,C,D}
L09	grass	next to farm track	-56.2	-7.8
L10	dec	beech-oak-forest	-52.3	GIPR ^{A,B,C,D}
L11	con	spruce forest with larches	-56.0	-7.5
L11	grass	cow pasture, sparse oaks	-56.0	GIPR ^{A,B,C,D}
L12	dec	acer forest with poplars, ashes and elder	-61.0	-7.9
L13	con	fir forest with swampy underground	-67.0	GIPR ^{A,B,C,D}
L13	dec	beech forest with sparse acers, birches, loamy underground	-67.0	OIPC ^{E,F,6}
L14	con	spruce-pine-forest with moss layer	-71.0	-8.7
L15	con	spruce forest, sparse birches, used as cattle run	-76.0	OIPC ^{E,F,6}
L15-1	dec1	acers, oaks, beeches, sparse firs, on partly pebbly, partly humus-rich floor	-76.0	OIPC ^{E,F,6}
L15-2	dec2	birch- and oak-belt at spruce forest edge, grass layer, also used as cattle run	-76.0	OIPC ^{E,F,6}
L16	dec	oak forest, sparse birches and larches	-73.0	-10.7
L16	dec		-73.0	OIPC ^{E,F,6}

^a Stump, C., Stichler, W., 2014. Analysis of long-term stable isotopic composition in German precipitation. *Journal of Hydrology* 517, 351–361.
^b IAEA/WMO, 2018. Global Network of Isotopes in Precipitation. The GNIP Database, <https://nuclides.iaea.org/wiser>.
^c van Geldern, R., Baier, A., Subert, H.L., Kowol, S., Balk, L., Barth, J.A.C., 2014. (Table S1) Stable isotope composition of precipitation sampled at Erlangen, Germany between 2010 and 2013 for station Geozentrum located at Erlangen city center, in: Supplement to: Van Geldern, R. et al. (2014): Pleistocene Paleo-Groundwater as a Pristine Fresh Water Resource in Southern Germany – Evidence from Stable and Radiogenic Isotopes. *Science of the Total Environment*, 496, 107–115, <https://doi.org/10.1016/j.scitotenv.2014.06.016>. PANGAEA.

^d Umweltbundesamt GmbH, 2018. Erhebung der Wasserhärte in Österreich gemäß Hydrographengesetz i.d.F. des BGBl. Nr. 252/90 (ültig bis Dezember 2006) bzw. Gewässerzustandsüberwachung in Österreich gemäß Wasserrechtsgesetz, BGBl. I Nr. 123/06, i.d.F.; BMLFUW, Sektion IV / Abteilung 3 N, Öffentliche Qualitätsdaten-Abfrage.

^e Bowen, G.J., 2018. The Online Isotopes in Precipitation Calculator, version 3.1, <http://www.waterisotopes.org>.

^f IAEA/WMO, 2015. Global Network of Isotopes in Precipitation. The GNIP Database, <https://nuclides.iaea.org/wiser>.

^g Bowen, G.J., Revenaugh, J., 2003. Interpolating the isotopic composition of modern meteoric precipitation. *Water Resources Research* 39, 1–13.

50 Tab. S2. Climate station data.

Location	Vegetation	Station ID	Name	Latitude (decimal °)	Longitude (decimal °)	Altitude (m)	Observation begin (YYYYMMDD)	Observation end (YYYYMMDD)	T _{aw} (°C)	T _{sw} (°C)	Observation begin (YYYYMMDD)	Observation end (YYYYMMDD)	T _{aw} (°C)	T _{sw} (°C)	Station ID	Name	Latitude (decimal °)
L01	con	3730	Oberstdorf	47.40	10.28	806	19480101	20171231	6.5 ^A	11.5 ^A	n.n.	n.n.	14.2 ^A	n.n.	n.n.	n.n.	n.n.
L01	dec	3730	Oberstdorf	47.40	10.28	806	19480101	20171231	6.5 ^A	11.5 ^A	n.n.	n.n.	14.2 ^A	n.n.	n.n.	n.n.	n.n.
L02	con	2290	Hohenpeißenberg	47.80	11.01	977	19470101	20171231	7.0 ^A	11.4 ^A	n.n.	n.n.	12.7 ^A	n.n.	n.n.	n.n.	n.n.
L03	dec	2522	Karlsruhe	49.04	8.36	112	19480101	20081102	10.5 ^A	15.3 ^A	n.n.	n.n.	17.8 ^A	n.n.	n.n.	n.n.	n.n.
L03	grass	2522	Karlsruhe	49.04	8.36	112	19480101	20081102	10.5 ^A	15.3 ^A	n.n.	n.n.	17.8 ^A	n.n.	n.n.	n.n.	n.n.
L04	dec	3761	Öhringen	49.21	9.52	276	19550101	20171231	9.6 ^A	14.4 ^A	n.n.	n.n.	16.8 ^A	n.n.	n.n.	n.n.	n.n.
L04	grass	3761	Öhringen	49.21	9.52	276	19550101	20171231	9.6 ^A	14.4 ^A	n.n.	n.n.	16.8 ^A	n.n.	n.n.	n.n.	n.n.
L05	dec	5906	Mannheim	49.51	8.56	98	19480101	20171231	10.6 ^A	15.4 ^A	n.n.	n.n.	17.9 ^A	n.n.	n.n.	n.n.	n.n.
L06	dec	3231	Meinigen	50.56	10.38	450	19790101	20171231	7.8 ^A	12.7 ^A	n.n.	n.n.	14.7 ^A	n.n.	n.n.	n.n.	n.n.
L06-1	con1	3231	Meinigen	50.56	10.38	450	19790101	20171231	7.8 ^A	12.7 ^A	n.n.	n.n.	14.7 ^A	n.n.	n.n.	n.n.	n.n.
L06-2	con2	3231	Meinigen	50.56	10.38	450	19790101	20171231	7.8 ^A	12.7 ^A	n.n.	n.n.	14.7 ^A	n.n.	n.n.	n.n.	n.n.
L07	dec	2667	Köln-Bonn	50.86	7.16	92	19600101	20171231	10.1 ^A	14.4 ^A	n.n.	n.n.	16.7 ^A	n.n.	n.n.	n.n.	n.n.
L07	grass	2667	Köln-Bonn	50.86	7.16	92	19600101	20171231	10.1 ^A	14.4 ^A	n.n.	n.n.	16.7 ^A	n.n.	n.n.	n.n.	n.n.
L08	con	2483	Kahler Asten	51.18	8.49	839	19510101	20171231	5.3 ^A	9.6 ^A	n.n.	n.n.	10.9 ^A	n.n.	n.n.	n.n.	n.n.
L08	dec	2483	Kahler Asten	51.18	8.49	839	19510101	20171231	5.3 ^A	9.6 ^A	n.n.	n.n.	10.9 ^A	n.n.	n.n.	n.n.	n.n.
L08	grass	2483	Kahler Asten	51.18	8.49	839	19510101	20171231	5.3 ^A	9.6 ^A	n.n.	n.n.	10.9 ^A	n.n.	n.n.	n.n.	n.n.
L09	dec	2014	Hannover	52.46	9.68	55	19490101	20171231	9.2 ^A	13.7 ^A	n.n.	n.n.	15.9 ^A	n.n.	n.n.	n.n.	n.n.
L09	grass	2014	Hannover	52.46	9.68	55	19490101	20171231	9.2 ^A	13.7 ^A	n.n.	n.n.	15.9 ^A	n.n.	n.n.	n.n.	n.n.
L10	dec	691	Bremen	53.05	8.80	4	19490101	20171231	9.2 ^A	13.6 ^A	n.n.	n.n.	15.7 ^A	n.n.	n.n.	n.n.	n.n.
L11	con	4466	Schleswig	54.53	9.55	43	19510101	20171231	8.4 ^A	12.6 ^A	n.n.	n.n.	14.4 ^A	n.n.	n.n.	n.n.	n.n.
L11	grass	4466	Schleswig	54.53	9.55	43	19510101	20171231	8.4 ^A	12.6 ^A	n.n.	n.n.	14.4 ^A	n.n.	n.n.	n.n.	n.n.
L12	dec	06120	Odense Lufthavn	55.48	10.33	15	19610101	20001231	8.3 ^C	12.5 ^C	n.n.	n.n.	n.a.	n.n.	n.n.	n.n.	n.n.
L13	con	30110	Spodsbjerg	55.98	11.85	34	19610101	19901231	8.0 ^C	12.5 ^C	n.n.	n.n.	n.a.	n.n.	n.n.	n.n.	n.n.
L13	dec	30110	Spodsbjerg	55.98	11.85	34	19610101	19901231	8.0 ^C	12.5 ^C	n.n.	n.n.	n.a.	n.n.	n.n.	n.n.	n.n.
L14	con	74180	Hagshult Mo	57.29	14.13	169	19430101	20180601	5.8 ^F	10.8 ^F	n.n.	n.n.	n.a.	n.n.	n.n.	n.n.	n.n.
L15	con	84580	Snavlunda	58.97	14.90	144/140	19440101	19830901	5.4 ^F	10.8 ^F	n.n.	n.n.	13.9 ^F	85460	Kettstaka A	58.72	n.n.
L15-1	dec1	84580	Snavlunda	58.97	14.90	144/140	19440101	19830901	5.4 ^F	10.8 ^F	n.n.	n.n.	13.9 ^F	85460	Kettstaka A	58.72	n.n.
L15-2	dec2	84580	Snavlunda	58.97	14.90	144/140	19440101	19830901	5.4 ^F	10.8 ^F	n.n.	n.n.	13.9 ^F	85460	Kettstaka A	58.72	n.n.
L16	dec	85330	Motala Kraftverk	58.55	15.08	94	19340101	19901228	6.4 ^F	11.6 ^F	n.n.	n.n.	14.9 ^F	84310	Karlsborg Mo	58.51	n.n.

n.n. = not needed/see information further left

n.a. = not available

^A DWD Climate Data Center, 2018a. Historical hourly station observations of 2m air temperature and humidity for Germany, version v006.

^B DWD Climate Data Center, 2018b. Historical annual precipitation observations for Germany, version v007.

^C Laursen, E.V., Thomsen, R.S., Cappelen, J., 1999. Observed Air Temperature, Humidity, Pressure, Cloud Cover and Weather in Denmark - with Climatological Standard Normals, 1961-90.

^D Cappelen, J., 2002. Danish Climatological Normals 1971-2000 - for selected stations.

^E Frich, P., Rosenørn, S., Madsen, H., Jensen, J.J., 1997. Observed Precipitation in Denmark, 1961-90.

^F Swedish Meteorological and Hydrological Institute, 2018. SMHI Open Data Meteorological Observations, <https://opendata-download-metobs.smhi.se/explore/>.

51 Tab. S2. continuation...

Longitude (decimal °)	Altitude (m)	Observation begin (YYYYMMDD)	Observation end (YYYYMMDD)	RH _{low} (%)	RH _{low} (%)	RH _{low} (%)	Name	Latitude (decimal °)	Longitude (decimal °)	Altitude (m)	Observation begin (YYYYMMDD)	Observation end (YYYYMMDD)	P _{max} (mm)	Source
n.n.	n.n.	n.n.	n.n.	82 ^A	80 ^A	70 ^A	n.n.	n.n.	n.n.	n.n.	n.n.	n.n.	1769 ^B	DWD
n.n.	n.n.	n.n.	n.n.	82 ^A	80 ^A	70 ^A	n.n.	n.n.	n.n.	n.n.	n.n.	n.n.	1769 ^B	DWD
n.n.	n.n.	n.n.	n.n.	78 ^A	77 ^A	73 ^A	n.n.	n.n.	n.n.	n.n.	n.n.	n.n.	1173 ^B	DWD
n.n.	n.n.	n.n.	n.n.	77 ^A	73 ^A	63 ^A	n.n.	n.n.	n.n.	n.n.	n.n.	n.n.	758 ^B	DWD
n.n.	n.n.	n.n.	n.n.	77 ^A	73 ^A	63 ^A	n.n.	n.n.	n.n.	n.n.	n.n.	n.n.	758 ^B	DWD
n.n.	n.n.	n.n.	n.n.	77 ^A	74 ^A	65 ^A	n.n.	n.n.	n.n.	n.n.	n.n.	n.n.	816 ^B	DWD
n.n.	n.n.	n.n.	n.n.	77 ^A	74 ^A	65 ^A	n.n.	n.n.	n.n.	n.n.	n.n.	n.n.	816 ^B	DWD
n.n.	n.n.	n.n.	n.n.	75 ^A	71 ^A	61 ^A	n.n.	n.n.	n.n.	n.n.	n.n.	n.n.	658 ^B	DWD
n.n.	n.n.	n.n.	n.n.	79 ^A	75 ^A	67 ^A	n.n.	n.n.	n.n.	n.n.	n.n.	n.n.	660 ^B	DWD
n.n.	n.n.	n.n.	n.n.	79 ^A	75 ^A	67 ^A	n.n.	n.n.	n.n.	n.n.	n.n.	n.n.	660 ^B	DWD
n.n.	n.n.	n.n.	n.n.	79 ^A	75 ^A	67 ^A	n.n.	n.n.	n.n.	n.n.	n.n.	n.n.	660 ^B	DWD
n.n.	n.n.	n.n.	n.n.	77 ^A	74 ^A	65 ^A	n.n.	n.n.	n.n.	n.n.	n.n.	n.n.	809 ^B	DWD
n.n.	n.n.	n.n.	n.n.	77 ^A	74 ^A	65 ^A	n.n.	n.n.	n.n.	n.n.	n.n.	n.n.	809 ^B	DWD
n.n.	n.n.	n.n.	n.n.	87 ^A	84 ^A	78 ^A	n.n.	n.n.	n.n.	n.n.	n.n.	n.n.	1417 ^B	DWD
n.n.	n.n.	n.n.	n.n.	87 ^A	84 ^A	78 ^A	n.n.	n.n.	n.n.	n.n.	n.n.	n.n.	1417 ^B	DWD
n.n.	n.n.	n.n.	n.n.	87 ^A	84 ^A	78 ^A	n.n.	n.n.	n.n.	n.n.	n.n.	n.n.	1417 ^B	DWD
n.n.	n.n.	n.n.	n.n.	80 ^A	76 ^A	68 ^A	n.n.	n.n.	n.n.	n.n.	n.n.	n.n.	650 ^B	DWD
n.n.	n.n.	n.n.	n.n.	80 ^A	76 ^A	68 ^A	n.n.	n.n.	n.n.	n.n.	n.n.	n.n.	650 ^B	DWD
n.n.	n.n.	n.n.	n.n.	80 ^A	77 ^A	69 ^A	n.n.	n.n.	n.n.	n.n.	n.n.	n.n.	699 ^B	DWD
n.n.	n.n.	n.n.	n.n.	80 ^A	77 ^A	69 ^A	n.n.	n.n.	n.n.	n.n.	n.n.	n.n.	699 ^B	DWD
n.n.	n.n.	n.n.	n.n.	83 ^A	80 ^A	72 ^A	n.n.	n.n.	n.n.	n.n.	n.n.	n.n.	900 ^B	DWD
n.n.	n.n.	n.n.	n.n.	83 ^A	80 ^A	72 ^A	n.n.	n.n.	n.n.	n.n.	n.n.	n.n.	900 ^B	DWD
n.n.	n.n.	n.n.	n.n.	81 ^C	76 ^C	63 ^C	n.n.	n.n.	n.n.	n.n.	n.n.	n.n.	572 ^E	DMI
n.n.	n.n.	n.n.	n.n.	84 ^C	80 ^C	74 ^C	n.n.	n.n.	n.n.	n.n.	n.n.	n.n.	554 ^E	DMI
n.n.	n.n.	n.n.	n.n.	84 ^C	80 ^C	74 ^C	n.n.	n.n.	n.n.	n.n.	n.n.	n.n.	554 ^E	DMI
n.n.	n.n.	n.n.	n.n.	86 ^F	79 ^F	68 ^F	n.n.	n.n.	n.n.	n.n.	n.n.	n.n.	554 ^E	DMI
n.n.	n.n.	n.n.	n.n.	82 ^F	75 ^F	68 ^F	Snavlundia D	n.n.	n.n.	n.n.	n.n.	n.n.	717 ^F	SMHI
15.03	225	19950801	20180601	82 ^F	75 ^F	68 ^F	Snavlundia D	58.95/58.97/58.97	14.91/14.90/14.90	135/144/140	19440101	20150101	693 ^F	SMHI
15.03	225	19950801	20180601	82 ^F	75 ^F	68 ^F	Snavlundia D	58.95/58.97/58.97	14.91/14.90/14.90	135/144/140	19440101	20150101	693 ^F	SMHI
15.03	225	19950801	20180601	82 ^F	75 ^F	68 ^F	Snavlundia D	58.95/58.97/58.97	14.91/14.90/14.90	135/144/140	19440101	20150101	693 ^F	SMHI
14.51	95	20130101	20180601	83 ^F	78 ^F	71 ^F	Motala	58.56/58.55/58.55	15.02/15.01/15.08	95/95/94	19310101	20180501	557 ^F	SMHI

52 **Tab. S3.** GDGT data. Crenarcheol and brGDGTs in µg/g dry weight.

Location	Vegetation	pH (H ₂ O)	Crenarcheol ^a (ng/g dry weight)	IIIa ^a (ng/g dry weight)	IIIb ^a (ng/g dry weight)	IIIc ^a (ng/g dry weight)	IIIa ^a (ng/g dry weight)	IIIb ^a (ng/g dry weight)	IIIc ^a (ng/g dry weight)	IIa ^a (ng/g dry weight)	IIb ^a (ng/g dry weight)	IIc ^a (ng/g dry weight)	IIa ^a (ng/g dry weight)	IIb ^a (ng/g dry weight)	IIc ^a (ng/g dry weight)	Ic ^a (ng/g dry weight)
L01	con	4.5	2	194	3	0	645	34	1	531	38	7	531	38	7	7
L01	con	4.0	1	109	1	0	556	7	3	687	37	10	687	37	10	10
L02	con	6.5	38	128	9	1	329	81	4	160	86	79	160	86	79	79
L03	grass	4.3	16	55	0	0	617	17	5	1289	30	9	1289	30	9	9
L03	grass	5.2	12	28	0	0	142	8	1	124	12	2	124	12	2	2
L04	dec	5.9	13	60	4	1	185	37	3	137	33	6	137	33	6	6
L04	grass	6.0	208	54	7	3	131	105	8	79	92	27	79	92	27	27
L05	dec	4.1	15	25	0	0	204	2	1	380	5	1	380	5	1	1
L06	dec	7.3	16	226	26	1	304	184	6	66	66	5	66	66	5	5
L06-1	con1	4.5	2	116	0	0	585	18	7	549	21	1	549	21	1	1
L06-2	con2	6.0	19	332	24	2	695	197	7	295	97	12	295	97	12	12
L07	dec	3.6	149	67	1	1	506	10	4	677	16	5	677	16	5	5
L07	grass	4.2	18	19	0	0	141	1	1	183	2	1	183	2	1	1
L08	con	3.3	29	213	0	0	2265	26	19	3287	32	13	3287	32	13	13
L08	dec	3.6	11	84	0	0	821	12	5	1450	21	8	1450	21	8	8
L08	grass	4.3	0	232	0	0	996	11	2	884	21	6	884	21	6	6
L09	dec	3.6	64	101	1	0	943	13	5	1513	19	8	1513	19	8	8
L09	grass	4.3	16	26	1	0	169	1	1	275	5	1	275	5	1	1
L10	dec	3.0	1084	157	33	4	463	68	17	816	23	8	816	23	8	8
L11	con	3.5	512	76	0	1	353	6	0	406	8	2	406	8	2	2
L11	grass	5.9	19	89	0	0	579	26	2	714	44	5	714	44	5	5
L12	dec	4.9	735	450	16	2	2219	418	36	1642	476	142	1642	476	142	142
L13	con	3.2	0	56	0	3	619	0	6	993	13	20	993	13	20	20
L13	dec	3.7	0	150	0	0	1422	28	16	3165	46	19	3165	46	19	19
L14	con	3.6	0	103	2	0	1180	5	9	2077	17	4	2077	17	4	4
L15	con	3.6	0	207	3	1	2866	48	26	5695	98	35	5695	98	35	35
L15-1	dec1	5.0	7	192	2	0	933	41	4	658	58	22	658	58	22	22
L15-2	dec2	4.1	5	210	1	0	1896	24	14	2541	41	13	2541	41	13	13
L16	dec	4.3	0	54	0	0	349	5	1	424	9	2	424	9	2	2

^a structures can be found in Fig. S5
^b BIT index was calculated according to Hopmans, E.C., Weijers, J.W.H., Schefuß, E., Herfort, L., Sinninghe Damsté, J.S., Schouten, S., 2004. A novel proxy for terrestrial organic matter in sediments based on branched and isoprenoid tetraether lipids. *Earth and Planetary Science Letters* 224, 107–116.
^c MBT', CBT, reconstructed *T_{amb}*, and pHCBT according to Petersen, F., van der Meer, J., Schouten, S., Weijers, J.W.H., Fierer, N., Jackson, R.B., Kim, J.H., Sinninghe Damsté, J.S., 2012. Revised calibration of the MBT-CBT paleotemperature proxy based on branched tetraether membrane lipids in surface soils. *Geochimica et Cosmochimica Acta* 96, 215–229.

53 **Tab. S3.** continuation...

brGDGT concentration ($\mu\text{g/g}$ dry weight)	BIT	MBT	CBT	reconstructed T_{max} ($^{\circ}\text{C}$)	pH_{ref}
1.65	1.00	0.35	1.3	4.3	5.37
1.39	1.00	0.53	1.4	9.0	5.05
0.88	0.94	0.37	0.5	9.8	6.98
2.02	0.99	0.66	1.6	12.1	4.74
0.32	0.96	0.43	1.1	7.9	5.69
0.47	0.97	0.38	0.7	8.9	6.59
0.51	0.56	0.40	0.0	13.0	7.84
0.62	0.98	0.63	2.0	9.0	4.01
0.90	0.97	0.17	0.2	5.1	7.54
1.29	1.00	0.44	1.5	6.3	5.04
1.66	0.99	0.25	0.5	5.5	6.86
1.29	0.89	0.54	1.7	8.2	4.63
0.35	0.95	0.53	2.0	5.9	3.90
5.86	1.00	0.57	2.0	7.2	4.00
2.40	1.00	0.62	1.8	9.4	4.26
2.15	1.00	0.42	1.8	3.8	4.39
2.60	0.98	0.59	1.9	8.5	4.19
0.48	0.97	0.59	1.9	8.5	4.23
1.59	0.57	0.55	1.2	11.2	5.63
0.85	0.62	0.49	1.7	6.2	4.50
1.46	0.99	0.52	1.3	9.8	5.40
5.40	0.85	0.42	0.6	10.2	6.65
1.71	1.00	0.60	2.1	7.6	3.78
4.85	1.00	0.67	1.8	11.3	4.37
3.40	1.00	0.62	2.2	7.7	3.64
8.98	1.00	0.65	1.8	10.9	4.42
1.91	1.00	0.39	1.2	6.0	5.52
4.74	1.00	0.55	1.8	7.4	4.29
0.84	1.00	0.52	1.7	6.9	4.46

54 **Tab. S4.** Measured *n*-alkane $\delta^2\text{H}$ and sugar $\delta^{18}\text{O}$ data along with calculations and reconstruction
 55 results.

Location	Vegetation	<i>n</i> -alkane $\delta^2\text{H}$ (‰)	sugar $\delta^{18}\text{O}$ (‰)	ϵ_r , alkanes/precipitation (‰)	ϵ_{sugar} /precipitation (‰)	reconstructed $\delta^2\text{H}_{\text{source-water}}$ (‰)	reconstructed $\delta^{18}\text{O}_{\text{source-water}}$ (‰)	reconstructed RH_{IPDY} (%)
L01	con	-216.2	34.17	-149	45.5	-139	-18.7	34
L01	dec	-190.6	35.95	-121	47.3	-100	-13.8	42
L02	con	-169.4	32.95	-103	43.7	-49	-7.3	66
L03	dec	-176.8	34.54	-127	42.8	-67	-9.6	56
L03	grass	n.a.	29.96	n.a.	38.1	n.a.	n.a.	n.a.
L04	dec	n.a.	35.30	n.a.	43.7	n.a.	n.a.	n.a.
L04	grass	-208.6	30.80	-160	39.2	-110	-14.9	52
L05	dec	-169.6	32.95	-121	41.1	-47	-7.1	66
L06	dec	n.a.	34.30	n.a.	43.9	n.a.	n.a.	n.a.
L06-1	con1	-201.5	34.27	-146	43.9	-113	-15.3	42
L06-2	con2	-191.0	34.39	-135	44.0	-94	-13.0	48
L07	dec	-170.4	36.07	-124	43.8	-62	-9.0	54
L07	grass	n.a.	31.28	n.a.	39.2	n.a.	n.a.	n.a.
L08	con	-168.3	38.42	-113	48.1	-72	-10.2	45
L08	dec	-156.3	36.19	-101	45.8	-40	-6.2	61
L08	grass	-184.2	31.51	-130	41.1	-71	-10.1	63
L09	dec	-177.8	31.66	-129	39.8	-57	-8.4	66
L09	grass	-191.6	28.30	-144	36.4	-69	-9.8	71
L10	dec	-171.6	39.45	-126	47.3	-79	-11.1	40
L11	con	-183.6	33.56	-135	41.8	-77	-10.8	55
L11	grass	-194.1	27.67	-146	35.8	-71	-10.1	72
L12	dec	-177.4	37.30	-124	46.4	-83	-11.6	44
L13	con	-182.9	36.62	-124	46.6	-90	-12.5	44
L13	dec	-183.8	28.79	-125	38.7	-57	-8.4	74
L14	con	-190.3	36.85	-128	47.4	-103	-14.1	39
L15	con	-201.1	32.13	-135	43.3	-103	-14.1	51
L15-1	dec1	-201.6	33.41	-136	44.6	-110	-15.0	45
L15-2	dec2	-209.7	33.05	-145	44.2	-123	-16.6	42
L16	dec	-191.6	28.41	-128	39.2	-69	-9.9	71

n.a. = not available

56

C. Manuscript 3: Hepp et al. (2017)

published in *Quaternary International*

<https://doi.org/10.1016/j.quaint.2017.03.059>



Contents lists available at ScienceDirect

Quaternary International

journal homepage: www.elsevier.com/locate/quaint

Late Quaternary relative humidity changes from Mt. Kilimanjaro, based on a coupled ^2H - ^{18}O biomarker paleohygrometer approach



Johannes Hepp^{a, b, *}, Roland Zech^{c, 1}, Kazimierz Rozanski^d, Mario Tuthorn^{a, b, 2}, Bruno Glaser^b, Markus Greule^e, Frank Keppler^e, Yongsong Huang^c, Wolfgang Zech^f, Michael Zech^{a, b, g, 3}

^a Department of Soil Physics and Chair of Geomorphology, University of Bayreuth, Universitätsstrasse 30, D-95440, Bayreuth, Germany

^b Institute of Agronomy and Nutritional Sciences, Soil Biogeochemistry, Martin-Luther University Halle-Wittenberg, Von-Seckendorff-Platz 3, D-06120, Halle, Germany

^c Department of Geological Sciences, Brown University, Providence, RI, 02912, USA

^d Faculty of Physics and Applied Computer Science, AGH University of Science and Technology, Al. Mickiewicza 30, 30-059, Kraków, Poland

^e Institute of Earth Sciences, University of Heidelberg, Im Neuenheimer Feld 236, D-69120, Heidelberg, Germany

^f Institute of Soil Science and Geography, University of Bayreuth, 95445 Bayreuth, Universitätsstrasse 30, D-95440, Bayreuth, Germany

^g Institute of Geography, Chair of Landscape- and Geoecology, Technical University of Dresden, Helmholtzstrasse 10, D-01062, Dresden, Germany

ARTICLE INFO

Article history:

Received 6 August 2016

Received in revised form

27 February 2017

Accepted 19 March 2017

Available online 11 April 2017

Keywords:

Paleohydrology

Paleosol

Deuterium

Oxygen-18

Leaf water

Evapotranspirative enrichment

ABSTRACT

Our understanding of African paleoclimate/hydrological history is mainly based on lake level and lake sediment studies. It improved during the last decade thanks to emerging stable isotope techniques such as compound-specific deuterium analysis of sedimentary leaf wax biomarkers ($\delta^2\text{H}_{\text{leaf-wax}}$). Here we present the results from a multi-proxy biomarker study carried out on a ~100 ka loess-like paleosol sequence preserved in the Maundi crater at ~2780 m a.s.l. on the southeastern slopes of Mt. Kilimanjaro in equatorial East Africa.

The Maundi stable isotope records established for hemicellulose-derived sugars, lignin- and pectin-derived methoxyl groups, leaf wax-derived fatty acid and *n*-alkane biomarkers ($\delta^{18}\text{O}_{\text{sugars}}$, $\delta^2\text{H}_{\text{methoxyl}}$ groups, $\delta^2\text{H}_{\text{fatty-acids}}$ and $\delta^2\text{H}_{\text{n-alkanes}}$, respectively) reveal similar patterns, but also some distinct differences are obvious. The periods from ~70 to 60 ka, the Last Glacial Maximum (LGM) and the Younger Dryas (YD) are characterized by more positive δ values, whereas during the Holocene, and around 30, 39, and 56 ka BP more negative δ values are determined. The application of a 'coupled $\delta^2\text{H}_{\text{n-alkane}}-\delta^{18}\text{O}_{\text{sugar}}$ paleohygrometer' approach allows us to derive information about Late Quaternary changes of air relative humidity at the Maundi study site. Reconstructed changes of mean day-time relative humidity (RH_D) are in good agreement with pollen results from the study area. Apart from the overall regional moisture availability, the intensification versus weakening of the trade wind inversion, which affects the diurnal montane atmospheric circulation on the slopes of Mt. Kilimanjaro, is suggested as a local factor which may contribute to the observed variability of RH_D at Maundi study site.

The combined usage of $\delta^2\text{H}_{\text{n-alkanes}}$ and $\delta^{18}\text{O}_{\text{sugars}}$ allowed us to reconstruct $\delta^2\text{H}/\delta^{18}\text{O}$ of source water utilized by plants in the study area, which is directly linked to local precipitation. The results of this reconstruction caution against a straightforward interpretation of $\delta^2\text{H}_{\text{leaf-wax}}$ and $\delta^{18}\text{O}_{\text{sugars}}$ records as proxies for isotopic composition of local precipitation because variable and primarily RH-dependent isotopic evaporative enrichment of leaf water can mask changes of $\delta^2\text{H}_{\text{prec}}/\delta^{18}\text{O}_{\text{prec}}$ in the past. The biomarker-based $\delta^2\text{H}/\delta^{18}\text{O}_{\text{source-water}}$ records derived for the Maundi site revealed a discernible link with the reconstructed RH_D record; lower RH_D values were generally observed during periods characterized by more negative $\delta^2\text{H}/\delta^{18}\text{O}_{\text{source-water}}$ values, indicating a reverse relationship with the expected precipitation amount. This indicates that the empirical relationship between amount of rainfall and its

* Corresponding author. Present address: Chair of Geomorphology, University of Bayreuth, Universitätsstrasse 30, D-95440, Bayreuth, Germany.

E-mail address: johannes-hepp@gmx.de (J. Hepp).

¹ Present address: Institute of Geography, Chair of Physical Geography, Friedrich-Schiller University of Jena, Löbdergraben 32, D-07743 Jena, Germany.

² Present address: Thermo Fisher Scientific, Bremen, Germany.

³ Present address: Institute of Geography, Chair of Landscape- and Geoecology, Technical University of Dresden, Helmholtzstrasse 10, D-01062 Dresden, Germany.

isotopic composition, observed nowadays on monthly timescale in the East African region, might not be valid on millennial time scale.

© 2017 Elsevier Ltd and INQUA. All rights reserved.

1. Introduction

East Africa and its Late Quaternary climate and vegetation history has received much attention during the last decades. Evidence for dramatic environmental and hydrological changes come from various types of archives, such as ice cores (Thompson et al., 2002) and glacial deposits (Mark and Osmaston, 2008; Shanahan and Zreda, 2000), lake sediments (e.g. Berke et al., 2012; Cockerton et al., 2015; Gasse, 2000; Gasse et al., 2008; Scholz et al., 2007; Street-Perrott et al., 2004; Trauth et al., 2003; Verschuren et al., 2009) and marine sediments (e.g. Schefuß et al., 2011; Tierney and deMenocal, 2013). The equatorial and northern East Africa, as well as the east Saharan region, experienced multiple lake level high-stands and humid conditions, especially during the Early Holocene (African Humid Period - AHP). The East African monsoon is responsible for rainy periods in East Africa and is controlled by low-latitude insolation changes occurring on orbital timescales. However, the forcing of the East African monsoon on millennial timescales is still a matter of debate. Evidence for precession forcing, including half-precession effects, have been presented in numerous studies (e.g. Trauth et al., 2003; Verschuren et al., 2009). However, many influencing factors and controlling mechanisms on East African paleoclimate are not yet fully understood. This concerns the teleconnection with high-latitude boundary conditions, for instance during the Younger Dryas period, the possible influence of the Indian Ocean Dipole (IOD) and the El Niño Southern Oscillation (ENSO) phenomena, and the possible influence of a migrating Congo air boundary (Abram et al., 2007; Castañeda et al., 2007; Konecky et al., 2011; Schefuß et al., 2011; Stager et al., 2011; Tierney et al., 2008, 2011). The multitude of possible controls of East African climate in the past stimulate the ongoing research efforts addressing exact timing, abruptness and spatial/temporal variability of East African monsoon precipitation.

During the last decade, the hydrogen isotopic composition of sedimentary leaf waxes ($\delta^2\text{H}_{\text{leaf-wax}}$) became a widely used proxy that was also explored in East African paleoclimate/hydrological archives. There are two major assumptions underlying most interpretations of $\delta^2\text{H}_{\text{leaf-wax}}$ records originating from this region. First, $\delta^2\text{H}$ values of leaf waxes extracted from lake sediments reflect the isotopic composition of paleoprecipitation ($\delta^2\text{H}_{\text{prec}}$) (e.g. Konecky et al., 2011; Tierney et al., 2010, 2011). Second, $\delta^2\text{H}_{\text{leaf-wax}}$ records retrieved from sedimentary archives can be interpreted in terms of an 'amount effect', as inferred from modern precipitation in the tropics (e.g. Schefuß et al., 2005, 2011; Tierney et al., 2008; Tierney and deMenocal, 2013).

However, the first assumption may not be as robust as previously thought. For instance, the ^2H content of leaf wax-derived *n*-alkane biomarkers, studied in a modern topsoil climate transect along the southern slopes of Mt. Kilimanjaro, does not follow the expected 'altitude effect' for $\delta^2\text{H}$ of local precipitation (Zech et al., 2015). The *n*-alkanes were rather found to reflect the isotopic composition of leaf water ($\delta^2\text{H}_{\text{leaf-water}}$), as it was previously suggested by Kahmen et al. (2013). Given that ^2H -enrichment of leaf water strongly depends on relative air humidity (Farquhar et al., 2007; Flanagan et al., 1991; Roden et al., 2000), large changes of this parameter may thus mask climatically-driven fluctuations of $\delta^2\text{H}_{\text{prec}}$.

The second assumption is based on the observation that for

present-day climate monthly means of $\delta^2\text{H}_{\text{prec}}$ ($\delta^{18}\text{O}_{\text{prec}}$) values in the tropics are inversely correlated with the precipitation amount collected at a given site (e.g. Rozanski et al., 1993). This is also true for East Africa (Rozanski et al., 1996). However, on an inter-annual basis, which is the relevant timescale for (paleo-)climatic considerations, such correlation is very poor or not-existent, at least for the East African region (Rozanski et al., 1996), and validation of a long-term 'amount effect' is in fact lacking for this area. Alternatively, Konecky et al. (2011) suggested that moisture source and transport history dominated the $\delta^2\text{H}_{\text{leaf-wax}}$ record at Lake Malawi, whereas rainfall amount played a secondary role.

In order to overcome ambiguities associated with the interpretations of $\delta^2\text{H}_{\text{leaf-wax}}$ records, Zech et al. (2013) suggested a coupled $\delta^2\text{H}_{n\text{-alkane}}\text{-}\delta^{18}\text{O}_{\text{sugar}}$ biomarker approach, where $\delta^{18}\text{O}_{\text{sugar}}$ is determined by compound-specific $\delta^{18}\text{O}$ -analyses of the hemicellulose-derived sugar biomarkers, such as arabinose, fucose, xylose and rhamnose (Zech and Glaser, 2009). This coupled approach opens up new possibilities: (i) in combination with known biosynthetic fractionation factors (ϵ_{bio}) it enables the reconstruction of the isotopic composition of leaf water [$\delta^2\text{H}_{\text{leaf-water}} = \delta^2\text{H}_{\text{leaf-wax}} - \epsilon_{\text{bio}}$ (*n*-alkanes); $\delta^{18}\text{O}_{\text{leaf-water}} = \delta^{18}\text{O}_{\text{sugars}} - \epsilon_{\text{bio}}$ (sugars)]. (ii) The evapotranspirative ^2H and ^{18}O enrichment of leaf water – characterized by the deuterium-excess of leaf water – can be used to quantify relative humidity of the local atmosphere for the periods when stomata are open and the transpiration process is in operation. Relative air humidity appears to be a decisive factor controlling the extent of this isotope enrichment. Finally, (iii) the intersect of the local leaf water evaporation line (LLEL) with the local meteoric water line (LMWL) can be used to reconstruct $\delta^2\text{H}/\delta^{18}\text{O}$ source water values more robustly than previously done, based on $\delta^2\text{H}_{\text{leaf-wax}}$ records alone. Recently, Tuthorn et al. (2015) validated this coupled $\delta^2\text{H}\text{-}\delta^{18}\text{O}$ biomarker approach by applying it to an Argentinean climate topsoil transect. Their findings corroborate that the 'coupled $\delta^2\text{H}_{n\text{-alkane}}\text{-}\delta^{18}\text{O}_{\text{sugar}}$ paleohygrometer' is a promising proxy for reconstructing day-time relative humidity of local atmosphere (RH_D).

The aim of this study was (i) to establish a multi-proxy stable isotope biomarker record spanning the last ~ 100 ka by investigating a loess-like paleosol sequence from the Maundi crater situated on the southeastern slopes of Mt. Kilimanjaro, equatorial East Africa, (ii) to compare the Maundi $\delta^2\text{H}_{n\text{-alkane}}$ record with the $\delta^2\text{H}$ records of fatty acids and lignin-/pectin-derived methoxyl groups ($\delta^2\text{H}_{\text{fatty-acid}}$ and $\delta^2\text{H}_{\text{methoxyl}}$, respectively) as well as with published $\delta^2\text{H}$ biomarker records from East African lakes, (iii) to reconstruct the past history of the RH_D at the Maundi study site using the 'coupled $\delta^2\text{H}_{n\text{-alkane}}\text{-}\delta^{18}\text{O}_{\text{sugar}}$ paleohygrometer', and (iv) to reconstruct and interpret the $\delta^2\text{H}/\delta^{18}\text{O}_{\text{source water}}$ record for the Maundi loess-like paleosol sequence in terms of paleoclimate.

2. Materials and methods

2.1. Study area – the Maundi crater

A detailed description of the study area, as well as an age-depth model of the Maundi loess-like paleosol sequence, were previously presented by Schüller et al. (2012). In brief, Maundi is an ancient volcanic crater of ~60 m diameter and 20–30 m depth that is located on the southeastern slopes of Mt. Kilimanjaro at ~2780 m

a.s.l. (Fig. 1; $3^{\circ}10'27.5''S$, $37^{\circ}31'05.8''E$). The surrounding vegetation represents the transition from closed forest (upper montane forest) to open *Erica* bush (subalpine heathland) (Fig. 1b). The bottom of the crater is occupied by a seasonal swamp, which only holds standing water during the rainy season (Schüler et al., 2012). There are two rainy seasons in the area caused by the seasonal migration of the ITCZ (Fig. 1a); the long rainy season from March to May with subsequently prevailing southeasterly trade winds and the short rainy season from November to December with subsequently prevailing northeasterly trade winds. Apart from seasonal climate variability, pronounced diurnal atmospheric circulation changes are observed along the slopes of Mt. Kilimanjaro (Appelhans et al., 2015; Duane et al., 2008; Pepin et al., 2010). Strong upslope moisture transport occurs during the day, whereas downslope transport and drying occurs at night. The study site is located above the RH maxima of the montane zone, as depicted by Fig. 1c. Mean annual precipitation at Maundi is ~1800 mm and mean annual temperature is about $9^{\circ}C$ (Hemp, 2006b). Mean day-time temperature from a close-by meteorological field station is slightly higher at $\sim 14^{\circ}C$ (cf. Appelhans et al., 2015).

During the Late Quaternary, the Maundi crater served as trap for aeolian and colluvial sediments. In July 2007, samples were taken from a 240 cm deep soil pit and additionally from further down to 646 cm depth using a piston corer. While Schüler et al. (2012) established their age-depth model by adapting a linear trend line through all 11 available calibrated AMS radiocarbon ages, we chose

a linear interpolation between each individual ^{14}C data for the upper 3 m of the sequence and a linear extrapolation for the lower part of the sequence (Fig. 2). The extrapolation suggests that the lowermost part of the core at 6.46 m depth may be as old as ~100 ka BP. Pollen, total organic carbon (TOC) and glycerol dialkyl glycerol tetraether (GDGT) biomarker results were published previously by Schüler et al. (2012) and Zech et al. (2012). The position of sugar, methoxyl and leaf wax (fatty acids and *n*-alkanes) samples are shown in Fig. 2.

2.2. Biomarker and compound-specific $\delta^{18}O/\delta^2H$ analyses

A total of 38 samples were prepared for $\delta^{18}O$ analyses of hemicellulose-derived sugar biomarkers according to Zech and Glaser (2009) at the Department of Soil Physics and the Chair of Geomorphology at the University of Bayreuth. In brief, the hemicelluloses were hydrolytically extracted with 4 M trifluoroacetic acid (TFA) (Amelung et al., 1996); the extracted sugars were cleaned using XAD-7 and Dowex 50WX8 columns; the purified sugars were freeze-dried and afterwards derivatized by adding methylboronic acid (MBA; 4 mg in 400 μ l pyridine) and heating for 1 h at $60^{\circ}C$. The compound-specific $\delta^{18}O$ measurements were performed at the Institute of Agronomy and Nutritional Sciences, Soil Biogeochemistry, Martin-Luther University Halle-Wittenberg, using a Trace GC 2000 gas chromatograph (GC; Thermo Fisher Scientific, Bremen, Germany) coupled to a Delta V Advantage isotope ratio mass

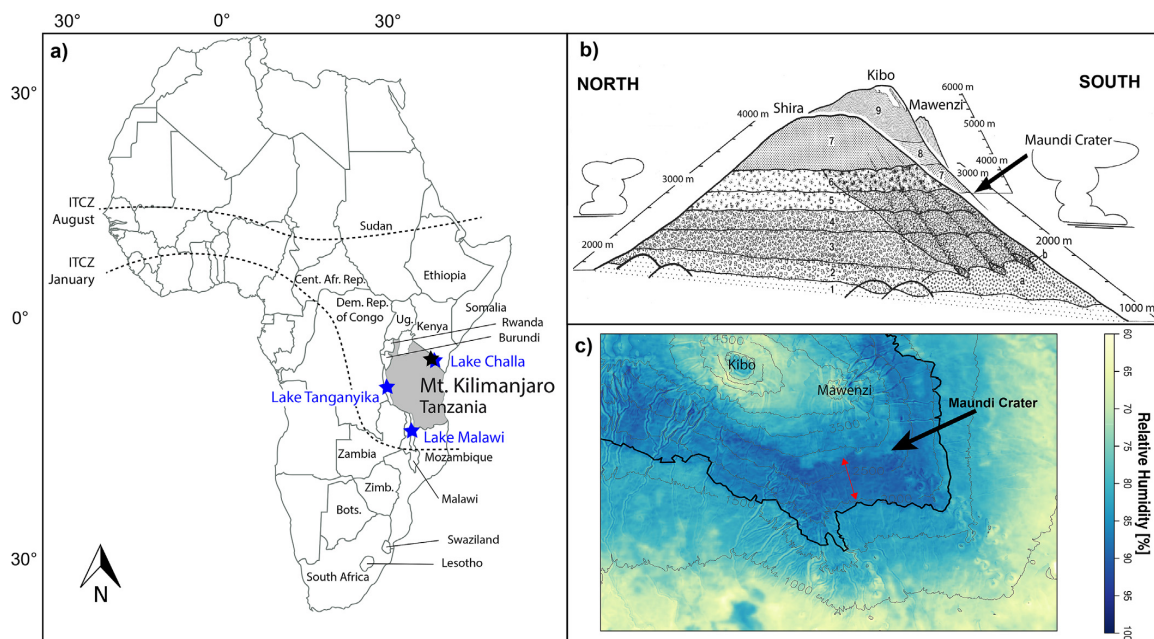


Fig. 1. a) Overview map of Africa depicting the study area Mt. Kilimanjaro, Tanzania. The black star shows the location of Maundi crater. Blue stars indicate locations of Lake Malawi, Lake Tanganyika, and Lake Challa. The dashed lines represent approximate positions of the ITCZ during August and January, respectively. b) North-south profile of the western slope of Mt. Kilimanjaro, showing the three volcanic cones Shira, Kibo and Mawenzi as well as the main altitudinal zones, vegetation types and the Maundi crater. 1: colline (savanna) zone; 2: submontane zone with *Croton-Calodendrum* forest; a: coffee-banana plantations in the submontane zone on the southern slope; b: submontane gorge forests on the southern slope; 3: lower montane zone with *Cassipourea* forests on the northern slope and *Agauria-Syzygium-Ocotea* forests on the southern slope; 4: middle montane zone with *Cassipourea* forests on the northern slope and *Ocotea* forests on the southern slope; 5: upper montane zone with *Juniperus* forests on the northern slope and *Podocarpus-Ocotea* forests on the southern slope; 6: subalpine zone with *Juniperus* forests on the northern slope and *Podocarpus* forests on the southern slope; 7: subalpine zone with heathlands (*Erica* bush); 8: lower alpine zone with *Helichrysum* cushion vegetation; 9: upper alpine and nival zone, mainly bare of vegetation (modified according to Hemp, 2006a). c) Relative humidity map illustrating the characteristic altitudinal hillside RH gradients and the RH maxima in the montane zone (red double arrow) (Appelhans et al., 2015; modified). Subfigures a) and b) reprinted and modified according to Schüler et al. (2012). (For interpretation of the references to colour in this figure legend, the reader is referred to the web version of this article.)

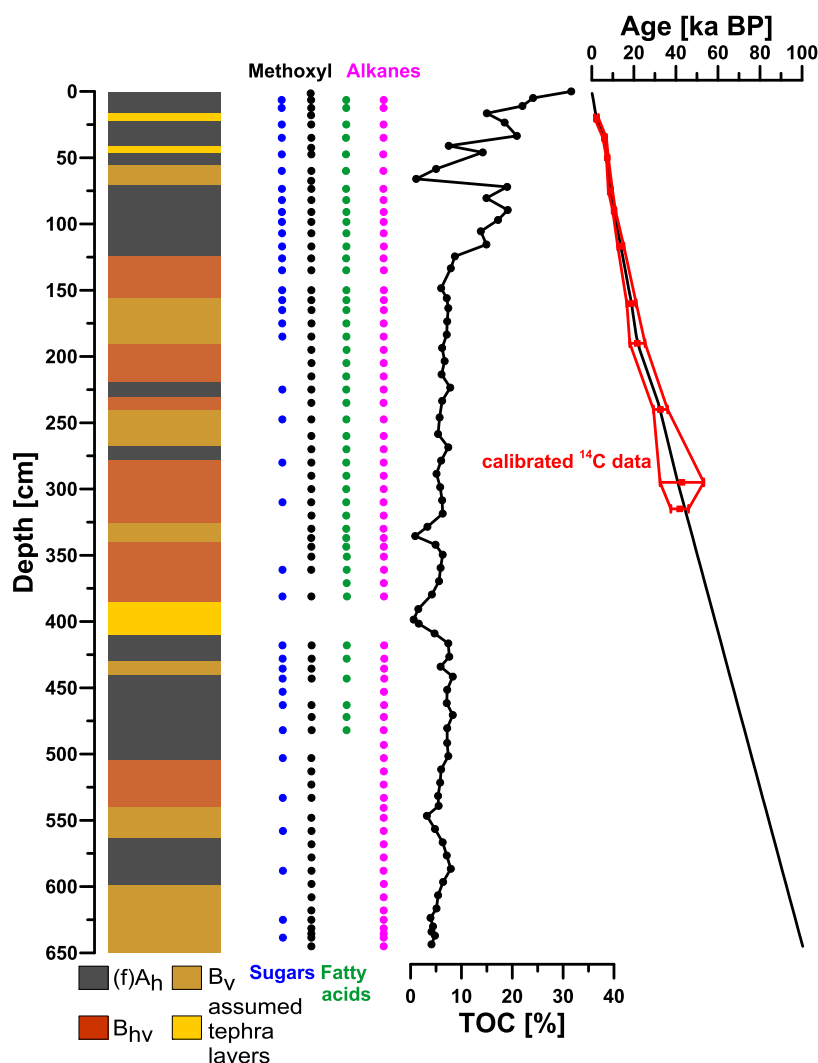


Fig. 2. Left: Stratigraphy of the Maundi loess-like paleosol sequence (modified according to Zech et al., 2012). (f)Ah_v: (fossil) dark soil horizons; B_v: weathered, brown soil horizons; B_{hv}: weathered, dark brown soil horizons; assumed tephra layers: yellowish smeary sandy silt (presumably strongly weathered tephra layers); and position of sugar (blue dots), methoxyl (black dots) and leaf wax (fatty acids as green dots and *n*-alkanes as magenta dots) samples. Middle: Total organic carbon (TOC) depth profile. Right: Revised age-depth model (black line) based on 11 calibrated AMS radiocarbon data (modified according to Schüller et al., 2012). Red squares display the calibrated ¹⁴C data with associated measurement uncertainties and uncertainty band (thin red lines). (For interpretation of the references to colour in this figure legend, the reader is referred to the web version of this article.)

spectrometer (IRMS; Thermo Fisher Scientific, Bremen, Germany) via an ¹⁸O-pyrolysis reactor and a GC/TC III interface (Thermo Fisher Scientific, Bremen, Germany). While arabinose, fucose and xylose yielded peak areas that were high enough for robust peak integrations in the chromatograms, rhamnose was excluded from further data evaluation due to too low peak areas. Mean standard errors for triplicate measurements of all 38 samples are 0.90‰, 1.46‰ and 0.97‰ for arabinose, fucose and xylose, respectively. The three sugars yielded very similar results with correlation coefficients ranging from 0.6 to 0.8 ($p < 0.001$; $n = 38$). In the following, we use the weighted mean $\delta^{18}\text{O}_{\text{sugars}}$ values of arabinose, fucose and xylose and refer to as $\delta^{18}\text{O}_{\text{sugars}}$, relative to Vienna

Standard Mean Ocean Water (VSMOW).

Laboratory work for the leaf wax analyses on 74 samples and compound-specific $\delta^2\text{H}$ measurements followed standard procedures at the Department of Geological Sciences, Brown University. In brief, free lipids were extracted using accelerated solvent extraction (Dionex ASE 200) with dichloromethane (DCM) and methanol (MeOH, 9:1). Lipids were separated over pipette columns filled with aminopropyl silica gel (Supelco, 45 μm). *n*-Alkanes were eluted with hexane, polar lipids with DCM and MeOH (1:1), and fatty acids with acetic acid in diethyl ether (1:19). The fatty acids were methylated using 5% acetyl chloride in methanol of a known isotopic composition, yielding the corresponding fatty acid methyl

esters (FAMES). These were recovered by liquid-liquid extraction using hexane and further purified over silica columns. Quantification of the leaf wax-derived long-chain *n*-alkanes and *n*-fatty acids was done on a HP 6890 GC coupled to a flame ionization detector (Agilent, Santa Clara, CA, USA). Compound-specific $\delta^2\text{H}$ measurements of the *n*-alkanes *n*-C₂₉ and *n*-C₃₁ and the *n*-fatty acids *n*-C₂₆ and *n*-C₂₈ (dominant peaks/compounds and considered to derive from terrestrial higher plants) were performed on a GC-Pyrolysis-IRMS system consisting of HP 6890 GC coupled to a Delta^{PLUS}XL (Thermo-Quest Finnigan, Bremen, Germany). Mean standard errors for triplicate measurements of all 74 *n*-alkane samples were 0.9‰ and 1.1‰ for *n*-C₂₉ and *n*-C₃₁, respectively, and 0.9‰, each, for the fatty acids *n*-C₂₆ and *n*-C₂₈ measured in triplicate for 45 samples. During the course of the measurements the H_3^+ factor stayed constant. The $\delta^2\text{H}$ results of the *n*-alkanes *n*-C₂₉ and *n*-C₃₁ correlate with $R = 0.6$ ($p < 0.001$); their weighted mean values are reported in the following as $\delta^2\text{H}_{n\text{-alkanes}}$, relative to VSMOW. The $\delta^2\text{H}$ results of the fatty acids *n*-C₂₆ and *n*-C₂₈ correlate with $R = 0.8$ ($p < 0.001$); their mean values are reported as $\delta^2\text{H}_{\text{fatty-acids}}$, corrected for the methyl group added during methylation and also relative to VSMOW.

Although methoxyl groups are not specific compounds *sensu stricto*, they originate mostly from lignin and/or pectin. Given that their $\delta^2\text{H}$ values ($\delta^2\text{H}_{\text{methoxyl}}$) were found to reflect $\delta^2\text{H}_{\text{prec}}$, $\delta^2\text{H}_{\text{methoxyl}}$ was recently suggested as a paleoclimate proxy (Anhäuser et al., 2014; Keppler et al., 2007). The respective analysis was described previously by Greule et al. (2008). In brief, methoxyl groups are converted to gaseous methyl iodide (CH₃I) by the addition of hydroiodic acid (HI) and heating of the samples to 130 °C for 30 min. The $\delta^2\text{H}_{\text{methoxyl}}$ measurements for the Maundi samples were performed using an HP 6890N GC (Agilent, Santa Clara, CA, USA) equipped with an A200S auto-sampler (CTC Analytics, Zwingen, Switzerland), coupled to a Delta^{PLUS}XL IRMS (Thermo-Quest Finnigan, Bremen, Germany) via a pyrolysis reactor and a GC Combustion III interface (Thermo-Quest Finnigan, Bremen, Germany).

3. The coupled $\delta^2\text{H}$ - $\delta^{18}\text{O}$ biomarker paleohygrometer and reconstruction of $\delta^{18}\text{O}$ and $\delta^2\text{H}$ of source water

The coupled $\delta^2\text{H}_{n\text{-alkane}}\text{-}\delta^{18}\text{O}_{\text{sugar}}$ approach was previously described in detail by Zech et al. (2013) and Tuthorn et al. (2015). Leaf water undergoes evaporation through stomata openings. This process is associated with equilibrium and kinetic isotope effects, which causes isotopic enrichment of leaf water (Dongmann et al., 1974). Due to its small dimensions, the leaf water reservoir at evaporation sites quickly reaches isotope steady-state in which the isotopic composition of water vapor leaving the leaf surface is identical to the isotopic composition of the ‘source’ water pumped by plants from the ground in the course of the transpiration process (Flanagan et al., 1991; Roden and Ehleringer, 1999). In most cases the water used up by plants is directly linked through soil water and shallow groundwater to the local precipitation.

If the isotope steady-state of the leaf water reservoir is assumed, its ^2H and ^{18}O isotope composition can be then calculated using a ‘terminal lake analogue’ (cf. Zech et al., 2013 adopted from Gat and Bowser, 1991):

$$\delta_{\text{leaf-water}} \cong \delta_{\text{source-water}} + (1 - h_N)\epsilon^* + \Delta\epsilon \quad (1)$$

where $\delta_{\text{leaf-water}}$ and $\delta_{\text{source-water}}$ is the isotopic composition of leaf water and source (transpired) water, respectively, expressed in (‰), h_N is the relative humidity of the local atmosphere, normalized to the leaf water temperature; $\epsilon^* = (1 - 1/\alpha_{LV})10^3$ is the equilibrium isotope enrichment where α_{LV} stands for equilibrium isotope

fractionation between the liquid and gaseous phase (‰), and $\Delta\epsilon$ is the kinetic isotope enrichment [$\Delta^{18}\epsilon = C_k^{18}(1 - h_N)$; $\Delta^2\epsilon = C_k^2(1 - h_N)$] where C_k^{18} , C_k^2 stand for kinetic enrichment parameters, for ^{18}O and ^2H , respectively.

When $\delta^2\text{H}_{\text{leaf-water}}$ and $\delta^{18}\text{O}_{\text{leaf-water}}$ values are known, the d-excess parameter for the leaf water reservoir ($d_{\text{leaf-water}}$) undergoing evaporation, defined as $d = \delta^2\text{H} - 8 \cdot \delta^{18}\text{O}$, can be calculated using Eq. (1):

$$d_{\text{leaf-water}} = d_{\text{source-water}} + (1 - h_N)\left(\epsilon_2^* - 8 \cdot \epsilon_{18}^* + C_k^2 - 8 \cdot C_k^{18}\right) \quad (2)$$

where $d_{\text{source-water}}$ is the d-excess of the source water. It is apparent from Eq. (2) that the d-excess of leaf water is primarily controlled by the relative humidity of the local atmosphere when stomata are open and the transpiration process is in operation.

If the d-excess of leaf water is quantified through $\delta^2\text{H}$ and $\delta^{18}\text{O}$ measurements of relevant biomarkers and the d-excess of source water is known or can be assumed, the relative humidity of the local atmosphere can be estimated from Eq. (2):

$$h_N = 1 - \frac{\Delta d}{\epsilon_2^* - 8 \cdot \epsilon_{18}^* + C_k^2 - 8 \cdot C_k^{18}} \quad (3)$$

where $\Delta d = d_{\text{leaf-water}} - d_{\text{source-water}}$ stands for the difference of the d-excess values of the leaf water and the source water. Although kinetic enrichment parameters, C_k , can vary widely depending on the aerodynamic conditions characterizing a given evaporation process, maximum values of those parameters (25.1‰ and 28.5‰ for C_k^2 and C_k^{18} , respectively; Merlivat, 1978) seem to be most suitable for leaf water evaporation (see Zech et al. (2013) for further discussion). Equilibrium isotope enrichments, ϵ_2^* and ϵ_{18}^* , as a function of temperature can be calculated using empirical equations (Horita and Wesolowski, 1994; Majoube, 1971). It is to be noted here that evaporation of leaf water takes place when stomata are open i.e. during photosynthetic activity of a plant. While the biomarkers are synthesized during day-time in C_3 plants, which are of relevance here, the relative humidity defined by Eq. (3) (h_N) is in fact a proxy for day-time relative humidity (RH_D) of the local atmosphere seen by transpiring plants.

Equation (3) provides a useful tool to establish relative humidity records from sedimentary archives provided that: (i) ^2H and ^{18}O isotope composition of leaf water reservoir can be reconstructed using the measured δ values of *n*-alkanes and sugars and respective biosynthetic fractionation factors (ϵ_{bio}), and (ii) the d-excess of local source water (precipitation) can be evaluated. As far as point (i) is considered, we are aware that the biosynthetic fractionation factors for biosynthesis of *n*-alkanes and sugars in plants are strictly speaking not constant, however, we consider the respective ϵ_{bio} values not to be substantially variable (Sternberg, 2014 vs. Zech et al., 2014a). We therefore apply an ϵ_{bio} value of -160‰ for reconstructing $\delta^2\text{H}_{\text{leaf-water}}$ from measured $\delta^2\text{H}$ of *n*-alkanes (Sachse et al., 2006; Sessions et al., 1999) and an ϵ_{bio} value of $+27\text{‰}$ for reconstructing $\delta^{18}\text{O}_{\text{leaf-water}}$ from measured $\delta^{18}\text{O}$ of sugars (Cernusak et al., 2003; Gessler et al., 2009; Schmidt et al., 2001; Sternberg et al., 1986; Yakir and DeNiro, 1990). Note that interspecies variation in the fractionation between leaf water and leaf wax $\delta^2\text{H}$ (Kahmen et al., 2013), as well as other potentially biological processes related to their life forms can influence the hydrogen isotope composition of plant leaf water (Shu et al., 2008), besides leaf water enrichment. This represents further potentially uncertainty sources when using leaf wax $\delta^2\text{H}$ to reconstruct leaf water $\delta^2\text{H}$ (and therefore ultimately the $\delta^2\text{H}$ of source water, see below).

The reconstruction of the isotopic composition of leaf water and the day-time relative humidity values using Equations (1)–(3) are also based on the assumption that sugars and *n*-alkanes derive their ^{18}O and ^2H isotope composition from leaf water at the evaporation sites. This is where carbohydrate metabolism and gas exchange take place (e.g. Roden and Ehleringer, 1999; Sachse et al., 2012). Although the leaf water reservoir is isotopically not-uniform (Flanagan et al., 1991; Roden and Ehleringer, 1999; Santrucek et al., 2007), we assume that measured $\delta^{18}\text{O}_{\text{sugars}}$ and $\delta^2\text{H}_{n\text{-alkanes}}$ values are essentially controlled by $\delta^{18}\text{O}$ and $\delta^2\text{H}$ of leaf water at the sites where it undergoes evaporation and that are described by the ‘terminal lake’ approach applied here. The standard uncertainty of the reconstructed RH_D values [Eq. (3)], derived from the uncertainty propagation law and the analytical uncertainties of the measured $\delta^2\text{H}_{n\text{-alkanes}}$ and $\delta^{18}\text{O}_{\text{sugars}}$, varies between 3 and 20% (Table 1). This uncertainty does not include uncertainties associated with the adopted values of the biosynthetic fractionation factors, and the uncertainties associated with the simplifying assumptions discussed above.

If not measured, the isotopic composition of the source water can be evaluated when the slope of the local leaf water evaporation line (LLEL) is known and the local meteoric water line is defined by direct measurements or can be assumed. The slope of LLEL can be obtained from Eq. (1):

$$S_{\text{leaf-water}} = \frac{\delta_{\text{LW}}^2 - \delta_{\text{SW}}^2}{\delta_{\text{LW}}^{18} - \delta_{\text{SW}}^{18}} = \frac{(1 - h_N)\epsilon_2^* + \Delta\epsilon_2}{(1 - h_N)\epsilon_{18}^* + \Delta\epsilon_{18}} = \frac{\epsilon_2^* + C_k^2}{\epsilon_{18}^* + C_k^{18}} \quad (4)$$

It is worth mentioning here that, with the simplifying assumptions underlying Eqs. (1) and (4), i.e. full isotope steady-state of the leaf water reservoir undergoing evaporation and isotopic equilibrium at ground-level temperature between source water utilized by plants and the local atmospheric water vapor, the slope of LLEL depends only on equilibrium and kinetic fractionation for both isotopes. Slight temperature dependence of the slope is hidden in the temperature dependence of the equilibrium fractionation factors for ^2H and ^{18}O . Assuming present day-time mean surface air temperature for the elevation of Maundi site (+14 °C, cf. Appelhans et al., 2015), the slope of LLEL calculated using Eq. (4) is equal to 2.83. Lowering this temperature by 5 °C, to account for a possible drop of surface air temperature during the glacial period (Sacred Lake, Mt. Kenya: Loomis et al., 2012; Lake Malawi: Woltering et al., 2011; Congo Basin: Weijers et al., 2007; Lake Tanganyika: Tierney et al., 2008; Burundi highlands: Bonnefille et al., 1992), increases the slope derived from Eq. (4) to 2.94. Low LLEL slopes (~2.5 or even lower) were measured in some field studies, too (e.g. Allison et al., 1985; Flanagan et al., 1991). To account for possible uncertainties we therefore generated $\delta^2\text{H}/\delta^{18}\text{O}_{\text{source water}}$ records for

Table 1

Weighted mean $\delta^2\text{H}$ values of leaf wax-derived *n*-alkanes (*n*-C₂₉ and *n*-C₃₁) and weighted mean $\delta^{18}\text{O}$ values of hemicellulose-derived sugars (arabinose, fucose, and xylose). The reported uncertainties represent the weighted mean standard uncertainties. Also calculated/reconstructed $\delta^2\text{H}/\delta^{18}\text{O}_{\text{leaf-water}}$, deuterium-excess_{leaf-water}, mean day-time relative humidities (RH_D), and $\delta^2\text{H}/\delta^{18}\text{O}_{\text{source-water}}$ values are displayed. The reported uncertainties of deuterium-excess_{leaf-water} and RH_D represent expanded uncertainties calculated using the uncertainty propagation law.

Measured				Calculated/Reconstructed						
Depth [cm]	Age [ka BP]	$\delta^2\text{H}_{n\text{-alkanes}}$ [‰]	$\delta^{18}\text{O}_{\text{sugars}}$ [‰]	$\delta^2\text{H}_{\text{leaf-water}}$ [‰]	$\delta^{18}\text{O}_{\text{leaf-water}}$ [‰]	deuterium-excess _{leaf-water} [‰]	RH_D [%]	$\delta^2\text{H}_{\text{source-water}}$ [‰]	$\delta^{18}\text{O}_{\text{source-water}}$ [‰]	
6.5	0.7	-157.3 ± 1.0	36.4 ± 0.9	3.2	9.1	-70.0 ± 7.0	58 ± 7	-41.0	-7.0	
12.5	1.4	-159.3 ± 1.7	34.2 ± 1.0	0.9	7.0	-55.0 ± 8.0	65 ± 8	-35.8	-6.3	
25.0	3.5	-159.3 ± 1.1	34.0 ± 0.9	0.8	6.8	-54.0 ± 7.0	66 ± 7	-35.2	-6.3	
35.0	6.1	-161.0 ± 1.7	32.6 ± 1.2	-1.1	5.5	-45.0 ± 9.0	70 ± 9	-32.4	-5.9	
47.5	7.2	-170.7 ± 0.9	33.6 ± 1.6	-12.7	6.5	-64.0 ± 13.0	60 ± 13	-54.2	-8.6	
60.0	8.1	-165.6 ± 1.0	35.1 ± 1.1	-6.7	7.9	-70.0 ± 9.0	58 ± 9	-51.0	-8.2	
73.5	8.9	-166.6 ± 1.3	36.7 ± 1.2	-7.9	9.4	-83.0 ± 9.0	51 ± 9	-59.2	-9.2	
82.0	9.7	-158.5 ± 1.2	35.7 ± 0.8	1.8	8.5	-66.0 ± 6.0	60 ± 6	-40.5	-6.9	
91.0	10.8	-155.8 ± 0.7	41.3 ± 1.3	5.0	13.9	-106.0 ± 11.0	40 ± 11	-58.3	-9.1	
98.5	11.6	-156.0 ± 1.3	38.2 ± 1.6	4.7	10.9	-82.0 ± 13.0	51 ± 13	-46.2	-7.6	
107.0	12.6	-153.1 ± 1.2	38.3 ± 0.5	8.2	11.0	-80.0 ± 5.0	53 ± 5	-41.3	-7.0	
117.0	13.8	-149.6 ± 0.6	36.9 ± 1.1	12.4	9.6	-64.0 ± 9.0	60 ± 9	-29.1	-5.5	
126.0	14.8	-158.0 ± 1.5	38.0 ± 0.4	2.4	10.7	-84.0 ± 3.0	51 ± 3	-49.1	-8.0	
135.0	15.9	-152.4 ± 1.4	37.5 ± 0.5	9.0	10.2	-73.0 ± 4.0	56 ± 4	-37.0	-6.5	
150.0	17.7	-148.2 ± 0.5	42.0 ± 0.4	14.0	14.6	-103.0 ± 4.0	41 ± 4	-47.7	-7.8	
157.5	18.6	-147.6 ± 1.1	41.0 ± 0.4	14.8	13.6	-94.0 ± 4.0	46 ± 4	-42.1	-7.1	
165.0	19.4	-151.6 ± 0.7	37.8 ± 0.9	10.0	10.5	-74.0 ± 7.0	55 ± 7	-36.7	-6.4	
175.0	20.3	-154.5 ± 1.3	41.3 ± 0.5	6.5	13.9	-105.0 ± 5.0	40 ± 5	-56.1	-8.9	
185.0	21.2	-154.0 ± 0.1	42.0 ± 1.1	7.2	14.6	-110.0 ± 9.0	38 ± 9	-58.1	-9.1	
225.0	29.4	-154.7 ± 0.4	32.9 ± 1.2	6.4	5.8	-40.0 ± 10.0	73 ± 10	-22.3	-4.6	
247.5	33.6	-153.1 ± 1.7	40.9 ± 1.5	8.2	13.5	-100.0 ± 12.0	43 ± 12	-52.0	-8.3	
280.0	38.6	-155.0 ± 1.9	34.1 ± 0.7	5.9	6.9	-49.0 ± 6.0	68 ± 6	-27.7	-5.3	
310.0	43.5	-159.1 ± 1.7	37.7 ± 0.6	1.0	10.4	-83.0 ± 5.0	51 ± 5	-49.9	-8.1	
361.0	52.1	-147.3 ± 1.2	35.2 ± 1.8	15.1	8.0	-49.0 ± 14.0	68 ± 14	-18.3	-4.1	
381.0	55.5	-146.9 ± 2.1	31.9 ± 0.7	15.5	4.8	-23.0 ± 6.0	81 ± 6	-4.2	-2.4	
418.0	61.8	-138.3 ± 1.8	36.5 ± 0.7	25.8	9.2	-48.0 ± 6.0	69 ± 6	-7.1	-2.7	
428.0	63.5	-133.8 ± 1.3	46.7 ± 1.7	31.1	19.2	-122.0 ± 14.0	31 ± 14	-40.7	-6.9	
435.5	64.8	-141.7 ± 0.9	37.2 ± 1.0	21.8	10.0	-58.0 ± 8.0	64 ± 8	-16.3	-3.9	
443.0	66.0	-137.4 ± 1.7	46.8 ± 2.4	26.9	19.3	-127.0 ± 19.0	29 ± 19	-47.5	-7.8	
453.0	67.7	-144.2 ± 1.0	33.3 ± 1.3	18.8	6.1	-30.0 ± 10.0	77 ± 10	-4.9	-2.5	
463.0	69.4	-142.0 ± 1.0	40.4 ± 0.7	21.5	13.1	-83.0 ± 5.0	51 ± 5	-29.8	-5.6	
482.0	72.6	-154.5 ± 1.4	39.1 ± 1.1	6.6	11.8	-88.0 ± 9.0	49 ± 9	-47.0	-7.7	
503.0	76.2	-148.7 ± 0.4	35.0 ± 0.7	13.4	7.8	-49.0 ± 5.0	68 ± 5	-19.9	-4.3	
533.0	81.3	-151.8 ± 0.4	37.9 ± 0.5	9.7	10.6	-75.0 ± 4.0	55 ± 4	-37.4	-6.5	
558.0	85.5	-156.3 ± 0.5	36.2 ± 1.2	4.4	8.9	-67.0 ± 10.0	59 ± 10	-38.4	-6.6	
588.0	90.6	-158.2 ± 0.5	36.2 ± 0.6	2.1	9.0	-70.0 ± 5.0	58 ± 5	-42.1	-7.1	
625.0	96.9	-153.0 ± 0.5	35.6 ± 1.6	8.4	8.4	-59.0 ± 13.0	63 ± 13	-30.1	-5.6	
638.5	99.2	-154.3 ± 0.8	37.6 ± 1.4	6.7	10.4	-76.0 ± 12.0	55 ± 11	-40.9	-7.0	

the Maundi site using three different LLEL slopes: 2.50, 2.75 and 3.00.

The local meteoric water line (LMWL) derived for precipitation collected on the southern slopes of Mt. Kilimanjaro is $\delta^2\text{H} = 8.0 \cdot \delta^{18}\text{O} + 14.8$ (Zech et al., 2015). The intersection of LLEL drawn through the data point representing present-day leaf water at Maundi site (reconstructed using the uppermost sample from 6.5 cm depth; Fig. 2; Table 1), with the LMWL noted above, should provide a good estimation of modern source water at the site. Analogous procedures can be repeated for all reconstructed leaf water data points shown in Fig. 3, leading to a reconstruction of local $\delta^2\text{H}/\delta^{18}\text{O}$ source water values for the entire time span covered by the investigated loess-like paleosol sequence. This in turn can be linked to temporal variations of $\delta^2\text{H}$ and $\delta^{18}\text{O}$ of local precipitation at the study area.

It should be noted that the slope and intercept (d-excess) of LMWL for Maundi site most likely have not been constant during the time period covered by the investigated loess-like paleosol sequence. This potentially affects both our reconstructed RH_D values and $\delta^2\text{H}/\delta^{18}\text{O}_{\text{source-water}}$ records for the Maundi site. However, the variability of d-excess of precipitation recorded in Greenland and Antarctic ice cores during the last 100 ka was not larger than $\pm 4\text{‰}$ (Masson-Delmotte et al., 2005; Stenni et al., 2010). This is much smaller compared to the standard uncertainty of the reconstructed d-excess values of leaf water. The latter was calculated using the analytical uncertainties of the measured $\delta^{18}\text{O}_{\text{sugar}}$ and $\delta^2\text{H}_{n\text{-alkane}}$, plugged into the uncertainty propagation law. The calculated uncertainties of the d-excess values of leaf water were in the range from 3.4‰ to 19.5‰ (Table 1).

^2H and ^{18}O isotope composition of the global ocean fluctuated during the Quaternary, responding to climatically-controlled net transfer of water between the global ocean and the cryosphere. During glacial periods, with the global cryosphere at its maximum, the ocean became isotopically enriched. The maximum extent of

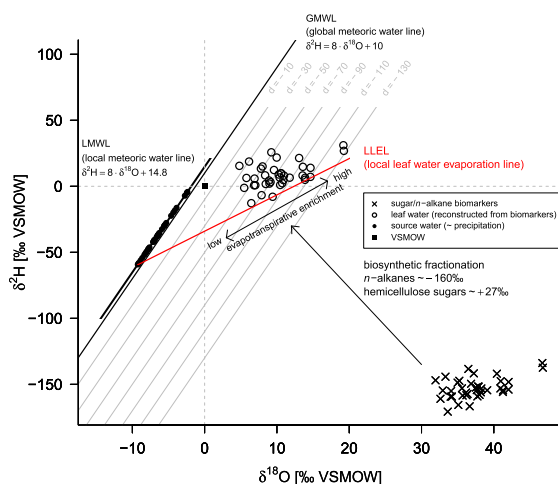


Fig. 3. $\delta^2\text{H}$ versus $\delta^{18}\text{O}$ diagram illustrating the coupled $\delta^2\text{H}_{n\text{-alkane}}-\delta^{18}\text{O}_{\text{sugar}}$ approach to reconstruct mean day-time relative humidity values and isotopic composition of plant source water. Data points are plotted for measured $\delta^2\text{H}_{n\text{-alkane}}/\delta^{18}\text{O}_{\text{sugar}}$ values (crosses), for reconstructed $\delta^2\text{H}/\delta^{18}\text{O}_{\text{leaf water}}$ values (open circles) and for reconstructed $\delta^2\text{H}/\delta^{18}\text{O}_{\text{source water/prec}}$ values (filled circles). Accordingly, (i) $\delta^2\text{H}/\delta^{18}\text{O}_{\text{leaf-water}}$ is calculated from the n -alkane and sugar biomarkers using biosynthetic fractionation factors, (ii) the distance of leaf water to the local meteoric water line (LMWL) – expressed as deuterium-excess – is used to calculate day-time air relative humidity (RH_D), and (iii) $\delta^2\text{H}/\delta^{18}\text{O}_{\text{source-water}}$ is calculated as intersect of the local leaf water evaporation lines (LLEL) with the LMWL (modified according to Zech et al., 2013).

this isotope enrichment was evaluated to be around one per mil for ^{18}O (Schrage et al., 1996, 2002). Since the zero point of the δ scale used for measurements of the isotopic composition of water is defined by the VSMOW standard, which is close to present-day mean isotope composition of the global ocean, appropriate correction is needed when isotopic composition of precipitation (δ_{prec}) for the glacial period is reconstructed and compared with the present-day δ_{prec} values. We applied the correction procedure according to Stenni et al. (2010) which assumes that local factors can be ignored and the d-excess of seawater is set to zero during transitions from glacial to interglacial conditions. The seawater $\delta^{18}\text{O}$ record from Bintanja et al. (2005) was used. This record represents the benthic stack from Lisiecki and Raymo (2005), compiled from 57 globally distributed marine sediment cores, corrected for deep water temperature changes.

4. Results and discussion

4.1. The Maundi multi-proxy stable isotope records ($\delta^{18}\text{O}_{\text{sugars}}$, $\delta^2\text{H}_{\text{methoxyl}}$, $\delta^2\text{H}_{\text{fatty-acids}}$, $\delta^2\text{H}_{n\text{-alkanes}}$)

The stable isotope records plotted on a time axis are illustrated in Fig. 4. The $\delta^{18}\text{O}_{\text{sugars}}$ values show great variability during the last 100 ka BP ranging from $+31.9$ to $+46.8\text{‰}$ (Fig. 4; Table 1). While the Holocene is characterized by a $\delta^{18}\text{O}_{\text{sugars}}$ minimum ($+32.6$ to $+36.7\text{‰}$), the Younger Dryas (YD) and the Last Glacial Maximum (LGM, from 17.5 to 26.5 ka BP, according to Schüler et al., 2012; Clark et al., 2009; respectively) show distinct $\delta^{18}\text{O}_{\text{sugars}}$ maxima (YD: $+38.2$ – 41.3‰ ; LGM: $+37.8$ – 42.0‰). The pre-LGM portion of the record reveals a pronounced $\delta^{18}\text{O}_{\text{sugars}}$ minimum around 30, 38 and 56 ka BP ($+32.9\text{‰}$, $+34.1\text{‰}$ and $+31.9\text{‰}$) and a pronounced $\delta^{18}\text{O}_{\text{sugars}}$ maximum around 34 ka BP (40.9‰). The most positive $\delta^{18}\text{O}_{\text{sugars}}$ values occur between 60 and 70 ka BP (peaks with $+46.7\text{‰}$ and $+46.8\text{‰}$).

The $\delta^2\text{H}_{\text{methoxyl}}$ record (Fig. 4), ranging from -160.6 to -74.3‰ (excluding the uppermost data point), has the most positive values between 60 and 73 ka BP (-106.9 to -74.3‰). Although much less pronounced, the YD and the LGM are also characterized by elevated $\delta^2\text{H}_{\text{methoxyl}}$ values (YD: -120.1 to -116.1‰ ; LGM: -115.5 to -108.4‰). $\delta^2\text{H}_{\text{methoxyl}}$ shows only minor variability between 17.5 and 40 ka and a pronounced negative shift for the youngest part of the sequence comprising the modern topsoil (-22.4‰ ; cf. Fig. 4). In contrast to the older sections of the core, the bulk of the topsoil consists mainly of organic matter (TOC > 30%, whereas most other section show TOC between 5 and 10%; cf. Fig. 2) and potentially includes a large fraction of methoxyl groups e.g. from wood lignin (with more negative $\delta^2\text{H}_{\text{methoxyl}}$ values). Under tropical conditions these components might be readily available for decomposition by wood rooting fungi. However, the reasons for the observed large shift of the $\delta^2\text{H}_{\text{methoxyl}}$ of the topsoil and the higher range shown in the Maundi $\delta^2\text{H}_{\text{methoxyl}}$ values ($\sim 80\text{‰}$; cf. Fig. 4) compared to the $\delta^2\text{H}_{\text{fatty-acid}}$ and $\delta^2\text{H}_{n\text{-alkane}}$ records ($\sim 40\text{‰}$) are currently unclear. In contrast to leaf waxes, which are known to record only a fraction of the leaf water evapotranspirative enrichment (cf. Section 4.3; Gamarra et al., 2016), a higher sensitivity of the methoxyl groups could possibly explain the larger variability.

The $\delta^2\text{H}_{\text{fatty-acid}}$ values range from -161.3 to -126.1‰ (Fig. 4) resembling well the variability of $\delta^2\text{H}_{n\text{-alkane}}$ values ranging from -170.7 to -133.9‰ (Fig. 4; Table 1). There is a good overall agreement between the n -alkanes and the fatty acids ($R = 0.7$; $p < 0.001$). Both records reveal pronounced $\delta^2\text{H}$ minima during the early Holocene, slight maxima during the YD and the LGM, little variability during the pre-LGM period and, like the $\delta^{18}\text{O}_{\text{sugar}}$ and the $\delta^2\text{H}_{\text{methoxyl}}$ records, more positive values between 60 and 70 ka BP.

The uppermost sample of the Maundi loess-like paleosol

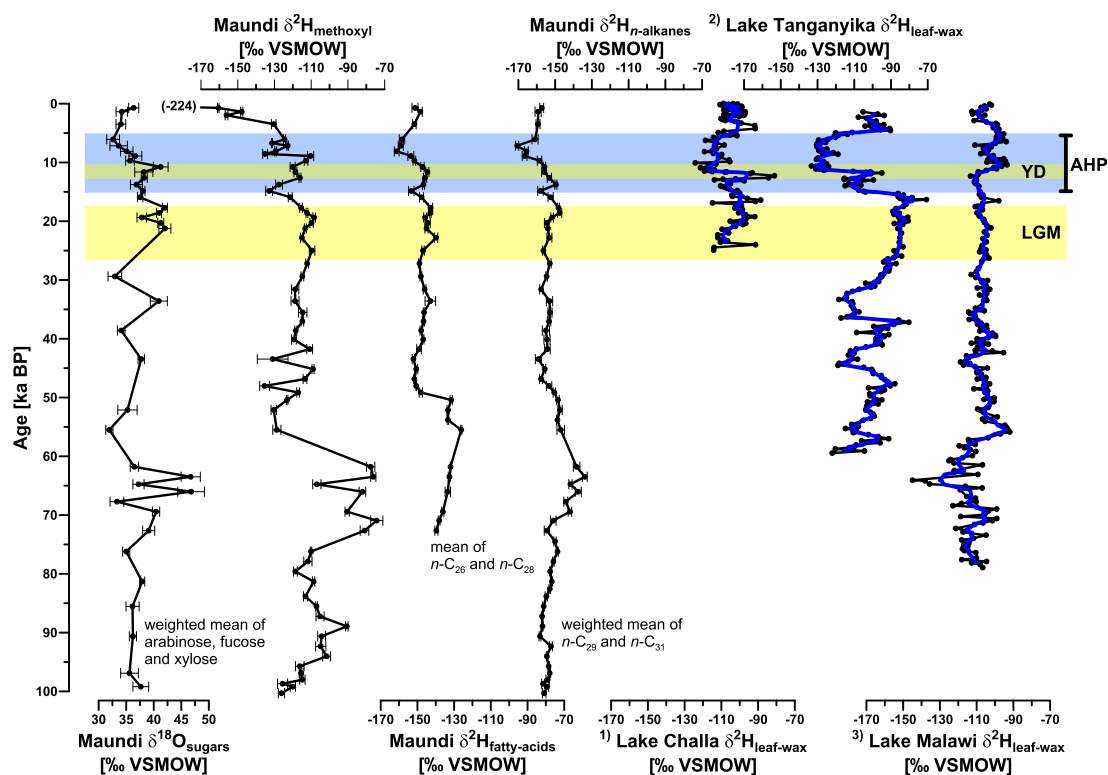


Fig. 4. The stable isotope records of Maundi comprising $\delta^{18}\text{O}_{\text{sugars}}$, $\delta^2\text{H}_{\text{methoxyyl}}$, $\delta^2\text{H}_{\text{fatty-acids}}$ and $\delta^2\text{H}_{\text{n-alkanes}}$ results and comparison with other equatorial East African $\delta^2\text{H}_{\text{leaf-wax}}$ records, ¹ from Tierney et al. (2011), ² from Tierney et al. (2008), ³ from Konecky et al. (2011). Running means are applied to the original data (7-point, 3-point and 5-point averaging for Lake Challa, Lake Tanganyika and Lake Malawi, respectively) in order to enhance the comparability to the Maundi record. The blue bar highlights the time period of the African Humid Period (AHP, from 5 to 15 ka BP; Junginger et al., 2014), the yellow bars highlight the time periods of the Last Glacial Maximum (LGM, from 17.5 to 26.5 ka BP; according to Clark et al., 2009; Schüler et al., 2012) and the Younger Dryas (YD, from 10.3 to 12.9 ka BP). According to Rasmussen et al. (2014) the YD is defined from 11.7 to 12.9 ka b2k in the Greenland ice cores. However, we suggest that considering the age uncertainties of the Maundi paleosol sequence and possible atmospheric and/or oceanic tele-connctive time lags, the Maundi $\delta^{18}\text{O}_{\text{sugar}}$ maximum (10.8 ka cal BP according to the age-depth model) very likely corresponds with the YD. We therefore chose a wider age range of 10.3–12.9 ka BP for defining and depicting the YD in Figs. 4–6. (For interpretation of the references to colour in this figure legend, the reader is referred to the web version of this article.)

sequence, reflecting the modern topsoil, yielded $\delta^2\text{H}_{\text{fatty-acid}}$ and $\delta^2\text{H}_{\text{n-alkane}}$ values of -151‰ and -156‰ , respectively (Fig. 4). For comparison, Peterse et al. (2009) reported on $\delta^2\text{H}_{\text{leaf-wax}}$ values of -133‰ for topsoils at this altitude on the southern slopes of Mt. Kilimanjaro and Zech et al. (2015) reported on $\delta^2\text{H}_{\text{n-alkanes}}$ values of $\sim -140\text{‰}$ for topsoils from the same transect and altitude. Given their similarity, the Maundi $\delta^2\text{H}_{\text{fatty-acid}}$ and $\delta^2\text{H}_{\text{n-alkane}}$ records can both be interpreted as reflecting Maundi $\delta^2\text{H}_{\text{leaf-wax}}$ record.

4.2. Comparison of the Maundi $\delta^2\text{H}_{\text{leaf-wax}}$ records with other equatorial East African $\delta^2\text{H}_{\text{leaf-wax}}$ records

Compared to other equatorial East African $\delta^2\text{H}_{\text{leaf-wax}}$ records, the Maundi record is characterized by overall more negative $\delta^2\text{H}_{\text{leaf-wax}}$ values (Fig. 4). The mean $\delta^2\text{H}_{\text{fatty-acid}}$ and $\delta^2\text{H}_{\text{n-alkane}}$ values for Maundi are -145‰ and -153‰ , respectively, whereas mean $\delta^2\text{H}_{\text{leaf-wax}}$ values for Lake Challa (Tierney et al., 2011), Lake Tanganyika (Tierney et al., 2008) and Lake Malawi (Konecky et al., 2011) are -105‰ , -104‰ and -108‰ , respectively. This can be attributed to differences in elevation of those sites: Maundi is located at 2780 m a.s.l., whereas Lake Challa, Lake Tanganyika and Lake Malawi are located at 880 m a.s.l., 773 m a.s.l. and 474 m a.s.l.,

respectively. This corresponds to a total difference of -47‰ for ~ 2100 m, and thus to a $\delta^2\text{H}_{\text{leaf-wax}}$ lapse rate of -22.4‰ km^{-1} , which is in good agreement with reported $\delta^2\text{H}_{\text{prec}}$ lapse rates ranging from ~ -10 – 40‰ km^{-1} according to Araguás-Araguás et al. (2000). For Mt. Cameroon and Mt. Kilimanjaro, Gonfiantini et al. (2001) and Zech et al. (2015) found $\delta^2\text{H}_{\text{prec}}$ lapse rates of -14.1‰ km^{-1} (entire altitude span of ca. 4000 m) and -14.9‰ km^{-1} (above ca. 2000 m a.s.l.), respectively.

Apart from this overall offset, which is well understood, the Maundi $\delta^2\text{H}_{\text{leaf-wax}}$ record has one striking feature in common with Lake Challa and Lake Tanganyika $\delta^2\text{H}_{\text{leaf-wax}}$ records, namely a pronounced $\delta^2\text{H}_{\text{leaf-wax}}$ minimum during the early Holocene as part of the AHP. While this also occurs further north at the Horn of Africa (Tierney and deMenocal, 2013), it is much less pronounced in Lake Malawi and even reversed further south in the catchment of the Zambezi River (Schefuß et al., 2011). This discrepancy dividing central tropical from southern tropical East Africa, has been referred to as the ‘meteorological equator’ or the ‘climate hinge zone’ (e.g. Gasse, 2000; Gasse et al., 2008; Konecky et al., 2011, and references therein), which is represented by a lateral boundary broadly between the Lakes Tanganyika and Malawi. This zone separates the northern equatorial region and the proposed anti-

phase changes in the south, both insolation-driven paleoprecipitation regimes (e.g. Patridge et al., 1997; Barker et al., 2002). Higher amplitude in the Lake Tanganyika $\delta^2\text{H}_{\text{leaf-wax}}$ variability since ~10 ka BP compared to those of Lake Challa and Maundi might indicate a feedback mechanism associated with a variable Lake Kivu (1460 m a.s.l.) discharge (Cohen et al., 1997; Felton et al., 2007). Accordingly, higher precipitation amounts might result in more terrestrial organic material formed at higher elevations being transported from the Lake Kivu catchment via the Ruzizi River into Lake Tanganyika, thus leading to more negative $\delta^2\text{H}_{\text{leaf-wax}}$ values in the sediments of this lake. However, it is challenging to derive more detailed paleoclimate implications from the Maundi $\delta^2\text{H}_{\text{leaf-wax}}$ records alone due to the large number of processes influencing them: e.g. moisture transport history (Konecny et al., 2011; Tierney et al., 2011), precipitation amount (Scheffuß et al., 2011, 2005; Tierney et al., 2008; Tierney and deMenocal, 2013) and leaf water enrichment caused by evapotranspiration (Kahmen et al., 2013; Tierney et al., 2010). Therefore, the coupled $\delta^2\text{H}_{\text{n-alkane}}-\delta^{18}\text{O}_{\text{sugar}}$ approach seems to be a valuable tool for (i) quantifying this leaf water enrichment effect and (ii) getting the relative day-time humidity and the isotopic composition of plant source water as new paleoclimate proxies.

4.3. Day-time relative humidity history at Maundi

The reconstructed d-excess values of leaf water for the Maundi profile range from -127 to -23‰ (Table 1), with the lowest value recorded at ca. 66 ka and the highest at ca. 55 ka. Changes of RH_D

mirror the changes of the d-excess_{leaf-water}. The biomarker-based day-time relative humidity record [RH_D ; derived from Eq. (3)] from the Maundi paleosol sequence reveals large variability for the last ~100 ka BP. RH_D ranges from 29% to 81% (Fig. 5). The modern topsoil sample (6.5 cm depth) yields an RH_D value of 58% ($\pm 3.7\%$; Table 1). For comparison, Pepin et al. (2010) reported for this elevation on the southern slopes of Mt. Kilimanjaro, a higher mean annual free-air relative humidity of approximately 65%. The measured ground-level mean annual relative humidity values are reported to be much higher, between 88% and 96% (Duane et al., 2008; Appelhans et al., 2015; cf. Fig. 1c). This apparent discrepancy is addressed below.

The proposed coupled ' $\delta^2\text{H}_{\text{n-alkane}}-\delta^{18}\text{O}_{\text{sugar}}$ paleohygrometer' is prone to uncertainties resulting from analytical uncertainties of $\delta^2\text{H}_{\text{n-alkane}}$ and $\delta^{18}\text{O}_{\text{sugar}}$ measurements (Fig. 4) and the uncertainties of $\delta^2\text{H}_{\text{n-alkane}}$ and $\delta^{18}\text{O}_{\text{sugar}}$ biosynthetic fractionation factors. Although we consider the temperature dependence of the biosynthetic fractionation factors to be negligible (Zech et al., 2014a), it is very likely that an ϵ_{bio} value of $+27\text{‰}$ for reconstructing $\delta^{18}\text{O}_{\text{leaf-water}}$ from arabinose and xylose underestimates the true ϵ_{bio} value (cf. Zech et al., 2014b, and discussion therein). A slightly higher ϵ_{bio} value of $+29\text{‰}$ would increase the reconstructed RH_D for the uppermost sample of Maundi from 58% to 66%. Similarly, an increase of ϵ_{bio} for deuterium by 10‰ (from -160‰ to -170‰) would lead to a corresponding increase of RH_D by 6%. Therefore, the reconstructed RH_D values should be considered as minimum estimates based on these considerations.

On the other hand, it might be worth trying to account for

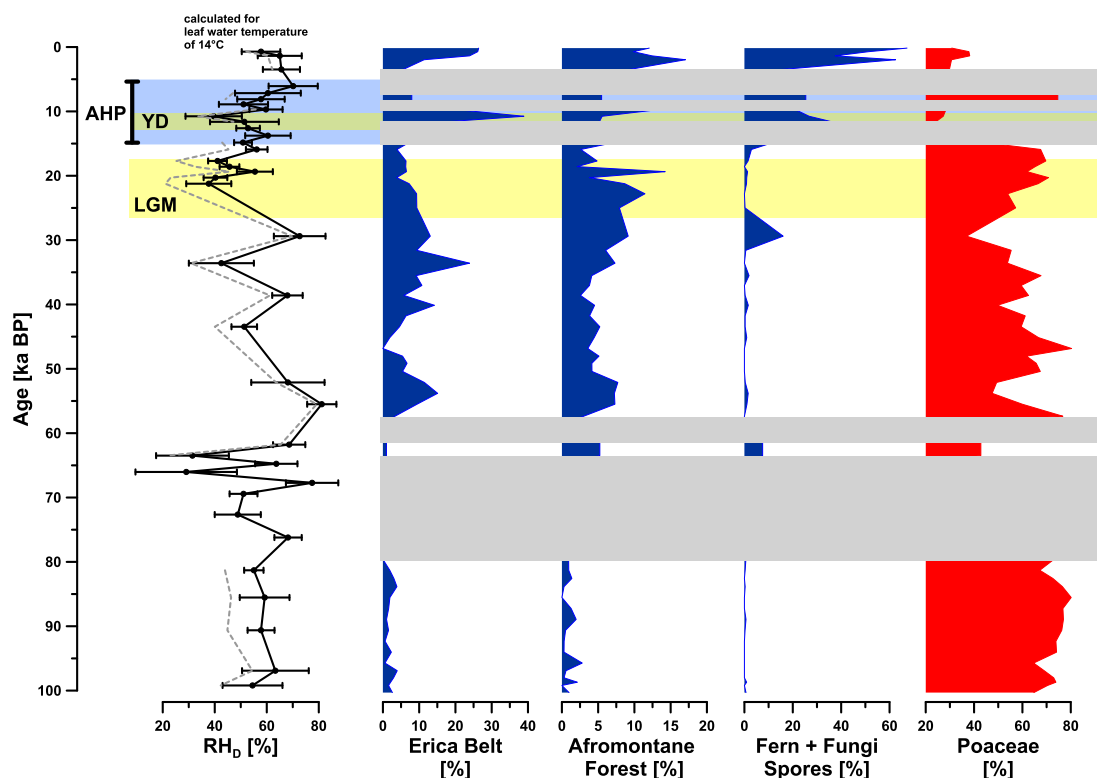


Fig. 5. Reconstructed day-time relative humidity record (RH_D) for the Maundi paleosol sequence. Error bars indicate expanded uncertainties derived from the uncertainty propagation law. Also pollen records for Maundi site are shown (Schüler et al., 2012).

variable contributions of grass-derived biomarkers, because it is reported that grass-derived *n*-alkane and sugar biomarkers are not (fully) sensitive for recording the evapotranspirative enrichment signal of leaf water (Helliker and Ehleringer, 2002; McInerney et al., 2011). This effect can be presumably explained with the grass leaf growth from a basal intercalary meristem, where leaf water enrichment is diluted by non-enriched stem water. Based on findings of Helliker and Ehleringer (2002) we assumed that 35% of the leaf water enrichment is lost during hemicellulose sugar biosynthesis; and based on findings of Gamarra et al. (2016) and Kahmen et al. (2013) we assumed that 50% of the leaf water enrichment is lost/not seen during *n*-alkane biosynthesis of leaves. Assuming furthermore that the *Poaceae* pollen concentration (Fig. 5) corresponds to the *Poaceae* biomarker contribution (which is surely not correct but may serve as rough approximation and is without alternative at the current state of knowledge), an isotope mass balance calculation can be applied. The thus “corrected” RH_D record (albeit underlying many assumptions and uncertainties) yields on average 6.9% lower RH_D values (Fig. 5, grey dotted line, maximum offset 17.2% around 85 ka BP) than the uncorrected RH_D record. Nevertheless, these consideration and results overall corroborate the robustness of our paleohygrometer approach and even amplify most of the uncorrected RH_D variability (Fig. 5).

Furthermore, as discussed above, the proposed paleohygrometer is a proxy for mean day-time values of air relative humidity, i.e. when stomata are open, the transpiration process is at its maximum and biomarker synthesis takes place (e.g. Tuthorn et al., 2015). The relative humidity of air on the slopes of Mt Kilimanjaro exhibits strong altitudinal gradients with the maximum coinciding well with the altitudinal precipitation maximum (Fig. 1c). Also, it is subject to pronounced seasonal as well as diurnal variability (Appelhans et al., 2015; Duane et al., 2008; Pepin et al., 2010). While the seasonal variability of relative humidity is controlled by the migration of the ITCZ, the strong diurnal variability of this parameter at Maundi site is caused by specific circulation patterns of the local atmosphere, with upslope moisture transport during the day and downslope transport and drying at night (see Fig. 11 in Pepin et al., 2010). We suggest that the Maundi RH_D record depicted in Fig. 5 reflects the long-term variability of mean day-time values of air relative humidity.

Finally, the apparent offset between the reconstructed RH_D values and the ground-level instrumental data, seen at Maundi site, may largely stem from the fact that when biomarkers are biosynthesized predominantly within the canopy (Zech et al., 2015) they will record canopy-level rather than ground-level relative humidity values. As demonstrated by Graham et al. (2014) the differences in morning-time (9 a.m.–12 p.m.) relative humidity recorded in tropical forest at ground-level (0–5 m), and at canopy-level (>5 m), may easily reach 20%. This would imply grasses to record the higher ground-level relative humidity as opposed to trees, which incorporate the lower canopy-level relative humidity values. This effect points in the same direction as the correction made above (due to relatively insensitive grasses concerning recording leaf water evapotranspirative enrichment). Considering high uncertainties associated to this correction, a further adjustment seems not to be needed or is already covered.

The most outstanding feature of the lower part of the Maundi RH_D record shown in Fig. 5 is the reduction of this parameter during the period from ca. 70 to 60 ka BP. This extreme drought period is corroborated by the absence of pollen, which is interpreted in terms of poor pollen preservation due to dry conditions (Schüler et al., 2012). Within dating uncertainties, this pronounced drought period might correspond to low stands of Lake Malawi (Scholz et al., 2007) and Lake Challa (Moernaut et al., 2010).

Although the resolution of Maundi RH_D record is relatively low

from 60 to 25 ka BP, the recorded variability of this parameter is also corroborated by the Maundi pollen results (Fig. 5). The two pronounced RH_D maxima around ~55 and during the pre-LGM around ~30 ka BP coincide with *Poaceae* minima, whereas humid-indicating taxa of the *Erica* belt, the Afromontane forest and fern and fungi spores reveal maxima. By contrast, the onset of the LGM is characterized by a marked decline of the latter taxa and a marked increase of the *Poaceae* taxa, in line with RH_D minima; a first one from ~22 to 20 ka BP and a second one around ~17.5 ka BP (Fig. 5). The first minimum coincides with a lake level drop of Lake Tanganyika of 300 m at around 21 ka BP (Gasse et al., 1989) or at least ~260 m during the LGM (32–14 ka BP; McGlue et al., 2007), while Lake Victoria was nearly desiccated at that time (Talbot and Livingstone, 1989). Within dating uncertainties of the investigated loess-like paleosol sequence, the second arid spell is consistent with one of the most extreme lake-level low stands reported for Lake Challa, dated to ~17.0–16.4/16.9–16.3 ka BP (Moernaut et al., 2010; Verschuren et al., 2009).

A late glacial shift to more humid conditions is evident both in the reconstructed Maundi RH_D record and the pollen spectra. This shift is in agreement with the onset of the AHP and equatorial East African lake transgressions (Gasse, 2000; Junginger et al., 2014; and references therein) as well as rainfall modeling results (Otto-Bliesner et al., 2014). A pronounced arid spell during the YD is only visible in the RH_D record, not in pollen, which partly suffers from pollen preservation in the upper part of the investigated loess-like paleosol sequence. Such pronounced arid climatic conditions during the YD seem to have been a widespread phenomenon in East Africa (Gasse et al., 2008) and were for instance reported for the close-by sedimentary record of Lake Challa (Tierney et al., 2011; Verschuren et al., 2009).

The reconstructed RH_D values increase during the Holocene and reach a maximum during the middle Holocene. This is in accord with pollen results showing a *Poaceae* maximum and still moderate abundance of *Erica* and Afromontane forest taxa during the early Holocene. Only during the middle and the late Holocene, when the AHP ended, the RH_D record stays still high and the Afromontane forest, fern and fungi taxa reach their maximum indicating very humid conditions. The same Holocene climate history is recorded in the WeruWeru pollen study site, located in the montane forest at an elevation of 2650 m on the southern slopes of Mt. Kilimanjaro. According to Schüler (2013), drought tolerant *Cassipourea* forests prevailed here during the early Holocene. Over the course of the Holocene montane forest taxa typical for the wetter southern slopes, which also form the forests today, became more abundant (Schüler, 2013). Lake levels in equatorial East African, reached their maximum during the early Holocene and dropped over the course of the Holocene (Gasse, 2000; Junginger et al., 2014; and references therein). This apparent discrepancy is addressed in Section 4.5.

The uppermost sample, representing the modern topsoil, suggests again more arid climatic condition (Fig. 5). This is well in agreement with climate and environmental observations indicating considerably decreasing amounts of precipitation and relative humidity on Mt. Kilimanjaro during the last century (Hemp, 2005; Mólög et al., 2009).

4.4. Reconstructed $\delta^2\text{H}/\delta^{18}\text{O}_{\text{source-water}}$ and its paleoclimate implications

Apart from reconstructing mean day-time relative humidity, the coupled $\delta^2\text{H}_{n\text{-alkane}}-\delta^{18}\text{O}_{\text{sugar}}$ approach allows also the assessment of $\delta^2\text{H}$ and $\delta^{18}\text{O}$ values of water used up by plants being the source of biomarkers analysed in this study (cf. Fig. 3). In order to address potential uncertainty of the reconstructed $\delta^2\text{H}/\delta^{18}\text{O}_{\text{source-water}}$

values associated with the slope of the local leaf water evaporation line (LLEL), we used three different values of this slope: 2.50, 2.75 and 3.00. The values of $\delta^2\text{H}/\delta^{18}\text{O}_{\text{source-water}}$ reported in Table 1 were derived with the slope of LLEL equal to 2.75. The reconstructed Maundi $\delta^2\text{H}/\delta^{18}\text{O}_{\text{source-water}}$ records are shown in Fig. 6. For comparison, the figure depicts also the RH_D record and the $\delta^2\text{H}/\delta^{18}\text{O}_{\text{leaf-water}}$ record.

The modern topsoil sample of Maundi yields $\delta^2\text{H}_{\text{source-water}}$ and $\delta^{18}\text{O}_{\text{source-water}}$ values of -41‰ and -7‰ , respectively using a LLEL slope of 2.75 (Fig. 6; Table 1). A direct comparison with present-day isotope precipitation signal at this site cannot be made due to the lack of data. Modern $\delta^2\text{H}/\delta^{18}\text{O}_{\text{prec}}$ values recorded on south-western slopes of Mt. Kilimanjaro at the elevation of 2800 m a.s.l., approximately 30 km to the west of Maundi, are significantly less negative: $\sim -22\text{‰}$ and $\sim -5\text{‰}$, respectively (Zech et al., 2015). This apparent offset may stem from local differences in altitude gradient of $\delta^2\text{H}/\delta^{18}\text{O}_{\text{prec}}$, induced by differences in atmospheric circulation and/or local moisture recycling (cf. discussion in Section 4.3). It is worth noting that the vertical extent of the montane rainforest belt on the south-eastern slopes of Mt. Kilimanjaro is

significantly smaller than that observed at southern and south-western slopes (Hemp and Beck, 2001), which may result in a lower degree of moisture recycling and a higher $\delta^2\text{H}/\delta^{18}\text{O}_{\text{prec}}$ altitude gradient at the Maundi location.

It is also apparent from Fig. 6 that the reconstructed Maundi $\delta^2\text{H}/\delta^{18}\text{O}_{\text{source-water}}$ records do not closely resemble the corresponding $\delta^2\text{H}/\delta^{18}\text{O}_{\text{leaf-water}}$ records (and thus the biomarker records). The entire $\delta^{18}\text{O}_{\text{source-water}}$ record has a weak negative correlation with $\delta^{18}\text{O}_{\text{sugars}}$ ($R = -0.26$; $p = 0.001$); the correlation is positive for $\delta^2\text{H}_{\text{source-water}}$ and $\delta^2\text{H}_{n\text{-alkanes}}$, yet the coefficient of correlation is also quite low ($R = 0.26$; $p < 0.001$). This suggests that changes in $\delta^{18}\text{O}_{\text{sugar}}$ and $\delta^2\text{H}_{\text{leaf-wax}}$ records are to some extent decoupled from changes in $\delta^2\text{H}/\delta^{18}\text{O}_{\text{prec}}$ at least in those cases where paleohumidity, and thus the isotopic enrichment of leaf water, is highly variable.

4.5. Controls on paleohumidity and $\delta^2\text{H}/\delta^{18}\text{O}$ of paleoprecipitation on the southeastern slopes of Mt. Kilimanjaro

The Maundi paleohumidity record shows some broad

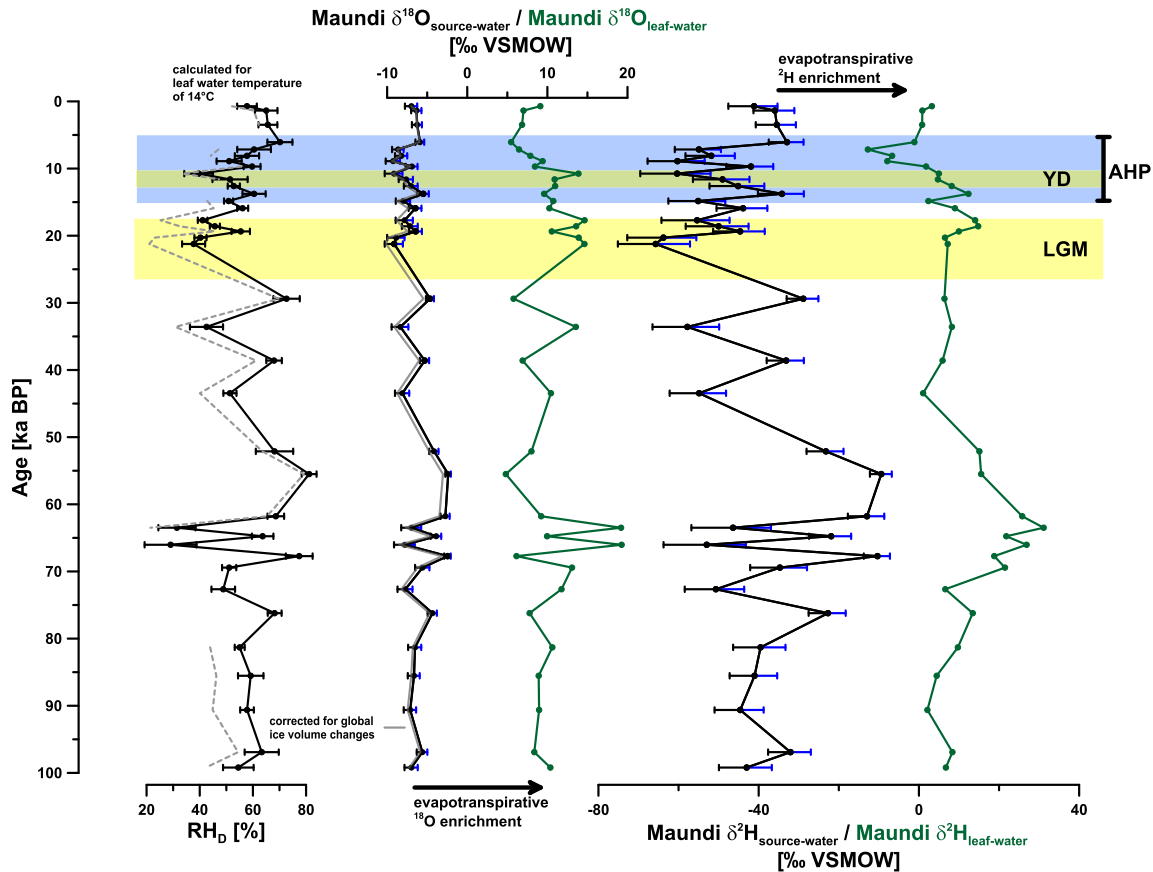


Fig. 6. Climatic records reconstructed for Maundi site. Left: Mean day-time relative air humidity (RH_D). Error bars indicate expanded uncertainties derived from the uncertainty propagation law. The grey dotted line depicts a “corrected” RH_D record, that accounts for vegetation changes (contribution of grass-derived n -alkane and sugar biomarkers, see text Section 4.3 for details). Middle: Record of $\delta^{18}\text{O}_{\text{source-water}}$ reconstructed using local leaf water evaporation line slope (LLEL) of 2.75 (blue and black error bars represent the confidence interval calculated using LLEL slopes of 2.50 and 3.00, respectively) and $\delta^{18}\text{O}$ values of leaf water. The $\delta^{18}\text{O}_{\text{source-water}}$ curve corrected for ice-volume effect is also shown (in grey). $\delta^{18}\text{O}_{\text{leaf-water}}$ is shown in green. Right: Record of $\delta^2\text{H}_{\text{source-water}}$ reconstructed for a LLEL slope of 2.75 (blue and black error bars represent LLEL slopes of 2.50 and 3.00, respectively), corrected for ice-volume effect. $\delta^2\text{H}_{\text{leaf-water}}$ is shown in green. (For interpretation of the references to colour in this figure legend, the reader is referred to the web version of this article.)

similarities to previously published regional paleoprecipitation records (East African lake-level history and local pollen records; cf. Section 4.3). This suggests that one important factor for Maundi RH_D record is the overall regional moisture availability that is associated with the precipitation provided by the East African monsoon system. However, as mentioned above, discrepancies appear between Maundi RH_D record and the lake stand record. Lake level high-stands during the early Holocene are followed by lake level regressions during the late Holocene, whereas Maundi RH_D values reach their maximum only in the middle Holocene, in line with the pollen records from the same site (Schüler et al., 2012) and the WeruWeru study site at 2650 m a.s.l. (Schüler, 2013). This apparent discrepancy can be reconciled by taking into account local factors. Mölg et al. (2009) speculated that the altitudinal belt of maximum precipitation, which is located at present at about ~2200 m a.s.l. on the southern slopes of Mt. Kilimanjaro, might have migrated vertically in the past. We propose that this belt, and thus also the belt of maximum RH_D, migrated uphill along the slopes of Mt. Kilimanjaro in direction to the Maundi study site at ~2780 m a.s.l. over the course of the Holocene. The vertical migration of the belt could be controlled by increasing moisture availability and also by variable inversion – a concept described by Augstein et al. (1974) as ‘trade wind inversion’ for the Atlantic Ocean. During the early Holocene, the trade wind inversion of the southeast trades was presumably strongly developed due to the 30°N summer insolation maximum and thus enhanced latent heat transfer into the higher atmospheric layers in the northern African tropics. As a consequence of the well-developed trade wind inversion during the early Holocene, the diurnal thermal circulation on Mt. Kilimanjaro, and thus also the cloud formation in the subalpine zone where the Maundi study site is located, was suppressed (cf. Fig. 11 in Pepin et al., 2010). However, the shifts in the Maundi RH_D record does not follow the maxima in equatorial or the Northern Hemisphere summer insolation. The prominent drought period (ca. 70–60 ka BP, Fig. 5) cannot be explained via orbital forcing either and its cause remains unclear.

Concerning the factors controlling variability of $\delta^2\text{H}/\delta^{18}\text{O}$ of paleoprecipitation, a straightforward application of the ‘amount effect’, as we know it from modern precipitation, may not be applicable for the Maundi precipitation record. Apart from the fact that a long-term/interannual isotope ‘amount effect’ in tropical precipitation is by no means clear from the instrumental data (Rozanski et al., 1996), an apparent positive correlation of RH_D record with $\delta^2\text{H}/\delta^{18}\text{O}_{\text{source-water}}$ is visible in the presented data (Fig. 6, $R = 0.60$; $p < 0.001$). This effect could be generated by the local vegetation, particularly the montane rainforest. The isotopic composition of transpired moisture is similar to that of plant source water under steady-state conditions (e.g. Bariac et al., 1991; Flanagan et al., 1991), thus being isotopically much heavier than the vapor of marine origin. Along the southern slopes of Mt. Kilimanjaro, $\delta^2\text{H}_{\text{prec}}$ has a local maximum in the montane rainforest at about 2000–2200 m a.s.l. (Zech et al., 2015). This maximum can be interpreted in terms of an increasing proportion of transpired, i.e. isotopically enriched moisture. At Mt. Kilimanjaro, the montane rainforest is an important atmospheric moisture source under present climatic conditions (Pepin et al., 2010), and we suggest it contributed also in the past to the precipitation at Maundi site, with the importance varying in accordance with the fluctuation of its size and vertical extent. This could explain that maxima of the reconstructed RH_D record generally coincide with an increase in Afromontane pollen taxa and more isotopically enriched source water (precipitation). During arid periods the Afromontane forest belt descended and/or diminished, which resulted in more isotopically depleted precipitation at the Maundi site. A rough

assessment based on modern $\delta^2\text{H}_{\text{prec}}$ transect presented in Fig. 3b of Zech et al. (2015) shows that this local effect could be in the order of 20‰ and 2.5‰ for $\delta^2\text{H}_{\text{prec}}$ and $\delta^{18}\text{O}_{\text{prec}}$, respectively.

Apart from the local effect associated with montane rainforest, changes in the isotopic composition of precipitation at Maundi site could be also influenced by regional effects associated with the regional biosphere as an important factor controlling moisture recycling over the East African continent. Dry conditions at the vicinity of Maundi site, as well as further south and southeast of Mt. Kilimanjaro, towards the coast of the Indian Ocean, most probably resulted in scarce vegetation and consequently a reduced source of isotopically heavy water vapor for the regional atmosphere. This would mean that even reduced precipitation during dry periods might lead to higher effective rainout of moist air masses of marine origin and the resulting depletion of heavy isotope content in precipitation falling on the southern and eastern slopes of Mt. Kilimanjaro. The importance of the biosphere-modulated recycling of water for continental water balance is clearly seen in present-day Europe. The gradient of $\delta^2\text{H}/\delta^{18}\text{O}_{\text{prec}}$ across the European continent during summer is nowadays significantly weaker than it would be without the transpiration flux operated on continental scale (Rozanski et al., 1982). Similar modulation of the extent of continental effect in $\delta^2\text{H}/\delta^{18}\text{O}_{\text{prec}}$ in response to varying biospheric feedback, can be expected along the passage of East African monsoon all the way to the Maundi site.

5. Conclusions

The Maundi loess-like paleosol sequence provides a valuable paleoclimate/environmental archive roughly comprising the last 100 ka. We summarize our results as follows:

- The records of $\delta^{18}\text{O}_{\text{sugars}}$, $\delta^2\text{H}_{\text{methoxy}}$, $\delta^2\text{H}_{\text{fatty-acids}}$ and $\delta^2\text{H}_{\text{n-alkanes}}$ reveal similar patterns. The periods from ~70 to 60 ka, the LGM and YD are characterized by relatively positive δ values, whereas during the Holocene relatively negative δ values occurred. The important differences comprise higher variability of the $\delta^{18}\text{O}_{\text{sugar}}$ record, timing of the Holocene minima, and larger fluctuations in $\delta^2\text{H}_{\text{methoxy}}$ values, as well as a shift to very negative values in the modern topsoil.
- Comparison of the Maundi $\delta^2\text{H}_{\text{leaf-wax}}$ record with other available equatorial East African $\delta^2\text{H}_{\text{leaf-wax}}$ records (Lake Challa, Lake Tanganyika) shows that they all reveal distinct $\delta^2\text{H}_{\text{leaf-wax}}$ minima within the AHP, but the pattern, timing and amplitude are somewhat different. The most striking difference among them is a clear regional ‘altitude effect’ resulting in the Maundi $\delta^2\text{H}_{\text{leaf-wax}}$ record being shifted to more negative δ values with respect to those recorded in lake sediments.
- The various influences on $\delta^2\text{H}_{\text{leaf-wax}}$ records from East Africa (e.g. moisture transport history, precipitation amount, evapotranspirative enrichment) challenge a straightforward interpretation in terms of paleoclimate. We suggest that the coupled $\delta^2\text{H}_{\text{n-alkane}}-\delta^{18}\text{O}_{\text{sugar}}$ approach could provide more robust proxies, namely the day-time relative humidity (RH_D) and the isotopic composition of plant source water ($\delta^2\text{H}/\delta^{18}\text{O}_{\text{source-water}}$), by accounting for the leaf water enrichment.
- The reconstructed day-time relative humidity record for Maundi site is generally in agreement with the Maundi pollen results (Schüler et al., 2012), suggesting arid climatic conditions from ~70 to 60 ka, during the LGM and the YD, whereas the pre-LGM, the Late Glacial and the middle and late Holocene were characterized by more humid climatic conditions. Apart from the overall regional moisture availability, we suggest that the intensification/weakening of the trade wind inversion, which

affects the diurnal montane atmospheric circulation on the slopes of Mt. Kilimanjaro, is a local process, which may influence changes of relative humidity recorded at the Maundi study site.

- The results of the coupled $\delta^2\text{H}_{n\text{-alkane}}-\delta^{18}\text{O}_{\text{sugar}}$ approach presented here caution against directly interpreting $\delta^2\text{H}_{\text{leaf-wax}}$ (as well as $\delta^{18}\text{O}_{\text{sugar}}$) records as proxies of $\delta^2\text{H}_{\text{prec}}$ ($\delta^{18}\text{O}_{\text{prec}}$). Changes in relative humidity and the resulting variations in isotopic evapotranspirative enrichment of leaf water (Fig. 6) can mask changes of $\delta^2\text{H}_{\text{prec}}$ ($\delta^{18}\text{O}_{\text{prec}}$).
- Strong positive correlation between RH_D and $\delta^2\text{H}/\delta^{18}\text{O}_{\text{source-water}}$ observed at the Maundi site on millennial time scale (Fig. 6), suggests that a straightforward application of the ‘amount effect’, as we know it from modern precipitation, cannot explain the reconstructed isotopic composition of local precipitation. Effects associated with the impact of local and regional biosphere on the isotopic composition of atmospheric moisture and precipitation need to be called on to understand $\delta^2\text{H}/\delta^{18}\text{O}_{\text{source-water}}$ records on millennial time scale. They involve expansion/shrinking or complete disappearance of montane rainforest on the southeastern slopes of Mt. Kilimanjaro as well as expansion/shrinking of regional vegetation cover in response to climatic changes in the region.

Clearly, further work is needed to improve our understanding of isotope biomarkers records preserved in continental archive. This is particularly true for the East African region.

Acknowledgements

We kindly thank Prof. B. Huwe (University of Bayreuth) and Prof. L. Zöller (University of Bayreuth) for logistic support. We are also very grateful to M. Benesch (Martin-Luther University Halle-Wittenberg) for laboratory assistance during compound specific $\delta^{18}\text{O}$ analyses of sugars. We are furthermore very grateful to Dr. L. Schüler (University of Göttingen) for kindly providing pollen data of the Maundi loess-like paleosol sequence, for providing Fig. 1a and b and for discussions on the pollen results. We also thank Dr. C. Lane (University of Manchester) for discussions on dating issues, Dr. T. Appelhans and F. Detsch (University of Marburg) for providing Fig. 1c, mean day-time ambient air temperature and above-ground air humidity data, and discussions on atmospheric circulation patterns. We acknowledge the comments of four anonymous reviewers on an earlier version of our manuscript and three anonymous reviewers for their constructive comments and feedback on this version of our manuscript. This study was partly financed by the German Research Foundation (ZE 844/1-2) and the SNF (119492). Involvement of K. Rozanski was supported by statutory funds of the AGH University of Science and Technology (project no. 11.11.220.01). J. Hepp also greatly acknowledges the support given by the German Federal Environmental Foundation.

References

Abram, N.J., Gagan, M.K., Liu, Z., Hantoro, W.S., McCulloch, M.T., Suwargadi, B.W., 2007. Seasonal characteristics of the Indian Ocean Dipole during the holocene epoch. *Nature* 445, 299–302. <http://dx.doi.org/10.1038/nature05477>.

Allison, G.B., Gat, J.R., Leaney, F.W.J., 1985. The relationship between deuterium and oxygen-18 delta values in leaf water. *Chem. Geol.* 58, 145–156.

Amelung, W., Cheshire, M.V., Guggenberger, G., 1996. Determination of neutral and acidic sugars in soil by capillary gas-liquid chromatography after trifluoroacetic acid hydrolysis. *Soil Biol. Biochem.* 28, 1631–1639.

Anhäuser, T., Sirocko, F., Greule, M., Esper, J., Keppler, F., 2014. D/H ratios of methoxyl groups of the sedimentary organic matter of Lake Holzmaar (Eifel, Germany): a potential palaeoclimate/hydrology proxy. *Geochimica Cosmochimica Acta* 142, 39–52.

Appelhans, T., Mwangomo, E., Otte, I., Detsch, F., Nauss, T., Hemp, A., 2015. Eco-meteorological characteristics of the southern slopes of Kilimanjaro, Tanzania. *Int. J. Climatol.* 36, 3245–3258. <http://dx.doi.org/10.1002/joc.4552>.

Araguás-Araguás, L., Froehlich, K., Rozanski, K., 2000. Deuterium and oxygen-18 isotope composition of precipitation and atmospheric moisture. *Hydrol. Process.* 14, 1341–1355. [http://dx.doi.org/10.1002/1099-1085\(20000615\)14:8<1341::AID-HYP983>3.0.CO;2-Z](http://dx.doi.org/10.1002/1099-1085(20000615)14:8<1341::AID-HYP983>3.0.CO;2-Z).

Augstein, E., Schmidt, H., Ostapoff, F., 1974. The vertical structure of the atmospheric planetary boundary layer in undisturbed trade winds over the Atlantic Ocean. *Boundary-Layer Meteorol.* 6, 129–150.

Bariac, T., Deleens, E., Gerbaud, A., Andre, M., Mariotti, A., 1991. La composition isotopique (^{18}O , ^2H) de la vapeur d'eau transpiree: etude en conditions asser-vies. *Geochimica Cosmochimica Acta* 55, 3391–3402.

Barker, P., Telford, R., Gasse, F., Thevenon, F., 2002. Late pleistocene and holocene palaeohydrology of Lake Rukwa, Tanzania, inferred from diatom analysis. *Palaeogeogr. Palaeoclimatol. Palaeoecol.* 187, 295–305. [http://dx.doi.org/10.1016/S0031-0182\(02\)00482-0](http://dx.doi.org/10.1016/S0031-0182(02)00482-0).

Berke, M.A., Johnson, T.C., Werne, J.P., Grice, K., Schouten, S., Sinninghe Damsté, J.S., 2012. Molecular records of climate variability and vegetation response since the late pleistocene in the lake Victoria basin, East Africa. *Quat. Sci. Rev.* 55, 59–74. <http://dx.doi.org/10.1016/j.quascirev.2012.08.014>.

Bintanja, R., van der Wal, R.S.W., Oerlemans, J., 2005. Modelled atmospheric temperatures and global sea levels over the past million years. *Nature* 437, 125–128. <http://dx.doi.org/10.1038/nature03975>.

Bonnefille, R., Chalié, F., Guiot, J., Vincens, A., 1992. Quantitative estimates of full glacial temperatures in equatorial Africa from palynological data. *Clim. Dyn.* 6, 251–257.

Castañeda, I.S., Werne, J.P., Johnson, T.C., 2007. Wet and arid phases in the southeast African tropics since the last glacial maximum. *Geology* 35, 823–826. <http://dx.doi.org/10.1130/G23916A.1>.

Cernusak, L.A., Wong, S.C., Farquhar, G.D., 2003. Oxygen isotope composition of phloem sap in relation to leaf water in *Ricinus communis*. *Funct. Plant Biol.* 30, 1059–1070.

Clark, P.U., Dyke, A.S., Shakun, J.D., Carlson, A.E., Clark, J., Wohlfarth, B., Mitrovica, J.X., Hostetler, S.W., McCabe, A.M., 2009. The last glacial maximum. *Science* 325, 710–714.

Cockerton, H.E., Street-Perrott, F.A., Barker, P.A., Leng, M.J., Sloane, H.J., Ficken, K.J., 2015. Orbital forcing of glacial/interglacial variations in chemical weathering and silicon cycling within the upper White Nile basin, East Africa: stable isotope and biomarker evidence from Lakes Victoria and Edward. *Quat. Sci. Rev.* 130, 57–71. <http://dx.doi.org/10.1016/j.quascirev.2015.07.028>.

Cohen, A.S., Talbot, M.R., Awramik, S.M., Dettman, D.L., Abell, P., 1997. Lake level and palaeoenvironmental history of Lake Tanganyika, Africa, as inferred from late Holocene and modern stromatolites. *Geol. Soc. Am. Bull.* 109, 444–460.

Dongmann, G., Nürnberg, H.W., Förstel, H., Wagener, K., 1974. On the enrichment of H_2^{18}O in the leaves of transpiring plants. *Radiat. Environ. Biophysics* 11, 41–52. <http://dx.doi.org/10.1007/BF01323099>.

Duane, W.J., Pepin, N.C., Losleben, M.L., Hardy, D.R., 2008. General characteristics of temperature and humidity variability on Kilimanjaro, Tanzania. *Arct. Antarct. Alp. Res.* 40, 323–334. [http://dx.doi.org/10.1657/1523-0430\(06-127\)](http://dx.doi.org/10.1657/1523-0430(06-127)).

Farquhar, G.D., Cernusak, L.A., Barnes, B., 2007. Heavy water fractionation during transpiration. *Plant Physiol.* 143, 11–18. <http://dx.doi.org/10.1104/pp.106.093278>.

Felton, A.A., Russell, J.M., Cohen, A.S., Baker, M.E., Chesley, J.T., Lezzar, K.E., McGlue, M.M., Pigati, J.S., Quade, J., Stager, J.C., Tiercelin, J.-J., 2007. Paleolimnological evidence for the onset and termination of glacial aridity from lake Tanganyika, tropical East Africa. *Palaeogeogr. Palaeoclimatol. Palaeoecol.* 252, 405–423. <http://dx.doi.org/10.1016/j.palaeo.2007.04.003>.

Flanagan, L.B., Comstock, J.P., Ehleringer, J.R., 1991. Comparison of modeled and observed environmental influences on the stable oxygen and hydrogen isotope composition of leaf water in *Phaseolus vulgaris* L. *Plant Physiol.* 588–596.

Gamarra, B., Sachse, D., Kahmen, A., 2016. Effects of leaf water evaporative ^2H -enrichment and biosynthetic fractionation on leaf wax *n*-alkane $\delta^2\text{H}$ values in C3 and C4 grasses. *Plant, Cell Environ. Environ.* 39, 2390–2403. <http://dx.doi.org/10.1111/pce.12789>.

Gasse, F., 2000. Hydrological changes in the African tropics since the last glacial maximum. *Quat. Sci. Rev.* 19, 189–211.

Gasse, F., Chalié, F., Vincens, A., Williams, M.A.J., Williamson, D., 2008. Climatic patterns in equatorial and southern Africa from 30,000 to 10,000 years ago reconstructed from terrestrial and near-shore proxy data. *Quat. Sci. Rev.* 27, 2316–2340. <http://dx.doi.org/10.1016/j.quascirev.2008.08.027>.

Gasse, F., Lédée, V., Massault, M., Fontes, J.-C., 1989. Water-level fluctuations of Lake Tanganyika in phase with oceanic changes during the last glaciation and deglaciation. *Nature* 342, 57–59.

Gat, J.R., Bowser, C.J., 1991. The heavy isotope enrichment of water in coupled evaporative systems. In: Tayler, H.P., O'Neil, J.R., Kaplan, I.R. (Eds.), *Stable Isotope Geochemistry: a Tribute to Samuel Epstein*. The Geochemical Society, Lancaster, pp. 159–168.

Gessler, A., Brandes, E., Buchmann, N., Helle, G., Rennberg, H., Barnard, R.L., 2009. Tracing carbon and oxygen isotope signals from newly assimilated sugars in the leaves to the tree-ring archive. *Plant, Cell & Environ.* 32, 780–795. <http://dx.doi.org/10.1111/j.1365-3040.2009.01957.x>.

Gonfiantini, R., Roche, M.-A., Olivry, J.-C., Fontes, J.-C., Zuppi, G.M., 2001. The altitude effect on the isotopic composition of tropical rains. *Chem. Geol.* 181, 147–167.

Graham, H.V., Patzkowsky, M.E., Wing, S.L., Parker, G.G., Fogel, M.L., Freeman, K.H., 2014. Isotopic characteristics of canopies in simulated leaf assemblages. *Geochimica Cosmochimica Acta* 144, 82–95. <http://dx.doi.org/10.1016/j.gca.2014.08.032>.

- Greule, M., Mosandl, A., Hamilton, J.T.G., Keppler, F., 2008. A rapid and precise method for determination of D/H ratios of plant methoxyl groups. *Rapid Commun. Mass Spectrom.* 22, 3983–3988. <http://dx.doi.org/10.1002/rcm>.
- Helliker, B.R., Ehleringer, J.R., 2002. Grass blades as tree rings: environmentally induced changes in the oxygen isotope ratio of cellulose along the length of grass blades. *New Phytol.* 155, 417–424.
- Hemp, A., 2006a. Continuum or zonation? Altitudinal gradients in the forest vegetation of Mt. Kilimanjaro. *Plant Ecol.* 184 (1), 27–42.
- Hemp, A., 2006b. Vegetation of Kilimanjaro: hidden endemics and missing bamboo. *Afr. J. Ecol.* 44, 305–328.
- Hemp, A., 2005. Climate change-driven forest fires marginalize the impact of ice cap wasting on Kilimanjaro. *Glob. Change Biol.* 49, 1013–1023. <http://dx.doi.org/10.1111/j.1365-2486.2005.00968.x>.
- Hemp, A., Beck, E., 2001. *Erica excelsa* as a fire-tolerating component of Mt. Kilimanjaro's forests. *Phytocoenologia* 449–475.
- Horita, J., Wesolowski, D.J., 1994. Liquid-vapor fractionation of oxygen and hydrogen isotopes of water from the freezing to the critical temperature. *Geochimica Cosmochimica Acta* 58, 3425–3437.
- Junginger, A., Roller, S., Olaka, L.A., Trauth, M.H., 2014. The effects of solar irradiation changes on the migration of the Congo air boundary and water levels of paleo-Lake Suguta, Northern Kenya Rift, during the African humid period (15–5 ka BP). *Palaeogeogr. Palaeoclimatol. Palaeoecol.* 396, 1–16. <http://dx.doi.org/10.1016/j.palaeo.2013.12.007>.
- Kahmen, A., Scheffuß, E., Sachse, D., 2013. Leaf water deuterium enrichment shapes leaf wax *n*-alkane δD values of angiosperm plants I: experimental evidence and mechanistic insights. *Geochimica Cosmochimica Acta* 111, 39–49.
- Keppler, F., Harper, D.B., Kalin, R.M., Meier-Augenstein, W., Farmer, N., Davis, S., Schmidt, H.-L., Brown, D.M., Hamilton, J.T.G., 2007. Stable hydrogen isotope ratios of lignin methoxyl groups as a paleoclimate proxy and constraint of the geographical origin of wood. *New Phytol.* 176, 600–609.
- Konecny, B.L., Russell, J.M., Johnson, T.C., Brown, E.T., Berke, M.A., Werne, J.P., Huang, Y., 2011. Atmospheric circulation patterns during late Pleistocene climate changes at Lake Malawi, Africa. *Earth Planet. Sci. Lett.* 312, 318–326. <http://dx.doi.org/10.1016/j.epsl.2011.10.020>.
- Lisiecki, L.E., Raymo, M.E., 2005. A Pliocene-Pleistocene stack of 57 globally distributed benthic $\delta^{18}O$ records. *Palaeoceanography* 20, 1–17. <http://dx.doi.org/10.1029/2004PA001071>.
- Loomis, S.E., Russell, J.M., Ladd, B., Street-Perrott, F.A., Sinninghe Damsté, J.S., 2012. Calibration and application of the branched GDGT temperature proxy on East African lake sediments. *Earth Planet. Sci. Lett.* 257–258, 277–288. <http://dx.doi.org/10.1016/j.epsl.2012.09.031>.
- Majoube, M., 1971. Fractionation of oxygen-18 and of deuterium between water and its vapor. *J. Chem. Phys.* 68, 1423–1436.
- Mark, B.G., Osmaston, H.A., 2008. Quaternary glaciation in Africa: key chronologies and climatic implications. *J. Quat. Sci.* 23, 589–608. <http://dx.doi.org/10.1002/jqs>.
- Masson-Delmotte, V., Jouzel, J., Landais, A., Stievenard, M., Johnson, S.J., White, J.W.C., Werner, M., Sveinbjörnsdóttir, A., Fuhrer, K., 2005. GRIP deuterium excess reveals rapid and orbital-scale changes in Greenland moisture origin. *Science* 309, 118–121. <http://dx.doi.org/10.1126/science.1108575>.
- McGlue, M.M., Lezzar, K.E., Cohen, A.S., Russell, J.M., Tierceline, J.-J., Felton, A.A., Mbede, E., Nkotagu, H.H., 2007. Seismic records of late pleistocene aridity in lake Tanganyika, tropical East Africa. *J. Paleolimnol.* 40, 635–653. <http://dx.doi.org/10.1007/s10933-007-9187-x>.
- McInerney, F.A., Helliker, B.R., Freeman, K.H., 2011. Hydrogen isotope ratios of leaf wax *n*-alkanes in grasses are insensitive to transpiration. *Geochimica Cosmochimica Acta* 75, 541–554. <http://dx.doi.org/10.1016/j.gca.2010.10.022>.
- Merlivat, L., 1978. Molecular diffusivities of $H_2^{16}O$, $HD^{16}O$, and $H_2^{18}O$ in gases. *J. Chem. Phys.* 69, 2864–2871. <http://dx.doi.org/10.1063/1.436884>.
- Moernaut, J., Verschuren, D., Charlet, F., Kristen, I., Fagot, M., Batist, M. De, 2010. The seismic-stratigraphic record of lake-level fluctuations in Lake Challa: hydrological stability and change in equatorial East Africa over the last 140 kyr. *Earth Planet. Sci. Lett.* 290, 214–223. <http://dx.doi.org/10.1016/j.epsl.2009.12.023>.
- Mölg, T., Chiang, J.C.H., Gohm, A., Cullen, N.J., 2009. Temporal precipitation variability versus altitude on a tropical high mountain: observations and mesoscale atmospheric modelling. *Q. J. R. Meteorological Soc.* 135, 1439–1455. <http://dx.doi.org/10.1002/qj>.
- Otto-Bliessner, B.L., Russell, J.M., Clark, P.U., Liu, Z., Overpeck, J.T., Konecny, B., deMenocal, P., Nicholson, S.E., He, F., Lu, Z., 2014. Coherent changes of south-eastern equatorial and northern African rainfall during the last deglaciation. *Science* 346, 1223–1227.
- Patridge, T.C., deMenocal, P.B., Lorentz, S.A., Paiker, M.J., Vogel, J.C., 1997. Orbital forcing of climate over South Africa: a 200,000-year rainfall record from the pretoria saltpan. *Quat. Sci. Rev.* 16, 1125–1133.
- Pepin, N.C., Duane, W.J., Hardy, D.R., 2010. The montane circulation on Kilimanjaro, Tanzania and its relevance for the summit ice fields: comparison of surface mountain climate with equivalent reanalysis parameters. *Glob. Planet. Change* 74, 61–75. <http://dx.doi.org/10.1016/j.gloplacha.2010.08.001>.
- Peterse, F., van der Meer, M.T.J., Schouten, S., Jia, G., Ossebaer, J., Blokker, J., Sinninghe Damsté, J.S., 2009. Assessment of soil *n*-alkane δD and branched tetraether membrane lipid distributions as tools for paleoelevation reconstruction. *Biogeosciences* 6, 2799–2807.
- Rasmussen, S.O., Bigler, M., Blockley, S.P., Blunier, T., Buchardt, S.L., Clausen, H.B., Cuvjajnovic, I., Dahl-Jensen, D., Johnsen, S.J., Fischer, H., Gkinis, V., Guillevic, M., Hoek, W.Z., Lowe, J.J., Pedro, J.B., Popp, T., Seierstad, I.K., Peder Steffensen, J., Svensson, A.M., Vallelonga, P., Vinther, B.M., Walker, M.J.C., Wheatley, J.J., Winstrup, M., 2014. A stratigraphic framework for abrupt climatic changes during the Last Glacial period based on three synchronized Greenland ice-core records: refining and extending the INTIMATE event stratigraphy. *Quat. Sci. Rev.* 106, 14–28. <http://dx.doi.org/10.1016/j.quascirev.2014.09.007>.
- Roden, J.S., Ehleringer, J.R., 1999. Observations of hydrogen and oxygen isotopes in leaf water confirm the Craig-Gordon model under wide-ranging environmental conditions. *Plant Physiol.* 120, 1165–1173.
- Roden, J.S., Lin, G., Ehleringer, J.R., 2000. A mechanistic model for interpretation of hydrogen and oxygen isotope ratios in tree-ring cellulose. *Geochimica Cosmochimica Acta* 64, 21–35.
- Rozanski, K., Araguás-Araguás, L., Gonfiantini, R., 1996. Isotope patterns of precipitation in the East African region. *Limnol. Climatol. Paleoclimatology East Afr. Lakes* 79–94.
- Rozanski, K., Araguás-Araguás, L., Gonfiantini, R., 1993. Isotopic patterns in modern global precipitation. *Clim. Change Cont. Isotopic Rec.* 1–36.
- Rozanski, K., Sonntag, C., Münnich, K.O., 1982. Factors controlling stable isotope composition of European precipitation. *Tellus* 34, 142–150. <http://dx.doi.org/10.1111/j.2153-3490.1982.tb01801.x>.
- Sachse, D., Billault, I., Bowen, G.J., Chikaraishi, Y., Dawson, T.E., Feakins, S.J., Freeman, K.H., Magill, C.R., McInerney, F.A., van der Meer, M.T.J., Polissar, P., Robins, R.J., Sachs, J.P., Schmidt, H.-L., Sessions, A.L., White, J.W.C., West, J.B., 2012. Molecular paleohydrology: interpreting the hydrogen-isotopic composition of lipid biomarkers from photosynthesizing organisms. *Annu. Rev.* 40, 221–249. <http://dx.doi.org/10.1146/annurev-earth-042711-105535>.
- Sachse, D., Radke, J., Gleixner, G., 2006. δD values of individual *n*-alkanes from terrestrial plants along a climatic gradient – implications for the sedimentary biomarker record. *Org. Geochem.* 37, 469–483. <http://dx.doi.org/10.1016/j.orggeochem.2005.12.003>.
- Santruckce, J., Kveton, J., Setlik, J., Bulickova, L., 2007. Spatial variation of deuterium enrichment in bulk water of snowgum leaves. *Plant Physiol.* 143, 88–97. <http://dx.doi.org/10.1104/pp.106.089284>.
- Scheffuß, E., Kuhlmann, H., Mollenhauer, G., Prange, M., Pätzold, J., 2011. Forcing of wet phases in southeast Africa over the past 17,000 years. *Nature* 480, 509–512. <http://dx.doi.org/10.1038/nature10685>.
- Scheffuß, E., Schouten, S., Schneider, R.R., 2005. Climatic controls on central African hydrology during the past 20,000 years. *Nature* 437, 1003–1006. <http://dx.doi.org/10.1038/nature03945>.
- Schmidt, H.-L., Werner, R.A., Roßmann, A., 2001. ^{18}O Pattern and biosynthesis of natural plant products. *Phytochemistry* 58, 9–32. [http://dx.doi.org/10.1016/S0031-9422\(01\)00017-6](http://dx.doi.org/10.1016/S0031-9422(01)00017-6).
- Scholz, C.A., Johnson, T.C., Cohen, A.S., King, J.W., Peck, J.A., Overpeck, J.T., Talbot, M.R., Brown, E.T., Kalindekale, L., Amoko, P.Y.O., Lyons, R.P., Shanahan, T.M., Castañeda, I.S., Heil, C.W., Forman, S.L., McHargue, L.R., Beuning, K.R., Gomez, J., Pierson, J., 2007. East African megadroughts between 135 and 75 thousand years ago and bearing on early-modern human origins. *PNAS* 104, 16416–16421.
- Schrag, D.P., Adkins, J.F., McIntyre, K., Alexander, J.L., Hodell, D.A., Charles, C.D., McManus, J.F., 2002. The oxygen isotopic composition of seawater during the last glacial maximum. *Quat. Sci. Rev.* 21, 331–342.
- Schrag, D.P., Hampt, G., Murray, D.W., 1996. Pore fluid constraints on the temperature and oxygen isotopic composition of the glacial ocean. *Science* 272, 1930–1932.
- Schüler, L., 2013. Studies on Late Quaternary Environmental Dynamics (Vegetation, Biodiversity, Climate, Soils, Fire and Human Impact) on Mt Kilimanjaro. *Geograph.-Universität Göttingen*. <http://hdl.handle.net/11858/00-1735-0000-0001-8B6E-F>.
- Schüler, L., Hemp, A., Zech, W., Behling, H., 2012. Vegetation, climate and fire-dynamics in East Africa inferred from the Maundi crater pollen record from Mt Kilimanjaro during the last glacial-interglacial cycle. *Quat. Sci. Rev.* 39, 1–13. <http://dx.doi.org/10.1016/j.quascirev.2012.02.003>.
- Sessions, A.L., Burgoyne, T.W., Schimmelmann, A., Hayes, J.M., 1999. Fractionation of hydrogen isotopes in lipid biosynthesis. *Org. Geochem.* 30, 1193–1200.
- Shanahan, T.M., Zreda, M., 2000. Chronology of quaternary glaciations in East Africa. *Earth Planet. Sci. Lett.* 177, 23–42.
- Shu, Y., Feng, X., Posmentier, E.S., Sonder, L.J., Faiia, A.M., Yakir, D., 2008. Isotopic studies of leaf water. Part 1: a physically based two-dimensional model for pine needles. *Geochimica Cosmochimica Acta* 72, 5175–5188. <http://dx.doi.org/10.1016/j.gca.2008.05.062>.
- Stager, J.C., Ryves, D.B., Chase, B.M., Pausata, F.S.R., 2011. Catastrophic drought in the Afro-Asian monsoon region during Heinrich event 1. *Science* 331, 1299–1303.
- Stenni, B., Masson-Delmotte, V., Selmo, E., Oerter, H., Meyer, H., Röthlisberger, R., Jouzel, J., Cattani, O., Falourd, S., Fischer, H., Hoffmann, G., Iacumin, P., Johnsen, S.J., Minster, B., Udisti, R., 2010. The deuterium excess records of EPICA Dome C and Dronning Maud Land ice cores (East Antarctica). *Quat. Sci. Rev.* 29, 146–159. <http://dx.doi.org/10.1016/j.quascirev.2009.10.009>.
- Sternberg, L.S.L., 2014. Comment on “Oxygen isotope ratios ($^{18}O/^{16}O$) of hemicellulose-derived sugar biomarkers in plants, soils and sediments as paleoclimate proxy I: insight from a climate chamber experiment” by Zech et al. (2014). *Geochimica Cosmochimica Acta* 141, 677–679. <http://dx.doi.org/10.1016/j.gca.2014.04.051>.
- Sternberg, L.S.L., DeNiro, M.J., Savidge, R.A., 1986. Oxygen isotope exchange between metabolites and water during biochemical reactions leading to cellulose synthesis. *Plant Physiol.* 82, 423–427.
- Street-Perrott, F.A., Ficken, K.J., Huang, Y., Eglinton, G., 2004. Late Quaternary

- changes in carbon cycling on Mt. Kenya, East Africa: an overview of the $\delta^{13}\text{C}$ record in lacustrine organic matter. *Quat. Sci. Rev.* 23, 861–879.
- Talbot, M.R., Livingstone, D.A., 1989. Hydrogen index and carbon isotopes of lacustrine organic matter as lake level indicators. *Palaeogeogr. Palaeoclimatol. Palaeoecol.* 70, 121–137. [http://dx.doi.org/10.1016/0031-0182\(89\)90084-9](http://dx.doi.org/10.1016/0031-0182(89)90084-9).
- Thompson, L.G., Mosley-Thompson, E., Davis, M.E., Henderson, K.A., Brecher, H.H., Zagorodnov, V.S., Mashiotta, T.A., Lin, P.-N., Mikhalenko, V.N., Hardy, D.R., Beer, J., 2002. Kilimanjaro ice core records: evidence of holocene climate change in tropical Africa. *Science* 298, 589–593. <http://dx.doi.org/10.1126/science.1073198>.
- Tierney, J.E., deMenocal, P.B., 2013. Abrupt shifts in Horn of Africa hydroclimate since the last glacial maximum. *Science* 342, 843–846. <http://dx.doi.org/10.1126/science.1240411>.
- Tierney, J.E., Russell, J.M., Huang, Y., 2010. A molecular perspective on Late Quaternary climate and vegetation change in the Lake Tanganyika basin, East Africa. *Quat. Sci. Rev.* 29, 787–800. <http://dx.doi.org/10.1016/j.quascirev.2009.11.030>.
- Tierney, J.E., Russell, J.M., Huang, Y., Sinninghe Damsté, J.S., Hopmans, E.C., Cohen, A.S., 2008. Northern Hemisphere controls on tropical southeast African climate during the past 60,000 years. *Science* 322, 252–255. <http://dx.doi.org/10.1126/science.1160485>.
- Tierney, J.E., Russell, J.M., Sinninghe Damsté, J.S., Huang, Y., Verschuren, D., 2011. Late quaternary behavior of the east African monsoon and the importance of the Congo air boundary. *Quat. Sci. Rev.* 30, 798–807. <http://dx.doi.org/10.1016/j.quascirev.2011.01.017>.
- Trauth, M.H., Deino, A.L., Bergner, A.G.N., Strecker, M.R., 2003. East African climate change and orbital forcing during the last 175 kyr BP. *Earth Planet. Sci. Lett.* 206, 297–313. [http://dx.doi.org/10.1016/S0012-821X\(02\)01105-6](http://dx.doi.org/10.1016/S0012-821X(02)01105-6).
- Tuthorn, M., Zech, R., Ruppenthal, M., Oelmann, Y., Kahmen, A., del Valle, H.F., Eglinton, T., Rozanski, K., Zech, M., 2015. Coupling $\delta^2\text{H}$ and $\delta^{18}\text{O}$ biomarker results yields information on relative humidity and isotopic composition of precipitation - a climate transect validation study. *Biogeosciences* 12, 3913–3924. <http://dx.doi.org/10.5194/bg-12-3913-2015>.
- Verschuren, D., Damsté, J.S.S., Moernaut, J., Kristen, I., Blaauw, M., Fagot, M., Haug, G.H., CHALLACEA project members, 2009. Half-precessional dynamics of monsoon rainfall near the East African Equator. *Nature* 462, 637–641. <http://dx.doi.org/10.1038/nature08520>.
- Weijers, J.W.H., Schefuß, E., Schouten, S., Sinninghe Damsté, J.S., 2007. Coupled thermal and hydrological evolution of tropical Africa over the last deglaciation. *Science* 315, 1701–1704. <http://dx.doi.org/10.1126/science.1138131>.
- Woltering, M., Johnson, T.C., Werne, J.P., Schouten, S., Sinninghe Damsté, J.S., 2011. Late pleistocene temperature history of southeast Africa: a TEX₈₆ temperature record from lake Malawi. *Palaeogeogr. Palaeoclimatol. Palaeoecol.* 303, 93–102. <http://dx.doi.org/10.1016/j.palaeo.2010.02.013>.
- Yakir, D., DeNiro, M.J., 1990. Oxygen and hydrogen isotope fractionation during cellulose metabolism in *Lemna gibba* L. *Plant Ecol.* 93, 325–332.
- Zech, M., Glaser, B., 2009. Compound-specific $\delta^{18}\text{O}$ analyses of neutral sugars in soils using gas chromatography-pyrolysis-isotope ratio mass spectrometry: problems, possible solutions and a first application. *Rapid Commun. Mass Spectrom.* 23, 3522–3532. <http://dx.doi.org/10.1002/rcm>.
- Zech, M., Mayr, C., Tuthorn, M., Leiber-Sauheitl, K., Glaser, B., 2014a. Reply to the comment of Sternberg on “Zech et al. (2014) Oxygen isotope ratios ($^{18}\text{O}/^{16}\text{O}$) of hemicellulose-derived sugar biomarkers in plants, soils and sediments as paleoclimate proxy I: insight from a climate chamber experiment. *GCA* 126, 614–623.” *Geochimica Cosmochimica Acta* 141, 680–682. <http://dx.doi.org/10.1016/j.gca.2014.04.051>.
- Zech, M., Mayr, C., Tuthorn, M., Leiber-Sauheitl, K., Glaser, B., 2014b. Oxygen isotope ratios ($^{18}\text{O}/^{16}\text{O}$) of hemicellulose-derived sugar biomarkers in plants, soils and sediments as paleoclimate proxy I: insight from a climate chamber experiment. *Geochimica Cosmochimica Acta* 126, 614–623. <http://dx.doi.org/10.1016/j.gca.2013.10.048>.
- Zech, M., Tuthorn, M., Detsch, F., Rozanski, K., Zech, R., Zöllner, L., Zech, W., Glaser, B., 2013. A 220 ka terrestrial $\delta^{18}\text{O}$ and deuterium excess biomarker record from an eolian permafrost paleosol sequence, NE-Siberia. *Chem. Geol.* <http://dx.doi.org/10.1016/j.chemgeo.2013.10.023>.
- Zech, M., Zech, R., Rozanski, K., Gleixner, G., Zech, W., 2015. Do n-alkane biomarkers in soils/sediments reflect the $\delta^2\text{H}$ isotopic composition of precipitation? A case study from Mt. Kilimanjaro and implications for paleoaltimetry and paleoclimate research. *Isotopes Environ. Health Stud.* 51, 508–524. <http://dx.doi.org/10.1080/10256016.2015.1058790>.
- Zech, R., Gao, L., Tarozo, R., Huang, Y., 2012. Branched glycerol dialkyl glycerol tetraethers in Pleistocene loess-paleosol sequences: three case studies. *Org. Geochem.* 53, 38–44. <http://dx.doi.org/10.1016/j.orggeochem.2012.09.005>.

D. Manuscript 4: Hepp et al. (2016)

published in *Organic Geochemistry*

<https://doi.org/10.1016/j.orggeochem.2016.05.012>



Contents lists available at ScienceDirect

Organic Geochemistry

journal homepage: www.elsevier.com/locate/orggeochem

A sugar biomarker proxy for assessing terrestrial versus aquatic sedimentary input



Johannes Hepp^{a,b,*}, Max Rabus^c, Tobias Anhäuser^d, Tobias Bromm^b, Christian Laforsch^c, Frank Sirocko^e, Bruno Glaser^b, Michael Zech^{b,f}

^a Chair of Geomorphology and BayCEER, University of Bayreuth, Universitätsstrasse 30, D-95440 Bayreuth, Germany

^b Institute of Agronomy and Nutritional Sciences, Soil Biogeochemistry, Martin-Luther University Halle-Wittenberg, von-Seckendorff-Platz 3, D-06120 Halle, Germany

^c Animal Ecology I and BayCEER, University of Bayreuth, Universitätsstrasse 30, D-95440 Bayreuth, Germany

^d Institute of Earth Sciences, Ruprecht Karls University Heidelberg, Im Neuenheimer Feld 234-236, D-69120 Heidelberg, Germany

^e Institute of Geosciences, Johannes Gutenberg University Mainz, J.-J.-Becher-Weg 21, D-55128 Mainz, Germany

^f Institute of Geography, Chair of Landscape- and Geoecology, Technical University of Dresden, Helmholtzstrasse 10, D-01062 Dresden, Germany

ARTICLE INFO

Article history:

Received 14 March 2016

Received in revised form 17 May 2016

Accepted 24 May 2016

Available online 27 May 2016

Keywords:

Lake sediments

Paleolimnology

Organic matter source

Algae

Indicator

Biomarkers

Sugars

Monosaccharides

ABSTRACT

One of the most important and at the same time most challenging issues in paleolimnological research is the differentiation between terrestrial and aquatic sedimentary organic matter (OM). We therefore investigated the relative abundance of the sugars fucose (fuc), arabinose (ara) and xylose (xyl) from various terrestrial and aquatic plants, as well as from algal samples. Algae were characterized by a higher abundance of fucose than vascular plants. Our results and a compilation of data from the literature suggest that fuc/(ara + xyl) and (fuc + xyl)/ara ratios may serve as complementary proxies in paleolimnological studies for distinguishing between terrestrial and aquatic sedimentary OM.

© 2016 Elsevier Ltd. All rights reserved.

1. Introduction

Lake sediments are valuable, often continuous and potentially high resolution, archives for studying past environmental and climate changes. This is highlighted by methods developed during the last few decades based on compound specific ¹⁸O and ²H results from hemicellulose/polysaccharide derived sugars and from leaf wax/aquatic plant derived *n*-alkanes, respectively (e.g. Rach et al., 2014; Zech et al., 2014b). Thereby, often one of the most crucial questions and challenges (Meyers and Ishiwatari, 1993) is to identify whether the origin of the sedimentary organic matter (OM) is allochthonous (terrestrial) or autochthonous (aquatic). The issue is typically addressed by way of different approaches and proxies in paleolimnological studies.

For instance, the C/N ratio of sedimentary total OM is frequently used to distinguish between algal and land derived material. This

proxy is based on the notion that land plants generally show markedly higher C/N values than lacustrine plants (Meyers and Ishiwatari, 1993). Further differentiation between input of C₃ vs. C₄ land plants is possible on the basis of the stable carbon isotopic composition ($\delta^{13}\text{C}$; Meyers, 1994; Meyers and Lallier-Vergès, 1999). However, both $\delta^{13}\text{C}$ and C/N values of terrestrial OM are affected by mineralization and degradation, resulting in more positive $\delta^{13}\text{C}$ values and lower C/N ratio (e.g. Zech et al., 2007). The latter could lead to a misinterpretation of soil OM transported by soil erosion into lacustrine systems as being aquatic-derived sedimentary OM. Similarly, other studies have demonstrated that the hydrogen index and oxygen index (HI, OI; derived from Rock-Eval analysis) may provide valuable information about the origin of sedimentary OM (Talbot and Livingstone, 1989; Meyers and Lallier-Vergès, 1999; Mügler et al., 2010). However, the indices are strongly affected by oxidation of the sedimentary OM and in addition strongly depend on the quality of terrestrial OM (waxy OM vs. cellulose rich OM; Lüniger and Schwark, 2002). Additional information and clarification about terrestrial vs. aquatic OM origin may be provided by lipid biomarkers. This is realized mainly by

* Corresponding author at: Chair of Geomorphology and BayCEER, University of Bayreuth, Universitätsstrasse 30, D-95440 Bayreuth, Germany. Tel.: +49 921 55 2172.

E-mail address: johannes-hepp@gmx.de (J. Hepp).

Table 1
Samples and concentrations of fucose (fuc), arabinose (ara) and xylose (xyl), sum of sugars (ara + fuc + xyl) and fuc/(ara + xyl) ratio. Median values of each group are given in the respective group row.

Sample	Name	Study site/origin	Fucose (mg/g sample)	Arabinose (mg/g sample)	Xylose (mg/g sample)	Sum of sugars (ara + fuc + xyl) (mg/g sample)	Fuc/(ara + xyl)
Terrestrial plants							
BS_Acer	Maple	Lake Bichlersee	0.54	26.20	21.75	50.42	0.01
BS_Buche	Beech	Lake Bichlersee	1.58	31.85	43.73	77.17	0.02
BS_Fichte	Spruce	Lake Bichlersee	0.00	32.93	66.98	99.91	0.00
BS_Gras1	Grass unspec.	Lake Bichlersee	0.41	30.77	21.75	52.93	0.01
BS_Gras2	Grass unspec.	Lake Bichlersee	0.00	268.45	512.35	780.81	0.00
BS_Tanne	Pine	Lake Bichlersee	0.00	31.80	105.99	137.79	0.00
GM6	Leaves sample (under water)	Lake Gemündener Maar	0.59	34.59	19.71	54.90	0.01
GM8	Leaves sample (shore area)	Lake Gemündener Maar	1.58	55.40	62.01	119.00	0.01
B1	Blackberry	Lake Gemündener Maar	0.47	22.13	27.82	50.42	0.01
B2	Blackberry	Lake Holzmaar	0.54	10.49	10.68	21.71	0.02
B3	Blackberry	Lake Holzmaar	0.38	10.28	12.77	23.42	0.01
B7	Blackberry	Lake Holzmaar	1.02	20.43	26.05	47.50	0.02
B8	Blackberry	Lake Holzmaar	0.17	9.57	19.20	28.95	0.00
HG1	Rose hip	Lake Holzmaar	0.64	12.07	14.47	27.18	0.02
HG2	Rose hip	Lake Holzmaar	0.90	15.23	7.90	24.02	0.03
			0.87	26.20	19.99	47.06	0.01
Emergent plants							
B51	Reed	Lake Bichlersee	0.00	54.33	98.35	144.73	0.00
B54	Juncus	Lake Bichlersee	0.00	179.24	608.63	787.87	0.00
B55	Carex roots	Lake Bichlersee	0.00	39.16	88.34	127.51	0.00
B56	Carex leaf	Lake Bichlersee	0.00	55.07	72.45	127.52	0.00
B59	Emergent plant unspec.	Lake Bichlersee	0.00	22.10	31.94	54.04	0.00
GM2	Cane green	Lake Bichlersee	1.02	22.77	12.12	35.91	0.03
GM3	Cane dead	Lake Gemündener Maar	0.00	232.45	452.81	685.25	0.00
GM4	<i>Iris pseudacorus</i> green	Lake Gemündener Maar	0.00	192.54	445.21	637.75	0.00
GM5	<i>Iris pseudacorus</i> death	Lake Gemündener Maar	0.00	17.35	37.50	54.84	0.00
HM_S1	Reed	Lake Holzmaar	0.00	57.25	136.54	193.79	0.00
HM_S2	Reed	Lake Holzmaar	0.00	20.81	38.56	59.37	0.00
HM_S3	Reed	Lake Holzmaar	0.00	23.70	57.70	81.40	0.00
P3	Reed	Pond near Rosenheim	0.00	53.58	108.36	161.94	0.00
P5	Carex	Pond near Rosenheim	0.00	108.91	390.74	499.66	0.00
			0.00	98.59	195.72	294.31	0.00
Mosses							
B57	Moss unspec.	Lake Bichlersee	0.54	17.66	18.45	36.65	0.02
P2	Moss unspec.	Pond near Rosenheim	0.28	18.45	20.48	39.21	0.01
			0.81	16.86	16.41	34.08	0.02
Submerged aquatic plants							
BS10	Water lily	Lake Bichlersee	0.65	12.10	12.47	25.31	0.02
BS11	Submerge plant unspec.	Lake Bichlersee	0.46	15.79	43.00	59.25	0.01
GM1	Submerge plant unspec.	Lake Gemündener Maar	1.66	11.11	10.17	22.95	0.08
GM7	Water lily	Lake Gemündener Maar	0.42	27.09	33.92	61.43	0.01
HF1	Submerge plant unspec.	Lake Hofstätter See	0.46	11.93	62.04	74.43	0.01
AL1	Stoneworts	Lake Holzmaar	0.11	24.92	29.62	54.66	0.00
AL2	Stoneworts	Lake Holzmaar	0.84	12.27	6.55	19.65	0.03
AL3	Stoneworts	Lake Holzmaar	1.73	14.33	11.62	27.68	0.05
PP2	Submerge root felt	Lake Panch Pokhari	1.08	9.09	4.48	14.65	0.06
P4	Elodea unspec.	Pond near Rosenheim	0.89	8.54	13.32	22.75	0.04
			0.18	9.79	7.87	17.85	0.01
Algae							
BS2	Algae	Lake Bichlersee	7.50	16.01	16.20	34.50	0.34
BS3	Algae	Lake Bichlersee	7.50	17.91	4.15	29.56	0.34
BS8	Algae	Lake Bichlersee	11.74	12.86	9.90	34.50	0.52
PP1	Algae crust	Lake Panch Pokhari	1.80	16.01	16.20	34.01	0.06
P1	Algae	Pond near Rosenheim	3.24	12.09	20.59	35.91	0.10
			50.77	32.02	52.73	135.53	0.60

(continued on next page)

Table 1 (continued)

Sample	Name	Study site/origin	Fucose (mg/g sample)	Arabinose (mg/g sample)	Xylose (mg/g sample)	Sum of sugars (ara + fuc + xyl) (mg/g sample)	Fuc/(ara + xyl)
Green algae							
Bot	<i>Botryococcus braunii</i>	Cultivated	2.36	1.55	2.20	5.50	0.33
Nano Jim16	<i>Nannochloropsis limnetica</i>	Cultivated	4.56	6.45	8.18	19.19	0.24
Nano Jim2	<i>Nannochloropsis limnetica</i>	Cultivated	2.14	1.18	1.35	4.67	0.65
Nano Jim9	<i>Nannochloropsis limnetica</i>	Cultivated	3.38	4.79	3.09	11.25	0.33
Ped	<i>Pediastrum boryanum</i>	Cultivated	4.06	2.83	2.20	9.08	0.62
Ped_bo	<i>Pediastrum boryanum</i>	Cultivated	0.00	1.41	0.86	2.26	0.00
Acut (former Scene)	<i>Acutodesmus obliquus</i>	Cultivated	0.57	1.55	2.00	4.12	0.12
			2.36	0.37	2.77	5.50	0.60
Diatoms							
Fra	<i>Fragilaria crotonensis</i>	Cultivated	3.28	1.00	5.68	10.14	0.41
Gom	<i>Gomphonema parvulum</i>	Cultivated	15.73	0.87	2.93	19.54	3.24
Gom6315	<i>Gomphonema parvulum</i>	Cultivated	2.71	1.41	6.28	10.39	0.28
Nav	<i>Navicula pelliculosa</i>	Cultivated	3.20	0.67	6.01	9.88	0.38
Nit	<i>Nitzschia palea</i>	Cultivated	6.84	1.13	8.91	16.87	0.54
Pin	<i>Pinnularia spec.</i>	Cultivated	3.35	0.00	4.52	7.87	0.59
Pin6315	<i>Pinnularia spec.</i>	Cultivated	3.96	1.35	5.63	10.94	0.45
Skel	<i>Skeletonema subsalsum</i>	Cultivated	5.27	2.21	5.73	13.21	0.52
Skel6315	<i>Skeletonema subsalsum</i>	Cultivated	0.78	0.62	3.87	5.27	0.14
Step	<i>Stephano discus minutulus</i>	Cultivated	0.62	0.53	1.64	2.78	0.22
			1.76	1.33	6.21	9.30	0.18

investigating the chain length of *n*-alkanes, *n*-alkanoic acids and *n*-alkanols (Rieley et al., 1991; Bourbonniere and Meyers, 1996; Ficken et al., 1998, 2000). Furthermore, particularly in the case of marine environments, the branched vs. isoprenoid tetraether (BIT) index (Hopmans et al., 2004) has become a frequently used tool for assessing fluvial terrestrial OM input (Schouten et al., 2013). High BIT values (>0.8) are commonly interpreted to reflect strong soil OM input, whereas low values are interpreted to reflect a weaker soil OM imprint. However, it is increasingly reported that soils and eolian sediments, especially under dry climatic conditions, can have very low BIT values (Dirghangi et al., 2013; Zech et al., 2013b). Thus, low BIT values originating from terrestrial soils may be misinterpreted in terms of aquatic/marine origin. This short introduction and overview reveals that every terrestrial vs. aquatic proxy approach has advantages, but also disadvantages and limitations. Therefore, it seems advisable to address the question of terrestrial vs. aquatic sedimentary OM with multi-proxy approaches.

In previous studies we found that the hemicellulose-derived neutral sugars arabinose (ara) and xylose (xyl) strongly predominate over fucose (fuc) in terrestrial soils and sediments (e.g. Zech et al., 2013a). By contrast, we found fuc to occur in similar abundance to ara and xyl in lacustrine sediments (Zech et al., 2014b; Hepp et al., 2015). We have therefore investigated and reviewed here neutral sugar patterns of various terrestrial and aquatic plants, including mosses as well as algal species. We aimed to answer the question whether the sugar biomarker patterns and particularly sugar biomarker ratios, such as for instance fuc/(ara + xyl), may serve as proxies for terrestrial vs. aquatic origin of sedimentary OM input.

2. Material and methods

2.1. Sample description

The terrestrial and aquatic plant and algal samples were collected from different sites/lakes. These are (Table 1) Lake Bichlersee in the Valley Inn [47°40'33.58"N; 12°7'19.50"E; 961 m above sea level (a.s.l.)] Lake Hofstätter See about 9 km northeast of Rosenheim (47°54'4.82"N; 12°10'26.94"E; 483 m a.s.l.), a pond near Rosenheim (47°51'36.26"N; 12°8'35.58"E; 470 m a.s.l.), Lake Gemündener Maar and Lake Holzmaar in the Western Eifel (50°10'39.85"N; 6°50'12.91"E; 406 m a.s.l. and 50°7'3.10"N; 6°52'42.31"E; 430 m a.s.l., respectively) and Lake Panch Pokhari in the Helambu Himal, Nepal (28°2'30.90"N; 85°43'4.01"E; 4050 m a.s.l.).

Additionally, eleven common freshwater green algae and diatoms were cultivated and harvested in the laboratory of the Chair of Animal Ecology I, University of Bayreuth. All were obtained from the SAG Culture Collection of Algae at Göttingen University. The green algae *Nannochloropsis limnetica* (SAG 18.99), *Pediastrum boryanum* (SAG 85.81) were cultivated on Basal Medium, *Botryococcus braunii* (SAG 807-1) was cultured on MiEB12 Medium, and *Acutodesmus obliquus* (SAG 276-3a) was cultivated on Z-Medium at a concentration of $\times 0.25$. The diatoms *Gomphonema parvulum* (SAG 1032-1), *Navicula pelliculosa* (SAG 1050-3), *Nitzschia palea* (SAG 1052-3a), *Pinnularia spec.* (SAG 2386), *Skeletonema subsalsum* (SAG 8.94) and *Stephano discus minutulus* (SAG 49.91) were cultivated on bacillariophycean medium, as was *Fragilaria crotonensis* (SAG 28.96) but with an added vitamin mix. For detailed information on the culture media, see the list of culture media of the SAG (<http://www.uni-goettingen.de/en/list-of-media-and-recipes/186449.html>). After harvesting, the algae were freeze dried (Christ BETA-RVC & ALPHA 2–4; Martin Christ Gefriertrocknungsanlagen GmbH, Osterode am Harz, Germany) and stored dry until analysis.

2.2. Sugar biomarker analysis

Analysis were carried out according to Zech and Glaser (2009). This method allows sugar quantification and simultaneously $\delta^{18}\text{O}$ analysis of the sugars. In brief, myoinositol was added first as internal standard. Then, the sugars were released hydrolytically from the samples using 4 M trifluoroacetic acid (TFA) for 4 h at 105 °C as described by Amelung et al. (1996). The extracted sugars were cleaned over glass fiber filters and purified using XAD and Dowex columns. After freezing and freeze-drying, derivatization was carried out with methylboronic acid (MBA; Knapp, 1979). Prior to derivatization, 3-O-methylglucose in dry pyridine was added to the samples as a second internal standard. Measurements of the individual sugars were performed at the Institute of Agronomy and Nutritional Sciences, Soil Biogeochemistry, Martin-Luther University Halle-Wittenberg using gas chromatography–pyrolysis–isotope ratio mass spectrometry (GC–Py–IRMS) with a Trace GC 2000 gas chromatograph (Thermo Fisher Scientific, Bremen, Germany) coupled to a Delta V Advantage isotope ratio mass spectrometer (Thermo Fisher Scientific, Bremen, Germany) via an ^{18}O -pyrolysis reactor and a GC/TC III interface (Thermo Fisher Scientific, Bremen, Germany). The monosaccharides were quantified using the myoinositol and 3-O-methylglucose internal standards.

3. Results

The relative abundances of ara, fuc and xyl in the samples are illustrated in a ternary diagram (Fig. 1a). The terrestrial and aquatic plants, including mosses, plotted close to the ara axis, whereas the algae and diatom samples plotted farther from the ara axis. This reveals that algae contain a higher relative amount of fuc than the vascular plants and mosses. According to Table 1, the algae here were characterized by fuc/(ara + xyl) ratio values >0.10 (except for samples Ped and BS8), whereas the vascular plant and moss samples were characterized by fuc/(ara + xyl) values <0.08. This finding suggests that the fuc/(ara + xyl) ratio may serve as a proxy for algal vs. vascular plant/moss origin of sedimentary OM.

The total sugar concentration (sum of ara, xyl and fuc) for the samples ranged (Table 1) from 2.26 mg/g sample (Ped, i.e. *P. boryanum* cultivated in the laboratory) to 787.87 mg/g sample (BS1, i.e. reed from Lake Bichlersee). Median total sugar concentration for grouped samples increased in the order green algae (laboratory) < diatoms (laboratory) < submerged aquatic plants < algae (lakes) < mosses < terrestrial plants < emergent plants (Fig. 2a).

4. Discussion

Our finding that ara and xyl predominate strongly over fuc in vascular plants and mosses confirms data (Fig. 1b) from D'Souza

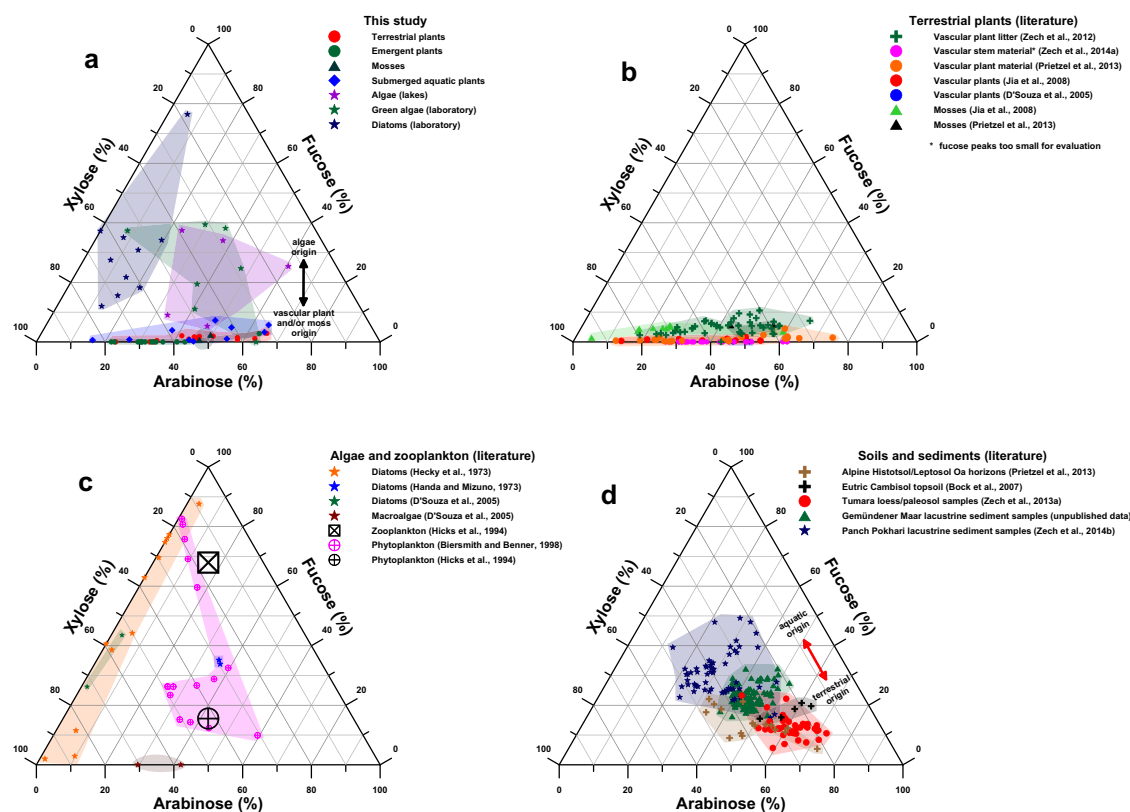


Fig. 1. Ternary diagrams depicting the relative abundance of arabinose, xylose and fucose. (a) Results from this study; (b) results of compiled terrestrial plant data from Jia et al. (2008), Zech et al. (2012, 2014a) and Prietzel et al. (2013); (c) results from a compilation of algal and zooplankton data from Handa and Mizuno (1973), Hecky et al. (1973), Hicks et al. (1994), Biersmith and Benner (1998) and D'Souza et al. (2005); (d) results from compiled soil and sediment data from Bock et al. (2007), Prietzel et al. (2013), Zech et al. (2013a, 2014b) and unpublished data.

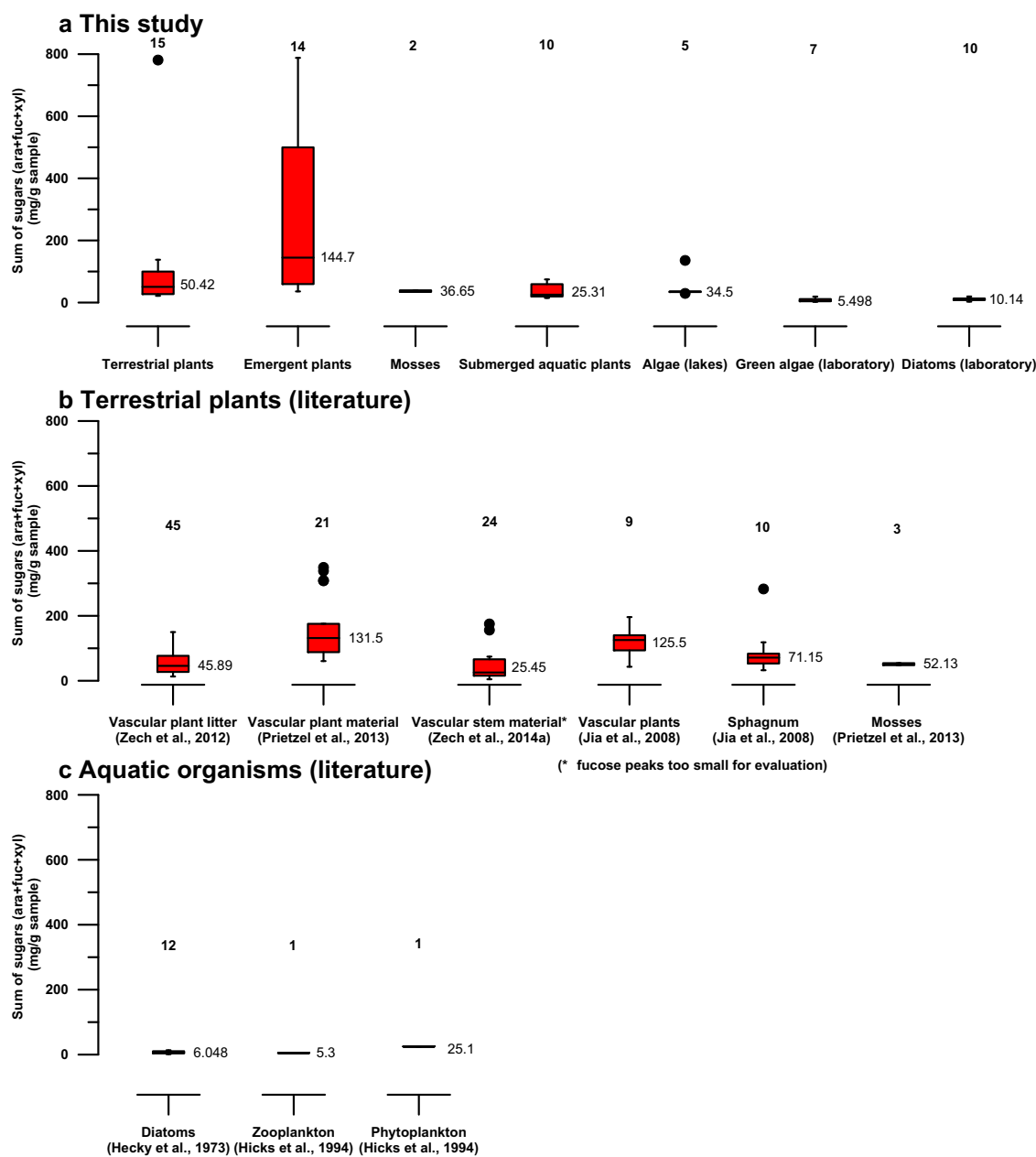


Fig. 2. Box plots of sugar concentration (sum of arabinose, fucose, and xylose). Bold numbers above the box plot represent the numbers of samples summarized in a group; numbers next to the box plot represent the median value for the group. (a) Results from own data set; (b) results from compiled terrestrial plant data from Jia et al. (2008), Zech et al. (2012, 2014a) and Prietz et al. (2013); (c) results from compiled aquatic organism data from Hecky et al. (1973) and Hicks et al. (1994).

et al. (2005), Jia et al. (2008), Zech et al. (2012, 2014a) and Prietz et al. (2013). Similarly, most of the published sugar biomarker data for algae (except for two macroalgae), as well as zooplankton (Fig. 1c), show higher relative amounts of fuc (Handa and Mizuno, 1973; Hecky et al., 1973; Hicks et al., 1994; Biersmith and Benner, 1998; D'Souza et al., 2005).

While the above compilation corroborates the proposed fuc/(ara + xyl) proxy, it may still be necessary to consider degradation

effects when interpreting sedimentary sugar biomarker results. After deposition in soils and sediments, plant- and algal-derived sugars are partly mineralized. At the same time, soil microorganisms biosynthesize sugars. Both processes may lead to post-depositional alteration of the sugar biomarker patterns of soils and sediments (Oades, 1984; Glaser et al., 2000; Ogier et al., 2001). Fig. 1d shows soil and sediment data available from the literature (Bock et al., 2007; Prietz et al., 2013; Zech et al., 2013a,

2014b) and our own unpublished data from the Lake Gemündener Maar. The Lake Panch Pokhari sugar pattern agrees well with the pattern reported by Ogier et al. (2001), measured on a sediment core from the eutrophic Lake Aydat. Accordingly, although the predominance of ara and xyl over fuc originating from plant material still exists in soils, it is slightly attenuated. These shifts could be partly explained by findings from Basler et al. (2015) indicating that ara is much more affected by microbial production than xyl. On the other hand, soil microorganisms seem to produce notable amounts of fuc (cf. review from Gunina and Kuzyakov, 2015). Nevertheless, the ternary diagram in Fig. 1d depicts that the soils can still be distinguished from lacustrine sediments on the basis of the sugar biomarker patterns.

It is noteworthy that the sediment samples from Gemündener Maar plot between the sediment samples from Lake Panch Pokhari and the soil samples. Both lakes are characterized by very small catchments (Sirocko et al., 2013; Zech et al., 2014b). However, while Lake Panch Pokhari is in a high alpine and sparsely vegetated environment and its sediment is very rich in diatoms (Krstić et al., 2012), the catchment of Gemündener Maar is densely vegetated with broadleaf trees. Hence, leaf litter input into Gemündener Maar presumably clearly dominates autochthonous OM production and explains the strong terrestrial signal for this dataset.

Our own dataset, the terrestrial plant data, as well as algae and zooplankton data from the literature (Fig. 1a–c), suggest that the ratio $fuc/(ara + xyl)$ is a valuable proxy for algal OM [$fuc/(ara + xyl) > 0.10$] vs. vascular plant/moss OM [$fuc/(ara + xyl) \leq 0.10$]. Additionally, the compiled soil and sediment data (Fig. 1d) indicate that the ratio $(fuc + xyl)/ara$ can help distinguish between terrestrial and aquatic sedimentary OM input. In the case of Lake Gemündener Maar, it can be concluded that fuc and xyl are primarily of aquatic origin, whereas ara is primarily of terrestrial origin. Moreover, the developed sugar biomarker ratios can help answer the question whether the sedimentary biomarkers are of autochthonous or allochthonous origin, when interpreted with compound specific $\delta^{18}O$ results.

The sugar concentration values for our own data set (Fig. 2a) are well within the range reported (Fig. 2b and c). The low sugar concentrations of lab-grown green algae and diatoms might be partly an underestimation of natural conditions. Bigogno et al. (2002) and Krienitz and Wirth (2006) found that harvesting algae in the log phase of growth, as well as specific cultural conditions, can also negatively influence algal fatty acid production. Despite limitations in the presented sugar biomarker proxies, such as different sugar concentrations characterizing different sugar sources (algal vs. terrestrial), a multi-proxy biomarker approach (suggested by e.g. Bechtel and Schubert (2009) for lake particulate organic matter) including our sugar biomarkers would provide more details on sedimentary OM sources.

5. Conclusions

The results show that the relative abundance of fucose vs. arabinose and xylose [$fuc/(ara + xyl)$] is much higher in algae and zooplankton than in vascular plants and mosses. In the course of mineralization and/or degradation by soil microorganisms, the initial sugar patterns of plants may be altered. Nevertheless, the compilation of literature data suggests that lacustrine sediments and terrestrial soils can be readily distinguished using a ternary diagram with the relative abundances of fucose, arabinose and xylose. Accordingly, increased abundance of arabinose in lake sediments indicates an input of terrestrial plant material, whereas fucose and xylose are primarily of aquatic origin. We therefore, in addition to the $fuc/(ara + xyl)$ ratio, propose the sugar biomarker ratio

$(fuc + xyl)/ara$ as a proxy for aquatic vs. terrestrial origin of sedimentary OM in paleolimnological studies. Ideally, both sugar ratio proxies should be used within multi-proxy approaches.

Acknowledgements

We are grateful to U. Wilczek (Animal Ecology I, University of Bayreuth) for handling the algal cultures, and to M. Benesch (Martin-Luther University Halle-Wittenberg) for laboratory assistance during sugar analysis. We are also grateful to P.A. Meyers and A. Bechtel for constructive comments on the manuscript. J.H. greatly acknowledges the funding provided by the journal *Organic Geochemistry* and the European Association of Organic Geochemists (EAOG) via the Elsevier Research Scholarship 2014.

Associate Editor—L.R. Snowdon

References

- Amelung, W., Cheshire, M.V., Guggenberger, G., 1996. Determination of neutral and acidic sugars in soil by capillary gas–liquid chromatography after trifluoroacetic acid hydrolysis. *Soil Biology & Biochemistry* 28, 1631–1639.
- Basler, A., Dippold, M., Helfrich, M., Dyckmans, J., 2015. Microbial carbon recycling: an underestimated process controlling soil carbon dynamics – Part 2: a C₃–C₄ vegetation change field labelling experiment. *Biogeosciences* 12, 5929–5940.
- Bechtel, A., Schubert, C.J., 2009. Biogeochemistry of particulate organic matter from lakes of different trophic levels in Switzerland. *Organic Geochemistry* 40, 441–454.
- Biersmith, A., Benner, R., 1998. Carbohydrates in phytoplankton and freshly produced dissolved organic matter. *Marine Chemistry* 63, 131–144.
- Bigogno, C., Khozin-Goldberg, I., Boussiba, S., Vonshak, A., Cohen, Z., 2002. Lipid and fatty acid composition of the green oleaginous alga *Parietochloris incisa*, the richest plant source of arachidonic acid. *Phytochemistry* 60, 497–503.
- Bock, M., Glaser, B., Millar, N., 2007. Sequestration and turnover of plant- and microbially derived sugars in a temperate grassland soil during 7 years exposed to elevated atmospheric pCO₂. *Global Change Biology* 13, 478–490.
- Bourbonniere, R.A., Meyers, P.A., 1996. Sedimentary geolipid records of historical changes in the watersheds and productivities of Lakes Ontario and Erie. *Limnology and Oceanography* 41, 352–359.
- D'Souza, F., Garg, A., Bhosle, N.B., 2005. Seasonal variation in the chemical composition and carbohydrate signature compounds of biofilm. *Aquatic Microbial Ecology* 41, 199–207.
- Dirghangi, S.S., Pagani, M., Hren, M.T., Tipple, B.J., 2013. Distribution of glycerol dialkyl glycerol tetraethers in soils from two environmental transects in the USA. *Organic Geochemistry* 59, 49–60.
- Ficken, K.J., Barber, K.E., Eglinton, G., 1998. Lipid biomarker, $\delta^{13}C$ and plant macrofossil stratigraphy of a Scottish montane peat bog over the last two millennia. *Organic Geochemistry* 28, 217–237.
- Ficken, K.J., Li, B., Swain, D.L., Eglinton, G., 2000. An n-alkane proxy for the sedimentary input of submerged/floating freshwater aquatic macrophytes. *Organic Geochemistry* 31, 745–749.
- Glaser, B., Turrión, M.-B., Solomon, D., Ni, A., Zech, W., 2000. Soil organic matter quantity and quality in mountain soils of the Alay Range, Kyrgyzia, affected by land use change. *Biology and Fertility of Soils* 31, 407–413.
- Gunina, A., Kuzyakov, Y., 2015. Sugars in soil and sweets for microorganisms: review of origin, content, composition and fate. *Soil Biology & Biochemistry* 90, 87–100.
- Handa, N., Mizuno, K., 1973. Carbohydrates from lake sediments. *Geochemical Journal* 7, 215–230.
- Hecky, R.E., Mopper, K., Kilham, P., Degens, E.T., 1973. The amino acid and sugar composition of diatom cell-walls. *Marine Biology* 19, 323–331.
- Hepp, J., Tuthorn, M., Zech, R., Mügler, I., Schlütz, F., Zech, W., Zech, M., 2015. Reconstructing lake evaporation history and the isotopic composition of precipitation by a coupled $\delta^{18}O$ – δ^2H biomarker approach. *Journal of Hydrology* 529, 622–631.
- Hicks, R.E., Owen, C.J., Aas, P., 1994. Deposition, resuspension, and decomposition of particulate organic matter in the sediments of Lake Itasca, Minnesota, USA. *Hydrobiologia* 284, 79–91.
- Hopmans, E.C., Weijers, J.W.H., Schefuß, E., Herfort, L., Sinnighe Damsté, J.S., Schouten, S., 2004. A novel proxy for terrestrial organic matter in sediments based on branched and isoprenoid tetraether lipids. *Earth and Planetary Science Letters* 224, 107–116.
- Jia, G., Dunggait, J.A.J., Bingham, E.M., Valiranta, M., Korhola, A., Evershed, R.P., 2008. Neutral monosaccharides as biomarker proxies for bog-forming plants for application to palaeovegetation reconstruction in ombrotrophic peat deposits. *Organic Geochemistry* 39, 1790–1799.
- Knapp, D.R., 1979. *Handbook of Analytical Derivatization Reactions*. John Wiley & Sons, New York, Chichester, Brisbane, Toronto, Singapore.
- Krienitz, L., Wirth, M., 2006. The high content of polyunsaturated fatty acids in *Nannochloropsis limnetica* (Eustigmatophyceae) and its implication for food web

- interactions, freshwater aquaculture and biotechnology. *Limnologia* 36, 204–210.
- Krstić, S.S., Zech, W., Obrecht, I., Svirčev, Z., Marković, S.B., 2012. Late Quaternary environmental changes in Helambu Himal, Central Nepal, recorded in the diatom flora assemblage composition and geochemistry of Lake Panch Pokhari. *Journal of Paleolimnology* 47, 113–124.
- Lüniger, G., Schwark, L., 2002. Characterisation of sedimentary organic matter by bulk and molecular geochemical proxies: an example from Oligocene maar-type Lake Enspel, Germany. *Sedimentary Geology* 148, 275–288.
- Meyers, P.A., 1994. Preservation of elemental and isotopic source identification of sedimentary organic matter. *Chemical Geology* 114, 289–302.
- Meyers, P.A., Ishiwatari, R., 1993. Lacustrine organic geochemistry – an overview of indicators of organic matter sources and diagenesis in lake sediments. *Organic Geochemistry* 20, 867–900.
- Meyers, P.A., Lallier-Vergès, E., 1999. Lacustrine sedimentary organic matter records of Late Quaternary paleoclimates. *Journal of Paleolimnology* 21, 345–372.
- Mügler, I., Gleixner, G., Günther, F., Mäusbacher, R., Daut, G., Schütt, B., Schwab, F., Schwark, L., Xu, B., Yao, T., Zhu, L., Yi, C., 2010. A multi-proxy approach to reconstruct hydrological changes and Holocene climate development of Nam Co, Central Tibet. *Journal of Paleolimnology* 43, 625–648.
- Oades, J.M., 1984. Soil organic matter and structural stability: mechanisms and implications for management. *Plant and Soil* 76, 319–337.
- Ogier, S., Disnar, J.-R., Albéric, P., Bourdier, G., 2001. Neutral carbohydrate geochemistry of particulate material (trap and core sediments) in an eutrophic lake (Aydat, France). *Organic Geochemistry* 32, 151–162.
- Prietzl, J., Dechamps, N., Spielvogel, S., 2013. Analysis of non-cellulosic polysaccharides helps to reveal the history of thick organic surface layers on calcareous Alpine soils. *Plant and Soil* 365, 93–114.
- Rach, O., Brauer, A., Wilkes, H., Sachse, D., 2014. Delayed hydrological response to Greenland cooling at the onset of the Younger Dryas in western Europe. *Nature Geoscience* 7, 109–112.
- Riele, G., Collier, R.J., Jones, D.M., Eglinton, G., 1991. The biogeochemistry of Ellesmere Lake, UK – I: source correlation of leaf wax inputs to the sedimentary lipid record. *Organic Geochemistry* 17, 901–912.
- Schouten, S., Hopmans, E.C., Sinninghe Damsté, J.S., 2013. The organic geochemistry of glycerol dialkyl glycerol tetraether lipids: a review. *Organic Geochemistry* 54, 19–61.
- Sirocko, F., Dietrich, S., Veres, D., Grootes, P.M., Schaber-Mohr, K., Seelos, K., Nadeau, M.-J., Kromer, B., Rothacker, L., Röhrner, M., Krbitschek, M., Appleby, P., Hambach, U., Rolf, C., Sudo, M., Grim, S., 2013. Multi-proxy dating of Holocene maar lakes and Pleistocene dry maar sediments in the Eifel, Germany. *Quaternary Science Reviews* 62, 56–76.
- Talbot, M.R., Livingstone, D.A., 1989. Hydrogen index and carbon isotopes of lacustrine organic matter as lake level indicators. *Palaeogeography, Palaeoclimatology, Palaeoecology* 70, 121–137.
- Zech, M., Glaser, B., 2009. Compound-specific $\delta^{18}\text{O}$ analyses of neutral sugars in soils using gas chromatography–pyrolysis–isotope ratio mass spectrometry: problems, possible solutions and a first application. *Rapid Communications in Mass Spectrometry* 23, 3522–3532.
- Zech, M., Zech, R., Glaser, B., 2007. A 240,000-year stable carbon and nitrogen isotope record from a loess-like palaeosol sequence in the Tumara Valley, Northeast Siberia. *Chemical Geology* 242, 307–318.
- Zech, M., Werner, R.A., Juchelka, D., Kalbitz, K., Buggle, B., Glaser, B., 2012. Absence of oxygen isotope fractionation/exchange of (hemi-) cellulose derived sugars during litter decomposition. *Organic Geochemistry* 42, 1470–1475.
- Zech, M., Tuthorn, M., Detsch, F., Rozanski, K., Zech, R., Zöller, L., Zech, W., Glaser, B., 2013a. A 220 ka terrestrial $\delta^{18}\text{O}$ and deuterium excess biomarker record from an eolian permafrost palaeosol sequence, NE-Siberia. *Chemical Geology* 360–361, 220–230.
- Zech, R., Zech, M., Marković, S.B., Hambach, U., Huang, Y., 2013b. Humid glacials, arid interglacials? Critical thoughts on pedogenesis and paleoclimate based on multi-proxy analyses of the loess-palaeosol sequence Crvenka, Northern Serbia. *Palaeogeography, Palaeoclimatology, Palaeoecology* 387, 165–175.
- Zech, M., Mayr, C., Tuthorn, M., Leiber-Sauheitl, K., Glaser, B., 2014a. Oxygen isotope ratios ($^{18}\text{O}/^{16}\text{O}$) of hemicellulose-derived sugar biomarkers in plants, soils and sediments as paleoclimate proxy I: insight from a climate chamber experiment. *Geochimica et Cosmochimica Acta* 126, 614–623.
- Zech, M., Tuthorn, M., Schlütz, F., Zech, W., Glaser, B., 2014b. A 16-ka $\delta^{18}\text{O}$ record of lacustrine sugar biomarkers from the High Himalaya reflects Indian Summer Monsoon variability. *Journal of Paleolimnology* 51, 241–251.

E. Manuscript 5: Hepp et al. (2019a)

published in *Climate of the Past*

<https://doi.org/10.5194/cp-15-713-2019>

Clim. Past, 15, 713–733, 2019
<https://doi.org/10.5194/cp-15-713-2019>
 © Author(s) 2019. This work is distributed under
 the Creative Commons Attribution 4.0 License.



How dry was the Younger Dryas? Evidence from a coupled $\delta^2\text{H}$ – $\delta^{18}\text{O}$ biomarker paleohygrometer applied to the Gemündener Maar sediments, Western Eifel, Germany

Johannes Hepp^{1,2,a}, Lorenz Wüthrich³, Tobias Bromm², Marcel Bliedtner^{3,b}, Imke Kathrin Schäfer³, Bruno Glaser², Kazimierz Rozanski⁴, Frank Sirocko⁵, Roland Zech^{3,b}, and Michael Zech^{2,6,c}

¹Department of Geomorphology and BayCEER, University of Bayreuth, Universitätsstrasse 30, 95440 Bayreuth, Germany

²Institute of Agronomy and Nutritional Sciences, Soil Biogeochemistry, Martin Luther University Halle-Wittenberg, Von-Seckendorff-Platz 3, 06120 Halle, Germany

³Institute of Geography and Oeschger Center for Climate Change Research, University of Bern, Hallerstrasse 12, 3012 Bern, Switzerland

⁴Faculty of Physics and Applied Computer Science, AGH University of Science and Technology, Al. Mickiewicza 30, 30-059 Kraków, Poland

⁵Institute of Geosciences, Group of Climate and Sediments, Johannes Gutenberg University of Mainz, J.-J.-Becher-Weg 21, 55128 Mainz, Germany

⁶Institute of Geography, Dresden University of Technology, Helmholtzstrasse 10, 01062 Dresden, Germany

^apresent address: Department of Geomorphology and BayCEER, University of Bayreuth, Universitätsstrasse 30, 95440 Bayreuth, Germany

^bpresent address: Institute of Geography, Department of Physical Geography, Friedrich Schiller University of Jena, Löbdergraben 32, 07743 Jena, Germany

^cpresent address: Institute of Geography, Dresden University of Technology, Helmholtzstrasse 10, 01062 Dresden, Germany

Correspondence: Johannes Hepp (johannes-hepp@gmx.de)

Received: 23 August 2018 – Discussion started: 5 September 2018

Revised: 23 February 2019 – Accepted: 8 March 2019 – Published: 9 April 2019

Abstract. Causes of the Late Glacial to Early Holocene transition phase and particularly the Younger Dryas period, i.e. the major last cold spell in central Europe during the Late Glacial, are considered to be keys for understanding rapid natural climate change in the past. The sediments from maar lakes in the Eifel, Germany, have turned out to be valuable archives for recording such paleoenvironmental changes.

For this study, we investigated a Late Glacial to Early Holocene sediment core that was retrieved from the Gemündener Maar in the Western Eifel, Germany. We analysed the hydrogen ($\delta^2\text{H}$) and oxygen ($\delta^{18}\text{O}$) stable isotope composition of leaf-wax-derived lipid biomarkers (*n*-alkanes C_{27} and C_{29}) and a hemicellulose-derived sugar biomarker (arabinose), respectively. Both $\delta^2\text{H}_{n\text{-alkane}}$ and $\delta^{18}\text{O}_{\text{sugar}}$ are suggested to reflect mainly leaf water of vegetation growing in the catchment of the Gemündener Maar. Leaf water re-

flects $\delta^2\text{H}$ and $\delta^{18}\text{O}$ of precipitation (primarily temperature-dependent) modified by evapotranspirative enrichment of leaf water due to transpiration. Based on the notion that the evapotranspirative enrichment depends primarily on relative humidity (RH), we apply a previously introduced “coupled $\delta^2\text{H}_{n\text{-alkane}}$ – $\delta^{18}\text{O}_{\text{sugar}}$ paleohygrometer approach” to reconstruct the deuterium excess of leaf water and in turn Late Glacial–Early Holocene RH changes from our Gemündener Maar record.

Our results do not provide evidence for overall markedly dry climatic conditions having prevailed during the Younger Dryas. Rather, a two-phasing of the Younger Dryas is supported, with moderate wet conditions at the Allerød level during the first half and drier conditions during the second half of the Younger Dryas. Moreover, our results suggest that the amplitude of RH changes during the Early Holocene was

more pronounced than during the Younger Dryas. This included the occurrence of a “Preboreal Humid Phase”. One possible explanation for this unexpected finding could be that solar activity is a hitherto underestimated driver of central European RH changes in the past.

1 Introduction

In order to evaluate the relevance of man-made climate change in the future, it is of great importance to study and understand large and rapid climate fluctuations in the past. Many studies have focused on the Late Glacial to Early Holocene transition phase, a period with various expressions in temperature, atmospheric circulation and hydrology worldwide (Alley, 2000; Brauer et al., 2008; Denton et al., 2010; Partin et al., 2015; Wagner et al., 1999). Explanation for the Younger Dryas (YD) period, i.e. the major last cold spell in central Europe during the Late Glacial just before the onset of the Holocene warm period (Denton et al., 2010; Heiri et al., 2014; Isarin and Bohncke, 1999), has long been considered crucial for understanding rapid natural climate change in the past (Alley, 2000). The sediments from maar lakes in the Eifel, Germany, have turned out to be valuable archives for paleoenvironmental reconstruction by providing high-resolution palynological, sedimentological and geochemical records for climate, vegetation and landscape history (Brauer et al., 2008; Brunck et al., 2015; Litt et al., 2003; Litt and Stebich, 1999; Sirocko et al., 2013; Zolitschka, 1998).

Lacustrine sedimentary lipid biomarkers such as n -alkanes, originating either from leaf waxes of higher terrestrial plants (Eglinton and Hamilton, 1967) or from aquatic organisms (Volkman et al., 1998), and especially their hydrogen isotope composition ($\delta^2\text{H}_{\text{leaf-wax}/n\text{-alkane}}$), are widely accepted as paleoclimate proxies (Huang et al., 2004; Mügler et al., 2008; Sachse et al., 2004, 2012; Sauer et al., 2001). It has been demonstrated that $\delta^2\text{H}_{\text{leaf-wax}/n\text{-alkane}}$ is well correlated with the hydrogen isotope composition of precipitation ($\delta^2\text{H}_{\text{prec}}$) (e.g. Hou et al., 2008; Rao et al., 2009). Similar to the well-known ice-core and speleothem records (Alley, 2000; Luetscher et al., 2015; Rasmussen et al., 2014), lacustrine $\delta^2\text{H}_{\text{leaf-wax}/n\text{-alkane}}$ records are therefore increasingly used to reconstruct $\delta^2\text{H}$ of past precipitation and thus for deriving paleoclimatic information (cf. Araguás-Araguás et al., 2000; Dansgaard, 1964; Rozanski et al., 1993). However, the alteration of $\delta^2\text{H}_{\text{prec}}$ either through evapotranspirative ^2H enrichment of leaf or lake water can challenge a robust $\delta^2\text{H}_{\text{prec}}$ reconstruction (e.g. Mügler et al., 2008; Zech et al., 2015). Apart from $\delta^2\text{H}_{n\text{-alkane}}$, the oxygen isotope composition of hemicellulose- or polysaccharide-derived sugars ($\delta^{18}\text{O}_{\text{sugar}}$) was established as a tool in paleoclimate research during recent years (Zech et al., 2011, 2013a, 2014a). Analogous to $\delta^2\text{H}_{n\text{-alkane}}$, $\delta^{18}\text{O}_{\text{sugar}}$ is affected by the isotope composition of source water, which is closely related to the local precipi-

tation ($\delta^{18}\text{O}_{\text{prec}}$) as well as by evapotranspirative ^{18}O enrichment (Tuthorn et al., 2014; Zech et al., 2013b, 2014b). Moreover, it was suggested that the coupling of $\delta^2\text{H}$ and $\delta^{18}\text{O}$ results can help to disentangle $\delta^2\text{H}/\delta^{18}\text{O}_{\text{prec}}$ changes and variable $^2\text{H}/^{18}\text{O}_{\text{leaf/lake-water}}$ enrichment (Henderson et al., 2010; Hepp et al., 2015, 2017; Tuthorn et al., 2015; Voelker et al., 2014, 2015; Zech et al., 2013a). For instance, Voelker et al. (2014) presented a framework for using $\delta^2\text{H}$ and $\delta^{18}\text{O}$ of tree-ring cellulose in order to infer relative air humidity (RH). Tuthorn et al. (2015) validated a previously suggested “coupled $\delta^2\text{H}_{n\text{-alkane}}-\delta^{18}\text{O}_{\text{sugar}}$ paleohygrometer approach”. Accordingly, the application of that approach to an Argentinian topsoil transect yielded a highly significant correlation of actual and biomarker-based reconstructed RH values ($R = 0.79$, $p < 0.001$, $n = 20$). Both approaches were successfully applied to loess–paleosol sequences (Hepp et al., 2017; Zech et al., 2013a) and subfossil wood (Voelker et al., 2015). By contrast, the application of the coupled $\delta^2\text{H}_{n\text{-alkane}}-\delta^{18}\text{O}_{\text{sugar}}$ paleohygrometer approach to a lacustrine archive is still missing.

Within this study, we aimed at applying the coupled $\delta^2\text{H}_{n\text{-alkane}}-\delta^{18}\text{O}_{\text{sugar}}$ paleohygrometer approach to the Late Glacial–Early Holocene sediment cores of the Gemündener Maar. More specifically, we addressed the following objectives: (i) source identification of the sedimentary organic matter and the investigated n -alkanes and sugars (aquatic vs. terrestrial), (ii) reconstructing leaf water isotope composition based on compound-specific $\delta^2\text{H}$ and $\delta^{18}\text{O}$ values of the n -alkane and sugar biomarkers, (iii) reconstructing RH changes using the coupled $\delta^2\text{H}_{n\text{-alkane}}-\delta^{18}\text{O}_{\text{sugar}}$ paleohygrometer approach, and (iv) inferring implications for central European paleoclimate history from the established Gemündener Maar RH record.

2 Material and methods

2.1 The Gemündener Maar and sampling

The Gemündener Maar is located in the Eifel volcanic fields in western Germany at an altitude of 407 m a.s.l. ($50^\circ 10' 39.853'' \text{ N}$, $6^\circ 50' 12.912'' \text{ E}$; Fig. 1a and b; Sirocko et al., 2013). The maar was formed during a phreatomagmatic explosion within the local Devonian siltstone (greywacke) around 20–25 ka (Büchel, 1993). The lake is 39 m deep at its maximum and has a diameter of roughly 300 m. Due to its formation conditions the lake is almost circular with a lake surface area of 75 000 m² and is surrounded by a small catchment (Fig. 1b), with an area of 430 000 m² (Scharf and Menn, 1992). The lake is fed by precipitation and groundwater (no surface inflow and outflow present). The sediments are, accordingly, not affected by fluvial sediment input. The catchment area is furthermore steep and densely vegetated with broadleaved trees (Fig. 1c). The investigated samples were taken from the 8 m Gemündener Maar core (GM1), which was taken at approximately 20 m water depth near the

centre of the maar (Fig. 1b) with a Livingston piston corer (UWITEC, Mondsee, Austria). The GM1 core was retrieved from a terrace on the steep slope of the maar exactly in a fan of an underwater erosion gully structure. The core is part of the Eifel Laminated Sediment Archive Project of the Institute for Geoscience at Johannes Gutenberg University Mainz (Sirocko et al., 2013, 2016).

2.2 Bulk analysis and pollen analysis

Bulk analyses were carried out on 112 samples, covering a section of 606 to 727 cm depth of the Gemündener Maar GM1 core. Total carbon (TC) and nitrogen (N), bulk carbon isotope composition ($\delta^{13}\text{C}_{\text{TC}}$), and nitrogen isotope composition ($\delta^{15}\text{N}$) were determined at the Institute of Agronomy and Nutritional Sciences, Soil Biogeochemistry, Martin Luther University Halle-Wittenberg, using EuroVector EA 3000 elemental analyser (Hekatech, Wegberg, Germany) coupled via a ConFlo III Interface to a Delta V Advantage isotope ratio mass spectrometer (IRMS; both from Thermo Fisher Scientific, Bremen, Germany). Additionally, total organic carbon (TOC) and bulk $\delta^{13}\text{C}$ of the total organic carbon ($\delta^{13}\text{C}_{\text{TOC}}$) were assessed after removal of carbonate with 32 % hydrochloric acid (HCl) fumigation followed by a neutralisation step with moist sodium hydroxide, both for 24 h under 60 °C and vacuum conditions. This allows calculating TOC/N atomic ratios. Laboratory standards from the International Atomic Energy Agency (IAEA) as well as from the United States Geological Survey (USGS) with known total carbon, nitrogen, ^{13}C and ^{15}N contents (IAEA N2, IAEA CH6, IAEA NO3, IAEA CH7, IAEA 305A, USGS 41) were used for calibration. The ^{13}C and ^{15}N contents are expressed in the common δ notation as relative to an international standard ($\delta^{13}\text{C}$: Vienna Pee Dee Belemnite, VPDB; $\delta^{15}\text{N}$: atmospheric N_2 , air).

For pollen analysis, 16 samples were investigated covering the relevant depth section. Each sample covered a depth range of 1 cm. Preparation was conducted by Frank Dreher according to standard procedures at the laboratory of the Group of Climate and Sediments, Institute of Geosciences, Johannes Gutenberg University of Mainz, using potassium hydroxide, HCl and hydrofluoric acid (Sirocko et al., 2016). Afterwards, acetic acid and a mixture of acetic anhydride and sulfuric acid (9 : 1) were used for acetolysis. The samples were then centrifuged at 3000 to 3500 rpm for 5 min and then sieved over a 200 and a 10 μm sieve. Afterwards, the samples were fixed with anhydrous glycerol for reliable identification, and a maximum magnification of 600 was used for counting the remains. Pollen results are reported in relative percentages (%).

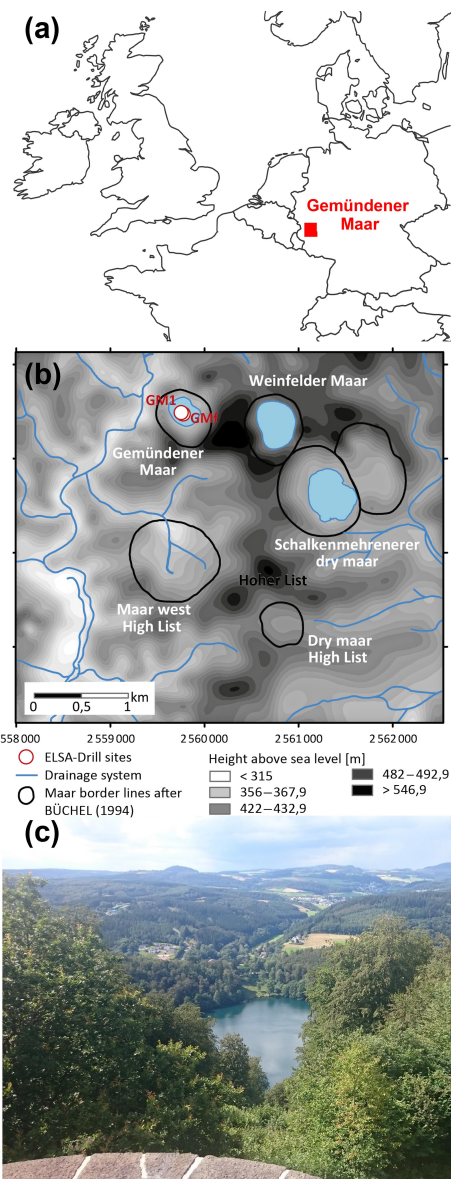


Figure 1. (a) Location of the Gemündener Maar in the Eifel region in Germany (generated using OpenStreetMap homepage, ©OpenStreetMap contributors, <https://www.openstreetmap.org>, last access: 15 August 2016). (b) Digital terrain model and drainage system of the immediate surroundings of the Gemündener Maar, with maar borders according to Büchel (1994) representing the size of the crater. In addition, the core position is displayed (GM1; $50^{\circ}10'39.853''\text{N}$, $6^{\circ}50'12.912''\text{E}$) along with the short core named GMf (not part of this study) marked as ELSA drill sites. Both cores are part of the Eifel Laminated Sediment Archive Project (ELSA project). (c) Photo of Gemündener Maar showing the steep and densely forested catchment (by Michael Zech, reproduced with his permission).

2.3 Age control

The investigated sediments are partially laminated. The first tie point to establish a chronology for the Gemündener Maar core is a radiocarbon-dated piece of charcoal in 727 cm core depth, which dates to $13\,800 \pm 110$ a cal BP (Fig. 2d). This age is derived from a ^{14}C age of $11\,950 \pm 65$ a BP as part of the Supplement of Sirocko et al. (2013), calibrated using CalPal software (Weninger and Jöris, 2008) calculated with the IntCal13 calibration curve (Reimer et al., 2013). The uncertainty of the calibrated ^{14}C age represents the 68 % probability range. The second tie point is the clearly visible Laacher See Tephra between 673 and 680 cm core depth (Fig. 2a and d). The latter can be used as chronological marker due to the varve-counted age of 12 880 a BP in the adjacent Meerfelder Maar (Brauer et al., 1999). The onset of the Younger Dryas period was set to 12 680 a BP (varve-counted in Meerfelder Maar sediments; Brauer et al., 1999; Litt et al., 2009) identified at a depth of 670 cm in the GM1 core due to a clear colour change (Fig. 2a and d). The onset of the Preboreal (Holocene) was found to date to 11 590 a BP in Meerfelder Maar by varve counting (Litt et al., 2009). This was used to wiggle-match the distinct changes in the pollen spectra (decreasing *Poaceae*, peaking *Artemisia*, increasing *Pinus* and *Betula*; Fig. 2b and c), the clear rise in TOC (Fig. 3a) and the colour change (Fig. 2a), which were identified at 643 cm depth (Fig. 2d). The Late Glacial to Preboreal (Holocene) transition is commonly well recorded in maar sediments from the Eifel region, i.e. clear changes in deposition as well as pollen pattern (Brauer et al., 1999; Litt et al., 2001, 2003; Litt and Stebich, 1999), dated to 11 600 a BP, e.g. in Holzmaar, by a combination of varve counting and ^{14}C dating (Zolitschka, 1998). The last time marker used to constrain the age model is the middle of the sharp increase in *Corylus* (hazel) pollen at 622 cm depth (Fig. 2b, c and d). We used this sharp increase as a marker for the Preboreal to Boreal transition, which is varve-counted by Litt et al. (2009) to 10 740 a BP in the Meerfelder Maar sediments. The offset of 60 years to the varve-counted Holzmaar record of Zolitschka (1998), as it is presented by Litt et al. (2009), is within the uncertainty of placing the onset of the Preboreal in the Gemündener Maar *Corylus* curve.

The investigated core section from 607 to 694 cm depth therefore covers the time between $\sim 13\,150$ and $10\,140$ a BP, i.e. the Allerød, the Younger Dryas, the Preboreal, and the beginning of the Boreal, with regard to the biomarkers (Fig. 2a and d). Assuming constant sedimentation rates between the markers, an average resolution of 51 a cm^{-1} can be calculated; the minimum and maximum resolution are 19 and 124 a cm^{-1} , respectively. The part above the Laacher See Tephra reveals a lower mean resolution (55 a cm^{-1}) than the section below (30 a cm^{-1}).

2.4 Biomarker and compound-specific isotope analysis

For $\delta^2\text{H}$ analyses of *n*-alkanes as well as $\delta^{18}\text{O}$ analyses of sugars, 59 samples were prepared from 607 to 694 cm depth of the Gemündener Maar GM1 core, in order to cover the core section with already high TOC content and the Late Glacial to Holocene transition (Figs. 2 and 3a). *n*-Alkanes were extracted from 1 to 6 g freeze-dried and ground samples by microwave extraction at 100°C for 1 h, using 15 mL of solvent (dichloromethane and methanol, at a ratio of 9 : 1). The resultant total lipid extracts were separated over amino-propyl silica gel (Supelco $45\ \mu\text{m}$) filled pipette columns. Non-polar compounds (including *n*-alkanes) were eluted with *n*-hexane. The fraction was spiked with a known amount of 5α -androstanone, used as an internal standard. Identification and quantification was carried out on an Agilent MS 5975 (EI) interfaced with an Agilent 7890 GC equipped with a 30 m fused silica capillary column (HP5-MS $0.25\ \text{mm i.d.}$, $0.25\ \mu\text{m}$ film thickness) and a split-splitless injector operating in splitless mode at 320°C . Carrier gas was helium and the temperature program was 1 min at 50°C , from 50 to 200°C at $30^\circ\text{C min}^{-1}$, from 200 to 320°C at 7°C min^{-1} , and 5 min at 320°C . Data recording comprised the total ion count (scan mode from m/z 40 to 600) and single-ion monitoring (m/z 57, 71, 85 and 99). Concentrations were calculated relative to the internal standard and to an external standard (*n*-C₂₁ to *n*-C₄₀ alkane mixture, Supelco), injected in different concentrations ($40, 4, 1, 0.4\ \text{ng }\mu\text{L}^{-1}$).

Prior to compound-specific isotope analyses, the *n*-alkanes were further purified. The non-polar fractions were passed over a pipette column filled with activated AgNO_3 impregnated silica gel and a pipette column filled with zeolite (Geokleen). After drying, the zeolite was removed using hydrofluoric acid and the *n*-alkanes were recovered by liquid-liquid extraction with hexane. The purified *n*-alkane fractions were measured for their compound-specific stable hydrogen isotope composition ($\delta^2\text{H}$). The measurements were performed at the Institute of Geography, University of Bern on an IsoPrime 100 IRMS, coupled to an Agilent 7890A GC via a GC5 pyrolysis or combustion interface operating in pyrolysis modus with a Cr (ChromeHD) reactor at 1000°C . Samples were injected with a split-splitless injector. The GC was equipped with 30 m fused silica column (HP5-MS, $0.32\ \text{mm}$ inner diameter, $0.25\ \mu\text{m}$ film thickness). The precision was checked by co-analysing a standard alkane mixture (*n*-C₂₇, *n*-C₂₉, *n*-C₃₃) with known isotope composition (Arndt Schimmelmann, University of Indiana), injected twice every six runs. The samples were analysed in three repetitions (except from the samples in 622 and 672 cm depth), and the analytical precision was generally better than 5 ‰. The stable hydrogen isotope compositions are given in the δ notation ($\delta^2\text{H}_{n\text{-alkane}}$) versus Vienna Standard Mean Ocean Water (VSMOW). The H_3^+ -correction factor was checked every 2 days and stayed stable over the course of measurements at 3.14. The $\delta^2\text{H}_{n\text{-alkane}}$ values refer to the area-weighted

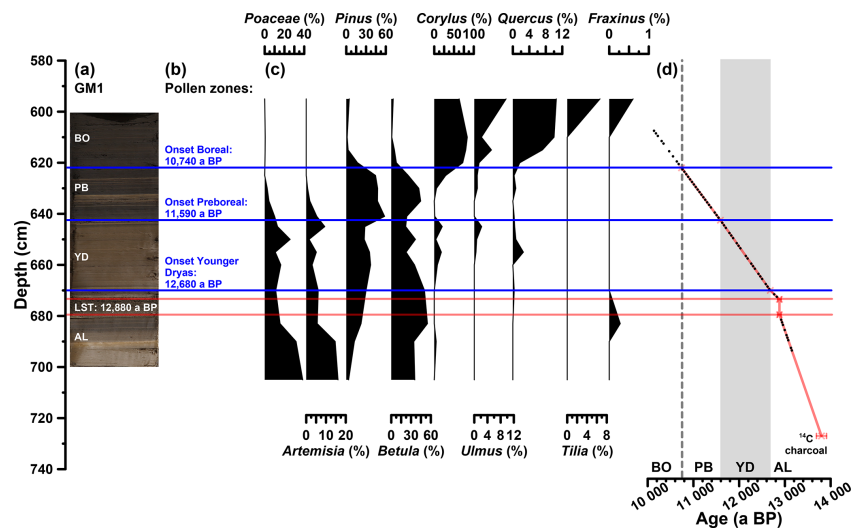


Figure 2. (a) Photo of the investigated GM1 core section, with regard to the biomarkers (607 to 694 cm depth), displaying the position of the Laacher See Tephra (LST), varve-counted to 12 880 a BP in the adjacent Meerfelder Maar (cf. Brauer et al., 1999). (b) Defined pollen zones according to Brauer et al. (1999) and Litt et al. (2009). (c) Pollen profiles of pollen groups, which were used for defining the pollen zones. Pollen analysis was carried out by Frank Dreher (Johannes Gutenberg University of Mainz). (d) Age–depth model of the full investigated GM1 section (606 to 727 cm depth) consisting of a ^{14}C -dated piece of charcoal, the LST and the onsets of the Younger Dryas, Preboreal and Boreal (Holocene). Additionally, the biomarker sampling points are displayed (black points). The error bars of the ^{14}C age and the LST represent the uncertainty of the calibration (68 % probability range) and the error during of the varve counting (± 40 a; Brauer et al., 1999), respectively.

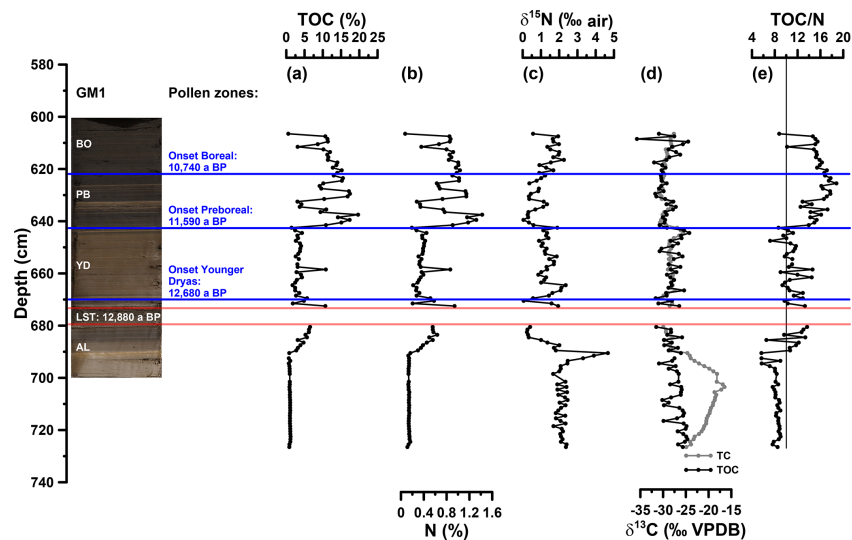


Figure 3. (a) Depth profiles of total organic carbon (TOC), (b) total nitrogen (N), (c) bulk stable nitrogen isotope composition ($\delta^{15}\text{N}$), (d) stable carbon isotope composition of total carbon (TC) and TOC ($\delta^{13}\text{C}_{\text{TC}}$, $\delta^{13}\text{C}_{\text{TOC}}$) and (e) carbon to nitrogen atomic ratio (TOC/N). The vertical line in (e) indicates a TOC/N atomic ratio threshold of 10 (Meyers, 2003). AL: Allerød; YD: Younger Dryas; PB: Preboreal; BO: Boreal.

mean of the $\delta^2\text{H}$ values of n -alkanes with 27 and 29 carbon atoms ($n\text{-C}_{27}$, $n\text{-C}_{29}$) because of their relatively high abundance in the samples (Fig. 4a).

The sample preparation for $\delta^{18}\text{O}$ analyses of hemicellulose- or polysaccharide-derived sugars followed standard procedures at the Institute of Agronomy and Nutritional Sciences, Soil Biogeochemistry, Martin Luther University Halle-Wittenberg, according to the method of Zech and Glaser (2009). The monosaccharide sugars were hydrolytically extracted from samples containing approximately 10 mg total organic carbon with 10 mL of 4 M trifluoroacetic acid at 105 °C for 4 h, applying the method described by Amelung et al. (1996). After filtration over glass fibre filters, the extracted sugars were cleaned using XAD-7 (to remove humic-like substances) and Dowex 50WX8 columns (to remove interfering cations). Afterwards, the purified samples were freeze-dried and derivatised by adding methylboronic acid (4 mg in 400 μL pyridine) for 1 h at 60 °C.

The compound-specific $\delta^{18}\text{O}$ measurements were performed using a Trace GC 2000 coupled to a Delta V Advantage IRMS via an ^{18}O -pyrolysis reactor (GC IsoLink) and a ConFlo IV interface (all devices from Thermo Fisher Scientific, Bremen, Germany). Each sample was measured in threefold repetition, embedded in-between co-derivatised sugar standards at various concentrations and known $\delta^{18}\text{O}$ values. The $\delta^{18}\text{O}$ values of the samples are expressed in δ notation ($\delta^{18}\text{O}_{\text{sugar}}$) versus VSMOW. The measured $\delta^{18}\text{O}_{\text{sugar}}$ values were corrected for drift, amount and area dependency and also for the hydrolytically introduced oxygen atoms that form carbonyl groups with the C1 atoms of the sugar molecules (Zech and Glaser, 2009). Mean standard errors for the triplicate measurements of all 59 samples are 0.6‰, 0.7‰ and 0.7‰ for arabinose, fucose and xylose, respectively. The $\delta^{18}\text{O}_{\text{sugar}}$ values refer to the $\delta^{18}\text{O}$ values of the monosaccharides arabinose, fucose and xylose (Fig. 4b). Rhamnose areas, or concentrations, were too low for reliable isotope measurements in most samples.

2.5 Conceptual framework of the coupled $\delta^2\text{H}_{n\text{-alkane}}\text{-}\delta^{18}\text{O}_{\text{sugar}}$ paleohygrometer approach

The coupled $\delta^2\text{H}_{n\text{-alkane}}\text{-}\delta^{18}\text{O}_{\text{sugar}}$ paleohygrometer approach was described in detail by Tuthorn et al. (2015) and Zech et al. (2013a). The most fundamental assumption of the approach is that the isotope composition of leaf water can be reconstructed by applying biosynthetic fractionation factors on the measured $\delta^2\text{H}_{n\text{-alkane}}$ and $\delta^{18}\text{O}_{\text{sugar}}$ values (Fig. 5). The concept is furthermore based on the observation that the isotope composition of global precipitation plots typically close to the global meteoric water line (GMWL; $\delta^2\text{H}_{\text{prec}} = 8 \cdot \delta^{18}\text{O}_{\text{prec}} + 10$; Dansgaard, 1964). In Germany, a local meteoric water line (LMWL_{Germany}) slightly deviating from GMWL was described by Stumpp et al. (2014) ($\delta^2\text{H}_{\text{prec}} = 7.72 \pm 0.13 \cdot \delta^{18}\text{O}_{\text{prec}} + 4.90 \pm 0.01$; Fig. 5), which we used as

the baseline for our calculations. The quite similar LMWLs for Trier ($\delta^2\text{H}_{\text{prec}} = 7.81 \pm 0.08 \cdot \delta^{18}\text{O}_{\text{prec}} + 5.06 \pm 0.60$) and Koblenz ($\delta^2\text{H}_{\text{prec}} = 7.80 \pm 0.07 \cdot \delta^{18}\text{O}_{\text{prec}} + 2.68 \pm 0.53$) as well as the GMWL are additionally displayed in Fig. 5 for comparison. The local precipitation is the source for soil water and shallow groundwater, which in turn acts as source water for plants. During daytime, however, leaf water is typically ^2H - and ^{18}O -enriched compared to the source water due to evapotranspiration through the stomata (Fig. 5; Allison et al., 1985; Bariac et al., 1994; Walker and Brunel, 1990). The leaf water reservoir at the evaporative sites quickly achieves steady-state conditions (Allison et al., 1985; Bariac et al., 1994; Gat et al., 2007; Walker and Brunel, 1990). Thus, the isotope composition of the transpired water vapour is equal to the isotope composition of the source water utilised by the plants during the transpiration process. The evaporative enrichment of leaf water under steady-state conditions can be described via a Craig–Gordon model (e.g. Flanagan et al., 1991; Roden and Ehleringer, 1999) by the following expression (e.g. Barbour et al., 2004):

$$\delta_e \approx \delta_s + \varepsilon^* + \varepsilon_k + (\delta_a - \delta_s - \varepsilon_k) \frac{e_a}{e_i}, \quad (1)$$

where δ_e , δ_s and δ_a are the hydrogen and oxygen isotope compositions of leaf water at the evaporative sites, in source water and in atmospheric water vapour, respectively; ε^* is the equilibrium enrichment expressed as $(1 - 1/\alpha_{L/V}) \times 10^3$ where $\alpha_{L/V}$ is the equilibrium fractionation between liquid and vapour in ‰; and ε_k is the kinetic fractionation parameters for water vapour diffusion from intracellular air space through the stomata and the boundary layer, both for ^2H and ^{18}O , respectively; and e_a/e_i is the ratio of atmospheric vapour pressure to intracellular vapour pressure. When leaf temperature is equal to air temperature, the e_a/e_i ratio represents the RH of the local atmosphere. If the plant source water and the local atmospheric water vapour are in isotopic equilibrium, the term $\delta_a - \delta_s$ can be approximated by $-\varepsilon^*$. Thus, Eq. (1) can be reduced to

$$\delta_e \approx \delta_s + (\varepsilon^* + \varepsilon_k)(1 - \text{RH}). \quad (2)$$

The kinetic fractionation parameters (ε_k) are typically related to stomatal and boundary layer resistances with respect to water flux (Farquhar et al., 1989). Since direct measurements of those plant physiological parameters can be hardly assessed in a paleo application, we used the kinetic enrichment parameters C_k instead, derived from a more generalised form of the Craig–Gordon model, for describing the kinetic isotope enrichment for ^2H and ^{18}O , which leads to Eq. (3) (Craig and Gordon, 1965; Gat and Bowser, 1991):

$$\delta_e \approx \delta_s + (\varepsilon^* + C_k)(1 - \text{RH}). \quad (3)$$

In a $\delta^2\text{H}\text{-}\delta^{18}\text{O}$ diagram, the hydrogen and oxygen isotope composition of leaf and source water can be described as a local deuterium (d) excess = $\delta^2\text{H} - 7.72 \cdot \delta^{18}\text{O}$ (Stumpp

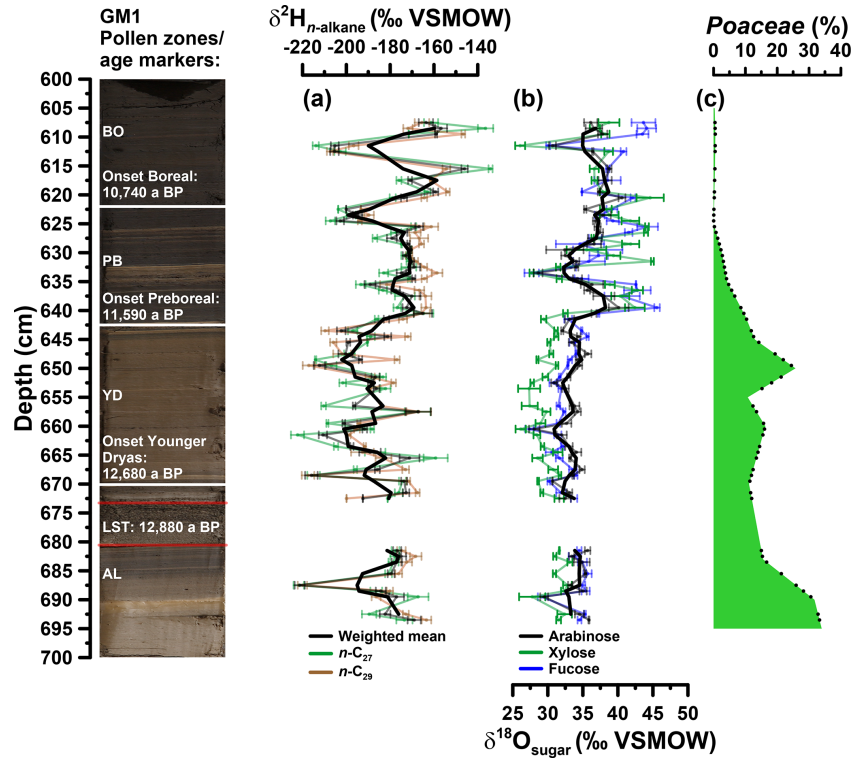


Figure 4. (a) Depth profiles of compound-specific stable hydrogen isotope composition of the individual alkanes $n\text{-C}_{27}$ and $n\text{-C}_{29}$ and the weighted mean ($\delta^2\text{H}_{n\text{-alkane}}$). (b) Compound-specific stable oxygen composition of the individual sugars arabinose, xylose and fucose ($\delta^{18}\text{O}_{\text{sugar}}$). Error bars show analytical standard errors; bold lines show three-point moving averages. (c) Depth profile of *Poaceae* pollen. Additionally, the resampled data points (black points) used for the grass correction procedures (Eqs. 10 and 11) are displayed. In addition, the GM1 core picture with the age markers used is displayed. AL: Allerød; LST: Laacher See Tephra; YD: Younger Dryas; PB: Preboreal; BO: Boreal.

et al., 2014) in one equation by using the slope of the LMWL_{Germany} (Eq. 4). This approach is comparable to the d excess definition from Dansgaard (1964), who used the equation $d = \delta^2\text{H} - 8 \cdot \delta^{18}\text{O}$ for a measure of the parallel deviation between a given point in the $\delta^2\text{H}$ – $\delta^{18}\text{O}$ diagram from the GMWL.

$$d_e \approx d_s + \left(\varepsilon_2^* - 7.72 \cdot \varepsilon_{18}^* + C_k^2 - 7.72 \cdot C_k^{18} \right) (1 - \text{RH}), \quad (4)$$

where d_e and d_s are the d excess values of the leaf water at the evaporative sites and the source water, respectively, and the equilibrium (ε_2^* and ε_{18}^*) and kinetic enrichment parameters (C_k^2 and C_k^{18}) are expressed for both isotopes. From Eqs. (1) to (4) the primary control of RH on the isotope composition of the leaf water is demonstrated when stomata are open through transpiration. If d_e can be derived from compound-specific $\delta^2\text{H}$ and $\delta^{18}\text{O}$ measurements of the n -alkane and sugar biomarkers, which derive $\delta^2\text{H}_e$ and $\delta^{18}\text{O}_e$ values for the purpose of calculating d_e values via the equa-

tion $d_e = \delta^2\text{H}_e - 7.72 \cdot \delta^{18}\text{O}_e$, the d_s can also be approximated from the d excess of the LMWL_{Germany} (= 4.9). Accordingly, Eq. (4) can be rearranged in order to calculate the RH of the local atmosphere normalised to leaf temperature as given by Eq. (5) (Hepp et al., 2017; Tuthorn et al., 2015; Zech et al., 2013a):

$$\text{RH} \approx 1 - \frac{\Delta d}{\left(\varepsilon_2^* - 7.72 \cdot \varepsilon_{18}^* + C_k^2 - 7.72 \cdot C_k^{18} \right)}, \quad (5)$$

where Δd is the distance between d_e and d_s , calculated as $\Delta d = d_e - d_s$. Equilibrium fractionation parameters (ε_2^* and ε_{18}^*) are derived from empirical equations of Horita and Wesolowski (1994), with mean daytime growth-period temperature of 14.8 °C (from 06:00 to 19:00 CET and April to October, derived from the Nürburg-Barweiler station, approx. 25 km northeast of Gemündener Maar; hourly data from 1995 to 2015 from Deutscher Wetterdienst, 2016). Equilibrium fractionation factors equal 83.8‰ and 10.15‰ for ^2H and ^{18}O , respectively. The kinetic fractionation pa-

rameters (C_k^2 and C_k^{18}) for ^2H and ^{18}O are set to 25.1‰ and 28.5‰, respectively, according to Merlivat (1978), who reported maximum values during the molecular diffusion process of water through a stagnant boundary layer. The assumption that maximum kinetic fractionation occurs seems to be most suitable for sedimentological application where a signal averaging over decades can be assumed (see above and discussion in Zech et al., 2013a). It should also be noted that ϵ_k values of broadleaf trees and shrubs over broad climatic conditions are well within the range of the C_k^2 and C_k^{18} values used, revealing 23.9‰ (± 0.9) and 26.7‰ (± 1.0) for $\delta^2\text{H}$ and $\delta^{18}\text{O}$, respectively (derived from the Supplement of Cernusak et al., 2016).

The numerator of Eq. (5) describes the parallel distance between the d excesses of LMWL and leaf water at the evaporative sites, which is converted into RH values, while the denominator is a combination of the slopes of LMWL and the local evaporation line (LEL). This means in turn that the quantification with Eq. (5) is done by obtaining the distance between the source water points, calculated via the intersects between the individual LELs and the LMWL_{Germany}, and the leaf water points. The underlying slope of those LELs can be derived from Eq. (6) via the Craig–Gordon model using the same assumptions as outlined above in a rearranged form (Eq. 6; Zech et al., 2013a). When using the fractionation parameters from above, the slope of the LEL is constant over time, independent of RH and equal to ~ 2.8 (Eq. 6). This agrees well with field and laboratory studies (Allison et al., 1985; Bariac et al., 1994; Gat et al., 2007; Tipple et al., 2013; Walker and Brunel, 1990).

$$S_{\text{LEL}} = \frac{\delta_e^2 - \delta_s^2}{\delta_e^{18} - \delta_s^{18}} \approx \frac{\epsilon_2^* + C_k^2}{\epsilon_{18}^* + C_k^{18}} \quad (6)$$

In order to provide an uncertainty interval in terms of measurement precision covering the Gemündener Maar RH record, we calculated an error propagation for d_e values according to Eq. (7), by using the analytical standard errors (SEs). Maximum and minimum values were then applied to Eq. (5) resulting in a lower and upper RH limit (blue-shaded area in Fig. 7a).

$$SEd_e = \sqrt{(\text{SE}\delta^2\text{H}_{n\text{-alkane}})^2 + 7.72 \cdot (\text{SE}\delta^{18}\text{O}_{\text{sugar}})^2} \quad (7)$$

3 Results and discussion

3.1 Source identification of bulk organic matter and of the investigated n -alkane and sugar biomarkers

For basic sedimentological characterisation, TOC, N, $\delta^{15}\text{N}$, $\delta^{13}\text{C}_{\text{TC}}$ and $\delta^{13}\text{C}_{\text{TOC}}$ values as well as the TOC/N atomic ratios (Fig. 3a to e) are displayed from 605 to 727 cm depth. TOC values range from 0.6% to 19.7%. N ranges from 0.1% to 1.4% and correlates highly significantly with TOC ($r = 0.99$, $p < 0.001$, $n = 110$). Higher TOC contents during

the Allerød, Preboreal and Boreal likely reflect warmer conditions being favourable for terrestrial and aquatic biomass production, whereas lower TOC values during the Younger Dryas likely reflect less favourable conditions for biomass production and possibly increasing minerogenic sedimentation. Interestingly, the Late Glacial–Early Holocene TOC patterns seem not to be the same for all maar lakes, because the Meerfelder Maar shows a clear TOC two-phasing during the Younger Dryas (Brauer et al., 1999) and the Holzmaar is lacking an Allerød TOC maximum (Lücke et al., 2003). The $\delta^{15}\text{N}$ values of the Gemündener Maar record range from 0‰ to 5‰, showing the maximum and minimum within the Allerød period. $\delta^{13}\text{C}_{\text{TC}}$ and $\delta^{13}\text{C}_{\text{TOC}}$ reveal values between -31 ‰ and -17 ‰ and -36 ‰ and -24 ‰, respectively. While $\delta^{13}\text{C}_{\text{TC}}$ shows maximum values at 703 cm depth, $\delta^{13}\text{C}_{\text{TOC}}$ is decreasing continuously from the beginning to the end of the Allerød, followed by increasing values during the Younger Dryas and the Preboreal and Boreal, interrupted by a short decrease around the beginning of the Holocene. $\delta^{13}\text{C}_{\text{TC}}$ clearly shows the presence of carbonate between 690 and 727 cm depth with less negative $\delta^{13}\text{C}_{\text{TC}}$ values compared to $\delta^{13}\text{C}_{\text{TOC}}$ values. TOC/N atomic ratios range from 6 to 19 with the end of the Allerød revealing increasing ratios, while the late Younger Dryas shows slightly decreasing ratios and the Preboreal is marked by the highest ratios.

The source of organic matter in lacustrine sediments of small lakes, as one of the most crucial questions and challenges when interpreting organic proxies from lacustrine sedimentary records (Meyers and Ishiwatari, 1993), can either be autochthonous (aquatic origin) or allochthonous (terrestrial origin). The TOC/N ratio and $\delta^{13}\text{C}$ values are the most common proxies for sedimentary source determination. While non-vascular aquatic organisms often reveal C/N atomic ratios between 4 and 10 (due to low amounts of cellulose and lignin), vascular plants commonly show C/N atomic ratios of 20 and higher (Meyers and Ishiwatari, 1993). According to Meyers (2003), a TOC/N atomic ratio of 10 is often used as threshold for identifying aquatic versus terrestrial input (Fig. 3e). Accordingly, the input from terrestrial organic matter increased during the Allerød, decreased slightly during the Younger Dryas and was highest during the Holocene. The Gemündener Maar $\delta^{13}\text{C}_{\text{TOC}}$ values (Fig. 3d) are well within the range of C_3 land plants and lacustrine algae (Meyers and Lallier-Vergés, 1999); evidence for the occurrence of C_4 land plants is missing. Overall, no clear additional information about the sedimentary organic matter origin of the Gemündener Maar sediments can be inferred neither from $\delta^{13}\text{C}_{\text{TOC}}$ alone (cf. Lücke et al., 2003) nor by combining $\delta^{13}\text{C}_{\text{TOC}}$ with TOC/N ratios (cf. Meyers and Lallier-Vergés, 1999). When considering that both $\delta^{13}\text{C}_{\text{TOC}}$ and TOC/N values of terrestrial organic matter are additionally affected by mineralisation and degradation, resulting in more positive $\delta^{13}\text{C}_{\text{TOC}}$ values and lower TOC/N ratios (e.g. Zech et al., 2007), a straightforward interpretation of those

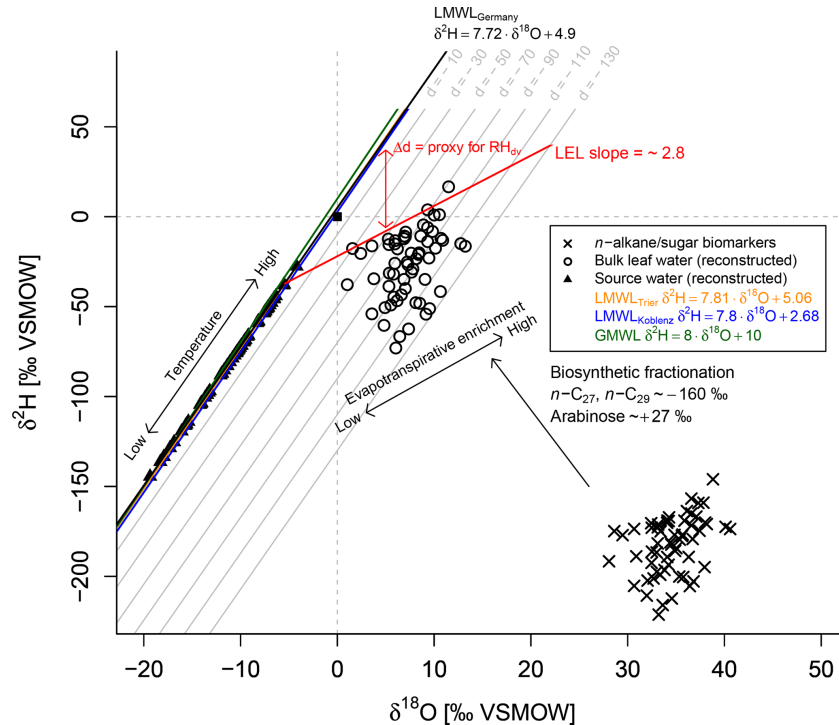


Figure 5. Conceptual framework of the coupled $\delta^2\text{H}_{n\text{-alkane}}-\delta^{18}\text{O}_{\text{sugar}}$ paleohygrometer approach displayed as $\delta^{18}\text{O}-\delta^2\text{H}$ diagram showing the measured n -alkanes (weighted mean of $n\text{-C}_{27}$ and $n\text{-C}_{29}$) and sugar (arabinose) biomarkers (black crosses), the reconstructed leaf water (open circles), the global meteoric water line (GMWL, green line), and the local meteoric water lines of Germany (LMWL_{Germany}, black line), Trier (LMWL_{Trier}, yellow line) and Koblenz (LMWL_{Koblenz}, blue line). The black arrows indicate natural processes of evapotranspirative enrichment of leaf water along local evaporation lines (LELs), biosynthetic fractionation during biomarker synthesis and the temperature effect on the source water isotope composition (\sim precipitation). Grey lines indicate the parallel distance between the individual reconstructed evaporative site leaf water points and the LMWL_{Germany}, expressed as $d = \delta^2\text{H} - 7.72 \cdot \delta^{18}\text{O}$. The difference between the leaf water and source water can serve as proxy for mean daytime vegetation period relative humidity (RH_{dv} ; red double arrow).

proxies seems to be challenging. Similarly, $\delta^{15}\text{N}$ has been investigated as proxy for sedimentary organic matter origin (Meyers and Ishiwatari, 1993; Meyers and Lallier-Vergés, 1999; Wolfe et al., 1999). However, numerous processes that may have an influence, like nitrogen uptake by plants, various nitrogen sources, discrimination during denitrification and diagenesis, complicate the use of $\delta^{15}\text{N}$ as a direct source determination proxy.

Despite the uncertainties presented above, concerning the origin of bulk sedimentary organic matter in the Gemündener Maar, the origin of the sedimentary biomarkers, namely n -alkanes and sugars, needs to be addressed. This is crucial because aquatic biomarkers incorporate the isotope composition of lake water, whereas terrestrial biomarkers incorporate the isotope composition of leaf water (Huang et al., 2004; Kahmen et al., 2013; Mügler et al., 2008; Sachse et al., 2004, 2012; Sauer et al., 2001; Tuthorn et al., 2014; Zech et al.,

2013b, 2014b). With regard to the n -alkane biomarkers, high amounts of the chain lengths $n\text{-C}_{27}$ and $n\text{-C}_{29}$ are characteristic of the epicuticular leaf wax layers of higher terrestrial plants (e.g. Eglinton and Hamilton, 1967). With regard to the sugar biomarkers, they were previously studied in detail by Hepp et al. (2016). According to the authors' own results and a compilation from the literature (including, e.g., Jia et al., 2008; Prietzel et al., 2013; Zech et al., 2012, 2014b), relatively high amounts of arabinose are a good indicator of a primarily terrestrial origin (higher vascular plants) of the sugars. This interpretation is in agreement with the Gemündener Maar being a small lake with densely forested steep crater walls (Fig. 1c). We therefore conclude and suggest that arabinose as well as $n\text{-C}_{27}$ and $n\text{-C}_{29}$ in our Gemündener Maar record are primarily of terrestrial rather than

aquatic origin and thus reflect $\delta^2\text{H}/\delta^{18}\text{O}_{\text{leaf-water}}$ rather than $\delta^2\text{H}/\delta^{18}\text{O}_{\text{lake-water}}$.

3.2 Reconstructing leaf water isotope composition based on $\delta^2\text{H}_{n\text{-alkane}}$ and $\delta^{18}\text{O}_{\text{sugar}}$

The $\delta^2\text{H}$ depth profiles reveal variations of -222‰ to -134‰ and -220‰ to -147‰ for $n\text{-C}_{27}$ and $n\text{-C}_{29}$, respectively (Fig. 4a). Their $\delta^2\text{H}$ patterns correlate highly significantly with each other ($r = 0.7$, $p < 0.001$, $n = 59$). Weighted mean $\delta^2\text{H}$ values were calculated using the relative amounts of $n\text{-C}_{27}$ and $n\text{-C}_{29}$. The Younger Dryas is characterised by the most negative $\delta^2\text{H}$ values (mean of -193‰), whereas the Allerød, the Preboreal and the Boreal yielded less negative values (-182‰ , -178‰ and -171‰ , respectively). Still, the Holocene part also reveals two pronounced $\delta^2\text{H}$ minima. Overall, our Gemündener Maar $\delta^2\text{H}_{n\text{-alkane}}$ resembles very well the $\delta^2\text{H}$ $n\text{-C}_{29}$ record of Rach et al. (2014) for Meerfelder Maar close by.

The $\delta^{18}\text{O}$ values for arabinose, xylose and fucose range from 28‰ to 41‰ , 26‰ to 45‰ and 27‰ to 46‰ , respectively (Fig. 4b). They reveal similar trends overall (arabinose vs. xylose: $r = 0.7$, $p < 0.001$, $n = 59$; arabinose vs. fucose: $r = 0.8$, $p < 0.001$, $n = 59$; xylose vs. fucose: $r = 0.8$, $p < 0.001$, $n = 59$). All sugar records show a clear shift to more positive values at the Younger Dryas–Holocene transition. While xylose and fucose exhibit a change of $\sim 8\text{‰}$ and 7‰ , arabinose $\delta^{18}\text{O}$ values show a less pronounced shift of $\sim 3\text{‰}$ (changes are based on the mean $\delta^{18}\text{O}$ values for the Younger Dryas compared to the Preboreal/Boreal period). Xylose is however slightly more negative throughout the Allerød and Younger Dryas compared to arabinose and fucose. Consistently less pronounced changes can be observed for the Allerød–Younger Dryas transition of 1.9‰ , 1.7‰ and 0.9‰ for xylose, fucose and arabinose, respectively (based on the mean $\delta^{18}\text{O}$ values for the Allerød compared to the Younger Dryas). A distinct minimum during the early Preboreal (633 cm depth) characterises all three $\delta^{18}\text{O}$ sugar records.

The isotope compositions of leaf wax $n\text{-alkanes}$ and leaf (hemi-)celluloses from higher plants are known to be strongly related to the water in which they are biosynthesised. They basically reflect the isotope composition of leaf water during photosynthetic activity (Barbour and Farquhar, 2000; Cernusak et al., 2005; Kahmen et al., 2013; Sachse et al., 2012). Hence, the isotope signature of the paleo leaf water, $\delta^{18}\text{O}_1$ and $\delta^2\text{H}_1$, respectively, can be reconstructed by using biosynthetic fractionation factors (Fig. 5; Eqs. 8 and 9). For this purpose, fractionation factors of -160‰ for the $n\text{-alkanes}$ $n\text{-C}_{27}$ and $n\text{-C}_{29}$ (ϵ_{bio}^2 ; Sachse et al., 2012; Sessions et al., 1999) and $+27\text{‰}$ for the hemicellulose sugar arabinose ($\epsilon_{\text{bio}}^{18}$; Cernusak et al., 2003; Schmidt et al., 2001; Sternberg et al., 1986; Yakir and DeNiro, 1990) seem to be appropriate (Eqs. 8 and 9).

$$\delta^{18}\text{O}_1 = (\delta^{18}\text{O}_{\text{arabinose}} - \epsilon_{\text{bio}}^{18}) / (1 + \epsilon_{\text{bio}}^{18}/1000) \quad (8)$$

$$\delta^2\text{H}_1 = (\delta^2\text{H}_{n\text{-alkane}} - \epsilon_{\text{bio}}^2) / (1 + \epsilon_{\text{bio}}^2/1000) \quad (9)$$

From the study of tree rings, it is known that stem cellulose does not show the full leaf water ^{18}O enrichment signal. Barbour and Farquhar (2000) related this signal dampening to the proportion of unenriched source water contributing to the local synthesis water (p_x) and to the proportion of exchangeable oxygen during cellulose synthesis (p_{ex}). The latter is often assumed to be rather constant around 0.40, as estimated from leaf and wood cellulose of *Eucalyptus globulus* and values compiled from the literature (Cernusak et al., 2005), meaning that around 40 % of the oxygens in the stem cellulose exchanged. Already Helliker and Ehleringer (2002) compared the signal transfer from leaf water to the cellulose of tree stems with the signal transfer occurring in grasses. And Liu et al. (2016) reported signal dampening in the range between 34 % and 53 % for the C_4 grass *Cleistogenes squarrosa*.

Figure 4c illustrates that *Poaceae* pollen concentrations ranged between 11 % and 33 % during the Allerød and the Younger Dryas in the Gemündener Maar record. Hence, a correction for the ^{18}O signal dampening may be required in order to take these vegetation changes into consideration. A respective correction procedure based on mass balance considerations is given in Eq. (10) in order to adjust $\delta^{18}\text{O}_1$ to $\delta^{18}\text{O}_1^\#$:

$$\delta^{18}\text{O}_1^\# = \left\{ \left(\delta^{18}\text{O}_1 - \delta^{18}\text{O}_s \right) / \left[f_{\text{non-grasses}} + (1 - 0.4) - f_{\text{non-grasses}} \cdot (1 - 0.4) \right] \right\} + \delta^{18}\text{O}_s. \quad (10)$$

The correction presented in Eq. (10) is based on assumptions that 40 % (0.4) of the leaf water enrichment is lost during hemicellulose biosynthesis of grass leaves, which is well within the range of values presented in the literature for cellulose synthesis in tree rings and grasses (Cernusak et al., 2005; Liu et al., 2016). Furthermore, the *Poaceae* pollen concentration in percentage is used to calculate the fraction of non-grassy pollen ($f_{\text{non-grasses}} = (100 - \textit{Poaceae})/100$) corresponding to the non-grassy biomarker contribution, which may serve as a rough approximation. For a paleo application, $\delta^{18}\text{O}_s$ remains a priori unknown. Therefore, the intercept between the individual LELs (Eq. 6) and the LMWL of Germany were used to generate $\delta^{18}\text{O}_s$ values. Note that the signal dampening effect described here for cellulose synthesis is likely not fully applicable to our approach using the sugar biomarker arabinose. In fact, pentoses like arabinose are biosynthesised via decarboxylation of the carbon at position six (C6) from glucose (Altermatt and Neish, 1956; Burget et al., 2003; Harper and Bar-Peled, 2002). Waterhouse et al. (2013) showed that the oxygens at C6 position in glucose moieties are most strongly affected by the exchange with a local water medium of 80 %, as indicated by

heterotrophic cellulose synthesis. Thus, arabinose has lost a strongly exchanged (dampened) oxygen and the remaining pentose shows less ^{18}O signal dampening.

With regard to the $\varepsilon_{\text{bio}}^2$ value of -160‰ , this biosynthetic fractionation factor is confirmed by climate chamber studies of dicotyledonous plants (Kahmen et al., 2011, 2013; Tipple et al., 2015). However, the latter studies also reveal a range of $\sim 35\text{‰}$, interpreted as species-specific effects during *n*-alkane biosynthesis. The difference between dicotyledonous and monocotyledonous C_3 plants is much more pronounced the regarding the degree to which the leaf water isotope enrichment is transferred into leaf *n*-alkanes (Gamarra et al., 2016; Kahmen et al., 2013). While dicotyledonous plants show signal transfer rates of 96 % on average (Kahmen et al., 2013), a larger range of between 38 % and 61 % is found for monocotyledonous plants (Gamarra et al., 2016). The latter implies that 39 % to 62 % of the ^2H leaf water enrichment is not recorded by the *n*-alkanes of grasses. Hence, like for $\delta^{18}\text{O}$, a correction may be requested to account for grass-derived *n*-alkanes:

$$\delta^2\text{H}_1^\# = \left\{ \left(\delta^2\text{H}_1 - \delta^2\text{H}_s \right) / \left[f_{\text{non-grasses}} + (1 - 0.5) - f_{\text{non-grasses}} \cdot (1 - 0.5) \right] \right\} + \delta^2\text{H}_s, \quad (11)$$

where $\delta^2\text{H}_1^*$ are the grass-corrected $\delta^2\text{H}_1$ values. The $\delta^2\text{H}_s$ values and the non-grassy pollen fraction are defined as in Eq. (10). The mass balance correction presented in Eq. (11) is based on assumptions that only 50 % of the leaf water enrichment is incorporated by the *n*-alkanes during biosynthesis in grass leaves.

In summary, the discussion outlined above allows reconstructing $\delta^2\text{H}/\delta^{18}\text{O}_{\text{leaf-water}}$ (and thus RH results with Eq. 5) for four scenarios (see also Table 1): (i) without signal dampening, (ii) with grass-corrected $\delta^2\text{H}$ values, (iii) with grass-corrected $\delta^{18}\text{O}$ values, and (iv) with grass-corrected $\delta^2\text{H}$ and $\delta^{18}\text{O}$ values.

3.3 Reconstructing relative humidity based on the coupled $\delta^2\text{H}_{n\text{-alkane}}-\delta^{18}\text{O}_{\text{sugar}}$ paleohygrometer approach

The biomarker-based leaf water values ($\delta_1 = \delta^2\text{H}_1$, $\delta^{18}\text{O}_1$ via Eqs. 8 and 9) result in *d* excess values of leaf water (d_1) ranging between -125‰ and -30‰ (Figs. 5 and 6a). This is well within the range that can be expected. For instance, Voelker et al. (2014) reported “deuterium deviations” (calculated as *d* excess of leaf water minus 10 ‰) ranging from 0 ‰ to -200‰ . And Mayr (2002) conducted climate chamber experiments with *Vicia*, *Brassica* and *Eucalyptus* during his dissertation and measured $\delta^2\text{H}$ and $\delta^{18}\text{O}$ of leaf water ($\delta^{18}\text{O}_{\text{leaf-water}}$ and $\delta^{18}\text{O}_{\text{sugars}}$ are published in Zech et al., 2014b). Accordingly, *d* excess of leaf water ranged from -38‰ to -171‰ and correlates highly significantly with RH (ranging from 21 % to 68 %).

Using the Gemündener Maar d_1 values as input for Eq. (5), RH values during daytime and vegetation period (RH_{dv}) can be calculated (scenario 1 in Table 1). Reconstructed RH_{dv} values range from 32 % to 82 % (Fig. 6b). The error bars covering the Gemündener Maar RH_{dv} record, calculated using pooled d_e standard errors ranging from 3.2 ‰ to 44.4 ‰ according Eq. (7), result in an RH uncertainty range of 1.7 % to 23.4 %. The RH_{dv} record shows quite large variability with no clear trend during the Allerød and the first half of the Younger Dryas. The late Younger Dryas and the early and the middle Preboreal are characterised by lower RH values. By contrast, the middle Preboreal reveals the most pronounced RH maximum. The mean reconstructed RH_{dv} value is 53 % (mean RH_{dv} upper limit = 45 %; mean RH_{dv} lower limit = 62 %; see Sect. 2.5). For comparison, the modern RH_{dv} value (06:00 to 19:00 CET from April to October) from the adjacent meteorological station Nürburg-Barweiler (approx. 25 km northeast of Gemündener Maar (GM); hourly data from 1995 to 2015 from Deutscher Wetterdienst, 2016) is 67 % (Fig. 6b). In addition, the range of the reconstructed RH_{dv} values of 50 % agrees well with the modern RH_{dv} variability of 45 %, within a range of 48 % to 93 % (definition and meteorological station details as above). As proposed, in the previous chapter, three correction scenarios can be applied when reconstructing d_1 and RH_{dv} values in order to account for ^2H and ^{18}O signal dampening occurring in grasses.

Accordingly, the full correction for grass-derived alkane and sugar biomarkers (scenario 4 in Table 1) results in 0.0 % to 6.3 % (mean 1.8 %) lower RH_{dv} values ($\text{RH}_{\text{dv}}^{\#}$ in Fig. 6b). This corresponds to d_1 decreases of 0.0 ‰ to -12.0‰ ($d_1^{\#}$ in Fig. 6a). Such small changes are still far below the pooled analytical standard errors. When only correcting for the ^{18}O signal dampening (scenario 3 in Table 1), d_1 values decrease by 0.0 ‰ to -22.7‰ , corresponding to RH decreases of 0.0 % to -12.0‰ ($d_1^\#$ and $\text{RH}_{\text{dv}}^\#$ in Fig. 6a and b, respectively). By contrast, when only correcting for the ^2H signal dampening (scenario 2 in Table 1), this leads to 0.0 ‰ to 10.6 ‰ more positive and 0.0 % to 5.6 % higher RH_{dv} values (d_1^* and RH_{dv}^* in Fig. 6a and b). Overall, these results suggest that the reconstructed RH_{dv} values are not strongly affected by ^2H and ^{18}O signal dampening of grasses.

We are aware that microclimatic conditions with higher RH values often develop in lower canopy levels of forests (Graham et al., 2014; Parker, 1995). This may result in RH overestimations when applying the coupled $\delta^2\text{H}_{n\text{-alkane}}-\delta^{18}\text{O}_{\text{sugar}}$ paleohygrometer approach. However, most leaf biomass is produced at higher canopy levels, which are exposed to sunlight and free-air RH values. This is in agreement with a study of Zech et al. (2015), who investigated *n*-alkanes in soils of the tropical montane rainforest of Mt Kilimanjaro. There, *n*-alkanes reflect $\delta^2\text{H}_{\text{leaf-water}}$ as calculated from free-air RH rather than as calculated from nearly saturated ground-level RH.

A basic assumption of our coupled $\delta^2\text{H}_{n\text{-alkane}}-\delta^{18}\text{O}_{\text{sugar}}$ paleohygrometer approach is isotopic equilibrium between

Table 1. Scenarios 1–4 used for reconstructing deuterium (d) excess of leaf water and corresponding RH_{dv} values in order to assess/estimate the effect of variable grass contributions on the reconstructed Gemündener Maar RH record (see also Fig. 6).

Scenario	Leaf water reconstructed from n -alkane or sugar biomarkers	Equations used for leaf water reconstruction	Resulting d excess of leaf water as input for Eq. (5)	Relative air humidity during daytime and vegetation period according Eq. (5)
1	$\delta^2H_1/\delta^{18}O_1$	(8) and (9)	d_1	RH_{dv}
2	$\delta^2H_1^*/\delta^{18}O_1$	(8) and (9) + (11)	d_1^*	RH_{dv}^*
3	$\delta^2H_1/\delta^{18}O_1^\#$	(8) + (10) and (9)	$d_1^\#$	$RH_{dv}^\#$
4	$\delta^2H_1^*/\delta^{18}O_1^\#$	(8) + (10) and (9) + (11)	$d_1^{\#\#}$	$RH_{dv}^{\#\#}$

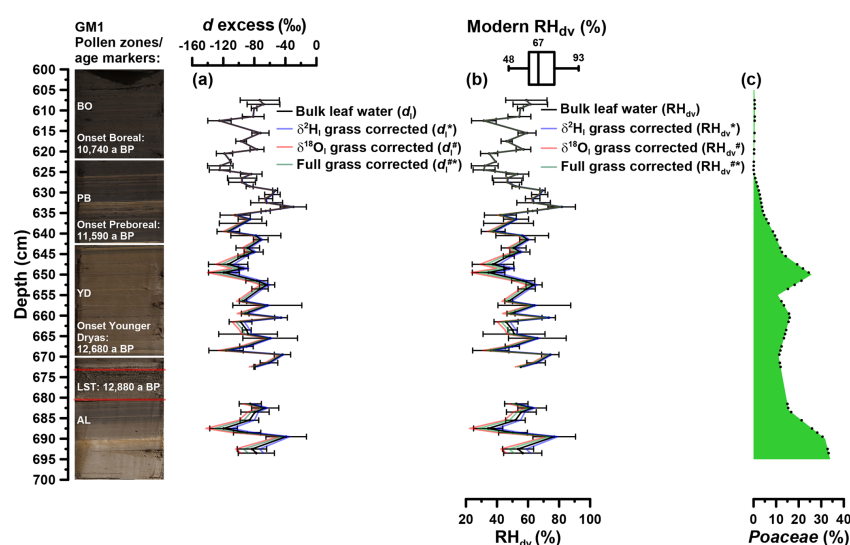


Figure 6. (a) Deuterium (d) excess depth profiles of reconstructed leaf water: d_1 (black line): no correction for grasses; d_1^* (light blue line): δ^2H corrected for grasses; $d_1^\#$ (light red line): $\delta^{18}O$ corrected for grasses; $d_1^{\#\#}$ (light green line): δ^2H and $\delta^{18}O$ corrected for grasses. The error bars of d_1 values are calculated according to Eq. (7). (b) Reconstructed RH_{dv} records. Modern RH variability during daytime and vegetation period (RH_{dv}) is displayed as a box plot derived from the adjacent meteorological station Nürburg-Barweiler, using monthly means from April to October between 06:00 and 19:00 CET (based on hourly data from 1995 to 2015; Deutscher Wetterdienst, 2016). The numbers within the box plot represent the maximum, median and minimum values. (c) Depth profile of *Poaceae* pollen. Additionally, the resampled data points (black points) are displayed. The GM1 core picture with the used age markers are displayed on the left. AL: Allerød; LST: Laacher See Tephra; YD: Younger Dryas; PB: Preboreal; BO: Boreal.

plant source water and water vapour. In order to test the robustness of this assumption and respective effects on reconstructed RH values, we used data of Jacob and Sonntag (1991), who measured the isotope composition of precipitation and of atmospheric water vapour in Heidelberg, Germany, during the period 1981 to 1989. The mean difference between the annual weighted means of precipitation (\approx plant source water) and the water vapour averaged over the vegetation period (April–October) was therefore calculated. Such derived apparent fractionation (ϵ_{ap}) amounts to 18.3‰ and 1.57‰ on average for 2H and ^{18}O , respectively. We used this ϵ_{ap} in Eq. (1) instead of the difference $\delta_a - \delta_s$

and recalculated the RH values. This recalculation leads to an average RH change of only -1.7% (± 0.9), which is far below the analytical errors of the d excess of leaf water.

Finally, the stability of the d excess and slope of the $LMWL_{Germany}$ through the past needs to be discussed. According to Stumpp et al. (2014), the long-term d excess of precipitation from 28 sites in Germany does not show pronounced relationships to local climate conditions of the site. All reported values are close to 10‰, which indicates that Atlantic air masses are the main moisture source for Germany (e.g. Rozanski et al., 1993). In addition, the d excess of precipitation from the stations Trier and Koblenz,

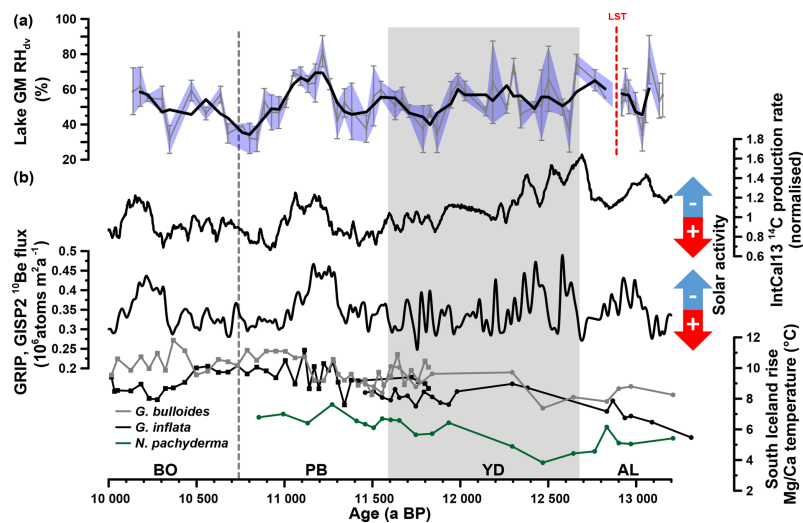


Figure 7. (a) Reconstructed Gemündener Maar (GM) RH_{dv} record. The bold line shows the three-point moving average. Error bars and the blue-shaded area indicate analytical uncertainties calculated according to error propagation (Eq. 7). (b) IntCal13 ^{14}C production rate, Greenland ice-core (GRIP, GISP2) ^{10}Be flux record (both from Muscheler et al., 2014) and South Iceland Rise planktic Mg/Ca-derived water temperatures from RAPiD-12-1K (squares; 10 000 to 11 800 a BP) and RAPiD-15-4P (circles; 10 900 to 13 200 a BP). RAPiD-12-1K and RAPiD-15-4P *G. bulloides* and *G. inflata* data from Thoralley et al. (2009) and Thoralley et al. (2010), respectively. RAPiD-15-4P *N. pachyderma* data from Thoralley et al. (2011). Note that each record is plotted on its own timescale (for planktonic Mg/Ca data, see Thoralley et al., 2009, 2010; for ^{10}Be data on GICC05, see Rasmussen et al., 2006; for ^{14}C data on IntCal13 calibration curve, see Reimer et al., 2013; for RH_{dv} data on GM age–depth model, see Fig. 2d). AL: Allerød, LST: Laacher See Tephra, YD: Younger Dryas, PB: Preboreal and BO: Boreal.

which are close to the Gemündener Maar, reveal rather small variability on a monthly, annual and long-term basis. For Trier monthly averaged d excess values (March to October) range from 5.3‰ to 8.7‰. Annually weighted mean d excess values range from 1.9‰ to 10.6‰, and the long-term weighted mean is 6.7‰ (± 2.2); for Koblenz the d excess values range between 2.1‰ and 6.4‰ and 1.4‰ and 8.7‰, and the long-term weighted mean is 4.1‰ (± 1.8) (derived from IAEA/WMO, 2018). Finally, d excess variability in Greenland and Antarctic ice cores does not exceed 4‰ over the timescale relevant here (Masson-Delmotte et al., 2005; Stenni et al., 2010). In addition, paleowater samples from Europe suggest that the d excess of precipitation was rather constant throughout the past 35 000 years, which implies that the principle atmospheric circulation patterns over the European continent did not change substantially (Rozanski, 1985). In summary, the variations in the slope of the LMWL of Germany are assumed to be rather small over longer timescales.

The detailed discussions in the above three sections address numerous uncertainties when using the coupled $\delta^2H_n\text{-alkane}-\delta^{18}O_{\text{sugar}}$ paleohygrometer approach. Conclusively, the reconstructed RH_{dv} history of the Gemündener Maar seems, however, robust enough to infer reliable paleoclimatic or hydrologic conclusions.

3.4 How dry was the Younger Dryas in western Europe?

While it is well known that the Younger Dryas was a cold spell occurring in the Northern Hemisphere during the Late Glacial (Denton et al., 2010; Heiri et al., 2014; Isarin and Bohncke, 1999), there is much less clear evidence concerning moisture supply or availability and RH changes during the Younger Dryas. The Gemündener Maar RH_{dv} record suggests quite some variability but on average moderate RH_{dv} conditions of $\sim 56\%$ during the end of the Allerød and the first half of the Younger Dryas. This is within the range of modern RH_{dv} values (Fig. 6b). In the second half of the Younger Dryas, a clear RH_{dv} decrease of $\sim 11\%$ occurred (Fig. 7a). Such a two phasing of the Younger Dryas has been suggested previously based on multiproxy climate data for western Europe (Isarin et al., 1998). In more detail, Isarin et al. (1998) reported a cold and humid first phase being followed by drier and warmer conditions. It is moreover speculated that a shift in the mean sea-ice margin during winter in the North Atlantic Ocean slightly to the north could have caused this two phasing. Reduced cyclonic activity and precipitation thereby primarily affected western Europe because this region was situated at the southern margin of the main storm tracks during the first Younger Dryas period (Isarin et al., 1998). The authors also presented evi-

dence for the strengthening of the westerly winds in western Europe as consequence of northward-shifted North Atlantic Ocean sea-ice margin during the late Younger Dryas period. This contradicts, however, with the interpretation of the Meerfelder Maar sedimentary record. Here, the thicker varves during the early Younger Dryas (between 12 680 and 12 240 varve a BP) are used along with geochemical results as indicator of stronger winter winds (Brauer et al., 2008). In line with this, Brauer et al. (1999) interpreted high biogenic opal contents and *Pediastrum* remains concentrations during the early Younger Dryas as enhanced aquatic productivity due to an increased nutrient supply caused by soil erosion and the reworking of littoral sediments. The varve formation throughout the second Younger Dryas period (between 12 240 and 11 590 varve a BP) is interpreted to be mainly controlled by snowmelt-driven surface runoff (Brauer et al., 1999). Moreover, the authors speculate if during that time the Meerbach began to drain into the Meerfelder Maar, which could be possibly linked to enhanced precipitation amounts. In summary, the interpretations derived from the Younger Dryas sediments of the Meerfelder Maar by Brauer et al. (2008, 1999) seem neither to be in accordance with the results of Isarin et al. (1998) nor with the established RH_{dv} record of the Gemündener Maar (Fig. 7a).

Recently, Rach et al. (2017) reconstructed RH changes and generally dry Younger Dryas climatic conditions by investigating δ^2H of terrestrially versus aquatically derived n -alkanes (published in Rach et al., 2014) from the Meerfelder Maar archive. At the current state of research, it can only be speculated about the reasons for this discrepancy, with our Gemündener Maar RH record not corroborating an overall dry Younger Dryas. While the uncertainties of the coupled $\delta^2H_{n\text{-alkane}}-\delta^{18}O_{\text{sugar}}$ paleohygrometer approach were discussed in detail in the previous sections, in our opinion the most important uncertainties affecting the dual-biomarker approach of Rach et al. (2014, 2017) are the following. First, lake water is assumed to reflect δ^2H of precipitation. Indeed, Holzmaar, which seems to be comparable to the Meerfelder Maar at least for the drainage conditions via one creek, shows a difference of 7.4‰ in δ^2H between inflow and lake water (Sachse et al., 2004). This lake water enrichment is likely to have been variable in the past, especially when including the speculation concerning the drainage of the Meerbach during the Younger Dryas (Brauer et al., 1999). Second, $n\text{-}C_{23}$ is interpreted to be of aquatic origin (from *Potamogeton*) and used for reconstructing $\delta^2H_{\text{lake-water}}$. However, there is increasing evidence that $n\text{-}C_{23}$ is also of terrestrial origin (Rao et al., 2014). For instance, Aichner et al. (2018) have recently shown for a lake in Poland that $n\text{-}C_{23}$ shows a variable mixture of aquatic and terrestrial origin in those Late Glacial and Early Holocene sediments. And birch as a pioneering and one of the dominant tree species during Late Glacial reforestation of central Europe is known to produce considerable amounts of mid-chain n -alkanes (Tarasov et al., 2013). Although they are not included in the latter publica-

tion, $n\text{-}C_{23}$ concentrations of *Betula exilis* and *Betula pendula* reached 653 and even 2323 $\mu\text{g g}^{-1}$ in that study. This is highly relevant, because the biosynthetic fractionation factor of aquatic n -alkanes is much smaller than the one of terrestrial n -alkanes. Minor changes in the contribution of terrestrial vs. aquatic n -alkanes will thus have a considerable impact on the reconstructed δ^2H $n\text{-}C_{23}$ record and in turn on reconstructed RH values when applying the dual-biomarker approach. Finally, it may worth acknowledging that Sachse et al. (2004) found no significant correlation for δ^2H of $n\text{-}C_{23}$ and lake water and precipitation along a European lake surface transect.

Also recently and also applying the dual-biomarker approach, Muschitiello et al. (2015) studied Younger Dryas lake sediments from Hässeldala Port in southern Sweden. Here, the authors used δ^2H of $n\text{-}C_{21}$ as a proxy for lake water and summer precipitation. The calculated difference between terrestrial and aquatic n -alkane δ^2H values suggests more humid conditions at the beginning of the Younger Dryas followed by a more or less steady trend towards drier conditions, peaking around 11 700 a BP (Muschitiello et al., 2015). Within age uncertainties, this would be in line with the Gemündener Maar RH_{dv} minimum between $\sim 11 700$ and 11 900 a BP. Last but not least, Gázquez et al. (2018) analysed triple oxygen and hydrogen isotopes of gypsum in the southern Pyrenees and thus reconstructed RH changes. Again, more humid conditions are reported for the beginning of the Younger Dryas.

In search of possible drivers or mechanisms for the observed Gemündener Maar RH_{dv} record, we came across the ^{14}C production and ^{10}Be flux rates (Fig. 7b), derived from IntCal13 and the Greenland ice cores (GRIP, GISP2), respectively (Muscheler et al., 2014). These records are commonly interpreted in terms of solar activity (and thus insolation) changes (Stuiver and Braziunas, 1988; Vonmoos et al., 2006) and reveal striking similarities with our Gemündener Maar RH_{dv} record. For instance, all three records reveal quite high centennial-scale variability during the Allerød and the first half of the Younger Dryas. Generally low RH_{dv} values during the second half of the Younger Dryas and the Early Preboreal coincide with high solar activity, whereas the pronounced RH_{dv} maximum from 11 260 to 11 050 a BP coincides within age uncertainties with a pronounced solar activity minimum (Fig. 7). We dub this wet period the “Preboreal Humid Phase”, which should not be confused with the Preboreal Oscillation (Björck et al., 1997). The Preboreal Oscillation is a short cold event recorded in Greenland ice cores $\sim 11 400$ ka (Rasmussen et al., 2007) and led to more arid conditions at least in the Netherlands according to palynological results (Bos et al., 2007; van der Plicht et al., 2004). These pollen records also show the existence of a pronounced humid phase thereafter, thus corroborating the Preboreal Humid Phase. Widespread glacial advances in the Alps are also attributed to the Preboreal Oscillation (Moran et al., 2017). However, given the dating uncertainties they

may actually rather reflect increased precipitation during the Preboreal Humid Phase.

It should be emphasised, that the described similarities between the Gemündener Maar RH_{dv} record and the solar activity records do not allow an a priori causality interpretation. It is widely accepted that the Younger Dryas and the Preboreal Oscillation are related to freshwater forcing in the North Atlantic (e.g. Fisher et al., 2002; Murton et al., 2010; Muschiello et al., 2015). However, the causes and mechanisms responsible for climate and environmental changes during the rest of the Holocene remain vague, and more research including paleoclimate modelling is clearly needed and encouraged to investigate the possible influence of solar activity (Renssen et al., 2007; Rind, 2002). We propose that both the North Atlantic Ocean temperature and solar activity (the latter triggering solar insolation) were the two main drivers for the RH_{dv} variability in central Europe. A key example might be the Preboreal Humid Phase. It can be expected that the North Atlantic Ocean, the main moisture source for central Europe, already had considerably higher temperatures during the Preboreal Humid Phase compared to the Younger Dryas, as indicated by a consistent $\sim 2^\circ\text{C}$ increase in Mg/Ca temperatures derived from planktonic foraminifera (*Globorotalia inflata*, *Globorotalia bulloides* and *Neogloboquadrina pachyderma*) in a marine sediment core south of Iceland (Fig. 7b, Thornalley et al., 2009, 2010, 2011). This led to an enhanced moisture content of the atmosphere. When these wet air masses were transported onto continental Europe, where low solar insolation inhibited warming up and drying of these air masses, pronounced humid climate conditions were established.

4 Conclusions

Referring to the underlying research questions and based on the presented results and the outlined discussion (including the cited literature), the following conclusions have to be drawn.

The terrestrial vs. aquatic origin of bulk sedimentary organic matter cannot be determined unambiguously for the Gemündener Maar. This is caused by the bulk proxies (TOC/N, $\delta^{13}\text{C}$ and $\delta^{15}\text{N}$) not being straightforwardly interpretable. By contrast, the alkane biomarkers with the chain-length *n*-C₂₇ and *n*-C₂₉ and the sugar biomarker arabinose can be most likely associated with the epicuticular leaf wax layers and the hemicellulose structures of higher terrestrial plants, respectively. Therefore, they are interpreted as originating primarily from leaf material of the Gemündener Maar catchment.

$\delta^2\text{H}/\delta^{18}\text{O}_{\text{leaf-water}}$ could be reconstructed from $\delta^2\text{H}_{n\text{-alkane}}$ (*n*-C₂₇ and *n*-C₂₉) and $\delta^{18}\text{O}_{\text{sugar}}$ (arabinose) by applying biosynthetic fractionation factors. We acknowledge that the assumption of constant fractionation factors introduces uncertainty as highlighted by the broad literature

discussion. A correction for the signal dampening of leaf water $^2\text{H}/^{18}\text{O}$ enrichment occurring in grasses is possible but seems negligible in the case of the Gemündener Maar record.

The detailed discussion of possible uncertainties of the applied coupled $\delta^2\text{H}_{n\text{-alkane}}-\delta^{18}\text{O}_{\text{sugar}}$ paleohygrometer approach suggests that robust RH reconstructions are possible for the Gemündener Maar record. The reconstructed RH values refer to daytime and vegetation period (RH_{dv}).

The established Gemündener Maar RH_{dv} record supports a two phasing of the Younger Dryas with moderate wet conditions at Allerød level during the first half and drier conditions during the second half of the Younger Dryas. Overall, dry climatic conditions characterising the Younger Dryas could not be corroborated. Unexpectedly, the amplitude of RH_{dv} changes during the Early Holocene was more pronounced than during the Younger Dryas and includes a pronounced Preboreal Humid Phase occurring from $\sim 11\,260$ to $11\,050$ a BP. We propose North Atlantic Ocean temperature and solar activity (and thus insolation) as the main drivers for Late Glacial–Early Holocene RH changes in central Europe and encourage respective paleoclimate modelling studies in order to validate or falsify our proposition.

Data availability. The data are available in the Supplement, including sampling depth, calculated ages, measured $\delta^2\text{H}_{n\text{-alkane}}$ and $\delta^{18}\text{O}_{\text{sugar}}$ values, reconstructed $\delta^2\text{H}/\delta^{18}\text{O}_{\text{leaf-water}}$, *d* excess of leaf water, RH_{dv}, and $\delta^2\text{H}/\delta^{18}\text{O}_{\text{source-water}}$ values.

Supplement. The supplement related to this article is available online at: <https://doi.org/10.5194/cp-15-713-2019-supplement>.

Author contributions. JH, LW and MZ wrote the paper; MZ and RZ acquired financial support. FS was responsible for lake coring and provided the chronology and stratigraphy. LW, JH, TB, MB and IKS carried out laboratory work and did data evaluation. MB, IKS, BG, KR, FS and RZ contributed to the discussion of the data and commented on the paper.

Competing interests. The authors declare that they have no conflict of interest.

Acknowledgements. We greatly acknowledge Raimund Muscheler (Lund University) for providing ^{10}Be flux as well as ^{14}C production rates data. We thank Marianne Benesch (Martin Luther University Halle-Wittenberg), Anna Kühnel (Technical University of Munich), Jana Zech (University of Bern), Frank Dreher (Johannes Gutenberg University of Mainz), Selina Lutz (University of Zurich), and Nevena Baltić and Paul Kretschmer (Martin Luther University Halle-Wittenberg) for their support during laboratory work and statistical analyses. We cordially thank Pieter M. Grootes (Kiel University) for valuable recommendations

during paper preparation and Keely Mills, Philip Meyers and an anonymous reviewer for their great editorial support and constructive and encouraging reviews. Our paper also greatly profited from short comments provided by Bernd Zolitschka, Andreas Lücke, Enno Schefuß, Dirk Sachse and Frederik Schenk (see SCs on discussion paper and our replies). The Swiss National Science Foundation (PP00P2 150590) funded Lorenz Wüthrich, Marcel Bliedtner, Imke Kathrin Schäfer and Roland Zech. The involvement of Kazimierz Rozanski was supported by AGH UST statutory task no. 11.11.220.01/1 within a subsidy of the Ministry of Science and Higher Education. Johannes Hepp greatly acknowledges the support given by the German Federal Environmental Foundation. This publication was funded by the publication fund of the Martin Luther University and of the University Hospital Halle (Saale) through reimbursement.

Review statement. This paper was edited by Keely Mills and reviewed by Philip Meyers and one anonymous referee.

References

- Aichner, B., Ott, F., Slowinski, M., Noryskiewicz, A. M., Brauer, A., and Sachse, D.: Leaf wax *n*-alkane distributions record ecological changes during the Younger Dryas at Trzechowskie paleolake (northern Poland) without temporal delay, *Clim. Past*, 14, 1607–1624, <https://doi.org/10.5194/cp-14-1607-2018>, 2018.
- Alley, R. B.: The Younger Dryas cold interval as viewed from central Greenland, *Quaternary Sci. Rev.*, 19, 213–226, [https://doi.org/10.1016/S0277-3791\(99\)00062-1](https://doi.org/10.1016/S0277-3791(99)00062-1), 2000.
- Allison, G. B., Gat, J. R., and Leaney, F. W. J.: The relationship between deuterium and oxygen-18 delta values in leaf water, *Chem. Geol.*, 58, 145–156, 1985.
- Altermatt, H. A. and Neish, A. C.: The biosynthesis of cell wall carbohydrates: III. Further studies on formation of cellulose and xylan from labeled monosaccharides in wheat plants, *Can. J. Biochem. Phys.*, 34, 405–413, <https://doi.org/10.1139/o56-042>, 1956.
- Amelung, W., Cheshire, M. V., and Guggenberger, G.: Determination of neutral and acidic sugars in soil by capillary gas-liquid chromatography after trifluoroacetic acid hydrolysis, *Soil Biol. Biochem.*, 28, 1631–1639, 1996.
- Araguás-Araguás, L., Froehlich, K., and Rozanski, K.: Deuterium and oxygen-18 isotope composition of precipitation and atmospheric moisture, *Hydrol. Process.*, 14, 1341–1355, [https://doi.org/10.1002/1099-1085\(20000615\)14:8<1341::AID-HYP983>3.0.CO;2-Z](https://doi.org/10.1002/1099-1085(20000615)14:8<1341::AID-HYP983>3.0.CO;2-Z), 2000.
- Barbour, M. M. and Farquhar, G. D.: Relative humidity- and ABA-induced variation in carbon and oxygen isotope ratios of cotton leaves, *Plant Cell Environ.*, 23, 473–485, 2000.
- Barbour, M. M., Roden, J. S., Farquhar, G. D., and Ehleringer, J. R.: Expressing leaf water and cellulose oxygen isotope ratios as enrichment above source water reveals evidence of a Péclet effect, *Oecologia*, 138, 426–435, <https://doi.org/10.1007/s00442-003-1449-3>, 2004.
- Bariac, T., Gonzalez-Dunia, J., Katerji, N., Béthenod, O., Bertolini, J. M., and Mariotti, A.: Spatial variation of the isotopic composition of water (^{18}O , ^2H) in the soil-plant-atmosphere system, 2. Assessment under field conditions, *Chem. Geol.*, 115, 317–333, 1994.
- Björck, S., Rundgren, M., Ingólfsson, O., and Funder, S.: The Preboreal oscillation around the Nordic Seas: terrestrial and lacustrine responses, *J. Quaternary Sci.*, 12, 455–465, [https://doi.org/10.1002/\(SICI\)1099-1417\(199711/12\)12:6<455::AID-JQS316>3.0.CO;2-S](https://doi.org/10.1002/(SICI)1099-1417(199711/12)12:6<455::AID-JQS316>3.0.CO;2-S), 1997.
- Bos, J. A. A., van Geel, B., van der Plicht, J., and Bohncke, S. J. P.: Preboreal climate oscillations in Europe: Wiggle-match dating and synthesis of Dutch high-resolution multi-proxy records, *Quaternary Sci. Rev.*, 26, 1927–1950, <https://doi.org/10.1016/j.quascirev.2006.09.012>, 2007.
- Brauer, A., Endres, C., Günter, C., Litt, T., Stebich, M., and Negen-dank, J. F. W.: High resolution sediment and vegetation responses to Younger Dryas climate change in varved lake sediments from Meerfelder Maar, Germany, *Quaternary Sci. Rev.*, 18, 321–329, [https://doi.org/10.1016/S0277-3791\(98\)00084-5](https://doi.org/10.1016/S0277-3791(98)00084-5), 1999.
- Brauer, A., Haug, G. H., Dulski, P., Sigman, D. M., and Negen-dank, J. F. W.: An abrupt wind shift in western Europe at the onset of the Younger Dryas cold period, *Nat. Geosci.*, 1, 520–523, <https://doi.org/10.1038/ngeo263>, 2008.
- Brunck, H., Sirocko, F., and Albert, J.: The ELSA-Flood-Stack: A reconstruction from the laminated sediments of Eifel maar structures during the last 60,000 years, *Global Planet. Change*, 142, 136–146, <https://doi.org/10.1016/j.gloplacha.2015.12.003>, 2015.
- Büchel, G.: Maars of the Westeifel, Germany, in: *Paleolimnology of European Maar Lake*, edited by: Negen-dank, L. and Zolitschka, B., Vol. 49, 1–13, Springer-Verlag, Berlin Heidelberg, 1993.
- Büchel, G.: Vulkanologische Karte der West- und Hocheifel 1 : 50 000, Landesvermessungsamt Rheinland-Pfalz, Koblenz, 1994.
- Burget, E. G., Verma, R., Mølhøj, M., and Reiter, W.-D.: The Biosynthesis of L-Arabinose in Plants: Molecular Cloning and Characterization of a Golgi-Localised UDP-D-Xylose 4-Epimerase Encoded by the MUR4 Gene of Arabidopsis, *Plant Cell*, 15, 523–531, <https://doi.org/10.1105/tpc.008425>, 2003.
- Cernusak, L. A., Wong, S. C., and Farquhar, G. D.: Oxygen isotope composition of phloem sap in relation to leaf water in *Ricinus communis*, *Funct. Plant Biol.*, 30, 1059–1070, 2003.
- Cernusak, L. A., Farquhar, G. D., and Pate, J. S.: Environmental and physiological controls over oxygen and carbon isotope composition of Tasmanian blue gum, *Eucalyptus globulus*, *Tree Physiol.*, 25, 129–146, <https://doi.org/10.1093/treephys/25.2.129>, 2005.
- Cernusak, L. A., Barbour, M. M., Arndt, S. K., Cheesman, A. W., English, N. B., Feild, T. S., Helliker, B. R., Holloway-Phillips, M. M., Holtum, J. A. M., Kahmen, A., Mcinerney, F. A., Munks-gaard, N. C., Simonin, K. A., Song, X., Stuart-Williams, H., West, J. B., and Farquhar, G. D.: Stable isotopes in leaf water of terrestrial plants, *Plant Cell Environ.*, 39, 1087–1102, <https://doi.org/10.1111/pce.12703>, 2016.
- Craig, H. and Gordon, L. I.: Deuterium and oxygen-18 variations in the ocean and the marine atmosphere, in: *Proceedings of a Conference on Stable Isotopes in Oceanographic Studies and Palaeotemperatures*, edited by: Tongiorgi, E., 9–130, Lischì and Figli, Pisa, 1965.
- Dansgaard, W.: Stable isotopes in precipitation, *Tellus*, 16, 436–468, <https://doi.org/10.1111/j.2153-3490.1964.tb00181.x>, 1964.
- Denton, G. H., Anderson, R. F., Toggweiler, J. R., Edwards, R. L., Schaefer, J. M., and Putnam, A. E.: The

- Last Glacial Termination, *Science*, 328, 1652–1656, <https://doi.org/10.1126/science.1184119>, 2010.
- Deutscher Wetterdienst: Climate data center, Nürnberg-Barweiler station, available at: <ftp://ftp-cdc.dwd.de/pub/CDC/>, last access: 10 August 2016.
- Eglinton, G. and Hamilton, R. J.: Leaf Epicuticular Waxes, *Science*, 156, 1322–1335, <https://doi.org/10.1126/science.156.3780.1322>, 1967.
- Farquhar, G. D., Hubick, K. T., Condon, A. G., and Richards, R. A.: Carbon Isotope Fractionation and Plant Water-Use Efficiency, in: *Stable Isotopes in Ecological Research. Ecological Studies (Analysis and Synthesis)*, edited by: Rundel, P. W., Ehleringer, J. R., and Nagy, K. A., Vol. 68, 21–40, Springer-Verlag, New York, 1989.
- Fisher, T. G., Smith, D. G., and Andrews, J. T.: Preboreal oscillation caused by a glacial Lake Agassiz flood, *Quaternary Sci. Rev.*, 21, 873–878, [https://doi.org/10.1016/S0277-3791\(01\)00148-2](https://doi.org/10.1016/S0277-3791(01)00148-2), 2002.
- Flanagan, L. B., Comstock, J. P., and Ehleringer, J. R.: Comparison of Modeled and Observed Environmental Influences on the Stable Oxygen and Hydrogen Isotope Composition of Leaf Water in *Phaseolus vulgaris* L., *Plant Physiol.*, 96, 588–596, 1991.
- Gamarra, B., Sachse, D., and Kahmen, A.: Effects of leaf water evaporative ^2H -enrichment and biosynthetic fractionation on leaf wax *n*-alkane $\delta^2\text{H}$ values in C₃ and C₄ grasses, *Plant Cell Environ.*, 39, 2390–2403, <https://doi.org/10.1111/pce.12789>, 2016.
- Gat, J. R. and Bowser, C. J.: The heavy isotope enrichment of water in coupled evaporative systems, in: *Stable Isotope Geochemistry: A Tribute to Samuel Epstein*, edited by: Tayler, H. P., O’Neil, J. R., and Kaplan, I. R., Vol. 3, 159–168, The Geochemical Society, Lancaster, 1991.
- Gat, J. R., Yakir, D., Goodfriend, G., Fritz, P., Trumborn, P., Lipp, J., Gev, I., Adar, E., and Waisel, Y.: Stable isotope composition of water in desert plants, *Plant Soil*, 298, 31–45, <https://doi.org/10.1007/s11104-007-9321-6>, 2007.
- Gázquez, F., Morellón, M., Bauska, T., Herwartz, D., Surma, J., Moreno, A., Staubwasser, M., Valero-Garcés, B., Delgado-Huertas, A., and Hodell, D. A.: Triple oxygen and hydrogen isotopes of gypsum hydration water for quantitative paleohumidity reconstruction, *Earth Planet. Sc. Lett.*, 481, 177–188, <https://doi.org/10.1016/j.epsl.2017.10.020>, 2018.
- Graham, H. V., Patzkowsky, M. E., Wing, S. L., Parker, G. G., Fogel, M. L., and Freeman, K. H.: Isotopic characteristics of canopies in simulated leaf assemblages, *Geochim. Cosmochim. Ac.*, 144, 82–95, <https://doi.org/10.1016/j.gca.2014.08.032>, 2014.
- Harper, A. D. and Bar-Peled, M.: Biosynthesis of UDP-Xylose. Cloning and Characterization of a Novel Arabidopsis Gene Family, UXS, Encoding Soluble and Putative Membrane-Bound UDP-Glucuronic Acid Decarboxylase Isoforms, *Gene*, 130, 2188–2198, <https://doi.org/10.1104/pp.009654>, 2002.
- Heiri, O., Koinig, K. A., Spötl, C., Barrett, S., Brauer, A., Drescher-Schneider, R., Gaar, D., Ivy-Ochs, S., Kerschner, H., Luetscher, M., Moran, A., Nicolussi, K., Preusser, F., Schmidt, R., Schoenich, P., Schwörer, C., Sprafke, T., Terhorst, B., and Tinner, W.: Palaeoclimate records 60–8 ka in the Austrian and Swiss Alps and their forelands, *Quaternary Sci. Rev.*, 106, 186–205, <https://doi.org/10.1016/j.quascirev.2014.05.021>, 2014.
- Helliker, B. R. and Ehleringer, J. R.: Grass blades as tree rings: environmentally induced changes in the oxygen isotope ratio of cellulose along the length of grass blades, *New Phytol.*, 155, 417–424, 2002.
- Henderson, A. K., Nelson, D. M., Hu, F. S., Huang, Y., Shuman, B. N., and Williams, J. W.: Holocene precipitation seasonality captured by a dual hydrogen and oxygen isotope approach at Steel Lake, Minnesota, *Earth Planet. Sc. Lett.*, 300, 205–214, <https://doi.org/10.1016/j.epsl.2010.09.024>, 2010.
- Hepp, J., Tuthorn, M., Zech, R., Mügler, I., Schlütz, F., Zech, W., and Zech, M.: Reconstructing lake evaporation history and the isotopic composition of precipitation by a coupled $\delta^{18}\text{O}$ - $\delta^2\text{H}$ biomarker approach, *J. Hydrol.*, 529, 622–631, 2015.
- Hepp, J., Rabus, M., Anhäuser, T., Bromm, T., Laforsch, C., Sirocko, F., Glaser, B., and Zech, M.: A sugar biomarker proxy for assessing terrestrial versus aquatic sedimentary input, *Organic Geochem.*, 98, 98–104, <https://doi.org/10.1016/j.orggeochem.2016.05.012>, 2016.
- Hepp, J., Zech, R., Rozanski, K., Tuthorn, M., Glaser, B., Greule, M., Keppler, F., Huang, Y., Zech, W., and Zech, M.: Late Quaternary relative humidity changes from Mt. Kilimanjaro, based on a coupled ^2H - ^{18}O biomarker paleohygrometer approach, *Quaternary Int.*, 438, 116–130, <https://doi.org/10.1016/j.quaint.2017.03.059>, 2017.
- Horita, J. and Wesolowski, D. J.: Liquid-vapor fractionation of oxygen and hydrogen isotopes of water from the freezing to the critical temperature, *Geochim. Cosmochim. Ac.*, 58, 3425–3437, [https://doi.org/10.1016/0016-7037\(94\)90096-5](https://doi.org/10.1016/0016-7037(94)90096-5), 1994.
- Hou, J., D’Andrea, W. J., and Huang, Y.: Can sedimentary leaf waxes record D/H ratios of continental precipitation? Field, model, and experimental assessments, *Geochim. Cosmochim. Ac.*, 72, 3503–3517, <https://doi.org/10.1016/j.gca.2008.04.030>, 2008.
- Huang, Y., Shuman, B., Wang, Y., and Iii, T. W.: Hydrogen isotope ratios of individual lipids in lake sediments as novel tracers of climatic and environmental change: a surface sediment test, *J. Paleolimnol.*, 31, 363–375, 2004.
- IAEA/WMO: Global Network of Isotopes in Precipitation, The GNIP Database, available at: <https://nucleus.iaea.org/wiser>, last access: 9 February 2018.
- Isarin, R. F. B. and Bohncke, S. J. P.: Mean July Temperatures during the Younger Dryas in Northwestern and Central Europe as Inferred from Climate Indicator Plant Species, *Quaternary Res.*, 51, 158–173, <https://doi.org/10.1006/qres.1998.2023>, 1999.
- Isarin, R. F. B., Renssen, H., and Vandenberghe, J.: The impact of the North Atlantic Ocean on the Younger Dryas climate in northwestern and central Europe, *J. Quaternary Sci.*, 13, 447–453, [https://doi.org/10.1002/\(sici\)1099-1417\(199809\)13:5<447::aid-jqs402>3.0.co;2-b](https://doi.org/10.1002/(sici)1099-1417(199809)13:5<447::aid-jqs402>3.0.co;2-b), 1998.
- Jacob, H. and Sonntag, C.: An 8-year record of the seasonal-variation of ^2H and ^{18}O in atmospheric water vapor and precipitation at Heidelberg, *Tellus B*, 43, 291–300, 1991.
- Jia, G., Dungait, J. A. J., Bingham, E. M., Valiranta, M., Korhola, A., and Evershed, R. P.: Neutral monosaccharides as biomarker proxies for bog-forming plants for application to palaeovegetation reconstruction in ombrotrophic peat deposits, *Org. Geochem.*, 39, 1790–1799, <https://doi.org/10.1016/j.orggeochem.2008.07.002>, 2008.
- Kahmen, A., Dawson, T. E., Vieth, A., and Sachse, D.: Leaf wax *n*-alkane δD values are determined early in the ontogeny of *Populus trichocarpa* leaves when grown under controlled en-

- vironmental conditions, *Plant Cell Environ.*, 34, 1639–1651, <https://doi.org/10.1111/j.1365-3040.2011.02360.x>, 2011.
- Kahmen, A., Schefuß, E., and Sachse, D.: Leaf water deuterium enrichment shapes leaf wax *n*-alkane δD values of angiosperm plants I: Experimental evidence and mechanistic insights, *Geochim. Cosmochim. Ac.*, 111, 39–49, 2013.
- Litt, T. and Stebich, M.: Bio- and chronostratigraphy of the lateglacial in the Eifel region, Germany, *Quaternary Int.*, 61, 5–16, [https://doi.org/10.1016/S1040-6182\(99\)00013-0](https://doi.org/10.1016/S1040-6182(99)00013-0), 1999.
- Litt, T., Brauer, A., Goslar, T., Merkt, J., Balaga, K., Müller, H., Ralska-Jasiewiczowa, M., Stebich, M., and Negendank, J. F. W.: Correlation and synchronisation of Lateglacial continental sequences in northern central Europe based on annually laminated lacustrine sediments, *Quaternary Sci. Rev.*, 20, 1233–1249, 2001.
- Litt, T., Schmincke, H.-U., and Kromer, B.: Environmental response to climatic and volcanic events in central Europe during the Weichselian Lateglacial, *Quaternary Sci. Rev.*, 22, 7–32, 2003.
- Litt, T., Schölzel, C., Kühl, N., and Brauer, A.: Vegetation and climate history in the Westeifel Volcanic Field (Germany) during the past 11 000 years based on annually laminated lacustrine maar sediments, *Boreas*, 38, 679–690, <https://doi.org/10.1111/j.1502-3885.2009.00096.x>, 2009.
- Liu, H. T., Gong, X. Y., Schäufele, R., Yang, F., Hirl, R. T., Schmidt, A., and Schnyder, H.: Nitrogen fertilization and $\delta^{18}O$ of CO_2 have no effect on ^{18}O -enrichment of leaf water and cellulose in *Cleistogenes squarrosa* (C_4) – is VPD the sole control?, *Plant Cell Environ.*, 39, 2701–2712, <https://doi.org/10.1111/pce.12824>, 2016.
- Lücke, A., Schleser, G. H., Zolitschka, B., and Negendank, J. F. W.: A Lateglacial and Holocene organic carbon isotope record of lacustrine palaeoproductivity and climatic change derived from varved lake sediments of Lake Holzmaar, Germany, *Quaternary Sci. Rev.*, 22, 569–580, [https://doi.org/10.1016/S0277-3791\(02\)00187-7](https://doi.org/10.1016/S0277-3791(02)00187-7), 2003.
- Luetscher, M., Boch, R., Sodemann, H., Spötl, C., Cheng, H., Edwards, R. L., Frisia, S., Hof, F., and Müller, W.: North Atlantic storm track changes during the Last Glacial Maximum recorded by Alpine speleothems, *Nat. Commun.*, 6, 6344, <https://doi.org/10.1038/ncomms7344>, 2015.
- Masson-Delmotte, V., Jouzel, J., Landais, A., Stievenard, M., Johnson, S. J., White, J. W. C., Werner, M., Sveinbjornsdottir, A., and Fuhrer, K.: GRIP Deuterium Excess Reveals Rapid and Orbital-Scale Changes in Greenland Moisture Origin, *Science*, 309, 118–121, <https://doi.org/10.1126/science.1108575>, 2005.
- Mayr, C.: Möglichkeiten der Klimarekonstruktion im Holozän mit $\delta^{13}C$ - und δ^2H -Werten von Baum-Jahrringen auf der Basis von Klimakammerversuchen und Rezentstudien, PhD thesis, GSF-Bericht 14/02, 152 pp., Ludwig-Maximilians-Universität, München, 2002.
- Merlivat, L.: Molecular diffusivities of $H_2^{16}O$, $HD^{16}O$, and $H_2^{18}O$ in gases, *J. Chem. Phys.*, 69, 2864–2871, <https://doi.org/10.1063/1.436884>, 1978.
- Meyers, P. A.: Applications of organic geochemistry to paleolimnological reconstructions: a summary of examples from the Laurentian Great Lakes, *Org. Geochem.*, 34, 261–289, 2003.
- Meyers, P. A. and Ishiwatari, R.: Lacustrine organic geochemistry – an overview of indicators of organic matter sources and diagenesis in lake sediments, *Org. Geochem.*, 20, 867–900, 1993.
- Meyers, P. A. and Lallier-Vergés, E.: Lacustrine Sedimentary Organic Matter Records of Late Quaternary Paleoclimates, *J. Paleolimnol.*, 21, 345–372, <https://doi.org/10.1023/A:1008073732192>, 1999.
- Moran, A. P., Ivy-Ochs, S., Vockenhuber, C., and Kerschner, H.: First ^{36}Cl exposure ages from a moraine in the Northern Calcareous Alps, *E&G Quaternary Sci. J.*, 65, 145–155, <https://doi.org/10.3285/eg.65.2.03>, 2017.
- Mügler, I., Sachse, D., Werner, M., Xu, B., Wu, G., Yao, T., and Gleixner, G.: Effect of lake evaporation on δD values of lacustrine *n*-alkanes: A comparison of Nam Co (Tibetan Plateau) and Holzmaar (Germany), *Org. Geochem.*, 39, 711–729, 2008.
- Murton, J. B., Bateman, M. D., Dallimore, S. R., Teller, J. T., and Yang, Z.: Identification of Younger Dryas outburst flood path from Lake Agassiz to the Arctic Ocean, *Nature*, 464, 740–743, <https://doi.org/10.1038/nature08954>, 2010.
- Muscheler, R., Adolphi, F., and Knudsen, M. F.: Assessing the differences between the IntCal and Greenland ice-core time scales for the last 14,000 years via the common cosmogenic radionuclide variations, *Quaternary Sci. Rev.*, 106, 81–87, <https://doi.org/10.1016/j.quascirev.2014.08.017>, 2014.
- Muschitiello, F., Pausata, F. S. R., Watson, J. E., Smittenberg, R. H., Salih, A. A. M., Brooks, S. J., Whitehouse, N. J., Karlatou-Charalampopoulou, A., and Wohlfarth, B.: Fennoscandian freshwater control on Greenland hydroclimate shifts at the onset of the Younger Dryas, *Nat. Commun.*, 6, 8939, <https://doi.org/10.1038/ncomms9939>, 2015.
- Parker, G. G.: Structure and Microclimate of Canopies, in: *Forest Canopies*, edited by: Lowman, M. D. and Nadkarni, N. M., 73–106, Academic Press, San Diego, 1995.
- Partin, J. W., Quinn, T. M., Shen, C.-C., Okumura, Y., Cardenas, M. B., Siringan, F. P., Banner, J. L., Lin, K., Hu, H.-M., and Taylor, F. W.: Gradual onset and recovery of the Younger Dryas abrupt climate event in the tropics, *Nat. Commun.*, 6, 8061, <https://doi.org/10.1038/ncomms9061>, 2015.
- Prietzl, J., Dechamps, N., and Spielvogel, S.: Analysis of non-cellulosic polysaccharides helps to reveal the history of thick organic surface layers on calcareous Alpine soils, *Plant Soil*, 365, 93–114, <https://doi.org/10.1007/s11104-012-1340-2>, 2013.
- Rach, O., Brauer, A., Wilkes, H., and Sachse, D.: Delayed hydrological response to Greenland cooling at the onset of the Younger Dryas in western Europe, *Nat. Geosci.*, 7, 109–112, 2014.
- Rach, O., Kahmen, A., Brauer, A., and Sachse, D.: A dual-biomarker approach for quantification of changes in relative humidity from sedimentary lipid *D/H* ratios, *Clim. Past*, 13, 741–757, <https://doi.org/10.5194/cp-13-741-2017>, 2017.
- Rao, Z., Zhu, Z., Jia, G., Henderson, A. C. G., Xue, Q., and Wang, S.: Compound specific δD values of long chain *n*-alkanes derived from terrestrial higher plants are indicative of the δD of meteoric waters: Evidence from surface soils in eastern China, *Org. Geochem.*, 40, 922–930, <https://doi.org/10.1016/j.orggeochem.2009.04.011>, 2009.
- Rao, Z., Jia, G., Qiang, M., and Zhao, Y.: Assessment of the difference between mid- and long chain compound specific $\delta D_{n\text{-alkanes}}$ values in lacustrine sediments as a paleoclimatic indicator, *Org. Geochem.*, 76, 104–117, <https://doi.org/10.1016/j.orggeochem.2014.07.015>, 2014.

- Rasmussen, S. O., Andersen, K. K., Svensson, A. M., Steffensen, J. P., Vinther, B. M., Clausen, H. B., Siggaard-Andersen, M.-L., Johnsen, S. J., Larsen, L. B., Dahl-Jensen, D., Bigler, M., Röthlisberger, R., Fischer, H., Goto-Azuma, K., Hansson, M. E., and Ruth, U.: A new Greenland ice core chronology for the last glacial termination, *J. Geophys. Res.-Atmos.*, 111, 1–16, <https://doi.org/10.1029/2005JD006079>, 2006.
- Rasmussen, S. O., Vinther, B. M., Clausen, H. B., and Andersen, K. K.: Early Holocene climate oscillations recorded in three Greenland ice cores, *Quaternary Sci. Rev.*, 26, 1907–1914, <https://doi.org/10.1016/j.quascirev.2007.06.015>, 2007.
- Rasmussen, S. O., Bigler, M., Blockley, S. P., Blunier, T., Buchardt, S. L., Clausen, H. B., Cvijanovic, I., Dahl-Jensen, D., Johnsen, S. J., Fischer, H., Gkinis, V., Guillevic, M., Hoek, W. Z., Lowe, J. J., Pedro, J. B., Popp, T., Seierstad, I. K., Steffensen, J. P., Svensson, A. M., Vallelonga, P., Vinther, B. M., Walker, M. J. C., Wheatley, J. J., and Winstrup, M.: A stratigraphic framework for abrupt climatic changes during the Last Glacial period based on three synchronized Greenland ice-core records: Refining and extending the INTIMATE event stratigraphy, *Quaternary Sci. Rev.*, 106, 14–28, <https://doi.org/10.1016/j.quascirev.2014.09.007>, 2014.
- Reimer, P., Bard, E., Bayliss, A., Beck, J., Blackwell, P., Ramsey, C., Buck, C., Cheng, H., Edwards, R., Friedrich, M., Grootes, P., Guilderson, T., Hafliðason, H., Hajdas, I., Hatté, C., Heaton, T., Hoffmann, D., Hogg, A., Hughen, K., Kaiser, K., Kromer, B., Manning, S., Niu, M., Reimer, R., Richards, D., Scott, E., Southon, J., Staff, R., Turney, C., and van der Plicht, J.: Intcal13 and Marine13 radiocarbon age calibration curves 0–50,000 years cal BP, *Radiocarbon*, 55, 1869–1887, https://doi.org/10.2458/azu_js_rc.55.16947, 2013.
- Renssen, H., Goosse, H., and Fichefet, T.: Simulation of Holocene cooling events in a coupled climate model, *Quaternary Sci. Rev.*, 26, 2019–2029, <https://doi.org/10.1016/j.quascirev.2007.07.011>, 2007.
- Rind, D.: The Sun's Role in Climate Variations, *Science*, 296, 673–677, <https://doi.org/10.1126/science.1069562>, 2002.
- Roden, J. S. and Ehleringer, J. R.: Observations of Hydrogen and Oxygen Isotopes in Leaf Water Confirm the Craig-Gordon Model under Wide-Ranging Environmental Conditions, *Plant Physiol.*, 120, 1165–1173, 1999.
- Rozanski, K.: Deuterium and oxygen-18 in European Groundwaters – Links to Atmospheric Circulation in the Past, *Chem. Geol.*, 52, 349–363, 1985.
- Rozanski, K., Araguás-Araguás, L., and Gonfiantini, R.: Isotopic Patterns in Modern Global Precipitation, in: *Climate Change in Continental Isotopic Records*, edited by: Swart, P. K., Lohmann, K. C., Mckenzie, J., and Savin, S., 1–36, Geophysical Monograph Series 78, American Geophysical Union (AGU), Washington DC, <https://doi.org/10.1029/GM078p0001>, 1993.
- Sachse, D., Radke, J., and Gleixner, G.: Hydrogen isotope ratios of recent lacustrine sedimentary *n*-alkanes record modern climate variability, *Geochim. Cosmochim. Ac.*, 68, 4877–4889, <https://doi.org/10.1016/j.gca.2004.06.004>, 2004.
- Sachse, D., Billault, I., Bowen, G. J., Chikaraishi, Y., Dawson, T. E., Feakins, S. J., Freeman, K. H., Magill, C. R., McInerney, F. A., van der Meer, M. T. J., Polissar, P., Robins, R. J., Sachs, J. P., Schmidt, H.-L., Sessions, A. L., White, J. W. C., and West, J. B.: Molecular Paleohydrology: Interpreting the Hydrogen-Isotopic Composition of Lipid Biomarkers from Photosynthesizing Organisms, *Annu. Rev.*, 40, 221–249, <https://doi.org/10.1146/annurev-earth-042711-105535>, 2012.
- Sauer, P. E., Eglinton, T. I., Hayes, J. M., Schimmelmann, A., and Sessions, A. L.: Compound-specific *D/H* ratios of lipid biomarkers from sediments as a proxy for environmental and climatic conditions, *Geochim. Cosmochim. Ac.*, 65, 213–222, [https://doi.org/10.1016/S0016-7037\(00\)00520-2](https://doi.org/10.1016/S0016-7037(00)00520-2), 2001.
- Scharf, B. W. and Menn, U.: Hydrology and morphometry, in: *Limnology of Eifel maar lakes*, edited by: Scharf, B. and Björk, S., 43–62, E. Schweizerbart, Stuttgart, Germany, 1992.
- Schmidt, H.-L., Werner, R. A., and Roßmann, A.: ¹⁸O Pattern and biosynthesis of natural plant products, *Phytochemistry*, 58, 9–32, [https://doi.org/10.1016/S0031-9422\(01\)00017-6](https://doi.org/10.1016/S0031-9422(01)00017-6), 2001.
- Sessions, A. L., Burgoyne, T. W., Schimmelmann, A., and Hayes, J. M.: Fractionation of hydrogen isotopes in lipid biosynthesis, *Org. Geochem.*, 30, 1193–1200, 1999.
- Sirocko, F., Dietrich, S., Veres, D., Grootes, P. M., Schabermohr, K., Seelos, K., Nadeau, M., Kromer, B., Rothacker, L., Röhner, M., Krbetschek, M., Appleby, P., Hambach, U., Rolf, C., Sudo, M., and Grim, S.: Multi-proxy dating of Holocene maar lakes and Pleistocene dry maar sediments in the Eifel, Germany, *Quaternary Sci. Rev.*, 62, 56–76, <https://doi.org/10.1016/j.quascirev.2012.09.011>, 2013.
- Sirocko, F., Knapp, H., Dreher, F., Förster, M. W., Albert, J., Brunck, H., Veres, D., Dietrich, S., Zech, M., Hambach, U., Röhner, M., Rudert, S., Schwibus, K., Adams, C., and Sigl, P.: The ELSA-Vegetation-Stack: Reconstruction of Landscape Evolution Zones (LEZ) from laminated Eifel maar sediments of the last 60,000 years, *Global Planet. Change*, 142, 108–135, <https://doi.org/10.1016/j.gloplacha.2016.03.005>, 2016.
- Stenni, B., Masson-Delmotte, V., Selmo, E., Oerter, H., Meyer, H., Röthlisberger, R., Jouzel, J., Cattani, O., Falourd, S., Fischer, H., Hoffmann, G., Iacumin, P., Johnsen, S. J., Minster, B., and Udisti, R.: The deuterium excess records of EPICA Dome C and Dronning Maud Land ice cores (East Antarctica), *Quaternary Sci. Rev.*, 29, 146–159, <https://doi.org/10.1016/j.quascirev.2009.10.009>, 2010.
- Sternberg, L. S. L., DeNiro, M. J., and Savidge, R. A.: Oxygen Isotope Exchange between Metabolites and Water during Biochemical Reactions Leading to Cellulose Synthesis, *Plant Physiol.*, 82, 423–427, 1986.
- Stuiver, M. and Braziunas, T. F.: The Solar Component of the Atmospheric ¹⁴C Record, in: *Secular Solar and Geomagnetic Variations in the Last 10,000 Years*, edited by: Stephenson, F. R. and Wolfendale, A. W., 245–266, Springer, Dordrecht, 1988.
- Stumpp, C., Klaus, J., and Stichler, W.: Analysis of long-term stable isotopic composition in German precipitation, *J. Hydrol.*, 517, 351–361, <https://doi.org/10.1016/j.jhydrol.2014.05.034>, 2014.
- Tarasov, P. E., Müller, S., Zech, M., Andreeva, D., Diekmann, B., and Leipe, C.: Last glacial vegetation reconstructions in the extreme-continental eastern Asia: Potentials of pollen and *n*-alkane biomarker analyses, *Quaternary Int.*, 290–291, 253–263, <https://doi.org/10.1016/j.quaint.2012.04.007>, 2013.
- Thornalley, D. J. R., Elderfield, H., and McCave, I. N.: Holocene oscillations in temperature and salinity of the surface subtropical North Atlantic, *Nature*, 457, 711–714, <https://doi.org/10.1038/nature07717>, 2009.
- Thornalley, D. J. R., McCave, I. N., and Elderfield, H.: Freshwater input and abrupt deglacial climate change

- in the North Atlantic, *Paleoceanography*, 25, 1–16, <https://doi.org/10.1029/2009PA001772>, 2010.
- Thornalley, D. J. R., Elderfield, H., and McCave, I. N.: Reconstructing North Atlantic deglacial surface hydrography and its link to the Atlantic overturning circulation, *Global Planet. Change*, 79, 163–175, <https://doi.org/10.1016/j.gloplacha.2010.06.003>, 2011.
- Tipple, B. J., Berke, M. A., Doman, C. E., Khachatryan, S., and Ehleringer, J. R.: Leaf-wax *n*-alkanes record the plant-water environment at leaf flush, *P. Natl. Acad. Sci. USA*, 110, 2659–2664, <https://doi.org/10.1073/pnas.1213875110>, 2013.
- Tipple, B. J., Berke, M. A., Hambach, B., Roden, J. S., and Ehleringer, J. R.: Predicting leaf wax *n*-alkane $^2\text{H}/^1\text{H}$ ratios: Controlled water source and humidity experiments with hydroponically grown trees confirm predictions of Craig-Gordon model, *Plant Cell Environ.*, 38, 1035–1047, <https://doi.org/10.1111/pce.12457>, 2015.
- Tuthorn, M., Zech, M., Ruppenthal, M., Oelmann, Y., Kahmen, A., del Valle, H. F., Wilcke, W., and Glaser, B.: Oxygen isotope ratios ($^{18}\text{O}/^{16}\text{O}$) of hemicellulose-derived sugar biomarkers in plants, soils and sediments as paleoclimate proxy II: Insight from a climate transect study, *Geochim. Cosmochim. Ac.*, 126, 624–634, <https://doi.org/10.1016/j.gca.2013.11.002>, 2014.
- Tuthorn, M., Zech, R., Ruppenthal, M., Oelmann, Y., Kahmen, A., del Valle, H. F., Eglinton, T., Rozanski, K., and Zech, M.: Coupling $\delta^2\text{H}$ and $\delta^{18}\text{O}$ biomarker results yields information on relative humidity and isotopic composition of precipitation – a climate transect validation study, *Biogeosciences*, 12, 3913–3924, <https://doi.org/10.5194/bg-12-3913-2015>, 2015.
- van der Plicht, J., van Geel, B., Bohncke, S. J. P., Bos, J. A. A., Blaauw, M., Speranza, A. O. M., Muscheler, R., and Björck, S.: The Preboreal climate reversal and a subsequent solar-forced climate shift, *J. Quaternary Sci.*, 19, 263–269, <https://doi.org/10.1002/jqs.835>, 2004.
- Voelker, S. L., Brooks, J. R., Meinzer, F. C., Roden, J., Pazdur, A., Pawelczyk, S., Hartsough, P., Snyder, K., Plavcova, L., and Santrucek, J.: Reconstructing relative humidity from plant $\delta^{18}\text{O}$ and δD as deuterium deviations from the global meteoric water line, *Ecol. Appl.*, 24, 960–975, <https://doi.org/10.1890/13-0988.1>, 2014.
- Voelker, S. L., Stambaugh, M. C., Guyette, R. P., Feng, X., Grimley, D. A., Leavitt, S. W., Panyushkina, I., Grimm, E. C., Marsicek, J. P., Shuman, B., and Brandon Curry, B.: Deglacial hydroclimate of midcontinental North America, *Quaternary Res.*, 83, 336–344, <https://doi.org/10.1016/j.yqres.2015.01.001>, 2015.
- Volkman, J. K., Barrett, S. M., Blackburn, S. I., Mansour, M. P., Sikes, E. L., and Gelin, F.: Microalgal biomarkers: A review of recent research developments, *Org. Geochem.*, 29, 1163–1179, [https://doi.org/10.1016/S0146-6380\(98\)00062-X](https://doi.org/10.1016/S0146-6380(98)00062-X), 1998.
- Vonmoos, M., Beer, J., and Muscheler, R.: Large variations in Holocene solar activity: Constraints from ^{10}Be in the Greenland Ice Core Project ice core, *J. Geophys. Res.-Space*, 111, 1–14, <https://doi.org/10.1029/2005JA011500>, 2006.
- Wagner, F., Bohncke, S. J. P., Dilcher, D. L., Kürschner, W. M., van Geel, B., and Visscher, H.: Century-Scale Shifts in Early Holocene Atmospheric CO_2 Concentration, *Science*, 284, 1971–1974, 1999.
- Walker, C. D. and Brunel, J.-P.: Examining Evapotranspiration in a Semi-Arid Region using Stable Isotopes of Hydrogen and Oxygen, *J. Hydrol.*, 118, 55–75, 1990.
- Waterhouse, J. S., Cheng, S., Juchelka, D., Loader, N. J., McCarroll, D., Switsur, V. R., and Gautam, L.: Position-specific measurement of oxygen isotope ratios in cellulose: Isotopic exchange during heterotrophic cellulose synthesis, *Geochim. Cosmochim. Ac.*, 112, 178–191, <https://doi.org/10.1016/j.gca.2013.02.021>, 2013.
- Weninger, B. and Jöris, O.: A ^{14}C age calibration curve for the last 60 ka: the Greenland-Hulu U/Th timescale and its impact on understanding the Middle to Upper Paleolithic transition in Western Eurasia, *J. Hum. Evol.*, 55, 772–781, <https://doi.org/10.1016/j.jhevol.2008.08.017>, 2008.
- Wolfe, B. B., Edwards, T. W. D., and Aravena, R.: Changes in carbon and nitrogen cycling during tree-line retreat recorded in the isotopic content of lacustrine organic matter, western Taimyr Peninsula, Russia, Holocene, 9, 215–222, <https://doi.org/10.1191/095968399669823431>, 1999.
- Yakir, D. and DeNiro, M. J.: Oxygen and Hydrogen Isotope Fractionation during Cellulose Metabolism in *Lemna gibba* L., *Plant Ecol.*, 93, 325–332, 1990.
- Zech, M. and Glaser, B.: Compound-specific $\delta^{18}\text{O}$ analyses of neutral sugars in soils using gas chromatography-pyrolysis-isotope ratio mass spectrometry: problems, possible solutions and a first application, *Rapid Commun. Mass Sp.*, 23, 3522–3532, <https://doi.org/10.1002/rcm.4278>, 2009.
- Zech, M., Zech, R., and Glaser, B.: A 240,000-year stable carbon and nitrogen isotope record from a loess-like palaeosol sequence in the Tumara Valley, Northeast Siberia, *Chem. Geol.*, 242, 307–318, <https://doi.org/10.1016/j.chemgeo.2007.04.002>, 2007.
- Zech, M., Zech, R., Bugge, B., and Zöller, L.: Novel methodological approaches in loess research – interrogating biomarkers and compound-specific stable isotopes, *E&G Quaternary Sci. J.*, 60, 13, <https://doi.org/10.3285/eg.60.1.12>, 2011.
- Zech, M., Werner, R. A., Juchelka, D., Kalbitz, K., Bugge, B., and Glaser, B.: Absence of oxygen isotope fractionation/exchange of (hemi-) cellulose derived sugars during litter decomposition, *Org. Geochem.*, 42, 1470–1475, <https://doi.org/10.1016/j.orggeochem.2011.06.006>, 2012.
- Zech, M., Tuthorn, M., Detsch, F., Rozanski, K., Zech, R., Zöller, L., Zech, W., and Glaser, B.: A 220 ka terrestrial $\delta^{18}\text{O}$ and deuterium excess biomarker record from an eolian permafrost palaeosol sequence, NE-Siberia, *Chem. Geol.*, 360–361, 220–230, <https://doi.org/10.1016/j.chemgeo.2013.10.023>, 2013a.
- Zech, M., Tuthorn, M., Glaser, B., Amelung, W., Huwe, B., Zech, W., Zöller, L., and Löffler, J.: Natural abundance of $\delta^{18}\text{O}$ of sugar biomarkers in topsoils along a climate transect over the Central Scandinavian Mountains, Norway, *J. Plant Nutr. Soil Sc.*, 176, 12–15, <https://doi.org/10.1002/jpln.201200365>, 2013b.
- Zech, M., Tuthorn, M., Schlütz, F., Zech, W., and Glaser, B.: A 16-ka $\delta^{18}\text{O}$ record of lacustrine sugar biomarkers from the High Himalaya reflects Indian Summer Monsoon variability, *J. Paleolimnol.*, 51, 241–251, <https://doi.org/10.1007/s10933-013-9744-4>, 2014a.
- Zech, M., Mayr, C., Tuthorn, M., Leiber-Sauheitl, K., and Glaser, B.: Oxygen isotope ratios ($^{18}\text{O}/^{16}\text{O}$) of hemicellulose-derived sugar biomarkers in plants, soils and sediments as paleoclimate proxy I: Insight from a climate chamber experiment, *Geochim. Cosmochim. Ac.*, 126, 614–623, <https://doi.org/10.1016/j.gca.2013.10.048>, 2014b.

J. Hepp et al.: How dry was the Younger Dryas?

733

Zech, M., Zech, R., Rozanski, K., Gleixner, G., and Zech, W.: Do *n*-alkane biomarkers in soils/sediments reflect the $\delta^2\text{H}$ isotopic composition of precipitation? A case study from Mt. Kilimanjaro and implications for paleoaltimetry and paleoclimate research, *Isot. Environ. Health. S.*, 51, 508–524, <https://doi.org/10.1080/10256016.2015.1058790>, 2015.

Zolitschka, B.: A 14,000 year sediment yield record from western Germany based on annually laminated lake sediments, *Geomorphology*, 22, 1–17, [https://doi.org/10.1016/S0169-555X\(97\)00051-2](https://doi.org/10.1016/S0169-555X(97)00051-2), 1998.

Supplement of *Clim. Past*, 15, 713–733, 2019
<https://doi.org/10.5194/cp-15-713-2019-supplement>
© Author(s) 2019. This work is distributed under
the Creative Commons Attribution 4.0 License.



Supplement of

How dry was the Younger Dryas? Evidence from a coupled $\delta^2\text{H}$ – $\delta^{18}\text{O}$ biomarker paleohygrometer applied to the Gemündener Maar sediments, Western Eifel, Germany

Johannes Hepp et al.

Correspondence to: Johannes Hepp (johannes-hepp@gmx.de)

The copyright of individual parts of the supplement might differ from the CC BY 4.0 License.

Tab. S1: Weighted mean $\delta^2\text{H}$ values of leaf wax-derived *n*-alkanes (*n*-C₂₇ and *n*-C₂₉) and $\delta^{18}\text{O}$ values of hemicellulose-derived sugar (arabinose). The reported standard errors represent the analytical uncertainties. Also calculated/reconstructed $\delta^2\text{H}/\delta^{18}\text{O}_{\text{leaf-water}}$, d-excess of leaf water, mean daytime vegetation period relative humidities (RH_{dv}), and $\delta^2\text{H}/\delta^{18}\text{O}_{\text{source-water}}$ values are displayed. The reported uncertainties of d-excess and RH represent expanded uncertainties calculated using the uncertainty propagation law.

Depth [cm]	Age [a BP]	Measured				Calculated/Reconstructed				
		$\delta^2\text{H}_{n\text{-alkane}}$ [‰]	$\delta^{18}\text{O}_{\text{sugar}}$ [‰]	$\delta^2\text{H}_{\text{leaf-water}}$ [‰]	$\delta^{18}\text{O}_{\text{leaf-water}}$ [‰]	d-excess of leaf water [‰]	RH _{dv} [%]	$\delta^2\text{H}_{\text{source-water}}$ [‰]	$\delta^{18}\text{O}_{\text{source-water}}$ [‰]	
607.5	10139	-163.7 ± 3.3	36.1 ± 0.9	-4.4	8.9	-73 ± 25	59 ± 13	-49	-7	
608.5	10180	-156.8 ± 2.7	36.6 ± 1.2	3.9	9.3	-68 ± 21	61 ± 11	-38	-6	
609.5	10222	-159.0 ± 0.5	37.8 ± 0.7	1.2	10.5	-80 ± 4	55 ± 2	-48	-7	
611.5	10305	-205.3 ± 1.8	30.7 ± 0.5	-53.9	3.6	-81 ± 14	54 ± 7	-104	-14	
612.5	10346	-205.4 ± 1.9	36.4 ± 0.1	-54.1	9.2	-125 ± 15	32 ± 8	-129	-17	
615.5	10470	-146.0 ± 1.4	38.8 ± 0.3	16.6	11.5	-72 ± 11	59 ± 6	-28	-4	
617.5	10553	-170.9 ± 0.9	38.2 ± 0.9	-13.0	10.9	-97 ± 7	46 ± 4	-72	-10	
619.5	10636	-159.2 ± 1.2	37.3 ± 0.2	0.9	10.0	-77 ± 9	57 ± 5	-46	-7	
620.5	10678	-173.7 ± 1.4	40.6 ± 0.5	-16.3	13.2	-118 ± 11	35 ± 6	-87	-12	
622.5	10761	-200.1 ± 0.0	35.3 ± 0.2	-47.7	8.1	-110 ± 0	39 ± 0	-114	-15	
623.5	10802	-194.9 ± 2.1	37.9 ± 1.0	-41.5	10.7	-124 ± 16	32 ± 9	-115	-16	
624.5	10844	-202.8 ± 1.7	36.8 ± 0.4	-50.9	9.5	-125 ± 13	32 ± 7	-125	-17	
625.5	10885	-166.8 ± 1.8	37.1 ± 0.4	-8.0	9.8	-84 ± 14	53 ± 7	-59	-8	
626.5	10927	-174.6 ± 2.4	37.4 ± 0.5	-17.4	10.1	-96 ± 19	47 ± 10	-75	-10	
627.5	10968	-179.2 ± 2.2	36.7 ± 1.0	-22.9	9.5	-96 ± 17	47 ± 9	-81	-11	
628.5	11010	-171.6 ± 0.6	36.6 ± 1.0	-13.8	9.4	-86 ± 5	52 ± 2	-66	-9	
629.5	11051	-170.4 ± 0.2	32.4 ± 2.7	-12.4	5.3	-53 ± 3	69 ± 2	-46	-7	
630.5	11092	-173.0 ± 1.3	32.5 ± 0.6	-15.4	5.3	-57 ± 10	68 ± 5	-51	-7	
631.5	11134	-170.2 ± 1.1	34.1 ± 0.4	-12.1	6.9	-65 ± 9	63 ± 5	-52	-7	
632.5	11175	-169.0 ± 2.7	34.1 ± 0.2	-10.7	6.9	-64 ± 21	64 ± 11	-50	-7	
633.5	11217	-174.8 ± 2.2	28.6 ± 0.6	-17.7	1.6	-30 ± 17	82 ± 9	-38	-6	
634.5	11258	-169.2 ± 0.8	34.2 ± 0.6	-11.0	7.0	-65 ± 6	63 ± 3	-51	-7	
635.5	11300	-189.2 ± 2.5	36.3 ± 1.6	-34.8	9.1	-105 ± 19	42 ± 10	-98	-13	
636.5	11341	-177.5 ± 2.0	35.6 ± 0.4	-20.9	8.4	-86 ± 15	52 ± 8	-73	-10	
637.5	11383	-170.1 ± 3.9	38.0 ± 1.5	-12.0	10.7	-95 ± 30	47 ± 16	-69	-10	
639.5	11466	-172.5 ± 1.9	40.1 ± 1.4	-14.8	12.8	-113 ± 15	38 ± 8	-83	-11	
640.5	11507	-165.1 ± 4.2	36.6 ± 0.3	-6.0	9.3	-78 ± 32	56 ± 17	-54	-8	
641.5	11549	-181.7 ± 1.2	33.1 ± 0.7	-25.8	5.9	-72 ± 9	60 ± 5	-70	-10	
643.5	11630	-202.3 ± 2.0	32.1 ± 0.2	-50.4	4.9	-88 ± 15	51 ± 8	-104	-14	
644.5	11669	-181.1 ± 1.6	34.4 ± 0.3	-25.1	7.2	-81 ± 12	55 ± 6	-74	-10	
645.5	11709	-199.1 ± 0.9	33.4 ± 0.4	-46.6	6.2	-94 ± 7	48 ± 4	-104	-14	
647.5	11788	-200.4 ± 3.3	35.7 ± 0.5	-48.1	8.5	-114 ± 25	37 ± 13	-116	-16	
648.5	11828	-193.5 ± 0.8	34.2 ± 0.2	-39.9	7.0	-94 ± 6	48 ± 3	-97	-13	
649.5	11867	-212.3 ± 2.6	34.6 ± 0.3	-62.3	7.4	-119 ± 20	35 ± 10	-134	-18	
651.5	11947	-186.7 ± 1.8	33.0 ± 0.2	-31.8	5.8	-77 ± 14	57 ± 7	-79	-11	
652.5	11986	-188.8 ± 1.3	30.9 ± 0.4	-34.3	3.8	-64 ± 10	64 ± 5	-74	-10	
653.5	12026	-186.3 ± 1.4	32.5 ± 0.5	-31.3	5.4	-73 ± 11	59 ± 6	-76	-10	
656.5	12145	-196.4 ± 0.6	33.8 ± 0.7	-43.4	6.6	-95 ± 5	48 ± 2	-101	-14	
657.5	12185	-167.2 ± 5.8	34.3 ± 0.4	-8.6	7.1	-63 ± 44	64 ± 23	-48	-7	
659.5	12264	-201.2 ± 0.6	32.7 ± 0.7	-49.0	5.5	-92 ± 5	49 ± 3	-105	-14	
660.5	12303	-191.6 ± 1.1	28.1 ± 0.8	-37.6	1.0	-46 ± 8	73 ± 4	-67	-9	
661.5	12343	-210.7 ± 1.9	32.0 ± 0.7	-60.4	4.8	-98 ± 15	46 ± 8	-119	-16	
663.5	12422	-197.5 ± 0.7	33.0 ± 0.5	-44.6	5.9	-90 ± 6	50 ± 3	-99	-13	
664.5	12462	-189.2 ± 4.9	34.1 ± 0.7	-34.8	6.9	-88 ± 38	51 ± 20	-88	-12	
665.5	12502	-171.2 ± 4.6	33.2 ± 0.1	-13.3	6.0	-60 ± 35	66 ± 19	-50	-7	
667.5	12581	-185.8 ± 1.1	34.9 ± 0.4	-30.8	7.7	-90 ± 9	50 ± 5	-85	-12	
668.5	12621	-216.0 ± 2.9	33.6 ± 0.1	-66.6	6.4	-116 ± 22	36 ± 12	-136	-18	
669.5	12660	-173.6 ± 1.4	30.7 ± 0.0	-16.2	3.6	-44 ± 11	74 ± 6	-44	-6	
671.5	12766	-172.7 ± 1.5	33.1 ± 0.4	-15.1	6.0	-61 ± 11	65 ± 6	-53	-8	
672.5	12823	-192.5 ± 0.0	32.5 ± 0.8	-38.7	5.3	-80 ± 1	55 ± 0	-87	-12	
673.5	LST	n.d. ± n.d.	n.d. ± n.d.	n.d.	n.d.	n.d. ± n.d.	n.d. ± n.d.	n.d.	n.d.	
679.5	LST	n.d. ± n.d.	n.d. ± n.d.	n.d.	n.d.	n.d. ± n.d.	n.d. ± n.d.	n.d.	n.d.	
681.5	12919	-176.8 ± 1.8	35.7 ± 0.4	-20.0	8.5	-85 ± 14	52 ± 8	-72	-10	
682.5	12938	-175.0 ± 2.3	33.4 ± 0.4	-17.8	6.2	-66 ± 17	63 ± 9	-59	-8	
683.5	12957	-177.0 ± 2.4	34.8 ± 1.1	-20.2	7.6	-79 ± 18	56 ± 10	-68	-9	
685.5	12996	-179.6 ± 1.5	35.4 ± 0.1	-23.3	8.2	-86 ± 12	52 ± 6	-76	-10	
687.5	13035	-221.3 ± 2.3	33.2 ± 0.3	-73.0	6.0	-120 ± 18	34 ± 9	-144	-19	
688.5	13054	-184.3 ± 2.3	35.0 ± 0.5	-28.9	7.8	-89 ± 18	50 ± 9	-83	-11	
689.5	13074	-177.1 ± 3.4	29.5 ± 0.6	-20.3	2.4	-39 ± 26	77 ± 14	-46	-7	
692.5	13132	-182.3 ± 2.4	34.5 ± 0.6	-26.6	7.3	-83 ± 19	54 ± 10	-77	-11	
693.5	13151	-169.0 ± 3.0	35.9 ± 0.1	-10.7	8.6	-77 ± 23	57 ± 12	-58	-8	

n.d. = not determined; LST = Laacher See Tephra

F. Manuscript 6: Hepp et al.

in preparation for *Journal of Paleolimnology*

1 **Late Glacial to Early Holocene $\delta^2\text{H}_{n\text{-alkane}}$ and $\delta^{18}\text{O}_{\text{sugar}}$ records from Lake Bergsee, Black Forest,**
2 **Germany – potential and limitations**

3
4 Johannes Hepp^{a,b,1,#}, Lucas Kämpf^{c,2}, Damien Rius^d, Mario Tuthorn^{b,3}, Lucas Bittner^b, Laurent Millet^d, Fanny
5 Duprat-Qualid^d, Bruno Glaser^b, Michael Zech^{b,e,4}

6
7 ^a*Chair of Geomorphology and BayCEER, University of Bayreuth, Universitätsstrasse 30, D-95440 Bayreuth,*
8 *Germany*

9 ^b*Institute of Agronomy and Nutritional Sciences, Soil Biogeochemistry, Martin-Luther-University Halle-*
10 *Wittenberg, Von-Seckendorff-Platz 3, D-06120 Halle, Germany*

11 ^c*Institute for Soil Science and Site Ecology, Site Ecology and Plant Nutrition, Piennner Strasse 19, D-01737*
12 *Tharandt, Germany*

13 ^d*CNRS UMR 6249, Laboratoire Chrono-Environnement, UFR des Sciences et Techniques, Universite de*
14 *Bourgogne-Franche-Comte, 16 Route de Gray, F-25030 Besancon, France*

15 ^e*Institute of Geography, Chair of Landscape- and Geoecology, Dresden University of Technology,*
16 *Helmholtzstrasse 10, D-01062 Dresden, Germany*

17
18 [#]*corresponding author: johannes-hepp@gmx.de*

¹ Present Address: *Chair of Geomorphology and BayCEER, University of Bayreuth, Universitätsstrasse 30, D-95440 Bayreuth, Germany*

² Present Address: *CNRS UMR 6249, Laboratoire Chrono-Environnement, UFR des Sciences et Techniques, Universite de Bourgogne-Franche-Comte, 16 Route de Gray, F-25030 Besancon, France*

³ Present Address: *Thermo Fisher Scientific, Hanna-Kunath-Str. 11, D-28199 Bremen, Germany*

⁴ Present Address: *Institute of Geography, Chair of Landscape- and Geoecology, Dresden University of Technology, Helmholtzstrasse 10, D-01062 Dresden, Germany*

19 **Keywords**

20 lacustrine sediments, biomarkers, source identification, oxygen isotopes, hydrogen isotopes, leaf water,
21 evaporative enrichment

22

23 **Abstract**

24 During the last decade, compound-specific $\delta^2\text{H}$ analyses of leaf wax-derived *n*-alkane biomarkers became
25 a popular tool in paleoclimate and particularly paleolimnological research. More recently, additionally
26 compound-specific $\delta^{18}\text{O}$ analyses of plant-derived sugar biomarkers emerged as paleoclimate proxy. By
27 applying both tools to the Late Glacial to Early Holocene sedimentary archive of Lake Bergsee, Black Forest,
28 Germany, we aimed at contributing to the paleoclimate reconstruction of Central Europe.

29 A prerequisite for the interpretation of $\delta^2\text{H}$ and $\delta^{18}\text{O}$ records obtained from sedimentary biomarkers is the
30 knowledge about the primarily terrestrial or aquatic origin of the investigated biomarkers. The long-chain
31 *n*-alkanes of Lake Bergsee reflect the vegetation history as derived from pollen results and can be
32 attributed with reasonable certainty to terrestrial sources/plants. Similarly, the high relative abundance
33 of fucose strongly suggests a primarily aquatic origin of the sugar biomarkers. By contrast, the origin of the
34 mid-chain *n*-alkane *n*-C₂₃ is prone to large uncertainty because it can be produced in high amounts by both
35 terrestrial plants such as birch and aquatic organisms. Moreover, a straightforward interpretation of the
36 terrestrial $\delta^2\text{H}_{n\text{-alkane}}$ and the aquatic $\delta^{18}\text{O}_{\text{sugar}}$ records of Lake Bergsee is challenging due to unknown degrees
37 of evapo(transpi)rative enrichment of leaf and lake water, respectively.

38 Finally, we tested the applicability of the recently proposed 'dual-biomarker approach' and the 'coupled
39 $\delta^2\text{H}_{n\text{-alkane}} - \delta^{18}\text{O}_{\text{sugar}}$ approach' as possible tools for reconstructing relative humidity and lake water
40 evaporation. Our discussion concerning possible uncertainties advises, however, caution. In the case of Lake
41 Bergsee, we refrain from applying the 'dual-biomarker approach' because (i) lake water enrichment cannot
42 be excluded but is rather very likely, (ii) *n*-C₂₃ is no robust aquatic biomarker and (iii) the $\varepsilon^2_{\text{bio}}$ value of
43 aquatic *n*-alkanes is an issue of major uncertainty. Minor changes in the contribution of aquatic versus
44 terrestrial *n*-C₂₃ are likely to have a significant influence on the $\delta^2\text{H}$ record of *n*-C₂₃. We also refrain from
45 applying the 'coupled $\delta^2\text{H}_{n\text{-alkane}} - \delta^{18}\text{O}_{\text{sugar}}$ approach', because neither a reliable pure terrestrial nor a
46 reliable pure aquatic $\delta^2\text{H}$ and $\delta^{18}\text{O}$ coupling is possible based on the source identification results for Lake
47 Bergsee.

48

49 1 Introduction

50 The analyses of lipid biomarkers became a popular tool in paleoenvironmental and -climate research (e.g.
51 Sachse et al. 2012; Diefendorf and Freimuth 2016). In paleolimnological studies, for instance, the hydrogen
52 isotopic composition from aquatic-derived lipids (aquatic $\delta^2\text{H}$ from short- and mid-chain *n*-alkanes and *n*-
53 alkanolic acids) from lacustrine sedimentary archives are used for reconstructing the hydrogen isotope
54 composition of lake water ($\delta^2\text{H}_{\text{lake-water}}$) and consequently precipitation (e.g. Jacob et al. 2007; Seki et al.
55 2011; Rach et al. 2014; Muschitiello et al. 2015). Due to lake evaporation, lake water can become
56 isotopically enriched, thus weakening the direct link to the precipitation signal (Hou et al. 2008; Hepp et
57 al. 2015). Alternatively, leaf wax-derived lipid biomarkers (e.g. long-chain *n*-alkanes and *n*-alkanoic) are
58 extracted from lacustrine sediments and measured in order to obtain terrestrial compound-specific $\delta^2\text{H}$
59 values (e.g. Sachse et al. 2006; Rao et al. 2014). Those values in turn reflect the isotope composition of leaf
60 water from higher terrestrial plants grown in the catchment, which can be related to precipitation
61 modified by leaf water ^2H enrichment caused by evapotranspiration (Kahmen et al. 2013; Zech et al. 2015).
62 The extent of leaf and lake water evapo(transpi)rative enrichment is mainly driven by relative humidity
63 normalized to leaf temperature (as e.g. reviewed by Cernusak et al. 2016) and inflow (input) to evaporation
64 ratio as well as relative humidity normalized to lake temperature (e.g. review by Gibson et al. 2016). When
65 leaf/lake water enrichment cannot be ruled out, the interpretation of $\delta^2\text{H}_{n\text{-alkane}}$ -based climate proxies have
66 to remain often qualitativ. Comparable to the $\delta^2\text{H}_{n\text{-alkane}}$, compound-specific oxygen stable isotope ($\delta^{18}\text{O}$)
67 analysis of individual sugar biomarkers offer insight into the isotopic composition of precipitation (Zech
68 and Glaser 2009; Zech et al. 2014b). When the sugars originate from aquatic sources, they reflect lake
69 water and can thus be interpreted either in terms of reflecting $\delta^{18}\text{O}$ of past precipitation or as
70 precipitation/evaporation proxy due to lake water evaporative ^{18}O enrichment (Hepp et al. 2015). When
71 sugars originate primarily from terrestrial sources, they reflect precipitation modified by
72 evapotranspirative enrichment of leaf water (Tuthorn et al. 2014; Zech et al. 2014a). The recently proposed
73 coupling of $\delta^2\text{H}_{n\text{-alkane}}$ results with $\delta^{18}\text{O}_{\text{sugar}}$ results (Zech et al. 2013; Tuthorn et al. 2015; Hepp et al. 2017)
74 as well as the 'dual-biomarker approach' (using the difference between terrestrial and aquatic *n*-alkane
75 $\delta^2\text{H}$ values; Rach et al. 2017) have the potential to overcome the above mentioned limitation/uncertainty
76 caused by unknown evapo(transpi)rative enrichment using single $\delta^2\text{H}_{n\text{-alkane}}$ and $\delta^{18}\text{O}_{\text{sugar}}$ records.
77 Moreover, such coupled approaches allow relative humidity reconstructions and may thus contribute to
78 respective quantitative paleoclimate research (Eley and Hren 2018; Gázquez et al. 2018).

79 With our study we aimed at contributing to the Late Glacial – Early Holocene paleoclimate reconstruction
80 of Central Europe by investigating the sedimentary archive of Lake Bergsee in the Black Forest, Germany.

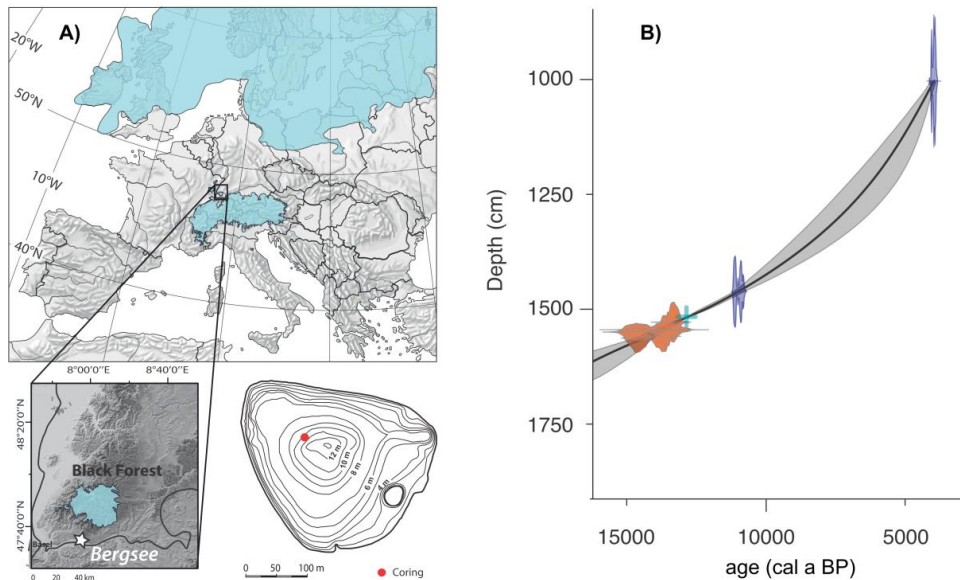
81 More specifically, we present (i) sedimentary bulk (total organic carbon/nitrogen, $\delta^{13}\text{C}$ and $\delta^{15}\text{N}$) and
82 biomarker (*n*-alkanes and sugars) proxies and discuss their potential/limitations for source identification,
83 (ii) $\delta^2\text{H}_{n\text{-alkane}}$ and $\delta^{18}\text{O}_{\text{sugar}}$ records and discuss their potential/limitations for reconstructing paleoclimatic
84 conditions and (iii) discuss the potential/limitations of applying the above introduced 'dual-biomarker
85 approach' and 'coupled $\delta^2\text{H}_{n\text{-alkane}} - \delta^{18}\text{O}_{\text{sugar}}$ approach' to our Lake Bergsee record.

86

87 **2 Material & Methods**

88 **2.1 Lake Bergsee**

89 Lake Bergsee (7°56'11"E, 47°34'20"N) is situated at 382 m a.s.l. on the foothill of the southern Black
90 Forest, Baden Württemberg, Germany (Becker et al. 2006), around 2 km north of Bad Säckingen (Fig. 1A).
91 The modern lake is maximum 335 m long and 250 m wide, representing the small lake surface area with
92 maximum water depth of 13 m. The natural catchment area is rather small with 0.162 km², restricted to
93 the surrounded slopes which are densely covered by forest vegetation. The lake has no natural inflow and is
94 only fed by precipitation and groundwater. The creek Seebächle is the natural outlet of the lake. Since
95 1802/1803 the water level of Lake Bergsee is controlled via a connection to the close-by creek
96 Schöpfenbach, which enlarged the catchment area by 10 km² (Becker et al. 2006). The lake is located in a
97 basin formed by the Riss glacier, embedded in the crystalline basement of mainly pre-Hercynian gneisses
98 (Becker and Angelstein 2004; Becker et al. 2006). Detailed pollen profiles of Lake Bergsee sediments are
99 published by Becker et al. (2006), up to the maximum depth of 20.7 m (covering approximately the last
100 30,000 a). Additionally, the authors show chironomid assemblages and geochemical results. Duprat-Oualid
101 et al. (2017) interpreted pollen results from a master core section between 1571 and 2850 cm
102 (corresponding to an age interval between 14,700 and 45,000 a cal BP) based on a most recent twin coring
103 campaign in November 2013. Pollen analysis, however, was already performed until a master core depth
104 of 1350 cm.



105

106 **Fig. 1:** A) Maps depicting the Lake Bergsee location in Europe and in the Southern Black Forest Region.
 107 Blue shaded areas show the glacier extend during the Last Glacial Maximum. Furthermore, the actual
 108 bathymetric map of Lake Bergsee is shown, highlighting the coring position with a red dot. B) Lake Bergsee
 109 Late Glacial/Holocene age-depth model, comprising the ¹⁴C dates obtained by Duprat-Oualid et al. (2017),
 110 shown in blue, the Laacher See Tephra is marked with a light blue cross and the orange areas mark 5 newly
 111 added ¹⁴C ages obtained from microfossils found during the core sampling campaign for this study, see
 112 Tab. 1.

113

114 Mean annual precipitation over the Lake Bergsee is 1159 mm. Typically, the January is the coldest month
 115 within the year, revealing a mean air temperature of 0.9°C. July is in average the warmest month with
 116 19.2°C. Data are means of the measuring period between 1981 to 2010 from the agrometeorological
 117 station Bad Säckingen at 339 m a.s.l. (Deutscher Wetterdienst).

118 2.2 Core details, sampling strategy and age-depth model

119 In the course of the project “Last Glacial Termination in Europe” two cores were retrieved (BER 13-01 &
 120 BER 13-02), close to the Livingston piston core BL2 of Becker et al. (2006), as overlapping twin cores
 121 (Duprat-Oualid et al. 2017). Coring was carried out with a Livingston piston corer (UWITEC, Mondsee,
 122 Austria) from a floating platform. The master core with 2850 cm length was established using magnetic

123 susceptibility measurements and high-resolution core imaging (Duprat-Oualid et al. 2017). The most
 124 recent cored Lake Bergsee sediments covers approximately the last 45,000 a, as derived from the age-
 125 depth model (Duprat-Oualid et al. 2017).

126 The samples investigated in this study originate from a 1.50 m long part of BER 13-01 representing a master
 127 core section between 1455 and 1605 cm depth. Samples were taken in 1 cm resolution. After sampling,
 128 the sediments were dried at 40°C and homogenized (grinded) before further analysis. All laboratory work
 129 and measurements were done at the Martin-Luther-University Halle-Wittenberg, Institute of Agronomy
 130 and Nutritional Sciences, Group of Soil Biogeochemistry.

131 For detailed information about the age-depth model the reader is referred to Duprat-Oualid et al. (2017).
 132 Within this study the age-depth model was refined by ¹⁴C analysis of 5 macrofossils found during core
 133 sampling (Tab. 1). Radiocarbon analysis and calibration was carried out in the Laboratory for the Analysis
 134 of Radiocarbon at the University of Bern, using accelerator mass spectrometry. In summary, the
 135 investigated core section is based on 5 ¹⁴C macrofossil dates and 2 of wood/needle and wood material in
 136 1461.7 and 1563 cm composite depth (Duprat-Oualid et al. 2017), and represents the Late Glacial to Early
 137 Holocene transition (16,000 to 10,750 a cal BP; Fig. 1B).

138 **Tab. 1:** New microfossil radiocarbon data obtained from Lake Bergsee sediment core BER 13-01.

composite depth (cm)	laboratory reference (Bern)	uncalibrated ages (¹⁴ C a BP)	calibrated ages (cal a BP; 2σ)
1528.2	7064.1.1	11,489 ± 178	13,384 ± 343
1544.7	7065.1.1	11,651 ± 407	13,782 ± 1058
1545.7	7066.1.1	11,770 ± 213	13,648 ± 476
1549.7	7067.1.1	12,460 ± 189	14,637 ± 638
1558.7	7068.1.1	11,892 ± 188	13,766 ± 451

139 Bern = Laboratory for the Analysis of Radiocarbon at the University Bern

140

141 **2.3 Bulk sedimentary analysis**

142 An EuroVector EA 3000 elemental analyzer (HeKatech, Wegberg, Germany) coupled via a ConFlo III
 143 Interface to a Delta V Advantage isotope ratio mass spectrometer (IRMS; both from Thermo Fisher
 144 Scientific, Bremen, Germany) was used for the analysis of total carbon (TC), total nitrogen (TN), carbon
 145 isotope composition ($\delta^{13}\text{C}_{\text{TC}}$) and nitrogen isotope composition ($\delta^{15}\text{N}$). For calibration, standard materials

146 from the International Atomic Energy Agency (IAEA) and United States Geological Survey (USGS) with
147 known total carbon, nitrogen, ^{13}C and ^{15}N contents were used (IAEA N2, IAEA CH6, IAEA NO3, IAEA CH7,
148 IAEA 305A, USGS 41). The isotope compositions are expressed relative to an international standard in the
149 common δ -notation (e.g. Coplen, 2011; ^{13}C : Vienna Pee Dee Belemnite, VPDB; ^{15}N : atmospheric N_2 , Air).

150

151 **2.4 Biomarker and compound-specific isotope analysis**

152 Free lipids were extracted 24 h using a soxhlet system (Behr Labor-Technik, R 106 S), constantly rinsed by
153 solvent (dichloromethane:methanol in a ratio of 9:1). After evaporation of the solvent by a rotary
154 evaporator, the total lipid extract was dissolved again and transferred to a pipette column filled with
155 aminopropyl silica gel (Supelco, 45 μm). Three different solvents of increasing polarity (*n*-hexane;
156 dichloromethane:methanol in a ratio of 1:1; diethyl ether + acetic acid in a ratio of 1:19) were used to
157 successively elute the fractions (nonpolar fraction, including *n*-alkanes; more polar fraction, including e.g.
158 alcohols; acids) from the pipette column. Quantification of *n*-alkanes was performed on a GC-2010 series
159 gas chromatograph equipped with a flame ionization detector (GC-FID; Shimadzu, Kyoto, Japan). A C_7 - C_{40}
160 saturated *n*-alkane standard mixture (Supelco 49452-U) in three different concentrations (10, 50 and 100
161 $\mu\text{g}/\text{ml}$) was co-analyzed in each batch several times, and used as quantification standards via linear
162 calibration. The compound-specific $\delta^2\text{H}_{n\text{-alkane}}$ analysis was realized on a Trace GC 2000 coupled to a Delta
163 V Advantage IRMS via a ^2H -pyrolysis reactor (GC IsoLink) and a ConFlo IV interface (all devices from Thermo
164 Fisher Scientific, Bremen, Germany). The reactor temperature was set to 1425°C. Samples were injected
165 with a split/splitless injector, operating in splitless mode. The precision was checked by a standard alkane
166 mixture (*n*- C_{27} , *n*- C_{29} , *n*- C_{33}) with known isotope composition (A. Schimmelmann, University of Indiana), co-
167 injected in three different concentrations after nine sample runs. The samples were analyzed in three- to
168 ninefold repetition and only $\delta^2\text{H}$ results for analytical uncertainty (standard deviation) better than 10‰
169 are shown, because a higher uncertainty is typically indicative for low concentrations (= measurement
170 areas) and/or not baseline separated peaks. The H_3^+ -correction factor was checked at least before and
171 after a sample batch and stayed stable throughout the measurement period. The stable hydrogen isotope
172 compositions are given in the δ -notation versus Vienna Standard Mean Ocean Water (VSMOW).

173 The sugar biomarker extraction followed the procedure described by Zech and Glaser (2009). Briefly, from
174 the grinded samples the monosaccharides were released hydrolytically using 4 M trifluoroacetic acid at
175 105°C for 4 h (Amelung et al., 1996). The solution was cleaned over glass fibre filters, XAD-7 columns and
176 finally over DOWEX 50WX8 columns. After freeze-drying, the samples were split for (i) methyloxime-

177 trimethylsilyl-derivatisation method (Andrews 1989), which enables the quantification of a large range of
178 sugars, and (ii) methylboronic acid (MBA) derivatization procedure for 1 h at 60°C (Knapp 1979), which
179 ensures that the investigated arabinose (ara), xylose (xyl), fucose (fuc) and rhamnose (rham) yield only one
180 peak in the $\delta^{18}\text{O}$ chromatograms (Gross and Glaser 2004). Quantification of the monosaccharides ara, fuc,
181 galactose (gal), glucose (glu), mannose (man), rham, ribose (rib) and xyl were realized on a GC-FID
182 (Shimadzu, Kyoto, Japan). Compound-specific $\delta^{18}\text{O}_{\text{sugar}}$ measurements were performed with the MBA
183 derivatized samples on a Trace GC 2000 coupled to a Delta V Advantage IRMS via an ^{18}O -pyrolysis reactor
184 (GC IsoLink) and a ConFlo IV interface (all devices from Thermo Fisher Scientific, Bremen, Germany). The
185 samples were measured in threefold repetition. Co-derivatized sugar standard batches are measured in-
186 between, containing ara, fuc, xyl, and rham in various concentrations of known $\delta^{18}\text{O}$ value (Zech and Glaser
187 2009). The $\delta^{18}\text{O}$ values of the samples were drift- and amount-corrected and a correction for the
188 hydrolytically introduced oxygen atoms on the carbonyl group at the C1 position of the sugar molecules
189 was applied (Zech and Glaser 2009). Standard uncertainties (deviations) for at least triplicate sample
190 measurements (excepted of 11 samples from which only duplicate measurements are available) are on
191 average 1.4, 1.4, 1.6‰ for ara (n = 130), fuc (n = 126) and xyl (n = 124), respectively. Sugars revealing $\delta^{18}\text{O}$
192 standard deviations higher than 6‰ were omitted from further interpretation, because sugar
193 concentration (= measurement area) was typically too low for robust evaluation (especially for most of the
194 rham peaks), which were finally excluded from further data evaluation. The $\delta^{18}\text{O}$ values of the
195 monosaccharides are expressed in common δ -notation versus the VSMOW.

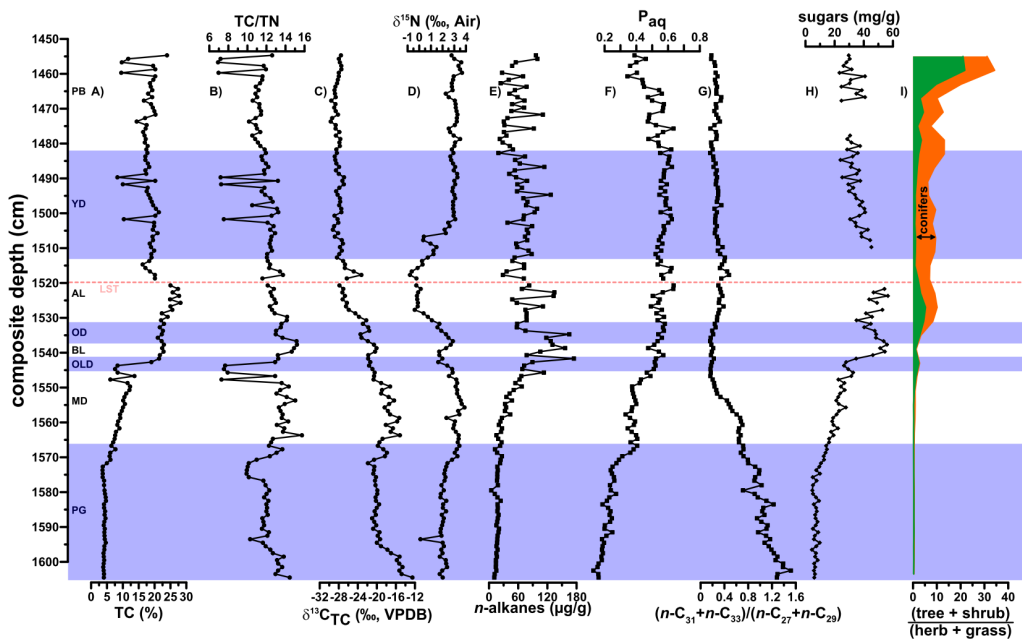
196

197 **3 Results & Discussion**

198 **3.1 Source identification of bulk sedimentary organic matter**

199 The TC contents of the investigated Lake Bergsee sediment section range between 4 and 28% (Fig. 2A).
200 The TN record highly resembles the TC depth variations ($r^2 = 0.92$, $p < 0.001$, $n = 149$) and is therefore not
201 displayed in Fig. 2. In order to infer information about the source of the sedimentary organic matter,
202 proxies derived from bulk analysis can potentially be used, i.e. TC to TN ratio (TC/TN), $\delta^{13}\text{C}_{\text{TC}}$ and $\delta^{15}\text{N}$ (Fig.
203 2B to D). The TC/TN ratio range between 7 and 16, with a slightly increasing trend from the top to the
204 bottom of the section (Fig. 2B). Using a threshold of > 12 as indicator for terrestrial input (Prahel et al. 1980),
205 no distinctive source can be identified since the bulk sedimentary TC/TN ratios plot all close to 12.
206 Moreover, the TC/TN proxy should not be over-interpreted, because mineralization and degradation are
207 well known to result in very low TC/TN values of terrestrial soils, too (Zech et al. 2007). Lake Bergsee
208 $\delta^{13}\text{C}_{\text{TC}}$ ranges from -30 to -13‰ (Fig. 2C). More positive values than -24‰ in the lower part of the core

209 cannot be explained with terrestrial C₃ plants as only sedimentary carbon source. Given that a C₄ plant
 210 contribution can be excluded (Duprat-Oualid et al. 2017), this points either to allochthonous (aeolian) or
 211 autochthonous anorganic carbonate, or to autochthonous organic (aquatic) matter contributing to TC. The
 212 δ¹⁵N values range between -1 and 4‰, with a minimum during the Allerød period (Fig. 2D). Albeit this
 213 minimum, which covers a composite depth of 1505 to 1535 cm, does not perfectly match the Bølling (BL)
 214 and Allerød (AL) TC maximum, it could be interpreted to reflect increased biomass production including
 215 N-fixation, be it aquatic or terrestrial. Moreover, numerous further factors such as e.g. denitrification and
 216 mineralisation can influence both terrestrial and lacustrine sedimentary δ¹⁵N values (Meyers and
 217 Ishiwatari 1993; Zech et al. 2011a). Hence, a robust source identification based on δ¹⁵N values seems to
 218 be challenging. Conclusively, a straightforward source identification of the bulk organic matter is not
 219 achievable for Lake Bergsee based on the here presented bulk proxies (Fig. 2A to D).



220

221 **Fig. 2:** Depth functions of Lake Bergsee. A) TC, B) TC/TN, C) δ¹³C, D) δ¹⁵N, E) total *n*-alkane concentration,
 222 F) P_{aq} (according to Ficken et al. 2000), G) *n*-alkane ratio $(n-C_{31}+n-C_{33})/(n-C_{27}+n-C_{29})$, H) total sugar
 223 concentration, and I) tree and shrub vs. herb and grass pollen ratio (green = sum of broadleaf trees and
 224 shrubs vs. herbs and grasses, orange = sum of broadleaf and coniferous trees and shrubs vs. herbs and
 225 grasses, orange minus green = coniferous proportion). Pollen results were taken from Duprat-Oualid et al.
 226 (2017). Background colors show time periods (according to Litt et al. 2001): PB = Preboreal, YD = Younger

227 Dryas, AL = Allerød, OD = Older Dryas, BL = Bølling, OLD = Oldest Dryas, MD = Meiendorf, PG = Pleniglacial.
228 LST = Laacher See Tephra.

229

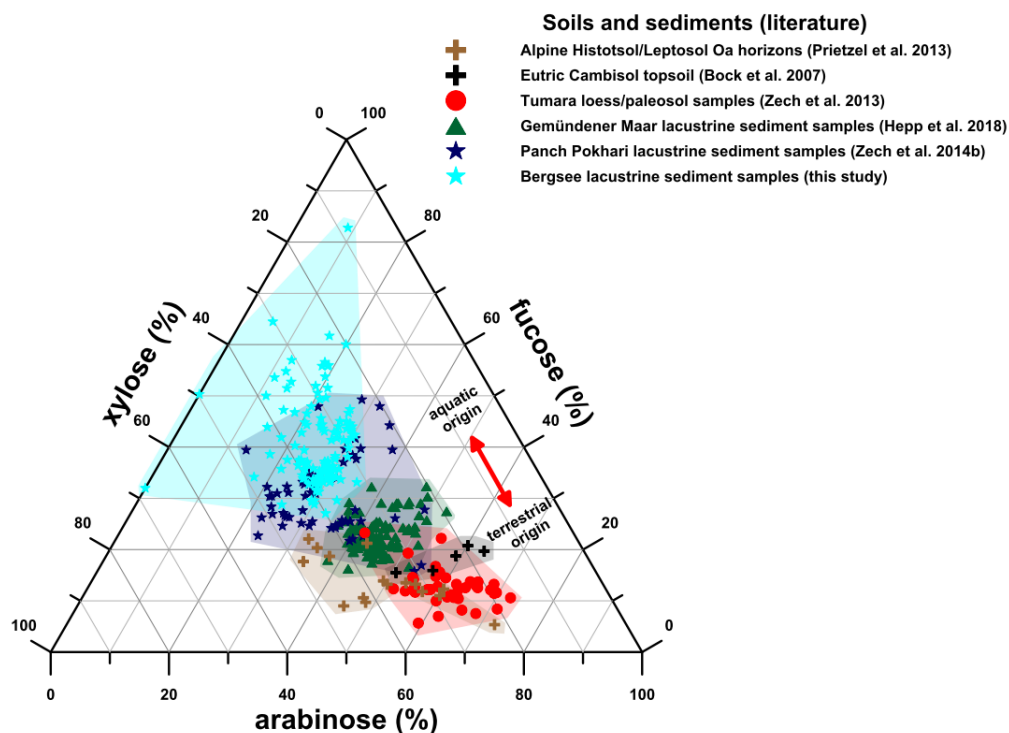
230 3.2 Source identification of *n*-alkane and sugar biomarkers

231 The total *n*-alkane concentrations shown in Fig. 2E range between 4 and 175 µg/g and generally reflect the
232 TC depth profile. In order to assess aquatic vs. terrestrial *n*-alkane input P_{aq} values were calculated
233 according to Ficken et al. (2000): $P_{aq} = (n-C_{23} + n-C_{25}) / (n-C_{23} + n-C_{25} + n-C_{29} + n-C_{31})$. The P_{aq} index was
234 established to distinguish between submerged and floating vs. emergent and terrestrial plant *n*-alkane
235 input. The Lake Bergsee P_{aq} record shows values ranging from 0.1 to 0.6 (Fig. 4F). Below 1550 cm depth,
236 P_{aq} values < 0.4 suggest a predominant input of *n*-alkanes that derived from emergent plants. One might
237 be tempted to interpret the P_{aq} values of > 0.4 above 1550 cm depth in terms of a predominant input of
238 aquatic-derived *n*-alkanes. This is based on the finding that higher terrestrial plants produce long-chain *n*-
239 alkanes in order to build up the epicuticular wax layer (Eglinton and Hamilton 1967). By contrast, short-
240 chain *n*-alkanes are often associated with algae (Gelpi et al. 1970) and mid-chain *n*-alkanes are often
241 assumed to originate from submerged macrophytes (Ficken et al. 2000). However, note that Aichner et al.
242 (2018) recently stressed that P_{aq} is no robust proxy for aquatic influx in lake sediments from North Poland.
243 Rather, the sedimentary mid-chain *n*-alkanes *n*-C₂₃ and *n*-C₂₅ originate either from a mixture of aquatic and
244 terrestrial sources (during Allerød and the Younger Dryas onset) or are predominantly of terrestrial origin
245 (during Younger Dryas and Early Holocene). Given that e.g. *Betula* as one of the main pioneering species
246 during Late Glacial reforestation at Lake Bergsee (Duprat-Qualid et al. 2017) is well known to produce quite
247 considerable amounts of *n*-C₂₃ and *n*-C₂₅ (Tarasov et al. 2013; van den Bos et al. 2018), we recommend
248 caution when interpreting P_{aq} values from sedimentary archives. In the case of Lake Bergsee, we consider
249 the respective interpretation to be not robust. Moreover, litter degradation by soil microorganisms is
250 reported to cause changes of both mid-chain and long-chain *n*-alkanes patterns (Tu et al. 2011; Zech et al.
251 2011b). Hence, soil erosion from the catchment should be considered when interpreting P_{aq} values, too.

252 Long-chain *n*-alkanes are furthermore used in chemotaxonomic studies in order to distinguish between
253 different vegetation types. This is based on the observation that in grass and herbaceous plant material
254 the *n*-C₃₁ and *n*-C₃₃ homologues are often dominating, whereas trees and shrubs often show higher relative
255 concentrations of *n*-C₂₇ and *n*-C₂₉ (Maffei 1996; Zech et al. 2009). We used here the ratio $(n-C_{31}+n-C_{33}) / (n-$
256 $C_{27}+n-C_{29})$, which range between 0.2 and 1.5 (Fig. 2G). This approach is comparable to the one of Schwark
257 et al. (2002), who used the *n*-C₂₇, *n*-C₂₉ and *n*-C₃₁ alkane distribution and pollen to reconstruct the Late

258 Glacial reforestation around Lake Steißlingen. While $(n\text{-}C_{31}+n\text{-}C_{33})/(n\text{-}C_{27}+n\text{-}C_{29})$ values > 1 can be
259 interpreted in terms of enhanced input of grass-derived leaf material (below 1570 cm depth), values < 1
260 suggest increased input of tree- and shrub-derived litter (above 1570 cm depth). The respective
261 interpretation is overall in agreement with the pollen record of Lake Bergsee (Fig. 2I; Duprat-Oualid et al.
262 2017) and corroborates that the investigated long-chain *n*-alkanes are primarily of terrestrial origin. Yet,
263 there seems to be a time lag between the $(n\text{-}C_{31}+n\text{-}C_{33})/(n\text{-}C_{27}+n\text{-}C_{29})$ ratio and the pollen record. The *n*-
264 alkane ratio declines most pronouncedly already during the Meiendorf Interstadial, whereas the tree and
265 shrub pollen increase starts at the end of Meiendorf (compare Fig. 2G vs. I). Possibly, this minor
266 discrepancy can be explained with shrub pollination rate having started with a delay compared to shrub
267 spreading.

268 Total sugar concentrations for Lake Bergsee range between 4 and 57 mg/g (Fig. 2H) and reveal a highly
269 significant correlation with TC ($r^2 = 0.88$, $p < 0.001$, $n = 128$). Recently, an approach was proposed for
270 distinguishing between aquatic versus terrestrial sedimentary input based on the relative abundances of
271 the sugar biomarkers ara, fuc and xyl (Hepp et al. 2016). Accordingly, $\text{fuc}/(\text{ara}+\text{xyl})$ ratios ranging between
272 0.4 and 4.8 for the Lake Bergsee record are clearly indicative for a primarily aquatic origin of the sugars.
273 Fig. 3 furthermore illustrates this interpretation in a ternary diagram where the relative abundances of
274 ara, fuc and xyl for Lake Bergsee are compared with soil and sediment data from the literature according
275 Hepp et al. (2016).



276

277 **Fig. 3:** Ternary diagram from Hepp et al. (2016) depicting the relative abundances of ara, xyl and fuc for
 278 Lake Bergsee sediment samples (this study) and comparative soil and sediment data compiled from the
 279 literature (Bock et al. 2007; Prietzal et al. 2013; Zech et al. 2013, 2014b; Hepp et al. 2018).

280

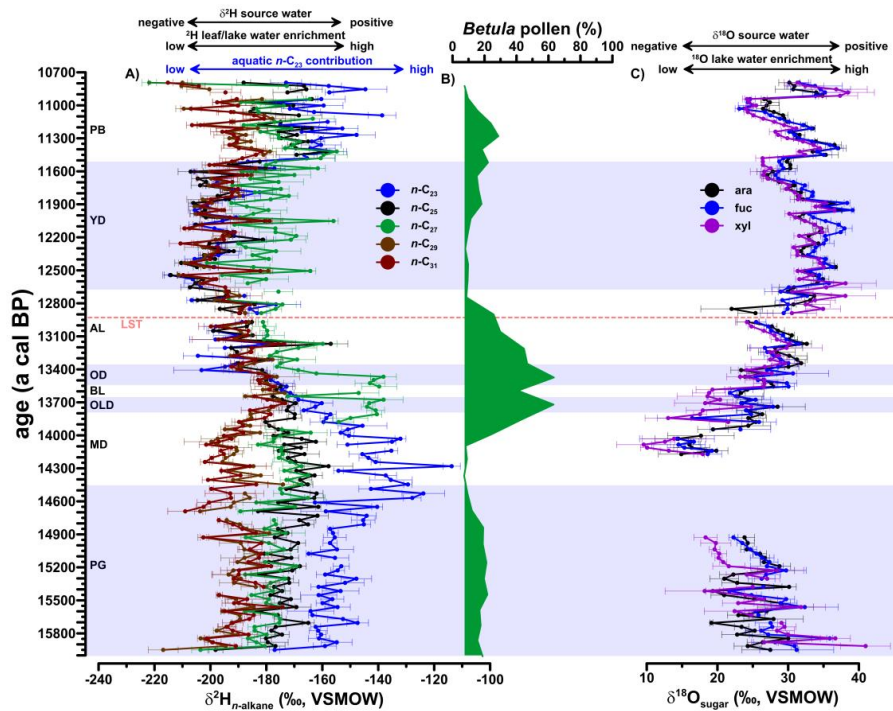
281 Summing up this subchapter, the long-chain *n*-alkanes *n*-C₂₇, *n*-C₂₉ and *n*-C₃₁ of the Lake Bergsee record
 282 are mainly of terrestrial origin, the sugar biomarkers ara, fuc and xyl are primarily of aquatic origin, and
 283 the mid-chain *n*-alkanes *n*-C₂₃ and *n*-C₂₅ in all likelihood represent a mixture of aquatic and terrestrial
 284 sources.

285

286 3.3 Lake Bergsee $\delta^2\text{H}_{n\text{-alkane}}$ record and its paleoclimatic interpretation

287 The $\delta^2\text{H}$ values of the investigated *n*-alkanes range between -215 to -173‰, -217 to -174‰, -222 to -
 288 138‰, -214 to -157‰ and -214 to -114‰ for *n*-C₃₁, *n*-C₂₉, *n*-C₂₇, *n*-C₂₅ and *n*-C₂₃, respectively (Fig. 4A). The
 289 *n*-C₂₉ and *n*-C₃₁ records show very similar $\delta^2\text{H}$ values. By contrast, *n*-C₂₇ yielded on average throughout the

290 record by +17‰ more positive $\delta^2\text{H}$ values. This could be explained with the different taxonomic origin of
 291 the alkane homologues. Leaf wax-derived long-chain *n*-alkanes are biosynthesized in the leaves of higher
 292 terrestrial plants, thus using mainly leaf water as hydrogen source, as e.g. reviewed by Sachse et al. (2012).
 293 Therefore, not only the plant source water is imprinted in terrestrial $\delta^2\text{H}_{n\text{-alkane}}$, moreover the leaf water
 294 evaporative enrichment plays an important role (Kahmen et al. 2013). As outlined above, grasses (e.g.
 295 *Poaceae*) are often characterized by highest relative abundances of *n*-C₃₁. At the same time, grass-derived
 296 *n*-alkanes (Fig. 2G) are known to be less sensitive recorders of leaf water enrichment compared to *n*-
 297 alkanes from other higher terrestrial plants (McInerney et al. 2011; Kahmen et al. 2013). The $\delta^2\text{H}$ offset
 298 between *n*-C₃₁ and *n*-C₂₇ is indeed largest during the Oldest Dryas and the early Older Dryas, when *Betula*,
 299 which is known to produce high amounts of *n*-C₂₇ (e.g. Tarasov et al. 2013) shows the highest pollen
 300 concentration (compare Fig. 4A and B) and *Poaceae* pollen concentration is decreasing (Duprat-Qualid et
 301 al. 2017).



302
 303 **Fig. 4:** A) $\delta^2\text{H}_{n\text{-alkane}}$ records (*n*-C₂₃, *n*-C₂₅, *n*-C₂₇, *n*-C₂₉ and *n*-C₃₁), B) *Betula* pollen record (Duprat-Qualid et
 304 al. 2017) and C) $\delta^{18}\text{O}_{\text{sugar}}$ records (ara, fuc, xyl) of Lake Bergsee. Background colors show time periods

305 according to Litt et al. (2001): PB = Preboreal, YD = Younger Dryas, AL = Allerød, OD = Older Dryas, BL =
306 Bølling, OLD = Oldest Dryas, MD = Meiendorf, PG = Pleniglacial. LST = Laacher See Tephra.

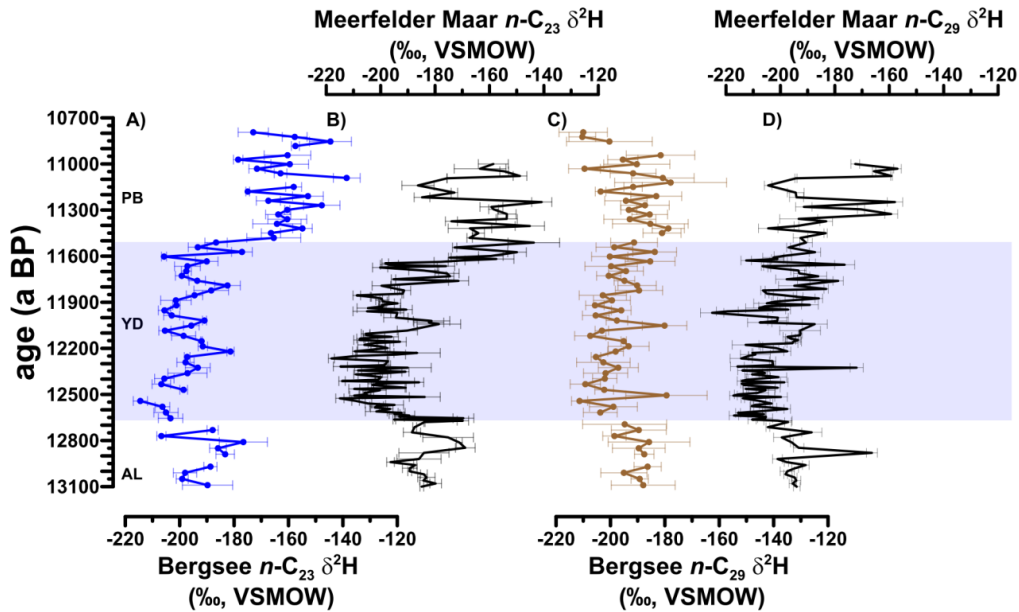
307

308 As outlined in section 3.2, $n\text{-C}_{23}$ in our Lake Bergsee record is most likely a mixture of terrestrial and aquatic
309 sources. The proposed partly aquatic origin of $n\text{-C}_{23}$ can help explaining the often more positive $\delta^2\text{H}$ values
310 of $n\text{-C}_{23}$ compared to the primarily terrestrial long-chain n -alkanes (Fig. 4A). While for long-chain n -alkanes
311 an biosynthetic fractionation factor (ϵ^2_{bio}) of -160‰ can be assumed (Sessions et al. 1999; Sachse et al.
312 2006), data from *Potamogeton* and surface sediments suggest an ϵ^2_{bio} fractionation factor of -82 to -88‰
313 for $n\text{-C}_{23}$ (Aichner et al. 2010). Accordingly, more positive $\delta^2\text{H}$ values of $n\text{-C}_{23}$ during the Pleniglacial,
314 Meiendorf and Preboreal of Lake Bergsee suggest a partly aquatic origin of $n\text{-C}_{23}$, whereas the absence of
315 an offset between $\delta^2\text{H}$ of $n\text{-C}_{23}$ and the long-chain n -alkanes during the Bølling, Older Dryas, Allerød and
316 Younger Dryas points to a primarily terrestrial origin of $n\text{-C}_{23}$. Therefore, the direct link between $\delta^2\text{H}$ values
317 of $n\text{-C}_{23}$ and $\delta^2\text{H}_{\text{lake-water}}$ (Aichner et al. 2010; Sachse et al. 2012) cannot be applied here.

318 In Fig. 5 the $n\text{-C}_{23}$ $\delta^2\text{H}$ record of Lake Bergsee is shown along with the $n\text{-C}_{23}$ $\delta^2\text{H}$ record from Lake
319 Meerfelder Maar (Rach et al. 2014) for comparison. Within age uncertainties, the $n\text{-C}_{23}$ $\delta^2\text{H}$ record of Lake
320 Bergsee resembles well the record from Lake Meerfelder Maar (Fig. 5A vs. B), which spans the time period
321 from 11,000 to 13,100 a varve BP (Rach et al. 2014). The $n\text{-C}_{23}$ $\delta^2\text{H}$ record from Lake Meerfelder Maar is
322 interpreted to reflect lake water and thus local precipitation. The lower $\delta^2\text{H}$ values of $n\text{-C}_{23}$ during the
323 Younger Dryas are therefore associated with lower regional air temperatures and by changes in $\delta^2\text{H}$ of the
324 moisture source associated with the freshwater input to the North Atlantic Ocean as well as with changes
325 in moisture source temperature and transport history (Rach et al. 2014). Importantly, for Lake Meerfelder
326 Maar the authors assumed the lake water enrichment was of minor importance. For Lake Bergsee,
327 however, lake water enrichment during drier periods is very likely, because the lake is characterized by
328 the absence of an inflowing creek (section 2.1). Fig. 5 also compares the $n\text{-C}_{29}$ $\delta^2\text{H}$ record of Lake Bergsee
329 with the $n\text{-C}_{29}$ $\delta^2\text{H}$ record from Lake Meerfelder Maar (Fig. 5C vs. D). Also these both records resemble
330 each other fairly well, except for larger fluctuations occurring in the Lake Meerfelder Maar record during
331 the Preboreal.

332 Summing up, the above outlined discussion reveals that the $\delta^2\text{H}_{n\text{-alkane}}$ record of Lake Bergsee cannot be
333 interpreted in a straightforward way. As illustrated in Fig. 4A, the main influencing factors which are
334 difficult to be disentangled and which cause $\delta^2\text{H}$ variations are: (i) $\delta^2\text{H}$ source water (\approx local precipitation)

335 changes, (ii) variable ^2H leaf/lake water enrichment, and (iii) variable contributions of aquatic versus
 336 terrestrial $n\text{-C}_{23}$.



337
 338 **Fig. 5:** Comparison between A) the $n\text{-C}_{23}$ $\delta^2\text{H}$ record of Lake Bergsee and B) the $n\text{-C}_{23}$ $\delta^2\text{H}$ record from Lake
 339 Meerfelder Maar (Rach et al. 2014) and comparison between C) the $n\text{-C}_{29}$ $\delta^2\text{H}$ record of Lake Bergsee and
 340 D) the $n\text{-C}_{29}$ $\delta^2\text{H}$ record from Lake Meerfelder Maar (Rach et al. 2014). Background colors show time
 341 periods according to Litt et al. (2001): PB = Preboreal, YD = Younger Dryas, AL = Allerød, OD = Older Dryas,
 342 BL = Bølling, OLD = Oldest Dryas, MD = Meiendorf, PG = Pleniglacial. LST = Laacher See Tephra.

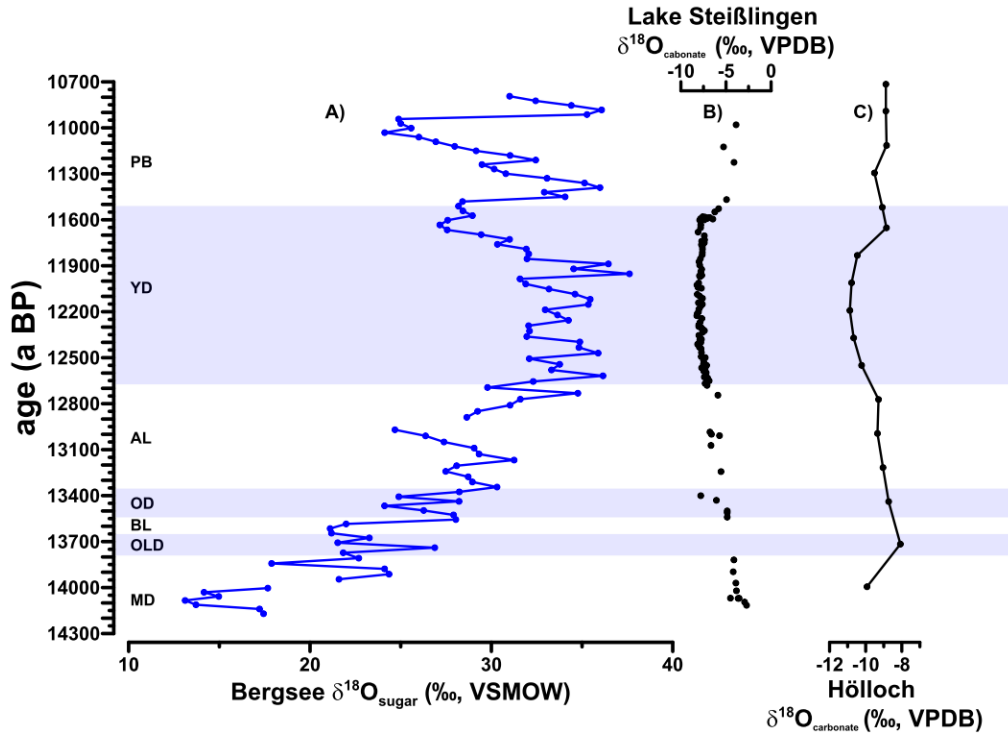
343

344 **3.4 Lake Bergsee $\delta^{18}\text{O}_{\text{sugar}}$ record and its paleoclimatic interpretation**

345 The $\delta^{18}\text{O}$ values of ara, fuc and xyl range from +14.4 to +37.6‰, +14.3 to +39.1‰ and +9.6 to +40.9‰,
 346 respectively, and resemble each other well (Fig. 4C). All three sugars are primarily of aquatic origin (see
 347 discussion in section 3.2). Hence, the $\delta^{18}\text{O}_{\text{sugar}}$ record of Lake Bergsee can be interpreted in terms of
 348 reflecting changes in (i) $\delta^{18}\text{O}$ source water (\approx local precipitation) and (ii) ^{18}O lake water enrichment (as
 349 illustrated in Fig. 4C).

350 The lake water enrichment can be directly linked to relative humidity when the lake input to evaporation
 351 ratio can be robustly defined (e.g. as terminal lake situation, input = evaporation; Gat 1971). This holds,

352 however, not valid for Lake Bergsee, due to the absence of a natural inflowing creek (see section 2.1).
353 Therefore, changes in the precipitation amount have to be taken into account, too (see section 3.2; Gibson
354 et al. 2016). Given that the $\delta^{18}\text{O}$ variability of precipitation (\approx source water) was unlikely larger than 8‰
355 during the Late Glacial-Holocene transition (von Grafenstein et al. 1998; Mayer and Schwark 1999), most
356 of the variability of the $\delta^{18}\text{O}_{\text{sugar}}$ record of Lake Bergsee can be attributed to variable lake water enrichment.
357 In order to highlight this, the $\delta^{18}\text{O}_{\text{sugar}}$ record of Lake Bergsee (calculated as weighted mean), is shown in
358 Fig. 6 in comparison to the $\delta^{18}\text{O}_{\text{carbonate}}$ record from Lake Steißlingen (Mayer and Schwark 1999) and the
359 stalagmite $\delta^{18}\text{O}_{\text{carbonate}}$ record from Hölloch Cave (Wurth et al. 2004). Those carbonate $\delta^{18}\text{O}$ records are
360 interpreted to reflect the local precipitation history. Lake Steißlingen is primarily fed by ground water via
361 submerged springs (Eusterhues et al. 2002) and the carbonate $\delta^{18}\text{O}$ values thus reflect mainly
362 precipitation. It is obvious that the $\delta^{18}\text{O}_{\text{sugar}}$ of Lake Bergsee shows opposite trends and a much higher
363 amplitude than the precipitation records (Fig. 8). The Younger Dryas-Preboreal transition reveals a shift of
364 around 5‰ towards more positive $\delta^{18}\text{O}_{\text{sugar}}$ values (Fig. 9A). This is in well in agreement with a
365 reconstructed $\delta^{18}\text{O}_{\text{lake-water}}$ shift of around 6‰ from Lake Goszcz in Central Poland as inferred from the
366 sedimentary cellulose (Rozanski et al. 2010).



367

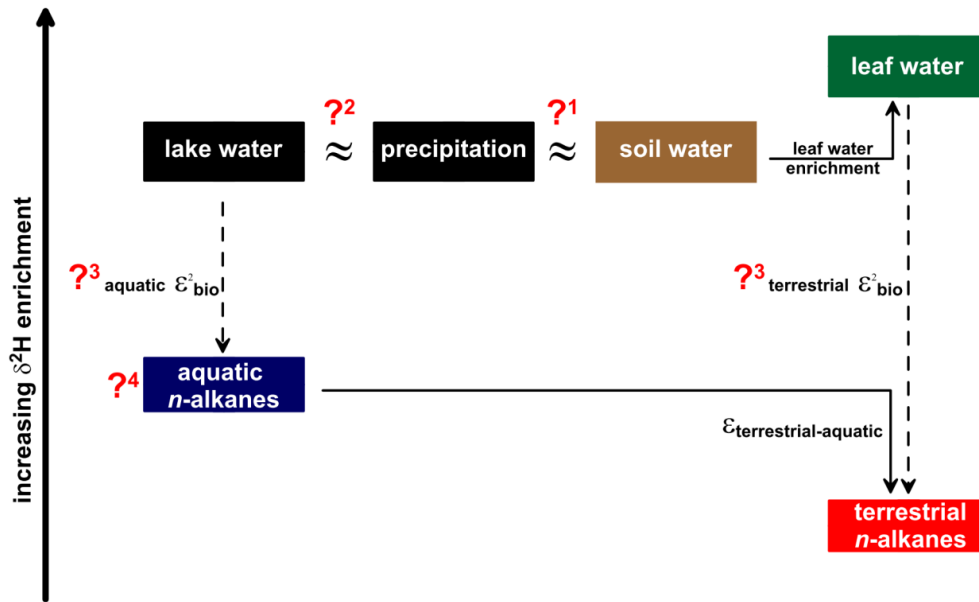
368 **Fig. 6:** Comparison between A) $\delta^{18}\text{O}_{\text{sugar}}$ record from Lake Bergsee and $\delta^{18}\text{O}_{\text{carbonate}}$ records from B) Lake
 369 Steißlingen (Mayer and Schwark 1999) and C) Hölloch cave stalagmite (Wurth et al. 2004). The $\delta^{18}\text{O}$ scale
 370 C is doubled compared to A and B due to a better visibility of the trends.

371

372 **3.5 'Dual-biomarker approach' based on terrestrial versus aquatic $\delta^2\text{H}_{n\text{-alkane}}$ records – potential
 373 and limitations**

374 The dual-biomarker approach was introduced by Rach et al. (2014, 2017) and uses the difference between
 375 terrestrial versus aquatic $\delta^2\text{H}_{n\text{-alkane}}$ values ($\epsilon_{\text{terrestrial-aquatic}}$). The basic assumption is that the long-chain *n*-
 376 alkanes such as *n*-C₂₉ are of terrestrial origin and reflect $\delta^2\text{H}$ of leaf water (precipitation altered by leaf
 377 water ²H enrichment), whereas *n*-C₂₃ is of aquatic origin and reflects $\delta^2\text{H}$ of lake water that is not ²H-
 378 enriched by evaporation (and thus reflects $\delta^2\text{H}$ of precipitation). When soil and lake water enrichment are
 379 negligible, such $\epsilon_{\text{terrestrial-aquatic}}$ values can be transferred into quantitative relative humidity values (Rach et
 380 al. 2017). Given that neither soil nor lake water ²H enrichment can be excluded for every study site, this
 381 represents one potential uncertainty of the dual-biomarker approach (Fig. 7). Especially lake water
 382 enrichment cannot be ruled out under dry and/or warm climatic conditions (see Fig. 8 in Hou et al. 2008).
 383 When lake water is/was affected by ²H enrichment in the past, the $\epsilon_{\text{terrestrial-aquatic}}$ values are no longer a

384 robust proxy for leaf water evapotranspirative enrichment. Another uncertainty concerns the hydrogen
385 fractionation during *n*-alkane biosynthesis (ϵ^2_{bio}) (Fig. 7). There is increasing evidence that this fractionation
386 is not constant between different species/organisms (e.g. review from Pedentchouk and Zhou, 2018). This
387 holds especially true for aquatic ϵ^2_{bio} values. While Muschitiello et al. (2015) and Rach et al. (2014) assume
388 that aquatic ϵ^2_{bio} is smaller than terrestrial ϵ^2_{bio} , Sachse et al. (2006), Jacob et al. (2007) and Seki et al.
389 (2011) set aquatic ϵ^2_{bio} equal to terrestrial ϵ^2_{bio} and Hou et al. (2008) show a case in which aquatic ϵ^2_{bio} is
390 larger than terrestrial ϵ^2_{bio} . Please note, that Jacob et al. (2007) called their difference between the
391 terrestrial $\delta^2\text{H}_{n\text{-alkane}}$ (C_{31}) and aquatic $\delta^2\text{H}_{n\text{-alkanoic}}$ (C_{16}) acid $\alpha_{\text{TA/wat}}$. They furthermore only mention the
392 fractionation factor between $\delta^2\text{H}_{n\text{-alkanoic}}$ (C_{16}) and source (lake) water to be -170‰. However, the ϵ^2_{bio}
393 between terrestrial $\delta^2\text{H}_{n\text{-alkane}}$ and $\delta^2\text{H}_{\text{leaf-water}}$ can be assumed to be close to that value, which is only slightly
394 larger than the commonly assumed -160‰ for terrestrial *n*-alkanes (see section 3.3; Sessions et al. 1999;
395 Freimuth et al. 2017). Finally, the paradigmatic source identification of the *n*-alkanes (long-chain *n*-alkanes
396 originate from terrestrial plants whereas mid-chain *n*-alkanes such as *n*- C_{23} originate from aquatic
397 organisms) may not always hold true (see sections 3.2 and 3.3). As mentioned above, also Aichner et al.
398 (2018) recently emphasized that *n*- C_{23} in a lacustrine sedimentary record from Poland is either completely
399 or at least partly of terrestrial origin. Given the above-discussed uncertainties, particularly including our
400 interpretation that *n*- C_{23} in Lake Bergsee is a mixture of aquatic and terrestrial sources, we consider the
401 dual-biomarker approach to be not robustly applicable to our $\delta^2\text{H}_{n\text{-alkane}}$ record and refrain from a
402 respective application.



403
 404 **Fig. 7:** Schematic diagram illustrating the ‘dual-biomarker approach’ for interpreting the difference
 405 between terrestrial versus aquatic $\delta^2\text{H}_{n\text{-alkane}}$ results, adopted from Sachse et al. (2006) and Rach et al.
 406 (2017). Uncertainties of the approach are marked with question marks and addressed in more detail in the
 407 text: 1 = it is assumed that $\delta^2\text{H}_{\text{soil water}}$ reflects $\delta^2\text{H}_{\text{precipitation}}$, 2 = it is assumed that lake water ^2H enrichment
 408 did not occur, 3 = robust knowledge concerning aquatic ϵ^2_{bio} values is actually lacking, 4 = mid-chain n -
 409 alkanes (C_{23}) are no exclusive aquatic biomarkers.

410
 411 **3.6 ‘Coupled $\delta^2\text{H}_{n\text{-alkane}}$ - $\delta^{18}\text{O}_{\text{sugar}}$ approach’ – potential and limitations**

412 A fundamental issue for this approach is again the question whether the investigated sedimentary
 413 biomarkers are primarily of autochthonous or of allochthonous origin. The concept for coupling $\delta^2\text{H}_{n\text{-alkane}}$
 414 with $\delta^{18}\text{O}_{\text{sugar}}$ results (Fig. 8) was originally developed for terrestrial biomarkers (Zech et al. 2013) but was
 415 adopted later on also for aquatic biomarkers (Hepp et al. 2015).

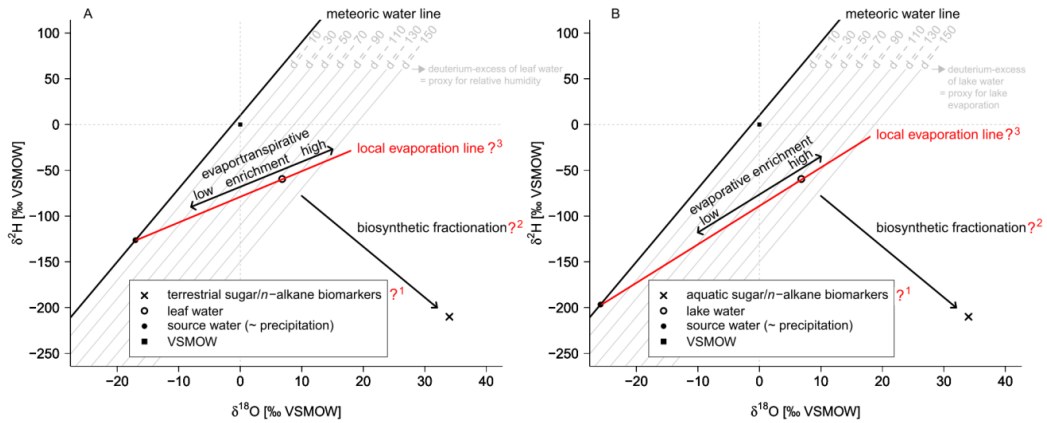
416 When applying the coupled $\delta^2\text{H}_{n\text{-alkane}}$ - $\delta^{18}\text{O}_{\text{sugar}}$ approach the following assumptions have to be made: (i)
 417 lake/leaf water $\delta^2\text{H}/\delta^{18}\text{O}$ values can be reconstructed from $\delta^2\text{H}_{n\text{-alkane}}$ and $\delta^{18}\text{O}_{\text{sugar}}$ values by applying
 418 constant biosynthetic fractionation factors. (ii) Lake/leaf water evapo(transpi)rative enrichment occur

419 along a local evaporation line, and the slope for such a line can be derived from a simplified Craig-Gordon
420 model. (iii) The $\delta^2\text{H}/\delta^{18}\text{O}$ values of plant/lake source water reflect precipitation, which typically plots along
421 a well-defined meteoric water line. The intersect between the local evaporation line throughout an
422 individual leaf/lake water point and the meteoric water thus allow the reconstruction of $\delta^2\text{H}/\delta^{18}\text{O}_{\text{source water}}$
423 ($\approx \delta^2\text{H}/\delta^{18}\text{O}_{\text{precipitation}}$). As such, the coupled $\delta^2\text{H}-\delta^{18}\text{O}$ approach is a promising tool to disentangle between
424 the leaf/lake water evapo(transpi)rative enrichment and the precipitation signal incorporated in the
425 biomarkers.

426 In the case of terrestrial biomarkers, the reconstructed $\delta^2\text{H}/\delta^{18}\text{O}_{\text{leaf-water}}$ can be used for calculating
427 deuterium-excess of leaf water. These deuterium-excess values can be converted into quantitative relative
428 humidity values. When aquatic biomarkers are used to reconstruct $\delta^2\text{H}/\delta^{18}\text{O}_{\text{lake-water}}$, those values allow
429 reconstructing the deuterium-excess of lake water. Those values can be used as lake water
430 evaporation/desiccation proxy. It should be noted that the deuterium-excess calculations follow the
431 formulation introduced by Dansgaard (1964). The coupled $\delta^2\text{H}_{n\text{-alkane}}-\delta^{18}\text{O}_{\text{sugar}}$ approach was successfully
432 applied to terrestrial sedimentary archives in order to derive relative humidity history (Zech et al. 2013;
433 Hepp et al. 2017). It was furthermore validated using a climate transect study by Tuthorn et al. (2015),
434 who called the $\delta^2\text{H}_{n\text{-alkane}}-\delta^{18}\text{O}_{\text{sugar}}$ coupling a 'paleohyrometer approach'. At the same time, Hepp et al.
435 (2015) realized the adoption of the coupled approach to a lacustrine sedimentary archive. Based on
436 aquatic biomarkers the authors reconstructed lake water evaporation history along with $\delta^2\text{H}/\delta^{18}\text{O}_{\text{precipitation}}$.

437 Apart from these potentials, the coupled $\delta^2\text{H}_{n\text{-alkane}}-\delta^{18}\text{O}_{\text{sugar}}$ approach has also limitations/uncertainties
438 (Fig. 8): (i) A clear source identification of the biomarkers is needed. (ii) The ϵ^2_{bio} and the oxygen
439 fractionation during sugar biosynthesis ($\epsilon^{18}_{\text{bio}}$) are assumed to be robust and constant. For a robust
440 deuterium-excess of leaf water interpretation also the soil water enrichment has to be ruled out.
441 Moreover, the slope of the local evaporation line has to be approximated. While for leaf water this seems
442 to be a minor issue due to rather small variations (Allison et al. 1985; Walker and Brunel 1990; Bariac et
443 al. 1994; Mayr 2002), the lake water local evaporation line seem to be much more variable (Gibson et al.
444 2008). This was taken into consideration by Hepp et al. (2015) by making reconstructions with different
445 slopes.

446 In the case of Lake Bergsee, we refrain from applying the coupled $\delta^2\text{H}-\delta^{18}\text{O}$ approach primarily because
447 we have neither (i) a reliable pure aquatic coupled $\delta^2\text{H}$ and $\delta^{18}\text{O}$ record (ii) nor a reliable pure terrestrial
448 $\delta^2\text{H}$ and $\delta^{18}\text{O}$ record.



449

450 **Fig. 8:** Schematic diagram illustrating the ‘coupled $\delta^2\text{H}_{n\text{-alkane}}-\delta^{18}\text{O}_{\text{sugar}}$ approach’ for A) interpreting
 451 terrestrial- or B) aquatic-derived n -alkane and sugar biomarkers (adopted from Zech et al. 2013 and Hepp
 452 et al. 2015). Uncertainties of this approach are marked with question marks and addressed in more detail
 453 in the text: 1 = robust knowledge about aquatic versus terrestrial source, 2 = robust knowledge concerning
 454 aquatic or terrestrial ϵ_{bio}^2 and $\epsilon_{\text{bio}}^{18}$ values, 3 = while the slope of the local evaporation line is quite robust
 455 for leaf water evapotranspirative enrichment, the slope is less robust for evaporative enrichment of lake
 456 water.

457

458 4 Conclusions

459 Our results and discussion on the Late Glacial to Early Holocene sedimentary record from Lake Bergsee
 460 allow the following conclusions:

461

- 462 • A straightforward source identification of the bulk organic matter is not achievable based on the
 463 bulk proxies TC/TN, $\delta^{13}\text{C}_{\text{TC}}$ and $\delta^{15}\text{N}$.
- 464 • While the long-chain n -alkanes are primarily of terrestrial origin and reflect the vegetation history
 465 as derived from pollen results, we suggest caution against the paradigmatic interpretation of the
 466 mid-chain n -alkane $n\text{-C}_{23}$ in terms of aquatic origin and the P_{aq} proxy.
- 467 • The abundant occurrence of fuc suggests that the sedimentary sugar biomarkers are primarily of
 468 aquatic origin.
- 469 • A straightforward paleoclimatic interpretation of the Lake Bergsee $\delta^2\text{H}_{n\text{-alkane}}$ and $\delta^{18}\text{O}_{\text{sugar}}$ records
 470 in terms of reflecting a paleoprecipitation signal is hindered by unknown and likely variably
 degrees of leaf and lake water enrichment, respectively.

471 During the last years, two concepts were developed in order to disentangle the precipitation from the
472 evaporation signal and to reconstruct relative humidity: the ‘dual-biomarker approach’ by Rach et al.
473 (2014) and the ‘coupled $\delta^2\text{H}_{n\text{-alkane}}\text{-}\delta^{18}\text{O}_{\text{sugar}}$ approach’ by Zech et al. (2013) and Hepp et al. (2015). Despite
474 the great potential of both approaches, we advise caution not to over-interpret sedimentary $\delta^2\text{H}_{n\text{-alkane}}$ and
475 $\delta^{18}\text{O}_{\text{sugar}}$ records. Fundamental assumptions underlying the two approaches may not be robust in every
476 case study. This concerns primarily:

- 477 • Lake water enrichment, which is assumed to be negligible in the dual-biomarker approach.
- 478 • Source identification of the biomarkers: In the case of Lake Bergsee, $n\text{-C}_{23}$ is in all likelihood a
479 mixture of aquatic and terrestrial sources and thus does not reflect $\delta^2\text{H}$ of lake water.
- 480 • Biosynthetic fractionation factors: there seems to be a large offset between terrestrial versus
481 aquatic ϵ^2_{bio} values (around -160 versus around -85‰). Hence, minor changes in the contribution
482 of terrestrial versus aquatic $n\text{-alkanes}$ are likely to have a large impact on the $\delta^2\text{H}$ record of $n\text{-C}_{23}$.

483 These state-of-the-art uncertainties clearly limit the robustness of both approaches and hindered their
484 application to the Lake Bergsee $\delta^2\text{H}_{n\text{-alkane}}$ and $\delta^{18}\text{O}_{\text{sugar}}$ records.

485

486 **Acknowledgement**

487 We are very grateful to M. Benesch (Martin-Luther-University Halle-Wittenberg) for her great support with
488 compound-specific $\delta^2\text{H}$ and $\delta^{18}\text{O}$ analyses. Furthermore, we greatly acknowledge the student support with
489 $n\text{-alkane}$ and sugar biomarker preparation by L. Boysen, M. Jakob, T.M. Jahn and A. Richter (all from
490 Technical University Dresden). J. Hepp greatly acknowledges the support given by the German Federal
491 Environmental Foundation. Financial support was partially given by the region Bourgogne-Franche-Comté.

492 **References**

- 493 Aichner B, Herzschuh U, Wilkes H, et al (2010) δD values of *n*-alkanes in Tibetan lake sediments and
 494 aquatic macrophytes - A surface sediment study and application to a 16 ka record from Lake
 495 Koucha. *Organic Geochemistry* 41:779–790. doi:
 496 <http://dx.doi.org/10.1016/j.orggeochem.2010.05.010>
- 497 Aichner B, Ott F, Słowiński M, et al (2018) Leaf wax *n*-alkane distributions record ecological changes
 498 during the Younger Dryas at Trzechowskie paleolake (Northern Poland) without temporal delay.
 499 *Climate of the Past Discussions* 1–29. doi: 10.5194/cp-2018-6
- 500 Allison GB, Gat JR, Leaney FWJ (1985) The relationship between deuterium and oxygen-18 delta values in
 501 leaf water. *Chemical Geology* 58:145–156
- 502 Amelung W, Cheshire MV, Guggenberger G (1996) Determination of neutral and acidic sugars in soil by
 503 capillary gas-liquid chromatography after trifluoroacetic acid hydrolysis. *Soil Biology and*
 504 *Biochemistry* 28:1631–1639
- 505 Andrews MA (1989) Capillary Gas-Chromatographi Analysis of Monosaccharides: Improvments and
 506 comparisons Trifluoroacetylation and Trimethylsilylation of sugar O-Benzyl- and O-Methyl-Oximes.
 507 *Carbohydrate Research* 194:1–19
- 508 Bariac T, Gonzalez-Dunia J, Katerji N, et al (1994) Spatial variation of the isotopic composition of water
 509 (^{18}O , 2H) in the soil-plant-atmosphere system, 2. Assessment under field conditions. *Chemical*
 510 *Geology* 115:317–333
- 511 Becker A, Ammann B, Anselmetti FS, et al (2006) Paleoenvironmental studies on Lake Bergsee, Black
 512 Forest, Germany. *Neues Jahrbuch für Geologie und Paläontologie - Abhandlungen* 240:405–445
- 513 Becker A, Angelstein S (2004) Rand- und subglaziale Rinnen in den Vorbergen des Süd-Schwarzwaldes bei
 514 Bad Säckingen , Hochrhein. *Eiszeitalter und Gegenwart* 54:1–19
- 515 Bock M, Glaser B, Millar N (2007) Sequestration and turnover of plant- and microbially derived sugars in
 516 a temperate grassland soil during 7 years exposed to elevated atmospheric pCO_2 . *Global Change*
 517 *Biology* 13:478–490. doi: 10.1111/j.1365-2486.2006.01303.x
- 518 Cernusak LA, Barbour MM, Arndt SK, et al (2016) Stable isotopes in leaf water of terrestrial plants. *Plant*
 519 *Cell and Environment* 39:1087–1102. doi: 10.1111/pce.12703
- 520 Coplen TB (2011) Guidelines and recommended terms for expression of stable-isotope-ratio and gas-
 521 ratio measurement results. *Rapid Communications in Mass Spectrometry* 25:2538–2560. doi:
 522 10.1002/rcm.5129
- 523 Dansgaard W (1964) Stable isotopes in precipitation. *Tellus* 16:436–468. doi: 10.1111/j.2153-

- 524 3490.1964.tb00181.x
- 525 Deutscher Wetterdienst Referenzstation Bad Säckingen. In: Agrarmeteorologische Station.
- 526 <http://www.wetter->
- 527 [bw.de/Internet/AM/inetcntrBw.nsf/cuhome.xsp?src=2060D27LT4&p1=title%3D1981-](http://www.wetter-bw.de/Internet/AM/inetcntrBw.nsf/cuhome.xsp?src=2060D27LT4&p1=title%3D1981-)
- 528 [2010~url%3D%2FInternet%2FAM%2FNotesDWD.nsf%2F%28Web_Refstat_n_BW_JM%29%2F87B8](http://www.wetter-bw.de/Internet/AM/inetcntrBw.nsf/cuhome.xsp?src=2060D27LT4&p1=title%3D1981-2010~url%3D%2FInternet%2FAM%2FNotesDWD.nsf%2F%28Web_Refstat_n_BW_JM%29%2F87B8)
- 529 [56CC9BE8B047C1257D4D003DB453%3FOpenDocument](http://www.wetter-bw.de/Internet/AM/inetcntrBw.nsf/cuhome.xsp?src=2060D27LT4&p1=title%3D1981-2010~url%3D%2FInternet%2FAM%2FNotesDWD.nsf%2F%28Web_Refstat_n_BW_JM%29%2F87B856CC9BE8B047C1257D4D003DB453%3FOpenDocument). Accessed 2 Aug 2018
- 530 Diefendorf AF, Freimuth EJ (2016) Extracting the most from terrestrial plant-derived *n*-alkyl lipids and
- 531 their carbon isotopes from the sedimentary record: A review. *Organic Geochemistry* 103:1–21. doi:
- 532 10.1016/j.orggeochem.2016.10.016
- 533 Duprat-Qualid F, Rius D, Bégeot C, et al (2017) Vegetation response to abrupt climate changes in
- 534 Western Europe from 45 to 14.7k cal a BP: the Bergsee lacustrine record (Black Forest, Germany).
- 535 *Journal of Quaternary Science* 32:1008–1021. doi: 10.1002/jqs.2972
- 536 Eglinton G, Hamilton RJ (1967) Leaf Epicuticular Waxes. *Science* 156:1322–1335. doi:
- 537 10.1126/science.156.3780.1322
- 538 Eley YL, Hren MT (2018) Reconstructing vapor pressure deficit from leaf wax lipid molecular distributions.
- 539 *Scientific Reports* 8:1–8. doi: 10.1038/s41598-018-21959-w
- 540 Eusterhues K, Lechterbeck J, Schneider J, Wolf-Brozio U (2002) Late- and post-glacial evolution of Lake
- 541 Steisslingen (I). Sedimentary history, palynological record and inorganic geochemical indicators.
- 542 *Palaeogeography, Palaeoclimatology, Palaeoecology* 187:341–371. doi: 10.1016/S0031-
- 543 0182(02)00486-8
- 544 Ficken KJ, Li B, Swain DL, Eglinton G (2000) An *n*-alkane proxy for the sedimentary input of
- 545 submerged/floating freshwater aquatic macrophytes. *Organic Geochemistry* 31:745–749. doi:
- 546 [http://dx.doi.org/10.1016/S0146-6380\(00\)00081-4](http://dx.doi.org/10.1016/S0146-6380(00)00081-4)
- 547 Freimuth EJ, Diefendorf AF, Lowell T V. (2017) Hydrogen isotopes of *n*-alkanes and *n*-alkanoic acids as
- 548 tracers of precipitation in a temperate forest and implications for paleorecords. *Geochimica et*
- 549 *Cosmochimica Acta* 206:166–183. doi: 10.1016/j.gca.2017.02.027
- 550 Gat JR (1971) Comments on the Stable Isotope Method in Regional Groundwater Investigations. *Water*
- 551 *Resources Research* 7:980–993
- 552 Gázquez F, Morellón M, Bauska T, et al (2018) Triple oxygen and hydrogen isotopes of gypsum hydration
- 553 water for quantitative paleo-humidity reconstruction. *Earth and Planetary Science Letters* 481:177–
- 554 188. doi: 10.1016/j.epsl.2017.10.020
- 555 Gelpi E, Schneider H, Mann J, Oró J (1970) Hydrocarbons of geochemical significance in microscopic
- 556 algae. *Phytochemistry* 9:603–612. doi: 10.1016/S0031-9422(00)85700-3

- 557 Gibson JJ, Birks SJ, Edwards TWD (2008) Global prediction of δ_A and $\delta^2\text{H}$ - $\delta^{18}\text{O}$ evaporation slopes for
558 lakes and soil water accounting for seasonality. *Global Biogeochemical Cycles* 22:1–12. doi:
559 10.1029/2007GB002997
- 560 Gibson JJ, Birks SJ, Yi Y (2016) Stable isotope mass balance of lakes: A contemporary perspective.
561 *Quaternary Science Reviews* 131:316–328. doi: 10.1016/j.quascirev.2015.04.013
- 562 Gross S, Glaser B (2004) Minimization of carbon addition during derivatization of monosaccharides for
563 compound-specific $\delta^{13}\text{C}$ analysis in environmental research. *Rapid Communications in Mass*
564 *Spectrometry* 18:2753–2764. doi: 10.1002/rcm.1684
- 565 Hepp J, Rabus M, Anhäuser T, et al (2016) A sugar biomarker proxy for assessing terrestrial versus
566 aquatic sedimentary input. *Organic Geochemistry* 98:98–104. doi:
567 10.1016/j.orggeochem.2016.05.012
- 568 Hepp J, Tuthorn M, Zech R, et al (2015) Reconstructing lake evaporation history and the isotopic
569 composition of precipitation by a coupled $\delta^{18}\text{O}$ – $\delta^2\text{H}$ biomarker approach. *Journal of Hydrology*
570 529:622–631
- 571 Hepp J, Wüthrich L, Bromm T, et al (2018) How dry was the Younger Dryas? Evidence from a coupled
572 $\delta^2\text{H}$ - $\delta^{18}\text{O}$ biomarker paleohygrometer, applied to the Lake Gemündener Maar sediments, Western
573 Eifel, Germany. *Climate of the Past Discussions* 1–44. doi: 10.5194/cp-2018-114
- 574 Hepp J, Zech R, Rozanski K, et al (2017) Late Quaternary relative humidity changes from Mt. Kilimanjaro,
575 based on a coupled ^2H - ^{18}O biomarker paleohygrometer approach. *Quaternary International*
576 438:116–130. doi: 10.1016/j.quaint.2017.03.059
- 577 Hou J, D’Andrea WJ, Huang Y (2008) Can sedimentary leaf waxes record D/H ratios of continental
578 precipitation? Field, model, and experimental assessments. *Geochimica et Cosmochimica Acta*
579 72:3503–3517. doi: 10.1016/j.gca.2008.04.030
- 580 Jacob J, Huang Y, Disnar JR, et al (2007) Paleohydrological changes during the last deglaciation in
581 Northern Brazil. *Quaternary Science Reviews* 26:1004–1015. doi: 10.1016/j.quascirev.2006.12.004
- 582 Kahmen A, Schefuß E, Sachse D (2013) Leaf water deuterium enrichment shapes leaf wax *n*-alkane δD
583 values of angiosperm plants I: Experimental evidence and mechanistic insights. *Geochimica et*
584 *Cosmochimica Acta* 111:39–49
- 585 Knapp DR (1979) *Handbook of Analytical Derivatization Reactions*. John Wiley & Sons, New York,
586 Chichester, Brisbane, Toronto, Singapore
- 587 Litt T, Brauer A, Goslar T, et al (2001) Correlation and synchronisation of Lateglacial continental
588 sequences in northern central Europe based on annually laminated lacustrine sediments.
589 *Quaternary Science Reviews* 20:1233,1249

- 590 Maffei M (1996) Chemotaxonomic significance of leaf wax *n*-alkanes in the umbelliferae, cruciferae and
591 leguminosae (subf. Papilionoideae). *Biochemical Systematics and Ecology* 24:531–545. doi:
592 10.1016/0305-1978(96)00037-3
- 593 Mayer B, Schwark L (1999) A 15,000-year stable isotope record from sediments of Lake Steisslingen,
594 Southwest Germany. *Chemical Geology* 161:315–337. doi: 10.1016/S0009-2541(99)00093-5
- 595 Mayr C (2002) Möglichkeiten der Klimarekonstruktion im Holozän mit $\delta^{13}\text{C}$ - und $\delta^2\text{H}$ -Werten von Baum-
596 Jahrringen auf der Basis von Klimakammerversuchen und Rezentstudien. PhD thesis, Ludwig-
597 Maximilians-Universität München. GSF-Bericht 14/02, 152 pp
- 598 McInerney FA, Helliker BR, Freeman KH (2011) Hydrogen isotope ratios of leaf wax *n*-alkanes in grasses
599 are insensitive to transpiration. *Geochimica et Cosmochimica Acta* 75:541–554. doi:
600 10.1016/j.gca.2010.10.022
- 601 Meyers PA, Ishiwatari R (1993) Lacustrine organic geochemistry - an overview of indicators of organic
602 matter sources and diagenesis in lake sediments. *Organic Geochemistry* 20:867–900
- 603 Muschitiello F, Pausata FSR, Watson JE, et al (2015) Fennoscandian freshwater control on Greenland
604 hydroclimate shifts at the onset of the Younger Dryas. *Nature Communications* 6:8939. doi:
605 10.1038/ncomms9939
- 606 Pedentchouk N, Zhou Y (2018) Factors Controlling Carbon and Hydrogen Isotope Fractionation During
607 Biosynthesis of Lipids by Phototrophic Organisms. In: Wilkes H (ed) *Hydrocarbons, Oils and Lipids:*
608 *Diversity, Origin, Chemistry and Fate. Handbook of Hydrocarbon and Lipid Microbiology.* Springer,
609 Cham, pp 1–24
- 610 Prahlg FG, Bennett JT, Carpenter R (1980) The early diagenesis of aliphatic hydrocarbons and organic
611 matter in sedimentary particulates from Dabob Bay, Washington. *Geochimica et Cosmochimica*
612 *Acta* 44:1967–1976. doi: 10.1016/0016-7037(80)90196-9
- 613 Prietzel J, Dechamps N, Spielvogel S (2013) Analysis of non-cellulosic polysaccharides helps to reveal the
614 history of thick organic surface layers on calcareous Alpine soils. *Plant and Soil* 365:93–114. doi:
615 10.1007/s11104-012-1340-2
- 616 Rach O, Brauer A, Wilkes H, Sachse D (2014) Delayed hydrological response to Greenland cooling at the
617 onset of the Younger Dryas in western Europe. *Nature Geoscience* 7:109–112. doi:
618 10.1038/ngeo2053
- 619 Rach O, Kahmen A, Brauer A, Sachse D (2017) A dual-biomarker approach for quantification of changes in
620 relative humidity from sedimentary lipid D/H ratios. *Climate of the Past* 13:741–757. doi:
621 10.5194/cp-2017-7
- 622 Rao Z, Jia G, Qiang M, Zhao Y (2014) Assessment of the difference between mid- and long chain

- 623 compound specific $\delta D_{n\text{-alkanes}}$ values in lacustrine sediments as a paleoclimatic indicator. *Organic*
624 *Geochemistry* 76:104–117. doi: 10.1016/j.orggeochem.2014.07.015
- 625 Rozanski K, Klisch MA, Wachniew P, et al (2010) Oxygen-isotope geothermometers in lacustrine
626 sediments: New insights through combined $\delta^{18}\text{O}$ analyses of aquatic cellulose, authigenic calcite
627 and biogenic silica in Lake Gościaz, central Poland. *Geochimica et Cosmochimica Acta* 74:2957–
628 2969. doi: 10.1016/j.gca.2010.02.026
- 629 Sachse D, Billault I, Bowen GJ, et al (2012) Molecular Paleohydrology: Interpreting the Hydrogen-Isotopic
630 Composition of Lipid Biomarkers from Photosynthesizing Organisms. *Annual Reviews* 40:221–249.
631 doi: 10.1146/annurev-earth-042711-105535
- 632 Sachse D, Radke J, Gleixner G (2006) δD values of individual *n*-alkanes from terrestrial plants along a
633 climatic gradient – Implications for the sedimentary biomarker record. *Organic Geochemistry*
634 37:469–483. doi: 10.1016/j.orggeochem.2005.12.003
- 635 Schwark L, Zink K, Lechterbeck J (2002) Reconstruction of postglacial to early Holocene vegetation
636 history in terrestrial Central Europe via cuticular lipid biomarkers and pollen records from lake
637 sediments. *Geology* 30:463–466. doi: 10.1130/0091-7613(2002)030<0463
- 638 Seki O, Meyers PA, Yamamoto S, et al (2011) Plant-wax hydrogen isotopic evidence for postglacial
639 variations in delivery of precipitation in the monsoon domain of China. *Geology* 39:875–878. doi:
640 10.1130/G32117.1
- 641 Sessions AL, Burgoyne TW, Schimmelmann A, Hayes JM (1999) Fractionation of hydrogen isotopes in
642 lipid biosynthesis. *Organic Geochemistry* 30:1193–1200
- 643 Tarasov PE, Müller S, Zech M, et al (2013) Last glacial vegetation reconstructions in the extreme-
644 continental eastern Asia: Potentials of pollen and *n*-alkane biomarker analyses. *Quaternary*
645 *International* 290–291:253–263. doi: 10.1016/j.quaint.2012.04.007
- 646 Tu TTN, Egasse C, Zeller B, et al (2011) Early degradation of plant alkanes in soils: A litterbag experiment
647 using ^{13}C -labelled leaves. *Soil Biology and Biochemistry* 43:2222–2228. doi:
648 10.1016/j.soilbio.2011.07.009
- 649 Tuthorn M, Zech M, Ruppenthal M, et al (2014) Oxygen isotope ratios ($^{18}\text{O}/^{16}\text{O}$) of hemicellulose-derived
650 sugar biomarkers in plants, soils and sediments as paleoclimate proxy II: Insight from a climate
651 transect study. *Geochimica et Cosmochimica Acta* 126:624–634. doi:
652 <http://dx.doi.org/10.1016/j.gca.2013.11.002>
- 653 Tuthorn M, Zech R, Ruppenthal M, et al (2015) Coupling $\delta^2\text{H}$ and $\delta^{18}\text{O}$ biomarker results yields
654 information on relative humidity and isotopic composition of precipitation - a climate transect
655 validation study. *Biogeosciences* 12:3913–3924. doi: 10.5194/bg-12-3913-2015

- 656 van den Bos V, Engels S, Bohncke SJP, et al (2018) Late Holocene changes in vegetation and atmospheric
657 circulation at Lake Uddelermeer (The Netherlands) reconstructed using lipid biomarkers and
658 compound-specific δD analysis. *Journal of Quaternary Science* 33:100–111. doi: 10.1002/jqs.3006
- 659 von Grafenstein U, Erlenkeuser H, Müller J, et al (1998) The cold event 8200 years ago documented in
660 oxygen isotope records of precipitation in Europe and Greenland. *Climate Dynamics* 14:73–81. doi:
661 10.1007/s003820050210
- 662 Walker CD, Brunel J-P (1990) Examining Evapotranspiration in a Semi-Arid Region using Stable Isotopes
663 of Hydrogen and Oxygen. *Journal of Hydrology* 118:55–75
- 664 Wurth G, Niggemann S, Richter DK, Mangini A (2004) The Younger Dryas and Holocene climate record of
665 a stalagmite from Hölloch Cave (Bavarian Alps, Germany). *Journal of Quaternary Science* 19:291–
666 298. doi: 10.1002/jqs.837
- 667 Zech M, Bimüller C, Hemp A, et al (2011a) Human and climate impact on ^{15}N natural abundance of plants
668 and soils in high-mountain ecosystems: a short review and two examples from the Eastern Pamirs
669 and Mt. Kilimanjaro. *Isotopes in environmental and health studies* 47:286–96. doi:
670 10.1080/10256016.2011.596277
- 671 Zech M, Buggle B, Leiber K, et al (2009) Reconstructing Quaternary vegetation history in the Carpathian
672 Basin, SE Europe, using *n*-alkane biomarkers as molecular fossils: problems and possible solutions,
673 potential and limitations. *Eiszeitalter und Gegenwart – Quaternary Science Journal* 58:148–155.
674 doi: 10.3285/eg.58.2.03
- 675 Zech M, Glaser B (2009) Compound-specific $\delta^{18}O$ analyses of neutral sugars in soils using gas
676 chromatography-pyrolysis-isotope ratio mass spectrometry: problems, possible solutions and a first
677 application. *Rapid Communications in Mass Spectrometry* 23:3522–3532. doi: 10.1002/rcm
- 678 Zech M, Mayr C, Tuthorn M, et al (2014a) Oxygen isotope ratios ($^{18}O/^{16}O$) of hemicellulose-derived sugar
679 biomarkers in plants, soils and sediments as paleoclimate proxy I: Insight from a climate chamber
680 experiment. *Geochimica et Cosmochimica Acta* 126:614–623. doi:
681 <http://dx.doi.org/10.1016/j.gca.2013.10.048>
- 682 Zech M, Pedentchouk N, Buggle B, et al (2011b) Effect of leaf litter degradation and seasonality on D/H
683 isotope ratios of *n*-alkane biomarkers. *Geochimica et Cosmochimica Acta* 75:4917–4928. doi:
684 <http://dx.doi.org/10.1016/j.gca.2011.06.006>
- 685 Zech M, Tuthorn M, Detsch F, et al (2013) A 220 ka terrestrial $\delta^{18}O$ and deuterium excess biomarker
686 record from an eolian permafrost paleosol sequence, NE-Siberia. *Chemical Geology* 360–361:220–
687 230. doi: <http://dx.doi.org/10.1016/j.chemgeo.2013.10.023>
- 688 Zech M, Tuthorn M, Schlütz F, et al (2014b) A 16-ka $\delta^{18}O$ record of lacustrine sugar biomarkers from the

- 689 High Himalaya reflects Indian Summer Monsoon variability. *Journal of Paleolimnology* 51:241–251.
690 doi: 10.1007/s10933-013-9744-4
- 691 Zech M, Zech R, Glaser B (2007) A 240,000-year stable carbon and nitrogen isotope record from a loess-
692 like palaeosol sequence in the Tumara Valley, Northeast Siberia. *Chemical Geology* 242:307–318.
693 doi: 10.1016/j.chemgeo.2007.04.002
- 694 Zech M, Zech R, Rozanski K, et al (2015) Do *n*-alkane biomarkers in soils/sediments reflect the $\delta^2\text{H}$
695 isotopic composition of precipitation? A case study from Mt . Kilimanjaro and implications for
696 paleoaltimetry and paleoclimate research. *Isotopes in Environmental and Health Studies* 51:508–
697 524. doi: 10.1080/10256016.2015.1058790
698

Additional publications

A list of additional publications not included in the cumulative PhD thesis is given below:

Johannes Hepp, Mario Tuthorn, Roland Zech, Ines Mügler, Frank Schlütz, Wolfgang Zech, Michael Zech (2015): Reconstructing lake evaporation history and the isotopic composition of precipitation by a coupled $\delta^{18}\text{O}$ - $\delta^2\text{H}$ biomarker approach. *Journal of Hydrology*, 529:622-631, <https://doi.org/10.1016/j.jhydrol.2014.10.012>.

Martin Bachmann, **Johannes Hepp**, Michael Zech, Michael Bulang, Annette Zeyner (2017): Application of natural wax markers in equine nutrition studies – current state, limitations and perspectives, *Livestock Science*, 208:77-89, <https://doi.org/10.1016/j.livsci.2017.12.010>.

Katja Osterloh, Nadine Tauchnitz, Oliver Spott, **Johannes Hepp**, Sabine Bernsdorf, Ralph Meissner (2018): Changes of methane and nitrous oxide emissions in a transition bog in central Germany (German National Park Harz Mountains) after rewetting, *Wetlands Ecology and Management*, 26:87-102, <https://doi.org/10.1007/s11273-017-9555-x>.

Versicherungen und Erklärungen

(§8 Satz 2 Nr. 3 PromO Fakultät)

Hiermit versichere ich eidesstattlich, dass ich die Arbeit selbstständig verfasst und keine anderen als die von mir angegebenen Quellen und Hilfsmittel benutzt habe (vgl. Art. 64 Abs. 1 Satz 6 BayHSchG).

(§8 Satz 2 Nr. 3 PromO Fakultät)

Hiermit erkläre ich, dass ich die Dissertation nicht bereits zur Erlangung eines akademischen Grades eingereicht habe und dass ich nicht bereits diese oder eine gleichartige Doktorprüfung endgültig nicht bestanden habe.

(§8 Satz 2 Nr. 4 PromO Fakultät)

Hiermit erkläre ich, dass ich Hilfe von gewerblichen Promotionsberatern bzw. – Vermittlern oder ähnlichen Dienstleistern weder bisher in Anspruch genommen habe noch künftig in Anspruch nehmen werde.

(§8 Satz 2 Nr. 7 PromO Fakultät)

Hiermit erkläre ich mein Einverständnis, dass die elektronische Fassung der Dissertation unter Wahrung meiner Urheberrechte und des Datenschutzes einer gesonderten Überprüfung unterzogen werden kann.

(§8 Satz 2 Nr. 8 PromO Fakultät)

Hiermit erkläre ich mein Einverständnis, dass bei Verdacht wissenschaftlichen Fehlverhaltens Ermittlungen durch universitätsinterne Organe der wissenschaftlichen Selbstkontrolle stattfinden können.

Ort, Datum, Unterschrift